The Rates and Mechanisms of Substitution from Ru(II) Complexes with Different Non-leaving Ligand Environments

MESHACK KITUYI SITATI

School of Chemistry and Physics

University of KwaZulu-Natal

Pietermaritzburg

December 2018

The Rates and Mechanisms of Substitution from Ru(II) Complexes with Different Non-leaving Ligand Environments

By

MESHACK KITUYI SITATI

Dip. Ed. (KSTC), BSc. (Hons) (JKUAT), MSc. (UKZN)

Submitted in partial fulfilment of the academic requirements for the degree of

Doctor of Philosophy

in the College of Agriculture, Engineering and Science

School of Chemistry and Physics

University of KwaZulu-Natal

Pietermaritzburg

December 2018

Declaration

I, MK Sitati declare that:

1. The research reported in this thesis, except where otherwise indicated, is my original research.

2. This thesis has not been submitted for any degree or examination at any other university.

3. This thesis does not contain other persons' data, pictures, graphs or other information, unless specifically acknowledged as being sourced from other persons.

4. This thesis does not contain other persons' writing, unless specifically acknowledged as being sourced from other researchers. Where other written sources have been quoted, then:

a. Their words have been re-written but the general information attributed to them has been referenced

b. Where their exact words have been used, then their writing has been placed in italics and inside quotation marks, and referenced.

5. This thesis does not contain text, graphics or tables copied and pasted from the Internet, unless specifically acknowledged, and the source being detailed in the thesis and in the References sections.

Signed: 

MK Sitati Date: 29/02/2019

We hereby certify that this is correct, and as the candidate's supervisor we have approved this thesis for submission

....

Dr. A. Mambanda **Prof D Jaganyi**

University Of KwaZulu-Natal
School of Chemistry and physics
Pietermaritzburg
December 2018

This work is dedicated to my loving family for their incredible patience and support

Table of Contents

Abstract

Results from multiple studies have confirmed that the nature of ligands on the metal centre determines the properties of an anti-cancer agent in a biological environment. Ligands affect solubility, substitution reactivity, stability of compound and product after substitution and the type of interaction between the agent and DNA among others properties. Due to competition for sulphur biomolecules by anti-cancer agents in the cells, substitution reactions of potential anti-cancer metal complexes with biologically relevant ligands sheds light on the possible interaction modes of the Ru(II) complexes and stability of the resulting products. This helps in the design, synthesis and administration of new pharmacological agents and in the concept of chemo-protection. On this basis, the study of rate of substitutions from the Ru(II) complexes by thiourea nucleophiles under *pseudo*-first order conditions was undertaken. The reactions were studied as a function of concentration and temperature using standard Stopped Flow technique for ultrafast reactions or UV-Visible Spectrophotometer.

The **first** series of the complexes investigated the role of arene ligands on the rate of substitutions in (aqua)(η^6-arene)Ru(II) complexes. The rate of substitution for the tri-aqua Ru(II) complexes was controlled by the π-acceptor ability of the arene ligands. For the complexes bearing 2,2'-bipyridyl co-ligand, the leaving aqua ligands are located *trans* to the arene ligands. For these complexes, the reactivity increase in accordance to the number and type of alkyl substituents on the η^6-arene ligands which donate inductively into the π-molecular orbitals, causing increased *trans* labialisation of the coordinated aquo co-ligand. Compared to the reactivity of tri-aquo complexes, the auxiliary bipyridyl ligands lower the rate of substitution for the later complex by a factor of about 100, due to its steric hindrance at the Ru(II) metal centre. The significantly negative activation entropies and positive activation enthalpies suggest that the activation process is dominated by bond making. In the **second** study, the role of arene and phosphino ligands on the rate of chloride substitution from Ru (II) complexes containing arene and phosphino co-ligands was investigated. It was observed that the coordinated arene ligand donates electrons towards the Ru(II) metal centre and its π-electron cloud presents an electrostatic repulsive effect onto and around the Ru centre as measured by the projected cone angle. The bidentate bis(diphenylphosphino)-methane ligand hinders the approach of nucleophiles during the substitution process. When the bis(diphenylphosphino)methane chelate is expanded through the introduction of a methylene carbon within the bridge, the steric hindrance to the approach of nucleophiles is reduced and

the ligand assumes a trough like conformation which traps the nucleophile within the coordination sphere. This enhances the reactivity by a factor of 10^3.

The rate of chloride substitution from 2,4,6-tris-(2-pyridyl)-1,3,5-triazineRu(PPh3)(Cl) and analogous complexes was done in the **third** study. The study showed that higher π-acceptor ability of *cis* ligands increase the electrophilicity of the metal centre resulting in enhanced reactivity. Electron donating substituents on the ligands at the cis position lower the π-acceptor ability of the ligand hence lower electrophilicity of the Ru(II) metal centre leading to slower rate of substitution. The investigation on the effect of 2-(2-Pyridyl)azole-based ancillary ligands (L) on the chloride substitution from $[Ru^{II}(tpy)(L)(Cl)]^+$ in the **fourth** study revealed that strong electronegative atoms (O or S) in the auxiliary ligands enhance their π-back-donation capacity thereby increasing the electrophilicity of the metal centre and hence the reactivity. On the other hand, the –NH group donate electron density to the metal centre by outer sphere proton donation causing *trans*-effect thereby which increases the reactivity more than in the former case. The **fifth** study sought to understanding the effect of substituents on rate of chloride substitution from Ru(II)tpy complexes. Ru(II)tpy complexes with the tpy having electron donating substituents trans to the labile ligand were dominated by *trans*-effect while those where the tpy bears electron accepting substituents had enhanced π-back-bonding controlling the reactivity. The rate of substitution from the Ru(II) complexes was more strongly affected by electron donating substituents. Electron donating ligands at the *cis* position slow down the rate of substitution from the Ru(II) metal centre.

Data from DFT calculations performed using Gaussian09 suite of programmes was used to support the observed rates of substitution from the Ru(II) complexes. Large negative values of entropies of activation and positive enthalpies of activation indicate associative mode of activation. On the other hand small positive values of entropies of activation indicate dissociatively activate interchange mode of substitutions. The studies were explored on model Ru(II) complexes with bio-relevant thiourea nucleophiles to predict possible interaction with biomolecules which has become part of the methods used in the endeavour to search for alternative anti-cancer agents with improved efficacy and higher spectrum of activity.

Acknowledgements

Firstly, this work would not have been possible by any means without God's grace and favour. Secondly, I am grateful to the University of KwaZulu-Natal for funding this project through to the end. I am especially indebted to Prof Deogratius Jaganyi whose exceptional mentorship skills, profound knowledge in chemistry, patience and love enabled this project to materialise. He mentored me and gave me a firm foundational basis that I applied in this project. As my teacher and mentor, he has taught me more than I could ever give him credit for here. He has shown me, by his own example, what a good scientist and person should be. I am so grateful to Dr Allen Mambanda for the supervisory role that he executed with great distinction. He offered unique expert advice and was always there for whatever kind of support I needed. My family have been supportive of my career goals and who worked actively to provide me with the protected academic time to pursue those goals. I would like to thank my parents Mr. John Sitati Wabwile and Mrs Mary Margaret Sitati, whose love and guidance are with me in whatever I pursue. They are the ultimate role models in my life. Importantly, I wish to thank my loving and supportive wife, Lydia Nasimiyu, and my four lovely kids: Larvin, Currie, Quincy and Leroy who provided unending inspiration by their resilience and patience during my absence. I am grateful to my brother Emmanuel Sasaka, my sisters Imelda Khakasa and Mercyline Namarome and their families for supporting me. My sister in-law Margaret Sasaka, niece Anne Mwenya, nephew Trevor Mwenya and the larger Wabwile family are unforgettable. My church family: Lighthouse Chapel International South Africa birthed me into a real hope, that of eternal life, what a great family! I cannot even begin to explain the love and comfort I have derived in this family under the able leadership of Bishop Larry Odonkor and Rev. Daniel Harley. To say thank you to this family is an understatement. I am grateful to all the academics and non-teaching staff in the school of Chemistry with whom I have had the pleasure to interact with on professional and other supportive matters throughout my stay. My interaction with academic staff, non-academic staff and postgraduate colleagues has taught me a great deal about both scientific research and life in general. I wish to single out a great friend and brother, Dr Isaac Masika Wekesa, through whom I learned of study opportunities in South Africa and successfully applied for this opportunity. He ushered me in the world of research. I will be forever indebted to this unselfish true friend. Finally, I have received great warmth and friendship from South Africans for the whole time I have been in this beautiful country. **God bless you**.

Publications and Conference Contributions

Publications

1. The reactivity of 4-substituted tpyPt(II) complexes with bio-relevant azole nucleophiles. A kinetic and mechanistic study. Inorganica Chimica Acta, 453 (2016) 531–537
3. The rate of aqua substitution from η^6-arene Ru(II) aqua complexes. Inorganica Chimica Acta, ICA_2018_1512 | Research Paper (2018)

Ready manuscripts from previous work and the work reported in this thesis ready for publication:

4. The role of Ruthenium Polypyridyl fragment on the reactivity of ethylene Pt(II) aqua unit with biological nucleophiles.
5. Reactivity of $[(\eta^6$-arene)(chloro)(phosphino)ruthenium(II)$]^+$ complexes towards thiourea nucleophiles
6. The rate of chloride substitution from Ru(II) complexes bearing triphenylphosphine and centrosymmetric 2,4,6-(substituted)-1,3,5-triazine tridentate ligands
7. Effect of 2-(2-Pyridyl)azole based auxiliary ligands (L) on the rate of chloride substitutions from $[Ru(II)(tpy)(L)(Cl)]^+$ complexes
8. Substituent effect on the rate of substitution from [(Dichloro)((4-substituted)-t erpyridine)(triphenylphosphino)Ruthenium(II)complexes

Conferences

1. University of KwaZulu-Natal postgraduate research day, Westville campus, 27/10/2014. *The role of ethylene polyglycoxyl pendant units on the tpy based Pt(II) complexes. A kinetic and mechanistic study*

2. The 9th International Conference of the Kenya Chemical Society, United States International University, Kenya, 10/5/2017. *The role of arene ligands on the rate of substitutions in mono-aqua η^6-arene Rut (II) complexes.*

3. The 1st education, science and technology symposium by the Kenya high commission to South Africa, University of KwaZulu-Natal Pietermaritzburg, 13/08/2016. *The role of Ru polypyridyl fragment on the reactivity of ethylene Pt(II) aqua units with biological nucleophiles.*

List of abbreviations and Symbols

DNA	Deoxyribonucleic acid
NMR	Nuclear Magnetic Resonance
Pt	Platinum
SAR	Structure Activity Relationship
Ru	Ruthenium
S	Sulphur
Nu	Nucleophile
Him	imidazole
NAMI	Na{*trans*-[Ru(III)Cl_4(DMSO)(Him)]}
NAMI-A	[H_2im][*trans*-Ru(III)Cl_4(DMSO)(Him)]
Fac	Facial
Dmso	Dimethylsulfoxide
tpy	2,2′:6′,2″-terpyridine
bpy	2,2′-bipyridine
mer-	Meridional
en	Ethylenediamine
dach	diaminocyclohexane
HT-29	Human colon cancer cell line
MCF-7	Michigan Cancer Foundation-7 (breast cancer cell line)
bpyMe	4,4′-dimethyl-2,2’-bipyridine
ROS	Reactive Oxygen Species
Bcl-2	B-cell lymphoma 2 (Regulator proteins that regulate cell death)
Cp	eta(5)-C_5H_5)
B3LYP	Hybrid Becke, 3-parameter, Lee-Young-Parr
LANL2DZ	Los Alamos National Laboratory 2 double ζ
Py	Pyridine
Pd	Palladium
PGM	Platinum Group Metals
UV/Vis	Ultraviolet/Visible
LCMS	Liquid Crystal Mass Spectrometer
HOMO	Highest Occupied Molecular Orbital
LUMO	Lowest Unoccupied Molecular Orbital

NBO	Natural Bond Orbital
DFT	Density functional theory
TOF	Time of Flight
m	Meta
P	Para
TU	Thiourea
DMTU	1,3-dimethyl-2-thiourea
TMTU	1,1,3,3-tetramethyl-2-thiourea
Å	Angstrong
eV	Electronvolt
ESI	Electron Spray Ionization
A	Associative mechanism of substitution
D	Dissociative mechanism of substitution
I	Interchange mechanism
I_A	Associatively activated interchange mechanism
I_D	Dissociatively activated interchange mechanism
C-PCM	Conductor Polarisable Continum
DMF	Dimethylformamide
K	Kelvin
E_a	Activation energy
e	Exponential
G	Guanine
HMG	High Mobility Group Protein
Ɛ	Molar absorptivity
$\Delta H^{\neq}$	Activation enthalpy
$\Delta S^{\neq}$	Activation entropy
η_{pt}	Nucleophilicity
k_2	Second order rate constant for the first substitution step
$k_{2'}$	Second order rate constant for the second substitution step
k_{obs}	Observed *pseudo* first order rate constant for the first substitution step
$k_{obs'}$	Observed *pseudo* first order rate constant for the second substitution step
L	Ligand
L1210	Murine Leukemia cell-line
M	Molarity ($moldm^{-3}$)

mL	Millilitre
PPh_3	Triphenylphosphine
Ppm	Parts Per Million
T	Temperature

List of figures

Chapter 1

Chapter 2

Chapter 3

Chapter 4

Chapter 5

Chapter 6

Chapter 7

Chapter 8

Chapter 9

List of Tables

Chapter 2

Chapter 3

Chapter 4

Chapter 5

Chapter 6

Chapter 7

List of Schemes

Chapter 1

Chapter 2

Chapter 3

Chapter 4

Chapter 5

Chapter 6

Chapter 7

Chapter 9

Chapter 1

The development of platinum (Pt) and ruthenium (Ru) anti-cancer drugs

1.0 Introduction

Cancer evolves from chemical damage to the genetics of cells which may prevent them from being responsive to normal cell growth and tissue controls.[1] Some types of cancer causes metastasis where the cancerous cells multiply rapidly into tumours of varying scales and spreads to other areas while other types occur as localised tumours. An anti-cancer agent must kill the rapidly dividing cells to slow and eventually stop the cancer from spreading.[2] Cisplatin has been the most successful in the treatment of some types of cancer than any other anti-cancer drug.[3] Some tumours are intrinsically resistant to its treatment or may develop the resistance after initial response. Cisplatin is toxic to the kidneys, liver and patients suffer severe side-effects, namely neurotoxicity, ototoxicity, nausea, vomiting, bone marrow dysfunction and nephrotoxicity, the latter being dose-limiting.[4] [5] [6] Cisplatin shortcomings have elicited not only a search for other better agents but effort towards understanding the transport of the drug in the body and its cellular uptake, as well as its mechanism of action inside the cell to inform the design of improved pharmaceuticals.

1.1 Cisplatin Mechanism of action

It is generally accepted that Pt drugs interact with the DNA within the cell and form DNA adducts.[7] The anti-cancer activity of Pt drugs is ascribed to DNA binding of the complexes.[8] These cisplatin-DNA adducts have been characterized using HPLC techniques with various mono- and di-adducts reported in literature confirming the binding of cisplatin to DNA in different modes.[9] [10] [11] The binding of the Pt complexes to DNA distort the normal helix structure of the later forming a kink which may be recognized by certain cellular proteins resulting in the repair of DNA or may be unrecognised triggering apoptosis and cell death.[12] [13] Formation of cisplatin-DNA adducts and kinking on the DNA structure at the Pt binding site were confirmed by NMR-techniques[14] and gel electrophoresis [15] respectively.

Notwithstanding the rapid binding of the Pt drugs onto the numerous S-containing bionucleophiles, its binding to the N7-donor atoms of guanine induce the anti-cancer cytotoxic effect. Thiols bind irreversibly, while the thioether have been shown to get

substituted by DNA species thus acting as chemo-protectors of the Pt drugs.[16] [17] [18] [19] Although Pt–S-adducts are kinetically preferred, the binding to nucleic acid bases does finally occur. The remaining platinum has been postulated to probably leave the cell via the Golgi apparatus.[20] The pathway of cisplatin in the cell is illustrated by Scheme 1.1.

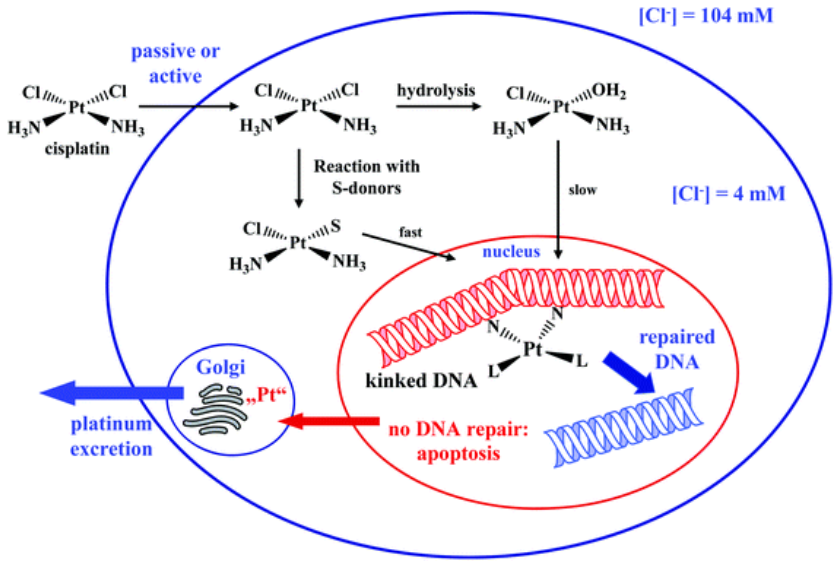

Scheme 1. 1 A simplified overview of the pathway of cisplatin in the cell[19]

1.2 Development of new platinum anticancer agents

1.2.1 Initial Platinum anti-cancer drugs

Numerous cisplatin analogues were synthesized and tested as anti-cancer agents though none of them has exhibited better qualities than cisplatin in anti-cancer chemotherapy. Structures of some of these analogues are presented in Figure 1.1. The most successful of these analogues was carboplatin.[21] It is preferred to cisplatin in the treatment of many platinum-sensitive malignancies because it has less toxicity.[21] Unfortunately it is cross-resistant with cisplatin. Its activity matches that of cisplatin in the treatment of ovarian cancers but inferior to cisplatin in the treatment of testicular, head and neck cancers.[21] Other drugs that have been approved for clinical use the world over are *cis*-diammine(glycolato)platinum(II) (nedaplatin) and (1R,2R-diaminocyclohexane)oxalatoplatinum(II) (oxaliplatin).[22] [23] [24] [25] Some of the aforementioned Pt complexes are shown in Figure 1.1.

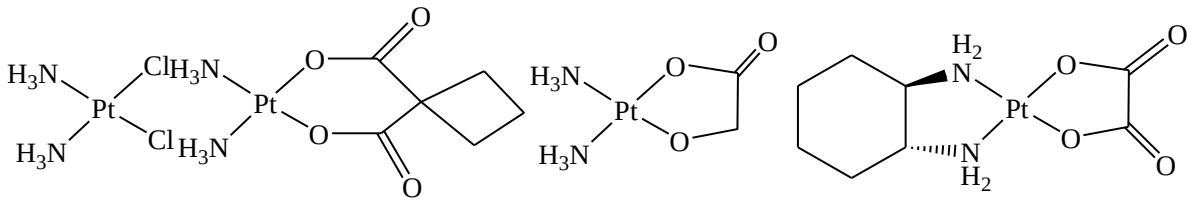

Figure 1. 1 Molecular structures of cisplatin and analogues that have been used or registered as anti-cancer agents

A common disadvantage of all analogues of cisplatin is that none offered better clinical advantages. These complexes were designed based on a common structure activity relationship and thus displayed similar activity profile to that of cisplatin. As a result the design shifted to other Pt complexes that would offer a different mechanism of action.

1.2.2 Pt(IV) complexes

Due to the problem of aqueous solubility of cisplatin and its analogues, oral administration was not possible. To tackle this problem, Pt(IV) complexes bearing lipophilic groups at axial positions that facilitated intestinal absorption of the drug were developed (Figure 1.2). These complexes were in fact pro-drugs which would undergo reduction by intracellular glutathione, ascorbic acid or other reducing agents upon entering the cell to produce active Pt(II) species.[26] [27] The most successful Pt(IV) complex is bis(acetato)amminedichlorido-(cyclohexylamine)platinum(IV) also known as satraplatin or JM216 which entered Phase III evaluation.[28] Its structure is shown in Figure 1.2.

1.2.3 Sterically hindered *cis*-Pt(II) complexes

Pt(II) complexes with capacity to sterically shield the metal centre from rapid deactivating process were designed in the search for active Pt drugs with reduced toxicity and proneness to development of resistance. An example was the complex *cis*-amminedichlorido(2-methylpyridine)platinum(II) (ZD0473 or AMD473). This analogue of cisplatin has a sterically shielding group (2-methyl pyridine) and did not exhibit any cross-resistance to cisplatin in *in vitro* tests carried out with human ovarian carcinoma cells.[29] Its structure and that of an analogue are shown in Figure 1.2. Despite lung and metastatic breast cancer patients showing good tolerability of the drug, it did not show greater efficacy over existing anti-cancer agents.[30] [31]

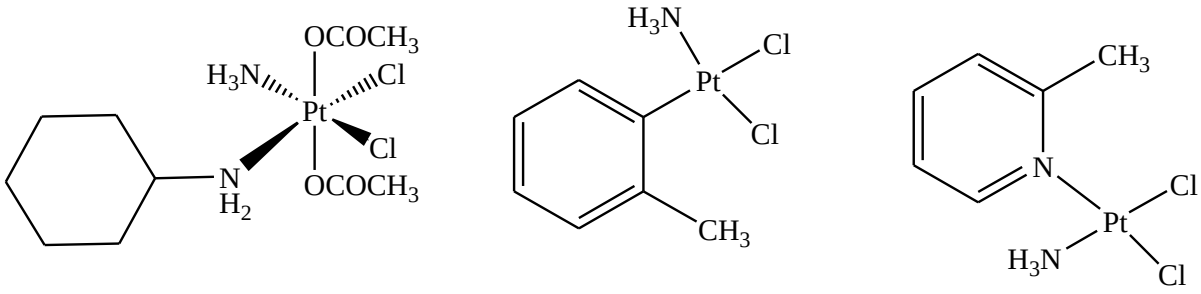

JM216 AMD437 ZD0437

Figure 1. 2 Chemical structures of Pt(II) complexes coordinated with shielding groups

1.2.4 *trans*- Pt(II) complexes

In an endeavour to look for Pt complexes which had a different mechanism to that of cisplatin, a series of *trans* Pt(II) compounds were investigated for anti-cancer activity. Active *trans* Pt(II) complexes included those with the general formula *trans*-[$PtCl_2$(L)(L')] where L, L' = N-aromatic planar ligand, amine, sulfoxide or L = L' = N-aromatic planar ligand[32] [33] or L = L' = branched aliphatic amines[34] [35] or L, L' = iminoether ligand, amine or imino-ether.[36] [37] There were also reports that replacement of one of transplatin amines in transplatine with a heterocyclic ligand such as piperidine, piperazine or 4-picoline, resulted in a radical enhancement of the cytotoxicity.[38] [39] Structures of some *trans*-platinum(II) complexes are shown in Figure 1.3.

All the *trans*-platinum complexes with bulky non-leaving groups were reported to show better cytotoxicity than cisplatin in some cases even better cytotoxicity than their respective *cis*-analogues.[32] The *trans* complexes showed an activity profile different from that of cisplatin and they often overcome resistance in cisplatin insensitive cell lines. In addition, these complexes caused different DNA alterations from those generated by *cis* Pt complexes.[3]

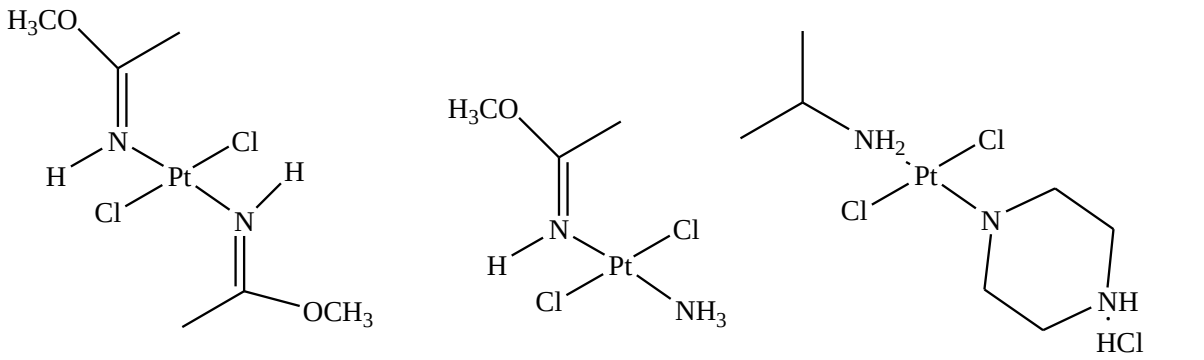

trans-[$PtCl_2${E-HN=C(OMe)Me}$_2$] *trans*-[$PtCl_2${E-HN=C(OMe)Me}(NH_3)] *trans*-[$PtCl_2$(ipa)(pz).HCl]

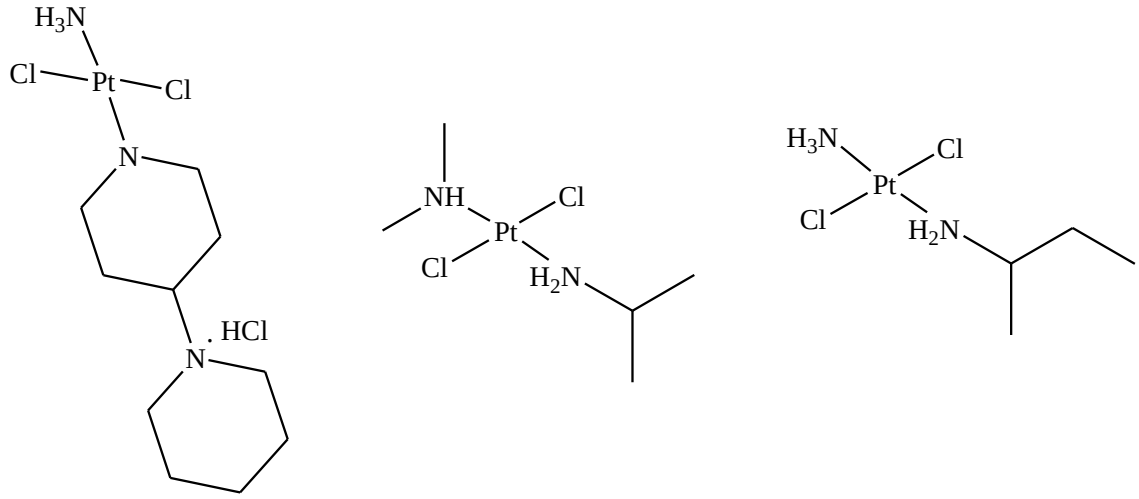

trans-[$PtCl_2(NH_3)$(pip-pip).HCl] *trans*-[$PtCl_2$(dma)(ipa)] *trans*-[$PtCl_2$(sba)($NH_{3)}$

Figure 1. 3 Structural formulas of some *trans* Pt(II) complexes

1.2.5 Dinuclear and polynuclear Pt(II) anti-cancer agents

Dinuclear and polynuclear Pt complexes were developed as a possible class of compounds with a drastically different DNA interaction to cisplatin. Several polynuclear complexes having a variety of structural features that could enable a different DNA binding and biological activity were developed. Some of the multinuclear complexes from literature are shown in Figure 1.4. These complexes vary in the number of metal centres, charge, and type of linkers (flexible or rigid). These poly-nuclear complexes displayed better antitumour activity than cisplatin with some even overcoming cisplatin resistance.[40] The dinuclear complexes with pyrazole and triazole as rigid linkers have been reported to display much higher *in vitro* cytotoxicity than cisplatin on several human tumour cell lines and to overcome cross-resistance to cisplatin.[41] [42] Tri-nuclear Pt(II) complex BBR3464 underwent phase II clinical trials after showing promising results at the pre-clinical evaluation. Due to its long

range intra-strand crosslink upon DNA, it was found to be very cytotoxically potent besides being effective against cisplatin-resistant tumours. The complex was found to affect tumours over a broad spectrum. However it was found to be acutely toxic.

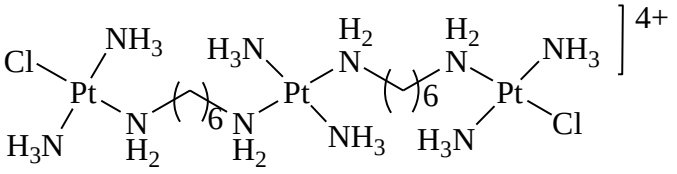

BBR3464

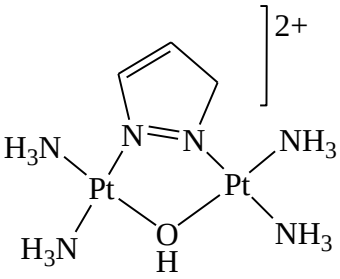

Pyrazole-bridged

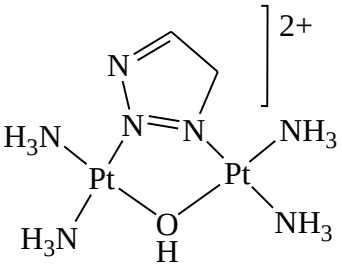

Triazole-bridged

Figure 1. 4 Chemical structures of some polynuclear Pt(II) complexes that have been reported to be cytotoxic

1.3 Ru as a possible alternative to platinum chemotherapy

In the search for metal-based anti-cancer agents with improved clinical effectiveness, reduced toxicity and a broader spectrum of activity, complexes of other metals have been considered. The idea was that some non-Pt active compounds may have different mechanisms of action, biodistribution and toxicity profiles against human malignancies that are resistance to Pt based chemotherapies. Indeed Ru complexes have shown promising *in vitro* and *in vivo* cytotoxicity even in cisplatin resistant cancers and are generally less toxic.[43]

Ru complexes have found numerous applications in bio-medical science. For example Ru complexes have been used for radio-diagnostic imaging.[44] *cis*-$[Ru(III)(NH_3)_4(HIm)_2]^{3+}$ is a potential immunosuppressant while Ru-organic drug conjugates such as $[Ru(II)Cl_2$-$(chloroquine)_2]$ are used as anti-microbials against malaria while others for the treatment of Chaga´s disease. [45] Ru complexes attached with organic antibiotic compounds like the Ru(III) conjugates of thiosemicarbazone are used as antibiotics against *Salmonellatyphi* and *Enterobacteria faecalis.* Polyaminocarboxylates Ru(III) complexes are nitrosyldelivery/-

scavengers and can potentially be used to treat stroke, septic shock, arthritis, epilepsy and diabetes or used as vasodilator/vasoconstrictor agents.[46]

Ru(II) and Ru(III) complexes exhibit similar ligand-exchange kinetics as Pt(II) complexes. This qualify them as alternatives to anti-cancer Pt(II) drugs.[46] [47] Before most metal drugs reach their biological targets, they undergo various bio-transformations which include substitution of their labile ligands by deactivating biomolecules. At the target cytotoxic sites such as DNA, metallo-drugs induce the desired therapeutic properties mainly through substitution of their labile ligands. Because of this, knowing the rate at which the drug bio-transforms and how fast it interacts at the target is key to understanding their anti-proliferation of cancers.

The multiple oxidation states accessible by Ru complexes include (Ru(II), Ru(III), Ru(IV) and Ru(V)) under physiological conditions. Majority of Ru complexes have an octahedral geometry. The type of ligands attached on a metal complex affect its redox potential thus this concept can be used to design desired compounds. In biological systems reducing agents such as glutathione, ascorbate and the single-electron-transfer proteins (like those involved in the mitochondrial electron-transfer chain) can reduce Ru(III) and Ru(IV)[48] depending on the electropotential of non-leaving ligand of the complex. Molecular dioxygen and cytochrome oxidase can oxidize Ru(II) in certain complexes.[49] [50] Thus, the redox potential of Ru compounds can be exploited to improve the effectiveness of Ru-based complexes in the clinic.[46] [47]

The reduction of Ru(III) to form Ru(II) by glutathione is a very slow process in healthy cells. However, in tumours where normal cell metabolism has been altered, this causes a lowering of oxygen concentration (hypoxia), which in turn make reduction products thermos-dynamically more stable and hence the process proceed expeditiously. This is thought to activate the inert Ru(III) complexes to Ru(II) species which can further react with DNA and proteins.[43] This reduction is catalysed by mitochondrial and microsomal single-electron-transfer proteins, amongst others. Ru(II) complexes selectively bind to cancerous cells which are under hypoxia condition because of the ability of the metal to bind to transferrin which partly accounts for its low toxicity.[46] [47] [43] [51] [52] Since rapidly dividing cells such as microbial infected or cancer cells have a greater requirement of iron, they increase the number of transferrin receptors on their surfaces. This implies that the amount of Ru taken up by these cancerous cells is greater than that taken up by healthy cells. This selectivity of the

drug towards the diseased cells accounts for a reduction on its general toxicity. The difference in ligand geometry leads to favourable Ru binding to DNA via interstrand crosslinking, which is different to cisplatin where intra-strand crosslinking is favoured.[53]

The first class of anti-cancer Ru complexes were designed to mimic the mechanism of action of the Pt drug cisplatin and targeting DNA as the cytotoxicity target. These complexes had ammine non-leaving groups and chlorido labile groups coordinated to Ru(II) or Ru(III) and were of general formula $[Ru(NH_3)_{6-x}Cl_x]^{Y+}$. The Ru(II) analogues were expected to bind to DNA in an analogous way to cisplatin, and indeed the first experiments performed with the complexes $[Ru(II)(NH_3)_5Cl]^+$ and $[Ru(II)(NH_3)_5(H_2O)]^{2+}$ confirmed this mode of binding.[54] [55] [56] Of this class, only *cis*-$[Ru(III)(NH_3)_4Cl_2]^+$ and *fac*-$[Ru(III)(NH_3)_3Cl_3]$ displayed comparable anti-tumour activity to that of cisplatin in some cell lines.[57] [58] The relatively inert Ru(III) complexes would bind to DNA after undergoing activation by reduction to less inert Ru(II) species followed by hydrolysis and final DNA binding.[48] However, most of the Ru(II) complexes were poorly soluble in aqueous media and were thus abandoned. Some of the amido chloride Ru complexes are shown in Figure 1.5.

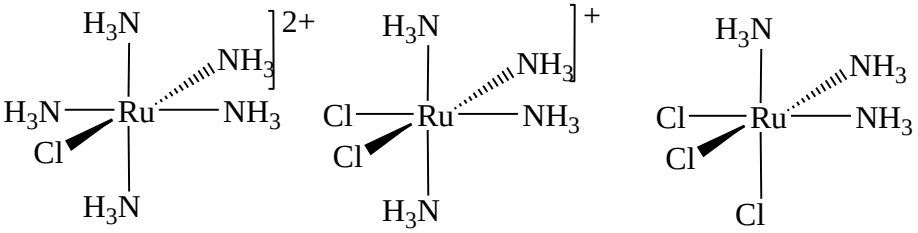

Figure 1. 5 Chemical structures of some amino-chlorido complexes of Ru

Replacement of the ammine ligands by dimethylsulphoxide (DMSO) molecules improved solubility of the Ru derivative. Just like cisplatin, both *cis*- and *trans*-$[Ru(II)Cl_2(DMSO)_4]$ showed a coordination to guanine residues of DNA via the N7 position.[59] The *trans* complex showed better activity both *in vitro* and *in vivo* in cytotoxicity tests attributed to its reactivity differences with its *cis* analogue. The *trans* isomer was found to overcome cisplatin resistance against P388 leukaemia cell line.[59] In addition, *trans*-$[Ru(II)Cl_2(DMSO)_4]$ shows a good activity against metastasis. [59] Thus, the *trans* Ru complexes could achieve remarkably better activity profile through a mechanism of action which is different from that of cisplatin.

Inspired by the promising activity of *trans*-[Ru(II)Cl_2(DMSO)$_4$], a series of chloride-dmso-Ru complexes were synthesized, key among them was Na{*trans*-[Ru(III)Cl_4(DMSO)-(Him)]}[60], (Him = imidazole), also called NAMI, and the more stable [H_2Im][*trans*-Ru(III)Cl_4(DMSO)(Him)], abbreviated NAMI-A. NAMI-A was the first Ru complex to undergo clinical trials as an anti-cancer drug. It is currently used in surgical removal of primary cancers. It is efficient against a broad range of tumours including lung metastasis.[61] Chemical structures of some (DMSO)(Cl)Ru(III) complexes which showed promising anti-cancer activity are shown in Figure 1.6.

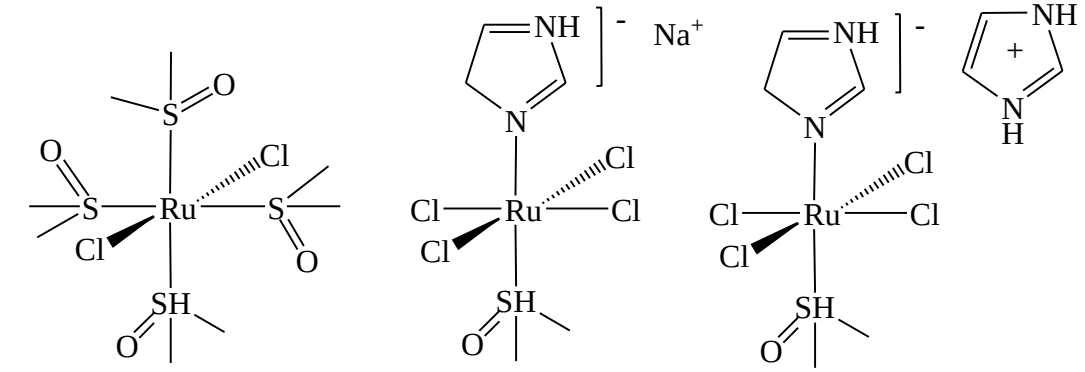

trans-[Ru(II)Cl_2(DMSO)$_4$] NAMI NAMI-A

Figure 1. 6 Chemical structures of some of the Ru dimethylsulphoxide complexes

It is hypothesised that the Ru(III) complexes are reduced to Ru(II) in the cells as evidenced from NAMI's loss of two of its chlorido ligands during hydrolysis. In addition to the binding of hydrated species of NAMI and NAMI-A to DNA and several biomolecules, these complexes are thought to have an anti-cancer mechanism of action that is different from cisplatin[62] [63] [53] [64] A series of NAMI-A analogues bearing a weakly basic heterocyclic nitrogen ligand *trans* to dmso were also synthesized[61] and found to be more hydrolytically stable than NAMI-A in slightly acidic solution with better *in vivo* effectiveness than that of the parent compound.

Keppler *et al.* prepared active anionic Ru(III) complexes with mono-dentate heterocyclic nitrogen donor ligands. The most promising sub-class of these complexes have the formula *trans*-[$RuCl_4(L)_2]^-$, where L is imidazole (KP418) or indazole (KP1019 and KP1339), with a counterion $(LH)^+$ or Na^+. KP1019 and KP1339 were effective in inhibiting Pt resistant colorectal carcinomas in rats[65] with complex KP1019 completing phase I clinical trials. The

mechanism of action of these complexes is thought to be different from that of cisplatin as there is involvement of the "activation-by-reduction" process. The transferrin-mediated transport into the cells seems to play an important role in the efficiency of the complexes[65] [51]as in the case of NAMI-A. The chemical structures of the Keppler type complexes are shown in Figure 1.7.

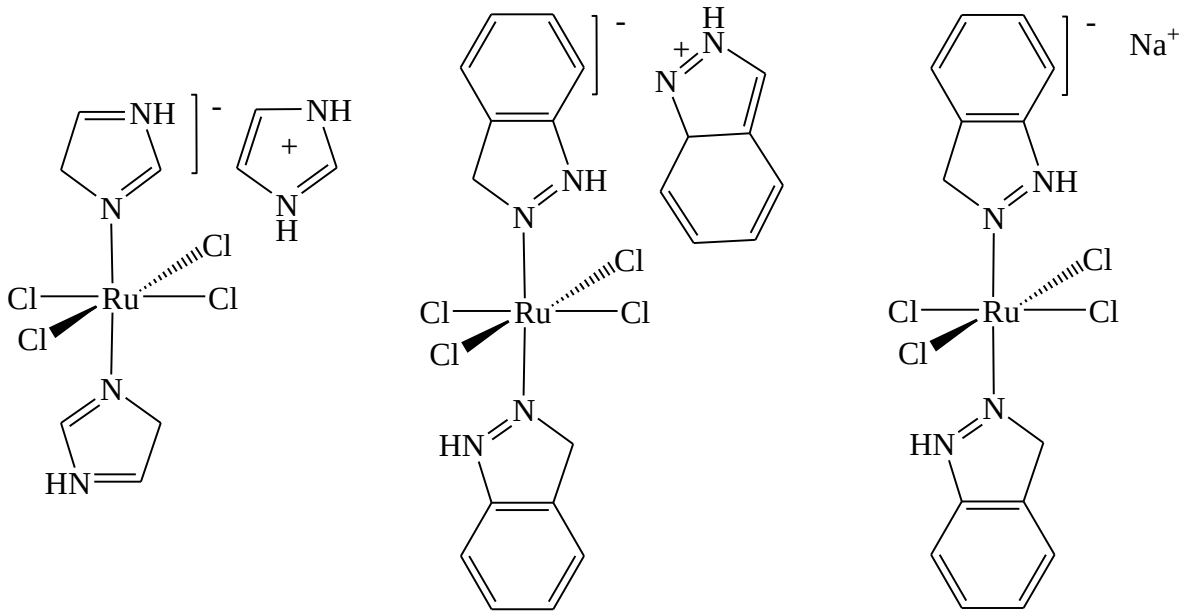

Figure 1. 7 Chemical structures of the "Keppler type" complexes

There has been growing interest in the use of Ru polypyridyl complexes as alternatives to the use of classical Pt chemotherapy.[66] [67] Polypyridyl complexes with one leaving group were shown to be good intercalators, they could coordinate DNA nucleobases in a similar fashion to cisplatin by first forming the aqua species before binding onto nucleobases.[68] Some of them such as *mer*-[Ru(tpy)Cl_3] and α-[Ru(azpy)$_2Cl_2$] (azpy = 2-phenylazopyridine,) (shown in Figure 1.8) were found to possess promising *in vitro* antitumor activity. They showed remarkably high cytotoxicity against several cell lines in which they were tested.[67] [69] The high activity of *mer*-[Ru(tpy)Cl_3] was postulated to be due to an energetically favourable binding of two guanine N-7 bases from two strands.[70] This was corroborated by the observation that its structural analogue [Ru(tpy)(bpy)Cl][Cl] also binds DNA after substitution of its *trans* chloro coligand displayed lower activity.[67]

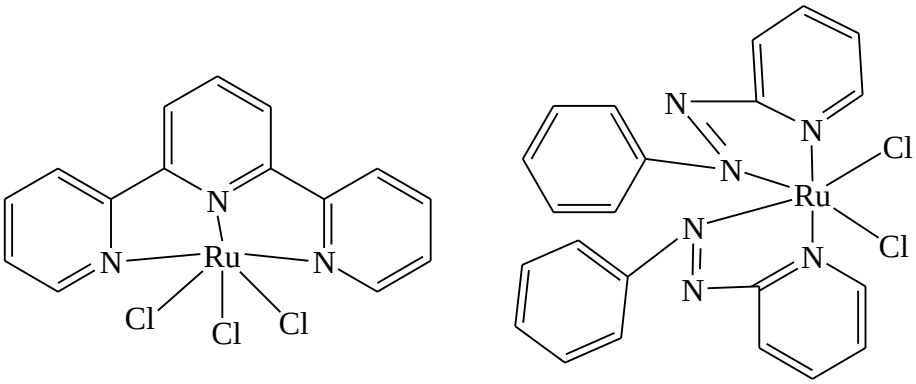

mer-[Ru(tpy)Cl_3] [Ru(azpy)$_2Cl_2$]

Figure 1. 8 Structures of some Ru polypyridyl complexes which have shown anti-tumour activity

Another class of Ru polypyridyl complexes examined for their DNA binding ability are the mono-chlorido-Ru(II) terpyridine complexes of the type *mer*-[Ru(tpy)(N-N)Cl]$^+$,these complexes were capped with a variety of N-N-donor bidentate ligands that include; 2,2'-bipyridyl (bpy), 4,4'-dimethyl-2,2'-bipyridine (bpyMe), 4,4'-diphenyl-2,2'-dipyridine-(biphbpy), 1,10-phenanthroline (phen), 3,4,7,8-tetramethyl-1,10-phenanthroline (tmephen), dipyrido[3,2-a:2',3'-c]phenazine (dppz), N,N,N',N'tetramethylethylenediamine (tmen), 2,2'-azobispyridine (apy), azpy and 2-phenylpyridinylmethyleneamine (impy). [71] [72] [73] [74] [75].The complexes could covalently bind to DNA forming mono-functional adducts, some of which could stop DNA replication.[67] [72]

Another sub-class of Ru polypyridyl complexes of the general formula *mer*-[Ru(L)(N-N)X][Y]^n were developed by Rilak *et. al.* where L is either tpy or Cl-tpy (4'-chloro-2,2':6',2''-terpyridine), X = Cl or dmso-S, N-N = en, dach or bpy, Y = Cl, PF_6 or CF_3SO_3 while n = 1 or 2, depending on the nature of X.[76] DNA (N7) guanine base could substitute chloride from [Ru(Cltpy)(en)Cl][Cl], [Ru(Cl-tpy)(dach)Cl][Cl] and [Ru(Cl-tpy)(bpy)Cl][Cl] (Figure 1.9) to form mono-functional adducts.[76] They strongly bind both covalently and non-covalently to CT DNA (K_b=10^4–10^5 M^{-1}), intercalating between base pairs.[77] The imidazole ring of L-histidine rapidly substituted chloride from [Ru(Cltpy)(en)Cl][Cl], and [Ru(Cl-tpy)(dach)Cl]-[Cl].[77] This is important given that the histidinyl residues of serum proteins play a crucial role in the transport and deactivation of Ru drugs.

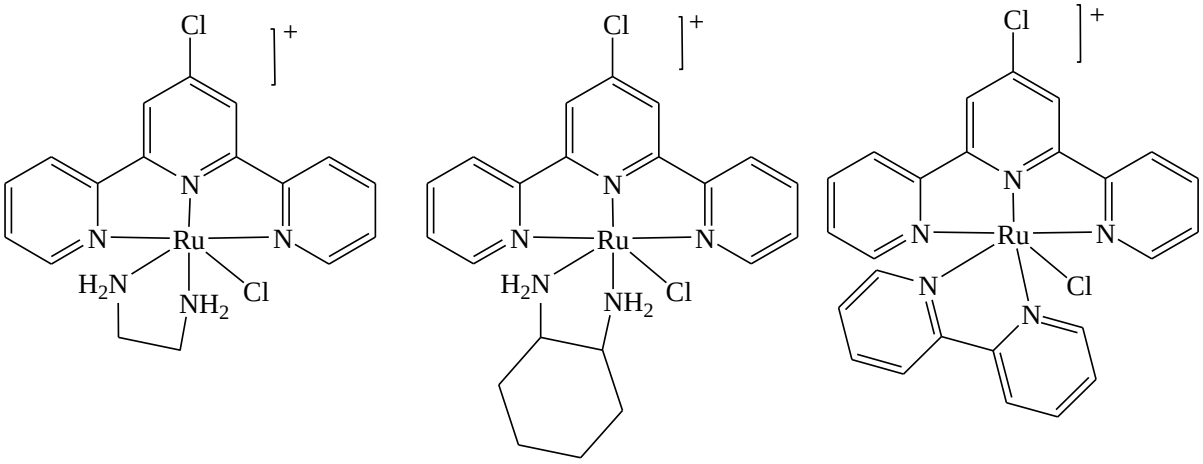

Figure 1. 9 Structures of the DNA binding chlorotpyRu(II) polypyridyl complexes

A detailed study conducted on their interactions with two major metal-transporting serum proteins, albumin (HSA) and transferrin (Tf) showed moderate-to-strong binding to the proteins with HSA appearing to be a more favourable binding partner for these compounds.[78] The higher reactivity of compounds containing en and dach towards HSA and Tf than the compound with bpy is possibly due to the former having more labile chlorides.[77] Investigations on their cytotoxicity with some cell lines showed high to moderate *in vitro* cytotoxicity.[77]

The study of (Cltpy)Ru(II) polypyridyl complexes was extended to complexes with 4'-the 4'-(4-Chrorophenyl)-2,2':6',2"-terpyridine (ClPhtpy) ligand in the place of 4'-chloro-2,2':6',2"-terpyridine. These had a general formula [Ru(ClPhtpy)(N-N)Cl][Cl] (where N-N = en, **1** dach, **2** or bpy, **3** as shown in Figure 1.10.[79] Evaluation of the anticancer activity of **1-3** against two different tumour cell lines (HeLa and A549), and one normal cell line (MRC-5) revealed that **3** is generally the most active.[79] A comparison with the previously studied Cltpy compounds [Ru(Cltpy)(dach)Cl]Cl and [Ru(Cltpy)(bpy)Cl]Cl showed lower activity for the former Ru complexes. [Ru(Cltpy)(en)Cl][Cl] and **3** are the most active in their respective sub-classes.[79] [77] This observation shows that the biological activity of Ru(II) polypyridyl complexes are affected by the nature of the meridional tridentate ligand. The introduction of the chlorophenyl substituent in the tpy ligand results in an increase in the anticancer activity. The *in vitro* activity of anti-cancer drugs can often be related in part, to their lipophilic character; higher hydrophobicity may contribute to an increased uptake of the

complex by the cells, thereby enhancing the anticancer activity.[80] This is confirmed by the fact that complex **3** which is most lipophilic is also most cytotoxic.

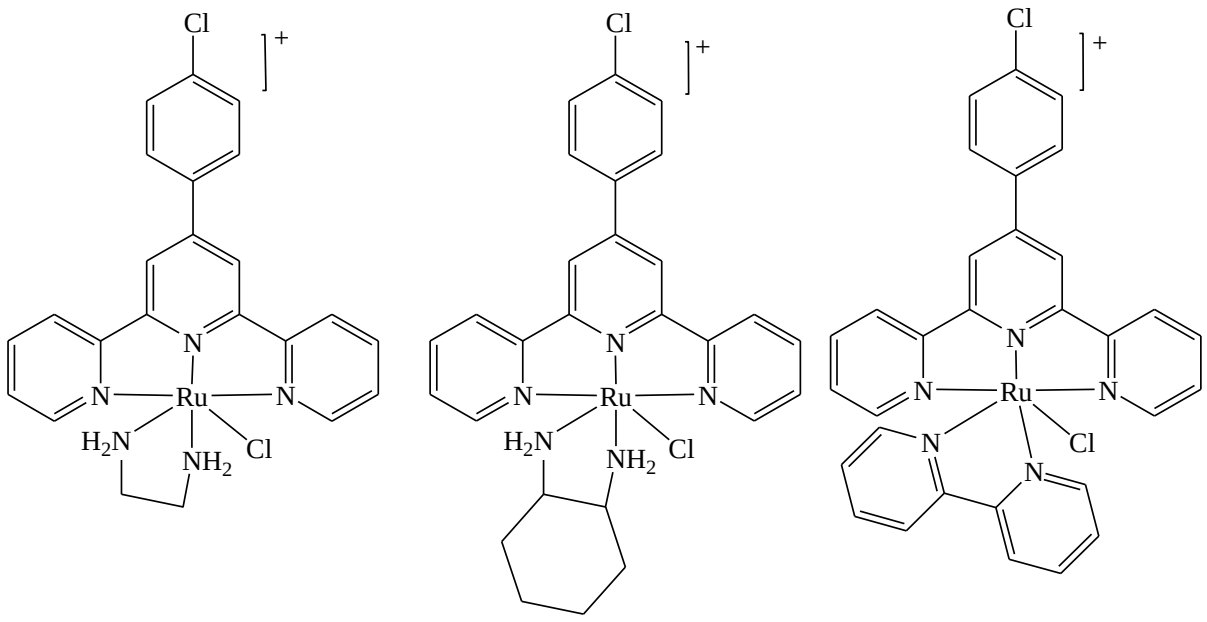

Figure 1. 10 Chemical structures of the chlorophenyl(tpy)Ru polypyridyl complexes with enhanced activity

Ru complexes without a labile ligand (Figure 1.11) were also found to possess significant biological activity against HT-29 and MCF-7 human cancer cells. This could not be attributed to coordinative binding of the Ru centre to biological targets. Rather their planar and rigid aromatic spectator ligands intercalate into the DNA base pairs. For example [Ru-(bpy)$_2$(dppn)][Cl$_2$] (dppn = benzo[*i*]dipyrido[3,2-a:2',3'-c]phenazine) was found to have anti-proliferative activity against HT-29 and MCF-7 human cancer cells comparable to that of cisplatin under identical conditions.[81] The mode of action of this compounds seems to involve interactions with cell membranes with consequent modification of cell membrane function through cell adhesion properties, rather than interactions with DNA i.e. intercalation of the dppn ligand. [Ru(bpy)(phpy)(dppz)]$^+$ was found to be rapidly taken up by cancer cells, and nearly 90% of the complex accumulated in the nuclei of cancer cells after a 2 h incubation.[82]

Further investigation on dppz-Ru coordination onto DNA by Han *et al.* using [Ru(bpMe)$_2$(dcdppz)](ClO$_4$)$_2$ (dcdppz = *h,j*-dichlorodipyrido[3,2-*a*:2',3'-*c*]phenazine) and [Ru(bpy)$_2$(dcdppz)](ClO$_4$)$_2$ (Figure 1.11)[83] showed the interaction of the complexes with

DNA by intercalative mode. $[Ru(bpyMe)_2(dcdppz)](ClO_4)_2$ showed higher cytotoxicity than $[Ru(bpy)_2(dcdppz)](ClO_4)_2$, but lower than cisplatin towards cancer cell lines.[83]

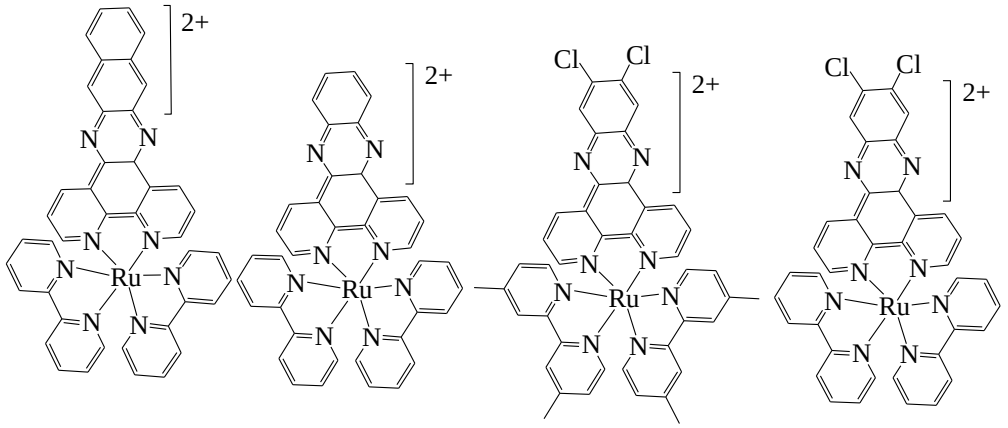

$[Ru(bpy)_2(dppn)][Cl_2]$ $[Ru(bpy)(phpy)(dppz)]^+$ [$Ru(bpMe)_2(dcdppz)](ClO_4)_2$ $[Ru(bpy)_2(dcdppz)](ClO_4)_2$

Figure 1. 11 Chemical structures of some substitutional inert Ru polypyridyl complexes

These Ru(II) complexes have shown high inhibitory effect on the growth of cancer cells.[84] In the quest to understand the mechanism of operation in inducing cancer apoptosis, a new ligand DQTT (DQTT = 12-(1,4-dihydroquinoxalin-6-yl)-4,5,9,14-tetraazabenzo[b]tri-phenylene) and its four Ru(II) complexes $[Ru(dmb)_2(DQTT)](ClO_4)_2$, $[Ru(bpy)_2(DQTT)]$-$(ClO4)_2$, $[Ru(phen)_2(DQTT)](ClO_4)_2$ and $[Ru(dmp)_2(DQTT)](ClO_4)_2$ (Figure 1.12) were synthesized by Zhang *et al*. Analysis of *in vitro* cytotoxic activity against various human cancer cell lines by MTT method [85] showed high cytotoxicity against BEL-7402 cells. The complexes can downregulate the expression of Bcl-x protein and upregulate the levels of Bad, Bid and Bim protein in BEL-7402 cells. Additionally, the results showed that the complexes induce BEL-7402 cells apoptosis through a ROS mediated mitochondrial dysfunction pathway, which was accompanied by regulation of the expression of Bcl-2 family proteins.[85]

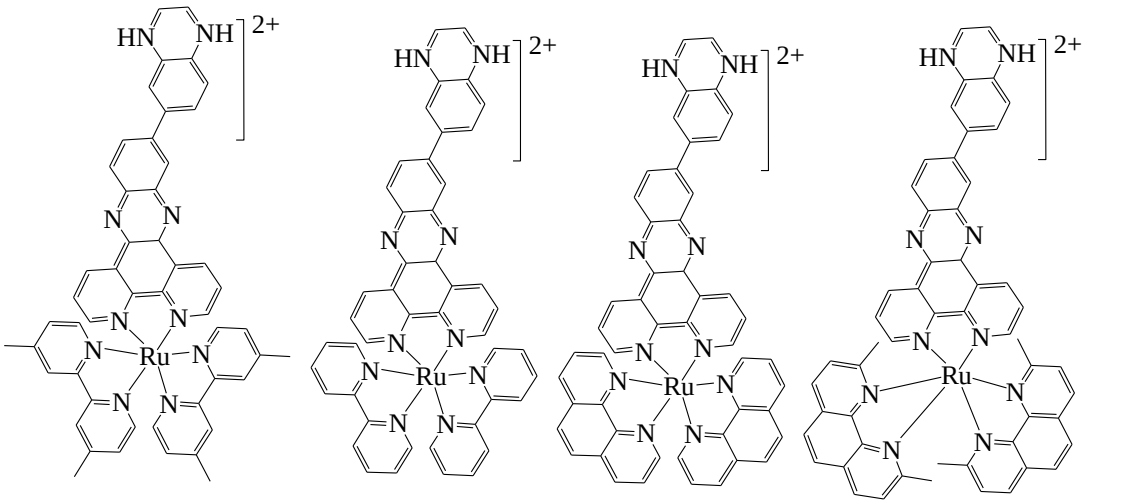

Figure 1. 12 Structures of other substitutionally inert Ru polypyridyl complexes which have shown anti-cancer activity

Another important class of Ru(II) complexes that has received attention as promising alternatives owing to their low toxicity, high antitumor activity and strong DNA-binding affinity is arene Ru(II) complexes.[86] [87] [88] [89] These complexes are also called half-sandwich complexes or piano stool complexes. The metal centres in these complexes are surrounded by three mono-dentate or one each of the mono and bidentate ligands besides the cyclic polyhapto hydrocarbon ligand. The arene complexes with general formular; [Ru(η^6-arene)(X)(Y)(Z)] which resemble a half-sandwich "piano-stool" in structure has the arene occupying the seat of the 'stool' and the remaining three coordinating sites can be occupied in three different ways, bidentate (X-Y) with monodentate (Z), tridentate (X-Y-Z) or three mono-dentate ligands (X)(Y)(Z) as shown in **A**, **B** and **C** respectively (Figure 1.13). The group Z represents the labile ligand (usually a chloro ligand) that is crucial for the activation process when undergoing hydrolysis. The manipulation of these ligands can give rise to a variety of complexes.[90] [91]

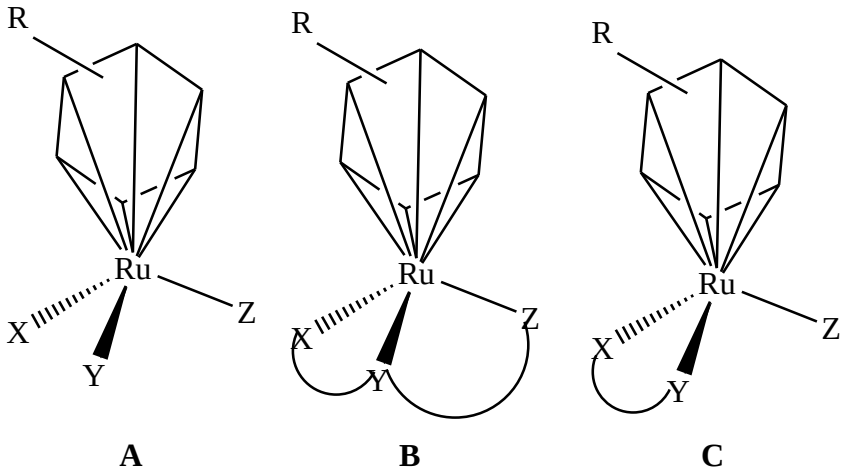

Figure 1. 13 General structures of Ru(II) "piano-stool" arene complexes

Their structures allow for variations of the three main types/groups of ligands around the metal centres, the mono-dentate ligand X, the bidentate ligand Z and the arene, to fine-tune the pharmacological properties.[92] The hydrophobic nature of the arene can help to influence cell uptake and interactions with potential cytotoxicity targets while a leaving group occupies a potential site for the complexes to bind to biomolecules.[92] Systematic modification of ligands in these complexes opens various possibilities for molecular design of Ru complexes with desirable physical, chemical and biological properties. This can be done mainly by changing the type of the arene ligand or introducing different chelating ligands, which will enhance selectivity towards tumour cells.[93] [81] [94] [95]

These organometallic compounds are easily synthesised under mild reaction conditions affording high yields. They are chemically stabile and have reasonably high solubility in aqueous media.[96] [97] Arene Ru(II) complexes have been shown to bind to and shown to disturb the replication of DNA.[98] [99] [100] The study by Sadler *et al.* indicated that $[(\eta^6\text{-arene})Ru^{II}(en)Cl]^+$ has inhibitory ability against various human tumour cells and can unwind the double strand helix of DNA by monofunctional adducts in intercalative mode. [93] [101] The activity of $[(\eta^6\text{-arene})Ru^{II}(en)Cl]^+$ increases with the size of the coordinated arene in the order benzene < p-cymene < biphenyl < dihydroanthracene < tetrahydroanthracene.[93] The biphenyl complex has similar cytotoxicity to the anticancer drug carboplatin while the tetrahydroanthracene complex is as active as cisplatin.[102] [103] [104] [105]

Further studies by Qiong Wu *et al.* on a series of arene Ru(II) complexes coordinated by phenanthroimidazole derivatives revealed that the complexes have reasonable inhibitory

activity against various tumour cells, especially MG-63 cells which made them potential activator of gene.[106] The Ru complexes containing multi-ring arenes bind to DNA not only through N7 atoms of guanine (G), but also interacted non-covalently through hydrophobic interactions between the arene and DNA.[107] [108] [109] These hydrophobic interactions might include intercalation of the non-coordinated arenes between DNA bases and minor-groove binding.[100] New complexes of the type $[Ru^{II}(\eta^6\text{-arene})(Cl)(en)]^+$ (arene = ortho-, meta-, or para-terphenyl) were investigated for cytotoxicity and DNA binding and it was observed that the complex containing paraterphenyl as the arene ligand exhibits promising cytotoxic effects in several human tumour cell lines, including those resistant to conventional cisplatin.[109] In contrast, complexes containing meta- or ortho-terphenyl arene ligands were much less cytotoxic.[109]

The complex $[(\eta_6\text{-toluene})Ru(II)(pta)Cl_2]$ (RAPTA-T), where pta 1,3,5-triaza-7-phospha-adamantane is a DNA-binding anti-metastatic drug from which a group of other water-soluble complexes were synthesized.[46] [110] The family of RAPTA compounds exhibit a *p*H dependent DNA binding profile and non-toxicity towards cancer cells (*in vitro*). However, RAPTA-T was found to inhibit lung metastases in mice bearing a mammary carcinoma, again with only mild effects on the primary tumours.

There is a huge prospect among Ru(II) arene complexes having cyclopentadienyl arene ligands ($\eta^5\text{-}C_5H_5$) in the place of benzene.[111] Four cationic Ru(II) complexes of the type $[Ru^{II}(\eta^5\text{-}C_5H_5)L(PPh_3)_2]^+$ (L = 5-phenyl-1H-tetrazole (TzH) 1, imidazole (ImH) 2, benzo[1,2-b;4,3-] dithio-phen-2-carbonitrile (Bzt) 3, and [5-(2-thiophen-2-yl)-vinyl]-thio-phene-2-carbonitrile] (Tvt) 4) were found to possess excellent antitumor activities.[112] Further, a new sub-classs of "RuCp" (Cp = eta(5)-C_5H_5) conjugates of bidentate N,O and N,N'- hetero-aromatic ligands showed outstanding cytotoxic properties against several human cell lines.[111] Another sub-class of these complexes with general formula $[Ru(\eta_5\text{-}C_5H_5)(PP)L]^+$ where L is a N-hetero-aromatic σ-bonded ligand also showed excellent cytotoxicity higher than cisplatin.[112] The study by Valente *et al.* on the polymer based Ru-cyclopentadienyl complex $[CpRu(P)(bpyPLA)]^+$ (Cp = cyclopentadienyl, P = triphenyl-phosphine, and bpyPLA = 2,2'-bipyridine-4,4'-D-glucose end-capped polylactide) revealed cytotoxicity which was six-fold higher than that of cisplatin especially for the MCF-7 cell lines.[113] Ru-cyclopentadienyl compounds bearing carbohydrate-derived ligands are emerging as anti-cancer agents for example η^5-cyclopentadienyl Ru(II)complexes of general

formula $[(\eta^5\text{-}C_5H_5)Ru(PP)(L)]^+$, isolated as PF_6^- salts, (L represents the galactose and fructose carbohydrate derivative ligands, functionalized with nitrile, tetrazole, and 1,3,4-oxadiazole N-coordinating moieties) showed very good activity.[114]

As just was the case with Pt complexes, binuclear Ru compounds were postulated to interact with DNA in a drastically different way to mononuclear analogues. The interaction of these complexes with DNA as well as their cellular processing were expected to be unique, and would involve long-range intra-strand cross-links upon DNA and van der Waals interactions within the minor groove of DNA. This would help overcome cisplatin resistance. Dimeric Ru cationic complexes bridged by heterocycles were studied electrochemically for their photophysical properties in the 1970s.[115] The dinuclear Ru complexes of the type $[\{trans\text{-}Ru(III)Cl_2(DMSO)L1L2\}_2(\mu\text{-}L3)]^{m-}$ (Figure 1.14) (L1, L2 are Cl or dmso. L3 is a nitrogen heterocyclic ligand with at least two nitrogen atoms (pyrazine (pyz), pyrimidine (pym), 4, 4´-bipyridine (bipy), 1,2-bis(4-pyridyl)ethane (etbipy), 1,2-bis(4-pyridyl)propane (prbipy) or *trans*-1,2-bis(4-pyridyl)ethylene (etilbipy) and m = 0, 1 or 2). Their coordination at each metal centre was designed to be similar to that of the mononuclear NAMI-A.[116] These complexes were found to have good chemical stability making them suitable for pharmacological formulation. They were also found to have a high anti-metastatic activity. Thus they were found to be useful in the treatment of tumours with a high degree of metastatic diffusion, such as mammary, lung or digestive tract carcinomas.[117] [118] [119] [120]

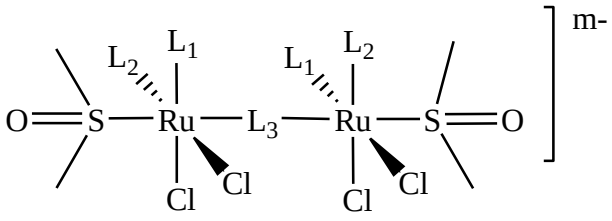

Figure 1. 14 General structure of Ru dinuclear complexes with antimetastatic activity

1.4 Importance of studying the rates of ligand exchange reactions

The sulphur biomolecules can react with anti-cancer agents in the cell through substitution of their labile ligands. These reactions determine as to whether the drugs will eventually interact with DNA to affect the necessary process of apoptosis. This study of substitution reactions of potential anti-cancer metal complexes with model ligands provide kinetic data and information on the possible interactional modes of the complexes with in-*vivo* targets..[121]

[122] [123] The data is helpful in the design, synthesis and administration of new pharmacological agents and the application of future tumour treatment procedures.[19] [124] This information also shade insight on the chemo-protection role of this used bio-nucleophiles and in respect to Ru(II) complexes metabolism. A lot of study has focused on DNA binding and cytotoxicity leaving gaps on the kinetic fate of compounds in biological systems. This study measures the rate of substitutions from Ru(II) complexes bearing different types of ligands with bio-relevant thiourea nucleophiles of different steric demands to mimic possible reactions of these compounds in biological systems. The nature of ligands coordinated on the metal centre is one of the key aspects that affect the behaviour of an anti-cancer agent in biological systems in terms of how it will interact with bio-nucleophiles be it proteins or nucleophiles such as DNA. Ligands affect solubility, lability of the leaving group, stability of complexes and the type of interaction between the agent and DNA among others properties.

It is evident from the literature survey that Ru complexes are equally competitive as anti-cancer agents in comparison to Pt based anti-cancer agents and potentially better in overcoming the shortcomings related with the existing drug cisplatin.

1.5 Aims and objectives of the study

1.5.1 To investigate the role of the substituents on the arene ligand as well as the effect of introducing the 2,2'-bipyridyl ligand onto the Ru(II)arene(aqua)$_3$ on the rate of aqua substitution from a series of arene-Ru(II) complexes. Their chemical structures are presented in Figure 1.15.

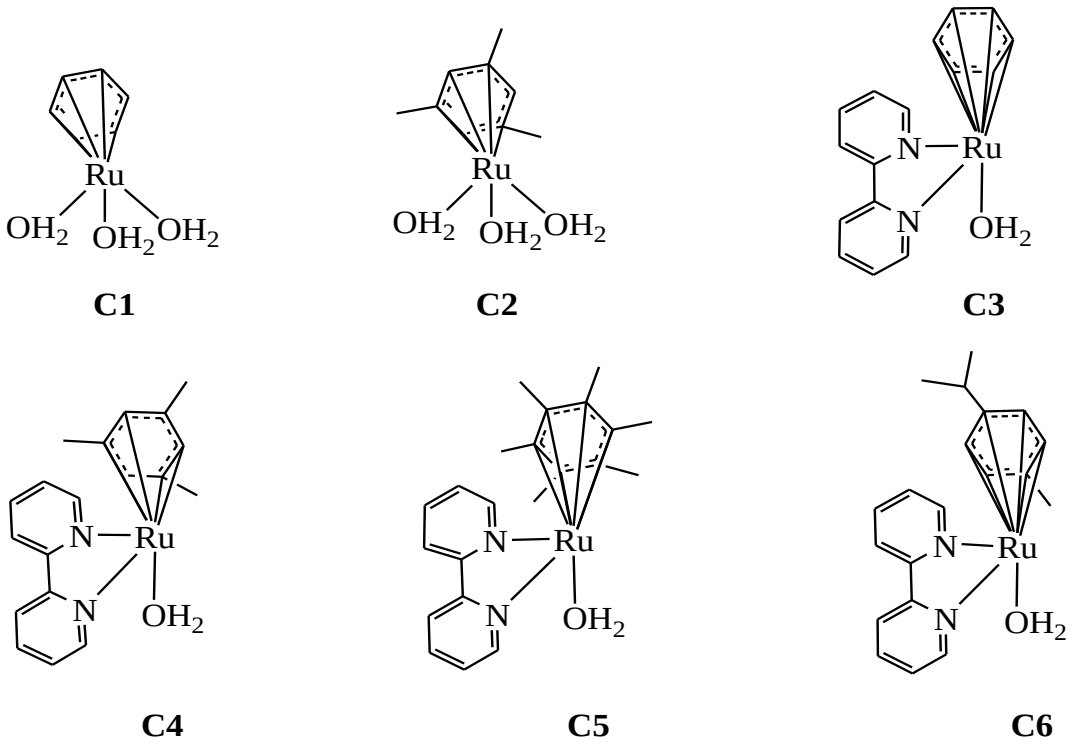

Figure 1. 15 Chemical structures of arene(triaquo)Ru(II) and aquo(arene)(bipyridine)Ru(II) complexes

The details of the study including synthetic work and rates of substitution reactions from the Ru(II) complexes will be reported in **chapter 3** of this thesis.

1.5.2 To investigate the role of non-labile arene and phosphane (L) ligands of arene Ru(II) complexes on the rate of substitution. The study seeks to establish the effect on the reactivity when there is variation of either the arene ligand or the phosphane ligand. Chemical structures of the Ru(II) complexes investigated are presented in Figure 1.16.

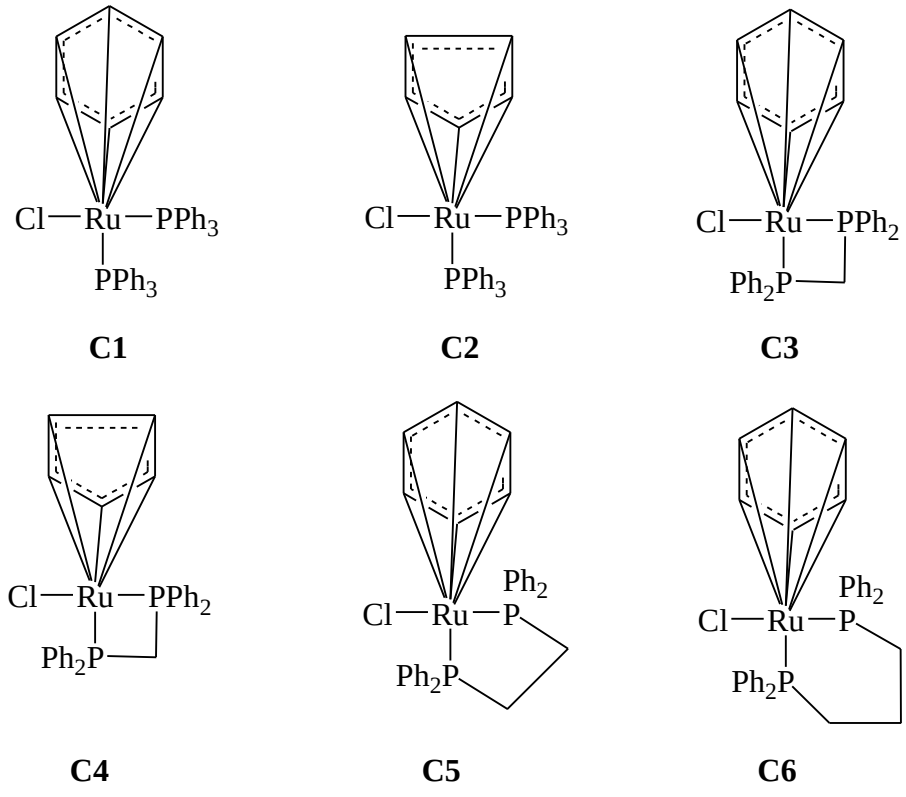

Figure 1. 16 Chemical structures of arene(chloro)(phosphine)Ru(II) complexes

The details of the study including synthetic work and substitution reactions from the Ru(II) complexes will be reported in **chapter 4** of this thesis.

1.5.3 To study the role of substituents on the rate of substitution from Ru(II) complexes having the strong σ-donor triphenylphosphine ligands and 2,4,6-tris(2-pyridyl)-1,3,5-triazine type of ligands. Chemical structures of the Ru(II) complexes investigated are presented in Figure 1.17.

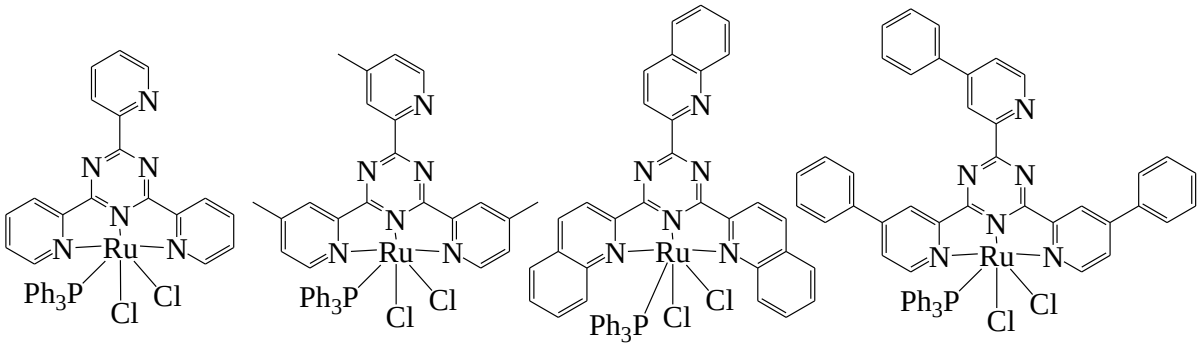

Figure 1. 17 Chemical structures of chloro(L)(triphenylphosphino)Ru(II) complexes

The details of the study including synthetic work and rates of substitution reactions from the Ru(II) complexes will be reported in **chapter 5** of this thesis.

1.5.4 To investigate how 2-(2-Pyridyl)azole auxiliary ligands (L) affect the rate of chloride substitution from chloro(L)(tpy)Ru(II) complexes. The structures of the Ru(II) complexes investigated are presented in Figure 1.18.

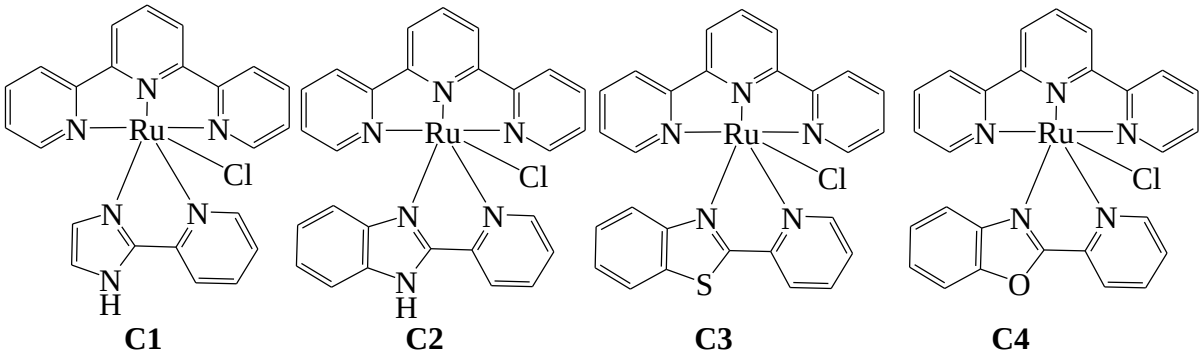

Figure 1. 18 Chemical structures of chloro(L)(tpy)Ru(II) complexes

The details of the study including synthetic work and rates of substitution reactions from the Ru(II) complexes will be reported in **chapter 6** of this thesis.

1.5.5 To study how substituents on the tpy affect the rate of substitution from dichlorido(terpy)Ru(II) complexes. It is of interest to understand how competing forces (σ-*trans*-effect/π-back donation) resulting from the substituents affect the rate of substitution

from the dichlorido(tpy)Ru(II) complexes. The structures of the complexes are presented in Figure 1.19.

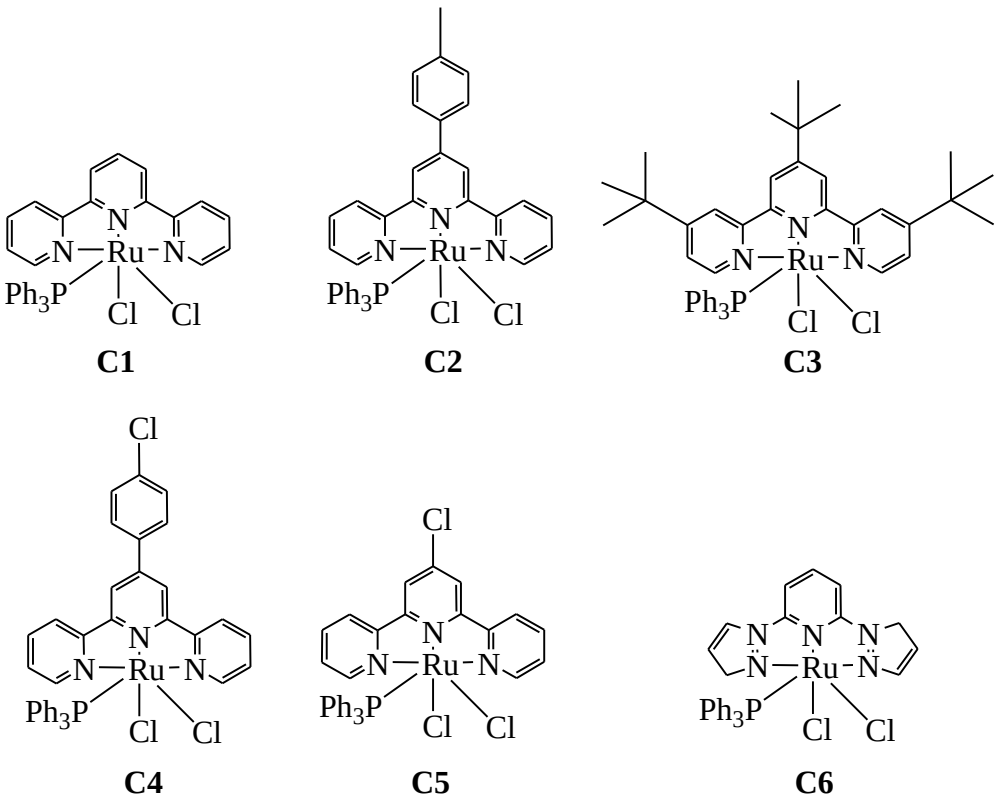

Figure 1. 19 Chemical structures of dichlorido(tpy)Ru(II) complexes

Details of the study including synthetic work and rates of substitution reactions from the Ru(II) complexes will be reported in **chapter 7** of this thesis.

DFT computations of the lowest conformations of all the Ru complexes were carried out using the B3LYP/LANL2DZ to get theoretical data that was used in support of the observed trends in the reactivity trends.

1.6 References

[1] I. Kostova, *Recent Patents on Anticancer Drug Discovery* **2006**, *1*, 1-22.

[2] O. S. Zhukova, I. Dobrynin, *Voprosy Onkologii* **2001**, *47*, 706-709.

[3] S. M. Aris, N. P. Farrell, *European Journal of Inorganic Chemistry* **2009**, *2009*, 1293-1302.

[4] N. J. Wheate, S. Walker, G. E. Craig, R. Oun, *Dalton Transactions* **2010**, *39*, 8113-8127.

[5] K. Kehe, L. Szinicz, *Toxicology* **2005**, *214*, 198-209.

[6] L. Kelland, *Nature Reviews Cancer* **2007**, *7*, 573-584.

[7] V. Brabec, *Progress in nucleic acid research and molecular biology* **2002**, *71*, 1-68.

[8] Z. D. Bugarcic, J. Bogojeski, B. Petrovic, S. Hochreuther, R. van Eldik, *Dalton transactions (Cambridge, England : 2003)* **2012**, *41*, 12329-12345.

[9] A. M. Fichtinger-Schepman, J. L. van der Veer, J. H. den Hartog, P. H. Lohman, J. Reedijk, *Biochemistry* **1985**, *24*, 707-713.

[10] A. Eastman, *Biochemistry* **1986**, *25*, 3912-3915.

[11] A. Eastman, *Pharmacology and Therapeutics* **1987**, *34*, 155-166.

[12] U. M. Ohndorf, M. A. Rould, Q. He, C. O. Pabo, S. J. Lippard, *Nature* **1999**, *399*, 708-712.

[13] Y. Jung, S. J. Lippard, *Chemical Reviews* **2007**, *107*, 1387-1407.

[14] J. Reedijk, *Inorganica Chimica Acta* **1992**, *198-200*, 873-881.

[15] J. A. Rice, D. M. Crothers, A. L. Pinto, S. J. Lippard, *Proceedings of the National Academy of Sciences of the United States of America* **1988**, *85*, 4158-4161.

[16] M. T. Kuo, H. H. Chen, I. S. Song, N. Savaraj, T. Ishikawa, *Cancer metastasis reviews* **2007**, *26*, 71-83.

[17] S. B. Howell, R. Safaei, C. A. Larson, M. J. Sailor, *Molecular Pharmacology* **2010**, *77*, 887-894.

[18] C. A. Puckett, R. J. Ernst, J. K. Barton, *Dalton Transactions* **2010**, *39*, 1159-1170.

[19] R. Jan, *European Journal of Inorganic Chemistry* **2009**, *2009*, 1303-1312.

[20] C. Molenaar, J. M. Teuben, R. J. Heetebrij, H. J. Tanke, J. Reedijk, *Journal of Biological Inorganic Chemistry* **2000**, *5*, 655-665.

[21] N. Thatcher, M. Lind, *Seminars in Oncology* **1990**, *17*, 40-48.

[22] Y. Hasegawa, S. Takanashi, K. Okudera, M. Aoki, K. Basaki, H. Kondo, T. Takahata, N. Yasui-Furukori, T. Tateishi, Y. Abe, K. Okumura, *Jpn J Clin Oncol* **2004**, *34*, 647-653.

[23] E.-I. Takaoka, K. Kawai, S. Ando, T. Shimazui, H. Akaza, *Jpn J Clin Oncol* **2006**, *36*, 60-63.

[24] Y. Sato, T. Takayama, T. Sagawa, T. Okamoto, K. Miyanishi, T. Sato, H. Araki, S. Iyama, S. Abe, K. Murase, R. Takimoto, H. Nagakura, M. Hareyama, J. Kato, Y. Niitsu, *Cancer chemotherapy and pharmacology* **2006**, *58*, 570-576.

[25] M. Shimada, H. Itamochi, J. Kigawa, *Cancer Management and Research* **2013**, *5*, 67-76.

[26] L. R. Kelland, G. Abel, M. J. McKeage, M. Jones, P. M. Goddard, M. Valenti, B. A. Murrer, K. R. Harrap, *Cancer Research* **1993**, *53*, 2581-2586.

[27] K. Lemma, J. Berglund, N. Farrell, L. I. Elding, *Journal of Biological Inorganic Chemistry* **2000**, *5*, 300-306.

[28] E. M. Bengtson, J. R. Rigas, *Drugs* **1999**, *58 Suppl 3*, 57-69.

[29] J. Holford, S. Y. Sharp, B. A. Murrer, M. Abrams, L. R. Kelland, *British journal of cancer* **1998**, *77*, 366-373.

[30] J. Treat, J. Schiller, E. Quoix, A. Mauer, M. Edelman, M. Modiano, P. Bonomi, R. Ramlau, E. Lemarie, *European Journal of Cancer* **2002**, *38*, S13-S18.

[31] K. A. Gelmon, T. A. Vandenberg, L. Panasci, B. Norris, M. Crump, L. Douglas, W. Walsh, S. J. Matthews, L. K. Seymour, *Annals of Oncology* **2003**, *14*, 543-548.

[32] U. Bierbach, Y. Qu, T. W. Hambley, J. Peroutka, H. L. Nguyen, M. Doedee, N. Farrell, *Inorganic Chemistry* **1999**, *38*, 3535-3542.

[33] M. E. Gore, R. J. Atkinson, H. Thomas, H. Cure, D. Rischin, P. Beale, P. Bougnoux, L. Dirix, W. M. Smit, *European Journal of Cancer* **2002**, *38*, 2416-2420.

[34] E. I. Montero, S. Díaz, A. M. González-Vadillo, J. M. Pérez, C. Alonso, C. Navarro-Ranninger, *Journal of Medicinal Chemistry* **1999**, *42*, 4264-4268.

[35] E. I. Montero, J. M. Pérez, A. Schwartz, M. A. Fuertes, J. M. Malinge, C. Alonso, M. Leng, C. Navarro-Ranninger, *European Journal of Chemical Biology* **2002**, *3*, 61-67.

[36] G. B. Onoa, G. Cervantes, V. Moreno, M. J. Prieto, *Nucleic Acids Research* **1998**, *26*, 1473-1480.

[37] A. Boccarelli, F. P. Intini, R. Sasanelli, M. F. Sivo, M. Coluccia, G. Natile, *Journal of Medicinal Chemistry* **2006**, *49*, 829-837.

[38] J. Kasparkova, O. Novakova, V. Marini, Y. Najajreh, D. Gibson, J. M. Perez, V. Brabec, *Journal of Biological Chemistry* **2003**, *278*, 47516-47525.

[39] M. Frybortova, O. Novakova, J. Stepankova, V. Novohradsky, D. Gibson, J. Kasparkova, V. Brabec, *Journal of Inorganic Biochemistry* **2013**, *126*, 46-54.

[40] A. P. Soares Fontes, R. Bandarage, N. Farrell, Y. Qu, H. Rauter, L. R. Kelland, *Journal of Medicinal Chemistry* **2000**, *43*, 3189-3192.

[41] S. Komeda, M. Lutz, A. L. Spek, M. Chikuma, J. Reedijk, *Inorganic Chemistry* **2000**, *39*, 4230-4236.

[42] S. Komeda, S. Bombard, S. Perrier, J. Reedijk, J. Kozelka, *Journal of Inorganic Biochemistry* **2003**, *96*, 357-366.

[43] M. J. Clarke, *Coordination Chemistry Reviews* **2002**, *232*, 69-93.

[44] I. Zanzi, S. C. Srivastava, G. E. Meinken, W. Robeson, L. F. Mausner, R. G. Fairchild, D. Margouleff, *Int J Rad Appl Instrum B* **1989**, *16*, 397-403.

[45] S. C. Srivastava, *Semin Nucl Med* **1996**, *26*, 119-131.

[46] C. S. Allardyce, P. J. Dyson, *Platinum Metals Review* **2001**, *45*, 62-69.

[47] M. Gielen, E. R. T. Tiekink, *Metallotherapeutic Drugs and Metal-based Diagnostic Agents: The Use of Metals in Medicine*, John Wiley & Sons, **2005**.

[48] M. J. Clarke, S. Bitler, D. Rennert, M. Buchbinder, A. D. Kelman, *Journal of Inorganic Biochemistry* **1980**, *12*, 79-87.

[49] D. M. Stanbury, O. Haas, H. Taube, *Inorganic Chemistry* **1980**, *19*, 518-524.

[50] D. M. Stanbury, D. Gaswick, G. M. Brown, H. Taube, *Inorganic Chemistry* **1983**, *22*, 1975-1982.

[51] C. G. Hartinger, S. Zorbas-Seifried, M. A. Jakupec, B. Kynast, H. Zorbas, B. K. Keppler, *Journal of Inorganic Biochemistry* **2006**, *100*, 891-904.

[52] K. Polec-Pawlak, J. K. Abramski, O. Semenova, C. G. Hartinger, A. R. Timerbaev, B. K. Keppler, M. Jarosz, *Electrophoresis* **2006**, *27*, 1128-1135.

[53] E. Gallori, C. Vettori, E. Alessio, F. G. Vilchez, R. Vilaplana, P. Orioli, A. Casini, L. Messori, *Archives of Biochemistry and Biophysics* **2000**, *376*, 156-162.

[54] M. J. Clarke, M. Buchbinder, A. D. Kelman, *Inorganica Chimica Acta* **1978**, *27*, L87-L88.

[55] M. J. Clarke, B. Jansen, K. A. Marx, R. Kruger, *Inorganica chimica acta* **1986**, *124*, 13-28.

[56] V. M. Rodriguez-Bailey, K. J. LaChance-Galang, P. E. Doan, M. J. Clarke, *Inorganic chemistry* **1997**, *36*, 1873-1883.

[57] J. R. Durig, J. Danneman, W. D. Behnke, E. E. Mercer, *Chemico-Biological Interactions* **1976**, *13*, 287-294.

[58] M. J. Clarke, F. Zhu, D. R. Frasca, *Chemical Reviews* **1999**, *99*, 2511-2534.

[59] E. Alessio, G. Mestroni, G. Nardin, W. M. Attia, M. Calligaris, G. Sava, S. Zorzet, *Inorganic Chemistry* **1988**, *27*, 4099-4106.

[60] I. Kostova, *Current medicinal chemistry* **2006**, *13*, 1085-1107.

[61] A. Bergamo, B. Gava, E. Alessio, G. Mestroni, B. Serli, M. Cocchietto, S. Zorzet, G. Sava, *International Journal of Oncology* **2002**, *21*, 1331-1338.

[62] A. Barca, B. Pani, M. Tamaro, E. Russo, *Mutation Research/Fundamental and Molecular Mechanisms of Mutagenesis* **1999**, *423*, 171-181.

[63] B. Sanna, M. Debidda, G. Pintus, B. Tadolini, A. M. Posadino, F. Bennardini, G. Sava, C. Ventura, *Archives of Biochemistry and Biophysics* **2002**, *403*, 209-218.

[64] L. Messori, P. Orioli, D. Vullo, E. Alessio, E. Iengo, *The FEBS Journal* **2000**, *267*, 1206-1213.

[65] S. Kapitza, M. Pongratz, M. A. Jakupec, P. Heffeter, W. Berger, L. Lackinger, B. K. Keppler, B. Marian, *Journal of Cancer Research and Clinical Oncology* **2005**, *131*, 101-110.

[66] J. Reedijk, *Proceedings of the National Academy of Sciences* **2003**, *100*, 3611-3616.

[67] O. Novakova, J. Kasparkova, O. Vrana, P. M. van Vliet, J. Reedijk, V. Brabec, *Biochemistry* **1995**, *34*, 12369-12378.

[68] T. Gianferrara, I. Bratsos, E. Alessio, *Dalton Transactions* **2009**, 7588-7598.

[69] A. H. Velders, H. Kooijman, A. L. Spek, J. G. Haasnoot, D. de Vos, J. Reedijk, *Inorganic chemistry* **2000**, *39*, 2966-2967.

[70] P. M. van Vliet, S. M. S. Toekimin, J. G. Haasnoot, J. Reedijk, O. Nováková, O. Vrána, V. Brabec, *Inorganica chimica acta* **1995**, *231*, 57-64.

[71] N. Grover, N. Gupta, H. H. Thorp, *Journal of the American Chemical Society* **1992**, *114*, 3390-3393.

[72] C. C. Cheng, W. L. Lee, J. G. Su, C. L. Liu, *Journal of the Chinese Chemical Society* **2000**, *47*, 213-220.

[73] E. Corral, A. C. G. Hotze, A. Magistrato, J. Reedijk, *Inorganic chemistry* **2007**, *46*, 6715-6722.

[74] E. Corral, A. C. G. Hotze, H. den Dulk, A. Leczkowska, A. Rodger, M. J. Hannon, J. Reedijk, *Journal of Biological Inorganic Chemistry* **2009**, *14*, 439-448.

[75] Y. Mulyana, G. Collins, R. Keene, *Journal of Inclusion Phenomena and Macrocyclic Chemistry* **2011**, *71*, 371-379.

[76] A. Rilak, I. Bratsos, E. Zangrando, J. Kljun, I. Turel, Z. D. Bugarcic, E. Alessio, *Inorganic Chemistry* **2014**, *53*, 6113-6126.

[77] D. Lazic, A. Arsenijevic, R. Puchta, Z. D. Bugarcic, A. Rilak, *Dalton Transactions* **2016**, *45*, 4633-4646.

[78] M. Nišavić, M. Stoiljković, I. Crnolatac, M. Milošević, A. Rilak, R. Masnikosa, *Arabian Journal of Chemistry* **2018**, *11*, 291-304.

[79] M. M. Milutinović, S. K. C. Elmroth, G. Davidović, A. Rilak, O. R. Klisurić, I. Bratsos, Ž. D. Bugarčić, *Dalton Transactions* **2017**, *46*, 2360-2369.

[80] F. Giannini, L. E. H. Paul, J. Furrer, B. Therrien, G. Süss-Fink, *New journal of chemistry* **2013**, *37*, 3503-3511.

[81] P. J. Dyson, G. Sava, *Dalton Transactions* **2006**, 1929-1933.

[82] H. Huang, P. Zhang, B. Yu, Y. Chen, J. Wang, L. Ji, H. Chao, *Journal of Medicinal Chemistry* **2014**, *57*, 8971-8983.

[83] B.-J. Han, G.-B. Jiang, J.-H. Yao, W. Li, J. Wang, H.-L. Huang, Y.-J. Liu, *Spectrochimica Acta Part A: Molecular and Biomolecular Spectroscopy* **2015**, *135*, 840-849.

[84] Y.-Y. Xie, H.-L. Huang, J.-H. Yao, G.-J. Lin, G.-B. Jiang, Y.-J. Liu, *European journal of medicinal chemistry* **2013**, *63*, 603-610.

[85] C. Zhang, B. J. Han, C. C. Zeng, S. H. Lai, W. Li, B. Tang, D. Wan, G. B. Jiang, Y. J. Liu, *Journal of Inorganic Biochemistry* **2016**, *157*, 62-72.

[86] P. C. Bruijnincx, P. J. Sadler, *Current opinion in chemical biology* **2008**, *12*, 197-206.

[87] D. Wesselinova, N. Kaloyanov, G. Dimitrov, *Journal of Medicinal Chemistry* **2009**, *44*, 5099-5102.

[88] C. Scolaro, A. B. Chaplin, C. G. Hartinger, A. Bergamo, M. Cocchietto, B. K. Keppler, G. Sava, P. J. Dyson, *Dalton Transactions* **2007**, 5065-5072.

[89] K. K.-W. Lo, T. K.-M. Lee, *Inorganic Chemistry* **2004**, *43*, 5275-5282.

[90] G. Suss-Fink, *Dalton Transactions* **2010**, *39*, 1673-1688.

[91] A. L. Noffke, A. Habtemariam, A. M. Pizarro, P. J. Sadler, *Chemical Communications* **2012**, *48*, 5219-5246.

[92] P. Kumar, R. K. Gupta, D. S. Pandey, *Chemical Society Reviews* **2014**, *43*, 707-733.

[93] R. E. Morris, R. E. Aird, S. Murdoch Pdel, H. Chen, J. Cummings, N. D. Hughes, S. Parsons, A. Parkin, G. Boyd, D. I. Jodrell, P. J. Sadler, *Journal of Medicinal Chemistry* **2001**, *44*, 3616-3621.

[94] A. F. Peacock, P. J. Sadler, *Chemistry- An Asian Journal* **2008**, *3*, 1890-1899.

[95] A. Bergamo, A. Masi, P. J. Dyson, G. Sava, *Int J Oncol* **2008**, *33*, 1281-1289.

[96] J. Canivet, G. Suss-Fink, *Green Chemistry* **2007**, *9*, 391-397.

[97] S. K. Singh, S. Joshi, A. R. Singh, J. K. Saxena, D. S. Pandey, *Inorganic Chemistry* **2007**, *46*, 10869-10876.

[98] H. K. Liu, P. J. Sadler, *Accounts of chemical research* **2011**, *44*, 349-359.

[99] O. Novakova, J. Kasparkova, V. Bursova, C. Hofr, M. Vojtiskova, H. Chen, P. J. Sadler, V. Brabec, *Chemistry and Biology* **2005**, *12*, 121-129.

[100] N. Olga, M. Jaroslav, S. Tereza, K. Jana, B. Tijana, S. P. J., B. Viktor, *Chemistry – A European Journal* **2010**, *16*, 5744-5754.

[101] S. W. Magennis, A. Habtemariam, O. Novakova, J. B. Henry, S. Meier, S. Parsons, I. D. H. Oswald, V. Brabec, P. J. Sadler, *Inorganic Chemistry* **2007**, *46*, 5059-5068.

[102] R. E. Aird, J. Cummings, A. A. Ritchie, M. Muir, R. E. Morris, H. Chen, P. J. Sadler, D. I. Jodrell, *British journal of cancer* **2002**, *86*, 1652-1657.

[103] S. Chatterjee, S. Kundu, A. Bhattacharyya, C. G. Hartinger, P. J. Dyson, *Journal of Biological Inorganic Chemistry* **2008**, *13*, 1149-1155.

[104] Y. Liu, R. Hammitt, D. A. Lutterman, L. E. Joyce, R. P. Thummel, C. Turro, *Inorganic Chemistry* **2009**, *48*, 375-385.

[105] K. S. M. Smalley, R. Contractor, N. K. Haass, A. N. Kulp, G. E. Atilla-Gokcumen, D. S. Williams, H. Bregman, K. T. Flaherty, M. S. Soengas, E. Meggers, M. Herlyn, *Cancer Research* **2007**, *67*, 209-217.

[106] Q. Wu, C. Fan, T. Chen, C. Liu, W. Mei, S. Chen, B. Wang, Y. Chen, W. Zheng, *European Journal of Medicina Chemistry* **2013**, *63*, 57-63.

[107] O. Novakova, H. Chen, O. Vrana, A. Rodger, P. J. Sadler, V. Brabec, *Biochemistry* **2003**, *42*, 11544-11554.

[108] O. Novakova, J. Kasparkova, V. Bursova, C. Hofr, M. Vojtiskova, H. Chen, P. J. Sadler, V. Brabec, *Chemistry and Biology* **2005**, *12*, 121-129.

[109] T. Bugarcic, O. Nováková, A. Halámiková, L. Zerzánková, O. Vrána, J. Kašpárková, A. Habtemariam, S. Parsons, P. J. Sadler, V. Brabec, *Journal of Medicinal Chemistry* **2008**, *51*, 5310-5319.

[110] W. H. Ang, E. Daldini, C. Scolaro, R. Scopelliti, L. Juillerat-Jeannerat, P. J. Dyson, *Inorganic Chememistry* **2006**, *45*, 9006-9013.

[111] T. S. Morais, T. J. L. Silva, F. Marques, M. P. Robalo, F. Avecilla, P. J. A. Madeira, P. J. G. Mendes, I. Santos, M. H. Garcia, *Journal of Inorganic Biochemistry* **2012**, *114*, 65-74.

[112] V. Moreno, J. Lorenzo, F. X. Aviles, M. H. Garcia, J. P. Ribeiro, T. S. Morais, P. Florindo, M. P. Robalo, *Bioinorganic Chemistry and Applications* **2010**, *2010*, 936834.

[113] A. Valente, M. H. Garcia, F. Marques, Y. Miao, C. Rousseau, P. Zinck, *Journal of Inorganic Biochemistry* **2013**, *127*, 79-81.

[114] P. Florindo, I. J. Marques, C. D. Nunes, A. C. Fernandes, *Journal of Organometallic Chemistry* **2014**, *760*, 240-247.

[115] C. Creutz, H. Taube, *Journal of the American Chemical Society* **1973**, *95*, 1086-1094.

[116] E. Iengo, G. Mestroni, S. Geremia, M. Calligaris, E. Alessio, *Journal of the Chemical Society, Dalton Transactions* **1999**, 3361-3371.

[117] E. Alessio, E. Iengo, S. Zorzet, A. Bergamo, M. Coluccia, A. Boccarelli, G. Sava, *Journal of inorganic biochemistry* **2000**, *79*, 173-177.

[118] B. Serli, E. Iengo, T. Gianferrara, E. Zangrando, E. Alessio, *Metal-Based Drugs* **2001**, *8*, 9-18.

[119] A. Bergamo, G. Stocco, C. Casarsa, M. Cocchietto, E. Alessio, B. Serli, S. Zorzet, G. Sava, *International journal of oncology* **2004**, *24*, 373-379.

[120] G. Mestroni, E. Alessio, G. Sava, E. Iengo, S. Zorzet, A. Bergamo, Google Patents, **2005**.

[121] P. del Socorro Murdoch, N. A. Kratochwil, J. A. Parkinson, M. Patriarca, P. J. Sadler, *Angewandte Chemie International Edition* **1999**, *38*, 2949-2951.

[122] M. El-Khateeb, T. G. Appleton, L. R. Gahan, B. G. Charles, S. J. Berners-Price, A.-M. Bolton, *Journal of inorganic biochemistry* **1999**, *77*, 13-21.

[123] M. E. Oehlsen, Y. Qu, N. Farrell, *Inorganic chemistry* **2003**, *42*, 5498-5506.

[124] Ž. D. Bugarčić, J. Bogojeski, B. Petrović, S. Hochreuther, R. van Eldik, *Dalton Transactions* **2012**, *41*, 12329-12345.

Chapter 2

The theory on the rate and mechanisms of substitution reactions in organometallic complexes

2.0 Introduction

Kinetics is a broad field of study mainly divided into physical and biochemical kinetics.[1] Physical kinetics measures the rate and mechanism of physical phenomena like adsorption, permeation etc. while biochemical kinetics investigates the rates and mechanism of biochemical reactions. The rate of a chemical reaction determines the time required to observe products or disappearance of reactants while the mechanism defines the route or reaction profile along the reaction coordinate.[2] This chapter reviews the theory of substitution reactions of coordination compounds. Kinetics of chemical and biochemical experiments measures the rate of reaction under specified conditions as well as theoretical to interpret the magnitudes of reaction rate.

2.1 Rate of reactions

The rate of a reaction is defined as the amount of reactant converted into product or product formed per unit time [1] Chemical kinetics concerns itself with speed of reactions and involves taking measurements under dynamic conditions in which the concentrations of the reactants and products are changing as a function of time.[2] [3] [4] [5] [6] [7] Controllable factors in reactions include, temperature, concentration, pressure, available surface area, solvent properties and presence of catalysts. Other factors inherent to the process which are beyond human control include identity of the chemical reagents or the set thermodynamic conditions. Both controllable factors and those beyond control must be taken into account to realistically explain the kinetics of a given process.[8]

2.2 Substitution reactions

A substitution reaction occurs when a ligand from the environment replaces a labile ligand on the coordination complexes.[9] [10] Substitution reactions proceed by any one of the following Langford and Gray mechanisms.[11]

2.2.1 Dissociative mechanism (D)

In this mechanism, the rate determining step is unimolecular and the rate depends only on the strength of the M-X bond and is independent of the nature and concentration of the incoming nucleophile.[12] [13] For a square planar geometry, a 14e$^-$ T-shaped intermediate ion is formed, from the dissociation of the M-X bond. This mechanism is rare but has been reported in square planar[14] [15] as well as octahedral Ru(II) complexes.[16] The dissociative mechanism of substitution is represented by equation 2.1.

$$MX_n \underset{+X}{\overset{-X}{\rightleftharpoons}} MX_{n-1} \underset{-Y}{\overset{+Y}{\rightleftharpoons}} MX_{n-1}Y \qquad 2.1$$

2.2.2 Associative mechanism (A)

In this mechanism, the rate determining step is bimolecular and involves nucleophilic process in which formation of the bond between the metal and incoming nucleophile triggers the breaking of the labile ligands. [17] This gives rise to an intermediate with an increased coordination number as shown in Equation 2.2.[18] [19] For the square planar geometry, a pentavalent intermediate is formed in the transition state[20] [21] [22] [23] [24] [25] [26] [27] while octahedral Ru complexes form a seven coordinate intermediate in the transition state.[28] [29] [30] The nature and concentration of the incoming nucleophile plays a key role in determining the rate of the reaction.

$$MX_n \underset{-Y}{\overset{+Y}{\rightleftharpoons}} MYX_n \underset{+X}{\overset{-X}{\rightleftharpoons}} MYX_{n-1} \qquad 2.2$$

2.2.3 Interchange Mechanism (I)

Between the limiting associative (**A**) and limiting dissociative (**D**) mechanisms lies a set of mechanisms consisting of a single activated complex. In this mechanism, bond formation between the metal centre and the incoming nucleophile and bond breaking between the metal and the leaving group are concurrent. These mechanisms are considered as interchange mechanisms.[1]

Associatively activated interchange mechanism (I_A)

In this mechanism, the rate of the reaction is dependent on the nature of the incoming ligand since the rate limiting step involves bond formation between the incoming ligand and the metal centre in the transition state. [18] Bond breaking is less important although the two steps

co-exist forming a single activated complex. This mechanism has been observed in octahedral Ru(II) complexes.[31] Figure 2.1 illustrates the progression of an associatively activated mechanism.

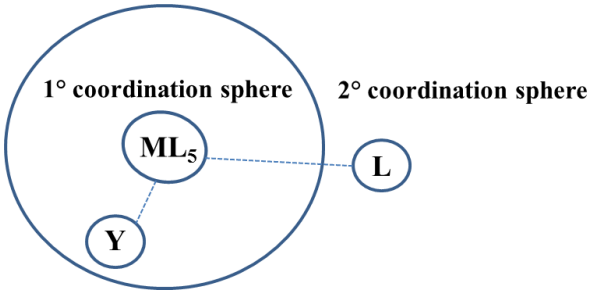

Where L = *labile ligand and* Y = *incoming ligand*

Figure 2. 1 Positions of the L and Y during the I_A mechanisms.

Dissociative activated interchange mechanism (I_D)

In this mechanism, the leaving group starts to break away from the inner coordination sphere to the outer coordination sphere as the entering group moves from the outer coordination sphere to the inner coordination sphere at the same time. If the concentration of the incoming ligand is much less than that of the solvent which is already in the inner coordination sphere, then the probability of the solvent coordinating to the metal centre is higher. Thus, the discrimination between the entering group and the solvent molecules should be minimized.

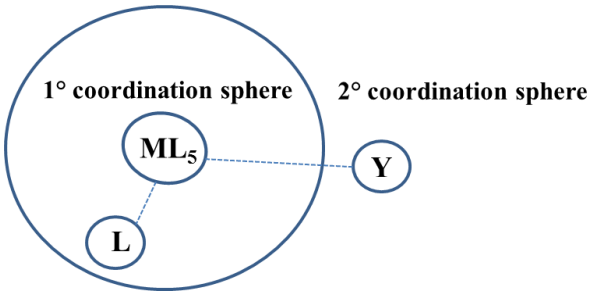

Where L = *labile ligand and* Y = *incoming ligand*

Figure 2. 2 Positions of L and Y ligands during the transition state

2.3 Factors affecting the rate of substitution reactions

There are a number of factors that can affect the rate of a given reaction[32] [33] [34] which include and not limited to;

2.3.1 Effect of the non-labile ligand

In a square planar geometry, commonly occurring for d^8 complexes a *trans* ligand can exert an axial effect on the bond between the metal and the leaving group and consequently on the rate of substitution and this effect is called the *trans*-effect.[35] [14] Alfred Werner[36] [37] and Chernayev and coworkers [38] were the first to use the *trans*-effect to explain the effect of non-labile ligands on the rate of substitution of ligands positioned *trans* to them in square planar Pt(II) complexes.[39] From the study of *trans*-effect of ligands in square planar Pt(II) complexes, ligands can be arranged in order of decreasing labializing strength as follows; CO, CN", C_2H_4 > PR_3, H > CH_3 > $SC(NH_2)_2$ > C_6H_5, NO_2 , I , SCN > Br , CI > py, NH_3, OH , H_2O.[40] *Trans*-effect has also been reported in substitution reactions of octahedral Ru(II) terpyridine complexes[41] as illustrated in Scheme 2.1.

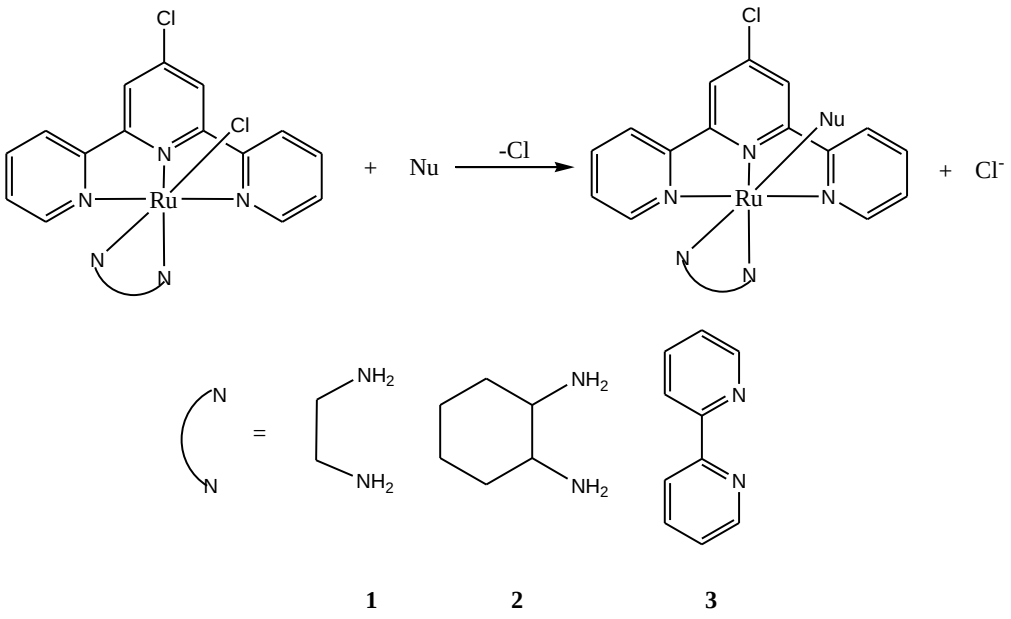

1 **2** **3**

Scheme 2. 1 Substitution reactions of ruthenium complexes exhibiting *trans* effect

Rate of chloro substitution for **1** and **2** is higher than **3** due to the strong *trans* influence of the aminoalkyl pure σ-donor ligands compared to the π-acceptor ligand in **3**.[42] These reactions and others [43] indicate that the strength of the metal-leaving group bond and the labializing influence of the *trans*-group play important roles in substitution reactions. The *trans* labializing ligand affects both ground state and transition states of the complex thereby affecting indirectly the rate of substituting the co-ligand from the complex. The labializing effect can be as large a factor as 10^6 in complexes with a mix of a strong *trans*-labializing ligand and a weak co-ligand.[44] *Trans* labialising effect can be due to σ-donating and/or π-accepting

properties of the ligand.[45] [46] For polarisable metal ions such as Pt, Pd, Ru, strong σ-donating ligand causes a weakening of the bond in the *trans* position (high ground state *trans*-influence) thereby increasing the rate of substitution.[14]

Some *trans* labialising ligands can receive electrons through metal ligand orbital interactions.[39] [47] The effect of π-back-bonding is stronger if the ligand has empty low energy delocalised π* molecular orbitals.[48] In a square planar complex, a good π-accepter ligand e.g. C_2H_4, CN^-, CO stabilises the five coordinate transition state because it accepts electrons donated from the filled *d* orbitals of the metal to the empty π^* orbitals of the ligands thereby facilitating the formation of the metal ion and bond with the incoming nucleophile. The same is applicable to an octahedral geometry in Ru complexes. The seven coordinate transition state is stabilized because the π-acceptor ligand accepts electrons from the filled *d* orbitals of the metal enabling formation of a bond between metal ion and incoming nucleophile. A number of studies have been keen to account for *trans*-effect with the π-bonding and the polarisation theories being the most common.[49]

The rate of substitution from square planar complexes is electronically less sensitive to the ligand *cis* to the leaving group than that in the *trans*-position. However, due to the close proximity of *cis* ligands (90° off axis), the rate will be influenced by the size as well as the spatial hindrance to the approach of the incoming nucleophile. Bulky ligands at *cis* positions strongly shield the co-ligand thus lowering the rate of substitution. Studies have shown that *trans*-activating ligands are poor *cis*-activators with exemptions though.[50] [51] [52]

2.3.2 Effect of incoming group

Because the associative mode of reaction is sensitive to the nature of incoming nucleophile, the rate of reaction is high for a nucleophile that can readily replace the co-labile ligand from the complex. For example the rate of anation of $[Ru(NH_3)_5(H_2O)]^+$ by various ligands shows a positive correlation to the nucleophilicity as well as the basicity of the incoming nucleophiles as shown in Table 2.1.[53] [54] [55] [56] [57]

Table 2. 1 Second order rate constants for the anation of $[Ru(NH_3)_5(H_2O)]^+$ by various ligands at 25 °C

Ligands	$k_2/10^2\ M^{-1}\ s^{-1}$
N_2O	7.2
N_2	7.1
Py	9.1
4-MePy	11.0
C_6H_5CN	26.8
CH_3CN	26.2
SCN	20.8
HCN	11.3

From the results, it is evident that the rate of a reaction for anation of $[Ru(NH_3)_5(H_2O)]^+$ is dependent on the nucleophilicity as well as the basicity of the incoming nucleophile. The nucleophiliciy varies with the nature of the ligand according to the general equation (2.3);

$$\eta_{pt} = \log\left(\frac{k_L}{k_S}\right) \tag{2.3}$$

Most reactive nucleophiles are "soft" (*i.e* are large, have low charge and are easily polarisable donor atoms such as S or I^-) and thus better donors than oxo (O^{2-}) or chloro (Cl^-), respectively in complexes of soft metals such as Pt(II) and Ru(II).[58] [59] A plot of $\log k_L$ verses η_{pt} according to equation 2.4 is a straight line whose slope, *s*, is called the nucleophilic discrimination factor.

$$\log k_L = s.\eta_{pt} + \log k_S \tag{2.4}$$

where k_L *= second order rate constant for the nucleophile, L,* s = *nucleophilic discrimination factor (slope) and log* k_s *= the intrinsic reactivity of the complex.*

The nucleophilic discrimination factor is specific for a complex and measures the sensitivity of the metal centre towards the entering nucleophile.[59] A large value of the slope means the reaction is more sensitive to the changes in the nucleophilic nature. The y-intercept gives the rate constant for the weakest nucleophile measured in a given solvent. A low value of k_S signifies that the complex is more sensitive to changes in the nucleophile. Ligands with

capacity to form dative π-bonding in the transition state exhibit high values of s (low values of k_S) which allows addition of electrons to the metal centre from incoming nucleophiles enhancing the reactivity.[59]

2.3.3 Nature of the leaving group

Effect of a leaving group is circumstantial.[60] If a reaction is dissociative, the bond between the leaving ligand and the metal complex breaks first at a rate that is universally correlated to its strength. In such cases, the rate would strongly depend on the nature of the leaving group for this mode of reaction.[60] But for an associative reaction, effect of the leaving group depends on the extent to which bond breaking occurs in the transition state which is variable. Effect of leaving group on reactivity is demonstrated in the hydrolysis reaction of $Rh(NH_3)_5X$ at 50 °C. A summary of the second order hydrolysis rate constants is shown in Table 2.2.

Table 2. 2 k_2 values for the substitutions of various ligands on $Rh(NH_3)_5X$[61] by the aqua ligand

X	k_2 X $10^3/s^{-1}$
Cl	5.63
Br	6.94
I	2.08

The rate of hydrolysis of the M-X (X = Cl^-, Br^-, I^-) depends inversely on the strength of the M-X bond and hence on the nature of the leaving group, X. Bond breaking in the transition state doesn't automatically lead to dissociative process but is required to facilitate bond formation between metal and incoming group.[60] Inertness of complexes increases when a high field strength co-ligand is the labile ligand.

2.3.4 Steric effect

Apart from the *cis*/*trans*-effect, the other aspect that affects ligand substitutions is the steric effects which are space-filling effects.[62] They are divided into steric bulk and steric hindrance. Steric bulk cause repulsive strain between atoms or a group of atoms due to a mutual repulsion in their electron densities when they are brought into a close-up proximity. When this happens around a central atom or site of reaction, this atom is considered overcrowded round it. The magnitude of this kind of steric effect is directly proportional to the spatial size (a volume effect) of the substituent causing it. If on the other hand, a

substituent or part of it causes a blockade in the approach of one reactant toward a site of reaction then steric hindrance is operational at the site of reaction. The site of the reaction is said to be shielded from a direct attack by an incoming nucleophile. Steric hindrance depends on the spatial size of the substituent (as measured by its volume) and its relative spatial orientation or configuration with respect to the targeted site of reaction. This is especially critical in d^8 square-planar metal complexes, where the geometry of the vacant orbitals on the metal centre requires that the nucleophile approach the central metal axially. The presence of axially configured substituents on the non-labile ligands usually shields the d^8 metal centre from attack by incoming nucleophile resulting in retarded rates of substitution.[63] The retardation on the rate of substitution is more prominent if the steric effect is brought about by a substituent in the *cis*-position relative to the leaving group. A typical example of a steric hindrance effect [64] on reactivity is demonstrated by the reduction in the rate of substitution of X by cyanide from cis-$Pt(PEt_3)_2RX$ (X = bromide, R = substituted phenyl ring) for a series of complexes in which methyl groups are added on the ligand architectural framework. The second order rate constant, $k_{2,}$ values are shown in table 2.3

Table 2. 3 The rate of substitution of X by cyanide from *cis*-[Pt(PEt3)2(R)X], the steric cis-effect by the aryl ligand

R	X	$10^3\, k_1/(s^{-1})$
	Br	6000
	Br	54.4
	Br	0.19

Increase in the overall spatial size of the co-ligand due to the increased number of methyl substituents leads to greater steric hindrance hence lower rate of substitution of the bromide leaving group.

2.3.5 Effect of the solvent

Depending on the nucleophilicity of solvent molecules, the solvent can compete with the incoming nucleophile to displace the labile ligand from the metal complex.[65] [49] So solvents are carefully chosen to minimize the interferences to the kinetics of the reaction by solvent

molecules. In the case where the solvent coordinates, the rate law will include a reaction path attributed to solvent attack. Results (Table 2.4) of rate of chloride exchange from *trans*-$[PtCl_2(py)_2]$ (equation 2.5) varies from one solvent to the other.[49]

$$trans-\left[Pt\left(py\right)_2Cl_2\right]+{}^{36}Cl \rightarrow trans-\left[Pt\left(py\right)_2Cl\left({}^{36}Cl\right)\right]+Cl^- \qquad (2.5)$$

Table 2. 4 A summary of the second order rate constants for the chloride exchange reactions illustrated by equation 2.5 in different solvents

Coordinating solvents	$k/10^{-5}$ **s**$^{-1}$	**weakly coordinating solvents**	$k/$**M**$^{-1}$ **s**$^{-1}$
DMSO	380	CCl_4	10000
H_2O	3.5	C_6H_6	100
CH_3NO_2	3.2	*i*-BuOH	0.1
EtOH	1.4	EtOAc	0.01
PrOH	0.42	$(CH_3)CO$	0.01
		DMF	0.001

Rate constants in strong aprotic coordinating solvents (first column) are 1-2 orders of magnitude higher than the alcohols. This shows that these solvents have a great effect on the substitution reactions in that the rate of substitution by solvent is greater as shown: $k_S >> k_{Cl}[^{36}Cl^-]$. The rates in weak coordinating solvents (second column) are solely due to the attack by incoming nucleophile hence $k_{Cl}[^{36}Cl^-] >> k_S$. In non-polar solvents, the rates are highest probably because the chloride is not solvated and hence making it more reactive.[49] For coordinating solvents, k_2 values go in the order;[48] DMSO > CH_3NO_2 ~ H_2O > ROH.

The significance of the order for coordinating solvents is that metal-solvent bond formation is more important than bond breaking in the transition state. If solvating the leaving group was the sole role of the solvent, then water would be superior to dmso in solvent effects. However, dmso is a more efficient nucleophile because sulphur is a better nucleophile than oxygen.[66]

2.4 The general chemistry of Ruthenium (Ru) complexes

Ru is a member of Group 8 metal elements of the periodic table along with iron and osmium and has an electronic configuration, [Kr] $4d^7$ $5s^1$. It is also a rare earth metal but the least

expensive among the PGM's[67] which includes platinum, osmium, palladium, iridium and rhodium. The chemistry of Ru more closely resembles that of osmium than that of iron.[68]

Ru can form complexes of different oxidation states and geometries with various ligands. Examples are $[Ru^{o}(CO)_5]$, $[R^{II}HCI(PPh_3)_2]$, $[Ru^{lll}(terpy)Cl_3]$ and $KRu^{v}F_6$ with geometries of the first and second complex being trigonal bipyramidal while for the rest, it is octahedral.[39] Most of these complexes are synthesized starting from $[(NH_3)_6Ru]Cl_3$ or $RuCl_3.3H_2O$.

The Ru complexes in aqueous media is dominated by Ru(II) and Ru(III) forms, with complexes containing N-donor ligands being the most stable. Most of these complexes have found applications in many areas which includes biomedical and biomolecular systems. Some of the Ru complexes such as *cis*-$[Cl_2(NH_3)_4Ru^{III}]Cl_2$ and (HIm)[*trans*-$(lm)_2CI_4Ru^{lll}$] (1m = imidazole) have shown a cytotoxic induction of DNA of cancer cell lines including their metastatics.[69]

2.4.1 Substitution from Octahedral Complexes

Most late transition metal (2^{nd} and 3^{rd}) ions form six coordinate octahedral complexes depending on the number of electrons in their valence *d* orbitals and the strength of the ligand crystal field.[70] For example, the d^3 and low-spin d^6 ions form predominantly octahedral complexes. So are the complexes of d^4 and d^9 metal ions. In the later class of complexes, a tetragonal distortion called the Jahn-Teller effect elongate the the bonds of the two axial ligands relative to the bond length of the four equatorial ligands of the an octahedral geometry.[70] This nature of distortions can have a great influence on the reactivity of the complexes.

Octahedral complexes are coordinatively saturated hence mechanism of their substitution reactions would tend towards dissociative (D) mode or dissociatively activated interchange mechanism (I_d).[71] However, numerous reports have appeared in literature where associatively activated substitution occurs in octahedral geometry.[30] [29] This is supported by entropy of activation values that are very negative, a dependency of the rate of substitution on the nature and concentration of incoming nucleophile etc. It has emerged in recent studies that the associative mode of activation may be possible for a range of geometries during the transition state.[72] Substitution reactions of the octahedral transition metal complexes are a more complex than those for square-planar complexes. For example, rate of substitution reactions from octahedral Co(llI), Cr(llI) and Ni(ll) complexes do not indicate high sensitivity

towards different nucleophile as observed for most associative reactions of square-planar d^8 metal complexes.[72]

2.4.2 Substitution Reactions of Ru Complexes

Studies on the rate of substitution from Ru complexes are dominated by those complexes with Ru in oxidation states (II) and (III), in particular Ru(II).[73] Data on the rate of substitution from Ru(II) is well reported for ligand exchange in $[Ru(NH_3)_5X]^{2+}$ where X = H_2O.[74] [75] The second order rate constants for the substitution process in these complexes with various neutral ligands at 25°C range from 2.7 to 302 x 10^{-3} M^{-1} S^{-1}.[76] [57] Taube and co-workers have shown that some substitution reactions of Ru(II) complexes proceed via a dissociative interchange mechanism.[75] An attempt to enhance the lability of the water molecule in $[Ru(NH_3)_5OH_2]^{2+}$ was made by replacing one of the ammine ligands with a field-strength ligand, L to form $[Ru(NH_3)_4L(OH_2)]^{2+}$, where L= CO, N_2, isonicotinamide (isn), pyridine (py), CN or SO_3^{2-}.[77] In general the reactivity and stability of the transition metal complexes depend on the oxidation state of the metal as well as the stereo-electronic properties of the ligand around the metal centre.

2.5 Differential rate laws

Since rate is the change in concentration per unit time, the unit for rate is mol dm^{-3} s^{-1} (M s^{-1}).[71] [72] [78] Consider a chemical reaction represented by equation 2.6,

$$aA + bB \rightarrow cC + dD \tag{2.6}$$

where a, b, c and d represent the stoichiometry of the reaction and A, B, C *and* D *represent formulae of chemical compounds.*

The general rate law for a reaction is represented by equation 2.7,

$$Rate = \frac{-d[reac\tan t]}{dt} = \frac{d[product]}{dt} \tag{2.7}$$

The negative sign in equation 2.7 represents the disappearance of the reactant with time. The rate law includes the concentration of all species that affect the rate.[79] When the reagents are included in the general rate law, equation 2.7 becomes equation 2.8,

$$Rate = -\frac{1}{a}\frac{d[A]}{dt} = -\frac{1}{b}\frac{d[B]}{dt} = \frac{1}{c}\frac{d[C]}{dt} = \frac{1}{d}\frac{d[D]}{dt} \quad (2.8)$$

In general the rate law is represented by equation 2.9;

$$Rate = -k\prod_i [A_i]^{\alpha_i}[X_j]^{\beta_j} \quad (2.9)$$

A_i is *reactants, k* is *rate constant,* X_j is *other species such as catalysts that may affect the rate and* α *and* β are *rate orders with respect to reagents, A and, B respectively determined experimentally.*

The order of a reaction is defined as:[80]

$$Order \quad of \quad reaction = \sum_i \alpha_i \quad (2.10)$$

The unit for the rate constant, *k*, depends on the reaction order. Reaction order is not always related to the stoichiometry of the reaction but can be only determined experimentally.

2.5.1 Integrated rate laws

Irreversible first-order reactions

Most of the reactions fall under the category of first order or are studied under conditions that approximate first-order conditions. For a first-order reaction, the rate is directly proportional to a single reactant concentration thus the kinetics follow a rate law with the reaction order being unity.[81] The rate constant for the forward reaction is much greater than that for the reverse reaction. A first-order reaction can simply be represented by the relation 2.11.

$$A \xrightarrow{k_1} B \quad (2.11)$$

The rate law for this reaction is given by equation 2.12.

$$Rate = \frac{-d[A]}{dt} = k_1[A]_t \quad (2.12)$$

Rearranging the equation gives equation 2.13,

$$\frac{-d[A]}{[A]_t} = k_1 dt \tag{2.13}$$

Integrating this equation from time, *t = 0* to *t = t* for changes in concentration from $[A]_0$ to $[A]_t$ leads to equations 2.15.

$$\int_{[A]_0}^{[A]_t} \frac{d[A]}{[A]_t} = -k_1 \int_o^t dt\,, \tag{2.14}$$

$$\ln \frac{[A]_t}{[A]_0} = -k_1 t \tag{2.15}$$

Equation 2.15 can be simplified to equation 2.16.

$$\ln[A]_t = -kt + \ln[A]_0 \tag{2.16}$$

Equation 2.16 can also be expressed as,

$$[A]_t = [A]_0 e^{-kt} \tag{2.17}$$

$[A]_0$ *and* $[A]_t$ *are concentrations of A at time* t = 0 *and* t = t, *respectively.*

From equation 2.16 which is consistent with the equation of a straight line $(y = mx + c)$, a plot of $\ln[A]_t$ verses *t* gives a straight line graph whose slope and intercept are equivalent to the rate constant, -*k*, and $\ln[A]_0$, respectively. Physical parameters that are proportional to the concentration including: absorbance, pressure, conductivity or volume could be applied directly in the determination of the rate constant for first-order reactions.[81] [82]

Reversible first-order reactions

A reaction that doesn't proceed to completion but establish equilibrium where some of the product which would have been formed is converted back into starting material as shown in equation 2.18 is described as a reversible reaction.[81] [83]

$$A \underset{k_{-1}}{\overset{k_1}{\rightleftharpoons}} B \tag{2.18}$$

where, k_1 and k_{-1} are rate constants for the forward and reverse reactions respectively.

The rate law for this reaction is given by equation 2.19,

$$Rate = \frac{d[B]}{dt} = \frac{-d[A]}{dt} = k_1[A]_t - k_{-1}[B]_t \tag{2.19}$$

At t = 0, $[B]_0 = 0$ and $[A]_t = [A]_0$ thus $[A]_0$, $[A]_t$ and $[B]_t$ are related by equation 2.20,

$$[B]_t = [A]_0 - [A]_t \tag{2.20}$$

Substituting for $[B]_t$ in equation 2.19 gives equation 2.21,

$$\frac{-d[A]}{dt} = k_1[A]_t - k_{-1}([A]_0 - [A]_t) \tag{2.21}$$

At equilibrium the net reaction is zero, hence equation 2.21 reduces to equation 2.22,

$$\frac{-d[A]}{dt} = 0 \tag{2.22}$$

Applying equations 2.21 and 2.22 to equation 2.19 leads to equation 2.23,

$$k_1[A]_{eq} = k_{-1}[B]_{eq} = k_{-1}\left([A]_0 - [A]_{eq}\right) \tag{2.23}$$

Equation 2.21 can be rearranged to form equation 2.24,

$$[A]_0 = \frac{k_1 + k_{-1}}{k_{-1}}[A]_{eq} \tag{2.24}$$

Substituting equation 2.24 in 2.21 forms equation 2.25,

$$\frac{-d[A]}{dt} = (k_1 + k_{-1})[A]_t - (k_1 + k_{-1})[A]_{eq} \tag{2.25}$$

Rearranging the equation gives equation 2.26,

$$\frac{d[A]}{([A]_t - [A]_{eq})} = -(k_1 + k_{-1})dt \tag{2.26}$$

Integrating equation 2.26 finally leads to equation 2.28,

$$\int_{[A]_0}^{[A]_t} \frac{d[A]}{([A]_t - [A]_{eq})} = -(k_1 + k_{-1}) \int_0^t dt\,, \tag{2.27}$$

Then,

$$\ln \frac{([A]_t - [A]_{eq})}{([A]_0 - [A]_{eq})} = -(k_1 + k_{-1})t \tag{2.28}$$

Rearranging equation 2.28 gives:

$$\ln([A]_t - [A]_{eq}) = -(k_1 + k_{-1})\ t\ +\ \ln([A]_0 - [A]_{eq}) \tag{2.29}$$

Equation 2.29 is linear and of the form: $y = mx + c$. A plot of $\ln([A]_t - [A]_{eq})$ against, t, is linear with the slope equal to $-(k_1 + k_{-1})$. To determine k_1 and k_{-1}, the equilibrium constant, K_{eq}, must be evaluated.

Since,

$$\frac{d[A]}{dt} = 0 = k_1[A]_{eq} - k_{-1}[B]_{eq}\text{, thus,}$$

$$K_{eq} = \frac{[B]_{eq}}{[A]_{eq}} = \frac{k_1}{k_{-1}} \tag{2.30}$$

The experimentally observed rate constant becomes;

$$k_{obs} = (k_1 + k_{-1}) \tag{2.31}$$

To apply equilibrium state calculations to first-order reversible reactions, $[A]_{eq}$ must be measured accurately.[83]

Consecutive first-order reactions

The reaction proceed through two reaction steps in which the product formed from the first reaction becomes the reactant for a subsequent reaction. Ligand substitution reactions normally do not stop after one substitution but proceed to form a more highly substituted complex.[82] Consider a simple consecutive reaction represented in equation 2.32,

$$A \xrightarrow{k_1} B \xrightarrow{k_2} C \tag{2.32}$$

The rate for the disappearance of A or formation of C or D is given by,

$$\frac{-d[A]}{dt} = k_1[A] \tag{2.33}$$

$$\frac{d[B]}{dt} = k_1[A] - k_2[B] \tag{2.34}$$

$$\frac{d[C]}{dt} = k_2[B] \tag{2.35}$$

At time t = 0, $[A] = [A]_0$ while $[B]_0 = [C]_0 = 0$ and after a time, *t*,

$$[A]_0 = [A]_t + [B]_t + [C]_t \tag{2.36}$$

Integrating equation 2.33 gives equation 2.37,

$$[A]_t = [A]_0 e^{-k_1 t} \tag{2.37}$$

Equation 2.37 is substituted in equation 2.34 to give 2.38,

$$\frac{d[B]}{dt} = k_1[A]e^{-k_1 t} - k_2[B]_t \tag{2.38}$$

Equation 2.39 is obtained by multiplying equation 2.38 an integrating factor $e^{-k_2 t}$, followed by rearrangement to give;

$$\frac{d[B]e^{k_2 t}}{dt} = k_1[A]_0 e^{(k_2 - k_1)t} - k_2[B]_t e^{k_2 t} \tag{2.39}$$

With the initial conditions, t = 0, $[B]_0 = 0$ the product rule is applied to equation 2.39 and subsequent integration proceeds as follows to give equation 2.40,

$$\int_0^t \frac{d}{dt}\left([B]_t e^{k_2 t}\right) = k_1[A]_0 \int_0^t e^{(k_2 - k_1)t}\, dt \quad ,$$

$$[B]_t = k_1[A]_0 \frac{\int_0^t e^{(k_2 - k_1)t}}{e^{k_2 t}},$$

$$[B]_t = \frac{[A]_0 k_1}{k_2 - k_1}[e^{k_1 t} - e^{k_2 t}] \tag{2.40}$$

The mass law is applied to equation 2.40 to give equation 2.41;

$$[C]_t = [A]_0\left(1 - \frac{k_2}{k_2 - k_1}e^{-k_1 t} + \frac{k_1}{k_2 - k_1}e^{-k_2 t}\right) \tag{2.41}$$

For the *steady state approximation* (an assumption used for consecutive reactions), [B] is assumed to be very small and doesn't change during the reaction thus, $k_1 < k_2$[83] based on this assumption, equation 2.34 gives equation 2.42,

$$\frac{d[B]}{dt} = k_1[A]_t - k_2[B]_t \cong 0 \tag{2.42}$$

This rearranges to equation 2.43,

$$[B]_t = \frac{k_1}{k_2}[A]_t \tag{2.43}$$

Substituting equation 2.37 into 2.43 gives equation 2.44,

$$[B]_t = \frac{k_1}{k_2}[A]e^{-k_1 t} \tag{2.44}$$

Making $[C]_t$ the subject of the formula in equation 2.36 gives; $[C]_t = [A]_0 - [A]_t - [B]_t$, which when substituted with equations 2.37 and 2.44 gives equation 2.45,

$$[C]_t = [A]_0\left[\ 1 - e^{-k_1 t} - \frac{k_1}{k_2} e^{-k_1 t}\ \right] \cong [A]_0[1 - e^{-k_1 t}] \tag{2.45}$$

Irreversible Second –Order reactions

Second-order reactions can be grouped into two types. For the first type the rate of the reaction is second order with respect to only one of the reactants while the second type is the rate of reaction is first-order with respect to two different reactants. Consider the type II second order reaction as shown in equation 2.46.

$$A + B \xrightarrow{k_2} C \tag{2.46}$$

The rate law for this reaction is given by equation 2.47,

$$Rate = k[A][B] \tag{2.47}$$

The rate law can be represented by equation 2.48,

$$Rate = \frac{d[C]}{dt} = -\frac{d[A]}{dt} = -\frac{d[B]}{dt} = k_2[A]_t[B]_t \tag{2.48}$$

If at t = 0, $[A] = [A]_0$ and $[B] = [B]_0$, and letting *x* be the amount of the reactants reacted after time, t, then concentration of [A] and [B] at time, t, will be, $[A]_t = ([A]_0 - x)$ and $[B]_t = ([B]_0 - x)$ respectively.

The rate after time, t, is therefore given by equation 2.49,

$$-\frac{d[A]}{dt} = k_2([A]_0 - x)([B]_0 - x) \tag{2.49}$$

Given that $\frac{dx}{dt} = -\frac{d[A]}{dt} = -\frac{d[B]}{dt}$, equation 2.49 can be represented by equation 2.50,

$$\frac{dx}{dt} = k_2([A]_0 - x)([B]_0 - x) \tag{2.50}$$

When variables are separated, the new form of this equation is given by equation 2.51,

$$\frac{dx}{([A]_0 - x)([B]_0 - x)} = k_2 dt \tag{2.51}$$

Integrating equation 2.51 between the limits $x = 0$ to $x = x$ and $t = 0$ to $t = t$ respectively through equation 2.52 solves to equation 2.53,

$$\int_0^x \frac{dx}{([A]_0 - x)([B]_0 - x)} = k_2 \int_0^t dt\,, \tag{2.52}$$

$$\frac{1}{[A]_0 - [B]_0} \ln \frac{[B]_0([A]_0 - x)}{[A]_0([B]_0 - x)} = k_2 t \tag{2.53}$$

Since $([A]_0 - x) = [A]_t$ and $([B]_0 - x) = [B]_t$, equation 2.53 changes to equation 2.54,

$$\frac{1}{[A]_0 - [B]_0} \ln \frac{[B]_0[A]_t}{[A]_0[B]_t} = k_2 t \tag{2.54}$$

For the second-order rate constant, k_2, to be calculated, $[A]_0$, $[B]_0$, $[A]_t$ and $[B]_t$ must be determined first (as implied in equation 2.54) and this is cumbersome.[82] [83] The rate law is thus commonly simplified by running reactions under *pseudo-first-order* conditions by having either concentration of *A* or *B* in excess (at least 10 fold). For example if $[B]_0 >> [A]_0$, then concentration of *B* remains relatively constant as the reaction proceeds. With the assumption that the reaction is *first-order* with respect to *A*, then equation 2.48 converts to equation 2.55,

$$\frac{-d[A]}{dt} = (k_2[B]_0)[A]_t\,,$$

$$\frac{-d[A]}{dt} = k_{obs}[A]_t \tag{2.55}$$

where k_{obs} *is the observed rate constant whose unit is per second* (s^{-1})

Integration of equation 2.55 leads to equation 2.15 from which a graph of $\ln[A]$ verses time, *t*, is a straight line with the slope equal to k_{obs}. If rate is measured at different initial concentrations of B (in excess fold of A) and the measured values of k_{obs} plotted against $[B]_0$ (according to equation 2.56) a straight line graph of slope equal to the second-order rate constant, k_2 ($M^{-1}s^{-1}$) is obtained.[84]

$$k_{obs} = k_2[B]_0 \tag{2.56}$$

Reversible Second-order Reactions

Some second order reactions may not proceed to completion. This leads to equilibrium state as illustrated by equation 2.57,

$$A + B \underset{k_{-2}}{\overset{k_2}{\rightleftharpoons}} C \tag{2.57}$$

If it is assumed that the forward reaction is second order while the reverse reaction is first order meaning that it is a complex multi-order reaction. The reaction is simplified by having pseudo first-order conditions for the forward reaction where $[B]_0 >> [A]_0$ which makes it resemble a reversible first-order reaction with rate given as, [84]

$$-\frac{d[A]}{dt} = -\frac{d[B]}{dt} = \frac{d[C]}{dt} \tag{2.58}$$

The rate of formation of C is given by equation 2.59,

$$Rate = k_2[A]_t[B]_t - k_{-2}[C]_t \tag{2.59}$$

Given the stoichiometry of the reaction is 1:1:1 and no product at time, $t = 0$, then after time, *t*, the masses remaining will be given by equations 2.60 and 2.61,

$$[A]_t = ([A]_0 - [C]_t) \tag{2.60}$$

$$[B]_t = ([B]_0 - [C]_t) \tag{2.61}$$

At equilibrium, the mass balances will be given by equations 2.62 and 2.63,

$$[A]_{eq} = ([A]_0 - [C]_{eq}) \tag{2.62}$$

$$[B]_{eq} = ([B]_0 - [C]_{eq}) \tag{2.63}$$

At equilibrium, the forward and reverse reactions are equal and opposite represented by equation 2.64,

$$-\frac{d[A]}{dt} = k_2[A]_{eq}[B]_{eq} - k_{-2}[C]_{eq} = 0\text{, thus,}$$

$$k_2[A]_{eq}[B]_{eq} = k_{-2}[C]_{eq} \tag{2.64}$$

Substituting for $[C]_{eq}$ gives equation 2.65,

$$k_2[A]_{eq}[B]_{eq} = k_{-2}([A]_0 - [A]_{eq}) \tag{2.65}$$

With this, the rate works out to equation 2.66,

$$k_{-2}[A]_0 = k_2[A]_{eq}[B]_{eq} + k_{-2}[A]_{eq},$$

$$[C]_t = ([A]_0 - [A]_t),$$

$$-\frac{d[A]}{dt} = k_2[A]_t[B]_t - k_{-2}([A]_0 - [A]_t) = k_2[A]_t[B]_t - k_{-2}[A]_0 + k_{-2}[A]_t,$$

$$= k_2[A]_t[B]_t - k_2[A]_{eq}[B]_{eq} - k_{-2}[A]_{eq} + k_{-2}[A]_t \tag{2.66}$$

Substituting for $[B]_t$ and $[B]_{eq}$ according to equations 2.61 and 2.63 and making the approximation that, $k_2[A]_0[A]_t \approx k_2[A]_{eq}[A]_0$ and $k_2[A]_t^2 \approx k_2[A]_{eq}^2$ gives equation 2.67,

$$-\frac{d[A]}{dt} = k_2[A]_t[B]_0 - k_2[A]_{eq}[B]_0 - k_{-2}[A]_{eq} + k_{-2}[A]_t \tag{2.67}$$

Factorizing this equation gives equation 2.68,

$$-\frac{d[A]}{dt} = \left(k_2[B]_0 + k_{-2}\right)\left([A]_t - [A]_{eq}\right) \tag{2.68}$$

Separating the variables and subsequent integration leads to equation 2.69,

$$\int_{[A]_0}^{[A]_t} \frac{d[A]}{\left([A]_t - [A]_{eq}\right)} = -\left(k_2[B]_0 + k_{-2}\right)\int_0^t dt\,,$$

$$\ln\left(\frac{[A]_t - [A]_{eq}}{[A]_0 - [A]_{eq}}\right) = -\left(k_2[B]_0 + k_{-2}\right)t = k_{obs}t \tag{2.69}$$

where $k_{obs} = k_2[B]_0 + k_{-2}$

A graph of k_{obs} verses $[B]_0$ is a straight line whose slope is k_2 and intercept equivalent to k_{-2}. The ratio of $k_2 : k_{-2}$ gives the value of the thermodynamic parameter.[84] Generally *pseudo*-first-order reactions are applied in the study of substitution reactions of square planar complexes.

2.6 Activation parameters

Temperature is one of the factors that directly affect the rate at which reactants can be converted to products depending on the amount of thermal energy required to activate the reaction.[84] [49] The rate can be accelerated or decelerated depending on the exothermicity or endothermicity of the reaction. Arrhenius studied the relationship between the rate and temperature and concluded that rate increased/decreased exponentially with change in temperature of the reaction medium.[49] [84]

2.6.1 The Arrhenius equation

The relationship between temperature and velocity of a reaction can be written as (Arrhenius equation 2.70):[85]

$$k = Ae^{-\frac{E_a}{\mathrm{RT}}} \tag{2.70}$$

Taking natural logarithm of the Arrhenius equation gives equation 2.71,

$$\ln k = \ln A - \frac{E_a}{\mathrm{R}}.\frac{1}{\mathrm{T}} \tag{2.71}$$

Where: A is *Arrhenius pre-exponential factor (M^{-1} s^{-1}), E_a* is *Arrhenius activation energy (J mol^{-1}),* R is *Gas constant (8.315 J K^{-1} mol^{-1}) and* T is *Absolute temperature (K)*

By varying temperature and measuring the rate constant a linear plot of $\ln k$ verses $\frac{1}{\mathrm{T}}$ is expected and the slope is equal to $-\frac{E_a}{\mathrm{T}}$ from which E_a can be determined. The rate constant is expected to increase or decrease with change in temperature.[86] The Arrhenius equation is useful for complex systems where the determined rate constant, *k,* is thought to be a composite of specific rate constants.[86]

2.6.2 The transition-state Theory

The transition-state theory was proposed by H. Eyring, M. Evans and M. Polanyi in 1936[87] [88] to account for thermal effect on rate of reactions of simple dissociation processes in gaseous phase. It is based on the assumption that most reactions proceed via established pre-equilibrium state as illustrated by equation 2.72,

$$A - B \overset{K^{\neq}}{\rightleftharpoons} \underbrace{[\ A \ldots\ldots B\ ]^*}_{\text{Activated complex}\ /\ \text{Transition state}} \rightarrow A + B \tag{2.72}$$

The reaction rate can be expressed by equation 2.73,

$$\frac{d[A]}{dt} = k_2\left[A - - - B\right]^* \tag{2.73}$$

Since $K^{\neq}$ is given by equation 2.74,

$$K^{\neq} = \frac{[A---B]^{*}}{[A-B]} \tag{2.74}$$

Equation 2.73 forms equation 2.75 after substituting for $[A\text{----}B]^{*}$.

$$\frac{d[A]}{dt} = k_2 K^{\neq}[A-B] = \frac{k_b \mathrm{T}}{h} K^{\neq}[A-B] \tag{2.75}$$

Where k_b is *Boltzmann's constant (1.38* x 10^{-23} *J* K^{-1}*) and h* is *Plank's constant (6.626* x 10^{-34} *J* s^{-1}*).*

The experimental rate constant can be incorporated in equation 2.75 to give equation 2.76,

$$\frac{d[A]}{dt} = k_{\exp}[A-B] \tag{2.76}$$

Where the experimental rate constant is given by equation 2.77,

$$k_{\exp} = \frac{k_b \mathrm{T}}{h} K^{\neq} \tag{2.77}$$

Given that Gibbs free energy of activation, $\Delta G^{\neq}$, is given by equation 2.78,

$$\Delta G^{\neq} = -\mathrm{RT} \ln K^{\neq},$$

$$= \Delta H^{\neq} - \mathrm{T}\Delta S^{\neq} \tag{2.78}$$

Substituting for $K^{\neq}$ in equation 2.77 gives equation 2.79,

$$k_{\exp} = \frac{k_b \mathrm{T}}{h} e^{\left(-\frac{\Delta G^{\neq}}{\mathrm{RT}}\right)} \tag{2.79}$$

Given that,

$-\mathrm{RT}\ln K^{\neq} = \Delta H^{\neq} - \mathrm{T}\Delta S^{\neq}$, where

$$K^{\neq} = e^{\left(\frac{-\Delta H^{\neq}}{RT}\right)} \quad e^{\left(\frac{\Delta S^{\neq}}{R}\right)},$$

Equation 2.79 could also give equation 2.80,

$$K_{\exp} = \frac{k_b T}{\mathrm{h}} \quad e^{\left(\frac{-\Delta H^{\neq}}{RT}\right)} \quad e^{\left(\frac{\Delta S^{\neq}}{R}\right)} \tag{2.80}$$

Rearranging, applying logarithms, linearization and simplifying equation 2.80 give equation 2.81,

$$\ln \left(\frac{K_{\exp}}{\mathrm{T}}\right) = \frac{-\Delta H^{\neq}}{\mathrm{R}} \frac{1}{\mathrm{T}} + \left[ln \left(\frac{K_b}{h}\right) + \frac{\Delta S^{\neq}}{\mathrm{R}}\right] \tag{2.81}$$

Substituting the values of k_b and h into $\ln\left(\frac{k_b}{h}\right)$ gives a value of ~23.8 hence equation 2.81 will eventually form equation 2.82,

$$\ln \left(\frac{K_{\exp}}{\mathrm{T}}\right) = \frac{-\Delta H^{\neq}}{\mathrm{R}} \frac{1}{\mathrm{T}} + \left[23.8 + \frac{\Delta S^{\neq}}{\mathrm{R}}\right] \tag{2.82}$$

A plot of $\ln\left(\frac{k_{\exp}}{\mathrm{T}}\right)$ verses $\frac{1}{\mathrm{T}}$ gives a graph known as Erying plot, of slope $-\frac{\Delta H^{\neq}}{\mathrm{R}}$ and an intercept equal to $23.8 + \frac{\Delta S^{\neq}}{\mathrm{R}}$ from which the thermal activation enthalpy change, $\Delta H^{\neq}$, and activation entropy change, $\Delta S^{\neq}$, can be determined respectively.[82] [89]

2.6.3 Determination of activated volume

The dependence of the rate constant on pressure provides another activation parameter of mechanistic utility. From thermodynamic point of view the relationship between pressure and volume is presented in equation 2.83;

$$dG = Vdp - SdT \tag{2.83}$$

where the partial derivative of the change in the free energy of a reaction, ΔG, with respect to the applied pressure for a reaction carried under isothermal conditions, can be written as,

$$\left(\frac{\partial(\Delta G)}{\partial p}\right)^{0}_{T} = \Delta V^{0} \tag{2.84}$$

ΔV^0, is the difference in the partial molar volumes between the products and the reactants. But $\Delta G = -RT \ln K$, thus equation 2.84 can be rewritten as equation 2.85:

$$\left(\frac{\partial(-RT \ln K)}{dT}\right)^{0}_{T} = \Delta V^{0} \tag{2.85}$$

$$\left(\frac{\partial(\ln K)}{\partial p}\right)^{0}_{T} = \frac{-\Delta V^{0}}{RT} \tag{2.85a}$$

$$\left(\frac{\partial\left(\frac{\ln k_{1}}{k-1}\right)}{\partial p}\right)^{0}_{T} = \tag{2.85b}$$

$$\left(\frac{\partial(\ln k_1)}{\partial p}\right) = \left(\frac{-\Delta V^{0}}{RT} + \frac{\partial \ln k_{-1}}{\partial p}\right) = \tag{2.85c}$$

Given that $\Delta V^{\#}$ is the volume of activation and is equal to the difference in the partial molar volumes between the transition state and the reactants and is considered independent of the applied pressure. Taking integrals both sides within the applied pressure range of P = 0 to P = P results to equation 2.86;

$$\ln k_1 = \ln(k_1)_0 - \frac{\Delta V^{\#}}{RT} P \tag{2.86}$$

A plot of $\ln k_1$ against applied pressure is linear with a slope of $\frac{-\Delta V^{\#}}{RT}$ from which the volume of activation can be attained. $\Delta V^{\#}$, is composed of two terms: the intrinsic component ($\Delta V_{int}^{\#}$), which stems from the changes in the first coordination sphere, and the electrostrictive one ($\Delta V_{el}^{\#}$), due to the changes in the electrostriction of the solvent. [90] In

practice, $\Delta V^{\#} \approx \Delta V_{int}^{\#}$, the $\Delta V_{el}^{\#}$ component becomes important only in reactions that proceed with no change in the overall charge between the reactants and the products.

Thus, for the reactions that proceed with no change in the overall charge, the volume of activation data can be positive or negative, and its sign is a valuable piece of mechanistic information.[91] Where the negative volume implies a mechanistic pathway proceeding via a contracted transition state involving a greater degree of bond making, corresponding to the decrease in volume effectively equal to partial molar volume of the entering ligand as it is lost from the inner shell ligand assemblage on forming the penta-coordinated transition state.[92] Whilst, a dissociately-activated process is indicated when an increase in the applied pressure cause a retardation in the observed in the observed rate of reaction such that $\Delta V^{\#}$ is positive resulting to a more expanded transition state resulting from a dominant bond breaking process.

2.7 Instrumentation for studying the rates of substitution from coordination complexes

Several methods are used to measure reaction rates depending on the speed of the reaction of interest. The best technique to study chemical kinetics must involve mixing reactants in a time negligible to the time scale of the reaction, measure a variable that is proportional to concentration of reactants or products as a function of time and accurately measure and control temperature or pressure at which a reaction happens.[83] A slow reaction can be studied by conventional methods of analysis to determine the concentration of a reactant or product as a function of time. Most reactions are too fast so that the reaction has to be stopped while the measurement is done (quenching) or use a technique that ensures continuous measurement of concentration as the reaction proceeds.

Quenching is achieved by lowering temperature which reduces thermal energy of the reacting particles allowing a measurement to be taken. This is cumbersome hence better conventional methods where a property (spectrophotometry, conductometry, potentiometry etc) that is proportional to the concentration is monitored continuously are preferred.[83] Many techniques are available for kinetic studies for example pulse methods, infrared spectroscopy (IR), nuclear magnetic resonance spectroscopy (NMR) etc. UV/Visible absorption spectroscopy and stopped-flow analysis were applied in this study hence the only ones discussed here.

2.7.1 UV/Visible Spectrophotometry

Light from a continuous source is dispersed on a monochromator, consisting of a prism or grating or even a filter which selects a wavelength. The selected photons of specific wavelength with incident intensity, I_o, are partially absorbed by sample held in a cuvette of length, l, and emerges at reduced intensity, I.[83] A double-beam spectrophotometer facilitates light to pass alternately through the sample cuvette and reference cuvette containing pure solvent. Absorption due to pure solvent is subtracted off the absorption of the sample before rationing it to the intensity of the incident beam.[83] As shown in Figure 2.3, the alternation of the beam between cuvettes is facilitated by a motor driven chopper which rotates a mirror into and out of the path of light. When the chopper is not deflecting the beam, light passes through the sample and the detector measures the intensity; however, when the chopper deflects the beam through the reference cuvette, the detector reads the reference value *i.e.* the beam is chopped several times per second.

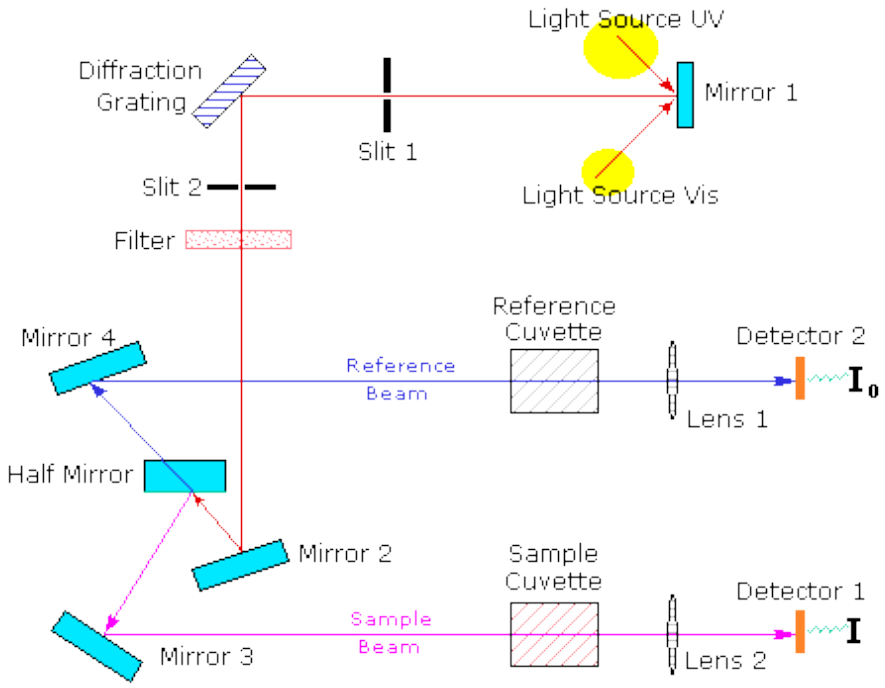

Figure 2. 3 A schematic diagram of a UV-Visible spectrophotometer.[93]

Transmittance, T, measured by a spectrophotometer is defined as the fraction of light passing through the sample given by equation 2.87,

$$T = \frac{I}{I_o} \tag{2.87}$$

where I_o is intensity of incident radiation and I is intensity of transmitted radiation

Absorbance which is a more useful quantity because of its direct relationship with concentration is given by equation 2.88,

$$A = \log \frac{I_0}{I} = -\log T \tag{2.88}$$

The absorbance is better expressed in terms of concentration by the Beer's law in equation 2.89,

$$A = \varepsilon CL \tag{2.89}$$

where A is optical absorbance (dimentionless), ε is molar absorptivity ($M^{-1}cm^{-1}$), C is concentration of the absorbing species (M) and L is path length (cm)

Consider a simple first-order reaction illustrated by equation 2.90,

$$X \xrightarrow{k_1} Y \tag{2.90}$$

Absorbance after a time, *t*, will be given by equation 2.91,

$$A_t = \varepsilon_X [X] + \varepsilon_Y [Y] \tag{2.91}$$

where A_t is absorbance at time, t, and $\varepsilon_X, \varepsilon_Y$ represent molar absorptivity of X and Y respectively

At the end of the reaction, the absorbance is given by equation 2.92,

$$A_\infty = \varepsilon_X [X]_0 + \varepsilon_Y [Y]_0 \tag{2.92}$$

where A_∞ = absorbance at infinity

Kinetic analysis of a reaction represented by equation 2.86, can be done by the relation in equation 2.93,

$$\ln \frac{[X]_0}{[Y]_0} = \ln\left(\frac{A_0 - A_\infty}{A_t - A_\infty}\right) = k_1 t \qquad (2.93)$$

An example of the reaction profile obtained from the UV/Visible spectrophotometer for the substitution of aqua ligand from [(aqua)2,2'-bipyridine(hexamethylbenzene)ruthenium(II)] perchlorate by thiourea (TU) nucleophile (studied in chapter 3) at 298 K is shown in Figure 2.4.The reaction was monitored within the wavelength range 200 to 800 nm wavelength.

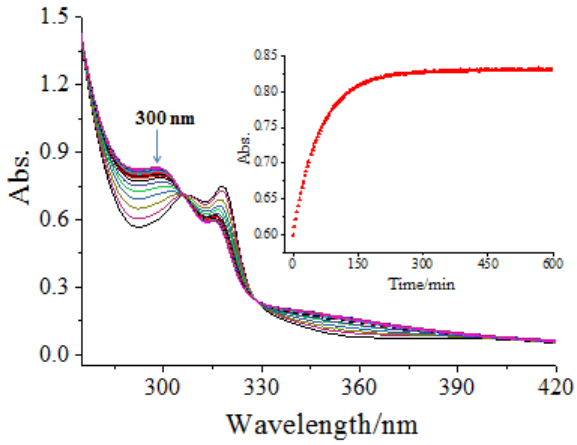

Figure 2.4 Graph of UV-Visible spectra for the reaction of aqua-2,2'-bipyridine-(hexamethylbenzene)ruthenium(II)perchlorate with TU at 298K (inset is the respective kinetic trace at 300 nm)

2.7.2 Flow methods

There are reactions that are ultrafast hence impossible to monitor by standard absorption spectroscopy. In such cases, techniques that can accomplish rapid mixing of reactants such as stopped-flow methods should be used. Stopped flow methods mix reagents rapidly and stopping the flow momentarily to allow analysis of equilibrium changes of concentration by monitoring a physical parameter which varies with concentration of a sample.[93] The functioning of the stopped-flow apparatus is illustrated in Figure 2.5.

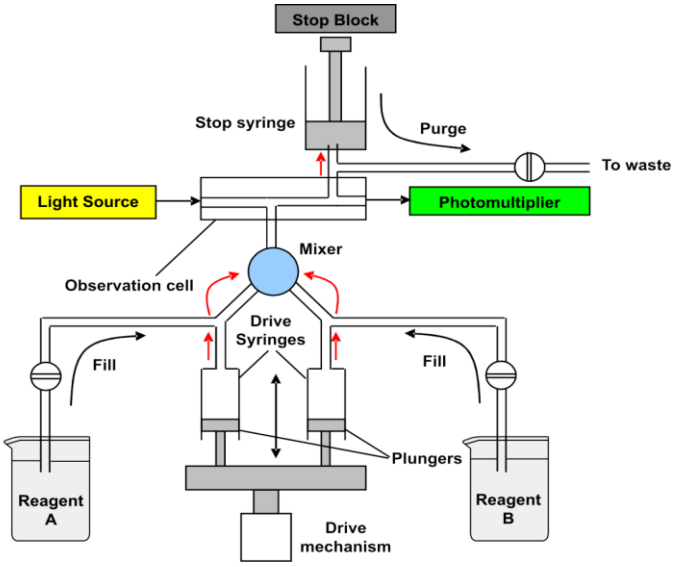

Figure 2. 5 Schematic diagram of mechanistic action of stopped-flow apparatus

Drive syringes are filled separately with the different reagents then the drive mechanism which is driven by a piston is activated causing the drive syringe plungers to go forward rapidly transferring equal volumes into the mixer region where they are mixed within milliseconds.[94] The solution passes onto the observation cell.[94] The reaction solution then passes into the stop syringe until the stop syringe fills causing the plunger to strike the stop block instantly to cease the flow. This leaves a thoroughly mixed plug of solution in the observation cell.[94]

The mixed solution is stationed in the observation cell allowing the recording of absorption or emission whose intensity changes as the reaction proceeds to completion.[93] A photomultiplier detector completes the current due to the primary photons striking its surface interpreted by a computer as an absorption/emission versus time spectrum which is analysed normally.[93] The stopped-flow analysis is a simple technique with several advantages:

- Rapid mixing of reactant thus allowing evolution of absorbance data to be collected for ultrafast reaction steps,
- it's easy to analyse with small volumes (≈ 0.2 ml) of solutions being used
- It permits the use of a number of different monitoring methods in conjunction with this technique.

Current research is shifting to Ru metal complexes as an alternative to Pt based anti-cancer drug. The importance of Ru metal complexes in optimising the therapeutic reactions and minimisation of resistance induced by deactivation pathways is useful in the anti-cancer

therapy. The kinetics of ruthenium metal complexes is less studied hence the need for further research.

2.8 References

[1] A. K. Connors, *Chemical Kinetics; The Study of reactions Rates in Solution*, Wiley-VCH, New York, **1990**.

[2] S. R. Logan, *Fundamentals of Chemical Kinetics*, Longman, , Essex, **1996**.

[3] D. M. W. D. A. Skoog, F. J. Holler and S. R. Crouch, *Fundamentals of Analytical Chemistry*, 8 ed., Brooks/Cole – Thomson Learning, Inc., U.S.A, **2004**.

[4] D. W. Ball, *Physical Chemistry*, Brooks/Cole, Pacific Groove, **2003**.

[5] M. M. a. P. Taylor, *Chemical Kinetics and Mechanism*, the Open University. Walton Hall, Miton Keys, MK76AA, London, **2002**.

[6] F. Wilkinson, *Chemical Kinetics and Reaction Mechanisms*, Van Nostrand Reinhold Company, New York, **1980**.

[7] O. M. S. a. G. I. L. E. T. Denisov, *Chemical Kinetics: Fundamentals and New Development*, Elsevier Science and Technology Books, **2003**.

[8] J. H. Espenson, *Chemical kinetics and Reaction mechanisms*, McGraw-Hill, New York, **1995**.

[9] M. L. T. J. Burgess, *Inorganic Reaction Mechanisms*, Addison Wesley Longman Ltd, Essex, **1999**.

[10] S. F. a. H. B. L. Arnaut, *Chemical Kinetics From Molecular Structure to Chemical Reactivity*, Elsevier, New York, **2007**.

[11] H. B. G. C.H. Langford, *Ligand Substitution Processes*, Benjamin Inc., Newyork, **1965**.

[12] H. B. G. C. H. Langford, *Ligand Substitution Processes*, W.A. Benjamin, Inc., New York, **1966**.

[13] T. O. P. Atkins, J. Rourke, M. Weller and F. Armstrong, *Shriver & Atkins Inorganic Chemistry* 4ed., Oxford University Press, New York, **2006**.

[14] A. Hofmann, L. Dahlenburg, R. van Eldik, *Inorganic chemistry* **2003**, *42*, 6528-6538.

[15] R. Romeo, M. R. Plutino, L. Monsù Scolaro, S. Stoccoro, G. Minghetti, *Inorganic Chemistry* **2000**, *39*, 4749-4755.

[16] L. R. Allen, P. P. Craft, B. Durham, J. Walsh, *Inorganic Chemistry* **1987**, *26*, 53-56.

[17] K. P. Beaumont, C. A. McAuliffe, *Inorganica Chimica Acta* **1974**, *8*, 105-127.

[18] M. L. Tobe, *Inorganic Reaction Mechanisms Studies in modern Chemistry*, Nelson, London, **1972**.

[19] G. Wulfsberg, *Inorganic chemistry*, university Science Books, U.S. A, **2000**.

[20] P. O. Ongoma, D. Jaganyi, *Dalton Transactions* **2013**, *42*, 2724-2734.

[21] A. Shaira, D. Reddy, D. Jaganyi, *Dalton Transactions* **2013**, *42*, 8426-8436.

[22] P. O. Ongoma, D. Jaganyi, *Transition Metal Chemistry* **2014**, *39*, 407-420.

[23] A. Shaira, D. Jaganyi, *Journal of Coordination Chemistry* **2014**, *67*, 2843-2857.

[24] I. M. Wekesa, D. Jaganyi, *Dalton Transactions* **2014**, *43*, 2549-2558.

[25] B. B. Khusi, A. Mambanda, D. Jaganyi, *Journal of Coordination Chemistry* **2016**, *69*, 2121-2135.

[26] W. P. Asman, D. Jaganyi, *International Journal of Chemical Kinetics* **2017**, *49*, 545-561.

[27] W. M. Mthiyane, A. Mambanda, D. Jaganyi, *Transition Metal Chemistry* **2017**, *42*, 739-751.

[28] M. Chrzanowska, A. Katafias, O. Impert, A. Kozakiewicz, A. Surdykowski, P. Brzozowska, A. Franke, A. Zahl, R. Puchta, R. van Eldik, *Dalton Transactions* **2017**, *46*, 10264-10280.

[29] M. M. Milutinović, S. K. C. Elmroth, G. Davidović, A. Rilak, O. R. Klisurić, I. Bratsos, Ž. D. Bugarčić, *Dalton Transactions* **2017**, *46*, 2360-2369.

[30] A. Rilak, I. Bratsos, E. Zangrando, J. Kljun, I. Turel, Z. D. Bugarcic, E. Alessio, *Inorganic Chemistry* **2014**, *53*, 6113-6126.

[31] F. Wang, H. Chen, S. Parsons, I. D. H. Oswald, J. E. Davidson, P. J. Sadler, *Chemistry–A European Journal* **2003**, *9*, 5810-5820.

[32] D. Banerjea, F. Basolo, R. G. Pearson, *Journal of the American Chemical Society* **1957**, *79*, 4055-4062.

[33] U. Belluco, L. Cattalini, F. Basolo, R. G. Pearson, A. Turco, *Journal of the American Chemical Society* **1965**, *87*, 241-246.

[34] J. Reedijk, *European Journal of Inorganic Chemistry* **2009**, *2009*, 1303-1312.

[35] K. M. Anderson, A. G. Orpen, *Chemical Communications* **2001**, 2682-2683.

[36] R. G. Pearson, *Journal of the American Chemical Society* **1963**, *85*, 3533-3539.

[37] R. G. Pearson, *Journal of Chemical Education* **1987**, *64*, 561.

[38] I. I. Chernyaev, *Ann. Inst. Plat.* **1928**.

[39] N. Kuznik, O. F. Wendt, *Journal of the Chemical Society, Dalton Transactions* **2002**, 3074-3078.

[40] Z. Chval, M. Sip, J. V. Burda, *Journal of Computational Chemistry* **2008**, *29*, 2370-2381.

[41] B. J. Coe, S. J. Glenwright, *Coordination Chemistry Reviews* **2000**, *203*, 5-80.

[42] A. Rilak, I. Bratsos, E. Zangrando, J. Kljun, I. Turel, Ž. D. Bugarčić, E. Alessio, *Inorganic Chemistry* **2014**, *53*, 6113-6126.

[43] M. M. Milutinović, S. K. C. Elmroth, G. Davidović, A. Rilak, O. R. Klisurić, I. Bratsos, Ž. D. Bugarčić, *Dalton transactions* **2017**, *46*, 2360-2369.

[44] S. Otto, L. I. Elding, *Journal of the Chemical Society, Dalton Transactions* **2002**, 2354-2360.

[45] J. Chatt, L. A. Duncanson, L. M. Venanzi, *Journal of the Chemical Society (Resumed)* **1955**, 4456-4460.

[46] L. E. Orgel, *Journal of Inorganic and Nuclear Chemistry* **1956**, *2*, 137-140.

[47] M. R. Plutino, S. Otto, A. Roodt, L. I. Elding, *Inorganic chemistry* **1999**, *38*, 1233-1238.

[48] U. Belluco, *Organometallic Coordination Chemistry of Platinum*, Academic Press, London, **1974**.

[49] D. Benson, *Mechanisms of Inorganic Reactions in Solution*, McGraw-Hill, London, **1968**.

[50] F. R. Hartley, *Chemical Society Reviews* **1973**, *2*, 163-179.

[51] F. Basolo, J. Chatt, H. B. Gray, R. G. Pearson, B. L. Shaw, *Journal of the Chemical Society (Resumed)* **1961**, 2207-2215.

[52] M. A. Tucker, C. B. Colvin, D. S. Martin Jr, *Inorganic Chemistry* **1964**, *3*, 1373-1383.

[53] J. N. Armor, H. Taube, *Journal of the American Chemical Society* **1969**, *91*, 6874-6876.

[54] H. Taube, J. N. Armor, *Journal of the American Chemical Society* **1970**, *92*, 6170-6174.

[55] R. J. Allen, P. C. Ford, *Inorganic Chemistry* **1972**, *11*, 679-685.

[56] R. E. Shepherd, H. Taube, *Inorganic Chemistry* **1973**, *12*, 1392-1401.

[57] J. F. Ojo, O. Olubuyide, O. Oyetunji, *Journal of the Chemical Society, Dalton Transactions* **1987**, 957-959.

[58] G. W. a. P. L. G. F. A. Cotton, *Basic Inorganic Chemistry* John Wiley & Sons, New York, **1995**.

[59] R. G. Pearson, *Journal of Chemical Education* **1968**, *45*, 643.

[60] H. B. Gray, R. J. Olcott, *Inorganic Chemistry* **1962**, *1*, 481-485.

[61] A. J. Poë, K. Shaw, M. J. Wendt, *Inorganica Chimica Acta* **1967**, *1*, 371-377.

[62] P. Y. Bruice, *Organic Chemistry*, 2nd Edition ed., Prentice Hall, **1998**.

[63] A. Mambanda, PhD Thesis thesis, University of Natal, Pietermaritzburg (South Africa), **2010**.

[64] R. Romeo, D. Minniti, M. Trozzi, *Inorganic Chemistry* **1976**, *15*, 1134-1138.

[65] C. W. Schwietert, J. P. McCue, *Coordination Chemistry Reviews* **1999**, *184*, 67-89.

[66] F. A. Cotton, R. Francis, *Journal of the American Chemical Society* **1960**, *82*, 2986-2991.

[67] H. Sigel, *Metal ions in biological systems, metal complexes as anticancer agents*, M. Dekker, **1980**.

[68] G. W. F. A Cotton, *Advanced Inorganic Chemistry*, 5 ed., John Wiley &
Sons, New York, **1988**.

[69] M. J. Clarke, F. Zhu, D. R. Frasca, *Chemical Reviews* **1999**, *99*, 2511-2534.

[70] M. L. Tobe, *Inorganic Reaction Mechanisms*, Addison Wesley Longman Limited, New York, **1999**.

[71] D. Atwood, *Inorganic and Organometallic Reaction Mechanisms*, 2 ed., Wiley VCR, Inc, New York, **1997**.

[72] R. B. Jordan, *Reaction Mechanisms ofInorganic and Organometallic Systems*, Oxford University Press, New York, **1991**.

[73] F. M. Foley, F. R. Keene, J. G. Collins, *Journal of the Chemical Society, Dalton Transactions* **2001**, 2968-2974.

[74] P. Byabartta, J. Dinda, P. K. Santra, C. Sinha, K. Panneerselvam, F.-L. Liao, T.-H. Lu, *Journal of the Chemical Society, Dalton Transactions* **2001**, 2825-2832.

[75] R. E. Shepherd, H. Taube, *Inorganic Chemistry* **1973**, *12*, 1392-1401.

[76] L. Dozsa, J. E. Sutton, H. Taube, *Inorganic Chemistry* **1982**, *21*, 3997-4000.

[77] S. S. Isied, H. Taube, *Inorganic Chemistry* **1976**, *15*, 3070-3075.

[78] D. Reddy, University of Natal (Pietermarizburg, South Africa), **2009**.

[79] R. Buchner, C. T. Cunningham, J. S. Field, R. J. Haines, D. R. McMillin, G. C. Summerton, *Journal of the Chemical Society, Dalton Transactions* **1999**, 711-718.

[80] B. G. Cox, *Modern Liquid Phase Kinetics*, Oxford University Press, New York, **1994**.

[81] K. T. Potts, D. A. Usifer, A. Guadalupe, H. D. Abruna, *Journal of the American Chemical Society* **1987**, *109*, 3961-3967.

[82] S. Asperger, *Chemical Kinetics and Inorganic Reaction Mechanisms*, 2 ed., Kluwer Academic/Plenum New York, **2003**.

[83] M. J. P. a. P. W. Seakins, *Reaction Kinetics*, Oxford Science Publications, Oxford, **1995**.

[84] P. A. a. J. d. Paula, *Atkins' Physical Chemistry*, 8 ed., Oxford University Press, Oxford, **2006**.

[85] R. G. Wilkins, *Kinetics and Mechanism of Reactions of Transition Metal Complexes*, 2 ed., VCH, Weinheim, London, **1991**.

[86] D. W. Ball, *Phsical Chemistry*, Brooks/Cole, Pacific grove, **2003**.

[87] H. Eyring, *The Journal of Chemical Physics* **1935**, *3*, 107-115.

[88] M. G. Evans, M. Polanyi, *Transactions of the Faraday Society* **1935**, *31*, 875-894.

[89] R. A. A. a. G. B. M. R. J. Silbey, *Physical Chemistry*, 4 ed., John Wiley & Sons, New York, **2005**.

[90] F. P. Rotzinger, *Chemical Reviews* **2005**, *105*, 2003-2038.

[91] L. Helm, A. E. Merbach, *Journal of the Chemical Society, Dalton Transactions* **2002**, 633-641.

[92] D. H. Powell, A. E. Merbach, I. Fabian, S. Schindler, R. van Eldik, *Inorganic Chemistry* **1994**, *33*, 4468-4473.

[93] D. C. Harris, *Quantitative Chemical Analysis*, 4 ed., W. H. Freeman & Co., New York, **1995**.

[94] M. S. Silberberg, *Chemistry. The Molecular Nature of Matter and Change*, 2 ed., McGraw-Hill, U.S.A, **2000**.

Chapter 3

The rate of aqua substitution from η^6-arene Ru(II) aqua complexes

3.0 Abstract

The rate and mechanism of substitution of the aqua ligand from η^6-arene-Ru(II) complexes by thiourea nucleophiles was studied under *pseudo* first order conditions in aqueous 0.1 M $NaClO_4$ at *p*H 2. The observed rate constants were measured as a function of nucleophile concentrations and temperature using UV-Visible absorption spectrophotometer or Stopped Flow Spectrophotometer for ultrafast reactions. The plots of k_{obs} versus nucleophile concentration were linear according to the equation $k_{obs} = k_2$[Nu]. The values of k_2 decreased in the order; **C1** > **C2** > **C5** > **C4** > **C6** > **C3**. **C1** is more reactive than **C2** due to the increased electron density at the Ru metal centre as a result of inductive donation by substituents on the arene ligand of **C2**. For the complexes **C3-C6** which bear 2,2'-bipyridyl as a common auxiliary ligand, the leaving aqua ligands are located trans to the arene ligands. For these complexes, the reactivity increase in accordance to the number and type of alkyl substituents on the η^6-arene ligands which donate inductively into the π-molecular orbitals, causing increased *trans* labialisation of the coordinated aquo co-ligand. the Compared to the reactivity of tri-aquo complex (**C1**), the auxiliary bipyridyl ligand of (**C3**) complexes lowers the rate of substitution for the later complex by a factor of about 100, possibly due to its steric hindrance at the Ru(II) metal centre. The significantly negative activation entropies and positive activation enthalpies suggest that the activation process is dominated by bond making. The reactivity of the nucleophiles follow the order DMTU > TU > TMTU.

3.1 Introduction

Interaction of transition metal complexes with DNA is one of the major known mechanistic pathway responsible for the anti-tumour activity.[1] [2] [3] [4] [5] Through such molecular mechanism of interaction, the prototype anti-cancer drug, cisplatin is active against several human cancer cell lines including those of the pancreatic, head, neck and testicular.[6] [7] However, it is acutely toxic to the kidneys and ineffective against several other cancers as well as being prone to development of resistance.

An attractive class of complexes that can be alternatives to Pt-based cancer drugs is ruthenium (Ru) complexes. Ru complexes are significantly less toxic because they can roleplay iron binding modes in biological systems.[8] [9] [10] [11] [12] Lead Ru complexes which

have been evaluated *in vitro* and *in vivo* [13] for cytotoxicity and showed promising activity profiles include imidazolium*trans*-[tetrachloro(dimethylsulfoxide)imidazoleruthenium-(III)] (NAMI-A) and indazolium *trans*-[tetrachlorobis(1H-indazole)ruthenium(III)] (KP 1019). They have also shown great anti-cancer potential in clinical trials.[14]

A subclass of Ru complexes that have been extensively evaluated for the anticancer activity are arene-Ru(II) complexes. Examples include [(η^6-/η^5-arene)(L)Ru(II)] such as [(η^6-biphenyl)Ru(en)Cl]$^+$ (en = ethylenediamine)[15], [(η^6-p-cymene)Ru(PTA)Cl_2] (PTA = 1,3,5-triaza-7-phosphaadamantane)[16] [17] [18]. These too have shown great potential as anticancer agents.[6] [19] [20] [21] [22] Numerous studies have linked their superior anti-cancer activity to the extra and favourable non-covalent interactions of arene ligands on the Ru complexes with hydrophobic components of cell membranes and at the ultimate nucleophilic target, DNA.[23] [24] [25] [26] Cytotoxicity of the arene-Ru complexes has been positively correlated to the nature of the substituents on the arene as well as rings on the parent arene ring. The hydrophobic face within the backbone of the non-leaving ligand of the complexes enhances bimolecular recognition on the non-polar receptor sites of the target macro-nucleophiles.[23] [27] [28] [29]Substitution of the labile halogen ligands by a chelating ligand can help to control the stability and ligand exchange kinetics of these complexes.[30] [31] [32] Previous studies as discussed in the previous sections have focused more on DNA binding and cytotoxicity studies leaving a gap on the kinetic properties of the complexes. Recognising the importance of the kinetic nature of compounds that applies at the interaction with DNA, this work investigated the rate of substitution of benzene(triaquo)ruthenium(II)perchlorate, **C1**, mesitylene(triaqua)ruthenium(II)perchlorate, **C2,** aquo(benzene)-2,2'-bipyridineruthenium(-II)perchlorate, **C3,** aquo-2,2'-bipyridine(mesitylene)ruthenium(II)perchlorate, **C4**, aqua-2,2'-bipyridine(hexamethylbenzene)ruthenium(II)perchlorate, **C5** and aqua-2,2'-bipyridine(*p*-cymene)ruthenium(II)perchlorate, **C6** by thiourea nucleophiles *viz* thiourea(**TU**), 1,3-dimethyl-2-thiourea(**DMTU**) and 1,1,3,3-tetramethyl-2-thiourea (**TMTU**). The study seeks to establish specifically the role of arene ligands and on the substitution reactions of these complexes. The chemical structures of the complexes used in this study are shown in Figure 3.1.

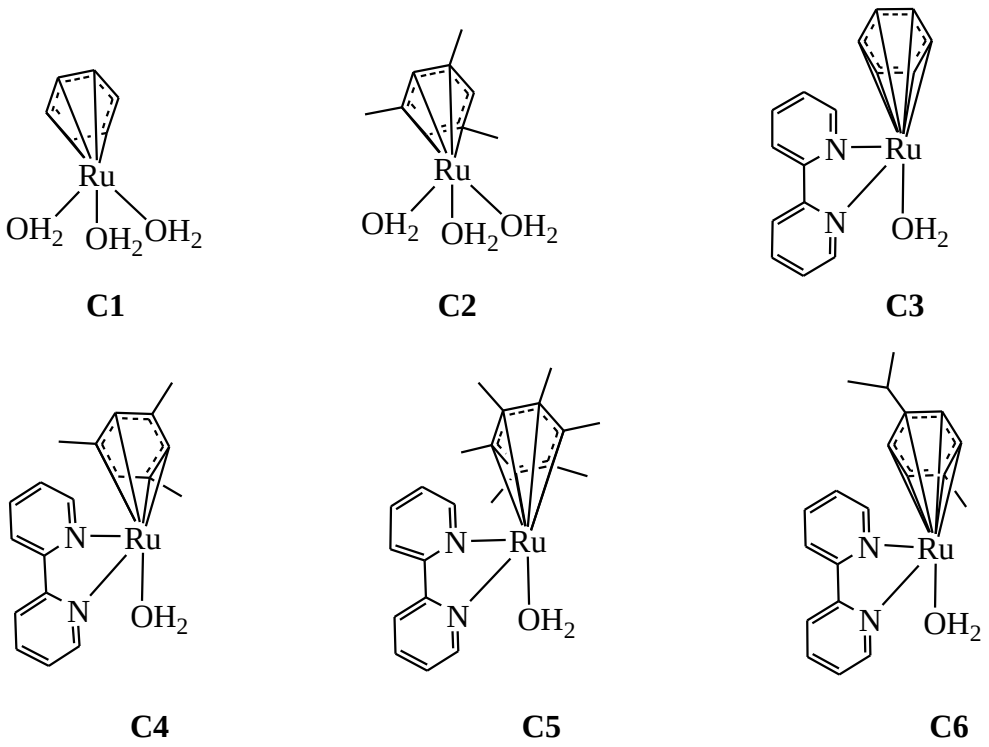

Figure 3. 1 Chemical structures of η^6-arene Ru(II) complexes

3.2 Experimental

3.2.1 Materials

All chemicals including ligands, the dichloro(arene)Ru(II) dimers, solvents, silver perchlorate and perchloric acid were purchased from Sigma Aldrich and used as received. The complexes; 2,2'-bipyridine(*p*-cymene)ruthenium(II) dichloride, Benzene-2,2'-bipyridine-ruthenium(II) dichloride, 2,2'-bipyridine(mesitylene)ruthenium(II) dichloride and 2, 2'-bipyridine(hexamethylbenzene)ruthenium(II) dichloride were synthesized according to published procedures.[33] The atomic numbering applied here is illustrated by Figure 3.3.

3.2.2 Synthesis of chloro complexes

2,2'-bipyridine(*p*-cymene)ruthenium(II) dichloride

An ethanolic solution (15 mL) of 2,2'-bipyridine (46.85 mg, 0.3 mmol) was mixed with dichloro(*p*-cymene)ruthenium(II) dimer (91.86 mg, 0.15 mmol) and the reaction mixture heated at reflux for 6 hours. The resulting solution was cooled to room temperature and precipitation of the respective complex done by addition of diethyl ether (60 mL). After filtration, the complex was washed with diethyl ether and pentane then dried in air. Yield: 127.62 mg (92%). ^{1}H NMR (400 MHz, CD_3OH) δ/ppm, J/Hz: 9.49 (d, 2H, 1, 1', J = 5.5);

8.51 (d, 2H, 4 4', J = 8.2); 8.25 (t, 2H, 3, 3', J = 15.8); 7.78 (dd, 2H, 2, 2', J = 5.6, J = 2.0); 6.12 (d, 2H, -CH_2, J = 6.2); 5.86 (d, 2H, -CH_2, J = 6.5); 2.64 (m, 1H, CH); 2.28 (S, 3H, -CH_3); 1.05 (d, 6H, -CH_3, J = 6.2). ^{13}C NMR (75 MHz, MeOH), δ/ppm: 17.55, 20.87, 30.96, 84.14, 86.82, 104.44, 104.65, 123.57, 127.49, 139.79, 154.98, 155.48. Anal. Calcd for $C_{20}H_{22}Cl_2N_2Ru$: C, 51.95; H, 4.80; N, 6.06; Found: C, 51.85; H, 5.01; N, 6.26. ESI^+ LCMS, m/z: 426 $[M + 1]^+$

Benzene-2,2'-bipyridineruthenium(II) dichloride

Synthesized following the same procedure as that of 2,2'-bipyridine(*p*-cymene)ruthenium(II) dichloride using 2,2'-bipyridine (46.85 mg, 0.3 mmol) and benzeneruthenium(II) chloride dimer (75.02 mg, 0.15 mmol). Yield: 97.50 mg (80%). ^{1}H NMR (400 MHz, CD_3OH) δ/ppm, J/Hz: 9.60 (d, 2H, 1, 1', J =5.4); 8.53 (d, 2H, 4,4', J = 7.9); 8.26 (t, 2H, 3,3', J = 15.8); 7.77 (dd, 2H, 2 2', J = 5.7, J = 2.3); 6.12 (s, 6H, -CH_3). ^{13}C NMR (75 MHz, MeOH), δ/ppm: 88.64, 125.03, 128.77, 141.28, 156.62, 157.07. Anal. Calcd for $C_{16}H_{14}Cl_2N_2Ru$: C, 47.30; H, 3.47; N, 6.90; Found: C, 47.18; H, 3.71; N, 6.88. ESI^+ LCMS, m/z: 371 $[M + 1]^+$

2,2'-bipyridine(mesitylene)ruthenium(II) dichloride

Synthesized following the same procedure as that of 2,2'-bipyridine(*p*-cymene)ruthenium(II) dichloride using 2,2'-bipyridine (46.85 mg, 0.3 mmol) and benzeneruthenium(II) chloride dimer (87.65 mg, 0.15 mmol). Yield: 93.48 mg (69.5%). ^{1}H NMR (400 MHz, CD_3OH) δ/ppm, J/Hz: 9.30 (d, 2H, 1,1', J =5.9); 8.44 (d, 2H, 4 4', J = 8.2); 8.17 (t, 2H, 3 3', J = 15.8); 7.73 (dd, 2H,2 2', J = 5.6, J = 2.0); 5.48 (s, 3H, -CH); 2.16 (s, 9H, -CH_3). ^{13}C NMR (75 MHz, MeOH), δ/ppm: 17.40, 79.40, 107.42, 123.03, 127.45, 139.63, 154.82, 155.35. Anal. Calcd for $C_{19}H_{20}Cl_2N_2Ru$: C, 50.90; H, 4.50; N, 6.25; Found: C, 50.51; H, 4.54; N, 6.45. ESI^+ LCMS, m/z: 413 $[M + 1]^+$

2,2'-bipyridine(hexamethylbenzene)ruthenium(II) dichloride

Synthesized following the same procedure as that of 2,2'-bipyridine(*p*-cymene)ruthenium(II) dichloride using 2,2'-bipyridine (46.85 mg, 0.3 mmol) and dichloro(hexamethylbenzene)-ruthenium(II) dimer (100.27 mg, 0.15 mmol). Yield: 118.62 mg (83%). ^{1}H NMR (400 MHz, CD_3OH) δ/ppm, J/Hz: 8.87 (d, 2H, 1,1', J =5.7); 8.37 (d, 2H, 4,4', J = 8.2); 8.10 (t, 2H, 3,3', J = 15.8); 7.69 (dd, 2H,2,2', J = 5.4, J = 1.2); 2.02 (s, 18H, -CH_3). ^{13}C NMR (75 MHz, MeOH), δ/ppm: 15.67, 97.39, 124.63, 128.91, 140.91, 155.05, 156. Anal. Calcd for $C_{22}H_{26}Cl_2N_2Ru$, %: C, 53.88; H, 5.34; N, 5.71; Found: C: 54.19; H: 5.42; N: 5.34. ESI^+ LCMS, m/z: 455 $[M + 1]^+$

The synthesized compounds were characterized giving satisfactory elemental analysis and spectroscopic data. They are stable in air as solids or their solutions. All compounds gave ^{1}H and ^{13}C NMR spectra corresponding to the proposed formulations. Mass spectrometric data gave single peaks corresponding to the masses of the complexes without the counter ions. The elemental analysis data was in agreement to the theoretical CHN values to within ± 0.40. The sample spectra for NMR and mass analyses are placed in the supporting information Figures SI 3.1-3.12. The results for NMR spectra, Mass spectra and elemental analyses are presented below.

3.2.3 Preparation of Aqua Ru(II) complexes (C1 - 6)

The desired solutions of the aqua complexes for kinetic studies were prepared from the chloride derivatives according to a literature procedure.[34] To a stirred solution of the chloro complexes in 0.01 M perchloric acid ($HClO_4$) (40 mL) was added silver perchlorate ($AgClO_4$). The moles of silver chloride added were slightly lower (< 0.1%) equivalent to the number of chloride ions in the complex. The mixture was stirred for 24 hours at 50° C in the dark, cooled and filtered using a 0.45 μm nylon membrane filter (Millipore) to remove the precipitated silver chloride. The filtrate was made up to 100 mL using 0.1 M $HClO_4$ which had an ionic strength of 0.1 M adjusted by dissolving 0.09 M $NaClO_4$ in 0.01 M perchloric acid. Kinetic analyses were done at pH 2 for all complexes as the pH titration showed that only aqua species of the complexes exist at this pH. [35]

3.2.4 Determination of p*K*a of Aqua complexes (C1 - 6)

The acidities of the aqua ligands were determined before kinetic analysis could be done. The p*K*a titrations were done spectrometrically as described in literature.[36] The pH titrations were started with solution of the aqua complexes of pH 2 (0.01 M $HClO_4$ solution) by addition of small amounts of NaOH until pH 9. To avoid errors due to dilution effect, a large volume (300 mL) of complex solution was used. Solid NaOH granules were used in the pH range of 1–3 solutions followed by dropwise addition of 0.5 M or 0.1 M or 0.05 M or 0.001 M of NaOH solution to adjust pH. After each addition of NaOH or acid, the solution was briefly stirred before recording the pH value. Vials were used to sample the solution (~2 mL) for pH measurements then the solution discarded to avoid *in situ* precipitation of the chloride. The aliquots from spectral acquisitions were returned to the titration solution. Both NaOH and perchloric acid were used to observe the reversibility of the spectra as proof of existence of the deprotonation of the aqua as defined by k_a.[35] The absorbance data was plotted against

pH giving a sigmoid curve from which the p*K*a values were determined by locating the inflection points. Figure 3.2 shows a typical UV–Visible spectrum recorded during spectrophotometric titration of the aqua complex solutions with NaOH and inset is the sigmoid curve.

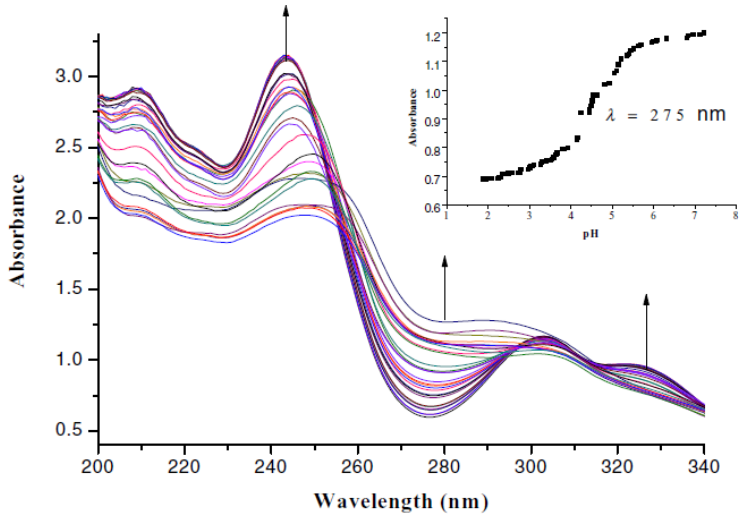

Figure 3. 2 UV–visible spectra of **C1** complex recorded as a function of pH in the range of 2–8 at 25°C. Inset is a plot of absorbance versus pH at λ = 275 nm

Table 3. 1 p*K*a values for the deprotonation of the aqua Ru(II) complexes

Complex	**pK_a**
Ru1	4.60 ± 0.01
Ru2	4.31 ± 0.02
Ru3	6.92 ± 0.01
Ru4	7.01 ± 0.02
Ru5	7.34 ± 0.01
Ru6	7.21 ± 0.01

The p*Ka* values in Table 3.1 indicate that the higher the alkylation of the arene moieties the lower the acidity. The p*K*a titration reactions of the aqua complexes with OH^- are illustrated in Scheme 3.1

$$[\text{X-(Bip)-Ru-OH}_2]^{n+} + OH^- \overset{K_a}{\rightleftharpoons} [\text{X-(Bip)-Ru-OH}]^{(n-1)+} + H_2O$$

X = Benzene or mesitylene or hexamethylbenzene or p-cymene

Scheme 3. 1 The p*K*a titration reactions of the aqua complexes with OH^-

3.2.5 Instrumentation

Physical measurements

NMR spectroscopy were recorded on a Bruker Avance DPX 400MHz spectrophotometer at 303 K and all chemical shift were referenced to those of $(CH_3)_4$. Low resolution electron spray ionization (ESI^+) mass spectra were recorded on the Waters Micromass LCT Premier Spectrometer or Shimadzu LCMS 2020. Elemental analyses were done on a ThermoScientific Flash 2000 elemental analyser. Kinetic measurements for fast reactions were performed on an Applied Photophysics SX20 stopped flow instrument coupled with an online data acquisition system whose temperature is controlled to within ± 0.1° C. The slow reactions were monitored using Varian Cary 100 Bio UV-Visible spectrophotometer with an attached Varian peltier temperature controller and online kinetic application. The same instrument was used for spectrometric titration. The UV-Visible spectrophotometer was also used to pre-determine the wavelengths at which the reactions on the Stop flow were monitored.

Computational modelling

The computations were done by Density Functional Theory (DFT) run on Gaussian 09 suite of programs.[37] The structures were optimised using the hybrid Becke, 3-parameter, Lee-Young-Parr (B3LYP) method with LANL2DZ (Los Alamos National Laboratory 2 double ζ) basis sets having inner core electrons of the Ru atom replaced by relativistic effective core potential (ECP).[38] [39] [40] DFT applies to physically observable electron density over a wave function in the determination of the properties of a system. Los Alamos National Laboratory 2 double ζ basis set exploits relativistic effective core potentials to account for effect of inner core 28 electrons ($[Ar]3d^{10}$) in Ru.[41] [42] To take into account of the solvent effects, the complexes were fully optimised in methanol using the conductor polarizable continuum model (C-PCM).[43] [44] The singlet states were used due to the low electronic spin state of

Ru(II) complexes. The complexes were considered to have an overall charge of +2. The chemical potential (μ) and molecular hardness (η) for each structure were calculated from the HOMO and LUMO energies. The global electrophilicities (ω) were determined by the relationship $\omega = \mu^2/2\eta$.[45] [46] The charge on each atom is expressed as a natural bond orbitals (NBO) .[47]

3.3 Results

3.3.1 Computational results

Density functional theory (DFT)[48] [49] calculated data for example electrophilicity index and NBO charges have provided information in support of the chemical reactivity. In this context, several reactivity descriptors have been proposed and used to analyse chemical reactivity and site selectivity. Hardness, η, electronic chemical potential, μ, electrophilicity, ω, are among the reactivity descriptors widely used to understand the global nature of molecules in terms of their stability and it is possible to gain knowledge about the reactivity of molecules. Atomic charges (NBO) are among the local reactivity descriptors, which provide information about the site selectivity.[50] [51]

In this study computational calculations and optimisation were carried out to gain information on the electronic and structural properties of the complexes. The DFT optimized structures of the complexes are shown in Table 1 and a summary of selected DFT data are presented in Table 3.2. Examining DFT diagrams in Table 1, the HOMO are located mainly on the ruthenium metal centre and partially on the arene and aqua ligands while the LUMO is entirely on the bipyridine ligand as reported in literature for other similar studies.[52]

Table 3. 2 DFT minimum energy structures and frontier molecular orbitals of the complexes

Optimised Structures		HOMO	LUMO
	**C1**	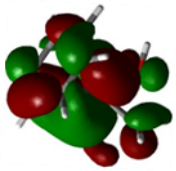	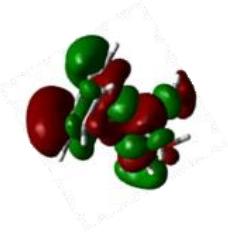
	**C2**	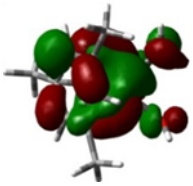	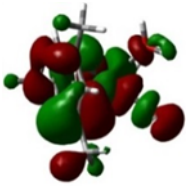
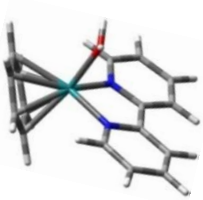	**C3**	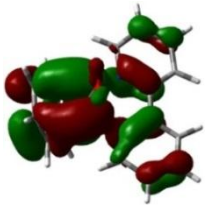	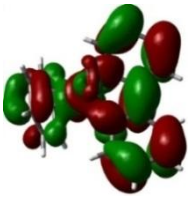
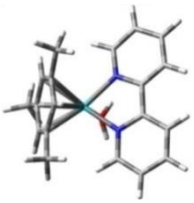	**C4**	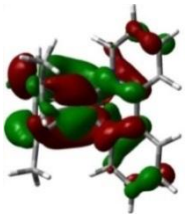	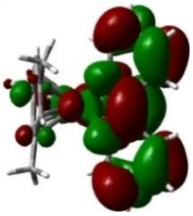
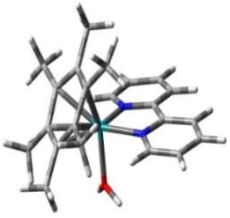	**C5**	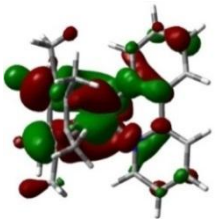	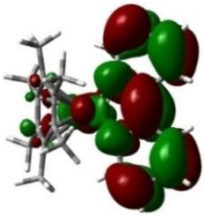
	**C6**	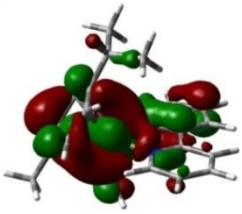	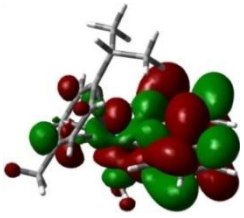

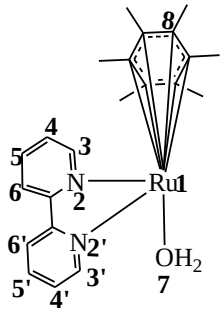

Figure 3. 3 An illustration of the numbering using **C5** as an example

Table 3. 3 Summary of DFT calculated data for the studied complexes

Parameters	**C1**	**C2**	**C3**	**C4**	**C5**	**C6**
Bond lengths (Å)						
Ru(1)-O(7)	2.13	2.15	2.15	2.15	2.17	2.15
Bond angles (°)						
C(8)-Ru(1)-O(7)	100.1	111.1	174.6	173.9	173.0	174.4
N(2)-Ru(1)-O(7)	-	-	85.2	85.8	85.9	84.4
NBO charges						
Ru(1)	0.430	0.377	0.276	0.281	0.314	0.280
O(7)	-0.710	-0.874	-0.859	-0.860	-0.869	-0.862
Orbital energy/eV						
HOMO	-7.720	-7.444	-7.018	-6.945	-6.718	-7.140
LUMO	-3.206	-2.908	-3.057	-3.007	-2.951	-3.070
$\Delta E_{HOMO-LUMO}$	4.514	4.536	3.961	3.938	3.767	4.072
Global chemical reactivity indices						
η/eV	2.257	2.268	1.981	1.969	1.884	2.036
μ/eV	-5.463	-5.176	-5.038	-4.976	-4.835	-5.204
ω/eV	6.612	4.998	6.406	6.288	6.203	6.4000

η = chemical hardness, μ = electronic chemical potential, ω = global electrophilicity index

3.3.2 Kinetic analysis

The rate of substitution of the aqua ligands from the complexes were carried out under *pseudo*-first-order conditions using at least a 10-fold excess of the entering nucleophile for complexes **C3**, **C4**, **C5** and **C6** and at least 30-fold excess for **C1** and **C2**. The kinetics of substituting the aqua ligands was investigated spectrophotometrically by following the change in absorbance with time using a UV-Visible spectrophotometer for slower reactions or stopped flow techniques for ultrafast reactions. All reactions were thermostated with a precision of ± 0.1 °C of the set temperature. The spectra data taken at a wavelength of maximum absorption changes were fitted to a first-order exponential decay function to obtain the observed *pseudo* first-order rate constants, k_{obs}, according to Equation 3.1.[44]

$$A_t = A_\circ + (A_\circ - A_\infty) \exp(-k_{obs}\, t) \qquad (3.1)$$

where; A_0 is initial absorbance of the mixture at time t = 0, A_t is absorbance of the reaction mixture at any time, t and A_∞ is final absorbance.

Typical absorbance spectra changes are illustrated in Figure 3.4 for the reaction of 0.01 mM **C4** with 0.5 mM TU. (Inset is the respective kinetic trace at 300 nm). Other kinetic traces are placed in the supporting information Figures SI 3.18, SI 3.21, SI 3.24 and SI 3.27.

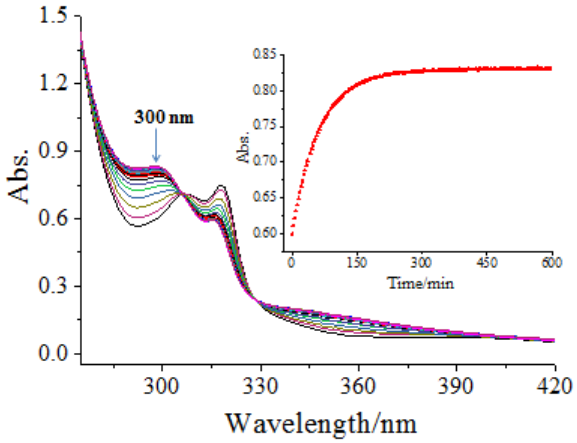

Figure 3. 4 UV-Visible spectra for the reaction of **C4** with TU at 298K (Inset is a kinetic trace at 300 nm)

The average values of observed rate constant were plotted against nucleophile concentrations according to Equation 3.2. The tabled data on the values of nucleophile concentration and k_{obs} are presented in supporting information Tables SI 3.1, SI 3.4, SI 3.7, SI 3.10, SI 3.12 and SI 3.14.

$$k_{obs} = k_2[Nu] + k_{-2}[Nu] \approx k_2[Nu] \tag{3.2}$$

The plots are linear with the slopes representing the second order rate constants, k_2. Typical plots of k_{obs} verses $[Nu]$ are shown in Figure 3.5 for the substitution reactions of **C6** with the thiourea nucleophiles at 298 K. More sample plots of observed rate constant, k_{obs}, verses concentration of nucleophile are presented in supporting information Figure SI 3.13, SI 3.14, SI 3.16, SI 3.19, SI 3.22, SI 3.25 and SI 3.28.

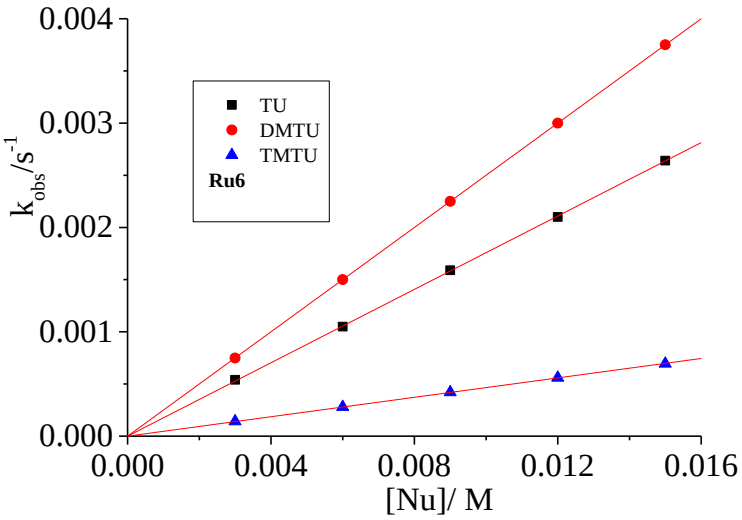

Figure 3. 5 Plots of k_{obs} versus nucleophile concentration for the reaction of **C6** with the thiourea nucleophiles at 298 K

Mechanism of substitution

From the kinetic analysis, the proposed mechanism of substitution for the complexes under investigation can be represented by Scheme 3.2 where (a) represents the mechanism for **C1** and **C2** and (b) for **C3**, **C4**, **C5** and **C6**

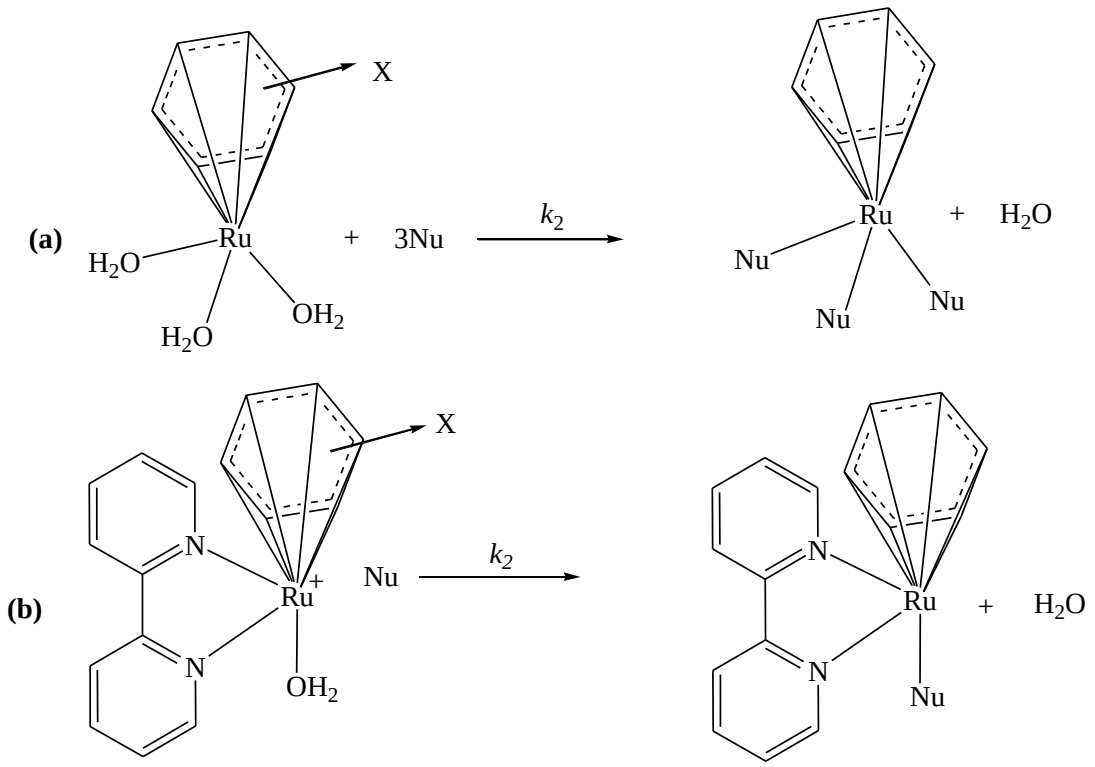

X = (a) benzene (**C1**) or mesitylene (**C2**). (b) benzene (**C3**), mesitylene (**C4**), hexamethylbenzene (**C5**) or *p*-cymene (**C6**). Nu = TU, DMTU or TMTU

Scheme 3. 2 Proposed mechanisms of substitution for complexes under investigation

The temperature dependence of the second order rate constants was studied over the temperature range of 20-40 °C in increments of 5 ^{o}C. Data was subjected to a linear plot of of $\ln(k_2/T)$ against T^{-1}/K^{-1} (the Eyring plot) according to the Equation 3.3;

$$\ln\left(\frac{k_{\exp}}{T}\right) = \frac{-\Delta H^{\neq}}{R}.\frac{1}{T} + \left[23.8 + \frac{\Delta S^{\neq}}{R}\right] \qquad (3.3)$$

Typical Eyring plots are shown in Figure 3.6 for the reactions of **C4** with the thiourea nucleophiles.

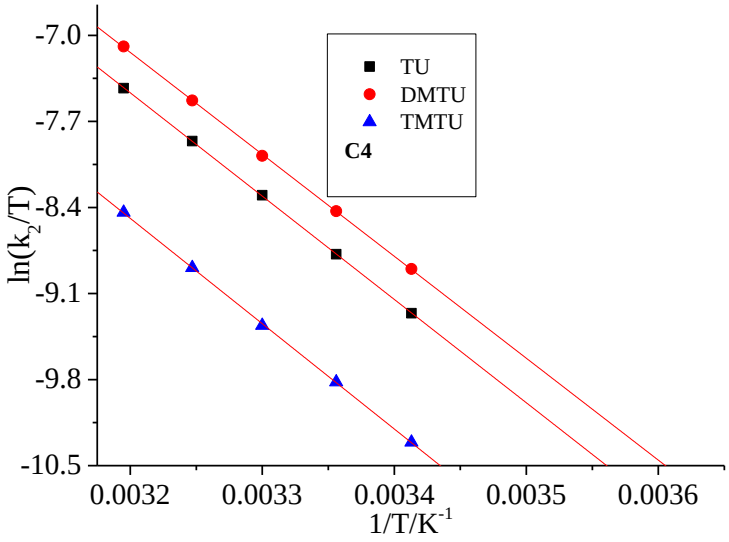

Figure 3. 6 Eyring plots for the reactions of **C4** with thiourea nucleophiles.

The slopes and intercepts of the Eyring plots, gave the enthalpy of activation, $\Delta H^{\neq}$, and entropy of activation, $\Delta S^{\neq}$, values, respectively. Values of the activation parameters are reported in Table 3.4. The rest of the Eyring plots are placed in supporting information Figures SI 3.15, SI 3.17, SI 3.20, SI 3.23 and SI 3.26, and the tables showing values of $\ln(k_2/T)$ and T^{-1}/K^{-1} are found in the supporting information in Tables SI 3.3, SI 3.6, SI 3.9, SI 3.11 and SI 3.13. The values of k_2, $\Delta H^{\neq}$ and $\Delta S^{\neq}$ are reported in Table 3.4.

Table 3. 4 Rate constants and activation parameters for studied reactions at 298 K

Complexes		*Nu.*	k_2 /M^{-1} s^{-1}x10^{-1}	$\Delta H_2^{\neq}$ /kJ mol^{-1}	$\Delta S_2^{\neq}$ /J K^{-1} mol^{1}
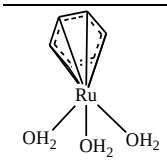	**C1**	***TU***	118 ± 2	44 ± 1	-57 ± 3
		DMTU	86 ± 3	56 ± 2	-20 ±5
		TMTU	45 ± 4	59 ± 1	-16 ± 3
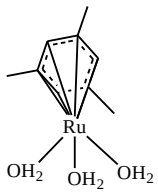	**C2**	***TU***	53.8 ± 0.07	68 ± 1	-41 ± 3
		DMTU	37.2 ± 0.05	68 ± 3	-18 ± 7
		TMTU	24.8 ± 0.03	75 ± 1	-10 ± 3
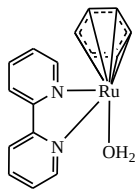	**C3**	***TU***	0.69 ± 0.004	68 ± 1	-32 ± 3
		DMTU	0.71 ± 0.002	65 ± 2	-31 ± 5
		TMTU	0.07 ± 0.001	69 ± 1	-31 ± 3
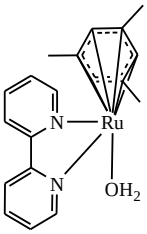	**C4**	***TU***	0.96 ± 0.004	66 ± 3	-36 ± 7
		DMTU	1.30 ± 0.002	70 ± 1	-33 ± 3
		TMTU	0.14 ± 0.005	71 ± 2	-40 ± 5
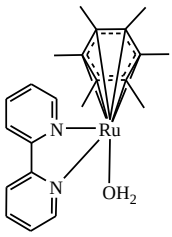	**C5**	***TU***	2.26 ± 0.001	60 ± 1	-56 ± 3
		DMTU	3.22 ± 0.001	58 ± 1	-59 ± 3
		TMTU	0.94 ± 0.003	65 ± 1	-47 ± 3
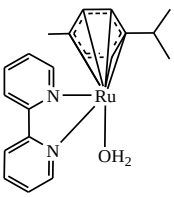	**C6**	***TU***	0.74 ± 0.001	63 ± 1	-50 ± 3
		DMTU	1.02 ± 0.001	64 ± 3	-45 ± 8
		TMTU	0.22 ± 0.002	67 ± 1	-46 ± 3

3.4 Discussion

The arene-Ru(II) complexes have η^6-arene ligands, whose extended π molecular orbitals (ring MOs) can side overlap with the metal *d* (σ-/or π-) atomic orbitals, contributing a total of

6π-electrons into the molecular orbitals of the complex. The other coordination sides are occupied by three aqua ligands (**C1-2**) or an N,N-bidentate ligand and the aqua labile group **(C3-6)**.[53] Substituents on the η^6-arene ligands affect the electron distribution in the ligand and thus the electron density around the Ru(II) metal centre and its effect on the leaving group. Lynda Dadci *et. al.*[54] made a similar point when the observed that alkylated η^6-arene ligands had stronger σ/π-donor character towards the metal centre.

The geometry in most arene complexes is *pseudo* octahedral, characterised by the arene and three other groups at the base of a piano stool.[54] [9] [29] [55] The other groups are spatially distributed so as to minimize electron repulsions between bonded and no-bonded electron pairs. However, introduction of the bipyridyl ligand in **C1** and **C2** further distorts the trigonal geometry to near T-geometry for complexes **C3-6** where in the aqua is directly *trans* to the face of the η^6-arene ligand as depicted in Figure 3.6. This positions the η^6-arene ligand where it has a stronger labializing effect on the aqua leaving group via a ground state destabilizing (the *trans* influence). This supposition is in line with the DFT-optimized structures of these complexes and a depiction of this geometry is shown in Figure 3.7 for **C3**. In the optimised structures of **C3-6**, the angle C8-Ru1-O7 is almost linear (180°) while angle N(2)-Ru(1)-O(7) is 90° (Table 3.3), showing the bipyridine ligand is perpendicular to the *trans* axis.

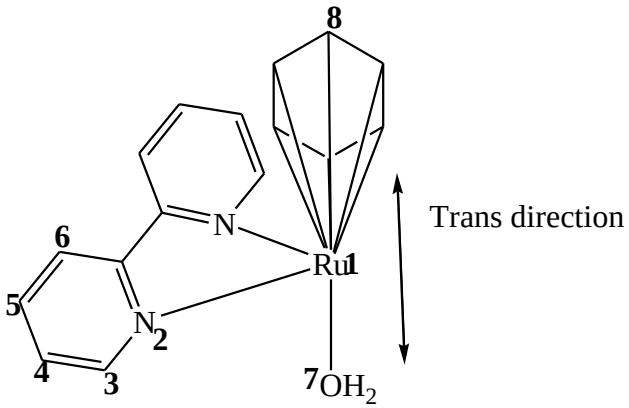

Figure 3. 7 Chemical structural of **C3** showing orientation of the Ru(II)-complexes

This geometry is corroborated by X-ray crystal structure literature data of **C3**.[56] Data in Table 3.4 shows that the order of reactivity of the complexes is: **C1** > **C2** > **C5** > **C4** > **C6** > **C3**. **C1** is more reactive than **C2** because of the inductive donor effect of the three methyl groups on the η^6-mesitylene ligand of **C2**. More electron density is received in it's extended

molecular orbitals, leading to a stronger Ru-(η^6-mesitylene) π-bonds compared to the same bonds in **C1**. As a result, electron density is also accumulated at its Ru metal centre thereby lowering the electrophilicity of the complex. This causes lower rates of substitution from **C2**. This is supported by the DFT calculated NBO charges showing higher charge for **C1** (0.430) compared to **C2** (0.377). The electrophilicity index of **C1** (6.612) is also higher than that of **C2** (4.998) (Table 3.3). A more positive metal centre pulls the incoming nucleophiles more strongly[57] hence the higher reactivity shown by **C1**. It is worth noting that the structures of **C1** and **C2** are trigonal pyramidal in geometry eliminating the possibility of aqua-arene *trans* orientation. The consequence is that *trans*-effect is minimal or non-existent in these complexes even though electrons are donated towards the ruthenium metal centre.

Other DFT calculated quantities including chemical hardness and electronic chemical potential further support the observed trend in the rate of substitution as envisaged in literature.[58] [58b] [59] [60] [61] The HOMO-LUMO energy gap for **C1**(4.514) is smaller than that of **C2** (4.536) which makes it easier for electron density to be transferred from the HOMO to the LUMO increasing the electrophilicity of the Ru(II) metal centre, thus the higher reactivity of **C1**. The stability of **C1** (2.257) is less than that of **C2** (2.268) which confirms the higher reactivity of **C1**. The electronic chemical potential of **C1** (-5.463) is lower than that of **C2** (-5.176) which indicates a less tendency for electrons to escape from the system in **C1** implying it is more positive than **C2** hence more reactive.

For the complexes **C3**-**C6** which bear 2,2'-bipyridyl as a common auxiliary ligand, the order of reactivity is; **C3** < **C6** < **C4** < **C5**. The rate of substitution increases with the number of alkyl substituents attached onto the η^6-arene ligand. The number of alkyl substituents attached directly onto the arene in the 2,2'-bypyridyl(η^6-arene)Ru(II) complexes increase in the order 0 (**C3**) > 2 (**C6**) > 3 (**C4**) > 6 (**C5**). The higher the number of alkyl groups on the η^6-arene ligand, the stronger the inductive donation of electron density into the π-group molecular orbitals of the ring and hence the more electron density flowing into the coordination bonds with Ru. This labializes the aqua groups through the *trans* influence. This is also raises the HOMO orbitals of the complexes in the same order while the LUMOs are hardly affected, showing the ground state labialisation effect on the properties of the complexes. This has been observed in literature for similar structured complexes exhibiting *trans* influence.[62] This inductive donation of electron density into the π-group molecular orbitals and towards the Ru centres also causes accumulation of electron density on the Ru

metal centre as supported by the decrease in electrophilicity indices, ω, of the 2,2'bypyridyl(η^6-arene)Ru(II) (6.203 (**C5**) > 6.288 (**C4**) > 6.400 (**C6**) > 6.406 (**C3**) with increase in the number of alkyl groups on the arene ligands.[63] The rest of DFT calculated data (Table 3.3) are consistent with the observed kinetic trends as envisioned in literature.[64] The HOMO-LUMO energy gaps of 2,2'bypyridyl(η^6-arene)Ru(II) increase in the order; 3.767 (**C5**) < 3.938 (**C4**) < 4.072 (**C6**) ~ 3.961 (**C3)**, signifying a decreased capacity of the arene ligands to receive electron density form the metals by π-back bonding leading to decreased reactivity in that order. The chemical hardness values increase in the same order as the energy gap: (1.884 (**C5**) < 1.969 (**C4**) < 2.036 (**C**6) ~ 1.981 (**C3**)). The electronic chemical potential (eV) values decrease (-4.835 (**C5**) > -4.976 (**C4**) > -5.204 (**C6**) ~ -5.038 (**C3**)) in the same trend as the rate of substitution reactivity.

The (triaqua)(η^6-arene)Ru(II) complexes **C1** and **C2** are approximately 10^2 more reactive than the their mono-aqua-Ru(II) counterparts **C3** and **C4** respectively. This is because the introduction of the bipyridyl ligand introduces steric hindrance at the Ru(II) metal centre which restricts the incoming nucleophiles, this effect has also been reported in literature.[54]

The values of $\Delta S^{\neq}$ are negative while the values of $\Delta H^{\neq}$ are positive and low hence the mode of substitution is associative and proceed through a seven-coordinate at the Ru(II) metal centre in the transition state. There is reported literature in support of this mechanism of substitution for octahedral Ru(II) complexes.[56] The thiourea nucleophiles substituted the aqua ligands in the order; DMTU > TU > TMTU. The DMTU reacts faster than TU because its two methyl groups donate electron density inductively towards the sulphur atom making it more nucleophilic hence more reactive. This has been reported in literature for similar studies.[65] [66] [67] [68] [69] [70]

3.5 Conclusions

The reactivity of the (η^6-arene)Ru(II)aqua complexes is driven mainly by electronic factors and in some cases by steric factors. The introduction of the bipyridyl ligand in **C3** and **C4** and the rest of the complexes distort their trigonal geometry of **C1** and **C2** closer to a T-geometry in which the aqua ligand is directly *trans* to the face of the η^6-arene. The bipyridyl ligand introduces steric hindrance at the Ru metal centre, lowering the reactivity of the complexes **C3-C6** compared to **C1** and **C2**. The alkylated η^6-arene ligands receive electron density by inductive donation into its extended molecular orbitals which can be π-donated to the Ru

metal centre. The higher the number of alkyl groups on the arene ligand, the stronger the inductive donation. The greater inductive electron donation in **C2** makes its metal centre less electropositive than that of **C1** hence less reactive. For the complexes **C3**-**C6** which bear 2,2'-bipyridyl as a common auxiliary ligand, the order of reactivity is; **C3** < **C6** < **C4** < **C5** in line with an increased labializing effect on the aqua co-ligand through the *trans* influence of the alkalyted η^6-arene ligands. The mode of substitution in these complexes is associative in nature.

3.6 References

[1] J. Reedijk, *Proceedings of the National Academy of Sciences* **2003**, *100*, 3611.

[2] Y. Zhao, W. He, P. Shi, J. Zhu, L. Qiu, L. Lin, Z. Guo, *Dalton Transactions* **2006**, 2617-2619.

[3] O. Novakova, H. Chen, O. Vrana, A. Rodger, P. J. Sadler, V. Brabec, *Biochemistry* **2003**, *42*, 11544-11554.

[4] E. I. Montero, J. M. Pérez, A. Schwartz, M. A. Fuertes, J. M. Malinge, C. Alonso, M. Leng, C. Navarro-Ranninger, *European Journal of Chemical Biology* **2002**, *3*, 61-67.

[5] E. Gallori, C. Vettori, E. Alessio, F. G. Vilchez, R. Vilaplana, P. Orioli, A. Casini, L. Messori, *Archives of Biochemistry and Biophysics* **2000**, *376*, 156-162.

[6] K. Sanjay, J. Shweta, A. R. S., K. S. Jitendra, S. P. Daya, *Inorganic Chemistry* **2007**, *46*.

[7] Z. H. Siddik, *Oncogene* **2003**, *22*, 7265-7279.

[8] W. Han Ang, P. J. Dyson, *European Journal of Inorganic Chemistry* **2006**, *2006*, 4003-4018.

[9] F. Wang, H. Chen, S. Parsons, I. D. H. Oswald, J. E. Davidson, P. J. Sadler, *Chemistry–A European Journal* **2003**, *9*, 5810-5820.

[10] C.-W. Jiang, H. Chao, H. Li, L.-N. Ji, *Journal of Inorganic Biochemistry* **2003**, *93*, 247-255.

[11] J. L. Beck, R. Gupta, T. Urathamakul, N. L. Williamson, M. M. Sheil, J. R. Aldrich-Wright, S. F. Ralph, *Chemical Communications* **2003**, 626-627.

[12] A. Ambroise, B. G. Maiya, *Inorganic Chemistry* **2000**, *39*, 4264-4272.

[13] C. G. Hartinger, P. J. Dyson, *Chemical Society Reviews* **2009**, *38*, 391-401.

[14] M. Groessl, C. G. Hartinger, K. Połeć-Pawlak, M. Jarosz, P. J. Dyson, B. K. Keppler, *Chemistry & Biodiversity* **2008**, *5*, 1609-1614.

[15] F. Wang, H. Chen, S. Parsons, I. D. Oswald, J. E. Davidson, P. J. Sadler, *Chemistry-A European Journal* **2003**, *9*, 5810-5820.

[16] P. J. Dyson, G. Sava, *Dalton Transactions* **2006**, 1929-1933.

[17] R. E. Morris, R. E. Aird, S. Murdoch Pdel, H. Chen, J. Cummings, N. D. Hughes, S. Parsons, A. Parkin, G. Boyd, D. I. Jodrell, P. J. Sadler, *Journal of Medicinal Chemistry* **2001**, *44*, 3616-3621.

[18] N. Olga, M. Jaroslav, S. Tereza, K. Jana, B. Tijana, S. P. J., B. Viktor, *Chemistry – A European Journal* **2010**, *16*, 5744-5754.

[19] K. S. M. Smalley, R. Contractor, N. K. Haass, A. N. Kulp, G. E. Atilla-Gokcumen, D. S. Williams, H. Bregman, K. T. Flaherty, M. S. Soengas, E. Meggers, M. Herlyn, *Cancer Research* **2007**, *67*, 209-217.

[20] S. W. Magennis, A. Habtemariam, O. Novakova, J. B. Henry, S. Meier, S. Parsons, I. D. H. Oswald, V. Brabec, P. J. Sadler, *Inorganic Chemistry* **2007**, *46*, 5059-5068.

[21] C. Scolaro, A. B. Chaplin, C. G. Hartinger, A. Bergamo, M. Cocchietto, B. K. Keppler, G. Sava, P. J. Dyson, *Dalton Transactions* **2007**, 5065-5072.

[22] K. K.-W. Lo, T. K.-M. Lee, *Inorganic Chemistry* **2004**, *43*, 5275-5282.

[23] A. F. Peacock, A. Habtemariam, R. Fernández, V. Walland, F. P. Fabbiani, S. Parsons, R. E. Aird, D. I. Jodrell, P. J. Sadler, *Journal of the American Chemical Society* **2006**, *128*, 1739-1748.

[24] Y. Liu, R. Hammitt, D. A. Lutterman, L. E. Joyce, R. P. Thummel, C. Turro, *Inorganic Chemistry* **2009**, *48*, 375-385.

[25] S. Chatterjee, S. Kundu, A. Bhattacharyya, C. G. Hartinger, P. J. Dyson, *Journal of Biological Inorganic Chemistry* **2008**, *13*, 1149-1155.

[26] R. E. Aird, J. Cummings, A. A. Ritchie, M. Muir, R. E. Morris, H. Chen, P. J. Sadler, D. I. Jodrell, *British journal of cancer* **2002**, *86*, 1652-1657.

[27] O. Novakova, J. Kasparkova, V. Bursova, C. Hofr, M. Vojtiskova, H. Chen, P. J. Sadler, V. Brabec, *Chemistry and Biology* **2005**, *12*, 121-129.

[28] H. K. Liu, P. J. Sadler, *Accounts of chemical research* **2011**, *44*, 349-359.

[29] P. Kumar, R. K. Gupta, D. S. Pandey, *Chemical Society Reviews* **2014**, *43*, 707-733.

[30] W. H. Ang, E. Daldini, C. Scolaro, R. Scopelliti, L. Juillerat-Jeannerat, P. J. Dyson, *Inorganic Chemistry* **2006**, *45*, 9006-9013.

[31] D. Wesselinova, N. Kaloyanov, G. Dimitrov, *Journal of Medicinal Chemistry* **2009**, *44*, 5099-5102.

[32] P. C. Bruijnincx, P. J. Sadler, *Current opinion in chemical biology* **2008**, *12*, 197-206.

[33] O. Dayan, S. Dayan, İ. Kani, B. Çetinkaya, *Applied Organometallic Chemistry* **2012**, *26*, 663-670.

[34] G. Enos, A. Mambanda, D. Jaganyi, *Journal of Coordination Chemistry* **2013**, *66*, 4280-4291.

[35] Ž. D. Bugarčić, B. V. Petrović, R. Jelić, *Transition Metal Chemistry* **2001**, *26*, 668-671.

[36] aS. Hochreuther, R. Puchta, R. van Eldik, *Inorganic Chemistry* **2011**, *50*, 8984-8996; bD. Jaganyi, F. Tiba, O. Q. Munro, B. Petrović, Ž. D. Bugarčić, *Dalton Transactions* **2006**, 2943-2949; cA. Mambanda, D. Jaganyi, *Dalton Transactions* **2011**, *40*, 79-91.

[37] R. A. Gaussian, *Inc., Wallingford CT* **2009**, *121*, 150-166.

[38] P. J. Hay, W. R. Wadt, *The Journal of chemical physics* **1985**, *82*, 270-283.

[39] C. Lee, W. Yang, R. G. Parr, *Physical Review B* **1988**, *37*, 785.

[40] A. D. Becke, *The Journal of chemical physics* **1993**, *98*, 5648-5652.

[41] M. Okamura, M. Yoshida, R. Kuga, K. Sakai, M. Kondo, S. Masaoka, *Dalton Transactions* **2012**, *41*, 13081-13089.

[42] M. Cossi, N. Rega, G. Scalmani, V. Barone, *Journal of computational chemistry* **2003**, *24*, 669-681.

[43] T. Le Bahers, T. Pauporté, G. Scalmani, C. Adamo, I. Ciofini, *Physical Chemistry Chemical Physics* **2009**, *11*, 11276-11284.

[44] A. Shaira, D. Jaganyi, *Journal of Coordination Chemistry* **2014**, *67*, 2843-2857.

[45] P. K. Chattaraj, U. Sarkar, M. Elango, R. Parthasarathi, V. Subramanian, *arXiv preprint physics/0509089* **2005**.

[46] A. Cedillo, R. Contreras, *Journal of the Mexican Chemical Society* **2012**, *56*, 257-260.

[47] E. Seifert, American Chemical Society Publications, **2014**.

[48] R. G. Parr, W. Yang, Oxford University Press, New York, **1989**.

[49] P. Geerlings, F. De Proft, W. Langenaeker, *Chemical Reviews* **2003**, *103*, 1793-1874.

[50] R. G. Parr, W. Yang, *Journal of the American Chemical Society* **1984**, *106*, 4049-4050.

[51] W. Yang, W. J. Mortier, *Journal of the American Chemical Society* **1986**, *108*, 5708-5711.

[52] S. Sangilipandi, D. Sutradhar, K. Bhattacharjee, W. Kaminsky, S. R. Joshi, A. K. Chandra, K. M. Rao, *Inorganica Chimica Acta* **2016**, *441*, 95-108.

[53] S. G. Warren, J. Clayden, *Solutions Manual to Accompany Organic Chemistry by Clayden, Greeves, Warren, and Wothers*, Oxford University Press, **2001**.

[54] L. Dadci, H. Elias, U. Frey, A. Hoernig, U. Koelle, A. E. Merbach, H. Paulus, J. S. Schneider, *Inorganic Chemistry* **1995**, *34*, 306-315.

[55] S. K. Tripathy, U. De, N. Dehury, S. Pal, H. S. Kim, S. Patra, *Dalton Transactions* **2014**, *43*, 14546-14549.

[56] F. Tiba, D. Jaganyi, A. Mambanda, *Journal of Coordination Chemistry* **2010**, *63*, 2542-2560.

[57] I. M. Wekesa, D. Jaganyi, *Dalton Transactions* **2014**, *43*, 2549-2558.

[58] aC. A. Mebi, *Journal of Chemical Sciences* **2011**, *123*, 727-731; bA. Vektariene, G. Vektaris, J. Svoboda, *Arkivoc: Online Journal of Organic Chemistry* **2009**.

[59] R. G. Parr, R. G. Pearson, *Journal of the American Chemical Society* **1983**, *105*, 7512-7516.

[60] S. Liu, *Journal of Chemical Sciences* **2005**, *117*, 477-483.

[61] R. E. Morris, R. E. Aird, P. del Socorro Murdoch, H. Chen, J. Cummings, N. D. Hughes, S. Parsons, A. Parkin, G. Boyd, D. I. Jodrell, *Journal of Medicinal Chemistry* **2001**, *44*, 3616-3621.

[62] B. J. Coe, S. J. Glenwright, *Coordination Chemistry Reviews* **2000**, *203*, 5-80.

[63] R. G. Parr, L. v. Szentpaly, S. Liu, *Journal of the American Chemical Society* **1999**, *121*, 1922-1924.

[64] D. Jaganyi, M. K. Sitati, I. M. Wekesa, *Inorganica Chimica Acta* **2016**, *453*, 531-537.

[65] W. P. Asman, D. Jaganyi, *International Journal of Chemical Kinetics* **2017**, *49*, 545-561.

[66] B. Petrović, Z. i. D. Bugarčić, A. Dees, I. Ivanović-Burmazović, F. W. Heinemann, R. Puchta, S. N. Steinmann, C. Corminboeuf, R. Van Eldik, *Inorganic Chemistry* **2012**, *51*, 1516-1529.

[67] M. M. Milutinović, S. K. C. Elmroth, G. Davidović, A. Rilak, O. R. Klisurić, I. Bratsos, Ž. D. Bugarčić, *Dalton Transactions* **2017**, *46*, 2360-2369.

[68] A. Rilak, I. Bratsos, E. Zangrando, J. Kljun, I. Turel, Ž. D. Bugarčić, E. Alessio, *Inorganic Chemistry* **2014**, *53*, 6113-6126.

[69] M. M. Milutinović, A. Rilak, I. Bratsos, O. Klisurić, M. Vraneš, N. Gligorijević, S. Radulović, Ž. D. Bugarčić, *Journal of Inorganic Biochemistry* **2017**, *169*, 1-12.

[70] M. Chrzanowska, A. Katafias, O. Impert, A. Kozakiewicz, A. Surdykowski, P. Brzozowska, A. Franke, A. Zahl, R. Puchta, R. van Eldik, *Dalton Transactions* **2017**, *46*, 10264-10280.

3.7 Supplementary Information

Included in the supplementary information are NMR spectra, mass spectra, tables, and various kinetic graphs for the synthetic and kinetic analysis of **C1, C2, C3, C4, C5** and **C6.**

3.7.1 Characterisation data

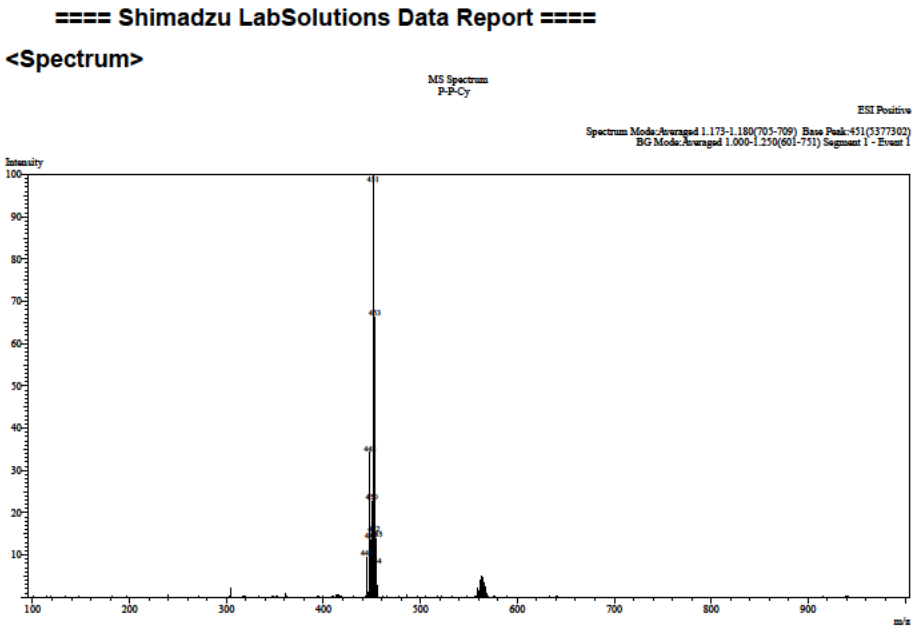

Figure SI 3.1 Low Res LC-Mass spectrum for [p-cym-Ru(Cl)-bp]

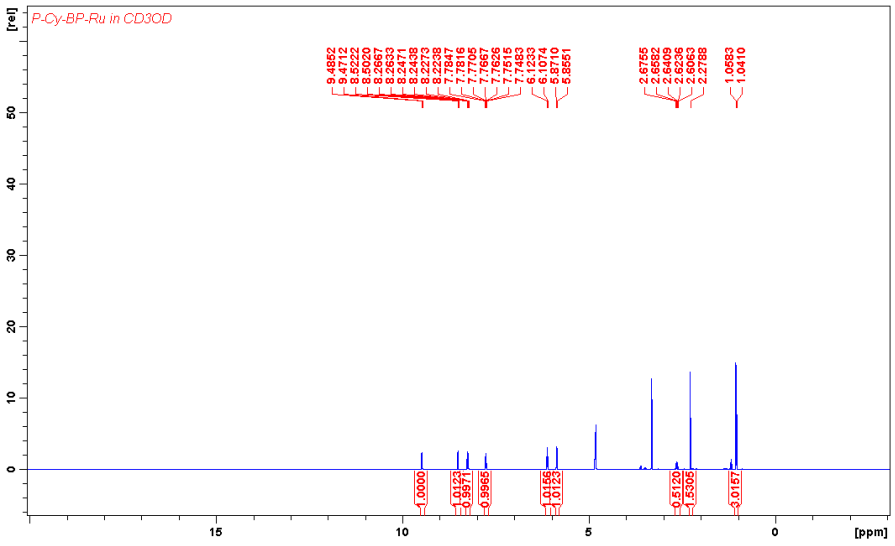

Figure SI 3.2 ^{1}H NMR spectrum for [p-cym-Ru(Cl)-bp]

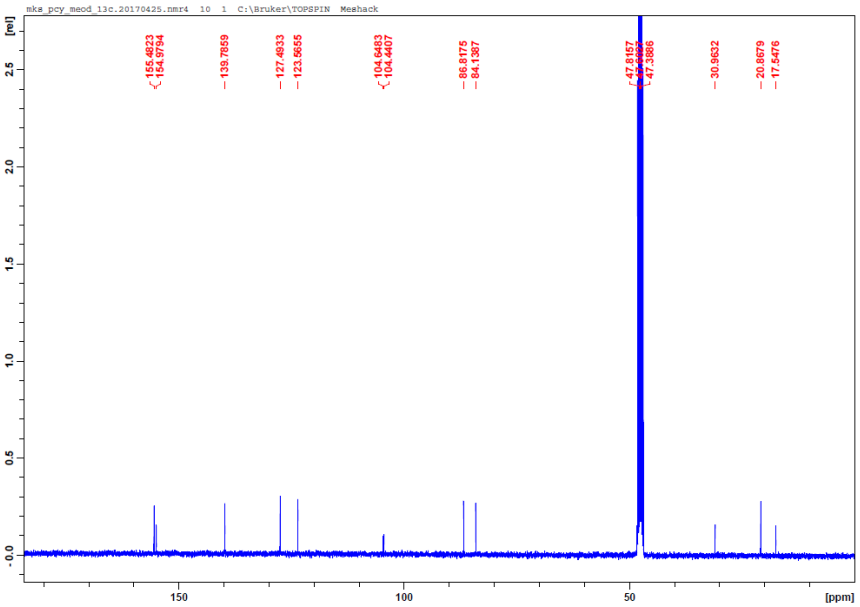

Figure SI 3.3 ^{13}C NMR spectrum for [p-cym-Ru(Cl)-bp]

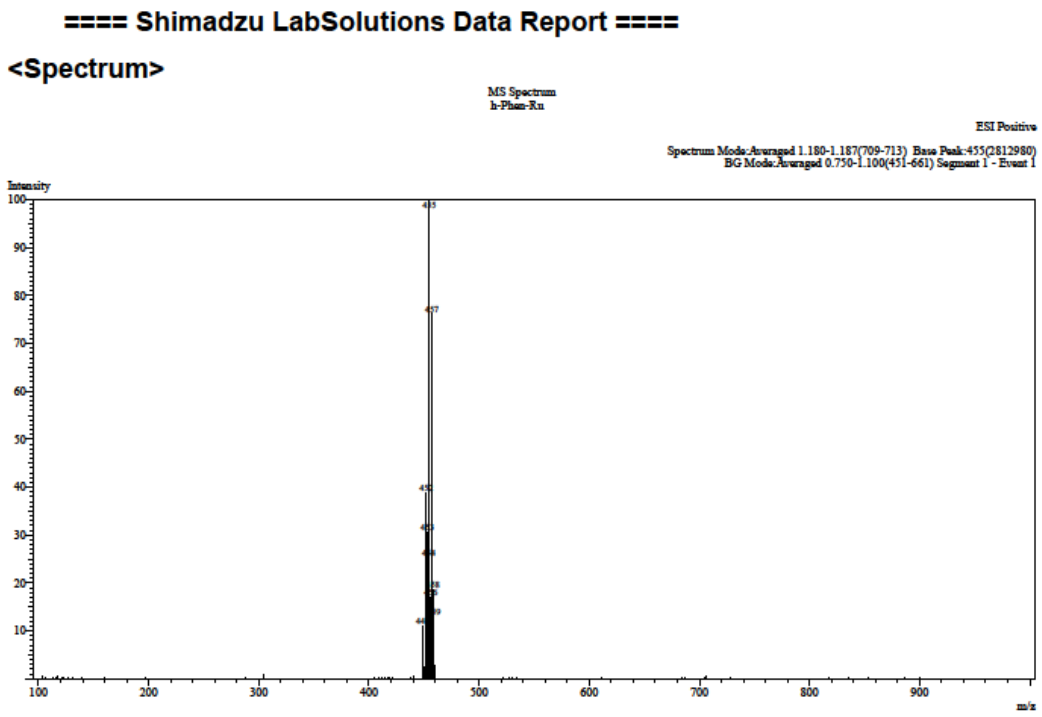

Figure SI 3.4 Low Res LC-Mass spectrum for [hexa-Ru(Cl)-bp]

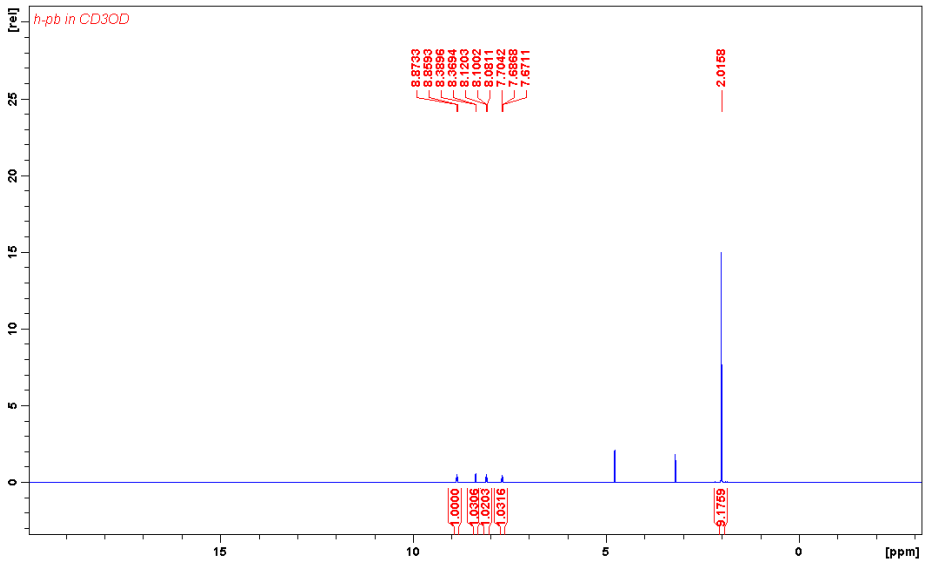

Figure SI 3.5 ^{1}H NMR spectrum for [hexa-Ru(Cl)-bp]

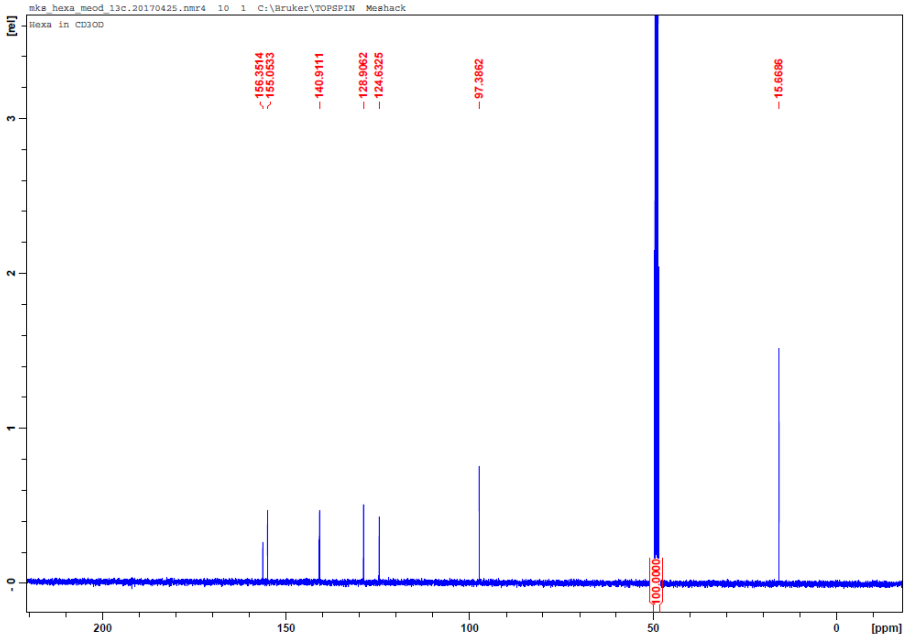

Figure SI 3.6 ^{13}C NMR spectrum for [hexa-Ru(Cl)-bp]

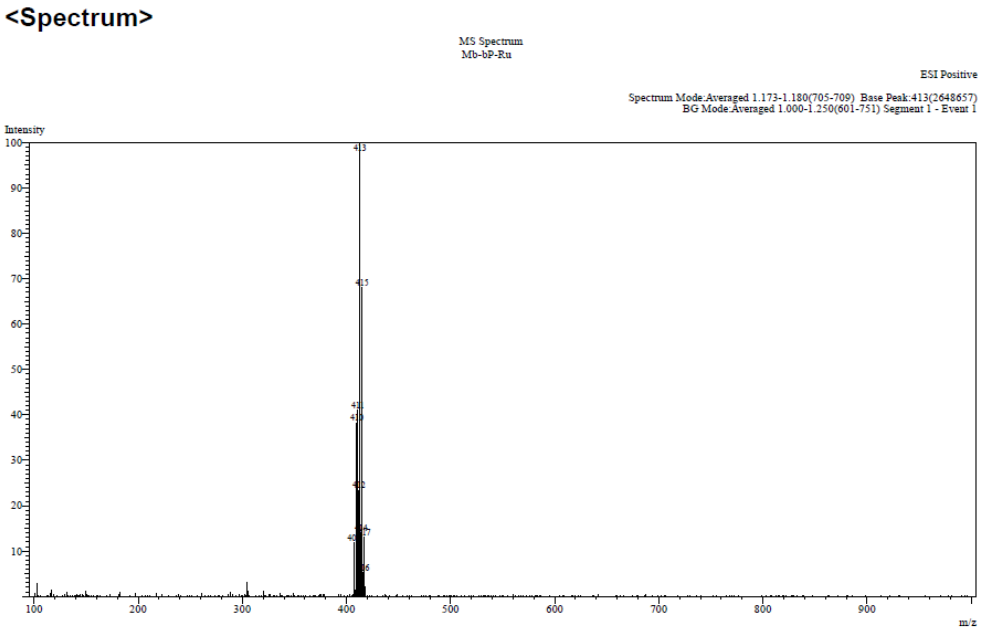

Figure SI 3.7 Low Res LC-Mass spectrum for [mesyt-Ru(Cl)-bp]

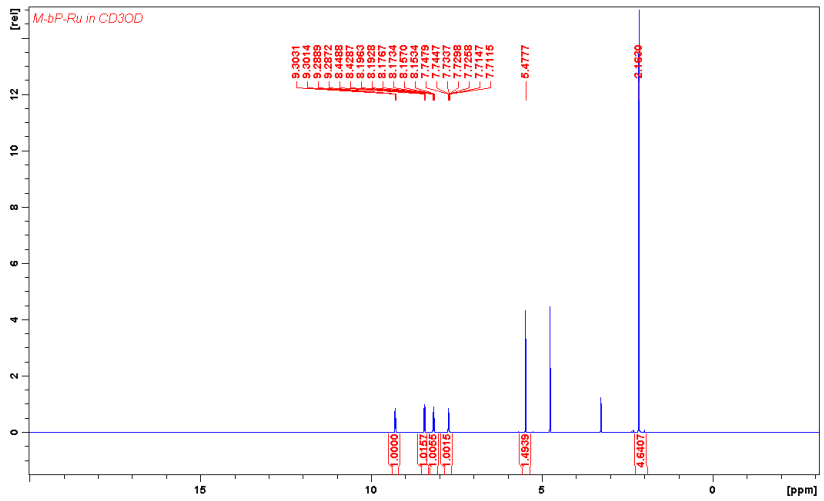

Figure SI 3.8 ^{1}H NMR spectrum for [mesyt-Ru(Cl)-bp]

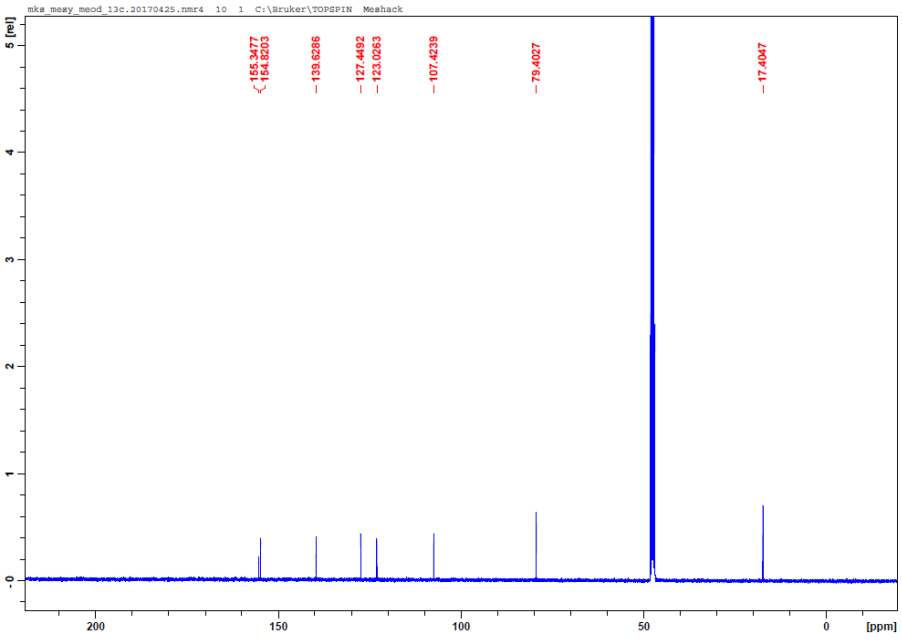

Figure SI 3.9 ^{13}C NMR spectrum for [mesyt-Ru(Cl)-bp]

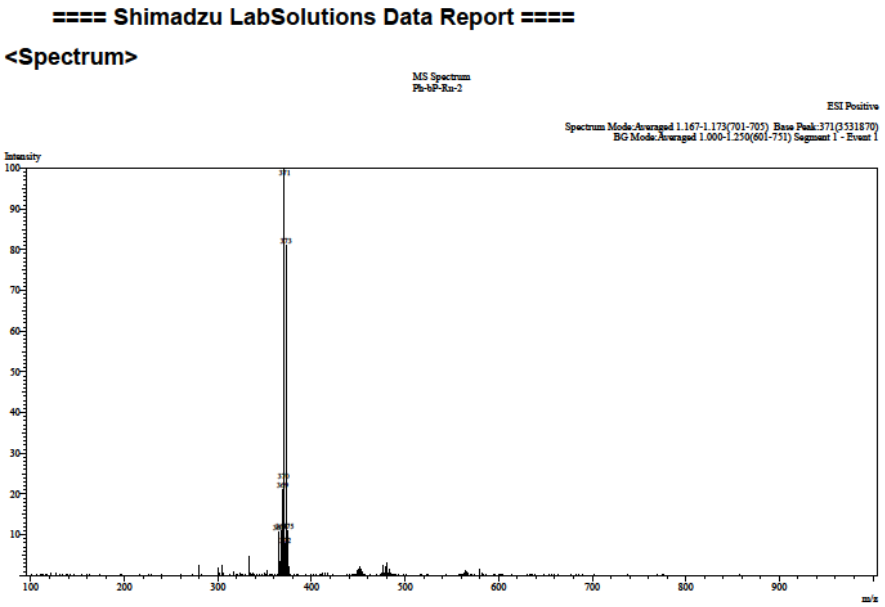

Figure SI 3.10 Low Res LC-Mass spectrum for [benz-Ru(Cl)-bp]

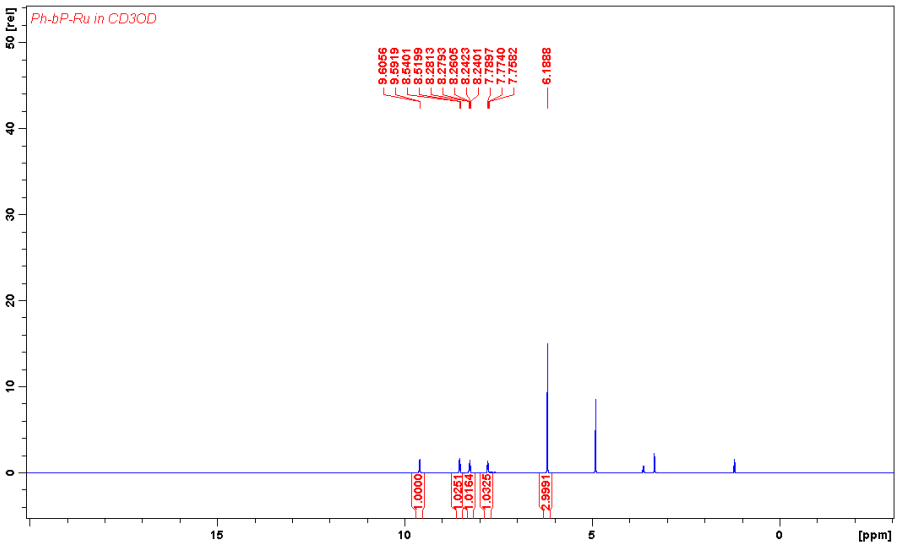

Figure SI 3.11 ^{1}H NMR spectrum for [benz-Ru(Cl)-bp]

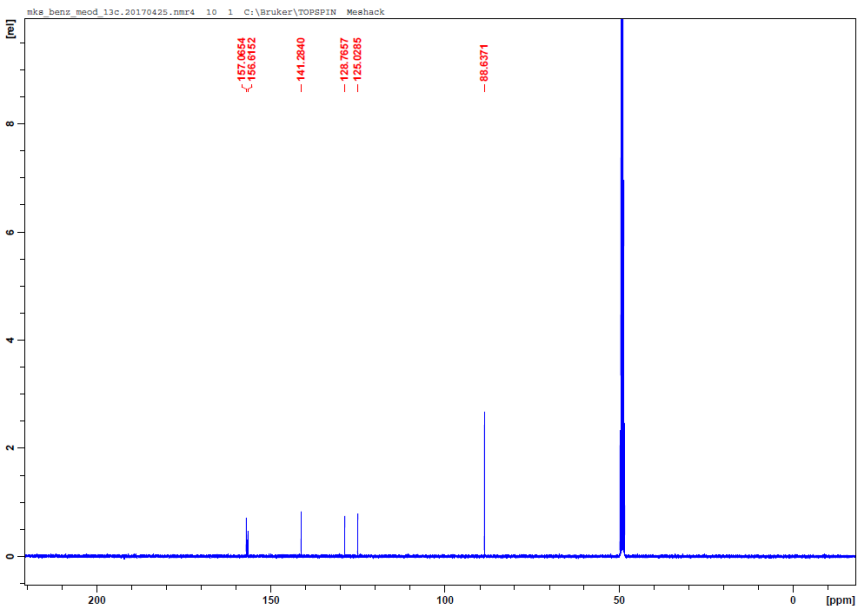

Figure SI 3.12 ^{13}C NMR spectrum for [benz-Ru(Cl)-bp]

3.7.2 Kinetic data and graphs

Mesitylene(triaqua)ruthenium(II)perchlorate (**C2**)

Table SI 3.1 Observed rate constants and the corresponding nucleophile concentrations

[Nu]/M	**k_{obs}/s-1 TU**	**k_{obs} /s-1 DMTU**	**[Nu]/M**	**k_{obs} /s-1 TMTU**
0.275	1.4791	1.02	0.110	0.2719
0.220	1.1843	0.8176	0.088	0.2174
0.165	0.8959	0.6193	0.066	0.165
0.110	0.5976	0.413	0.044	0.1087
0.055	0.289	0.2065	0.022	0.0545

Table SI 3.2 Wavelengths at which the kinetic progression were monitored

Nucleophile	**TU**	**DMTU**	**TMTU**
Wavelength/nm	405	405	345

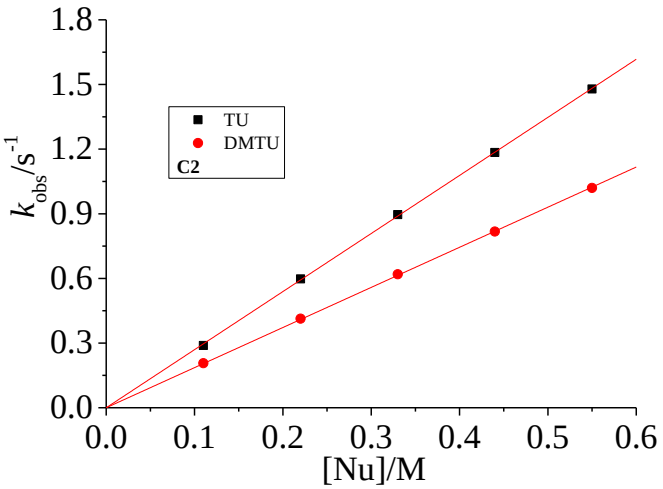

Figure SI 3.13 Concentration dependence plots for the reaction of C2 with DMTU and TU at 298 K

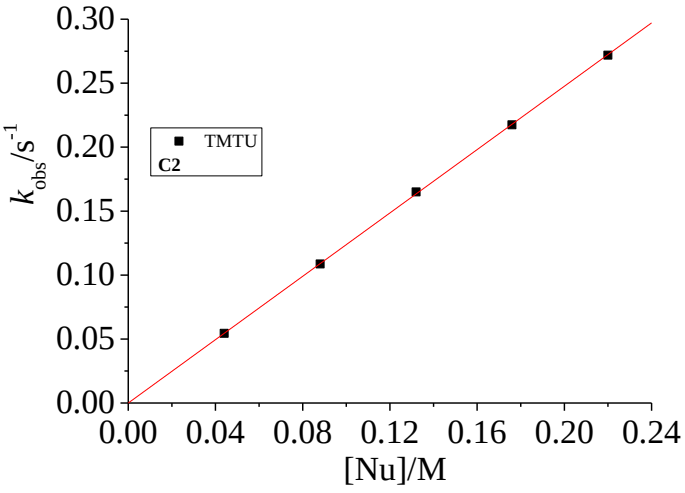

Figure SI 3.14 Concentration dependence plots for the reaction of **C2** with TMTU at 298 K

Table SI 3.3 Data of ln(k_2/T) and 1/T

1/T	ln(k_2/T) TU	ln(k_2/T) DMTU	ln(k_2/T) TMTU
0.00341	-4.37	-4.77	-5.26
0.00336	-3.98	-4.37	-4.82
0.0033	-3.49	-3.86	-4.27
0.00325	-3.06	-3.45	-3.82
0.00319	-2.6	-2.97	-3.27

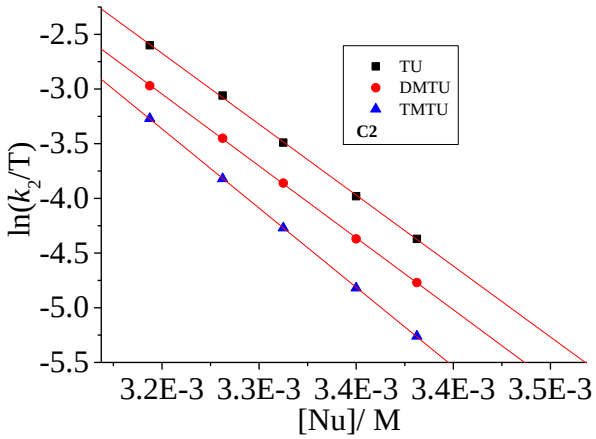

Figure SI 3.15 Temperature dependence plots for the reaction of **C2** with the thiourea nucleophiles

Benzene(triaquo)ruthenium(II)perchlorate (**C1**)

Table SI 3.4 Observed rate constants and the corresponding nucleophile concentrations

[Nu]/M	k_{obs}/s^{-1} TU	k_{obs} / s^{-1} DMTU	k_{obs} / s^{-1} TMTU
0.02	2.37	1.79	0.98
0.04	4.78	3.50	1.88
0.06	7.10	5.18	2.71
0.08	9.50	6.98	3.58
0.1	11.83	8.62	4.48

Table SI 3.5 Wavelengths at which the kinetic progression were monitored

Nucleophile	TU	DMTU	TMTU
Wavelength/nm	450	450	435

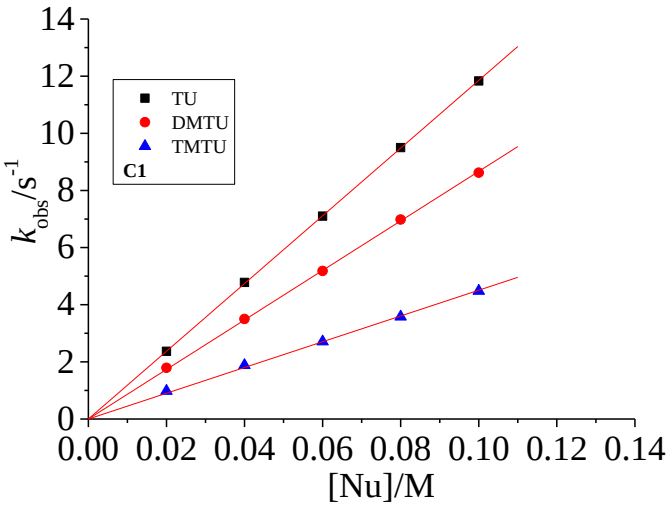

Figure SI 3.16 Concentration dependence plots for the reaction of **C1** with TMTU at 298 K

Table SI 3.6 Data of ln(k_2/T) and 1/T

1/T	**ln(k_2/T) TU**	**ln(k_2/T) DMTU**	**ln(k_2/T) TMTU**
0.00341	-0.85	-1.16	-1.84
0.00336	-0.53	-0.76	-1.41
0.0033	-0.26	-0.43	-1.06
0.00325	0.05	-0.02	-0.64
0.00319	0.32	0.31	-0.29

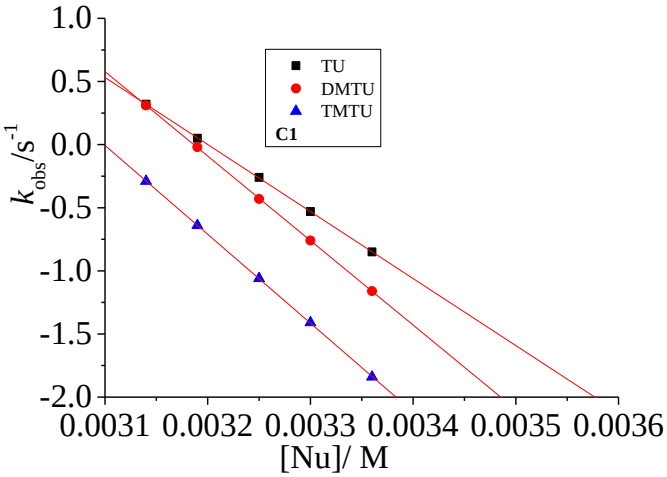

Figure SI 3.17 Temperature dependence plots for the reaction of **C1** with the thiourea nucleophiles

Aquo-(2,2'-bipyridine)(mesitylene)ruthenium(II)perchlorate (**C4**)

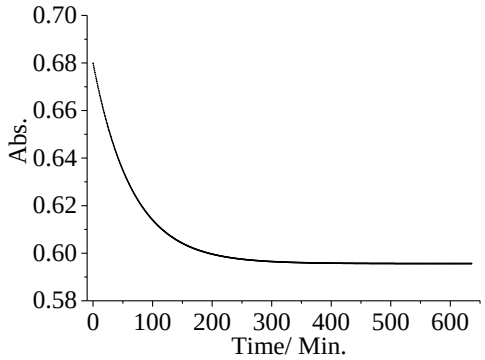

Figure SI 3.18 Kinetic trace for the reaction of **C4** with TU at 312 nm

Table SI 3.7 Observed rate constants and the corresponding nucleophile concentrations

[Nu]/M	**k_{obs} /s^{-1} TU**	**k_{obs} / s^{-1} DMTU**	**k_{obs} / s^{-1} TMTU**
0.015	7.16E-4	9.98E-4	2.43E-4
0.012	5.74E-4	7.98E-4	1.94E-4
0.009	4.3E-4	5.99E-4	1.46E-4
0.006	2.88E-4	4E-4	9.7E-5
0.003	1.44E-4	2E-4	4.85E-5

Table SI 3.8 Wavelengths at which the kinetic progression were monitored

Nucleophile	**TU**	**DMTU**	**TMTU**
Wavelength/nm	312	312	345

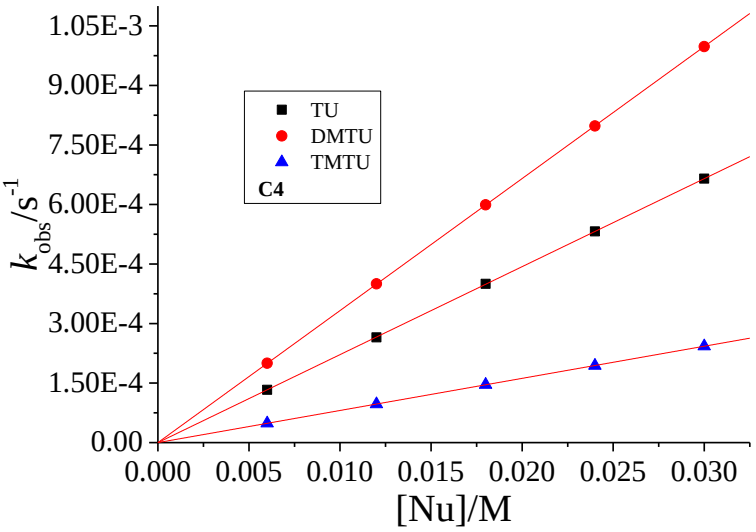

Figure SI 3.19 Concentration dependence plots for the reaction of **C4** with the thiourea nucleophiles at 298 K

Table SI 3.9 Data of ln(k_2/T) and 1/T

1/T	**ln(k_2/T) TU**	**ln(k_2/T) DMTU**	**ln(k_2/T) TMTU**
0.00341	-9.26	-8.9	-10.31
0.00336	-8.78	-8.43	-9.82
0.0033	-8.3	-7.98	-9.36
0.00325	-7.86	-7.53	-8.89
0.00319	-7.43	-7.09	-8.44

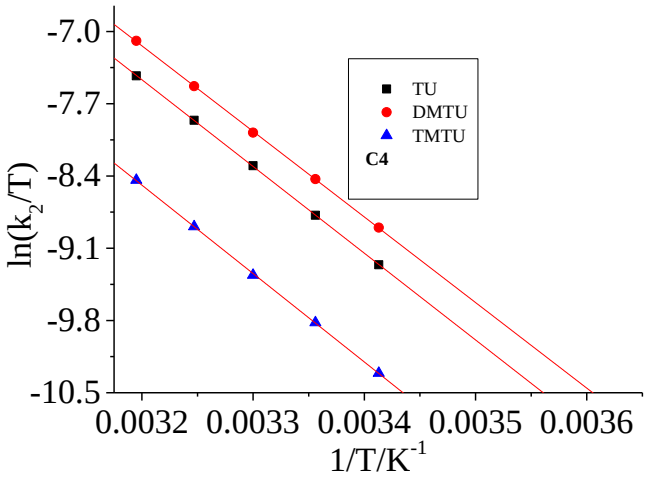

Figure SI 3.20 Temperature dependence plots for the reaction of **C4** with the thiourea nucleophiles

Aqua (2,2'-bipyridine)(hexamethylbenzene)ruthenium(II)perchlorate (**C5**)

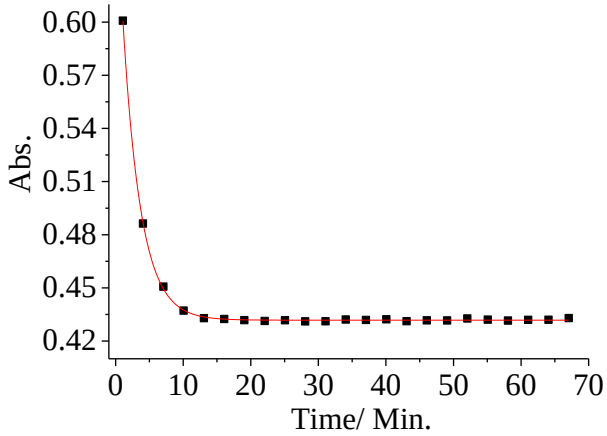

Figure SI 3.21 Kinetic trace for the reaction of **C5** with DMTU at 312 nm and 298 K

Table SI 3.10 Observed rate constants and the corresponding nucleophile concentrations

[Nu]/M	k_{obs}/ s^{-1} **TU**	k_{obs} / s^{-1} **DMTU**	k_{obs} / s^{-1} **TMTU**
0.015	0.0034	0.00481	0.00142
0.012	0.00272	0.00386	0.00114
0.009	0.00204	0.00289	8.48E-4
0.006	0.00135	0.00193	5.45E-4
0.003	6.83E-4	9.7E-4	2.83E-4

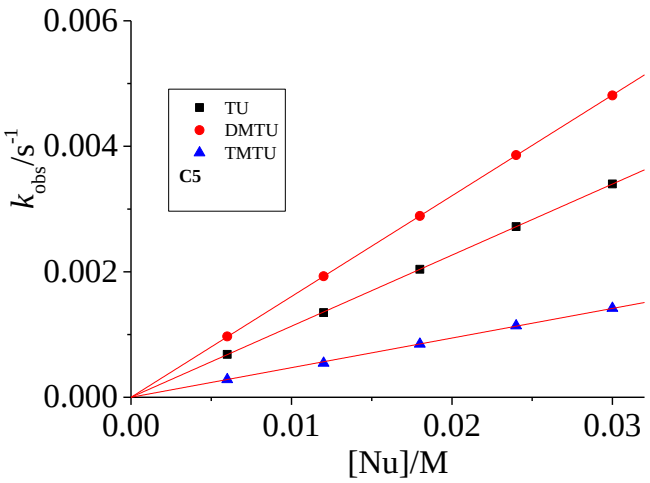

Figure SI 3.22 Concentration dependence plots for the reaction of **C5** with the thiourea nucleophiles at 298 K

Table SI 3.11 Data of ln(k_2/T) and 1/T

1/T	**ln(k_2/T) TU**	**ln(k_2/T) DMTU**	**ln(k_2/T) TMTU**
0.00341	-7.58	-7.23	-8.48
0.00336	-7.18	-6.83	-8.06
0.0033	-6.79	-6.46	-7.59
0.00325	-6.40	-6.09	-7.19
0.00319	-6.00	-5.69	-6.79

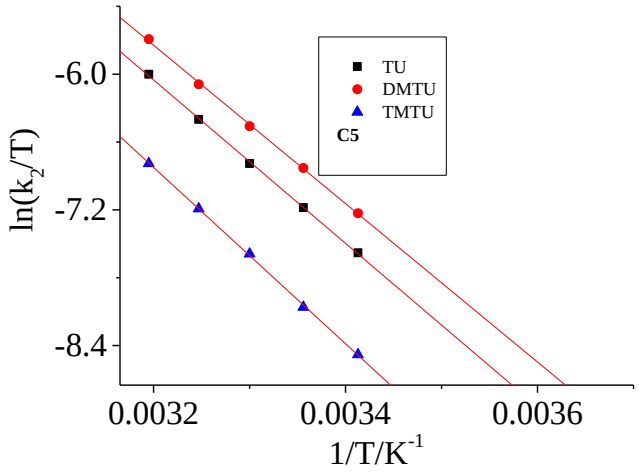

Figure SI 3.23 Temperature dependence plots for the reaction of **C5** with the thiourea nucleophiles

Aquo(2,2'-bipyridine)(*p*-cymene)ruthenium(II)perchlorate (**C6**)

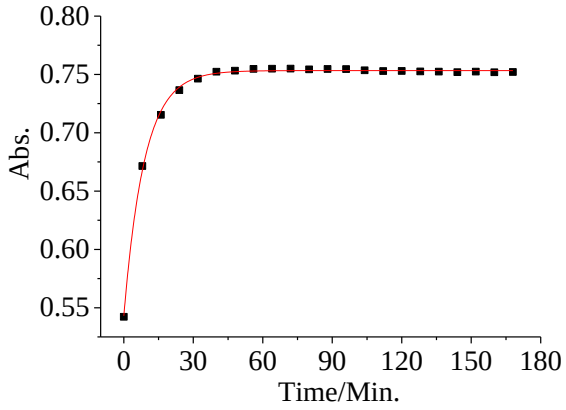

Figure SI 3.24 Kinetic trace for the reaction of **C6** with DMTU at 312nm and 298 K

Table SI 3.12 Observed rate constants and the corresponding nucleophile concentrations

[Nu]/M	k_{obs} /s^{-1} TU	k_{obs} / s^{-1} DMTU	k_{obs} / s^{-1} TMTU
0.00582	1.953E-4	2.997E-4	6.312E-5
0.01163	3.903E-4	5.993E-4	1.2548E-4
0.01745	5.846E-4	9.011E-4	1.891E-4
0.02326	7.965E-4	0.00121	2.498E-4
0.02908	9.876E-4	0.00149	3.133E-4

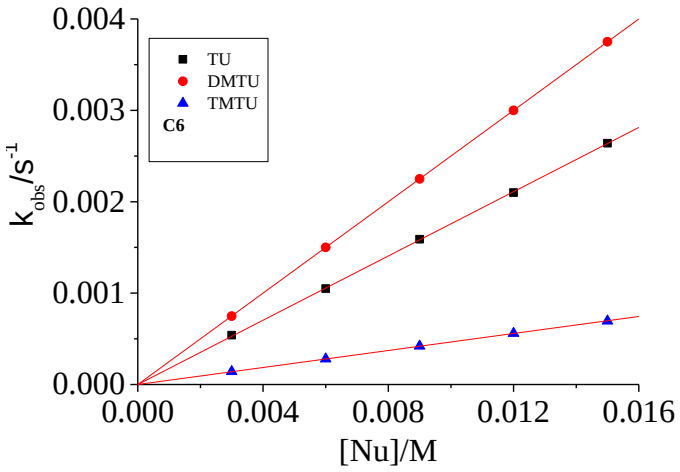

Figure SI 3.25 Concentration dependence plots for the reaction of **C6** with the thiourea nucleophiles at 298 K.

Table SI 3.13 Data of ln(k_2/T) and 1/T

1/T	ln(k_2/T) TU	ln(k_2/T) DMTU	ln(k_2/T) TMTU
0.00341	-8.13	-7.75	-9.46
0.00336	-7.68	-7.33	-9.01
0.0033	-7.3	-6.98	-8.53
0.00325	-6.87	-6.52	-8.13
0.00319	-6.47	-6.07	-7.69

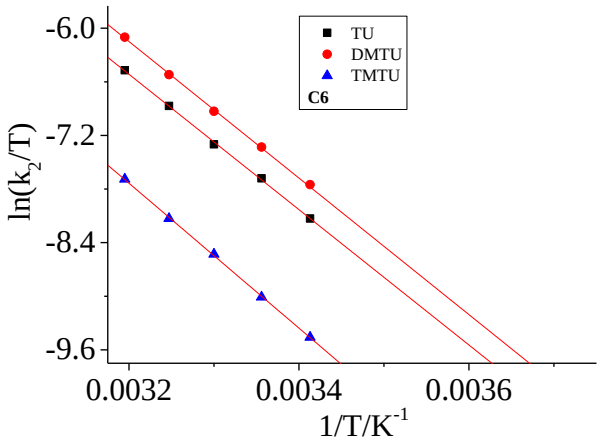

Figure SI 3.26 Temperature dependence plots for the reaction of **C6** with the thiourea nucleophiles

Aquo(benzene)(2,2'-bipyridine)ruthenium(II)perchlorate (**C3**)

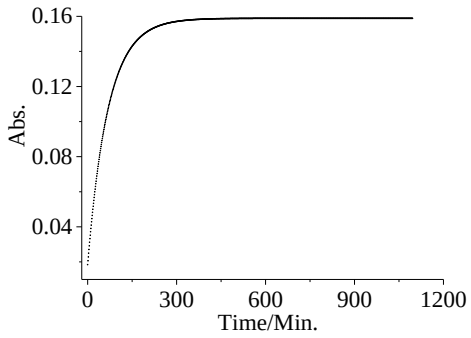

Figure SI 3.27 Kinetic trace for the reaction of **C3** with TMTU at 345nm and 298 K.

Table SI 3.14 Observed rate constants and the corresponding nucleophile concentrations

[Nu]/M	k_{obs}/ s^{-1} **TU**	k_{obs} / s^{-1} **DMTU**	k_{obs} / s^{-1} **TMTU**
0.0735	0.00505	0.0052	2.18E-4
0.0588	0.00404	0.00416	1.72E-4
0.0441	0.00304	0.0031	1.3E-4
0.0294	0.00202	0.00208	8.6E-5
0.0147	0.00101	0.001036	4.2E-5

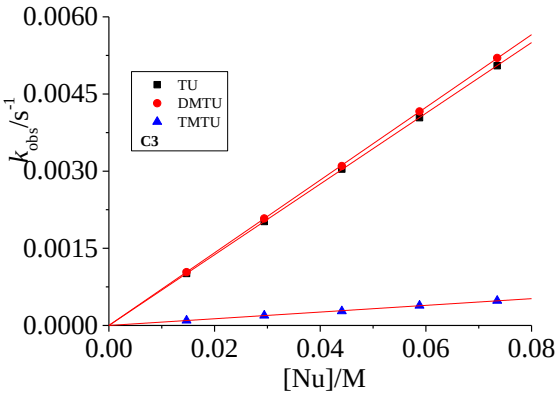

Figure SI 3.28 Concentration dependence plots for the reaction of **C3** with the thiourea nucleophiles at 298 K

Chapter 4

Reactivity of [(η^6-arene)(chloro)(phosphino)Ru(II)]$^+$ complexes towards thiourea nucleophiles

4.0 Abstract

Arene Ru(II) complexes; (η^6-Benzene)chloro-bis(triphenylphosphino)ruthenium(II) chloride, **C1**, (η^5-cyclopentadienyl)chloro-bis(triphenylphosphino)ruthenium(II) Chloride, **C2**, (η^6-Benzene)chloro{bis(diphenylphosphino)methane}ruthenium(II) Chloride, **C3**, (η^6-Benzene)-chloro{1,2-bis(diphenylphosphino)ethane}ruthenium(II) Chloride, **C5** and (η^6-Benzene)-chloro{1,3-bis(diphenylphosphino)propane}ruthenium(II) Chloride, **C6** were successfully synthesized by modified literature methods. The rate of chloro substitution and mechanism of reaction of the arene Ru(II) complexes by thiourea nucleophiles was studied under *pseudo* first order conditions in 0.1 M $NaClO_4$/LiCl methanol solution as a function of nucleophile concentration and temperature. The reactions were monitored using the UV-Vis absorption spectrophotometer or Stopped Flow Spectrophotometer for ultrafast reactions. The coordinated arene ligand donates electrons towards the Ru and it's π-electron cloud presents an electrostatic repulsive effect onto and around the Ru centre as measured by the projected cone angle. The bidentate bis(diphenylphosphino)methane ligand hinders the approach of nucleophiles during the substitution process. When the bis(diphenyl-phosphino)methane chelate is expanded through the introduction of a methylene carbon within the bridge, the steric hindrance to the approach of nucleophiles is reduced and the ligand assumes a trough like conformation which traps the nucleophile within the coordination sphere. This enhances the reactivity by a factor of 10^3.The observed reactivity trends are supported by DFT calculations. The entropy of activation values are positive indicating that the mechanism of substitution has interchange dissociative (I_D) character.

4.1 Introduction

Since the discovery of the anti-cancer properties of cisplatin, *cis*-$[PtCl_2(NH_3)_2]$,[1] [2] there has been concerted research efforts to improve on the clinical shortfalls of the drug. Cisplatin chemotherapy is shrouded by high toxicity, drug resistance and severe side effects of platinum-based anticancer drugs.[3] [4] Complexes of other metals such as Ru especially the arene-based Ru(II) have been considered as one of the most promising alternatives owing to their low toxicity, strong DNA-binding affinity and high antitumor activity.[4] [5] [6] [7]

Furthermore, arene-ruthenium complexes are stable, soluble in aqueous media and afforded under mild reaction conditions with high yields.[8] [9]

Most Ru(II)-arene complexes have shown good binding abilities which disrupt the replication of DNA.[10] [11] [12] For example, the complex $[(\eta^6\text{-arene})Ru^{II}(en)Cl]^+$ (en = ethylenediamine) inhibits the proliferation of human tumor cells and can unwind the double strand helix of DNA through a combination of intercalation and formation of mono-functional adducts with DNA. [13] [14] Studies have shown that increasing the size of the coordinated η^6-arene in the following order: benzene < p-cymene < biphenyl < dihydroanthracene < tetrahydro-anthracene caused a systematic increase in the anti-tumour activity.[13] Reactivity of the complexes also showed the same trend as the activity. The increase in activity with increasing number of rings on the coordinated arene supported the view that multi-ring arenes bind to DNA not only by coordination to the N7 atoms of guanine (G), but also non-covalently through hydrophobic interactions between the arene and DNA.[15] [16] [17] These hydrophobic interactions might include intercalation of the non-coordinated arenes between DNA bases or binding onto the minor-groove of DNA.[12] It was also observed that the biphenyl-Ru(II) complex has similar cytotoxicity to the anticancer drug carboplatin while the (tetrahydroanthracene)Ru(II)(en)Cl complex is as active as cisplatin.[18] [19] [20] [21]

DNA binding studies have also been done on complexes of the type $[Ru^{II}(\eta^6\text{-arene})(Cl)(en)]^+$ where arene is *o*-, *m*-, or *p*-terphenyl. The (*p*-terphenyl)Ru(II) complex exhibited promising cytotoxic effects in several human tumour cell lines, including those resistant to conventional cisplatin.[17] However, complexes containing *m*-, or *p*-terphenyl arene ligands were found to be less cytotoxic.[17] Similar studies on complexes coordinated by phenanthroimidazole derivatives revealed that they have substantial inhibitory activity against various tumour cells with potential application in cancer chemotherapy.[22]

Ru(II) complexes coordinated with cyclopentadienyl (η^5-C_5H_5) arene complexes have also been evaluated for activity against cancer.[23] For example (η^5-C_5H_5)(N,O or N,N-bidentate)Ru(II) revealed outstanding cytotoxic properties against several human cell lines.[23] [24] [25] Cytotoxicity of complexes of general form $[Ru(\eta_5\text{-}C_5H_5)(P\text{-}P)L]^+$ where L = σ-bonded N-heteroaromatic ligand and P-P = bidentate phosphine ligand were also evaluated.[26] The complexes bearing bidentate phosphine ligands and a mono-dentate N-donor ligand were found to have higher cytotoxicity than cisplatin against certain cell lines, indicating that DNA

is possibly one of the targets of their action inside the cells.[26] Another subclass of cyclopentadienyl Ru complexes which has been evaluated is the polymer based Ru(II)-cyclopentadienyl complex $[CpRu(P)(bpyPLA)]^+$ (Cp = η^5-C_5H_5, P = triphenyl-phosphine, and bpyPLA = 2,2'-bipyridine-4,4'-D-glucose end-capped polylactide). These were found to be six-fold more active than cisplatin in certain tumour cell lines.[27] Ru(III) hexaflourophosphate salts of the form; [(η^5-C_5H_5)Ru(PP)(L)]PF_6[28]; (L = galactose or fructose carbohydrate derivative ligands, functionalized with nitrile, tetrazole, or 1,3,4-oxadiazole N-coordinating moieties) displayed good anti-cancer activity.

The *pseudo*-octahedral geometry of Ru(II)-arene complexes can allow variations of the groups of ligands around the metal centre. For example, a mono-dentate ligand X, the bidentate ligand L and the arene itself permute to different complexes with various properties that can be useful for the anticancer activities of these compounds .[29] The leaving group controls the rate of hydrolysis of the complexes, the rate of substitution with non- targeted as well as targeted nucleophiles (*i.e*. reactions which triggers toxicity, resistance and ultimate activity, respectively).[29] Because of the hydrophobic nature of the coordinated arene, this influences favourable cell uptake through the hydrophobic membranes as well as non-covalent interactions with potential targets.

To date, arene-Ru(II) complexes have shown great potential as cancer therapeutics. Specifically, those coordinated with phosphine ligands have shown high activity that is comparable or even better than that of most of the existing Pt(II) metallo drugs. Moreso, some are not cross-resistant to cisplatin. Research studies on these complexes have focused mainly on testing their cytotoxicity. Not much the same has been done on their substitution reactivity yet there is literature evidence suggesting that their binding to DNA and interactions with other biomolecules underline their mechanism of action. The rate and mode of substitution of chloride from a series of (arene)Ru(II) with either triphenylphosphine or bidentate diphosphinoalkane as auxiliary ligands was studied using thiourea nucleophiles *viz* thiourea(**TU**), 1,3-dimethyl-2-thiourea(**DMTU**) and 1,1,3,3-tetramethyl-2-thiourea (**TMTU**). The chemical structures of the complexes used in this study are shown in Figure 4.1.

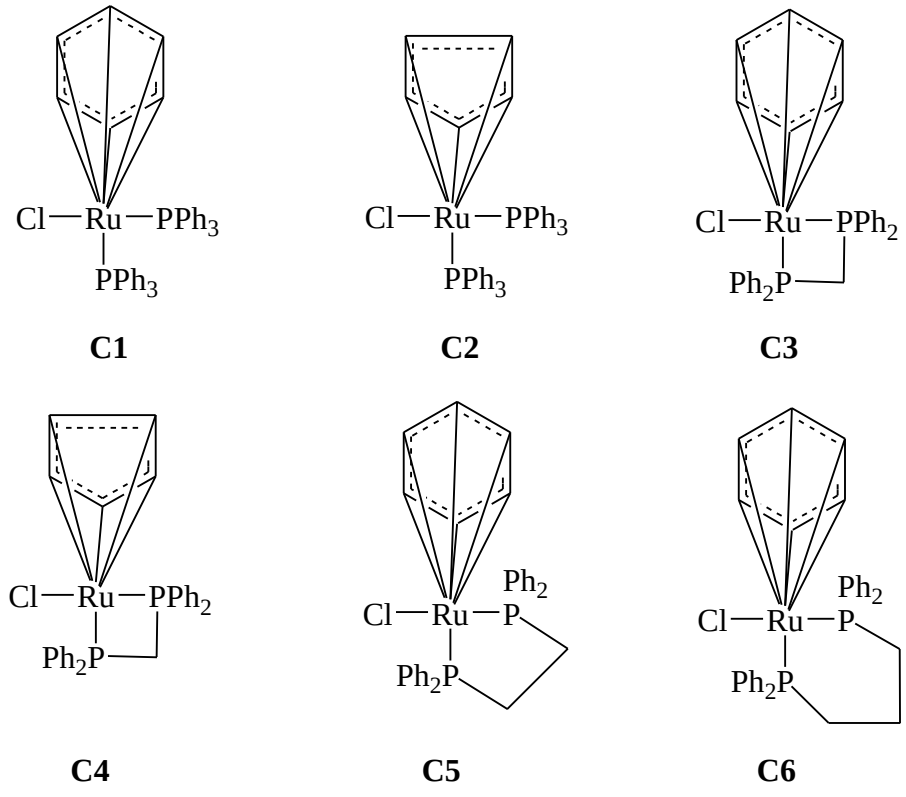

Figure 4. 1 The chemical structures of the arene-Ru(II) complexes

4.2 Experimental

4.2.1 Materials

All chemicals including (benzene)ruthenium(II) chloride dimer, bis(diphenylphosphino)-methane, bis(diphenylphosphinoethane, bis(diphenylphosphino)propane, triphenylphosphine, chloro(cyclopentadienyl)[bis(diphenylphosphino)methane]ruthenium(II-), ruthenium tri-chloride and cyclopentadiene, were purchased from Sigma Aldrich and used as received. The solvents were obtained from Merck and dried before use where needed.

4.2.2 Synthesis

All reactions were carried out under dry nitrogen atmosphere. All Ru complexes were prepared according to the literature methods, [30] [31] and characterized by elemental analysis and various spectroscopic techniques. The ^{1}H-NMR, ^{31}P-NMR and elemental spectral data confirmed successful synthesis of the complexes. Mass spectral data also gave peaks corresponding to the nominal mass of each complex. These are placed in the supporting information Figures SI 4.1- 4.15

(η^6-Benzene)chloro-bis(triphenylphosphino)ruthenium(II) chloride (C1)

A mixture of (η_6-benzene)Ru(II) chloride dimer and triphenylphosphine ligand in the ratio 1:4 in 30 ml of acetonitrile was refluxed for 1 h. The mixture was cooled to room temperature and the product precipitated by slow addition of 30 mL of cold ether. The orange product was collected by filtration, recrystallized from hot acetonitrile-ether, and dried in vacuo at room temperature. Yield: 0.065 g, (31.6%), Yellow powder. ^{1}H NMR (500 MHz, CD_2Cl_2, ppm) δ = 7.54 (m, 30H), 1.59 (s, 6H). ^{31}P NMR (500 MHz, CD_2Cl_2) δ/ppm δ = 28.69. LC-MS-ESI$^+$, m/z: 703.75 $[M -2Cl]^{2+}$. *Anal. Calc. For* $C_{42}H_{36}Cl_2P_2Ru$: C 65.12, H 4.68. *Found*: C 64.89, H 4.99.

(η^5-cyclopentadienyl)chlorobis(triphenylphosphino)ruthenium(II) chloride (C2)

A solution of 0.2 M $RuCl_3$ (1 mmol) in absolute ethanol was added to a boiling solution of triphenylphosphine (4 mmol) in absolute ethanol. After 5 min of refluxing, excess freshly distilled cyclopentadiene in a small volume of 95% ethanol was added. The solution was refluxed for 1 hour and cooled to room temperature to give orange crystals which were collected and washed with ethanol. Recrystallization from hot dichloromethane/n-hexane mixture gave compound **C2** as a pure orange solid. Yield: 0.105 g, (40.6%), Orange solid. ^{1}H NMR (400 MHz, CD_2Cl_2, ppm) δ = 7.29 (m, 30H), 1.71 (s, 5H). ^{31}P NMR (400 MHz, CD_2Cl_2) δ/ppm δ = 38.91. LC-MS-ESI$^+$, m/z: 691.14 $[M -2Cl]^{2+}$. *Anal. Calc. For* $C_{41}H_{35}Cl_2P_2Ru$: C 64.66, H 4.63. *Found*: C 64.78, H 4.59.

(η^6-Benzene)chloro{bis(diphenylphosphino)-methane}ruthenium(II) chloride (C3)

The complex was synthesised in the same way as **C1** using bis(diphosphino)methane ligand in the place of triphenylphosphine with the ratio of the reagents being 1:2. The yellow product was collected by filtration, recrystallized from acetonitrile-ether, and dried in vacuo at room temperature. Yield: 0.1 g, (41%), Yellow powder. ^{1}H NMR (500 MHz, CD_2Cl_2, ppm) δ = 7.92 (m, 6H), 7.22 (m, 20H), 1.57 (s, 2H). ^{31}P NMR(500 MHz, CD_2Cl_2) δ/ppm δ = 26.30. LC-MS-ESI$^+$, m/z: 634 $[M]^+$ 599.04 $[M^+ -Cl]^{2+}$. *Anal. Calc. For* $C_{31}H_{28}Cl_2P_2Ru$: C 58.68, H 4.45. *Found*: C 58.91, H 4.89

(η^6-Benzene)chloro{1,2-bis(diphenylphosphino)ethane}ruthenium(II) chloride (C5)

Complex **C5** was synthesized in the same manner as **C3** using bis(diphosphino)ethane ligand in the place of bis(diphosphino)methane. The yellow product was collected by filtration, recrystallized from acetonitrile-ether, and dried in vacuo at room temperature. Yield: 0.701 g, (91%), Yellow powder. ^{1}H NMR (500 MHz, CD_2Cl_2, ppm) δ = 7.43 (m, 20H), 2.74 (m, 6H),

1.5(m, 4H). ^{31}P NMR (500 MHz, CD_2Cl_2) δ/ppm δ = 23.90 LC-MS-ESI$^+$, m/z: 613.06 [M - Cl]$^+$. *Anal. Calc. For* $C_{32}H_{30}Cl_2P_2Ru$: C 59.27, H 4.46. *Found*: C 58.87, H 4.79.

(η^6-Benzene)chloro{1,3-bis(diphenylphosphino)propane}ruthenium(II)chloride (C6)

Complex **C6** was synthesized in the same manner as **C3** using bis(diphosphino)propane ligand in the place of bis(diphosphino)methane. The yellow product was collected by filtration, recrystallized from acetonitrile-ether, and dried in vacuo at room temperature. Yield: 0.760 g, (92.1%), Yellow powder. ^{1}H NMR (500 MHz, CD_2Cl_2, ppm) δ = 7.41 (m, 20H), 1.58 (s, 8H), 1.24 (m, 4H). ^{31}P NMR(500 MHz, CD_2Cl_2) δ/ppm δ = 24.00. LC-MS-ESI$^+$, m/z: 627.07 [M – Cl]$^+$. *Anal. Calc. For* $C_{32}H_{30}Cl_2P_2Ru$: C 59.82, H 4.87. *Found*: C 59.94, H 5.11.

4.2.3 Instrumentation and measurement

NMR spectroscopy were recorded on a Bruker Avance DPX 400 MHz spectrophotometer at 303 K and chemical shifts were referenced to those of $Si(CH_3)_4$. Low resolution electron spray ionization (ESI$^+$) mass spectra were recorded on the Waters Micromass LCT Premier Spectrometer or Shimadzu LCMS 2020. Elemental analyses were done on a ThermoScientific Flash 2000 elemental analyser. Kinetic measurements for fast reactions were performed on an Applied Photophysics SX20 stopped flow instrument coupled with an online data acquisition system whose temperature was controlled to within ± 0.1° C. The slow reactions were monitored using Varian Cary 100 Bio UV-visible spectrophotometer with an attached Varian peltier temperature controller and online kinetic application. The UV-vis spectrophotometer was also used to determine the wavelengths at which the reactions on the stopped low were monitored.

4.2.4 Computational modelling

The computations were done at the Density Functional Theory (DFT) level of theory run on Gaussian 09 suite of programs.[32] [33] DFT applies to physically observable electron density over a wave function in the determination of the properties of a system. The structures were optimised at the Becke hybrid exchange functional and the 3-parameter correlation functions of Lee-Young-Parr (B3LYP) method with LANL2DZ (Los Alamos National Laboratory 2 double ζ) basis sets having inner core electrons of the Ru atom replaced by relativistic effective core potential (ECP).[34] [35] Los Alamos National Laboratory 2 double ζ basis set exploits relativistic effective core potentials to account for effect of inner core 28 electrons

([Ar]$3d^{10}$) in Ru.[36] [37] To take into account the solvent effects, the systems were fully optimised in methanol using the conductor polarizable continuum model (C-PCM).[38] [39] The singlet states were used due to low electronic spin state of Ru(II) complexes. The complexes were considered to have an overall charge of +1. The chemical potential (μ) and molecular hardness (η) for each structure were obtained from the HOMO and LUMO energies. The global electrophilicities (ω) were determined by the relationship $\omega = \mu^2/2\eta$.[40] [41] The charge on each atom is expressed as a natural bond orbitals (NBO) .[42]

4.3 Results

4.3.1 Computational results

Density functional theory (DFT)[43] [44] calculated quantities for example electrophilicity index and NBO charges have provided information in support of the chemical reactivity. The DFT optimized structures of the complexes are shown in Table 4.1 and summarised data from DFT calculations are presented in Table 4.2. The complexes exhibit the familiar "three-legged piano-stool" geometry as shown by the DFT minimum energy structures in Table 4.1. The Ru metal centre is π-bonded to the aromatic ring of the arene ligand and σ-bonded to the phosphorus and chloride atoms. The complexes have *pseudo*-octahedral coordination in which the three sites accommodate the six electrons from the arene ligand and the remaining sites are bonded to two phosphorus atoms and a chloride.[45] The DFT frontier molecular orbitals in Table 4.1, shows that the HOMO are located mainly on the Ru metal centre and partially on the arene and chloro ligand while the LUMO are on the phenyl ligands.[46]

Table 4. 1 DFT minimum energy structures and frontier molecular orbitals of the complexes

Optimised Structures		HOMO	LUMO
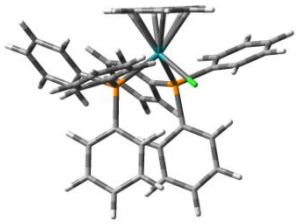	**C1**	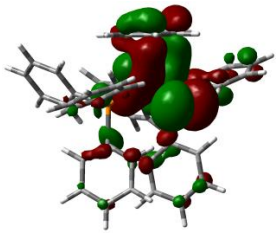	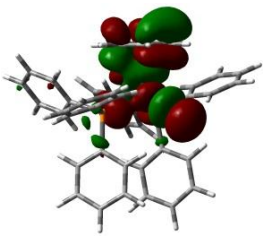
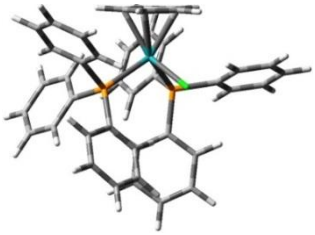	**C2**	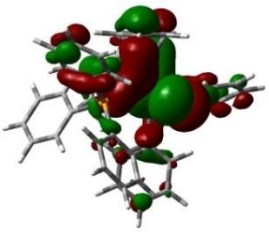	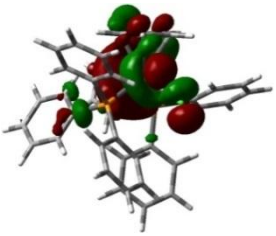
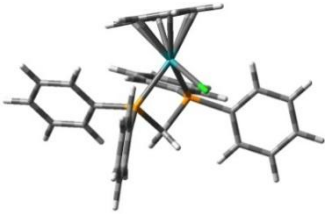	**C3**	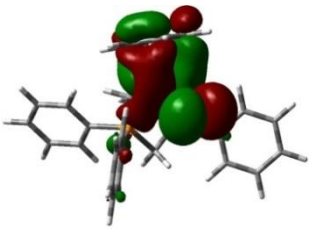	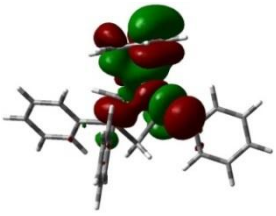
	**C4**	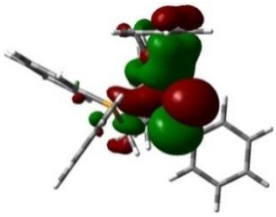	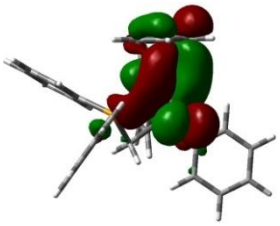
	**C5**	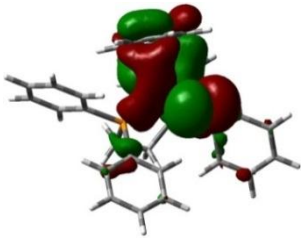	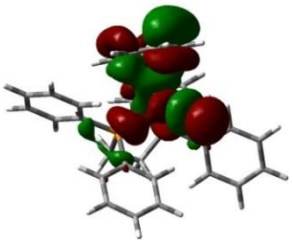
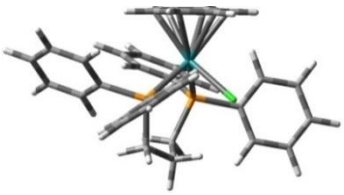	**C6**	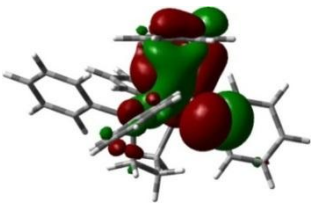	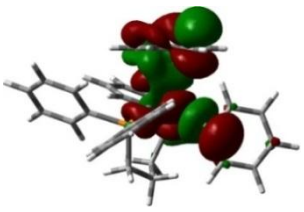

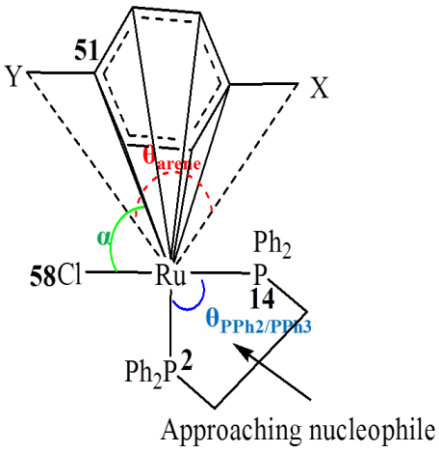

X and Y = H

Figure 4. 2 An illustration of the repulsive electrostatic effect around the metal centre due to the π-cloud of the arene, the 'cone angles' and an associated numbering using **C5** an example

Table 4. 2 Summary of DFT calculated data for the Ru(II) complexes

Parameters	**C1**	**C2**	**C3**	**C4**	**C5**	**C6**
Bond lengths (Å)						
Ru-Cl58	2.494	2.490	2.486	2.445	2.489	2.493
P2-P14	3.767	4.101	2.883	2.879	3.242	3.488
Bond angles (°)						
C51-Ru-Cl58, (α)	88.3	84.7	93.3	100.8	90.2	89.6
Y-Ru-X, (θ_{arene})	123.8	93.0	105.6	95.1	107.2	106.1
P14/2-Ru-Cl58	89.8	87.8	84.8	89.5	92.8	86.3
P2-Ru-P14, ($\theta_{PPh2/PPh3}$)	98.7	108.6	72.6	71.4	83.2	91.3
NBO charges						
Ru	-0.470	-0.282	-0.416	-0.268	-0.438	-0.486
Cl58	-0.317	-0.284	-0.313	-0.290	-0.333	-0.313
Orbital energy/eV						
HOMO	-6.548	-6.738	-6.476	-6.829	-6.395	-6.496
LUMO	-2.799	-3.673	-2.628	-3.427	-2.631	-2.731
$\Delta E_{HOMO-LUMO}$	3.749	3.065	3.849	3.401	3.764	3.865
Global chemical reactivity indices						
η/eV	1.875	1.533	1.924	1.701	1.882	1.933
μ/eV	-4.673	-5.205	-4.552	-5.128	-4.513	-4.564
ω/eV	5.825	8.840	5.384	7.731	5.410	5.388

η = chemical hardness, μ = electronic chemical potential, ω = electrophilicity index

Compounds with higher HOMO-LUMO energy gaps (Table 4.2) are likely be kinetically stable and chemically less reactive.[45] The calculated bond lengths and angles for the optimal Ru(II) complexes (Table 4.2) are comparable to those reported for complexes with similar structures.[45] [47] [48] The inter-ligand bond angles deviate significantly from the 90° as expected for perfect octahedral geometry. For example angle P2-Ru1-P14($\theta_{PPh2/PPh3}$) (Figure 4.2) is 98.7°, which is greater than the idealized angle because of marked distortions due to the steric demands of the coordinated ligands.[49] The NBO charges on the Ru metal centre are all negative showing that there is an overall charge transfer from the ligands to the Ru centre due to the inductive effects of the phosphine and π-donation of the arene ligands . Low elecrophilicity of the arene-Ru(II) complexes has been reported in literature[46]

DFT calculated changes on Ru show that complexes coordinated with bidentate α,ω-(diphosphino)alkane ligands have more negative charge due to the additional σ-donor effect of the alkyl chains on the P-donor atoms. The negative charge on the Ru atom increases with the length of the alkyl chain, pointing to greater electron donation towards the P atoms and finally to the Ru(II) metal centre. This effect is more pronounced when looking at arene-Ru(II) complexes having the benzene versus cyclopentadienyl rings i.e. **C1** versus **C2** or **C3** versus **C4**, where the negative charge on the former complexes is approximately 50 % more than that of the latter. It is also worth noting that introduction of the bidentate chelate diphosphino ligands (**C1** versus **C3** or **C2** versus **C4)** makes the Ru metal centre and the whole complex less negative as shown by the NBO charges and the global electrophilicity index. This can be attributed to the introduction of the lower σ-donor diphenylphosphino groups compared to the previous stronger σ-donating triphenylphosphino ligands.

The calculated inter-atomic separation distance in Table 4.2 also shows that the distance between the phosphino donor group is wider (longer) in **C2** than **C1**. This is because the π-electron cloud of the cyclopentadienyl group of **C2** is smaller hence project a smaller repulsive electrostatic effect defined by a projected "cone angle" over the Ru metal centre compared to the bigger π-electronic cloud of the benzene donor group in **C1**. The relative magnitude of the angle Y-Ru-X (θ_{arene}) [48] in the two complexes attest to this. This causes a reduction in the inter-shielding by the bulky triphenylphosphine ligands to spread more.

For complexes coordinated with then chelating bis(diphenylphospino)alkane ligands, the separation (Å) of phosphorus atoms about the Ru metal centre increases as the alkane chain of the P,P-chelate increases and occurs in the order; 3.488 (**C6**) > (3.242) **(C5)** > (2.883) **(C3)**). This effect leads to reduced steric hindrance to the approach of the nucleophile around the Ru.[48] Added to that, the smaller bis(diphenylphosphino)methane chelates in the complexes **C3** and **C4** restrict the spatial orientation of phosphine atoms, resulting in shorter P-P distance which has a net effect of increasing the steric hindrance to the approach of an incoming nucleophile. The inter-phosphine atomic distances are corroborated by the angles $\theta_{PPh2/PPh3}$ values (Table 4.2) which enlarges as the P-P separation increases.

4.3.2 Kinetic analysis

Kinetic measurements were done under *pseudo* first-order conditions using at least 10 fold excess of nucleophile in methanol with an ionic strength of 0.1 M provided by adding 0.01M

LiCl and 0.09 M $NaClO_4$ in dry methanol. The chloride ions from LiCl suppressed any possibility of solvolysis of the complexes. The perchlorate ion such a poor nucleophile and cannot competitively substitute the co-labile ligand ahead of the incoming thiourea ligands.[39] Kinetic solutions were prepared by dissolving required amounts of complexes in the methanolic solution. Nucleophile stock solutions were prepared at 50 times the concentration of the respective complex and diluted to afford concentrations of 40, 30, 20 and 10 times the concentration of the complexes for kinetic analysis

The rate of substituting the chloro ligand was investigated spectrophotometrically by following the change in absorbance with time using the UV-Visible Spectrophotometer for conventional and slower reactions or stopped flow technique for ultrafast reactions. Spectral changes due to the reactions were observed over the wavelength range 200-800 nm to establish a suitable wavelength at which the respective reaction for each metal complex could be followed. All reactions were thermostated within ± 0.1 °C of the set value. The changes in absorbance accompanying the reactions were analysed graphically using the software package OriginPro 9.1. An example of such spectral changes for the reaction of **C3** with thiourea nucleophile is shown in Figure 4.2. The inset to figure 4.3 is the kinetic trace of the reaction at 360 nm.

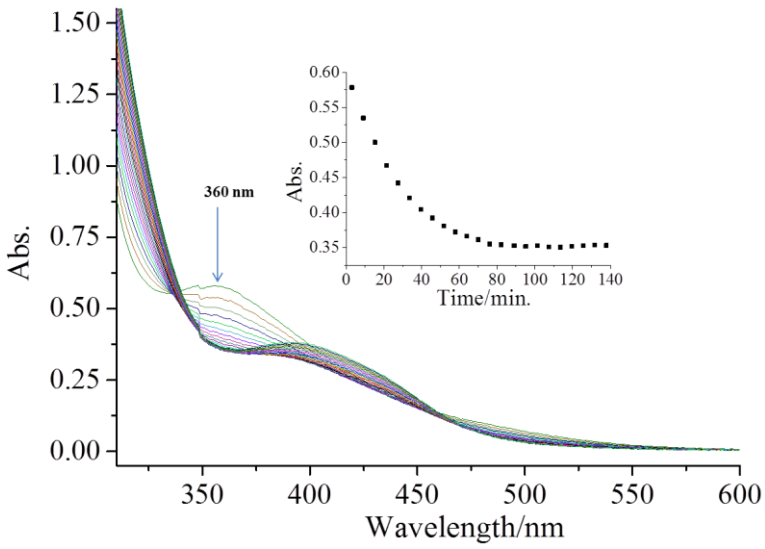

Figure 4. 3 Absorbance spectral changes for the reaction of **C3** and TU at 298 K (*Inset* is the kinetic trace of absorbance verses time for the reaction at 360 nm)

The observed first order rate constant, k_{obs}, were obtained from the fitted data consistent with equation 4.1 using OriginPro 9.1 program.

$$A_t = A_\circ + (A_\circ - A_\infty) \exp(-k_{obs}\, t) \tag{4.1}$$

where; A_0 is initial absorbance of the mixture, A_t is absorbance of the reaction mixture at time, t and A_∞ is final absorbance.

The rate of nucleophilic attack by the thiourea nucleophiles was measured by varying the concentration of the nucleophile at 25° C. The average value of the observed rate constant, k_{obs}, were plotted against [Nu] according to Equation 4.2. Linear plots of k_{obs} verses $[Nu]$ were obtained for all reactions and typical plots are shown in Figure 4.4 for the substitution reactions of **C2** with the thiourea nucleophiles at 298K

$$k_{obs} = k_2[Nu] + k_s \approx k_2[Nu] \tag{4.2}$$

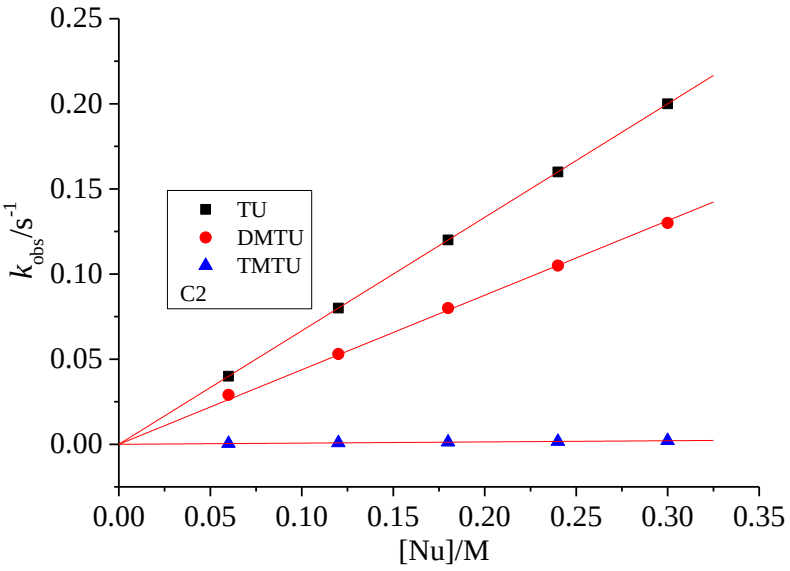

Figure 4. 4 Concentration dependence plots for reactions of **C2** and thiourea nucleophiles at 298 K

The slopes represent the second order rate constants, k_2, of the reaction of the respective nucleophile with **C2**. Other concentration dependence plots are presented in the

supplementary information Figures SI 4.16, 4.17, 4.19, 4.20, 4.22 and 4.24. Data of k_{obs} and respective nucleophile concentrations is presented in supplementary information Tables SI 4.1, 4.2, 4.4, 4.6, 4.8, 4.10.

Mechanism of substitution

The proposed mechanism of substitution of the chloro ligands from the Ru(II) complexes is illustrated in Scheme 4.1.

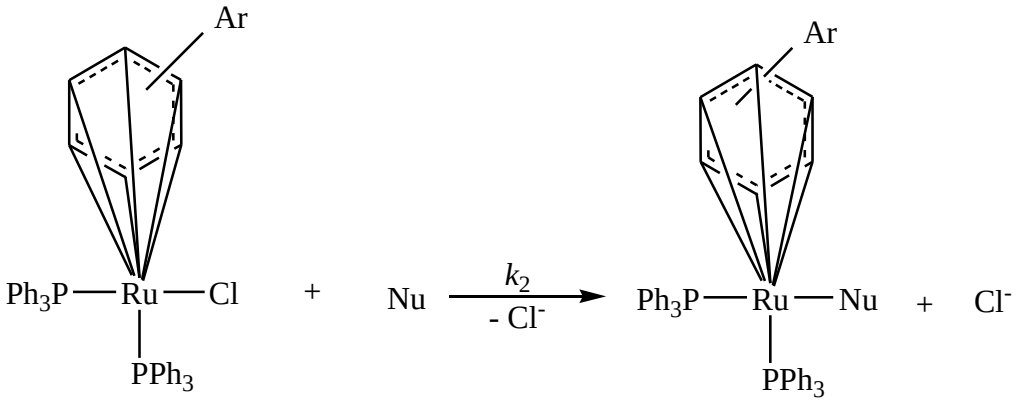

Ar. = Benzene (**C1**)or cyclopentadienyl(**C2**), Nu = TU, DMTU, TMTU

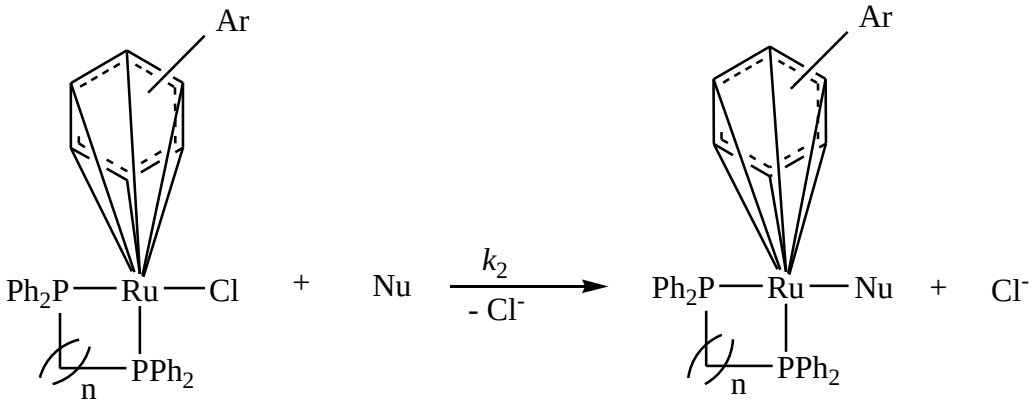

Ar. = cyclopentadienyl, n = 1(**C4**) or Benzene, n = 1(**C3**) or 2(**C5**) or 3(**C6**), Nu = TU, DMTU, TMTU

Scheme 4. 1 The mechanism of substitution of the complexes with thiourea nucleophiles

The rate constants were also measured over the temperature range of 25-45 °C in increments of 5° C. Graphs of $\ln(k_2/T)$ verses $1/T$ were plotted in accordance to the Eyring equation (Equation 4.3). Typical Eyring plots are shown in Figure 4.5 for the reaction of **C6** with the thiourea nucleophiles.

$$\ln\left(\frac{k_{exp}}{T}\right) = \frac{-\Delta H^{\neq}}{R}.\frac{1}{T} + \left[23.8 + \frac{\Delta S^{\neq}}{R}\right] \qquad (4.3)$$

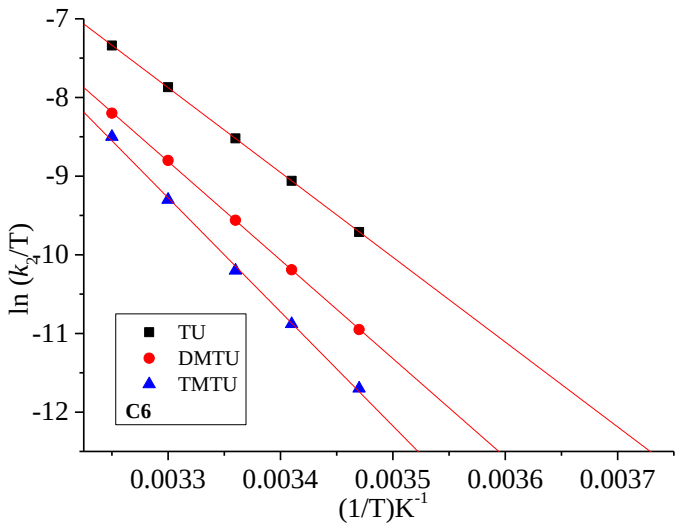

Figure 4. 5 Eyring plots for the reactions of **C6** with the thiourea nucleophiles

The enthalpy of activation, $\Delta H^{\neq}$, and entropy of activation, $\Delta S^{\neq}$, were calculated from the slope and the intercept of the Eyring plots. Other Eyring plots are presented in the supplementary information Figures SI 4.18, 4.21, 4.23 and 4.25. Data used for Eyring plots is presented in the supplementary information Tables SI 4.3, 4.5, 4.7, 4.9, 4.11. The values of k_2, $\Delta H^{\neq}$ and $\Delta S^{\neq}$ are summarise in Table 4.3.

Table 4. 3 Second order rate constants and activation parameters for the reactions

Complexes		Nu.	k_2 /10^{-2} M^{-1} s^{-1}	$\Delta H^{\neq}$ /kJ mol^{-1}	$\Delta S^{\neq}$ /$K^{-1}mol^{-1}$
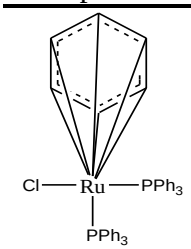	**C1**	TU	41.2 ± 0.1	117 ± 3	62 ± 8
		DMTU	27.4 ± 0.03	123 ± 1	109 ± 4
		TMTU	4.9 ± 0.01	129 ± 4	132 ± 13
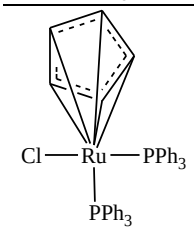	**C2**	TU	66.7 ± 0.01	100 ± 0.3	52 ± 1
		DMTU	43.8 ± 0.04	115 ± 0.4	101 ± 1
		TMTU	0.7 ± 0.001	123 ± 0.5	127 ± 2
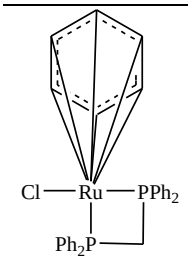	**C3**	TU	31.0 ± 0.1	100 ± 2	60 ± 7
		DMTU	10.2 ± 0.1	111 ± 1	93 ± 3
		TMTU	2.0 ± 0.01	140 ± 2	160 ± 7
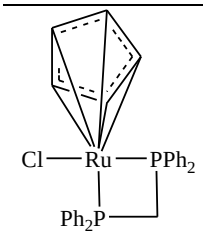	**C4**	TU	2.0 ± 0.1	103 ± 1	68 ± 4
		DMTU	0.4 ± 0.01	118 ± 0.7	94 ± 2
		TMTU	0.1 ± 0.01	143 ± 0.8	167 ± 3
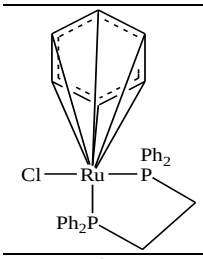	**C5**	TU	1998.0 ± 1	96 ± 0.5	53 ± 2
		DMTU	442.0 ± 1	111 ± 0.7	93 ± 2
		TMTU	559.0 ± 0.1	128 ± 1	139 ± 5
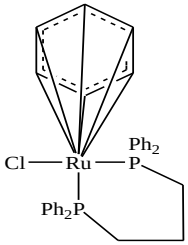	**C6**	TU	2796.0 ± 10	90 ± 0.2	32 ± 1
		DMTU	1550.0 ± 3	104 ± 1	73 ± 2
		TMTU	204.0 ± 1	121 ± 2	123 ± 8

4.2.3 Origin of Steric hindrance in the complexes

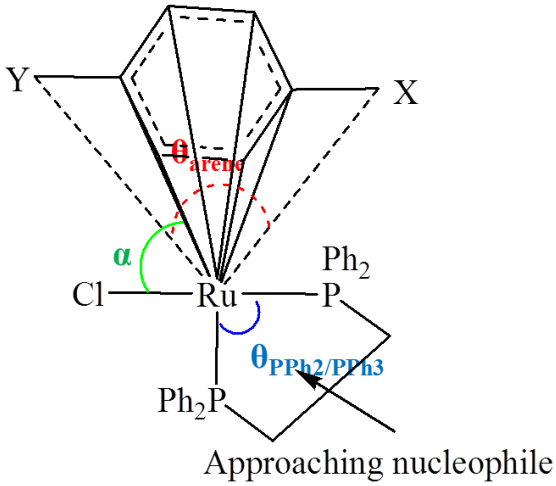

X and Y = H

Figure 4. 6 Chemical structure of complex **C5** illustrating atomic numbering and 'cone angles'

The electronic and steric properties of the phosphine ligands have been found to dramatically influence the reactivity of organometallic complexes.[50] [51] Tolman introduced the concept of "cone angle" as a quantitative measure of the steric hindrance of triphenylphosphine ligands in Ru metal complexes.[52] In the current study, the "cone angle" can be seen in two ways either as a projected electrostatic effect define by angle θ_{arene} in respect of the head of the arene π-electron cloud or as projected angle $\theta_{PPh2/PPh3}$ in respect of the head of the π-electron cloud of the coordinated phosphine ligands as shown in Figure 4.6.[53] In Ru(II) complexes with diphenylphosphine ligands, it has been estimated that the optimum range for the project angle $\theta_{PPh2/PPh3}$ (P-Ru-P) should lie between 90 ° and 101 °. Any deviation from this range causes steric strain in the complex resulting in higher steric hindrance.[50] [52] [53]

When angle θ_{arene} increases, the projected "cone" occupies a larger area causing increased steric hindrance at the Ru metal centre.[53] Steric demands for bidentate phosphine ligands have been modelled and have proven valuable in predicting reactivity trends.[54] The chelates in which diphenylphosphine groups are linked by long flexible polymethylene chain have been observed to form octahedral *trans*-complexes involving phosphine leading to *trans*-effect in such complexes depending on the nature of the other ligands.[50] [55] In case of the

one carbon methylene chain in diphenylphospshinomethane as in **C3** and **C4,** the complexes are normally strained due to smaller angle $\theta_{PPh2/PPh3}$ between them.[50] [56]

4.4 Discussion

The values of k_2 in the arene-Ru(II) complexes vary depending on the nature of the spectator ligands. The general trend of reactivity is as follows; **C6** > **C5** > **C2** > **C1** > **C3** > **C4**. The reactivity of the complexes will be discussed in groups, designated by arbitrary letters R, S and T. In the first group designated R (**C1, C2** and **C3**, **C4)**, the study seeks to look at the effect of varying the arene ligand on the reactivity. In group R, the difference between the structure of the complexes in each pair lies in the size of the π-electron cloud of the arene ligand. Considering the first pair, it is observed that **C2** has higher reactivity than **C1**. This is due to the smaller π- electron cloud of the cyclopentadiene arene in **C2** in comparison to that of the benzene arene in **C1**. This results in less electron donation by the arene in **C2** towards the metal centre leaving it relatively more electrophilic. Thus, during nucleophilic substitution **C2** is more stabilized in the transition state than **C1** and can accommodate the additional electron density from the incoming nucleophile better increasing reactivity.[57] [41] [40] This observation is supported by the lower DFT calculated Ru(II) NBO charges for **C2 (**-0.282) compared to that of **C1 (**-0.470) an indication that **C2** is more electrophilic than **C1**. This is also true for the electrophilicity indices where **C1** (5.825) has a lower value compared to **C2** (8.840). In addition the HOMO-LUMO energy gap and chemical hardness values for **C2** are smaller than those of **C1** supporting its higher reactivity.

The other factor that plays a role in this reactivity is the steric hindrance which is less in **C2** than in **C1** as measured by the sizes of the arene ligands. The projected Tolman's cone angles, θ_{arene}, on to the site of substitution for **C2** (91.7°) is smaller than **C1** (131.4°). Because of this, the molecular interactions between the triphenylphosphine results in wider P-P separation distances, being wider in **C2** (4.101 Å) compared to that in **C1** (3.767 Å). This is an indication that **C1** is more sterically hindered at the Ru metal centre, leading to lower rates of substitutions.

When the reactivity of **C3** is compared to **C4**, the former is more reactive than the later. Unlike **C1** and **C2**, both the complexes have a bis(diphenylphosphino)methane bidentate ligand. Their structures differ only in their arene groups.[58] [59] A reversal in the reactivity trend which was observed for the **C1**/**C2** pair is noted and can be accounted for by the steric

demands of the bidentate ligand. [60] [61] This causes angle α between the arene and the chloro to deviate from 90° by 11° in **C2** leaning towards the phosphines. This spatially blocks the path of the incoming nucleophile, resulting in lower reactivity. In case of **C3**, the deviation is smaller at 3°. In both sets of complexes in group R, the systems with monodentate triphenylphosphine ligands are more reactive than those having the bidentate bis(diphenylphosphino)alkane ligands i.e. **C1** and **C2** are more reactive than their respective analogues, **C3** and **C4**, respectively.

These complexes are regrouped as **C1**, **C3** or **C2**, **C4** denoted as S to investigate how the reactivity is influenced by the introduction of the bis(diphosphino)methane to the arene ruthenium(II) systems. The two pairs of complexes **C1**, **C3** and **C2**, **C4** have benzene and cyclopentadienyl heads respectively. The important feature of bis(diphenylphosphine)-methane chelate ligand that has been observed in other studies which is at play here is its *cis*-orientation to the labile chloro ligand.[50] [62] Its strong σ-electron donor effect lowers the electrophilicity of **C3** and **C4** relative to that of **C1** and **C2,** respectively. This lowers the reactivity of the former pair. This is in agreement with the DFT calculated NBO charges and electrophilicity indices ions; for which **C1** and **C2** have higher calculated NBO charges and electrophilicity indices hence are more positive and more reactive than **C3** and **C4**. Also in support of the observed reactivity trend is the lower HOMO-LUMO energy gap and chemical hardness for **C1**, **C2** than those of **C3**, **C4**.

Sterically, the data shows that the P-P distances are shorter and angle, A, smaller in **C3** and **C4** which means that these complexes experience more steric hindrance thereby lowering their reactivity compared to that of **C1** and **C2**. The spatial P-P distance is larger in **C1** and **C2** to minimize repulsion between the triphenyl groups compared to **C3** and **C4** where there are only two phenyl rings on each phosphine with a short bidentate diphosphinoalkyl chelate. What is also noted is that there is a drop in reactivity of the order of 10 between **C2** and **C4**. The reason for this is similar to those stated in group R.

The results of the Ru(II) complexes in group T show that the reactivity decreases as follows, **C6** > **C5** > **C1** > **C3**. The ligand systems of these complexes vary from the triphenylphosphine monodentate ligand in **C1** to the bis(diphenylphosphino)alkane bidentate ligands in **C3**, **C5** and **C6**. The reactivity between **C1** and **C3** has been explained in the previous section to be due to both electronic and steric factors with steric effect being

dominant due to the rigid bis(diphenylphosphino)methane ring around the Ru(II) metal centre in **C3**. The reactivity increases by a factor of 10^3 as the length of the ring increases from **C3** to **C6**. This huge increase is not electronic in nature as confirmed by the insignificant change in the DFT calculated NBO charges and electrophilicity indices. This indicates that the bis(diphenylphosphino)alky ligands have minimal effect in electron donation to the ruthenium centre through the phosphines. It is observed that along the series from **C3** to **C6**, there is successive increase in the P-P distances and angles, $\theta_{PPh2/PPh3}$, and a decrease in angle α. The outcome of this is a decrease in steric hindrance and creation of a trough like orientation that traps the incoming nucleophiles resulting in the high reactivity observed. This entrapment phenomenon has been reported in literature for platinum systems.[63] [64]

The enthalpies of activation values were large while the entropies of activation values were positive. This is a clear indication of the dissociative activated interchange mechanism ($\boldsymbol{I_D}$). Most organometallic Ru(II) complexes tend to react via dissociatively activated pathways.[61] Ru metal centres of the studied complexes have a high negative charge density due to the high σ/ andπ-donor effect of the attached ligand groups. However, coordination of strong π-acceptor ligands which accept electron density from the metal centre switches the activation to an associative interchange. The effect of π–back bonding is the increase charge on the Ru(II), thus partially oxidising to Ru(III) character.[61] [65] [66] This favours nucleophilic substitution. Hofman *et. al.* have also observed that reactions with some dissociative character benefit mostly from electron donors.[67] [68] [69] [70] [62] In this study, the Ru metal centre has a high negative charge density due to the high donor effect of the attached ligand groups making it adopt dissociative activated interchange mechanism ($\mathbf{I_D}$). The reactivity of the nucleophiles was influenced purely by steric demands and the order is as follows, TU > DMTU > TMTU. The trend in reactivity of the nucleophiles was replicated in all the complexes studied.

4.5 Conclusions

The reactivity of the Ru complexes is controlled by the electronic nature and steric hindrance due to the spectator ligands. Varying the the arene from benzene to cyclopentadienyl as happens from **C1** and **C3** lowers electron density donated towards the Ru centre. This also reduces the space occupied by the arene by narrowing the cone angle, θ_{arene}. As a result, the reactivity for **C1** is lower than **C2** due to a more negatively charged metal centre in **C1.** Introduction of the bidentate bis(diphenylphosphino)methane ligand around the Ru decreases

the phosphorus-phosphorus separation distance and angle $\theta_{PPh2/PPh3}$ between the phosphorus atoms. This results in the narrowing of the path of the incoming nucleophile which slows the reactivity. When the size of the ring formed by the bis(diphenylphosphino)alkane and Ru is increased, the substitution of the co-labile ligand is increased. An increase in P-P distance and the expansion of angle $\theta_{PPh2/PPh3}$, decrease the steric hindrance around Ru and results in the creation of a trough that traps the nucleophiles enhancing the reactivity. The observed reactivity trends are supported by DFT calculations. The mechanism of reactivity of these complexes is dissociative activated interchange mechanism ($\mathbf{I_D}$) which is mostly due to the steric nature around the ruthenium complex.

4.6 References

[1] M. Galanski, M. A. Jakupec, B. K. Keppler, *Current Medicinal Chemistry* **2005**, *12*, 2075-2094.

[2] Z. H. Siddik, *Oncogene* **2003**, *22*, 7265-7279.

[3] M. Markman, *Expert opinion on drug safety* **2003**, *2*, 597-607.

[4] P. C. Bruijnincx, P. J. Sadler, *Current opinion in chemical biology* **2008**, *12*, 197-206.

[5] D. Wesselinova, N. Kaloyanov, G. Dimitrov, *Journal of Medicinal Chemistry* **2009**, *44*, 5099-5102.

[6] C. Scolaro, A. B. Chaplin, C. G. Hartinger, A. Bergamo, M. Cocchietto, B. K. Keppler, G. Sava, P. J. Dyson, *Dalton Transactions* **2007**, 5065-5072.

[7] K. K.-W. Lo, T. K.-M. Lee, *Inorganic Chemistry* **2004**, *43*, 5275-5282.

[8] J. Canivet, G. Suss-Fink, *Green Chemistry* **2007**, *9*, 391-397.

[9] S. K. Singh, S. Joshi, A. R. Singh, J. K. Saxena, D. S. Pandey, *Inorganic Chemistry* **2007**, *46*, 10869-10876.

[10] H. K. Liu, P. J. Sadler, *Accounts of chemical research* **2011**, *44*, 349-359.

[11] O. Novakova, J. Kasparkova, V. Bursova, C. Hofr, M. Vojtiskova, H. Chen, P. J. Sadler, V. Brabec, *Chemistry and Biology* **2005**, *12*, 121-129.

[12] N. Olga, M. Jaroslav, S. Tereza, K. Jana, B. Tijana, S. P. J., B. Viktor, *Chemistry – A European Journal* **2010**, *16*, 5744-5754.

[13] R. E. Morris, R. E. Aird, S. Murdoch Pdel, H. Chen, J. Cummings, N. D. Hughes, S. Parsons, A. Parkin, G. Boyd, D. I. Jodrell, P. J. Sadler, *Journal of Medicinal Chemistry* **2001**, *44*, 3616-3621.

[14] S. W. Magennis, A. Habtemariam, O. Novakova, J. B. Henry, S. Meier, S. Parsons, I. D. H. Oswald, V. Brabec, P. J. Sadler, *Inorganic Chemistry* **2007**, *46*, 5059-5068.

[15] O. Novakova, H. Chen, O. Vrana, A. Rodger, P. J. Sadler, V. Brabec, *Biochemistry* **2003**, *42*, 11544-11554.

[16] O. Novakova, J. Kasparkova, V. Bursova, C. Hofr, M. Vojtiskova, H. Chen, P. J. Sadler, V. Brabec, *Chemistry and Biology* **2005**, *12*, 121-129.

[17] T. Bugarcic, O. Nováková, A. Halámiková, L. Zerzánková, O. Vrána, J. Kašpárková, A. Habtemariam, S. Parsons, P. J. Sadler, V. Brabec, *Journal of Medicinal Chemistry* **2008**, *51*, 5310-5319.

[18] R. E. Aird, J. Cummings, A. A. Ritchie, M. Muir, R. E. Morris, H. Chen, P. J. Sadler, D. I. Jodrell, *British journal of cancer* **2002**, *86*, 1652-1657.

[19] S. Chatterjee, S. Kundu, A. Bhattacharyya, C. G. Hartinger, P. J. Dyson, *Journal of Biological Inorganic Chemistry* **2008**, *13*, 1149-1155.

[20] Y. Liu, R. Hammitt, D. A. Lutterman, L. E. Joyce, R. P. Thummel, C. Turro, *Inorganic Chemistry* **2009**, *48*, 375-385.

[21] K. S. M. Smalley, R. Contractor, N. K. Haass, A. N. Kulp, G. E. Atilla-Gokcumen, D. S. Williams, H. Bregman, K. T. Flaherty, M. S. Soengas, E. Meggers, M. Herlyn, *Cancer Research* **2007**, *67*, 209-217.

[22] Q. Wu, C. Fan, T. Chen, C. Liu, W. Mei, S. Chen, B. Wang, Y. Chen, W. Zheng, *European Journal of Medicina Chemistry* **2013**, *63*, 57-63.

[23] T. S. Morais, T. J. L. Silva, F. Marques, M. P. Robalo, F. Avecilla, P. J. A. Madeira, P. J. G. Mendes, I. Santos, M. H. Garcia, *Journal of Inorganic Biochemistry* **2012**, *114*, 65-74.

[24] M. Daniels, R. U. Kirss, *Journal of Organometallic Chemistry* **2007**, *692*, 1716-1725.

[25] R. Lalrempuia, P. Govindaswamy, Y. A. Mozharivskyj, M. R. Kollipara, *Polyhedron* **2004**, *23*, 1069-1073.

[26] V. Moreno, J. Lorenzo, F. X. Aviles, M. H. Garcia, J. P. Ribeiro, T. S. Morais, P. Florindo, M. P. Robalo, *Bioinorganic Chemistry and Applications* **2010**, *2010*, 936834.

[27] A. Valente, M. H. Garcia, F. Marques, Y. Miao, C. Rousseau, P. Zinck, *Journal of Inorganic Biochemistry* **2013**, *127*, 79-81.

[28] P. Florindo, I. J. Marques, C. D. Nunes, A. C. Fernandes, *Journal of Organometallic Chemistry* **2014**, *760*, 240-247.

[29] P. Kumar, R. K. Gupta, D. S. Pandey, *Chemical Society Reviews* **2014**, *43*, 707-733.

[30] in *Inorganic Syntheses*.

[31] R. A. Zelonka, M. C. Baird, *Canadian Journal of Chemistry* **1972**, *50*, 3063-3072.

[32] R. A. Gaussian, *Inc., Wallingford CT* **2009**, *121*, 150-166.

[33] A. D. Becke, *The Journal of chemical physics* **1993**, *98*, 5648-5652.

[34] P. J. Hay, W. R. Wadt, *The Journal of chemical physics* **1985**, *82*, 270-283.

[35] C. Lee, W. Yang, R. G. Parr, *Physical Review B* **1988**, *37*, 785.

[36] M. Okamura, M. Yoshida, R. Kuga, K. Sakai, M. Kondo, S. Masaoka, *Dalton Transactions* **2012**, *41*, 13081-13089.

[37] M. Cossi, N. Rega, G. Scalmani, V. Barone, *Journal of computational chemistry* **2003**, *24*, 669-681.

[38] T. Le Bahers, T. Pauporté, G. Scalmani, C. Adamo, I. Ciofini, *Physical Chemistry Chemical Physics* **2009**, *11*, 11276-11284.

[39] A. Shaira, D. Jaganyi, *Journal of Coordination Chemistry* **2014**, *67*, 2843-2857.

[40] P. K. Chattaraj, U. Sarkar, M. Elango, R. Parthasarathi, V. Subramanian, *arXiv preprint physics/0509089* **2005**.

[41] A. Cedillo, R. Contreras, *Journal of the Mexican Chemical Society* **2012**, *56*, 257-260.

[42] E. Seifert, American Chemical Society Publications, **2014**.

[43] R. G. Parr, W. Yang, Oxford University Press, New York, **1989**.

[44] P. Geerlings, F. De Proft, W. Langenaeker, *Chemical Reviews* **2003**, *103*, 1793-1874.

[45] S. B. Jensen, S. J. Rodger, M. D. Spicer, *Journal of Organometallic Chemistry* **1998**, *556*, 151-158.

[46] S. Sangilipandi, D. Sutradhar, K. Bhattacharjee, W. Kaminsky, S. R. Joshi, A. K. Chandra, K. M. Rao, *Inorganica Chimica Acta* **2016**, *441*, 95-108.

[47] M. I. Bruce, I. R. Butler, W. R. Cullen, G. A. Koutsantonis, M. R. Snow, E. R. T. Tiekink, *Australian Journal of Chemistry* **1988**, *41*, 963-969.

[48] R. T. Hembre, J. S. McQueen, V. W. Day, *Journal of the American Chemical Society* **1996**, *118*, 798-803.

[49] M. Sato, M. Asai, *Journal of organometallic chemistry* **1996**, *508*, 121-127.

[50] C. P. Casey, G. T. Whiteker, *Israel journal of chemistry* **1990**, *30*, 299-304.

[51] B. Dutta, C. Scolaro, R. Scopelliti, P. J. Dyson, K. Severin, *Organometallics* **2008**, *27*, 1355-1357.

[52] C. A. Tolman, *Chemical Reviews* **1977**, *77*, 313-348.

[53] P. C. Möhring, N. J. Coville, *Journal of organometallic chemistry* **1994**, *479*, 1-29.

[54] M. T. Ashby, V. S. Asirvatham, A. S. Kowalski, M. A. Khan, *Organometallics* **1999**, *18*, 5004-5016.

[55] A. Rilak, I. Bratsos, E. Zangrando, J. Kljun, I. Turel, Ž. D. Bugarčić, E. Alessio, *Inorganic Chemistry* **2014**, *53*, 6113-6126.

[56] A. Habtemariam, M. Melchart, R. Fernández, S. Parsons, I. D. H. Oswald, A. Parkin, F. P. A. Fabbiani, J. E. Davidson, A. Dawson, R. E. Aird, *Journal of medicinal chemistry* **2006**, *49*, 6858-6868.

[57] M. C. Rezende, D. Millán, *Journal of the Brazilian Chemical Society* **2011**, *22*, 2078-2086.

[58] D. Michael, P. Mingos, P. C. Minshall, M. B. Hursthouse, K. M. A. Malik, S. D. Willoughby, *Journal of Organometallic Chemistry* **1979**, *181*, 169-182.

[59] J. A. Ibers, *Journal of Organometallic Chemistry* **1974**, *73*, 389-400.

[60] L. Dadci, H. Elias, U. Frey, A. Hoernig, U. Koelle, A. E. Merbach, H. Paulus, J. S. Schneider, *Inorganic Chemistry* **1995**, *34*, 306-315.

[61] F. Wang, H. Chen, S. Parsons, I. D. H. Oswald, J. E. Davidson, P. J. Sadler, *Chemistry–A European Journal* **2003**, *9*, 5810-5820.

[62] A. Hofmann, L. Dahlenburg, R. van Eldik, *Inorganic chemistry* **2003**, *42*, 6528-6538.

[63] A. Mambanda, D. Jaganyi, S. Hochreuther, R. van Eldik, *Dalton transactions* **2010**, *39*, 3595-3608.

[64] F. Wang, J. Xu, K. Wu, S. K. Weidt, C. L. Mackay, P. R. R. Langridge-Smith, P. J. Sadler, *Dalton Transactions* **2013**, *42*, 3188-3195.

[65] J. Chang, S. Meyerhoffer, L. R. Allen, B. Durham, J. L. Walsh, *Inorganic Chemistry* **1988**, *27*, 1602-1607.

[66] I. Rapaport, L. Helm, A. E. Merbach, P. Bernhard, A. Ludi, *Inorganic Chemistry* **1988**, *27*, 873-879.

[67] M. H. V. Huynh, J. M. Lasker, M. Wetzler, B. Mort, L. F. Szczepura, L. M. Witham, J. M. Cintron, A. C. Marschilok, L. J. Ackerman, R. K. Castellano, D. L. Jameson, M. R. Churchill, A. J. Jircitano, K. J. Takeuchi, *Journal of the American Chemical Society* **2001**, *123*, 8780-8784.

[68] M. H. V. Huynh, L. M. Witham, J. M. Lasker, M. Wetzler, B. Mort, D. L. Jameson, P. S. White, K. J. Takeuchi, *Journal of the American Chemical Society* **2003**, *125*, 308-309.

[69] C. A. Bessel, J. A. Margarucci, J. H. Acquaye, R. S. Rubino, J. Crandall, A. J. Jircitano, K. J. Takeuchi, *Inorganic Chemistry* **1993**, *32*, 5779-5784.

[70] R. A. Leising, J. S. Ohman, K. J. Takeuchi, *Inorganic Chemistry* **1988**, *27*, 3804-3809.

4.7 Supporting Information

Included in the electronic supplementary information (ESI) are NMR spectra, mass spectra, tables, and various kinetic graphs for the synthetic and kinetic analysis of the complexes *viz.* **C1, C2, C3, C4, C5** and **C6** investigated in this study.

4.7.1 Characterization

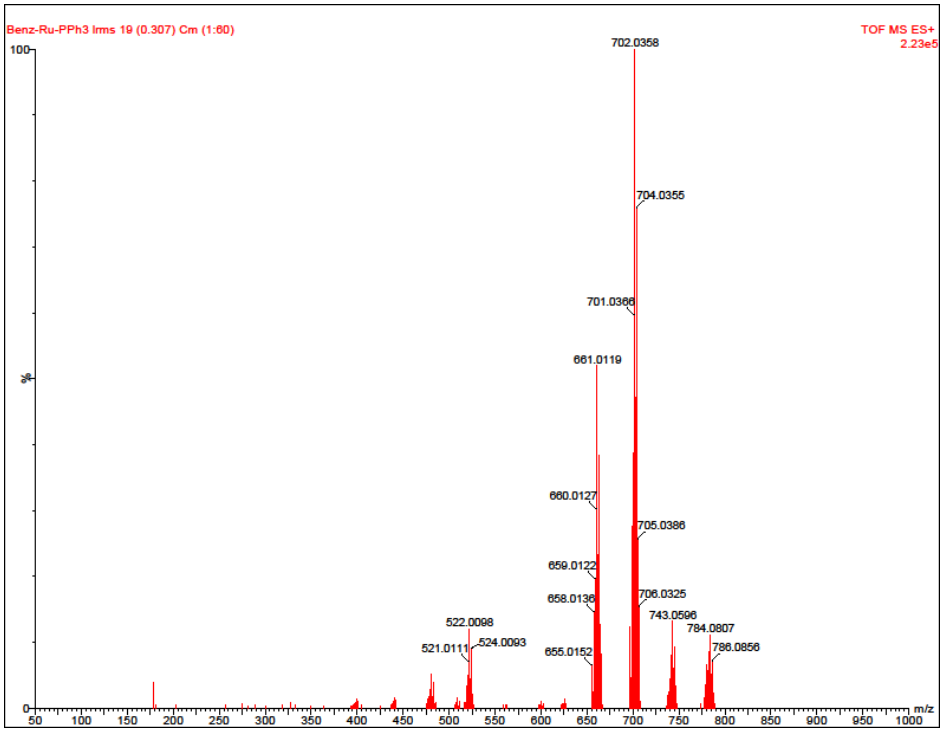

Figure SI 4.1 LC-MS Mass spectrum for **C1**

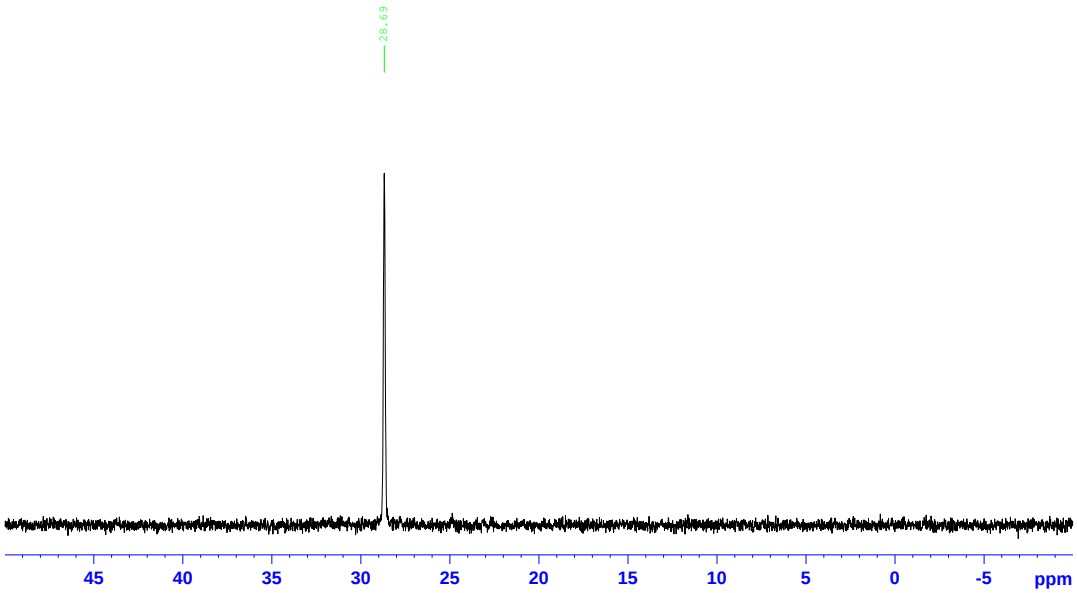

Figure SI 4.2 ^{31}P NMR spectrum for **C1**

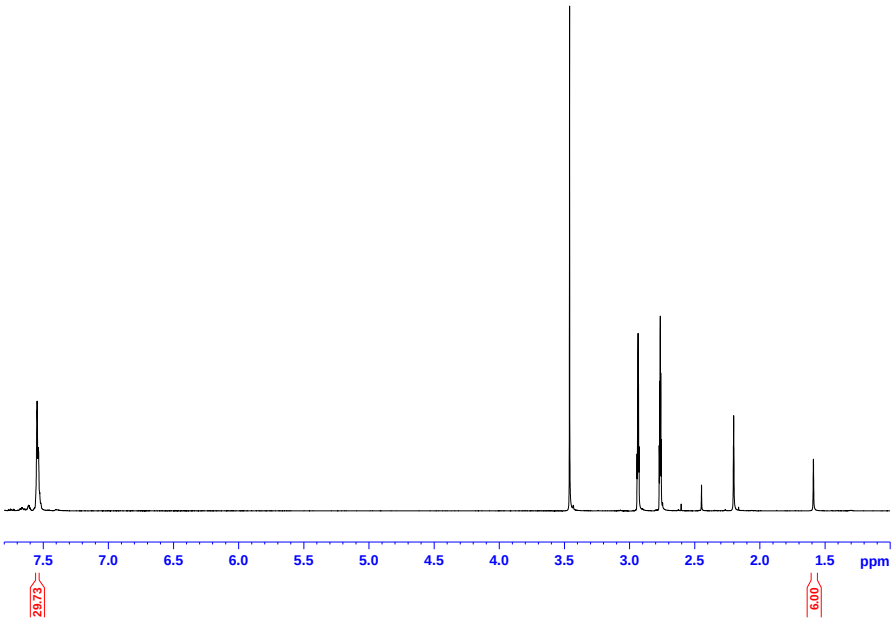

Figure SI 4.3 ^{1}H NMR spectra of **C1**

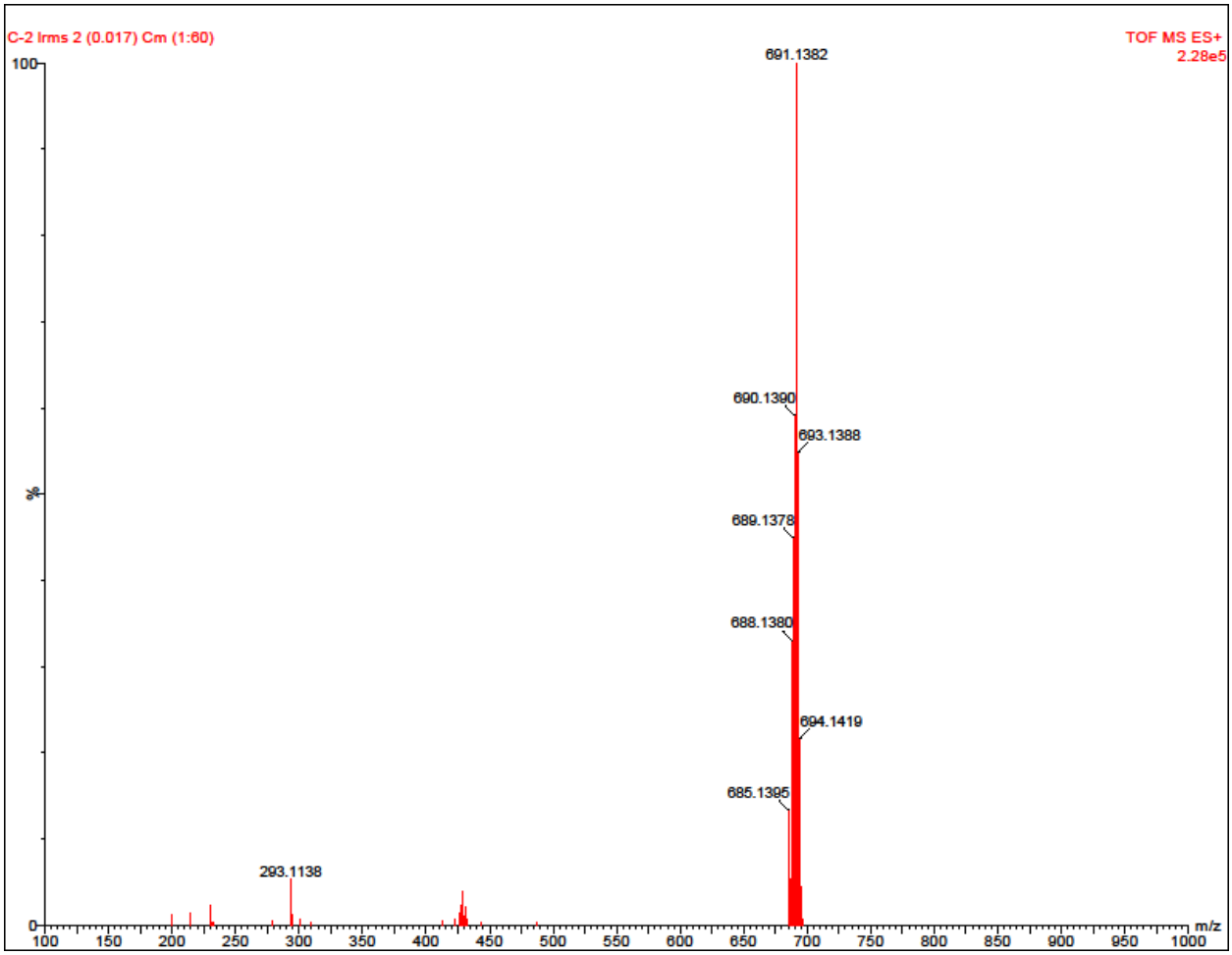

Figure SI 4.4 LC-MS Mass spectrum for **C2**

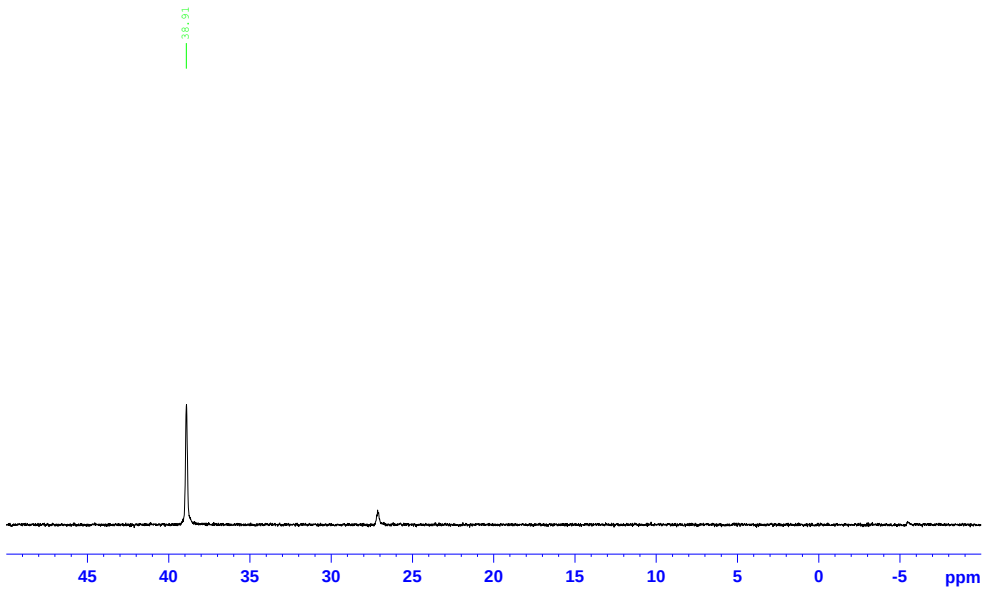

Figure SI 4.5 ^{31}P NMR spectrum for **C2**

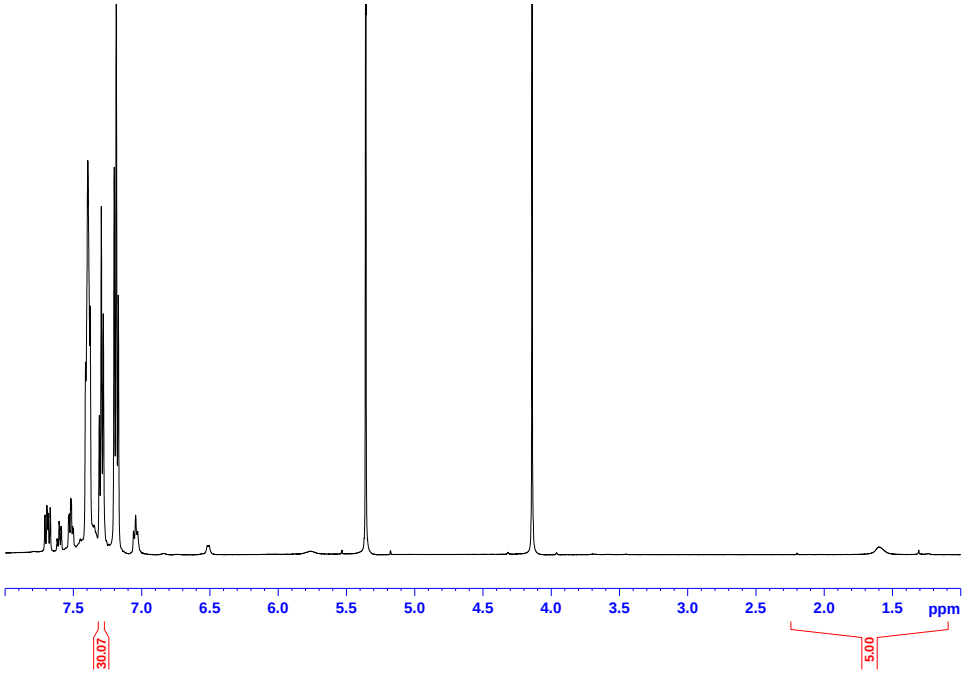

Figure SI 4.6 ^{1}H NMR spectra of **C2**

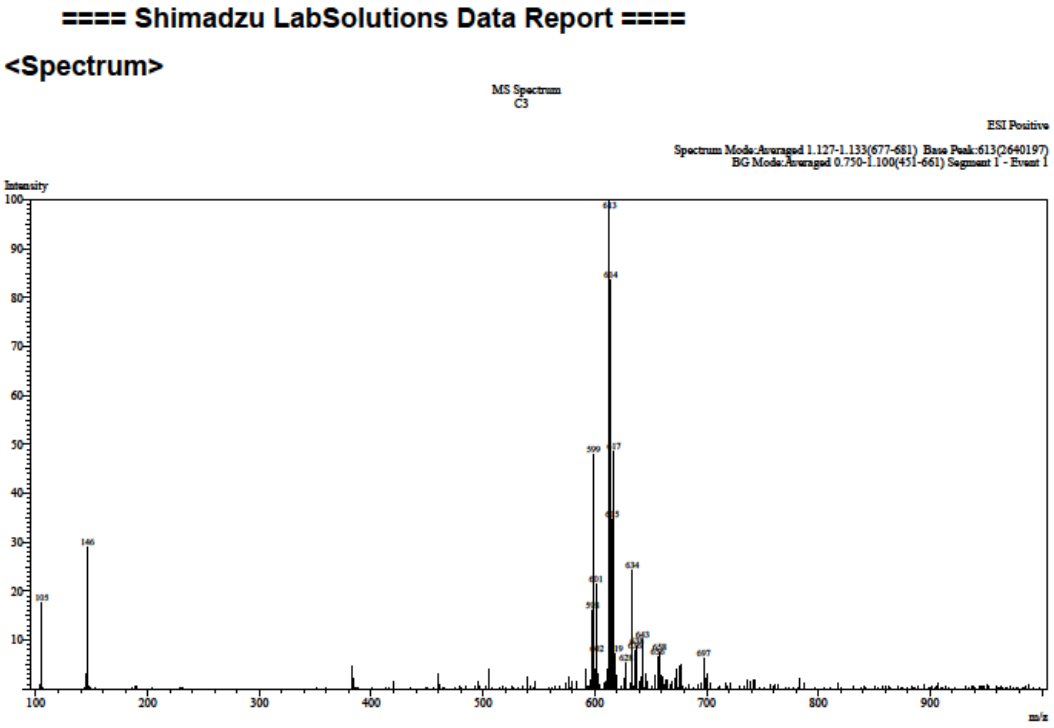

Figure SI 4.7 LC-MS Mass spectrum for **C3**

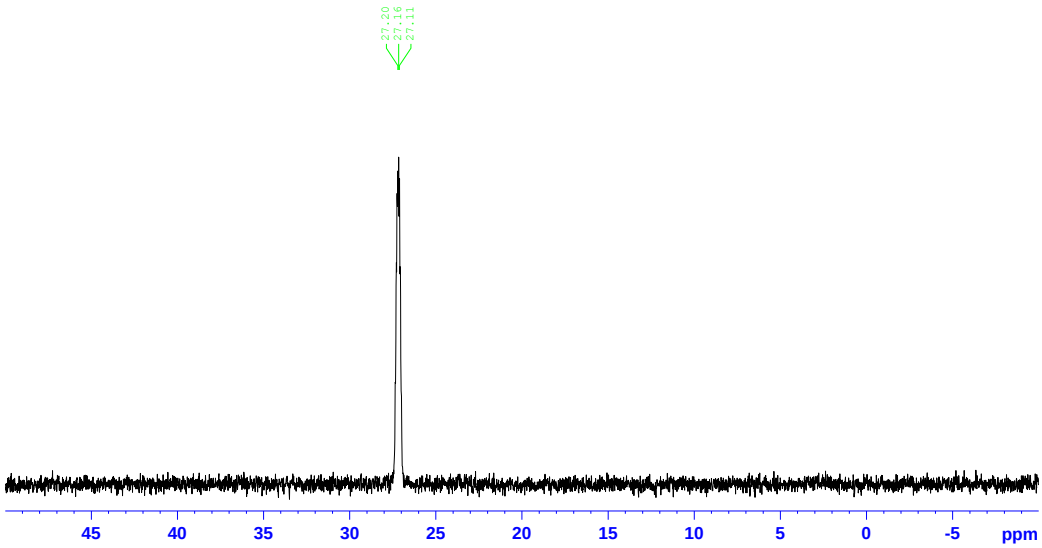

Figure 4.8 ^{31}P NMR spectrum for **C3**

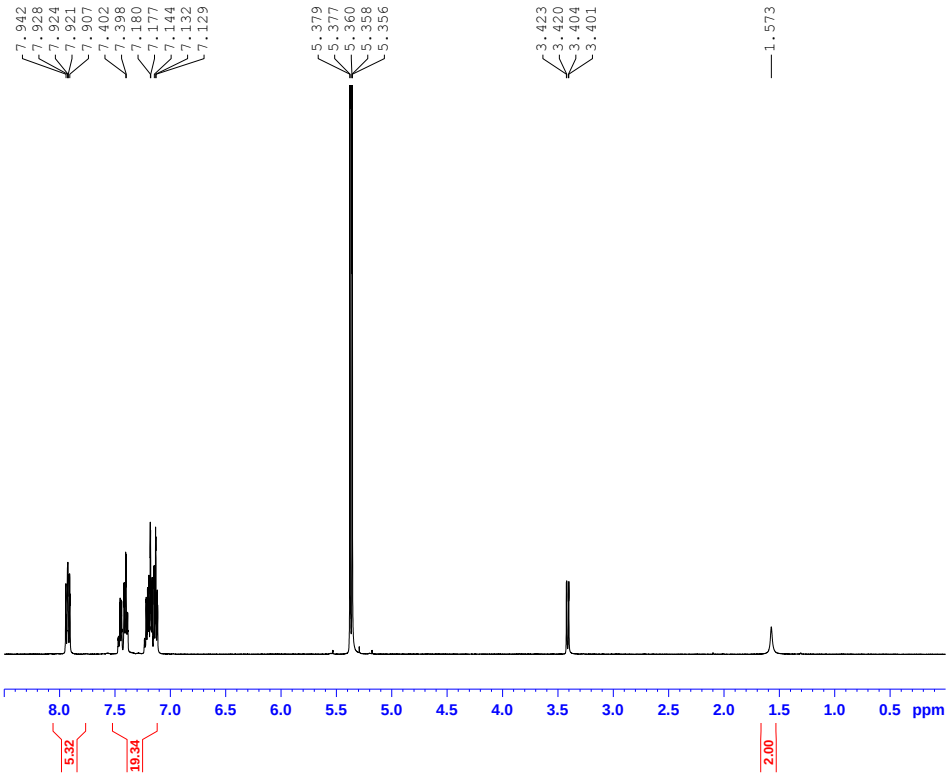

Figure SI 4.9 ^{1}H NMR spectra of **C3**

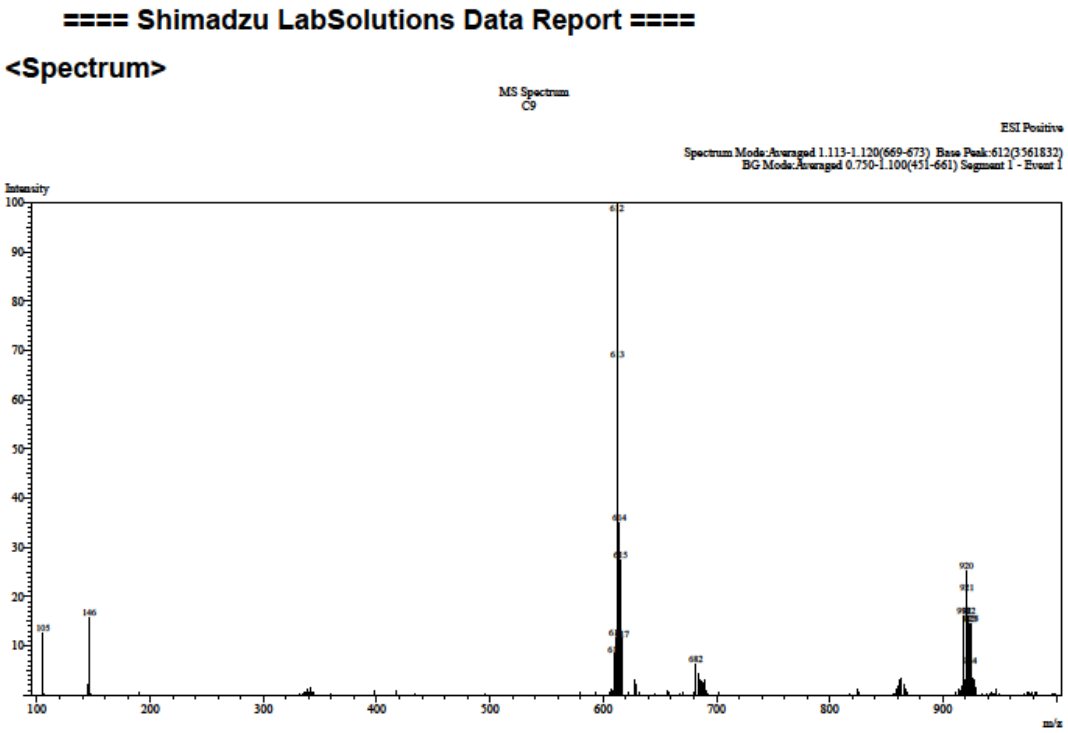

Figure SI 4.10 LC-MS Mass spectrum for **C5**

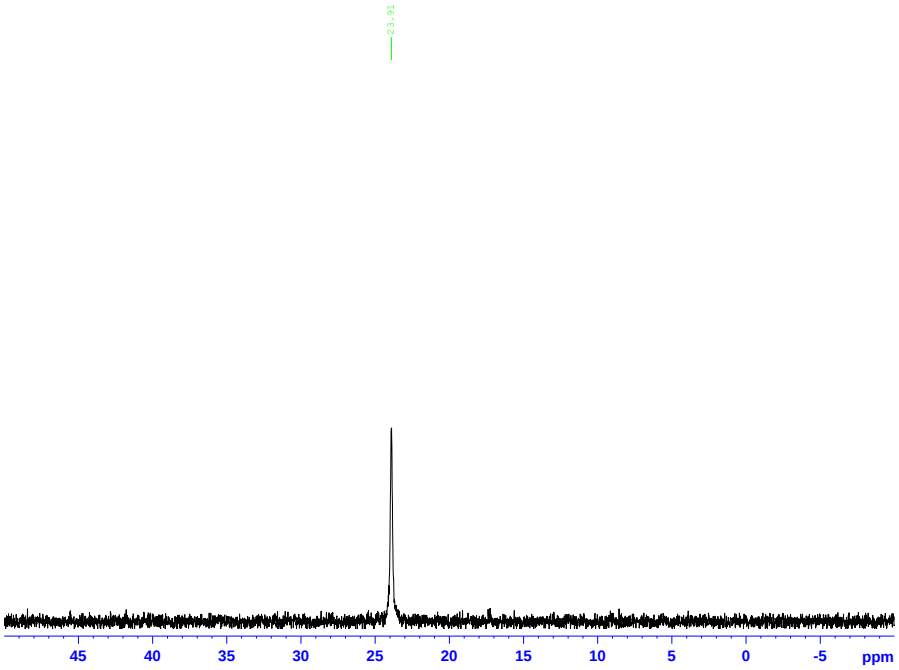

Figure SI 4.11 ^{31}P NMR spectrum for **C5**

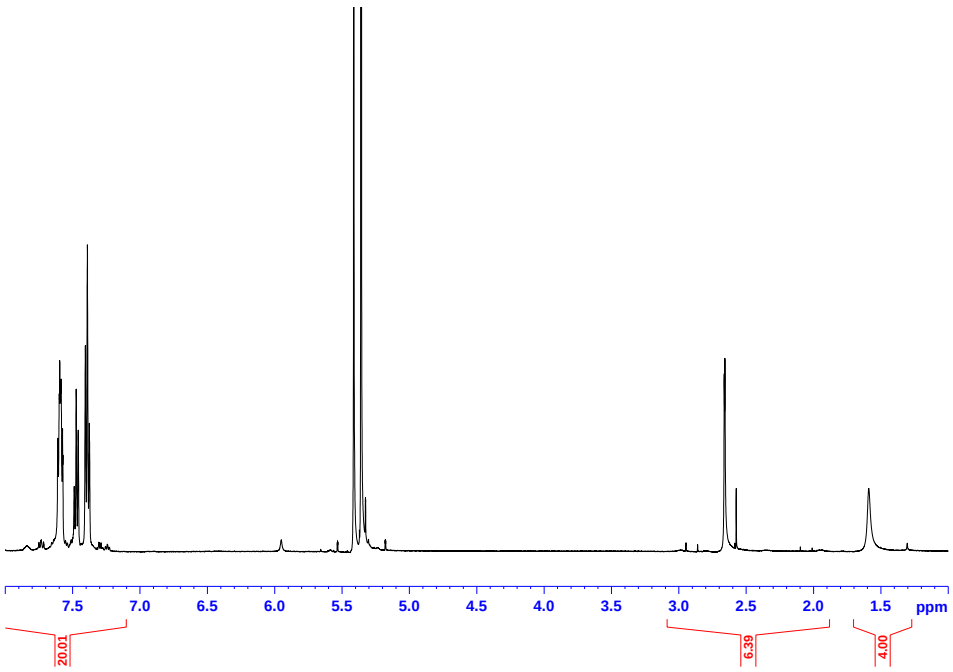

Figure SI 4.12 ^{1}H NMR spectra of **C5**

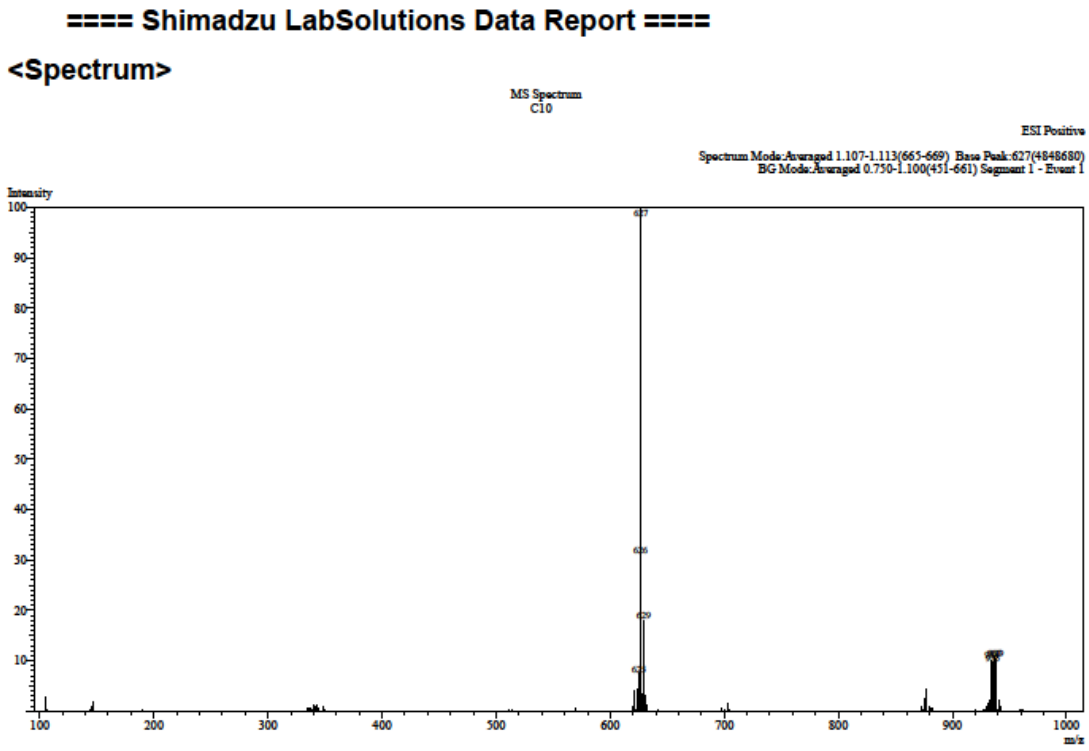

Figure SI 4.13 LC-MS Mass spectrum for **C6**

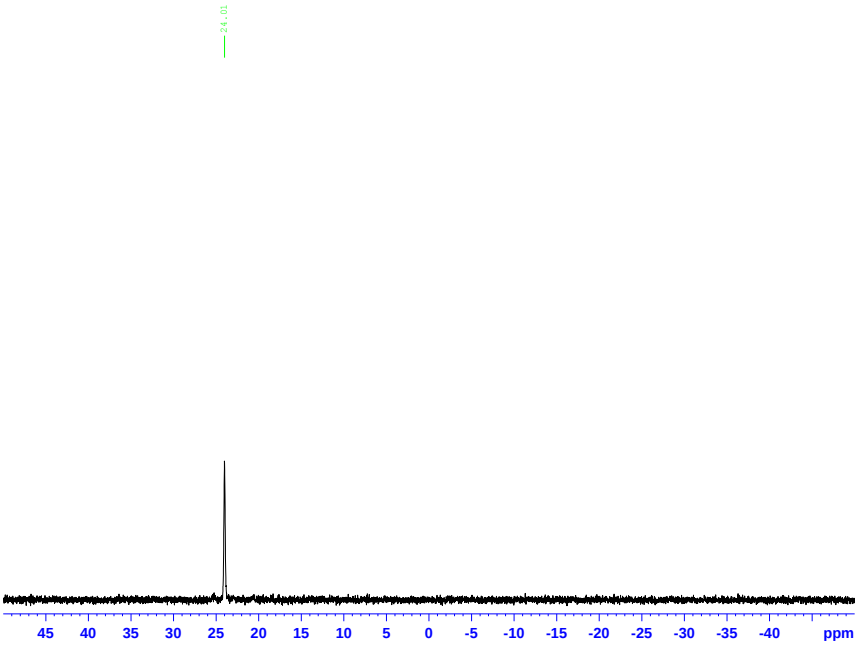

Figure SI 4.14 ^{31}P NMR spectrum for **C6**

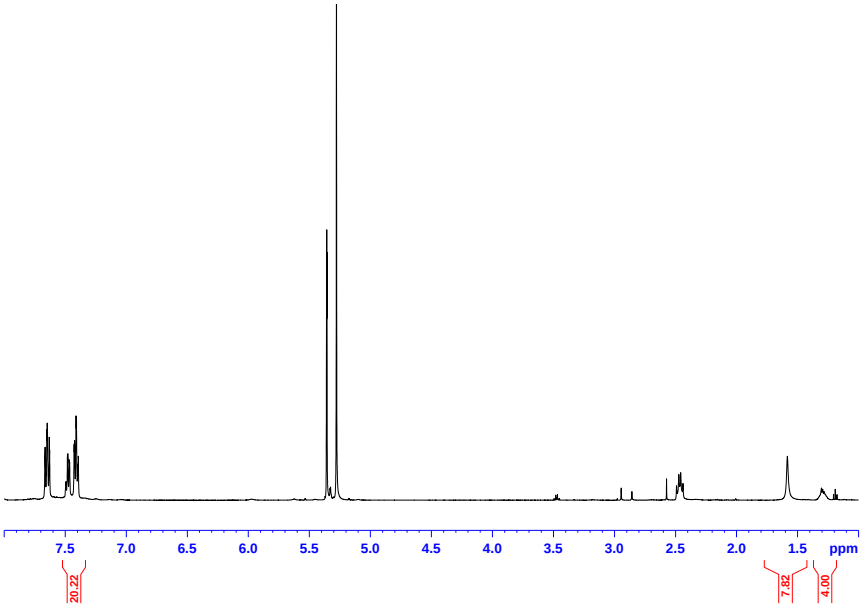

Figure SI 4.15 ^{1}H NMR spectra of **C6**

4.7.2 Kinetic data

(η^6-Benzene)chlorobis(triphenylphosphino)ruthenium(II) chloride (C1)

Table SI 4.1 Observed rate constants and the corresponding nucleophile concentrations for complex **C1**

[Nu]/M	k_{obs}/ s^{-1} TU	k_{obs} / s^{-1} DMTU	k_{obs} / s^{-1} TMTU
0.01	0.0038	0.00175	3.88E-4
0.02	0.00778	0.0035	7.75E-4
0.03	0.0117	0.0052	0.00115
0.04	0.0155	0.00694	0.00154
0.05	0.0193	0.00875	0.00194

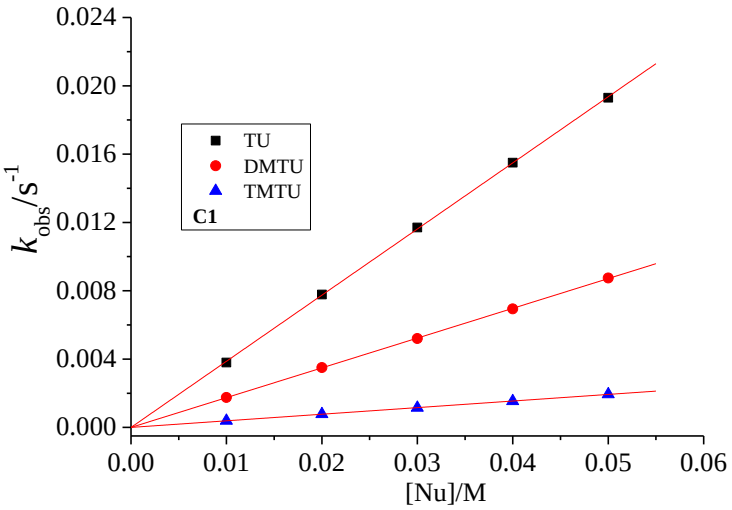

Figure SI 4.16 Concentration dependence plots for the reaction of **C1** with thiourea nucleophiles at 298 K

(η^5-cyclopentadienyl)chlorobis(triphenylphosphino)ruthenium(II) chloride (C2)

Table SI 4.2 Observed rate constants and the corresponding nucleophile concentrations for complex **C2**

[Nu]/M	**k_{obs} / s^{-1} TU**	**k_{obs} / s^{-1} DMTU**	**k_{obs} / s^{-1} TMTU**
0.06	0.04	0.029	4.2E-4
0.12	0.08	0.053	8.4E-4
0.18	0.12	0.080	0.00125
0.24	0.16	0.105	0.00167
0.3	0.2	0.13	0.0021

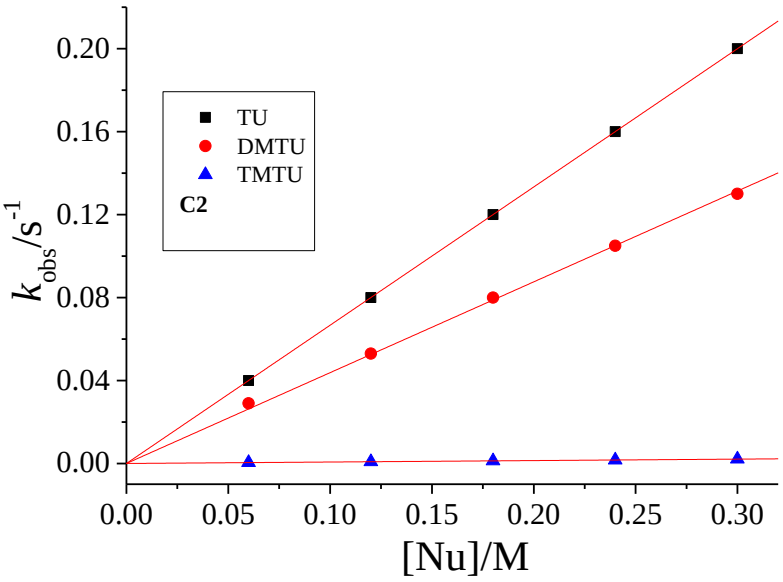

Figure SI 4.17 Concentration dependence plots for the reaction of **C2** with thiourea nucleophiles at 298 K

Table SI 4.3 Data of ln(k_2/T) and 1/T for complex **C2**

1/T	**ln(k_2/T) TU**	**ln(k_2/T) DMTU**	**ln(k_2/T) TMTU**
0.00336	-10.37	-10.55	-10.67
0.0033	-9.65	-9.72	-9.77
0.00325	-9.05	-9.05	-9.05
0.00319	-8.31	-8.21	-8.16
0.00314	-7.7	-7.52	-7.4

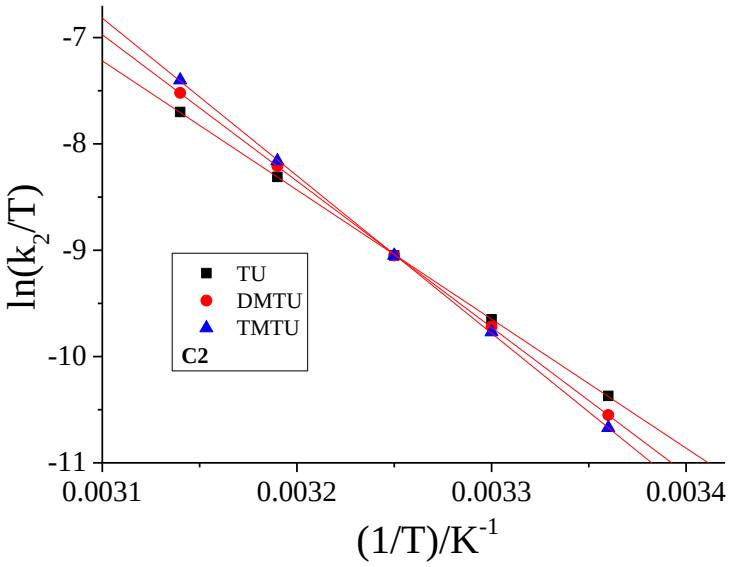

Figure SI 4.18 Eyring plots for the reaction of **C2** with thiourea nucleophiles

(η^6-Benzene)chloro{bis(diphenylphosphino)-methane} ruthenium(II) chloride (C3)

Table SI 4.4 Observed rate constants and the corresponding nucleophile concentrations for complex **C3**

[Nu]/M	k_{obs}/ s^{-1} TU	k_{obs} / s^{-1} DMTU	k_{obs} / s^{-1} TMTU
1E-3	3.1E-4	1.1E-4	2E-5
0.002	6.4E-4	2.15E-4	4E-5
0.003	9.6E-4	3.25E-4	6.1E-5
0.004	0.00125	4.3E-4	7.99E-5
0.005	0.00157	5.45E-4	1E-4

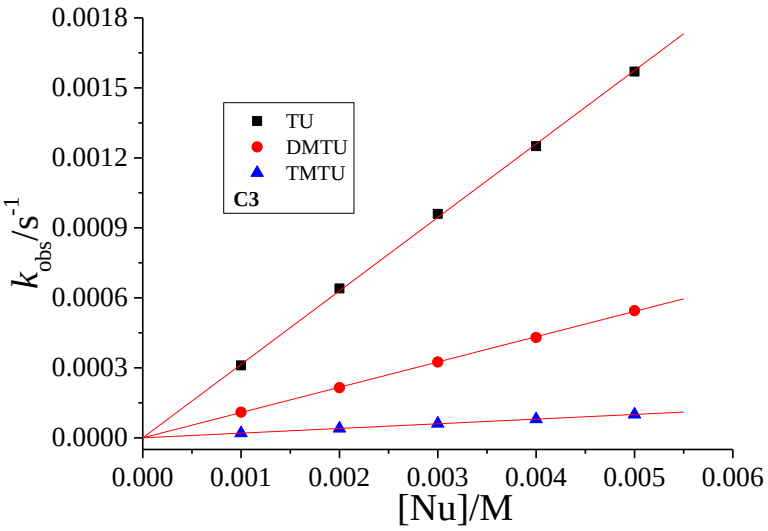

Figure SI 4.19 Concentration dependence plots for the reaction of **C3** with thiourea nucleophiles at 298 K

Table SI 4.5 Data of ln (k_2/T) and 1/T for complex **C3**

1/T	**ln(k_2/T) TU**	**ln(k_2/T) DMTU**	**ln(k_2/T) TMTU**
0.00347	-13.2	-13.48	-17.75
0.00341	-12.6	-12.86	-17
0.00336	-12.1	-12.36	-16.45
0.0033	-11.5	-11.75	-15.74
0.00325	-11	-11.24	-15.2

Chloro(cyclopentadienyl)[bis(diphenylphosphino)methane]ruthenium(II)

Table SI 4.6 Observed rate constants and the corresponding nucleophile concentrations for complex **C4**

[Nu]/M	k_{obs} / s^{-1} TU	k_{obs} / s^{-1} DMTU	k_{obs} / s^{-1} TMTU
0.036	7.2E-4	1.38E-4	3.3E-5
0.072	0.00144	2.7E-4	6.6E-5
0.108	0.00216	4.05E-4	9.9E-5
0.144	0.00288	5.4E-4	1.32E-4
0.18	0.0036	6.75E-4	1.65E-4

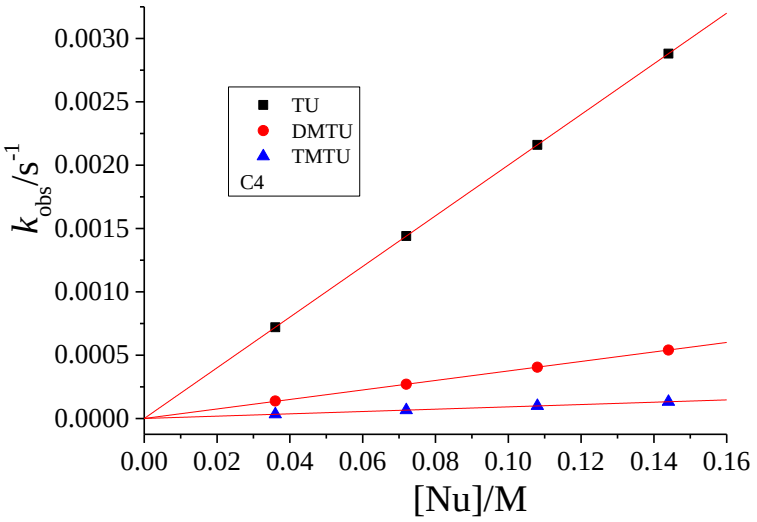

Figure SI 4.20 Concentration dependence plots for the reaction of **C4** with thiourea nucleophiles at 298 K

Table SI 4.7 Data of ln(k_2/T) and 1/T for complex **C4**

1/T	ln(k_2/T) TU	ln(k_2/T) DMTU	ln(k_2/T) TMTU
0.00336	-9.61	-12.52	-14
0.0033	-8.89	-11.66	-12.97
0.00325	-8.3	-10.93	-12.1
0.00319	-7.54	-10.1	-11.1
0.00314	-6.88	-9.4	-10.2

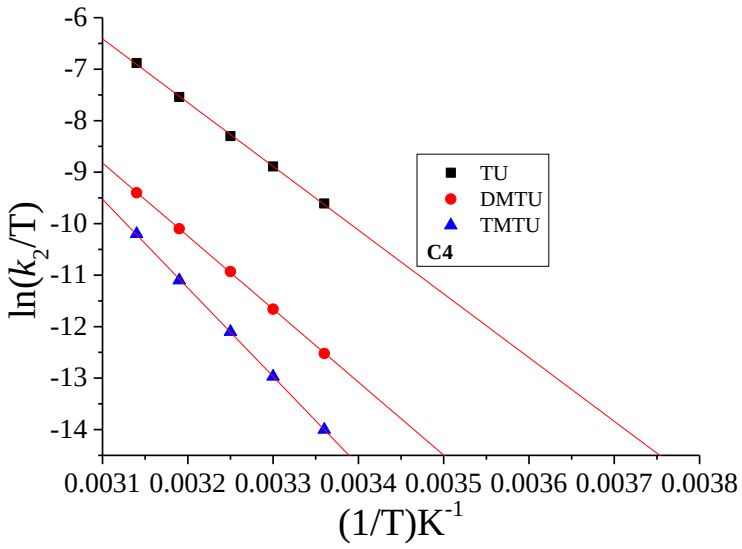

Figure SI 4.21 Eyring plots for the reaction of **C4** with thiourea nucleophiles

(η^6-Benzene)chloro{1,2-bis(diphenylphosphino)ethane}ruthenium(II) chloride (C5)

Table SI 4.8 Observed rate constants and the corresponding nucleophile concentrations for complex **C5**

[Nu]/M	k_{obs} / s^{-1} TU	k_{obs} / s^{-1} DMTU	k_{obs} / s^{-1} TMTU
5E-5	9.98E-4	0.00022	0.000028
1E-4	0.00200	0.00044	0.000056
1.5E-4	0.00300	0.00066	0.000083
2E-4	0.00400	0.00088	0.000112
2.5E-4	0.00499	0.00111	0.000140

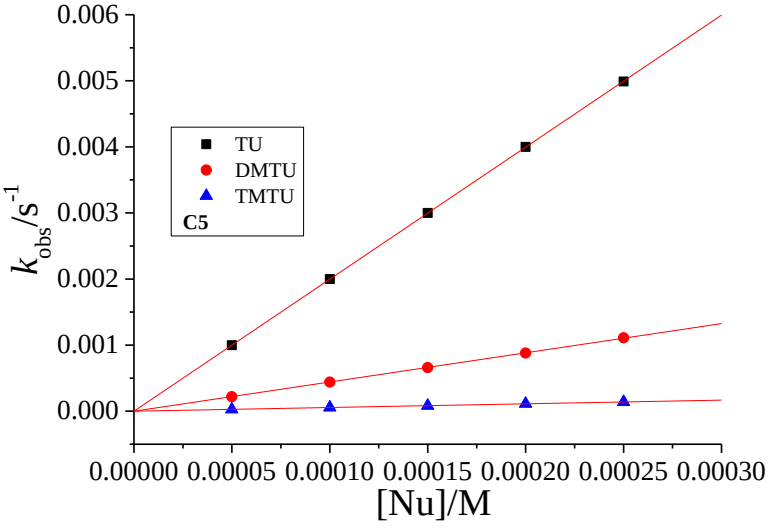

Figure SI 4.22 Concentration dependence plots for the reaction of **C5** with thiourea nucleophiles at 298 K

Table SI 4.9 Data of ln(k_2/T) and 1/T for complex **C5**

1/T	ln(k_2/T) TU	ln(k_2/T) DMTU	ln(k_2/T) TMTU
0.00347	-9.85	-11.4	-12.75
0.00341	-9.15	-10.6	-11.89
0.00336	-8.57	-9.91	-11.1
0.0033	-7.9	-9.14	-10.15
0.00325	-7.3	-8.45	-9.4

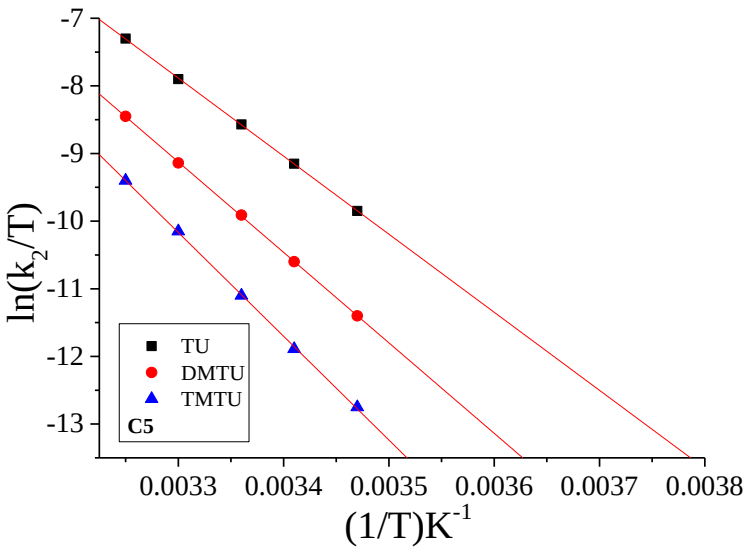

Figure SI 4.23 Eyring plots for the reaction of **C5** with thiourea nucleophiles

(η^6-Benzene)dichloro{1,3-bis(diphenylphosphino)propane}ruthenium(II) (C6)

Table SI 4.10 Observed rate constants and the corresponding nucleophile concentrations for complex **C6**

[Nu]/M	k_{obs} /s^{-1} TU	k_{obs} / s^{-1} DMTU	k_{obs} / s^{-1} TMTU
5E-5	0.0014	9.74E-4	0.000102
1E-4	0.0028	0.00194	0.000204
1.5E-4	0.00415	0.00294	0.000307
2E-4	0.0056	0.0039	0.000408
2.5E-4	0.00701	0.00487	0.000510

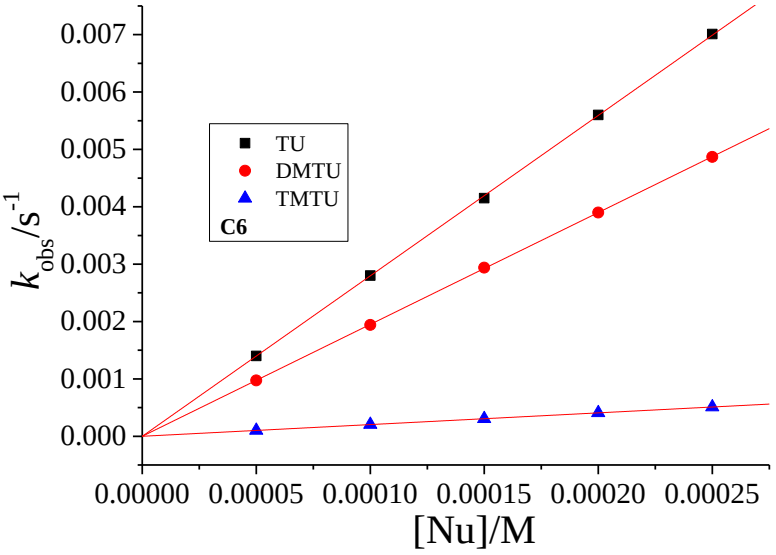

Figure SI 4.24 Concentration dependence plots for the reaction of **C6** with thiourea nucleophiles at 298 K

Table SI 4.11 Data of ln(k_2/T) and 1/T for complex **C6**

1/T	ln(k_2/T) TU	ln(k_2/T) DMTU	ln(k_2/T) TMTU
0.00347	-9.71	-10.95	-11.7
0.00341	-9.06	-10.19	-10.88
0.00336	-8.52	-9.56	-10.2
0.0033	-7.87	-8.8	-9.3
0.00325	-7.34	-8.2	-8.5

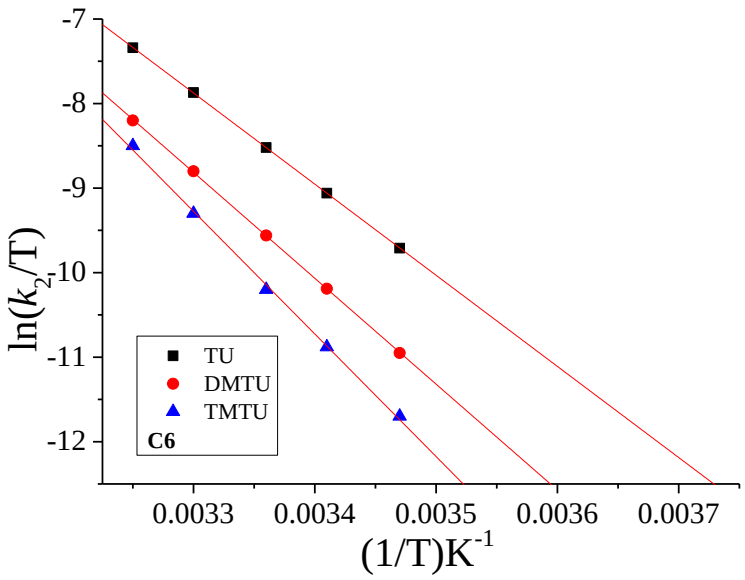

Figure SI 4.25 Eyring plots for the reaction of **C6** with thiourea nucleophiles

Chapter 5

The rate of chloride substitution from Ru(II) complexes bearing the triphenylphosphine and centrosymmetric 2,4,6-(substituted)-1,3,5-triazine tridentate ligands

5.0 Abstract

The study of rate of substitution of the labile chloride ligands from Ru(II) complexes (**C1-C4**) and of the form $[Ru(\kappa^3\text{-}L)(PPh_3)Cl_2]$, where L = 2,4,6-tris(2-pyridyl)-1,3,5-triazine (**L1**) or 2,4,6-tris(4-methyl-2-pyridyl)-1,3,5-triazine (**L2**) 2,4,6-tris(2-quinolyl)-1,3,5-triazine (**L3**) or 2,4,6-tris(4-phenyl-2-pyridyl)-1,3,5-triazine (**L4**), respectively by biologically relevant thiourea nucleophiles was measured. This was done under *pseudo* first order conditions in 0.1 M $NaClO_4$ methanol solution as a function of nucleophile concentrations and temperature. UV-Visible spectrophotometer or Stopped Flow spectrophotometer was used to monitor the reactions. The observed *pseudo* first order rate constants for the ultrafast and slower reaction steps are consistent with the rate law, $k_{obs/obs'} = k_{2/2'}$[Nu], where k_2 and $k_{2'}$ are rate constants for the first and second substitution steps respectively. The magnitudes of k_2 and $k_{2'}$ for the substitution reactions from the Ru(II) complexes decreased in the order: **C3** > **C4** > **C1** > **C2**. The two step substitution reactions follow the same reaction order. An increase in the π-conjugation of the C_3 symmetric (2,4,6-(phenyl-2-pyridyl)-1,3,5-triazine tridentate increase the π-back-bonding of the chelate backbone making the Ru(II) complexes more electrophilic, thereby accelerating the reactivity of the compound as observed in the reactivity of complex **C3** compared to **C1**. The 2-methyl pyridyl substituents on the ligand of **C2** leads to electron donation into the pyridyl rings thereby lowering their π-acceptor capacity. The complex becomes less electrophilic hence less reactive than **C1**. The introduction of phenyl substituents at the 4-positions on the pyridyl ligands in **C1** forms **C4** which is 10-15 times more reactive than **C1**. In **C4**, the three phenyl substituents **L4**, assume a trough like structural orientation that may facilitate trapping up of incoming nucleophiles. The reactivity of the complexes is not affected by the substituents on the pyridyl at the 4-position of the central 1,2,3-triazine ligand because they are far from the reaction centre. This substituent is not directly connected to the Ru(II) metal centre, hence the negligible effect on the substitution reactions. The second step is however 10^3 slower than the first step due to a decrease in the electrophilicity of the metal centre and increased steric hindrance upon

coordination of the first thiourea nucleophile. Additionally, the chloro co-ligand substituted in the second step is influenced by a weaker π-acceptor triphenylphosphino co-ligand. Both reaction steps proceeded by the associative mode of substitution mechanism as evidenced from the measured values which are significantly negative (activation entropies) and positive (activation enthalpies). The reactivity trends are also supported by DFT calculations. The reactivity of the nucleophiles follow the order TU > DMTU > TMTU

5.1 Introduction

Ru(II) complexes bearing multiple pyridyl ligands have attracted attention because of their various uses including their application in medicine due to their DNA and protein binding abilities.[1] The type of ligands coordinated to the Ru(II) metal centre determine the properties of the complex and its use.[2] The use of different types of ligands on the Ru centres has led to the design of complexes with different properties. Tridentate ligands such as 2,2':6,6''-terpyridine and its analogues have been extensively employed to obtain Ru(II) complexes with quite promising abilities to non-covalently interact with DNA.[3] Additionally, if the nature of the metal used is changed, the properties such as the charge, chirality, steric demand and electronic properties of the resultant complex also change thus fine tuning the structural and electronic character of a complex.

Among the polypyridyl ligands, the C_3-centrosymetric tridentate 2,4,6-tris(2-pyridyl)-1,3,5-triazine ligand has drawn interest because of its coordinating versatility.[4] Apart from forming mononuclear complexes it can coordinate as a bridging ligand, where it can ligate as a bidentate at one end and tridentate at the other end.[5] Studies have also reported cases of complexes where the ligand is in tri-nucleating mode.[6] A mononuclear complex of Ru(IV) incorporating the ligand has been found to chemically cleave DNA.[7] While this ligand primarily coordinates tridentately just like terpyridine, it coordinates to several metals ions in many ways to form complexes of different nucleicity and coordination stabilities. Investigations on the DNA binding capacity of cationic complexes of the form $[Ru(\kappa^3\text{-tptz})(EPh_3)_2Cl]^+$ (where tptz = 2,4,6-tris(2-pyridyl)-1,3,5-triazine, E = P or As)[8] showed that they had relatively poor binding strength to nucleosides due to steric hindrance caused by the bulky triphenylphosphine ligands. The phenyl rings on the phosphine ligands restricted the intercalating properties of the complexes.[8-9] That notwithstanding, the complexes were found to inhibit DNA topoisomerase II of the filarial parasite.[8] Reactions of the ligand with

a (Ru(acetylacetonate)$_3$ precursor formed various complexes with different modes of binding and mixed valences.[5]

[Ru(κ^3-tptz)(PPh_3)Cl_2], a neutral and a variation complex coordinated with a single triphenylphosphine ligand was investigated for its inhibitory effect on the DNA-Topoisomerase II activity of filarial parasite.[10] It exhibited greater DNA binding behaviour and inhibitory effect on the parasite than its counterpart with two triphenylphosphine groups. Thus the reduction in steric hindrance enhances its binding effect.[10]

In this study, the complex [Ru(κ^3-tptz)(PPh_3)Cl_2] with three other complexes bearing 2,4,6-substituted derivatives of 1,3,5-triazine were synthesized. The complexes (**C1**-**C4**) which are of the form [Ru(κ^3-L)(PPh_3)Cl_2] (where L = 2,4,6-tris(2-pyridyl)-1,3,5-triazine, **L1**, 2,4,6-tris(4-methyl-2-pyridyl)-1,3,5-triazine, **L2**, 2,4,6-tris(2-quinolyl)-1,3,5-triazine, **L3** or 2,4,6-tris(4-phenyl-2-pyridyl)-1,3,5-triazine, **L4**) were synthesised to study their rate of substitution reactions. The study sought to determine the role of *cis*-ligands on the substitution of the chloride co-ligands from the Ru(II) complexes using S-donor nucleophiles as the substituting nucleophiles. The substitution reactions mimic their interaction with S-containing biomolecules. The structures of the complexes are shown in Figure 5.1.

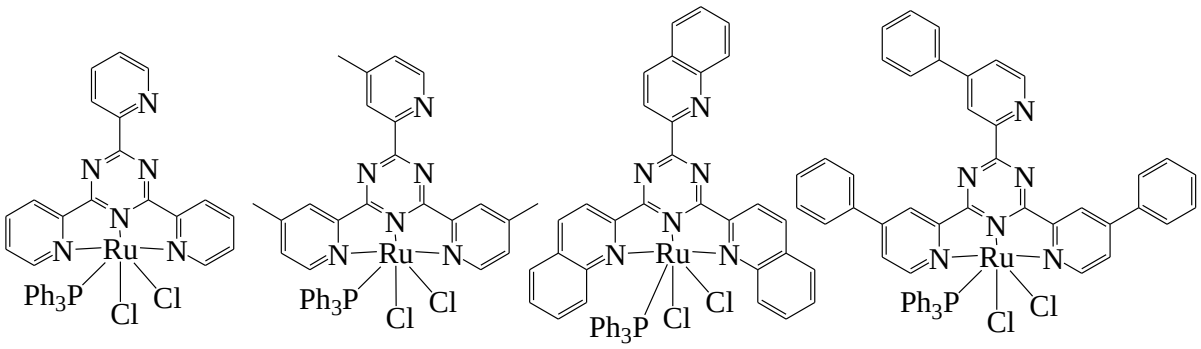

Figure 5. 1 Structures of the Ru(II) complexes under investigation

5.2 Experimental

5.2.1 Reagents

Synthetic experiments were performed under an inert atmosphere of nitrogen in deaerated solvents. Solvents (benzene, diethyl ether, ethanol, acetonitrile, chloroform, ethanol, dimethylformamide and acetone) were purchased from Sigma-Aldrich and dried by standard methods prior to use. Tris(triphenylphosphine) ruthenium(II)dichloride, 2,4,6-tris(2-pyridyl)-1,3,5-triazine (**L1**), sodium hydride, alumina, 2-cyanoquinoline, 4-methyl-2-cyanopyridine, 4-phenyl-2-cyanopyridine, sodium perchlorate monohydrate, lithium chloride and thiourea (TU), 1,3-dimethyl-2-thiourea (DMTU) and 1,1,3,3-tetramethyl-2-thiourea were obtained from Sigma-Aldrich and used without further purification. The ligands and complexes were characterized and gave satisfactory results consistent with their structure and formulae. The mass and NMR (^{1}H and ^{31}P) data are placed in the supporting information Figures SI 5.1-5.21

5.2.2 Synthesis

Synthesis of ligands and complexes was done according to modified literature methods.[11] [12]

5.2.2.1 Synthesis of ligands

2,4,6-tris(4-methyl-2-pyridyl)-1,3,5-triazine (**L2**)

4-methyl-2-cyanopyridine (6 g, 0.05 mol) and sodium hydride (0.1 g, 0.004 mol) were placed in a round bottomed flask and the mixture heated at 130 °C for 6 hours in a nitrogen atmosphere. The solid residue was then dissolved in chloroform and eluded through alumina. The chloroform solution was concentrated by rotary evaporation and the product precipitated using cold diethyl ether. The solid was obtained by filtration and washed with diethyl ether and dried. Yield: 1.1 g, (18.6 %). ^{1}H NMR (400 MHz, $CDCl_3$, ppm) δ = 8.80 (d, 3H); 8.70 (s, 3H); 7.38 (d, 3H); 2.56 (s, 9H). TOF MS-ES^{+}, m/z: 377.2 $[L + Na]^{+}$, 731.4 $(2L + Na)^{+}$. *Anal. Calc. For* $C_{21}H_{18}N_6$: C 71.17, N 23.71, H 5.12. *Found*: C 70.50, N 23.65, H 5.09.

2,4,6-tris(2-quinolyl)-1,3,5-triazine (**L3**)

2-cyanoquinoline (8 g, 0.05 mol) and sodium hydride (0.1 g 0.004 mol) were placed in a round bottomed flask and the mixture heated at 160 °C for 5 hours in a nitrogen atmosphere. The reaction mixture was then extracted with hot benzene. The benzene solution was concentrated by rotary evaporation and the product precipitated using diethyl ether. The solid was filtered and washed with diethyl ether and dried. Yield: 1.8 g, (23.3%). ^{1}H NMR (400 MHz, $CDCl_3$, ppm) δ = 8.33 (d, 3H); 8.20 (m, 3H); 7.92 (d, 3H); 7.87 (t, 3H); 7.73 (H, 6 m).

TOF MS-ES$^+$, m/z: 485.2 [L + Na]$^+$, 947.3 (2L+Na)$^+$. *Anal. Calc. For* $C_{30}H_{18}N_6$: C 77.91, N 18.17, H 3.92. *Found*: C 77.66, N 18.46, H 3.86.

2,4,6-tris(4-phenyl-2-pyridyl)-1,3,5-triazine (**L4**)

4-phenyl-2-cyanopyridine (4.2 g, 0.023 mol) and sodium hydride (0.1 g, 0.004 mol) were placed in a round bottomed flask and the mixture heated at 120 °C for 6 hours in a nitrogen atmosphere. The solid residue was then dissolved in chloroform and eluded through alumina. The chloroform solution was concentrated by rotary evaporation and the product precipitated using diethyl ether. The solid was obtained by filtration and washed with diethyl ether and dried. It was purified by recrystallization from benzene. Yield: 1.65 g, (39.3%). ^{1}H NMR (400 MHz, $CDCl_3$ ppm) δ = 9.12 (s, 3H); 9.02 (d, 3H); 7.82 (m 9H); 7.55 (s, 9H). TOF MS-ES$^+$, m/z: 563.2 [L + Na]$^+$. *Anal. Calc. For* $C_{36}H_{24}N_6$: C 79.98, N 15.55, H 4.47. *Found*: C 79.56, N 15.15, H 5.09.

5.2.2.2 Synthesis of Ru(II) complexes

Dichloro(2,4,6-tris(2-pyridyl)-1,3,5-triazine)(triphenylphosphino)Ru(II) (**C1**)

A suspension of equimolar amounts of tris(triphenylphosphine)ruthenium(II)dichloride (958.8 mg, 1 mmol) and **L1** (312.3 mg, 1 mmol) in benzene was heated under reflux for 6 hours. The solution was cooled to room temperature and the solid suspension filtered off and repeatedly washed with benzene and diethyl ether then dried. Yield: 500.2 mg, (67.0 %). ^{1}H NMR (400 MHz, DMF) δ/ppm, J/Hz: δ = 9.38 (m, 3H); 8.91 (m, 3H); 8.38 (m, 3H); 8.21 (m, 9H); 7.64 (m, 3H); 7.42 (m, 6H). ^{31}P NMR (400 MHz, DMF) δ/ppm δ = 35.93. LC-MS ESI$^+$, m/z: 746.05 (M), 711.01 [M – Cl]$^+$. *Anal. Calc. For* $C_{36}H_{27}Cl_2N_6PRu$: C 57.90, N 11.26, H 3.61. *Found*: C 57.64, N 11.05, H 3.31.

Dichloro(2,4,6-tris(4-methyl-2-pyridyl)-1,3,5-triazine)(triphenylphosphino)Ru(II) (**C2**)

The complex was synthesized in the same way as **C1** using **L2** (354.41 mg, 1 mmol) in the place of **L1.** Yield: 492.3 mg, (62.4 %). ^{1}H NMR (400 MHz, DMF) δ/ppm: δ = 9.23 (d, 3H); 7.52 (m, 3H); 7.32 (m, 9H); 7.24 (m, 9H); 2.61 (d, 9H). ^{31}P NMR (400 MHz, DMF) δ/ppm δ = 37.01. LC-MS ESI$^+$, m/z: 788.67 [M], 753.22 [M – Cl]$^+$ *Anal. Calc. For* $C_{39}H_{33}Cl_2N_6PRu.H_2O$: C 59.39, N 10.66, H 4.22. *Found*: C 59.70, N 10.32, H 3.91.

Dichloro(2,4,6-tris(2-quinolyl)-1,3,5-triazine)(triphenylphosphino)Ru(II) (**C3**)

The complex was synthesized in the same way as **C1** using **L3** (462.5 mg, 1 mmol) in the place of **L1**. Yield: 460.5 mg, (51.4 %). ^{1}H NMR (400 MHz, DMF) δ/ppm: δ = 9.20 (m, 3H);

9.03 (m, 3H); 8.58 (m, 3H); 8.41 (s, 3H); 7.85 (m, 9H); 7.19 (s, 3H); 7.17 (t, 3H); 7.01 (t, 6H). ^{31}P NMR (400 MHz, DMF) δ/ppm δ = 33.13. LC MS ESI$^+$, m/z: 896.77 (M), 861.11 [M –Cl]$^+$. *Anal. Calc. For* $C_{48}H_{33}Cl_2N_6PRu$: C 64.29, N 9.39, H 3.71. *Found*: C 64.61, N 9.50, H 3.70.

Dichloro(2,4,6-tris(4-phenyl-2-pyridyl)-1,3,5-triazine)(triphenylphosphino)Ru(II) (**C4**)
The complex was synthesized in the same way as **C1** using **L4** (540.62 mg, 1 mmol) in the place of **L1**.Yield: 712.1 mg, (73.0 %). ^{1}H NMR (400 MHz, DMF) δ/ppm: δ = 9.09 (m, 3H); 8.33 (m, 3H); 7.66 (m, 12H); 7.58 (m, 6H); 7.32, (m, 6H); 7.28 (m, 9H). ^{31}P NMR (400 MHz, DMF) δ/ppm δ = 35.81. LC-MS ESI$^+$, m/z: 974.88 [M], 939.20 [M – Cl]$^+$. *Anal. Calc. For* $C_{54}H_{39}Cl_2N_6PRu$: C 66.53, N 8.62, H 4.03. *Found*: C 66.91, N 8.33, H 3.67.

5.2.3 Instrumentation and physical measurements

NMR spectroscopy were recorded on a Bruker Avance DPX 400MHz spectrophotometer at 303 K and all chemical shift were referenced to those of $Si(CH_3)_4$. Low resolution electron spray ionization (ESI$^+$) mass spectra were recorded on the Waters Micromass LCT Premier Spectrometer or Shimadzu LCMS 2020. Elemental analyses were done on a ThermoScientific Flash 2000 elemental analyser. Kinetic measurements for fast reactions were performed on an Applied Photophysics SX20 Stopped Flow instrument coupled with an online data acquisition system whose temperature is controlled to within ± 0.1° C. The slow reactions were monitored using Varian Cary 100 Bio UV-Visible Spectrophotometer with an attached Varian Peltier temperature controller and online kinetic application. The UV-Visible spectrophotometer was also used to pre-determine the wavelengths at which the reactions on the Stopped Flow were monitored.

5.2.4 Computational modelling

The computations were done by Density Functional Theory (DFT) run on the Gaussian 09 suite of programs.[13] The structures were optimised using the hybrid Becke, 3-parameter, Lee-Young-Parr (B3LYP) method with LANL2DZ (Los Alamos National Laboratory 2 double ζ) basis sets having inner core electrons of the Ru atom replaced by relativistic effective core potential (ECP).[14] [15] [16] DFT applies to physically observable electron density over a wave function in the determination of the properties of a system. Los Alamos National Laboratory 2 double ζ basis set exploits relativistic effective core potentials to account for effect of inner core 28 electrons ([Ar]3d^{10}) in Ru.[17] [18] To take into account of

the solvent effects, the complexes were fully optimised in methanol using the conductor polarizable continuum model (C-PCM).[19] [20] The singlet states were used due to the low electronic spin state of Ru(II) complexes. The complexes were considered to have an overall charge of +2. The chemical potential (μ) and molecular hardness (η) for each structure were calculated from the HOMO and LUMO energies. The global electrophilicities (ω) were determined by the relationship $\omega = \mu^2/2\eta$.[21] [22] The charge on each atom is expressed as a natural bond orbitals (NBO).[23]

5.3 Results

5.3.1 Computational results

Density functional theory (DFT)[24] [25] calculated data for example electrophilicity index and NBO charges have provided information in support of the trends in chemical reactivity of metal complexes. Several reactivity descriptors have been proposed and used to analyse trends in chemical reactivity and site selectivity. Hardness, electronegativity and electrophilicity are among the reactivity descriptors which have been used to understand the global nature of molecules in terms of their stability. Atomic charges is among the local reactivity descriptors, which provide information about the site selectivity.[26] [27] In this study computational calculations and optimisation were carried out to gain information on the electronic and structural properties of the complexes. The DFT optimized structures of the complexes are shown in Table 5.1 and a summary of selected DFT parameters are presented in Table 5.2. The DFT frontier molecular orbitals presented in Table 5.1 show that the HOMO are located mainly on the Ru metal centre and partially on the chloro ligand while the LUMO on the *cis* ligands as reported in literature for other similar studies.[28]

Table 5. 1 DFT optimized minimum energy structures and frontier molecular orbitals of the complexes

Tubular Structures		HOMO	LUMO
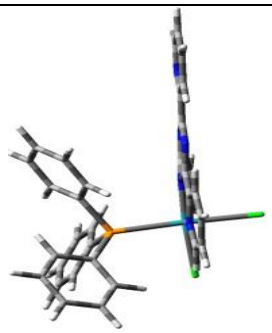	**C1**	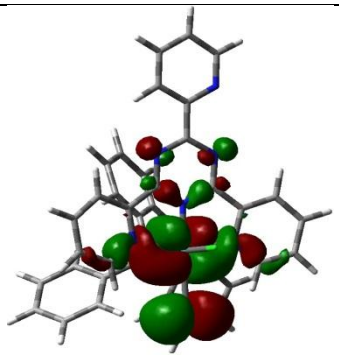	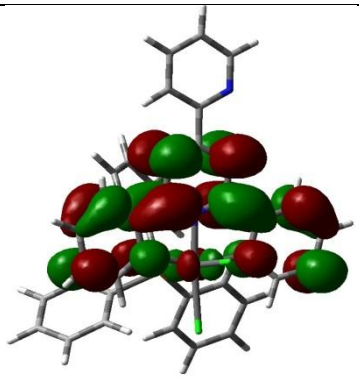
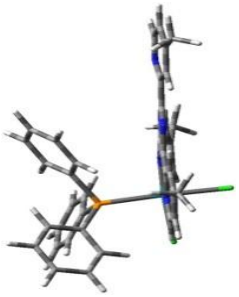	**C2**	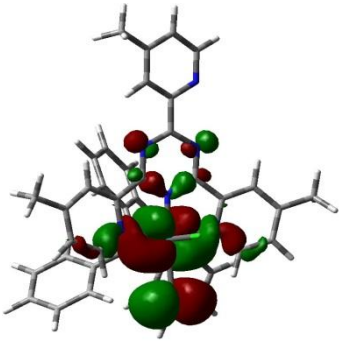	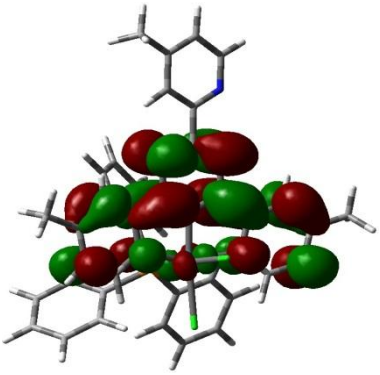
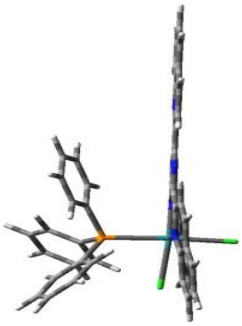	**C3**	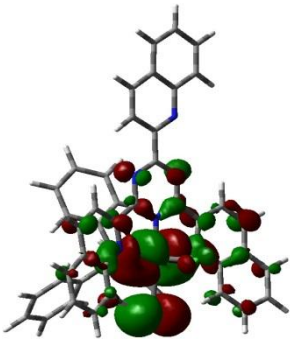	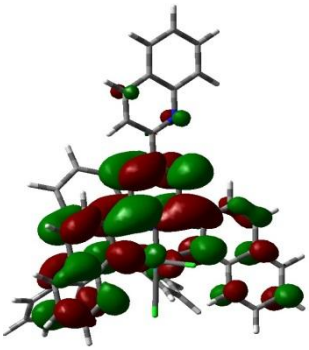
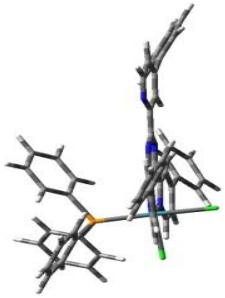	**C4**	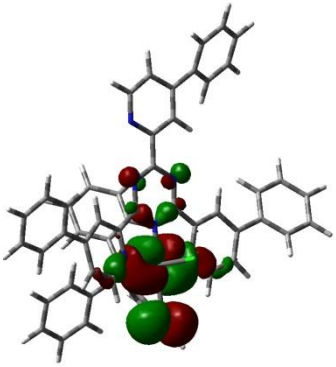	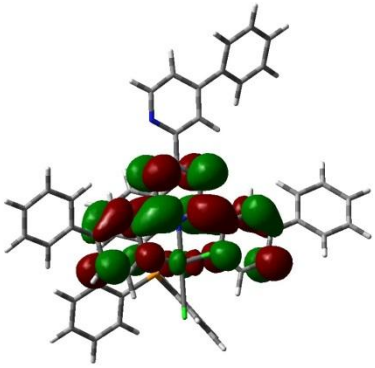

Table 5. 2 Summary of DFT calculated data for the complexes investigated

Parameters	**C1**	**C2**	**C3**	**C4**
Bond lengths (Å)				
Ru1-Cl44	2.56	2.56	2.61	2.56
Ru1-Cl103	2.54	2.55	2.53	2.55
Ru1-N11	1.94	1.94	1.95	1.94
Ru1-N16	2.12	2.12	2.21	2.10
Bond angles (°)				
N25-Ru1-N16	157.4	157.3	154.1	157.4
N16-Ru1-N11	78.9	78.8	77.7	79.2
N11-Ru1-Cl44	175.4	174.9	175.7	175.0
Cl44-Ru1-Cl103	90.0	89.5	93.0	89.7
NBO charges				
Ru1	0.188	0.184	0.192	0.190
Orbital energy/eV				
HOMO	-5.732	-5.658	-5.881	-5.713
LUMO	-3.096	-3.026	-3.275	-3.094
$\Delta E_{HOMO-LUMO}$	2.636	2.632	2.606	2.619
Global chemical reactivity indices				
η/eV	1.318	1.316	1.303	1.310
μ/eV	-4.414	-4.324	-4.578	-4.404
ω/eV	7.391	7.163	8.040	7.401

where; η = Chemical Hardness μ = Electronic chemical potential ω = Electrophilicity index

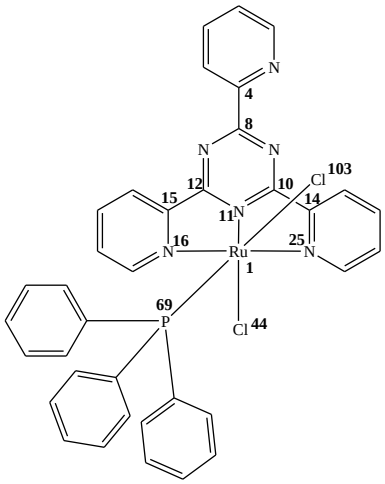

Figure 5. 2 Structure of **C1** including the atomic numbering adopted from the DFT optimized structural numbering

The HOMO-LUMO energy gap can predict accurately the relative kinetic inertness and chemical reactivity of a family of structurally related compounds. A compound whose energy gap is wide is kinetically inert and less reactive.[29] The coordination geometry at the Ru(II) metal centre in the mononuclear complexes under this study is distorted octahedral. The computed geometric angles and data are in agreement with literature data on Ru(II) complexes with similar coordination chelates.[10] The Ru is bonded at the tridentate site of the ligands through the pyridyl nitrogen atoms N25 and N16 and the triazyl nitrogen N11. The angles N11-Ru1-N16 and N11-Ru1-N25 are 79° which is 11° less than the expected 90°. This distortion is to accommodate steric repulsions and causes equatorial pyridyl groups to bend inward. The intra-ligand *trans* angles N25-Ru1-N16 (157.4°, 157.3°, 154.1° and 157.4°), Cl103-Ru1-P69 (177°) and Cl44-Ru1-N11 (175°) deviate from the expected 180°, giving further evidence of steric strain.[10] The angles $Cl^{\mathbf{44}}$-Ru1-$Cl^{\mathbf{103}}$ are 90° in all the complexes showing that the chloride co-ligands are *cis*-oriented. This is in agreement with what has been reported on similar complexes.[10] It's worth noting that the length of Ru1-N11 is about 0.16Å shorter than Ru1-N16 and Ru1-N25 bond lengths, a further confirmation of distortion of the octahedral geometry. The theoretically calculated physical measurements for **C1** are consistent with crystallographic data in the findings of Sanjeev Sharma *et. al.*[10].

To test if the 4-substituents on the triazine ligand had any significant effect on the rate of substitution reactions, preliminary DFT calculations were done on complexes **C2*-C4*** *i.e.* theoretical derivatives of **C2-C4** were their 4-substituents of the triazine all replaced by a

pyridyl ring as shown in Figure 5.3. A comparison of key DFT data between the theoretically studied compounds **C2*-C4*** and that of the experimentally investigated complexes **C2-C4** (Tables 5.3) revealed no noticeable difference in the NBO charges. The HOMO-LUMO energy gap and electrophilicity indices as tabulated in Table 5.3 were the same. This comparison revealed that the uncoordinated substituents (pyridyl (**C1**), 4-methylpyridyl (**C2**), 2-quinolyl (**C3**) or 4-phenylpyridyl (**C4**)) at the 4-position of 1,3,4-triazine have either no effect or negligible impact on the rate of substitution of the complexes. Therefore, it was pre-concluded that whatever differences in the substitution of the two chlorides is due to the substituents at the 2- and 6-positions of the 1,3,5-triazine rings. This is so because the moieties of the triazine ligands at their 2- and 6-positions are directly coordinated to the Ru(II) metal centres. Since the triphenylphosphine ligands is not varied then the effect on the rate of substitution from the Ru(II) complexes should be viewed in terms of its cis-effect in reference to Cl[44] and *trans* in reference to Cl[103]**.** A closer examination of the HOMO and LUMO diagrams shows that the uncoordinated 4-substituent groups of the triazine are neither the HOMO nor LUMO, corroborating the idea that these 4-substituents of the triazines have negligible impact on the reactivity of the complexes.

Table 5. 3 Sample DFT calculated data for the theoretical complexes shown in Figure 5.3

	C2	**C2***	**C3**	**C3***	**C4**	**C4***
NBO charges						
Ru1	0.184	0.185	0.192	0.190	0.190	0.186
Orbital energy/eV						
HOMO	-5.658	-5.668	-5.881	-5.907	-5.713	-5.713
LUMO	-3.026	-3.036	-3.275	-3.274	-3.094	-3.094
$\Delta E_{HOMO-LUMO}$	2.632	2.633	2.606	2.633	2.691	2.620
Global chemical reactivity indices						
ω/eV	7.163	7.195	8.040	8.003	7.401	7.402

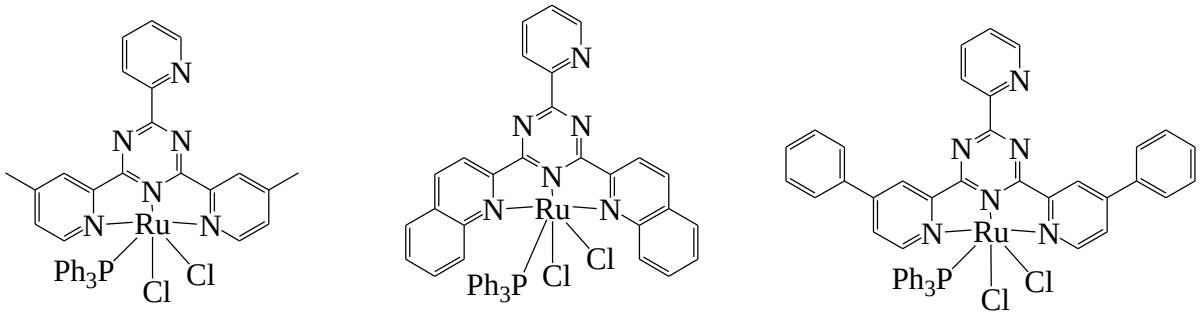

C2* **C3*** **C4***

Figure 5. 3 Chemical structures of **C2***, **C3*** and **C4*** without the substituents on the un-coordinated pyridyl ring

In all the complexes, the labile ligand Cl^{44} is *trans* to the meriodinally-coordinated triazine ligand while Cl^{103} is *trans* to the triphenylphosphine ligand. Due to the difference in the *trans* labilising abilities of the two spectator ligands, it is expected that the two chloride co-ligands would be substituted at two different rates as observed in the two-step reaction profiles of the substitution process for the complexes.

5.3.2 Kinetic Analysis

Kinetic measurements were done under *pseudo* first-order conditions using at least 20-fold excess of nucleophile in 0.1 M ionic solution consisting of 0.01M LiCl and 0.09 M $NaClO_4$ in dry methanol. The purpose of using lithium chloride was to suppress any possibility of solvolysis. The perchlorate ion is such a poor nucleophile it cannot competitively substitute the co-labile ligand ahead of the incoming thiourea ligands.[20] Kinetic solutions were prepared by dissolving required amounts of complexes in the ionic solution to achieve specific concentration. Nucleophile stock solutions were prepared at 100 times higher than the concentration of the respective complex and diluted to afford those that were 80, 60, 40 and 20 times higher than the concentration of the complexes.

The rate of substituting the chloride ligands was investigated spectrophotometrically by following the change in absorbance with time using a UV-Visible spectrophotometer for slower reactions or a stopped flow analyser for faster reactions. Spectral changes due to the reactions were observed over the wavelength range 200-800 nm to establish a suitable wavelength at which the respective substitution reaction for each metal complex and nucleophiles was followed. All reactions were done under a thermostated environment with a

temperature precision of ± 0.1 °C. The data obtained from the spectrophotometric studies were analysed graphically using the software package OriginPro 9.1. The data for the second and slower step were fitted to first-order exponential decay function to obtain the respective observed *pseudo* first-order rate constants, k_{obs}, according to Equation 5.1[20]

$$A_t = A_\circ + (A_\circ - A_\infty) \exp(-k_{obs}\, t) \qquad (5.1)$$

where; A_0 is initial absorbance of the mixture, A_t is absorbance of the reaction mixture at time, t and A_∞ is final absorbance.

A typical absorbance spectra change for the reaction of **C2** with DMTU is shown in Figure 5.4. The inset is the kinetic trace at 500 nm.

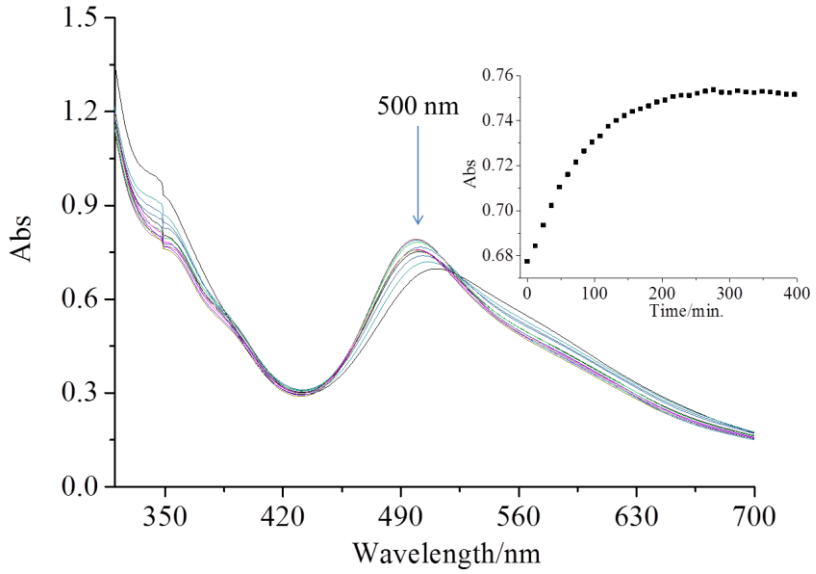

Figure 5. 4 Absorbance spectra changes for the substitution of the second chloride from **C2** by DMTU at 298 K (Inset is the kinetic trace of absorbance verses time for the reaction at 500 nm)

A typical kinetic trace from the stopped flow instrument is shown in Figure 5.5.

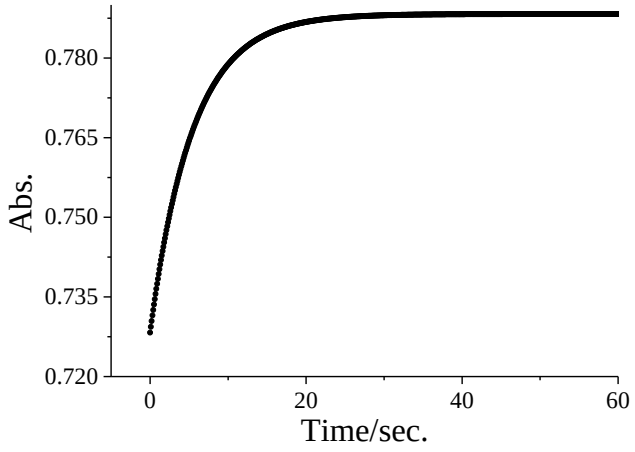

Figure 5. 5 Kinetic trace for the first substitution from **C4** by DMTU at 298 K obtained from the stopped flow analyser

The average values of the observed rate constants (k_{obs}/ $k_{obs'}$) for both the fast and slow reaction steps were plotted against nucleophile concentrations according to Equation 5.2. The linear plots gave slopes representing the second order rate constants, k_2 and k_2' for the first and second substitution steps, respectively. Typical plots of k_{obs} and $k_{obs'}$ verses $[Nu]$ are shown in Figure 5.6 for the first (a) and second (b) substitution reactions of **C1** with the thiourea nucleophiles at 298 K.

$$k_{obs/obs'} = k_{2/2'}[Nu] + k_s \approx k_{2/2'}[Nu] \quad (5.2)$$

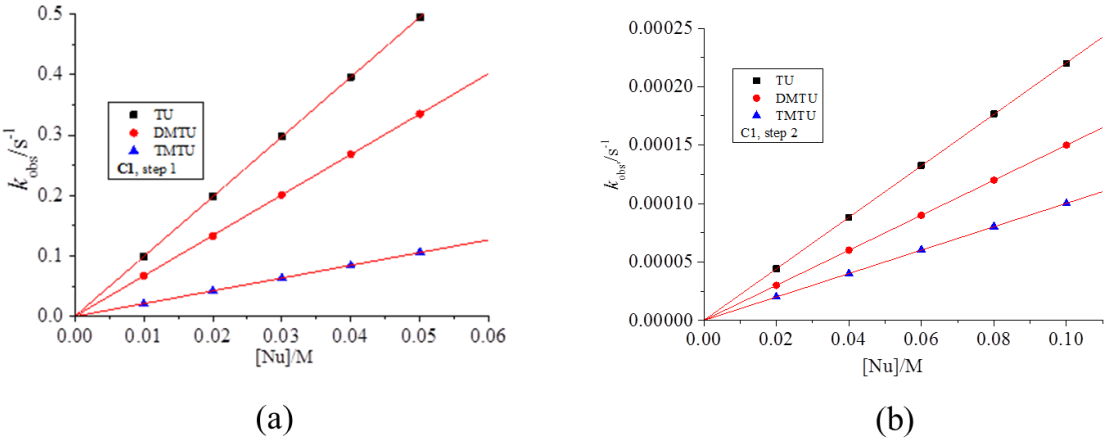

Figure 5. 6 Plots of k_{obs} (a) and k_{obs}' (b) versus [Nu] for the reactions of **C1** with the thiourea nucleophiles at 298 K

Other concentration dependence plots are presented in the supplementary information Figures SI 5.22, 5.23, 5.25, 5.26, 5.28 and 5.31. Tables of $k_{obs/obs}'$ and respective nucleophile concentrations are presented in supplementary information Tables SI 5.1, 5.2, 5.4, 5.5, 5.7, 5.8, 5.11 and 5.12.

Confirmation of the successive substitutions by ^{31}P NMR

The substitution of the two chloride ligands occurs in two successive steps as supported by the ^{31}P NMR kinetics spectra data presented in Figure 5.7 for the substitution reaction from **C4** by thiourea nucleophile.

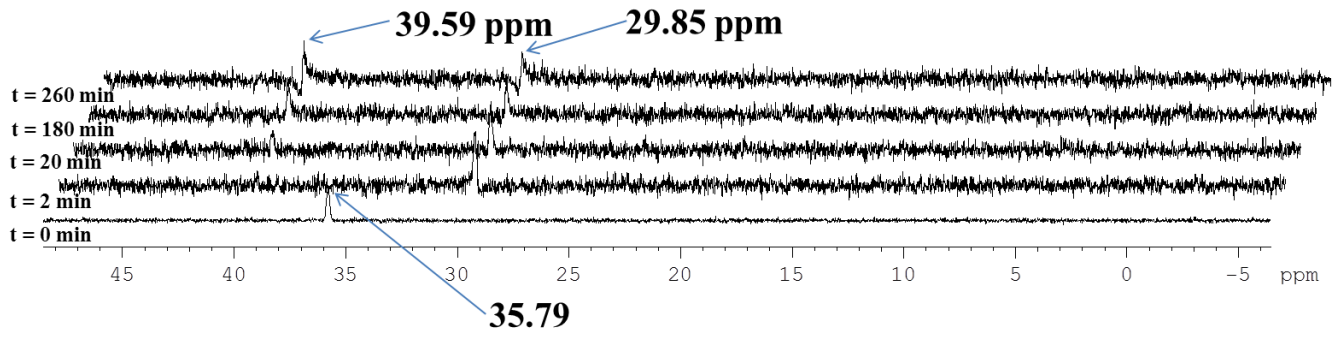

Figure 5. 7 ^{31}P NMR spectral array of the reaction progression of **C4** with thiourea

The ^{31}P NMR spectrum of **C4** shows a single chemical shift peak at 35.79 ppm. Immediately after mixing of complex with thiourea, there is a new peak at 29.85 ppm within 2 minutes with a concomitant disappearance of the 35.79 ppm resonance peak. The first chloride substitution from **C4** produced an intermediate coordinated with one chloro ligand substituted with a thiourea. This intermediate reacts with the second molecule of Tu at a much slower rate as evidenced by a decrease in its resonance at 29.85 ppm and concomitant growing of a resonance peak at 39.59 ppm. This resonance is due to $Ru(\kappa^3\text{-tptz})(PPh_3)Tu_2$ species.[30] The ^{31}P NMR peak characteristic of the free triphenylphosphine ligand (Figure 5.8) was not observed during the course of the substitution reaction.

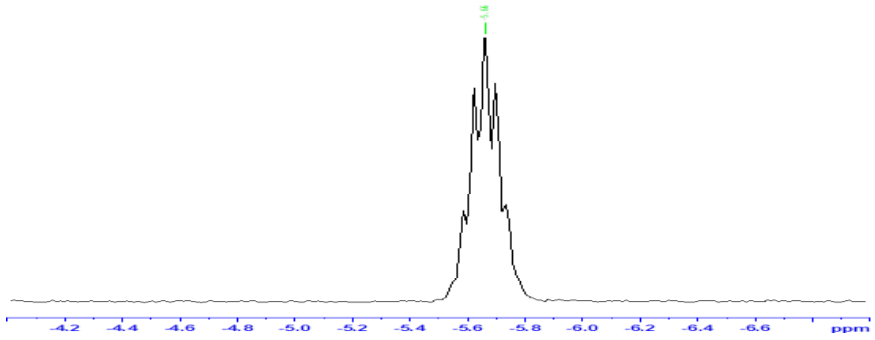

Figure 5. 8 ^{31}P NMR spectrum for free triphenylphosphine in DMF solvent

Based on the ^{31}P NMR data, the proposed mechanism of substitution for the complexes can be represented by Scheme 5.2.

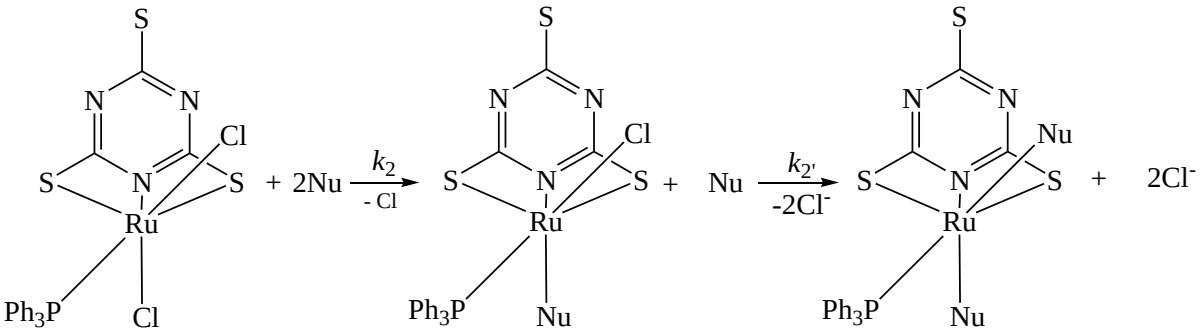

S = 2-pyridyl (**L1**) or 4-methyl-2-pyridyl (**L2**) or 2-quinolyl (**L3**) or 4-phenyl-2-pyridyl (**L4**),

Nu = TU, DMTU, TMTU

Scheme 5. 1 Proposed mechanism of substitution of the Ru(II) complexes with thiourea nucleophiles

The temperature dependence of the rate constants were studied over the temperature range of 25-45 °C in increments of 5 °C. Graphs of ($k_{2/2'}$/T) verses $1/T$ were plotted in accordance to the Eyring equation, Equation 5.3. Typical Eyring plots are shown in Figure 5.9 for the reactions of **C4** with the thiourea nucleophiles.

$$\ln\frac{k_2}{T} = \left(\frac{\Delta H^{\neq}}{R}\right)\frac{1}{T} + \left(23.8 + \frac{\Delta S^{\neq}}{R}\right) \tag{5.3}$$

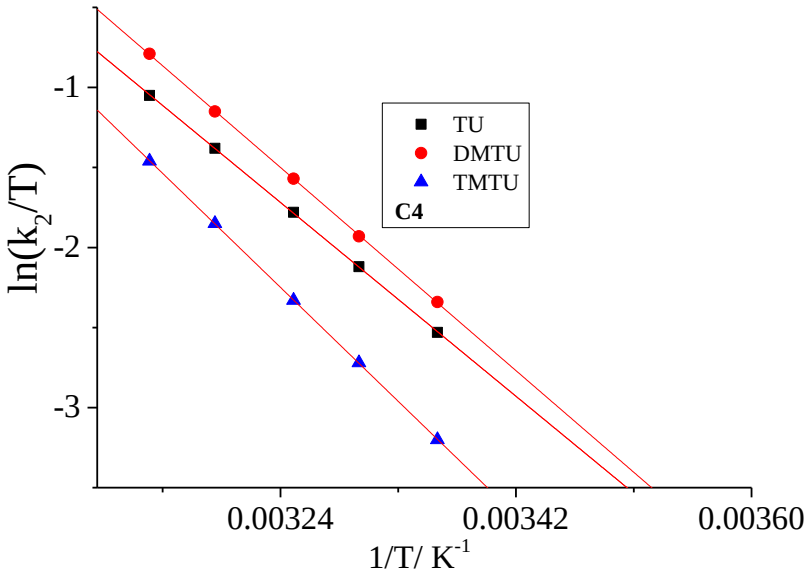

Figure 5. 9 Eyring plots for the reactions of **C4** with the thiourea nucleophiles

The enthalpy of activation, $\Delta H^{\neq}$, and entropy of activation, $\Delta S^{\neq}$, were calculated from the slopes and the intercepts of the Eyring plots. Other Eyring plots are presented in the supplementary information Figures SI 5.24, 5.27, 5.29, 5.30 and 5.32. Tables of $\ln(k_2/T)$ /(k_2'/T) and $1/T$ values are presented in the supplementary information Tables SI 5.3, 5.6, 5.9, 5.10, 5.13 and 5.14. The results of the kinetic analysis including the rate constants and thermodynamic parameters for steps 1 and 2 of substitution process are summarised in Table 5.4 and Table 5.5 respectively.

Table 5. 4 Second order rate constants and activation parameters for the first step

Complexes		Nu	k_2 / M^{-1} s^{-1}	$\Delta H_2^{\neq}$ /kJ mol^{-1}	$\Delta S_2^{\neq}$/ J K^{-1} mol^{-1}
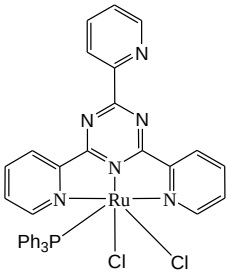	**C1**	TU	12.9 ± 0.06	52 ± 0.2	-47 ± 0.7
		DMTU	10.9 ± 0.04	61 ± 0.3	-20 ± 0.9
		TMTU	3.7 ± 0.01	72 ± 0.5	-14 ± 1.7
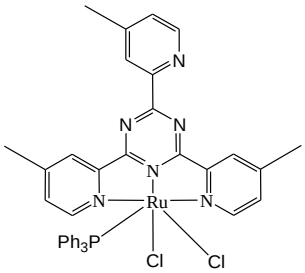	**C2**	TU	9.9 ± 0.02	55 ± 3	-34 ± 7
		DMTU	6.7 ± 0.02	65 ± 2	-17 ± 5
		TMTU	2.1 ± 0.01	78 ± 1	-14 ± 3
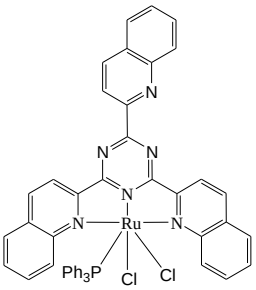	**C3**	TU	176.0 ± 0.1	22 ± 0.1	-128 ± 0.3
		DMTU	152.1 ± 0.5	24 ± 0.05	-122 ± 0.2
		TMTU	36.1 ± 0.05	47 ± 0.2	-53 ± 0.8
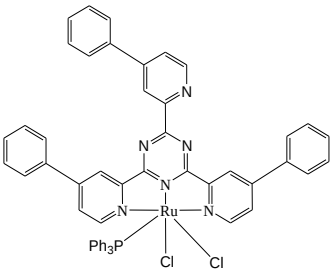	**C4**	TU	18.2 ± 0.02	47 ± 0.3	-63 ± 1
		DMTU	15.4 ± 0.02	57 ± 0.3	-29 ± 9
		TMTU	7.5 ± 0.01	67 ± 0.7	-24 ± 2.3

Table 5. 5 Second order rate constants and activation parameters for the second step

Complexes		Nu	$k_{2'}$/ 10^{-3} M^{-1} s^{-1}	$\Delta H_{2'}^{\neq}$ / kJ mol^{-1}	$\Delta S_{2'}$ / J K^{-1} mol^{-1}
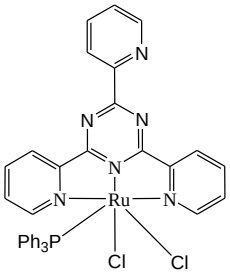	**C1**	TU	2.2 ± 0.01	72 ± 2	-29 ± 4
		DMTU	1.5 ± 0.01	76 ± 3	-12 ± 7
		TMTU	1.0 ± 0.01	86 ± 3	-9 ± 9
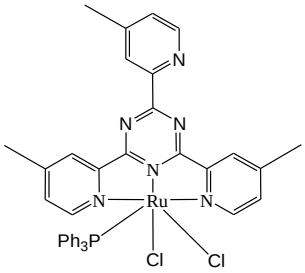	**C2**	TU	1.1 ± 0.01	77 ± 2.9	-26 ± 9.4
		DMTU	1.0 ± 0.01	80 ± 4.3	-11 ± 14
		TMTU	0.2 ± 0.01	90 ± 1	-5 ± 3
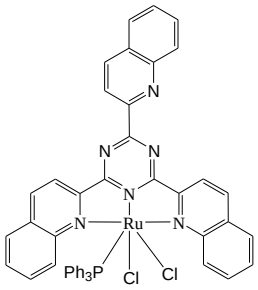	**C3**	TU	106.2 ± 0.1	54 ± 0.4	-99 ± 1.4
		DMTU	5.6 ± 0.01	60 ± 0.03	-88 ± 0.1
		TMTU	1.7 ± 0.01	83 ± 0.2	-20 ± 0.6
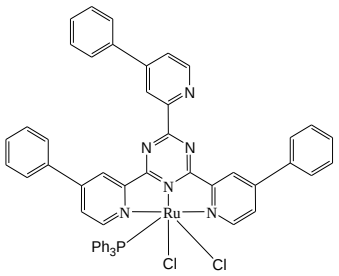	**C4**	TU	4.9 ± 0.2	68 ± 4.5	-67 ± 15
		DMTU	4.0 ± 0.02	73 ± 3	-17 ± 10
		TMTU	1.2 ± 0.01	85 ± 2.1	-10 ± 7

5.4 Discussion

The relative magnitudes of k_2 and $k_{2'}$ in Tables 5.5-5.6 shows that the stepwise substitution of the chloride ligands follow the same trend in rate of substitution for both steps. The order is: **C3** > **C4** > **C1** > **C2**. The rates of substitution from the complexes clearly depend on the π-acceptor abilities of the 2,6-substituents of the centrosymmetric 1,3,4-triazine of the ligands which are coordinated *cis* to Cl[44] in the equatorial plane of the octahedral geometry. The uncoordinated 4-substituents of the 1,3,4-triazine are far from the reaction site that they have no role in the substitution reactions as explained in the previous sections.

A comparison of the rate of substitution from **C2** versus **C1** shows that **C2** is marginally less reactive than **C1.** This is so because the two methyl groups at the 4-position on the *cis*-pyridyl donate electron density inductively into the pyridyl rings and thus reduces their π-acceptor abilities. This also leads to a slight accumulation of electron density on the Ru metal centre. Its charge is reduced, making it less electrophilic and hence less reactive. A similar trend has been reported for chloro Pt(II) complexes bearing tpy and tpy analogue ligands bearing a similarly derived ligand.[31] This observation is supported by the higher DFT calculated electrophilicity index for complex **C1** (7.391) compared to that of **C2**, (7.163).

When the C_3-symetrical tris(2-pyridyl)triazine ligand (L1) of **C1** is changed to the 2-quinolyl derivative in **C3**, the latter is found to be more reactive than the former by factors of between 10-15 for all nucleophiles. The quinoline moieties add an extended π-conjugation at the 2- and 6-positions of the coordinated groups of the triazine compared to the pyridyl ligands in **C1.** This enhances π-back-bonding of the chelate ligand which increases the positive charge on the metal centre thereby increasing the attraction of incoming nucleophiles as observed in literature for reactions of complexes bearing similar π-acceptor *cis* ligands. [32] [21] [22] This favours the addition of a seventh ligand in the transition state since the donation of electron density from the filled *d*-orbitals of the Ru(II) metal centre to the π*-orbitals of the ligand relieves electron density at the metal centre which now accommodates more electron density from the incoming nucleophile. This observation has been discussed in several literature studies. [33] [34] [35] [36] [37] [38] [39] [40] [41] [42] [43] The observation is also supported by the higher DFT calculated electrophilicity index for complex **C3** (8.040) compared to that of **C1** (7.391). It is worth noting that quinoline has both σ-donor and π-acceptor properties with the dominant property controlling the reactivity.[44] In this particular instance, the π-acceptor capacity is dominant possibly due to C_3-symetry of the triazine core ligand.

The replacement of the pyridine substituents on the triazine ligand of in **C1** with 4-phenylpyridine substituents to form **C4** slightly increases the rate of substitution. The phenyl is slightly twisted, hence not in the same plane as the pyridine eliminating the possibility of increase in π-conjugation. This is illustrated in the DFT optimised structures in Table 5.1. The slightly higher reactivity of **C4** compared to **C1** is due to the difference in geometry. The DFT optimised structures show that the phenyl substituents curve to one side forming a trough like surface that may trap incoming nucleophiles resulting in the higher reactivity of **C4** compared to **C1**.

All the complexes showed a second substitution step which is of the order of 10^3 smaller than that of the first step. The sharp decrease in reactivity is due to a decrease in the formal charge of the metal centre upon coordination of the first thiourea nucleophile. The reduction of the electrophilicity of Ru(II) in the intermediate is due to the attachment of the electron rich thiourea nucleophile which donates electron density towards the metal centre. Further, the coordinated nucleophile introduces steric hindrance at the Ru(II) metal centre, hindering the approach of the second incoming nucleophile as observed in similar literature studies.[45] The first chloride to undergo substitution is the one within the plane of the ligand framework, $Cl^{\mathbf{44}}$, while the one perpendicular to the ligand plane, $Cl^{\mathbf{103}}$ is substituted last. This is because $Cl^{\mathbf{44}}$ being within the plane of the ligand is most influenced by the ligand π-back-bonding effects. This is confirmed by the DFT calculated bond distances between the metal centre and the chloride ligands showing that Ru-$Cl^{\mathbf{44}}$ bond is slightly longer than Ru-$Cl^{\mathbf{103}}$, hence weaker and most likely to be easier to break. Additionally, since the triphenylphosphine ligand *trans* to $Cl^{\mathbf{103}}$ is a weak π-acceptor,[46] [47] the substitution of the chloro ligand is slower.

The enthalpy of activation, $\Delta H^{\#}$, values for all the reactions are small and positive while the entropy of activation, $\Delta S^{\#}$, values are large and negative. This is indicative of associative mode of substitution mechanism for both reaction steps. This has been observed in other studies dealing with kinetic behaviour of ruthenium as well as platinum metal complexes.[48] [49] [50] [51] [52] [53] [54] [55]

5.5 Conclusions

The study has shown that increasing π-conjugation of the C_3 symmetric tris(2-pyridyl)-1,3,5-triazine by introduction of the quinolyl in place of the pyrydyl substituents increases π-back-bonding of the resultant chelate backbone making its Ru(II) metal centre more electrophilic,

thereby accelerating the substitution reactivity of the compound as observed for the reaction of **C3** compared to **C1**. The methyl substituents on the 2-pyridyl substituents of triazine ligand chelate increase electron density into the triazine ring by σ-induction effects. This lowers π-acceptor of the chelate capacity which results in a less electrophilic metal centre. As a result, it reacts slightly slower as observed in the relative reactivity of **C2** in comparison to the reference complex **C1**. The introduction of the phenyl in the 2,4,6-positions on the 2-pyridyl rings of the triazine ligand **L1**, increases the steric demands of the resultant triazine chelate ligand **L4,** forcing it to assume a trough like orientation at the metal centre. This may facilitate the trapping of incoming nucleophiles increasing reactivity. The study also revealed that the substituents on the pyridyl ligand at the 4-positions of the C_3-centrosymmetric 1,2,3-triazine ligands are far removed from the metal centres and therefore have negligible effect on the rate of the substitution reactions. This is supported by the DFT comparative data (Table 5.3). The substitution reactions proceeds via two steps and the trend for both decreases in the order: **C3** > **C4** > **C1** > **C3**. The reactivity of the second step is about 10^3 lower than the first step. Both reaction steps proceed via the associative mode of substitution.

5.6 References

[1] aA. Ambroise, B. G. Maiya, *Inorganic Chemistry* **2000**, *39*, 4264-4272; bR. Miao, M. T. Mongelli, D. F. Zigler, B. S. Winkel, K. J. Brewer, *Inorganic chemistry* **2006**, *45*, 10413-10415; cK. van der Schilden, F. Garcìa, H. Kooijman, A. L. Spek, J. G. Haasnoot, J. Reedijk, *Angewandte Chemie International Edition* **2004**, *43*, 5668-5670; dH. Xu, K.-C. Zheng, Y. Chen, Y.-Z. Li, L.-J. Lin, H. Li, P.-X. Zhang, L.-N. Ji, *Dalton Transactions* **2003**, 2260-2268; eC. A. Puckett, J. K. Barton, *Journal of the American Chemical Society* **2007**, *129*, 46-47; fJ. L. Beck, R. Gupta, T. Urathamakul, N. L. Williamson, M. M. Sheil, J. R. Aldrich-Wright, S. F. Ralph, *Chemical Communications* **2003**, 626-627; gX. W. Liu, J. Li, H. Deng, K. C. Zheng, Z. W. Mao, L. N. Ji, *Inorganica chimica acta* **2005**, *358*, 3311-3319.

[2] aE. A. Medlycott, G. S. Hanan, *Chemical Society Reviews* **2005**, *34*, 133-142; bH. Hofmeier, U. S. Schubert, *Chemical Society Reviews* **2004**, *33*, 373-399; cR. Zong, R. P. Thummel, *Journal of the American Chemical Society* **2004**, *126*, 10800-10801; dR. J. Crutchley, *Coordination Chemistry Reviews* **2001**, *219*, 125-155.

[3] C. Metcalfe, S. Spey, H. Adams, J. A. Thomas, *Journal of the Chemical Society, Dalton Transactions* **2002**, 4732-4739.

[4] R. Lalrempuia, P. Govindaswamy, Y. A. Mozharivskyj, M. R. Kollipara, *Polyhedron* **2004**, *23*, 1069-1073.

[5] S. Ghumaan, S. Kar, S. M. Mobin, B. Harish, V. G. Puranik, G. K. Lahiri, *Inorganic chemistry* **2006**, *45*, 2413-2423.

[6] I. Yenmez, H. Specker, *Fresenius' Zeitschrift für analytische Chemie* **1979**, *296*, 140-145.

[7] N. Gupta, N. Grover, G. A. Neyhart, P. Singh, H. H. Thorp, *Inorganic Chemistry* **1993**, *32*, 310-316.

[8] S. Sharma, M. Chandra, D. S. Pandey, *European Journal of Inorganic Chemistry* **2004**, *2004*, 3555-3563.

[9] aA. N. Sahay, D. S. Pandey, M. G. Walawalkar, *Journal of Organometallic Chemistry* **2000**, *613*, 250-256; bM. Chandra, A. Sahay, S. M. Mobin, D. S. Pandey, *Journal of organometallic chemistry* **2002**, *658*, 43-49.

[10] S. Sharma, S. K. Singh, D. S. Pandey, *Inorganic chemistry* **2008**, *47*, 1179-1189.

[11] F. H. Case, E. Koft, *Journal of the American Chemical Society* **1959**, *81*, 905-906.

[12] S. Sharma, S. K. Singh, D. S. Pandey, *Inorganic Chemistry* **2008**, *47*, 1179-1189.

[13] R. A. Gaussian, *Inc., Wallingford CT* **2009**, *121*, 150-166.

[14] P. J. Hay, W. R. Wadt, *The Journal of chemical physics* **1985**, *82*, 270-283.

[15] C. Lee, W. Yang, R. G. Parr, *Physical Review B* **1988**, *37*, 785.

[16] A. D. Becke, *The Journal of chemical physics* **1993**, *98*, 5648-5652.

[17] M. Okamura, M. Yoshida, R. Kuga, K. Sakai, M. Kondo, S. Masaoka, *Dalton Transactions* **2012**, *41*, 13081-13089.

[18] M. Cossi, N. Rega, G. Scalmani, V. Barone, *Journal of computational chemistry* **2003**, *24*, 669-681.

[19] T. Le Bahers, T. Pauporté, G. Scalmani, C. Adamo, I. Ciofini, *Physical Chemistry Chemical Physics* **2009**, *11*, 11276-11284.

[20] A. Shaira, D. Jaganyi, *Journal of Coordination Chemistry* **2014**, *67*, 2843-2857.

[21] P. K. Chattaraj, U. Sarkar, M. Elango, R. Parthasarathi, V. Subramanian, *arXiv preprint physics/0509089* **2005**.

[22] A. Cedillo, R. Contreras, *Journal of the Mexican Chemical Society* **2012**, *56*, 257-260.

[23] E. Seifert, American Chemical Society Publications, **2014**.

[24] R. G. Parr, W. Yang, Oxford University Press, New York, **1989**.

[25] P. Geerlings, F. De Proft, W. Langenaeker, *Chemical Reviews* **2003**, *103*, 1793-1874.

[26] R. G. Parr, W. Yang, *Journal of the American Chemical Society* **1984**, *106*, 4049-4050.

[27] W. Yang, W. J. Mortier, *Journal of the American Chemical Society* **1986**, *108*, 5708-5711.

[28] S. Sangilipandi, D. Sutradhar, K. Bhattacharjee, W. Kaminsky, S. R. Joshi, A. K. Chandra, K. M. Rao, *Inorganica Chimica Acta* **2016**, *441*, 95-108.

[29] S. B. Jensen, S. J. Rodger, M. D. Spicer, *Journal of Organometallic Chemistry* **1998**, *556*, 151-158.

[30] T. Ben-Hadda, C. Mountassir, H. Le Bozec, *Polyhedron* **1995**, *14*, 953-955.

[31] D. Reddy, K. J. Akerman, M. P. Akerman, D. Jaganyi, *Transition Metal Chemistry* **2011**, *36*, 593-602.

[32] M. C. Rezende, D. Millán, *Journal of the Brazilian Chemical Society* **2011**, *22*, 2078-2086.

[33] A. Shaira, D. Reddy, D. Jaganyi, *Dalton Transactions* **2013**, *42*, 8426-8436.

[34] A. Hofmann, D. Jaganyi, O. Q. Munro, G. Liehr, R. van Eldik, *Inorganic Chemistry* **2003**, *42*, 1688-1700.

[35] R. Romeo, M. R. Plutino, L. Monsù Scolaro, S. Stoccoro, G. Minghetti, *Inorganic Chemistry* **2000**, *39*, 4749-4755.

[36] A. Hofmann, L. Dahlenburg, R. van Eldik, *Inorganic chemistry* **2003**, *42*, 6528-6538.

[37] Ž. D. Bugarčić, S. T. Nandibewoor, M. S. A. Hamza, F. Heinemann, R. van Eldik, *Dalton Transactions* **2006**, 2984-2990.

[38] D. Jaganyi, D. Reddy, J. A. Gertenbach, A. Hofmann, R. van Eldik, *Dalton Transactions* **2004**, 299-304.

[39] I. M. Wekesa, D. Jaganyi, *Dalton Transactions* **2014**, *43*, 2549-2558.

[40] A. Djeković, B. Petrović, Ž. D. Bugarčić, R. Puchta, R. van Eldik, *Dalton Transactions* **2012**, *41*, 3633-3641.

[41] S. Jovanović, J. Bogojeski, M. Petković, Ž. D. Bugarčić, *Journal of Coordination Chemistry* **2015**, *68*, 3148-3163.

[42] D. Jaganyi, F. Tiba, *Transition Metal Chemistry* **2003**, *28*, 803-807.

[43] G. Kinunda, D. Jaganyi, *Transition Metal Chemistry* **2014**, *39*, 451-459.

[44] M. W. M., M. Allen, J. Deogratius, *International Journal of Chemical Kinetics* **2018**, *50*, 531-543.

[45] B. B. Khusi, A. Mambanda, D. Jaganyi, *Journal of Coordination Chemistry* **2016**, *69*, 2121-2135.

[46] T. Karlen, P. Dani, D. M. Grove, P. Steenwinkel, G. van Koten, *Organometallics* **1996**, *15*, 5687-5694.

[47] C. A. Tolman, *Journal of the American Chemical Society* **1970**, *92*, 2953-2956.

[48] A. Rilak, R. Puchta, Ž. D. Bugarčić, *Polyhedron* **2015**, *91*, 73-83.

[49] H. K. Mandal, P. K. Ghosh, A. Mahapatra, *Polyhedron* **2010**, *29*, 2867-2874.

[50] Z. D. Bugarcic, G. Liehr, R. van Eldik, *Journal of the Chemical Society, Dalton Transactions* **2002**, 2825-2830.

[51] J. Rosić, B. Petrović, M. I. Djuran, Ž. D. Bugarčić, *Monatshefte für Chemie-Chemical Monthly* **2007**, *138*, 1-11.

[52] V. Vasić, M. Čakar, J. Savić, B. Petrović, J. Nedeljković, Ž. Bugarčić, *Polyhedron* **2003**, *22*, 279-285.

[53] P. O. Ongoma, D. Jaganyi, *Transition Metal Chemistry* **2014**, *39*, 407-420.

[54] E. Hakan, P. Ralph, v. E. Rudi, *European Journal of Inorganic Chemistry* **2009**, *2009*, 1331-1338.

[55] Z. D. Bugarcic, F. W. Heinemann, R. v. Eldik, *Dalton Transactions* **2004**, 279-286.

5.7 Supporting information

Included in the supplementary information are NMR spectra, mass spectra, tables of kinetic data and various kinetic graphs for the synthetic and kinetic analysis of the complexes; **C1, C2, C3** and **C4** investigated in this study.

5.7.1 Synthesis

5.7.1.1 Ligands

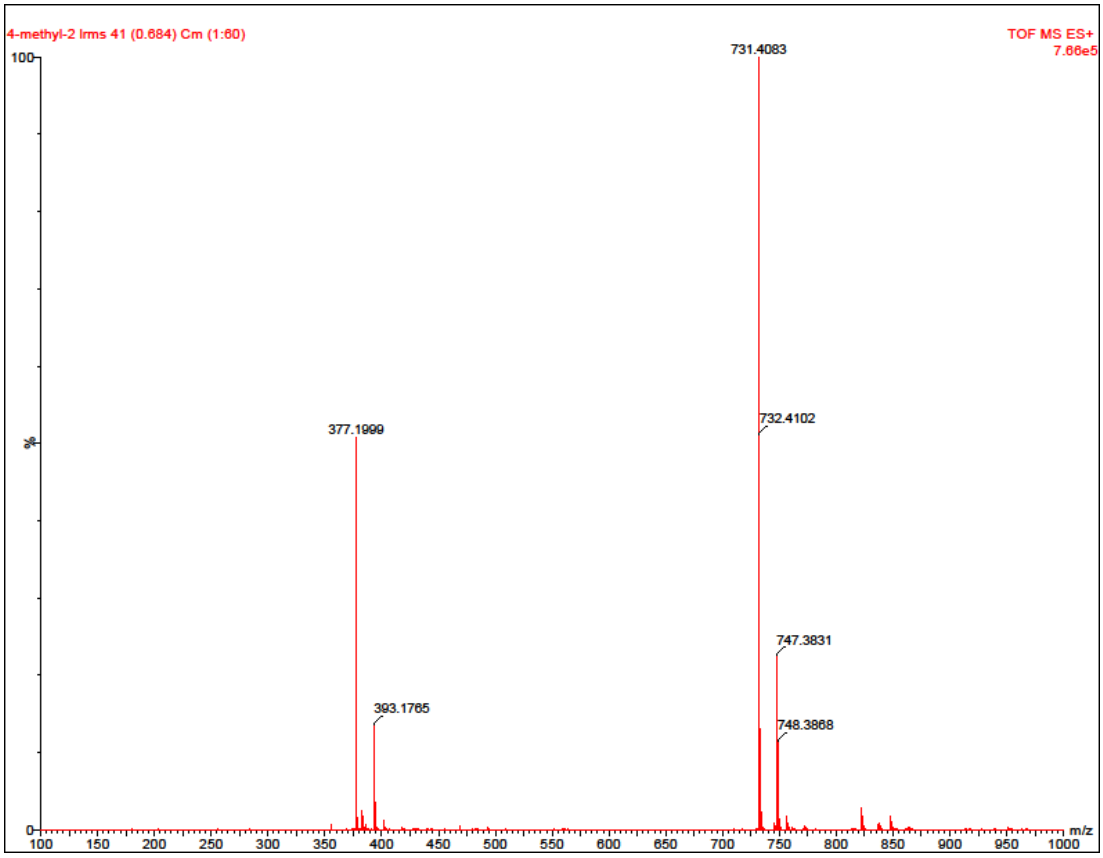

Figure SI 5.1 TOF mass spectrum for 2,4,6-tris(4-methyl-2-pyridyl)-1,3,5-triazine(**L2**) ligand

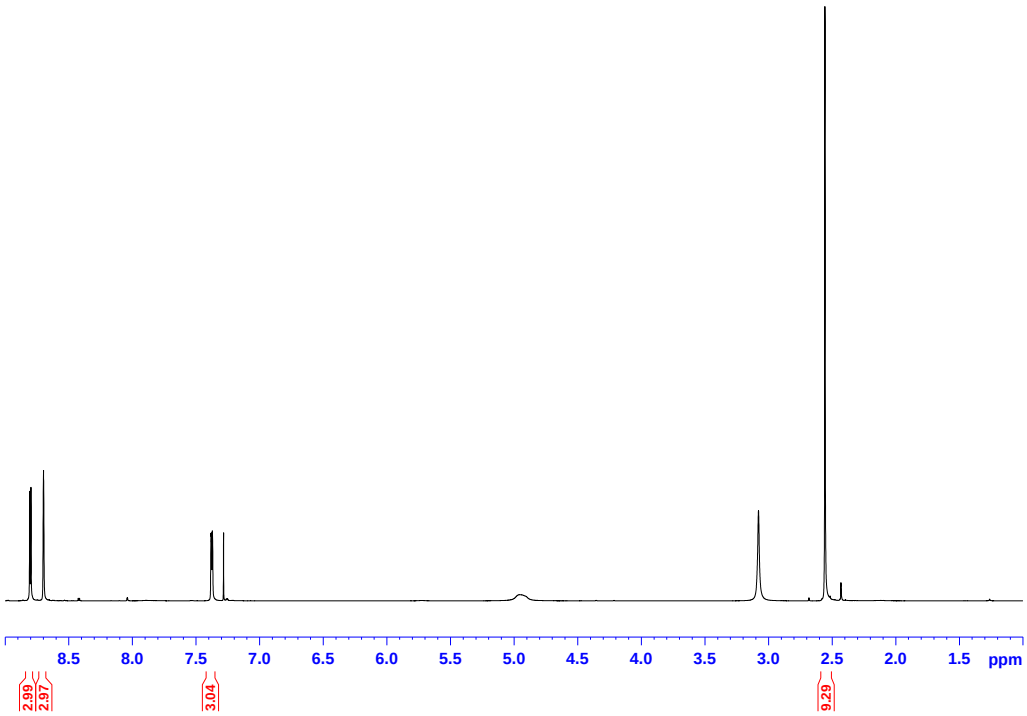

Figure SI 5.2 ^{1}H NMR for **L2** ligand

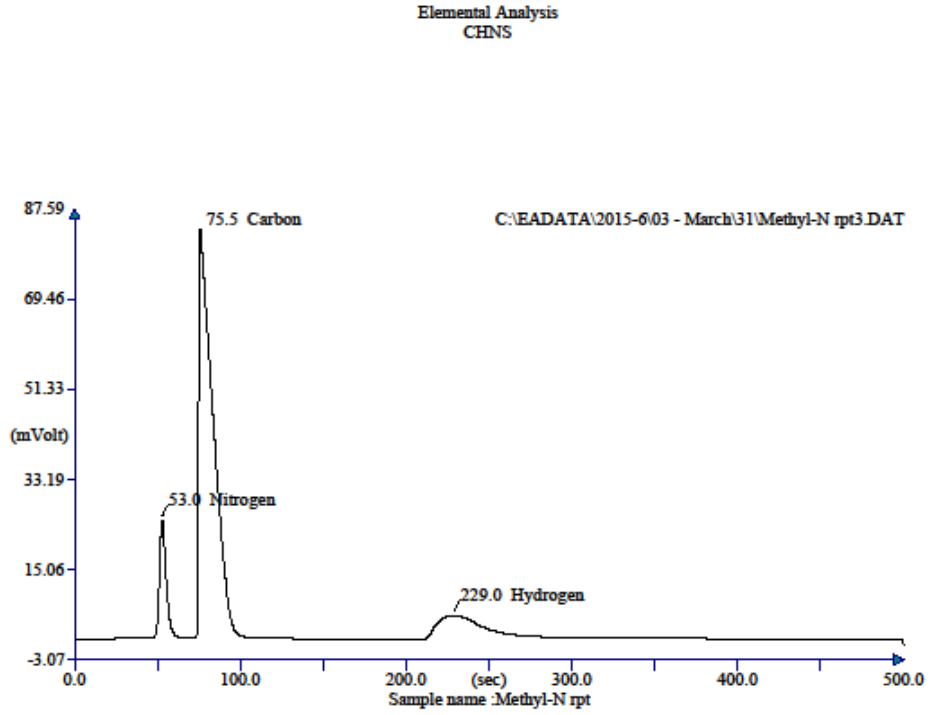

Retention Time (min)	Element Name	Element %
0.883	Nitrogen	23.651
1.258	Carbon	70.498
3.817	Hydrogen	5.093
		99.241

Figure SI 5.3 CHN spectrum for **L2** ligand

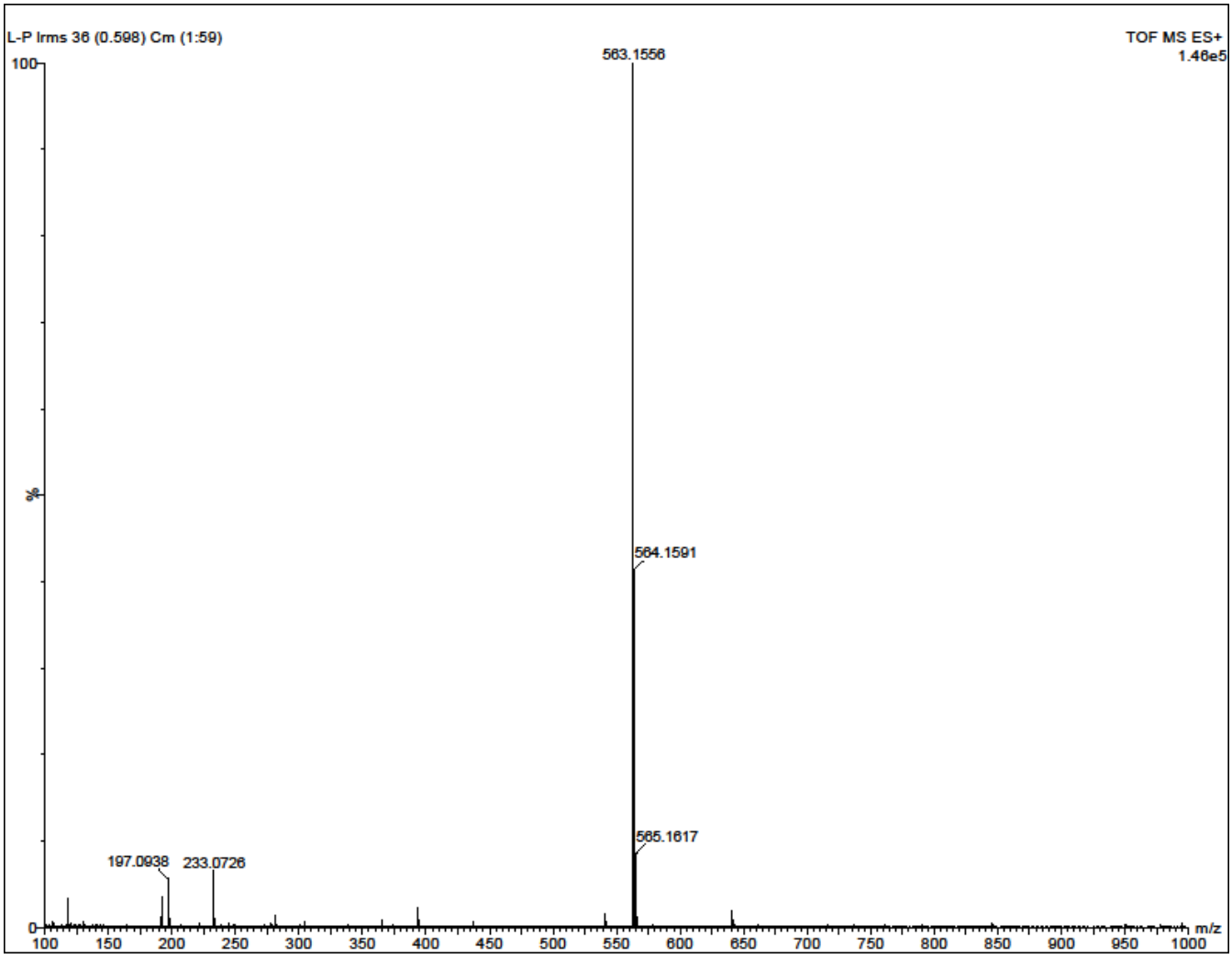

Figure SI 5.4 TOF mass spectrum for 2,4,6-tris(4-phenyl-2-pyridyl)-1,3,5-triazine(**L4**) ligand

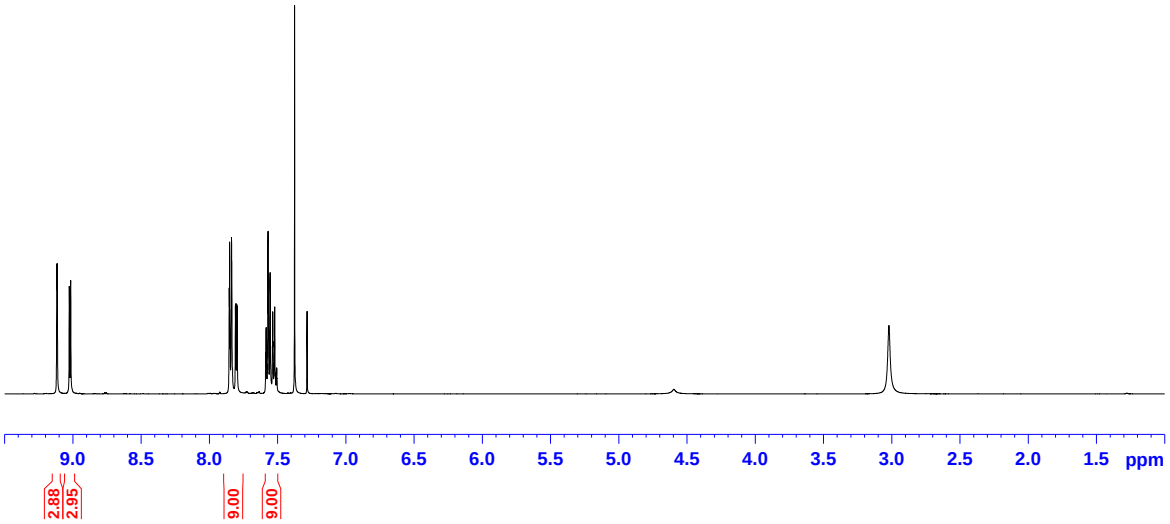

Figure SI 5.5 ^{1}H NMR for **L4** ligand

Figure SI 5.6 TOF mass spectrum for 2,4,6-tris(2-quinolyl)-1,3,5-triazine(**L3**) ligand

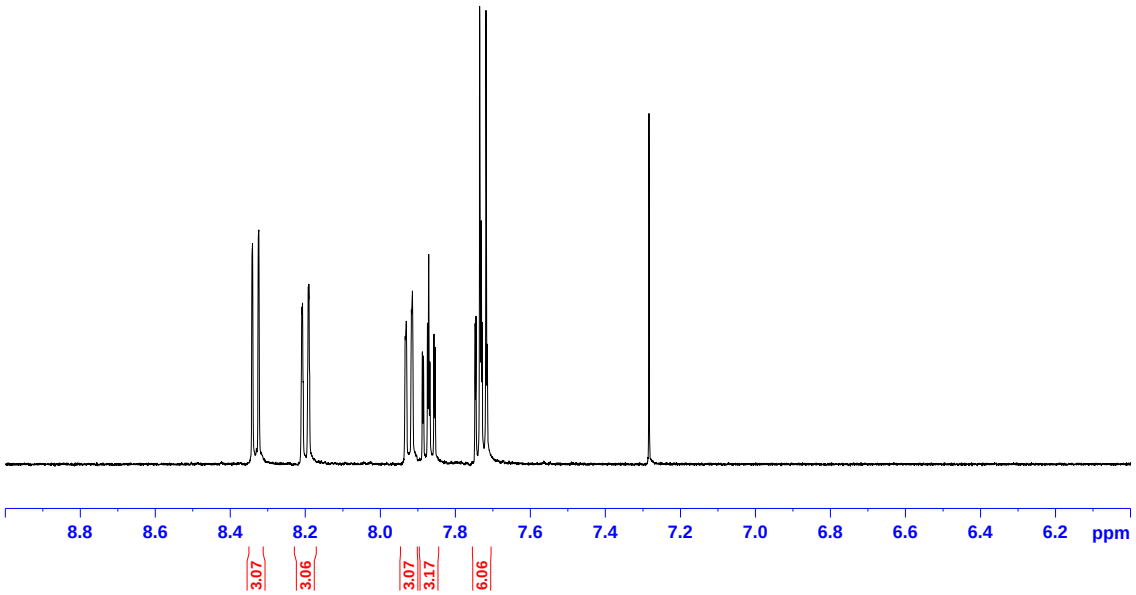

Figure SI 5.7 [1]H NMR for **L3** ligand

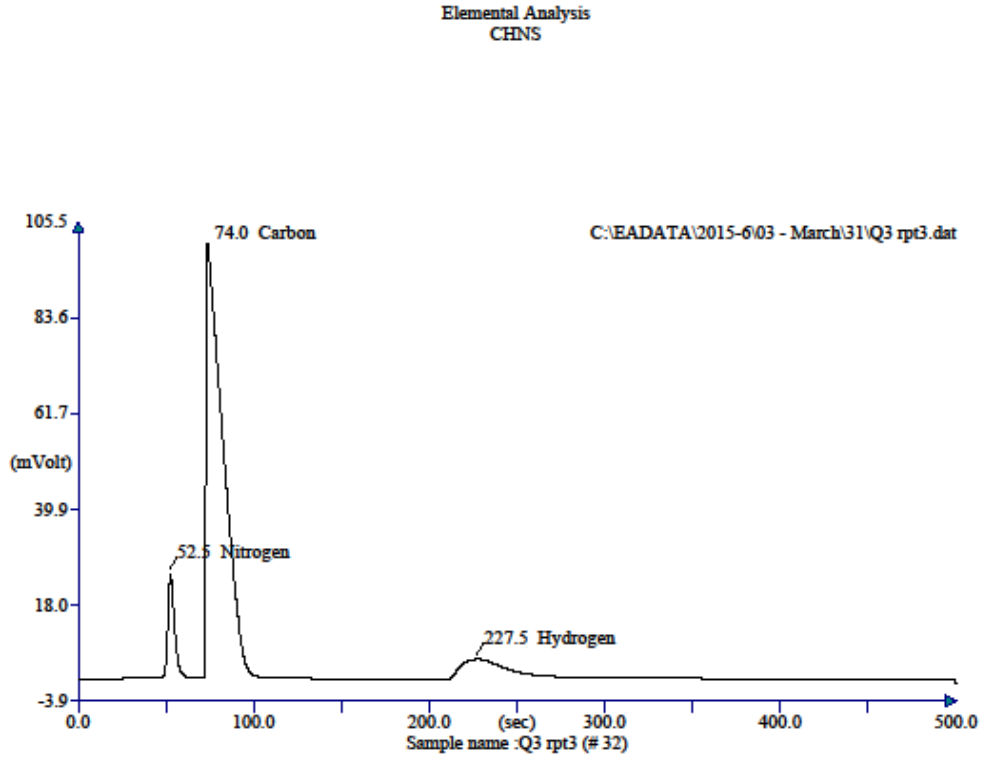

Retention Time (min)	Element Name	Element %
0.875	Nitrogen	18.455
1.233	Carbon	77.663
3.792	Hydrogen	3.858
		99.976

Figure SI 5.8 CHN spectrum for **L3** ligand

5.6.1.2 Complexes

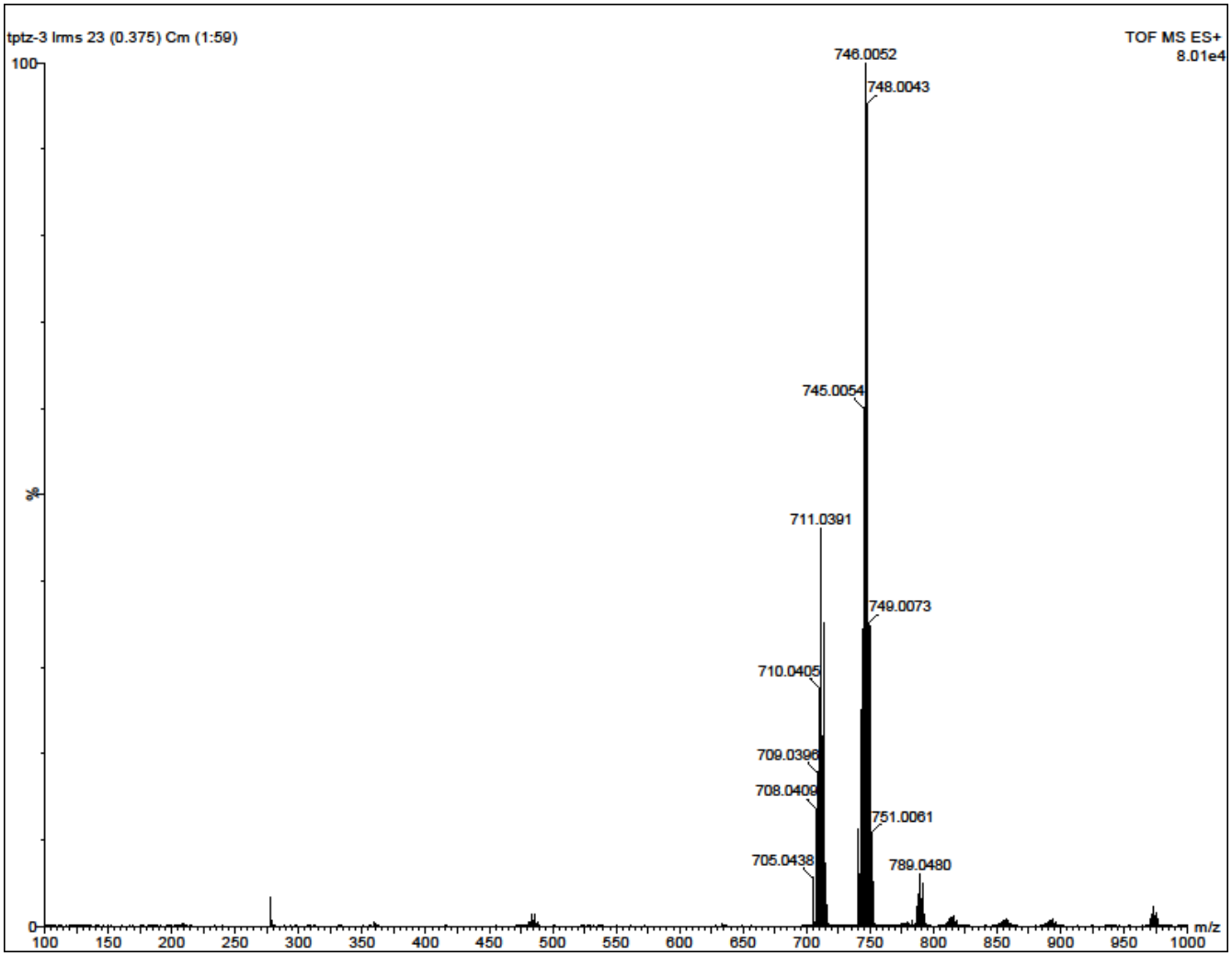

Figure SI 5.9 TOF mass spectrum for complex **C1**

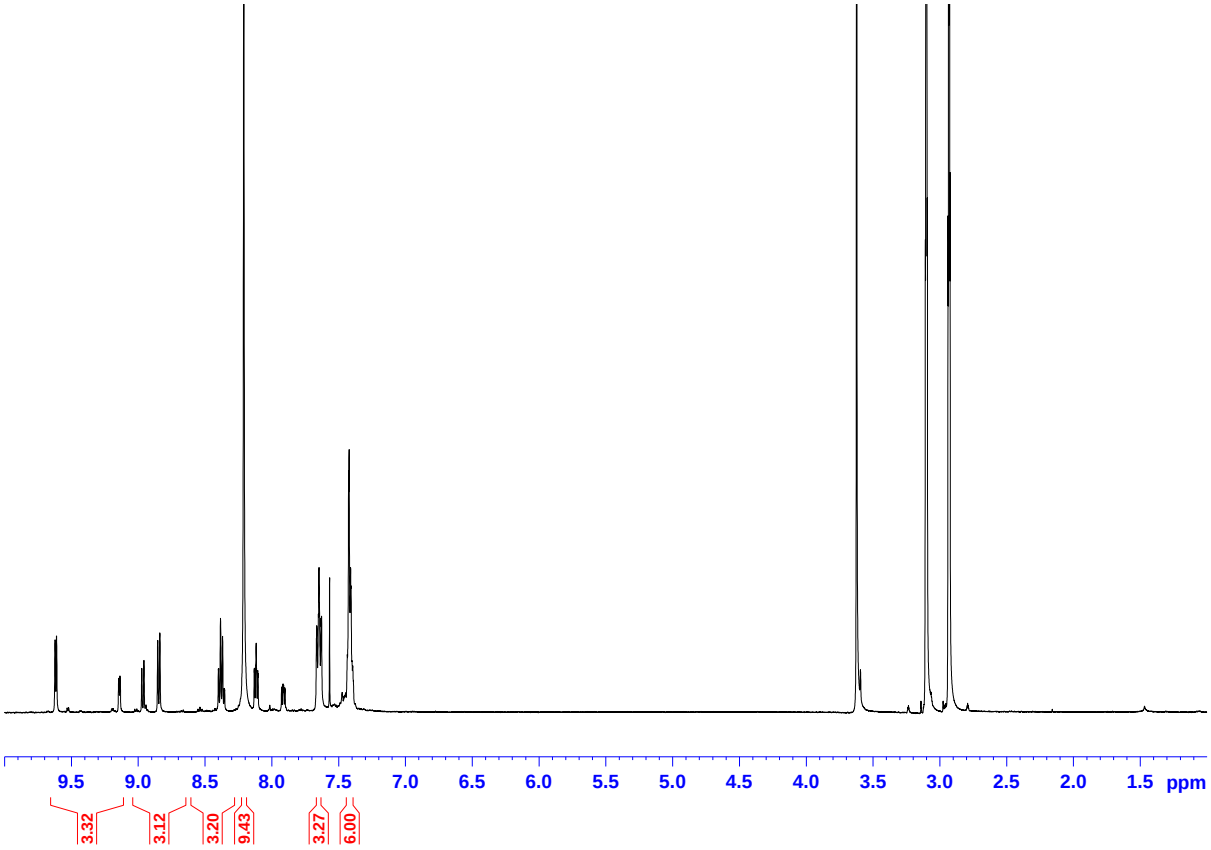

Figure SI 5.10 ^{1}H NMR for complex **C1**

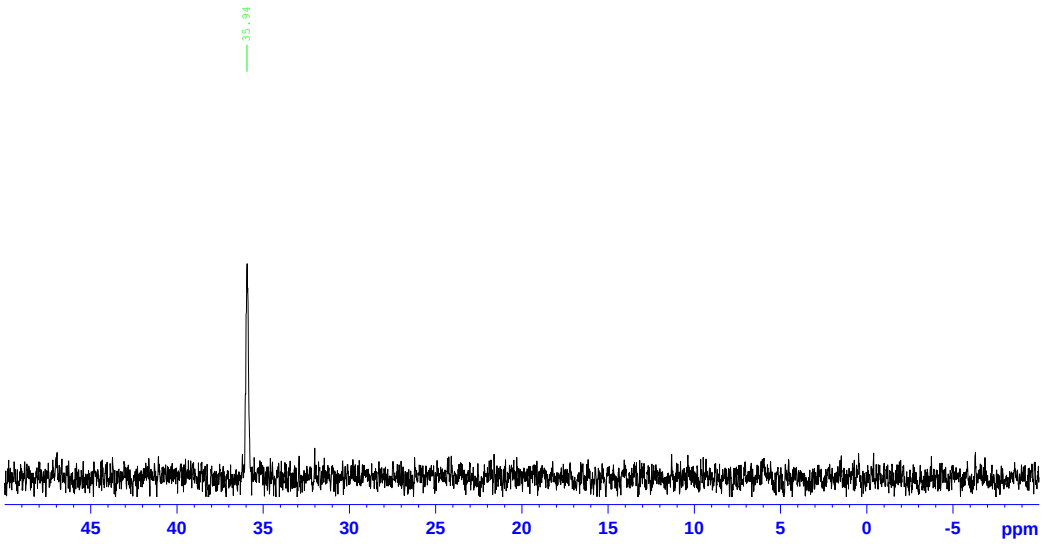

Figure SI 5.11 ^{31}P NMR spectrums for complex **C1**

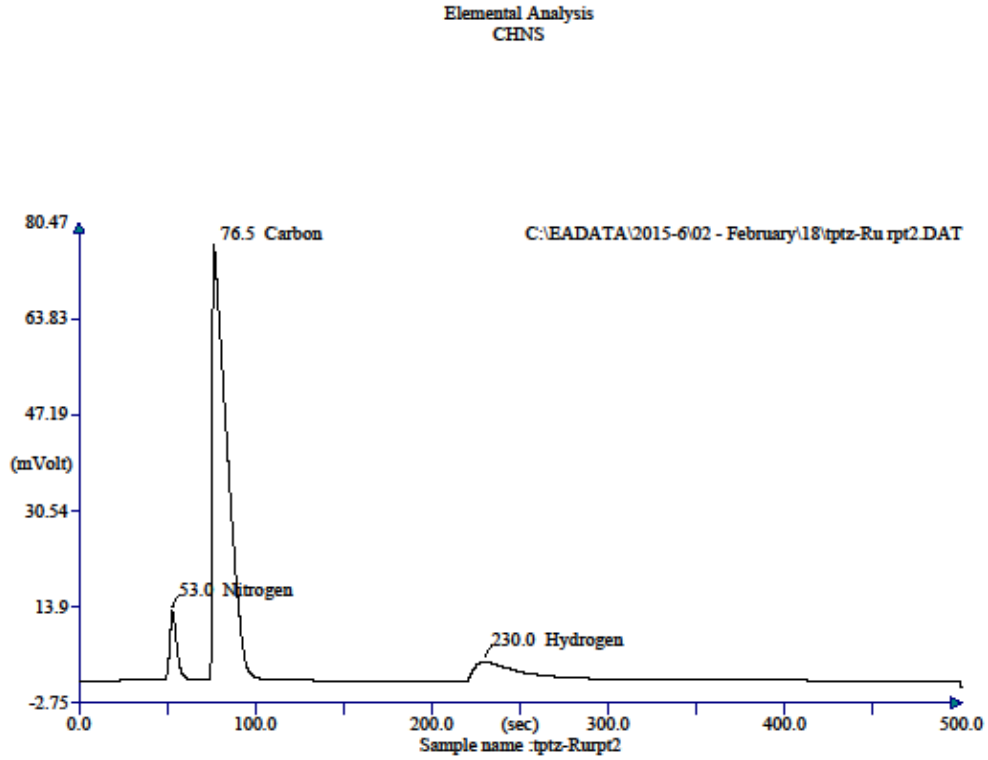

Retention Time (min)	Element Name	Element %
0.883	Nitrogen	11.049
1.275	Carbon	56.939
3.833	Hydrogen	3.305
		71.293

Figure SI 5.12 CHN spectrum for complex **C1**

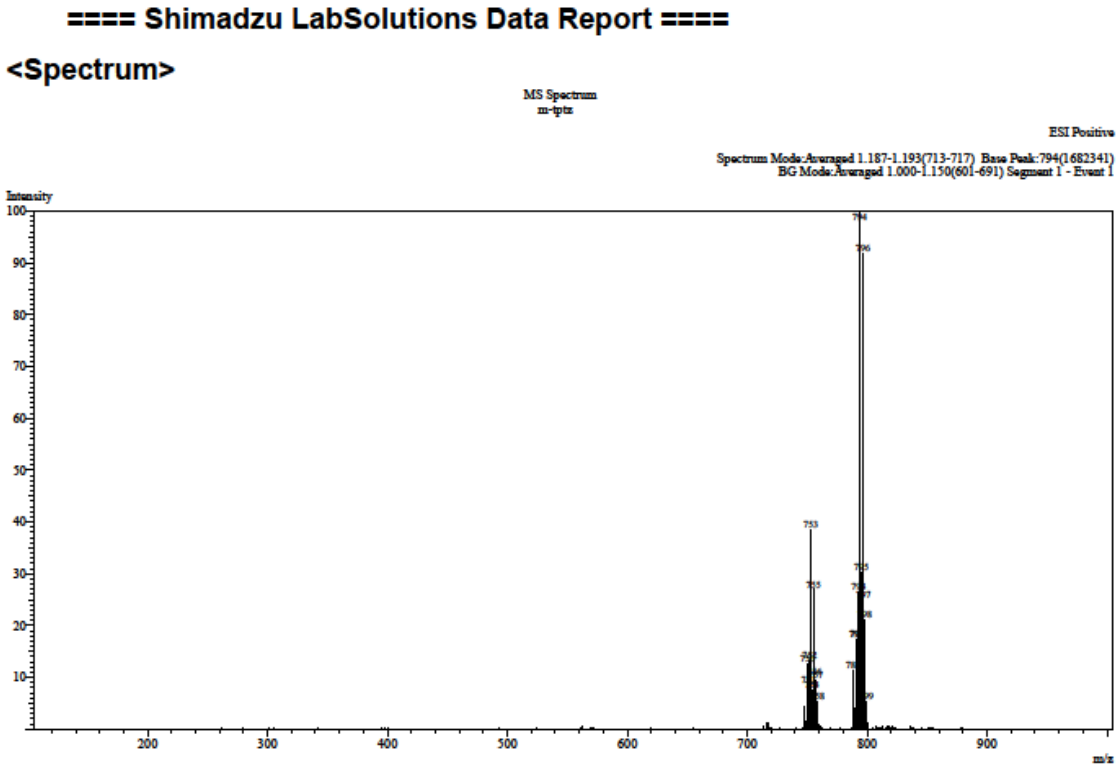

Figure SI 5.13 LC-MS mass spectrum for complex **C2**

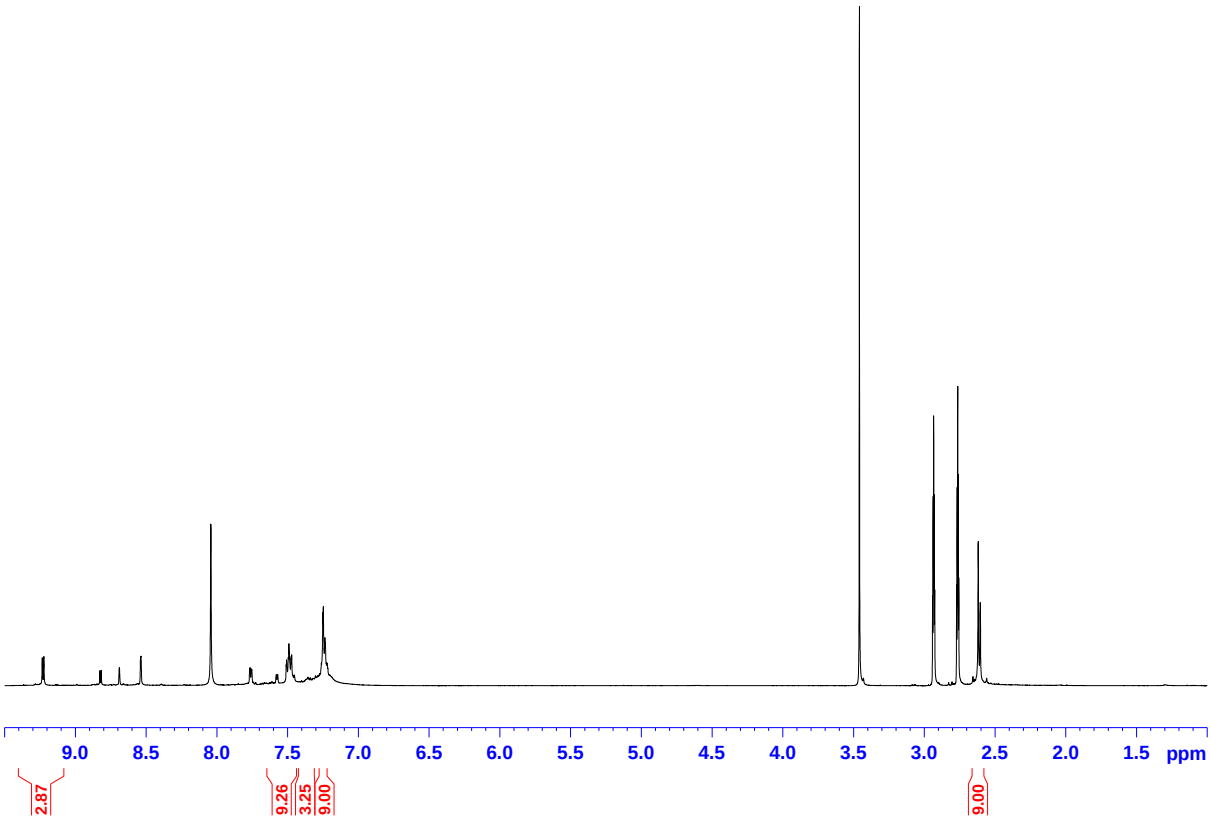

Figure SI 5.14 ^{1}H NMR for complex **C2**

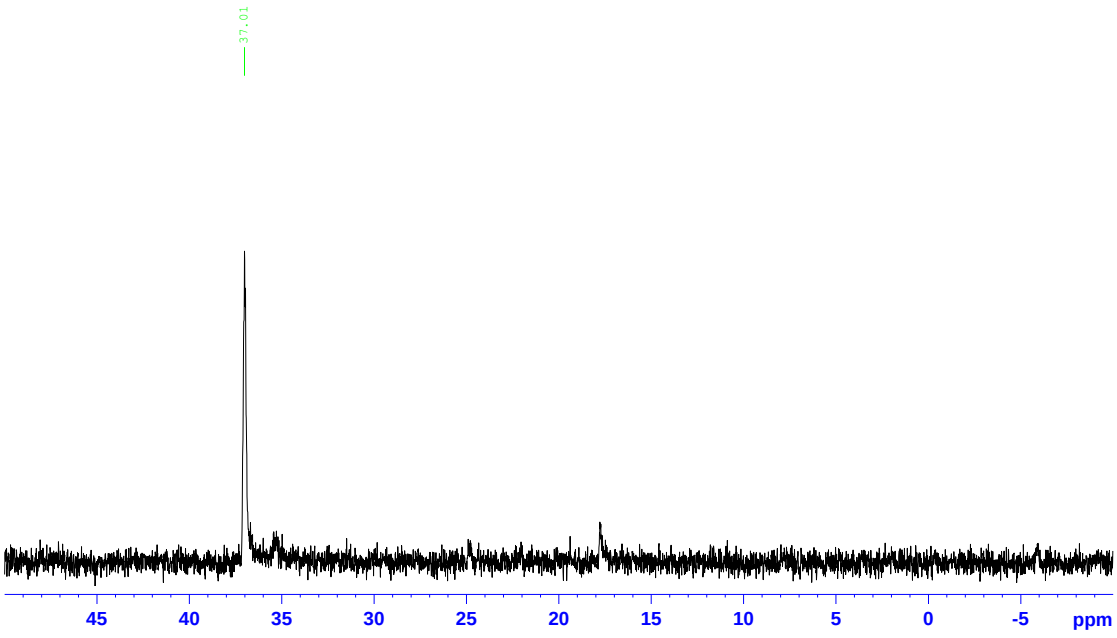

Figure SI 5.15 ^{31}P NMR spectrums for complex **C2**

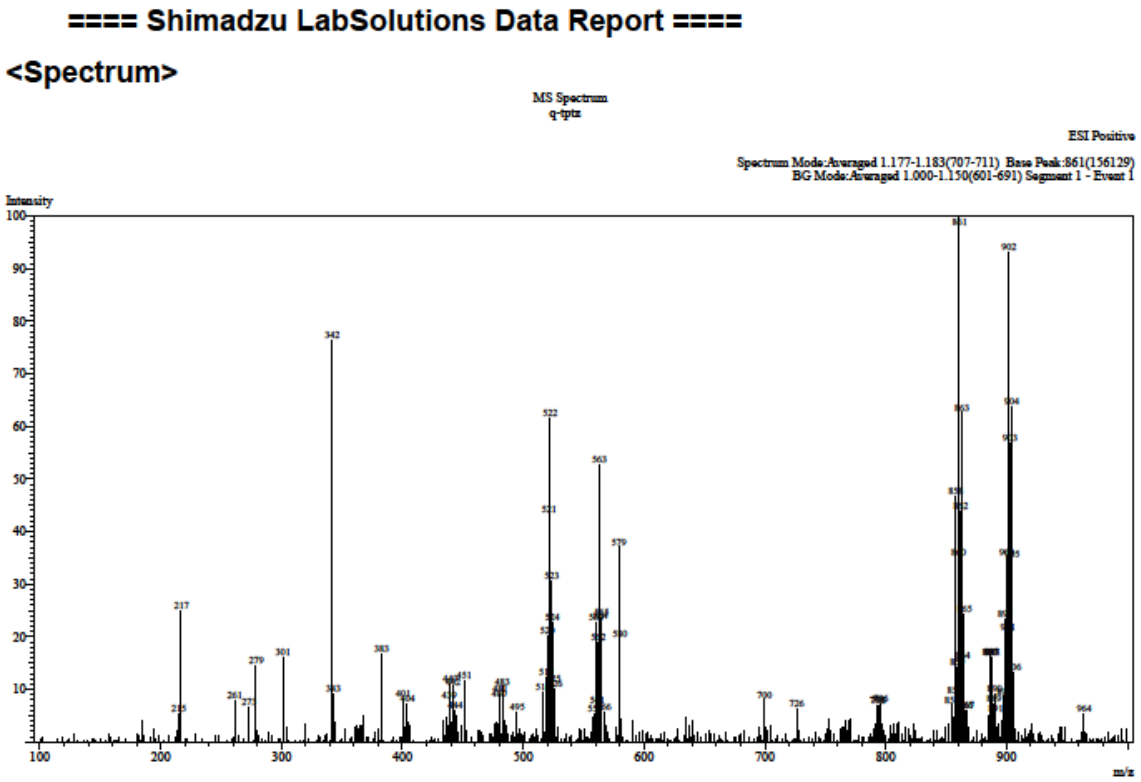

Figure SI 5.16 LC-MS mass spectrum for complex **C3**

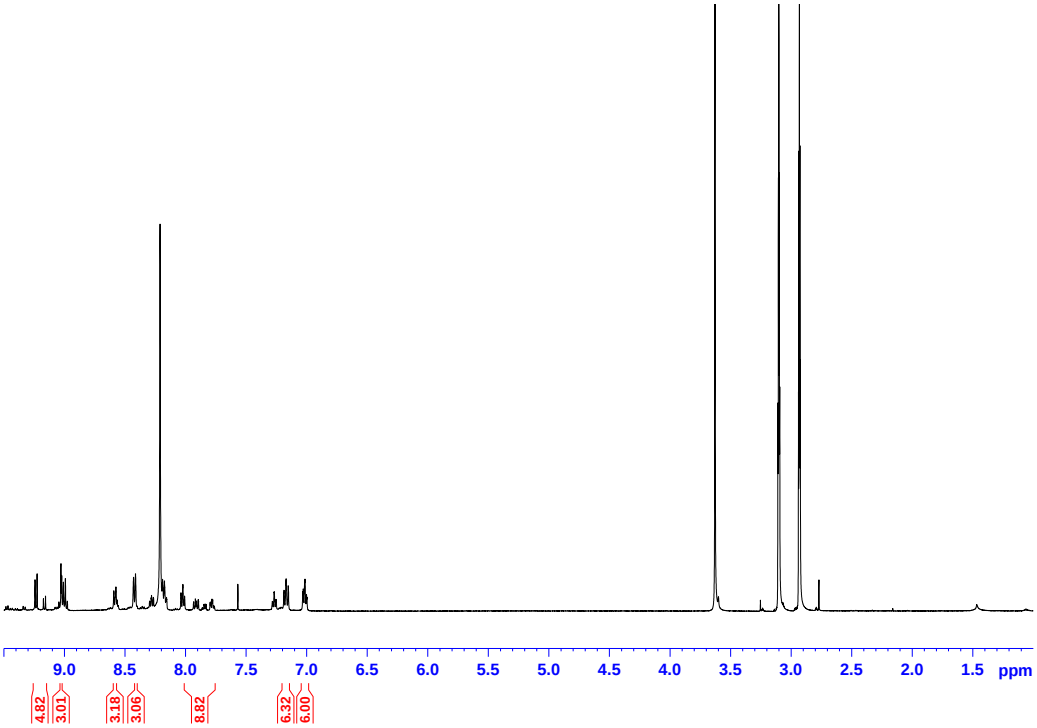

Figure SI 5.17 ^{1}H NMR for complex **C3**

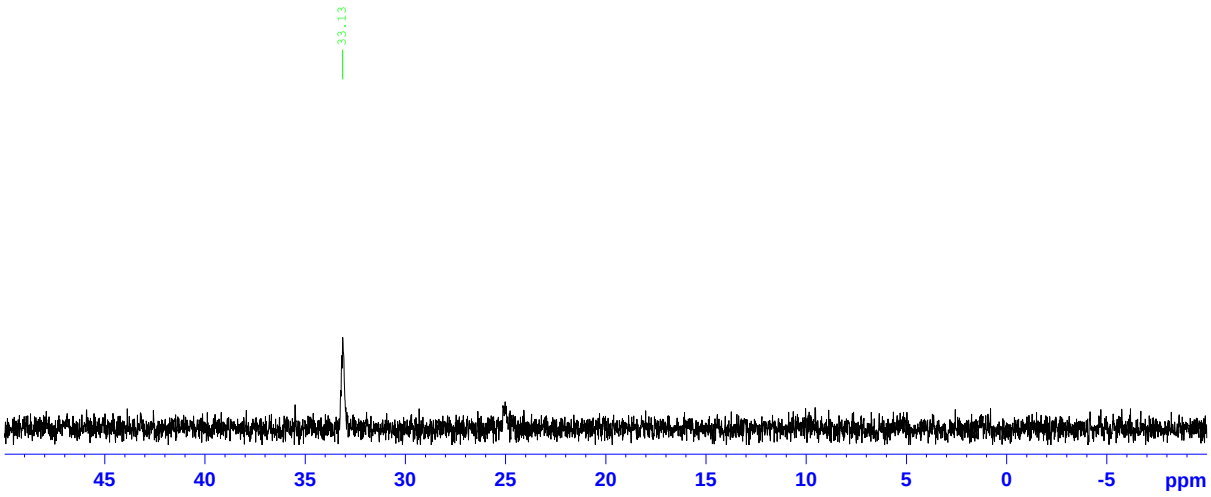

Figure SI 5.18 ^{31}P NMR spectrums for complex **C3**

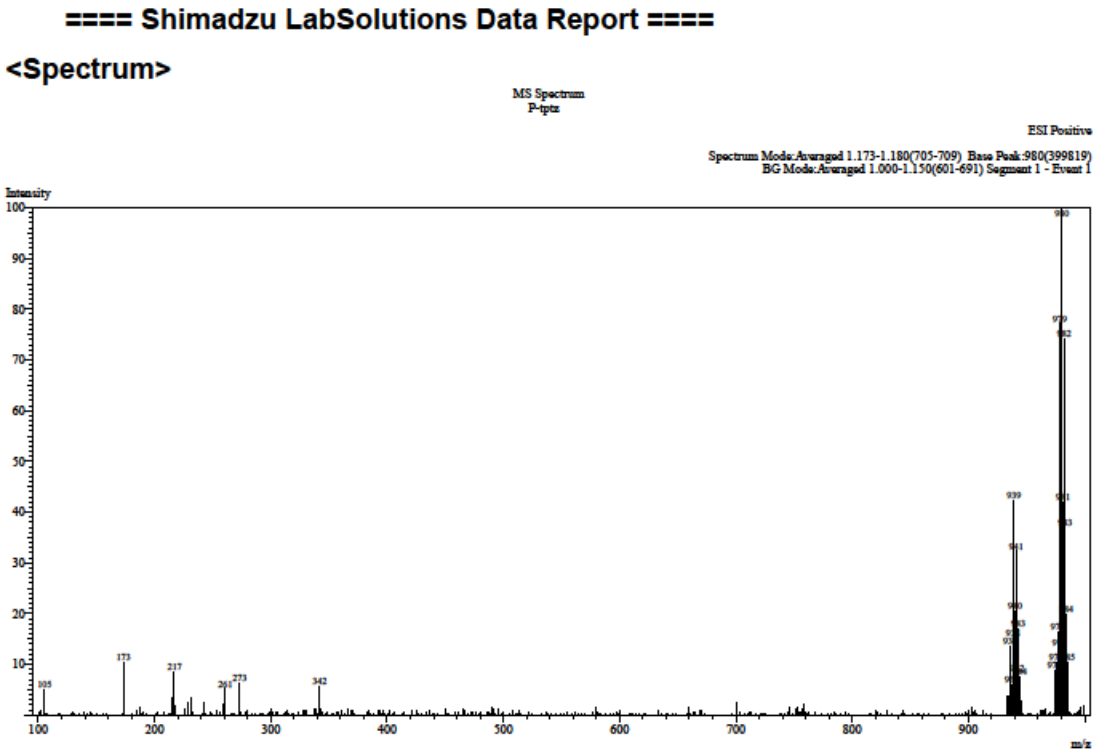

Figure SI 5.19 LC-MS mass spectrum for complex **C4**

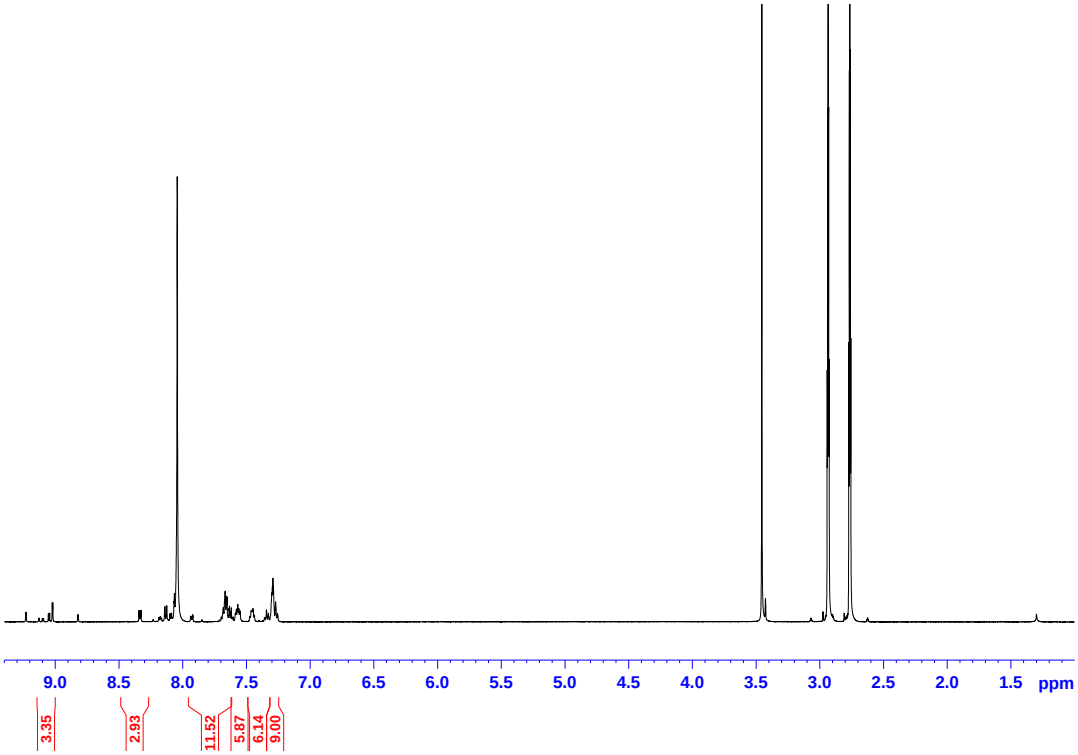

Figure SI 5.20 ^{1}H NMR for complex **C4**

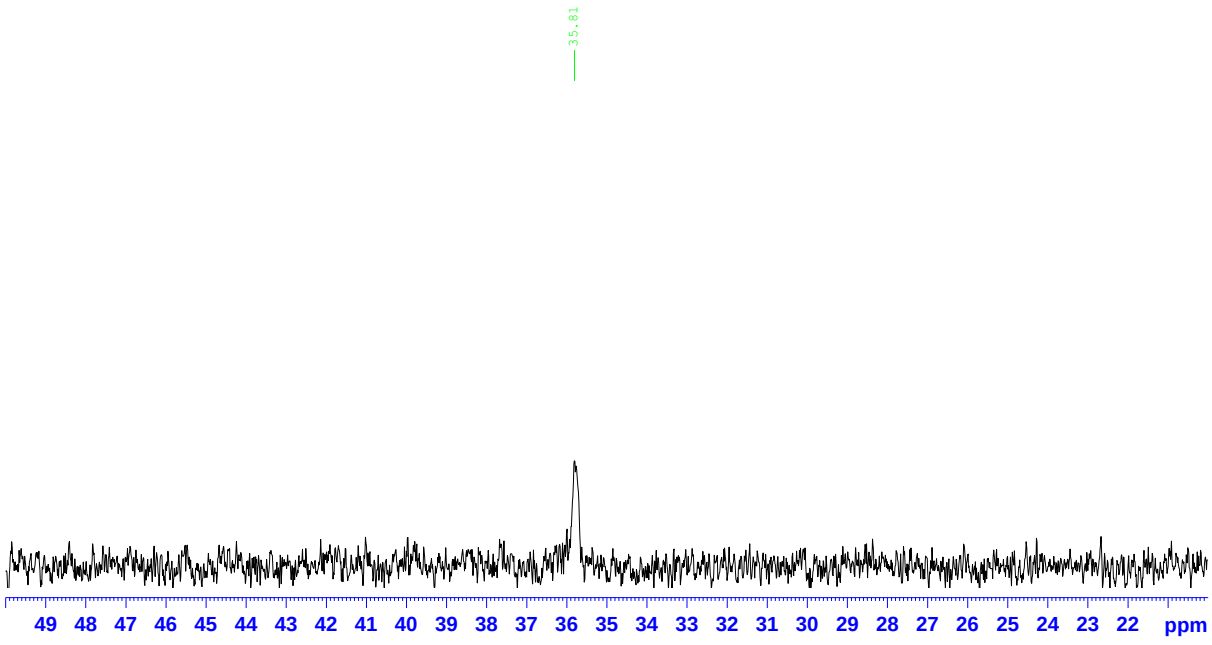

Figure SI 5.21 ^{31}P NMR spectrums for complex **C4**

5.7.2 Kinetic Data

Table SI 5.1 Observed rate constants and the corresponding nucleophile concentrations for step 1 of **C1**

[Nu]/M	k_{obs}/s^{-1} TU	[Nu]/M	k_{obs} / s^{-1} DMTU	[Nu]/M	k_{obs} / s^{-1} TMTU
0.0055	0.072	0.011	0.123	0.040	0.150
0.011	0.144	0.022	0.240	0.08	0.300
0.0165	0.215	0.033	0.364	0.12	0.445
0.022	0.28	0.044	0.480	0.16	0.593
0.0275	0.353	0.055	0.596	0.20	0.745

Table SI 5.2 Observed rate constants and the corresponding nucleophile concentrations for step 2 of **C1**

[Nu]/M	k_{obs}/ s^{-1} TU	k_{obs} / s^{-1} DMTU	k_{obs} / s^{-1} TMTU
0.02	4.42E-5	3E-5	2.01E-5
0.04	8.8E-5	6E-5	4E-5
0.06	1.327E-4	9E-5	6.03E-5
0.08	1.767E-4	1.2E-4	8.03E-5
0.1	2.2E-4	1.5E-4	1E-4

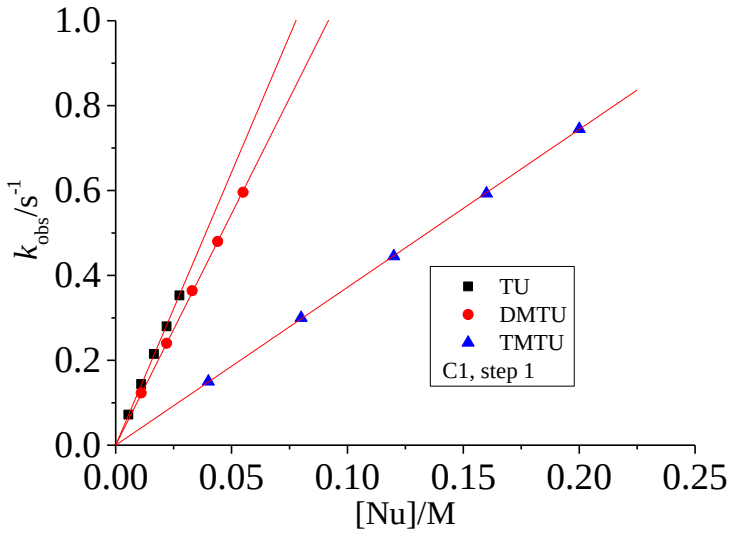

Figure SI 5.22 Step 1 concentration dependence plots for the reaction of **C1** with thiourea nucleophiles at 298 K

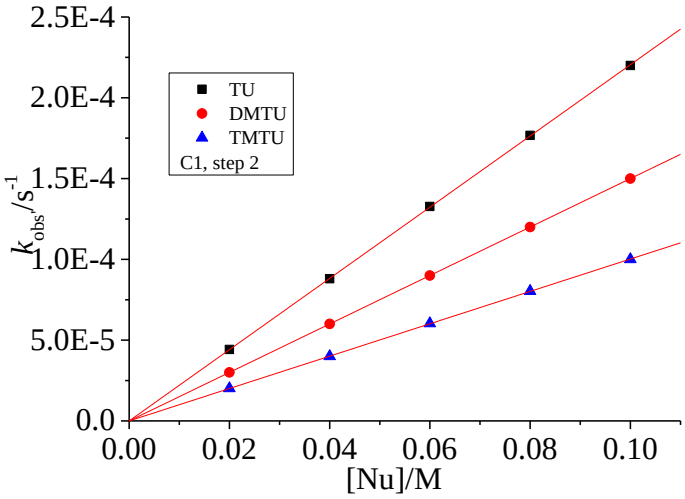

Figure SI 5.23 Step 2 concentration dependence plots for the reaction of **C1** with thiourea nucleophiles at 298 K

Table SI 5.3 Values of ln(k_2/T) and 1/T for step 1 of **C1**

1/T	**ln(k_2/T) TU**	**ln(k_2/T) DMTU**	**ln(k_2/T) TMTU**
0.00336	-2.89	-3.3	-4.6
0.0033	-2.52	-2.86	-4.08
0.00325	-2.2	-2.48	-3.64
0.00319	-1.82	-2.05	-3.15
0.00314	-1.5	-1.68	-2.7

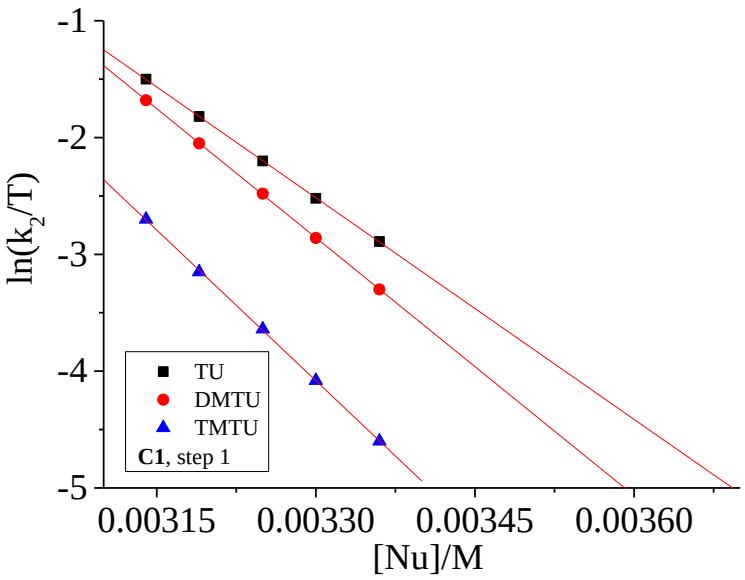

Figure SI 5.24 Step 1 temperature dependence plots for the reaction of **C1** with the thiourea nucleophiles

Table SI 5.4 Observed rate constants and the corresponding nucleophile concentrations for step 1 of **C2**

[Nu]/M	k_{obs}/s^{-1} **TU**	k_{obs} / s^{-1} **DMTU**	k_{obs} / s^{-1} **TMTU**
0.01	0.099	0.067	0.021
0.02	0.198	0.133	0.042
0.03	0.297	0.201	0.0633
0.04	0.396	0.2681	0.0841
0.05	0.495	0.335	0.106

Table SI 5.5 Observed rate constants and the corresponding nucleophile concentrations for step 2 of **C2**

[Nu]/M	k_{obs}/ s^{-1} **TU**	k_{obs} / s^{-1} **DMTU**	k_{obs} / s^{-1} **TMTU**
0.04	4.5E-5	8E-5	0.000007
0.08	9E-5	1.6E-4	0.000014
0.12	1.346E-4	2.4E-4	0.000021
0.16	1.8E-4	3.2E-4	0.000028
0.20	2.26E-4	4E-4	0.0000351

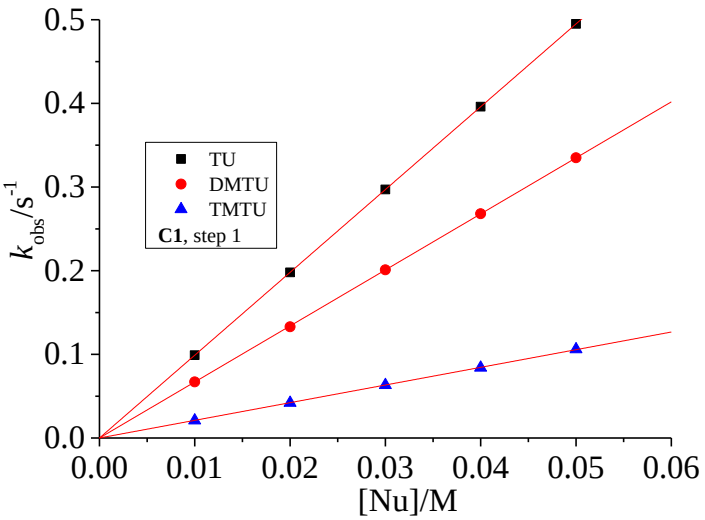

Figure SI 5.25 Step 1 concentration dependence plots for the reaction of **C2** with thiourea nucleophiles at 298 K

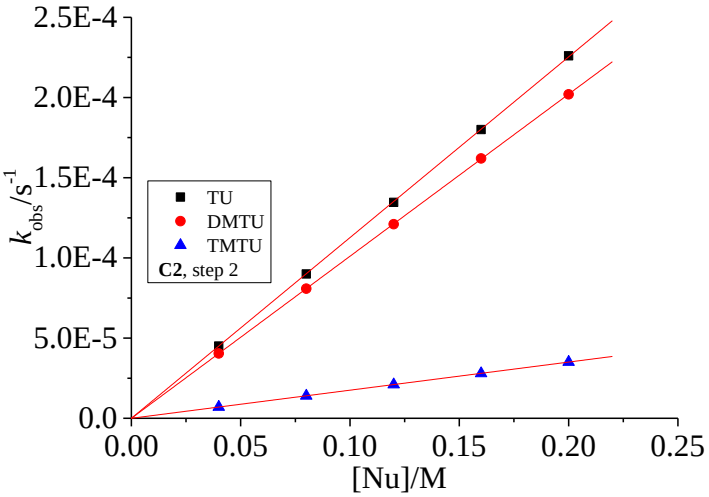

Figure SI 5.26 Step 2 concentration dependence plots for the reaction of **C2** with thiourea nucleophiles at 298 K

Table SI 5.6 Values of ln(k_2/T) and 1/T for step 2 of **C2**

1/T	**ln(k_2/T) TU**	**ln(k_2/T) DMTU**	**ln(k_2/T) TMTU**
0.00336	-11.3	-10.7	-13.11
0.0033	-10.73	-10.18	-12.5
0.00325	-10.25	-9.73	-11.92
0.00319	-9.69	-9.21	-11.28
0.00314	-9.2	-8.79	-10.75

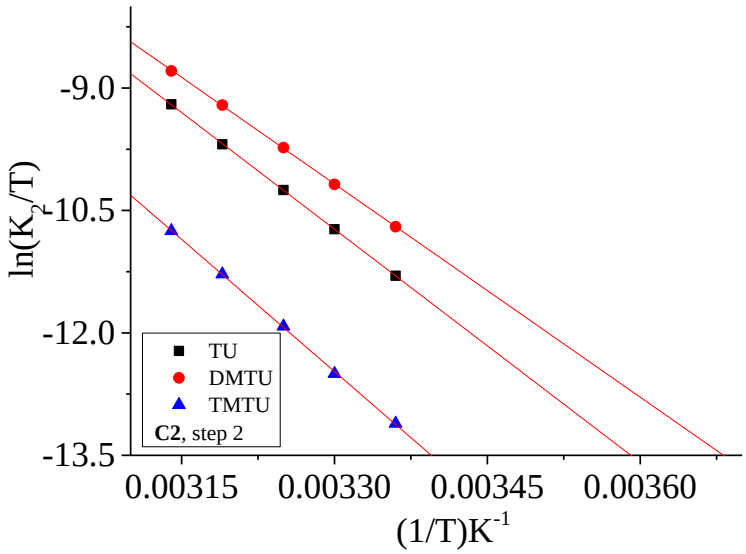

Figure SI 5.27 Step 2 temperature dependence plots for the reaction of **C2** with the thiourea nucleophiles

Table SI 5.7 Observed rate constants and the corresponding nucleophile concentrations for step 1 of **C3**

[Nu]/M	k_{obs}/s^{-1} TU	k_{obs} / s^{-1} DMTU	[Nu]/M	k_{obs} / s^{-1} TMTU
0.012	1.802	2.114	0.04	1.446
0.024	3.605	4.237	0.08	2.892
0.036	5.407	6.351	0.12	4.338
0.048	7.349	8.494	0.16	5.745
0.06	9.151	10.608	0.2	7.23

Table SI 5.8 Observed rate constants and the corresponding nucleophile concentrations for step 2 of **C3**

[Nu]/M	k_{obs} /s^{-1} TU	k_{obs} / s^{-1} DMTU	k_{obs} / s^{-1} TMTU
0.004	4.26E-4	2.26E-5	0.00000668
0.008	8.5E-4	4.5E-5	0.0000140
0.012	0.00128	6.75E-5	0.00002004
0.016	0.0017	9E-5	0.0000268
0.02	0.00212	1.128E-4	0.0000334

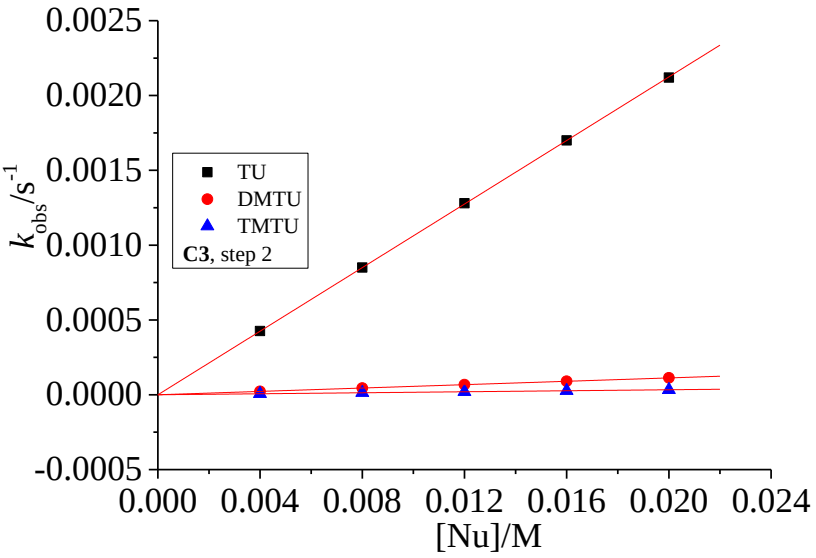

Figure SI 5.28 Step 2 concentration dependence plots for the reaction of **C3** with thiourea nucleophiles at 298 K

Table SI 5.9 Values of $\ln(k_2/T)$ and 1/T for step 1 of **C3**

1/T	**$\ln(k_2/T)$ TU**	**$\ln(k_2/T)$ DMTU**	**$\ln(k_2/T)$ TMTU**
0.00336	-0.6	-0.635	-1.68
0.0033	-0.44	-0.462	-1.35
0.00325	-0.303	-0.32	-1.06
0.00319	-0.146	-0.145	-0.72
0.00314	-0.015	-1E-3	-0.43

Table SI 5. 10 Values of ln(k_2/T) and 1/T for step 2 of **C3**

1/T	**ln(k_2/T) TU**	**ln(k_2/T) DMTU**	**ln(k_2/T) TMTU**
0.00336	-9.84	-10.88	-12.09
0.0033	-9.44	-10.45	-11.5
0.00325	-9.11	-10.09	-11
0.00319	-8.74	-9.66	-10.4
0.00314	-8.41	-9.3	-9.9

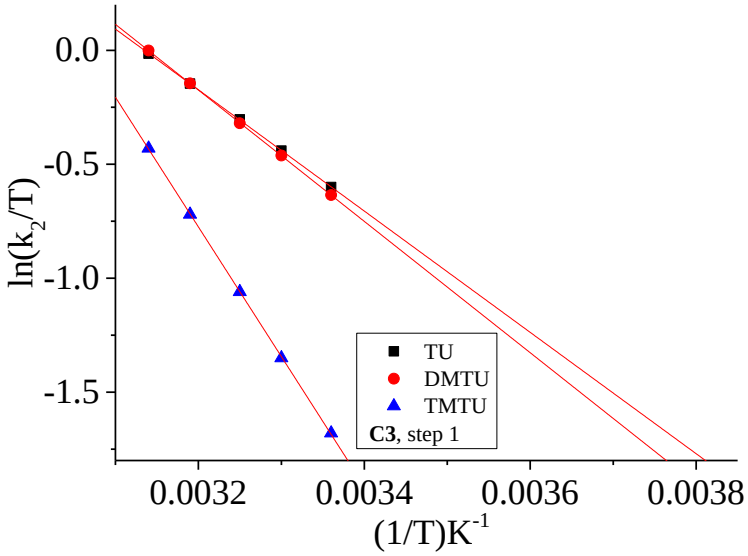

Figure SI 5.29 Step 1 temperature dependence plots for the reaction of **C3** with the thiourea nucleophiles

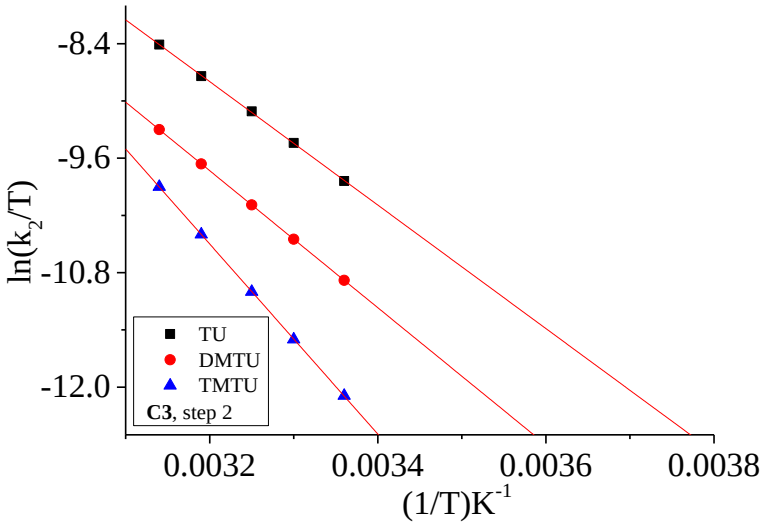

Figure SI 5.30 Step 2 temperature dependence plots for the reaction of **C3** with the thiourea nucleophiles

Table SI 5.11 Observed rate constants and the corresponding nucleophile concentrations for step 1 of **C4**

[Nu]/M	**k_{obs}/s^{-1} TU**	**[Nu]/M**	**k_{obs} / s^{-1} DMTU**	**[Nu]/M**	**k_{obs} / s^{-1} TMTU**
0.005	0.091	0.01	0.155	0.02	0.1665
0.01	0.183	0.02	0.309	0.04	0.333
0.015	0.272	0.03	0.460	0.06	0.4995
0.02	0.365	0.04	0.618	0.08	0.6716
0.025	0.456	0.05	0.770	0.1	0.8381

Table SI 5.12 Observed rate constants and the corresponding nucleophile concentrations for step 2 of **C4**

[Nu]/M	k_{obs}/ s^{-1} TU	k_{obs} / s^{-1} DMTU	k_{obs} / s^{-1} TMTU
0.04	4.5E-5	8E-5	0.000007
0.08	9E-5	1.6E-4	0.000014
0.12	1.346E-4	2.4E-4	0.000021
0.16	1.8E-4	3.2E-4	0.000028
0.20	2.26E-4	4E-4	0.0000351

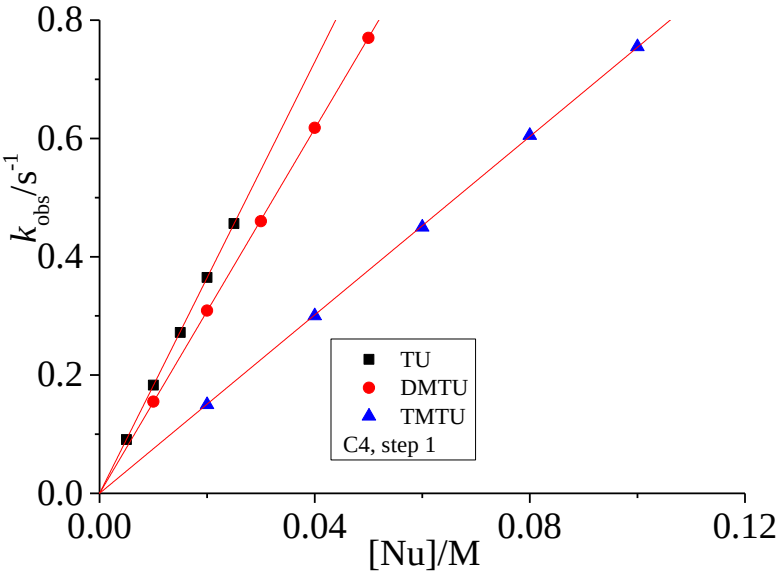

Figure SI 5.31 Step 1 concentration dependence plots for the reaction of **C4** with thiourea nucleophiles at 298 K

Table SI 5.13 Values of $\ln(k_2/T)$ and 1/T for step 1 of **C4**

1/T	ln(k_2/T) TU	ln(k_2/T) DMTU	ln(k_2/T) TMTU
0.00336	-2.65	-2.7	-3.45
0.0033	-2.3	-2.3	-2.99
0.00325	-2.02	-1.96	-2.58
0.00319	-1.69	-1.54	-2.07
0.00314	-1.41	-1.2	-1.68

Table SI 5.14 Values of $\ln(k_2/T)$ and 1/T for step 2 of **C4**

1/T	ln(k_2/T) TU	ln(k_2/T) DMTU	ln(k_2/T) TMTU
0.00336	-11.3	-10.7	-13.11
0.0033	-10.73	-10.18	-12.5
0.00325	-10.25	-9.73	-11.92
0.00319	-9.69	-9.21	-11.28
0.00314	-9.2	-8.79	-10.75

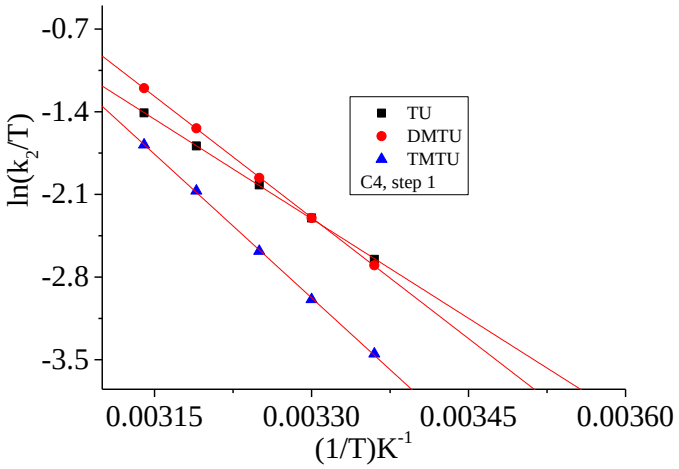

Figure SI 5.32 Step 1 temperature dependence plots for the reaction of **C4** with the thiourea nucleophiles

Chapter 6

Effect of 2-(2-Pyridyl)azole based auxillary ligands (L) on the rate of chloride substitutions from $[Ru(II)(tpy)(L)Cl]^+$ complexes

6.0 Abstract

The rate of substitution of the labile chloride ligands from Ru(II) complexes of the form $[Ru(II)(tpy)(L)Cl]^+$ (where L is an NN = 2-(1*H*-Imidazol-2-yl)pyridine(**L1**), 2-(2-pyridyl)-1*H*-benzimidazole(**L2**), 2-(2-pyridyl)benzoxazole (**L3**) or 2-(2-pyridyl)benzothiazole (**L4**), and tpy = 2,2':6',2''-terpyridine) by thiourea nucleophiles was studied under *pseudo* first order conditions in 0.1 M $NaClO_4$/LiCl methanol solution as a function of nucleophile concentration and temperature. The reactions were monitored using the UV-vis absorption spectrophotometer or stopped flow spectrophotometer for fast reactions. The rate of substitution of the chloride from the complexes follows the order: **C1** > **C2** > **C3** > **C4.** There are two electronic forces controlling the rates of substitutions in these complexes, π-donation in **C1** and **C2** and π-back-bonding in **C3** and **C4.** The 2-(1*H*-Imidazol-2-yl)pyridine ligand causes the strongest *trans*-effect that makes **C1** most reactive. In **C2**, the non-leaving ligand 2-(2-Pyridyl)benzimidazole in **C2** extents the π-space by an additional phenyl ring which lowers *trans*-effect and consequently the reactivity of **C2**. Additionally, the extended size of this ligand caused hindrance at the Ru metal centre in **C2** thus retarding its reactivity in comparison to **C1**. The highly electronegative sulphur and oxygen atoms in benzoxazole and benzothiazole ligands of **C3** and **C4** increase π-backbonding due to their enhanced π-acceptro abilities. This is supported by the DFT calculated electrophilicity indices of **C3** and **C4** which are higher compared to **C1** and **C2.** However the *trans*-effect experienced in **C1** and **C2** has greater magnitude and effect on reactivity than the π-back-bonding effect in **C3** and **C4** hence the higher reactivity of the former complexes. There is greater aromaticity in the 2-(2-Pyridyl)benzothiazole ligand in **C3** than in the 2-(2-Pyridyl)benzoxazole ligand of **C4** which accounts for the higher reactivity of **C3** compared to **C4**. This is supported by DFT calculated electrophiliciy index of **C3** which is higher than in **C4**. The greater π-acceptor capacity of **C3** is due to the azole end of its ancillary ligand *trans* to the leaving group with the opposite case in **C4**. The significantly negative activation entropies and positive activation enthalpies suggest an associative mechanism. The reactivity of the nucleophiles is controlled by steric properties according to the order TU > DMTU > TMTU.

6.1 Introduction

The research on metal based anti-cancer drugs has grown rapidly and extensively to include Ruthenum (Ru) polypyridyl complexes as possible complementary or alternative to Pt based chemotherapy. Some Ru complexes have shown promising antitumor activity certain cancer cell lines.[1] [2] Of the Ru complexes, octahedral polypyridyl coordinated complexes are the most studied because of their moderate reactivity, well known substitution chemistry and good photophysiscal properties well suited for anti-cancer agents.[3] Some Ru(II)(polypyridyl)X (X = Cl or H_2O) complexes bind to DNA after a labile exchange reaction.[2] [3] [4] The octahedral geometry and the many ways in which a wide range of non-leaving ligands can be permutated in these complexes helps in the design of many complexes for possible DNA binding trials.[5] These complexe coordinate DNA nucleobases in a two-step process like *cis*-platin.[2] [6] The nature of ligand(s) attached to the metal centres determines properties such as cellular uptake, geometry, cytotoxicity, rate of hydrolysis and ligand exchange as well as lipophilicity of the complex.[7] Complexes bound to ligands with higher denticity have been reported to be more cytotoxic compared to those with lower denticity. [8]

Ru(II) polypyridyl complexes which are kinetically inert have been reported to also bind to DNA.[9] For example, some Ru(II) polypyridyl complexes functionalized with $–OCH_3$ or $–NO_2$ substituents induced mitochondria mediated apoptosis in A375 human melanoma cells which was comparable to that of cisplatin.[10] [11] Even complexes which do not have labile ligands such as $[Ru(phen)_2(tpphz)]^{2+}$ and $[Ru(bpy)_2(tpphz)]^{2+}$ (where tpphz = tetra-pyridophenazine, phen = 1,10-phenanthrene and bpy = 2,2'-bipyridine) were found to display unusually high cytotoxicity against human cancer cell lines including certain cisplatin resistant ovarian cancer cell line.[12]

Cytotoxic evaluation of [Ru(tpy)(bpy)Cl][Cl], *cis*-$[Ru(bpy)_2Cl_2]$, and *mer*-$[Ru(tpy)Cl_3]$ (tpy = 2,2',6',2''-terpyridine and bpy = 2,2'-bipyridine)) against murine and human tumour cell lines revealed remarkably higher cytotoxicity by *mer*-$[Ru(tpy)Cl_3]$.[13] [2] This was attributed to its ability to form interstrand crosslinks with DNA through chloride exchange at the *trans* positions by N7 atoms of two guanines (a model nucleophile for DNA) in contrast to the monofunctional adducts which can form from the reactions of the other less active Ru(II) complexes.[14] On the other hand *cis*-$[Ru(bpy)_2Cl_2]$ only forms a mono adduct with 9-ethylguanine which has been confirmed by crystal structure of the adduct in literature.[15] [16]

Several DNA binding studies of some Ru(II) complexes with labile ligands of the general formula *mer*-$[Ru(tpy)(N\text{-}N)Cl]^+$ (N-N = bidentate nitrogen ligand) showed that the majority were able to bind coordinatively to DNA.[17] The binding studies were extended on other monofunctional Ru(II) polypyridyl complexes with various ligand moieties and these were found to be cytotoxic in murine and human tumour cell lines.[2] Further, DNA binding studies were done on complexes of the general formula *mer*-$[Ru(L)(N\text{-}N)X][Y]^n$ (L = tpy or Cl-tpy (4'-chloro-2, 2':6',2''-terpyridine), X = Cl or dmso-S, N-N = en, dach or bpy, Y = Cl, PF_6 or CF_3SO_3, and n = 1 or 2, depending on the nature of X).[18] [Ru(Cl-tpy)(en)Cl][Cl], [Ru(Cl-tpy)(dach)Cl][Cl] and [Ru(Cl-tpy)(bpy)Cl][Cl] were found to be capable of binding onto guanine derivatives after the dissociation of the monodentate ligand (Cl) forming mono-functional adducts.[18]

As reported in literature, some Ru polypyridyl complexes have displayed good interactions (both covalent and non-covalently) with DNA and displayed good abilities to decimate cancer cells (*in vitro*).This placed them in good state as potential anti-cancer agents. However the studies have focused mainly on DNA-binding potential. This does not provide a complete understanding on the pharmacokinetic behaviour under biological environments where their reactivity with both deactivating bionucleophiles and the targeted nucleophiles (for anti-tumour activity) have a direct effect on their ultimate cytotoxicity. A simple way to provide this data is to study their substitution reactivity with model biorelevant nucleophiles. This study focuses on measuring the rates and mechanisms of the substitution reactions from Ru(II) polypyridyl complexes of the form $[Ru(II)(tpy)(L)Cl]^+$ (where L = 2-(2-pyridyl)-benzoxazole (**L4**), 2-(2-pyridyl)benzthiazole (**L3**), 2-(2-pyridyl)-1*H*-benzimidazole (**L2**) and 2-(1*H*-Imidazol-2-yl)pyridine (**L1**)). Since these complexes have potential as anti-cancer agents, the study of their rates of substitution towards thiourea nucleophiles (thiourea (**TU**), 1,3-dimethyl-2-thiourea (**DMTU**) and 1,1,3,3-tetramethyl-2-thiourea (**TMTU**)) is helpful in understanding their reactivity toward potential nucleophilic competitors before binding to DNA. The structures of the complexes used in this study are shown in Figure 6.1

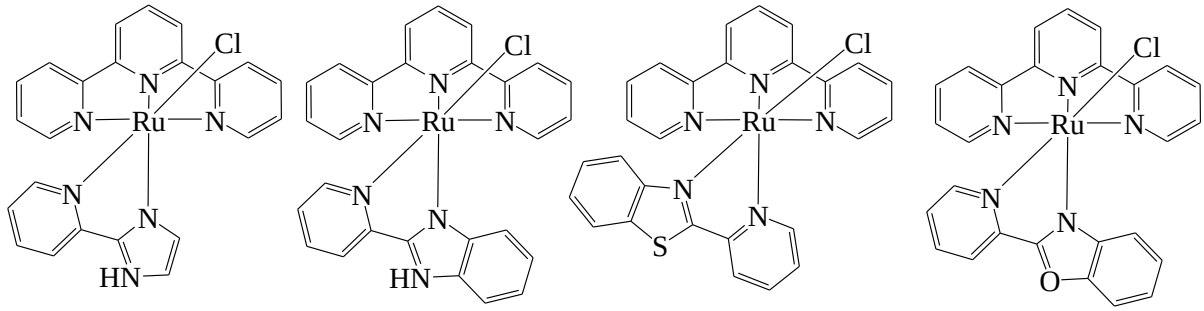

C1 **C2** **C3** **C4**

Figure 6. 1 Chemical structures of the cationic Ru complexes under investigation (charges and counter ions left out for clarity)

6.2 Experimental

6.2.1 Materials

The reagents including 2,2′:6′,2″-terpyridine (tpy), Dichloro(*p*-cymene)ruthenium(II) dimer, 2-(2-pyridyl)-1*H*-benzimidazole(**L2**), 2-(1*H*-Imidazol-2-yl)pyridine (**L1**), 2-aminophenol, 2-pyridine carboxylic acid, polyphosphoric acid, sodium carbonate and 2-aminothiophenol were obtained from Sigma Aldrich and used as received. The solvents: acetonitrile, diethyl ether, dichloromethane, hexane and pentane were obtained from Merck and dried before use where needed. All reactions were carried out under dry nitrogen atmosphere. All data for the synthesised ligands and complexes (elemental analysis, MS and NMR) corresponded to the proposed structures and formulations.

6.2.2 Synthesis of Ligands

The ligands **L3** and **L4** were synthesized following standard literature methods,[19]

2-(2-pyridyl)benzothiazole (L3)

To a solution of 2-pyridine-2-carboxylic acid (6.2 g, 50 mmols) in hot polyphosphoric acid (40 mL) was added *o*-aminothiophenol (6.2 g, 50 mmols). The reaction mixture was stirred at 180 °C for 2h, and then poured into ice/water slurry. The solution was neutralised with potassium hydroxide and the precipitate which formed was collected by filtration. The precipitate was purified by recrystallization from hot methanol to give a brown powder. Yield = 3.21 g (57%). ^{1}H NMR (400 MHz, $CDCl_3$): δ_H (ppm): 7.43 (dt, 2H); 7.54 (t, 1H); 7.88 (t, 1H); 7.99 (d, 1H); 8.13 (d, 1H); 8.43 (d, 1H); 8.72 (d, 1H). ESI^+ LCMS, m/z (%) 447 [$(M^+ + Na)^+$].

2-(2-pyridyl)benzoxale (L4)

The ligand was prepared by mixing 2-aminophenol (3.13 g, 25 mmol), 2-pyridine carboxylic acid (3.08 g, 25 mmol) and 10 mL of polyphosphoric acid (PPA) to give a paste. The reaction mixture was stirred at 200 °C for 4 h after which the temperature was decreased to 100 ^{o}C and the mixture transferred into a large volume of stirred water. The solution was neutralised with 10% sodium carbonate solution. The resulting precipitate was removed by filtration. The crude product was washed with sufficient with water, dried and recrystallized from n-hexane to obtain brown powder. Yield = 3.12 g (64%). ^{1}H NMR (DMSO-6): δ_H (ppm): 7.48 (t, 2H); 7.65 (t, 1H); 7.87 (dd, 2H); 8.08 (t, 1H); 8.35 (d, 1H); 8.81 (d, IH). ESI^{+} LCMS, m/z (%) 415 [(M^{+}+Na) $^{+}$].

6.2.3 Synthesis of complexes

Complexes were synthesized in two steps following the standard literature method by Osman *et. al.*[20]

[(acetonitrile)(dichloride)(2,2':6',2''-terpyridine)ruthenium(II)] [(CH_3CN)(Cl_2)(tpy)Ru (II)]

This precursor complex was prepared by dissolving a given amount of [$RuCl_2$(*p*-cymene)]$_2$ (122.5 mg, 0.2 mmol) in a small volume of acetonitrile and stirring for 10 min at room temperature. The terpyridine ligand (93.30 mg, 0.4 mmmol) was added to the solution and the resulting mixture refluxed overnight. After cooling the reaction mixture to room temperature, the excess solvent was removed under reduced pressure and the residue which formed was dissolved in dichloromethane (15 mL). The product was precipitated by slow addition of cold diethyl ether (30 mL). The product was filtered off and washed with diethyl ether (3 x 10 mL), pentane (3 x 10 mL) and dried under reduced pressure at 50° C for 1 h to yield a brown powder. Yield = 178.53 Mg (93.1%). ESI^{+} LCMS, m/z: 552.0 [M + 6]

[(dichloride)(2-(1*H*-Imidazol-2-yl)pyridine)(2,2':6',2''-terpyridine)ruthenium(II)] (C1)

An ethanolic solution (15 mL) of **[$RuCl_2$(tpy)(CH_3CN)]** (133.89 mg, 0.3 mmol) was mixed with **L1** (43.55 mg, 0.3 mmol)in the ratio 1:1 and the reaction mixture heated under reflux for 24 h. The mixture was then cooled to room temperature and precipitated by addition of diethyl ether (30 mL). The brown precipitate was obtained by filtration and washed with diethyl ether (3 x 10 ml) and pentane (3x10 ml). The solid was dried under reduced pressure at 50° C for 1 h. Yield: 99.07 mg (66%). ^{1}H NMR (400 MHz, DMF) δ/ppm, J/Hz: 16.34 (s,

1H); 10.31 (d, 1H); 9.13 (d, 2H); 9.01 (d, 1H); 8.90 (d, 2H); 8.32 (m, 1H); 8.28 (m, 2H); 8.13 (m, 2H); 7.90 (t, 1H); 7.68 (t, 2H); 7.45 (d, 1H); 7.11 (t, 1H). Anal. Calcd. for $C_{23}H_{18}Cl_2N_6Ru$: C, 50.19; H, 3.30; N, 15.27; Found: C, 50.20; H, 3.01; N, 15.26. ESI^+ LCMS, m/z: 514.95 $[M-Cl]^+$

[(dichloride)(2-(2-pyridyl)-1*H*-benzimidazole)(2,2':6',2''-terpyridine)ruthenium(II)] (C2)

C2 was prepared in the same way as **C1** using **$[RuCl_2(tpy)(CH_3CN)]$** (133.89 mg, 0.3 mmol) and **L2** (58.57 mg, 0.3 mmol). Yield: 127.90 mg (71%). ^1H NMR (400 MHz, DMF) δ/ppm, J/Hz: 9.50 (s, 1H); 9.29 (m, 2H); 9.07 (m, 2H); 8.90 (m, 2H); 8.60 (m, 1H); 8.40 (m, 2H); 8.17 (m, 2H); 8.01 (t, 1H); 7.81 (t, 1H); 7.72 (d, 1H); 7.64 (m, 2H); 7.59 (t, 2H); 7.27 (t, 1H). Anal. Calcd for $C_{27}H_{20}Cl_2N_6Ru$: C, 54.01; H, 3.36; N, 14.00; Found: C, 54.32; H, 3.71; N, 13.85. ESI^+ LCMS, m/z: 565.05 $[M-Cl]^+$

[(dichloride)(2-(pyridyl)benzothiazole)(2,2':6',2''-terpyridine)ruthenium(II)] (C3)

C3 was prepared in the same way as **C1** using **$[RuCl_2(tpy)(CH_3CN)]$** (133.89 mg, 0.3 mmol) and **L3** (63.68 mg, 0.3 mmol).Yield: 106.15 mg (57.3%). ^1H NMR (400 MHz, DMF) δ/ppm, J/Hz: 10.28 (m), 9.22 (d, 1H), 9.14 (m, 2H), 8.99 (d, 2H); 8.79 (m, 2H), 8.68 (m, 1H), 8.57 (t, 1H), 8.46 (m, 1H), 8.07 (m, 2H), 7.98 (t, 1H), 7.92 (d, 1H), 7.63 (m, 2H), 7.59 (m, 1H), 7.46 (m, 2H). Anal. Calcd for $C_{27}H_{19}Cl_2N_6SRu$: C, 52.52; H, 3.10; N, 11.34; Found: C, 52.32; H, 3.51; N, 11.75. ESI^+ LCMS, m/z: 582.06 $[M-Cl]^+$

[(**dichloride**)(**2-(pyridyl)benzoxale**)(**2,2':6',2''-terpyridine)ruthenium(II)] (C4)**

C4 was prepared in the same way as **C1** using **$[RuCl_2(tpy)(CH_3CN)]$** (133.89 mg, 0.3 mmol) and **L4** (58.86 mg, 0.3 mmol;).. Yield: 73.98 mg (41%). ^1H NMR (400 MHz, DMF) δ/ppm, J/Hz: 9.03 (m, 1H); 8.93 (d, 1H); 8.79 (m, 2H); 8.56 (m, 2H); 8.40 (t, 1H); 8.31 (m, 2H); 8.27 (m, 1H); 7.91 (m, 1H); 7.76 (m, 1H); 7.45 (m, 4H); 7.30 (m, 2H). Anal. Calcd for $C_{27}H_{19}Cl_2N_5ORu$: C, 53.92; H, 3.18; N, 11.64; Found: C, 53.51; H, 3.40; N, 11.90. ESI^+ LCMS, m/z: 566.03 $[M-Cl]^+$

Mass spectrometric data gave peaks corresponding to the masses of the complexes without the counter ions. The spectra for NMR and mass analyses are in the supporting information Figures SI 6.1-6.13

6.2.4 Instrumentation and measurement

NMR spectroscopy were recorded on a Bruker Avance DPX 400 MHz spectrophotometer at 303 K and chemical shifts were referenced to those of $Si(CH_3)_4$. Low resolution electron spray ionization (ESI^+) mass spectra were recorded on the Waters Micromass LCT Premier Spectrometer or Shimadzu2020 LCMS. Elemental analyses were done on a ThermoScientific Flash 2000 elemental analyser. Kinetic measurements were monitored using varian Cary 100 Bio UV-Viscible spectrophotometer with an attached Varian peltier temperature controller and online kinetic application.

6.2.5 Computational modelling

The computations were done by Density Functional Theory (DFT) run on Gaussian 09 suite of programs.[21] The structures were optimised using the hybrid Becke, 3-parameter, of Lee-Young-Parr (B3LYP) method with LANL2DZ (Los Alamos National Laboratory 2 double ζ) basis sets for which inner core electrons of the Ru atom are replaced by relativistic effective core potential (ECP).[22] [23] [24] Los Alamos National Laboratory 2 double ζ basis set exploits relativistic effective core potentials to account for effect of inner core 28 electrons ($[Ar]3d^{10}$) in Ru.[25] [26] To take into account of the solvent effects, the complexes were fully optimised in methanol using the conductor polarizable continuum model (C-PCM).[27] [28] The singlet states were used due to the low electronic spin state of Ru(II) complexes. The complexes were considered to have an overall charge of +1. The chemical potential (μ) and molecular hardness (η) for each structure were calculated from the HOMO and LUMO energies. The global electrophilicities (ω) were determined by the relationship $\omega = \mu^2/2\eta$.[29] [30] The charge on each atom is expressed as a natural bond orbitals (NBO) .[31]

6.3 Results

6.3.1 Computed/optimised structures of the Ru(II)complexes

DFT calculated properties of metal complexes (Table 6.2) have been used in literature to explain trends in substitutional kinetics. [32] [33] For example, electronic chemical potential, μ, chemical hardness, η, and electrophilicity index, ω, were used to account for observed trends in rates of substitution reactions. For this reason, geometry optimisation of the Ru complexes was carried out to gain information on the ground state electronic and structural properties of the complexes. The DFT optimized structures of the complexes are shown in Table 6.1 and a summary of selected DFT parameters are presented in Table 6.2. A close examination of the DFT diagrams in Table 6.1 reveals that the HOMOs are located mainly on the Ru metal

centre and partially on the chloro ligand. It is observed that the HOMOs partially extent to the auxillary bidentate ligands in **C1** and **C2,** pointing to the electron rich character of these ligands. The LUMOs lie entirely on the azole ring of the bidentate based ligands in **C3** and **C4** and on the terpyridine ligands in **C1** and **C2**.

Table 6. 1 DFT minimum energy structures and frontier molecular orbitals of the complexes

Optimised Structures		HOMO	LUMO
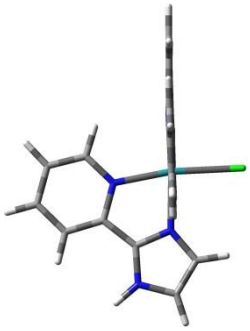	**C1**	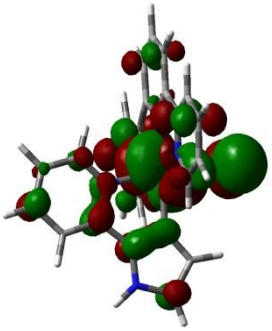	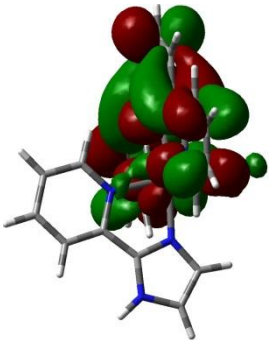
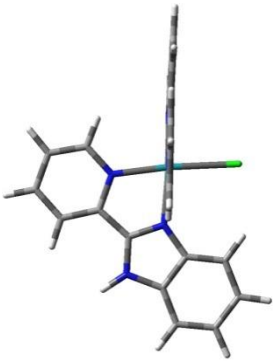	**C2**	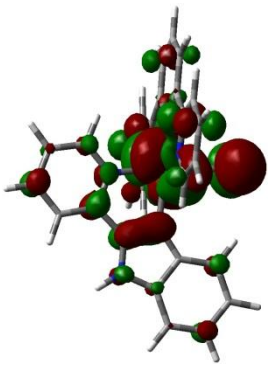	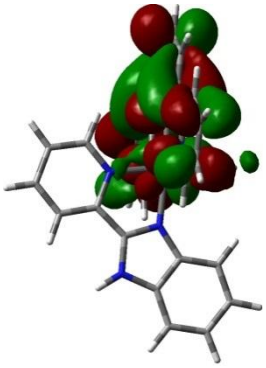
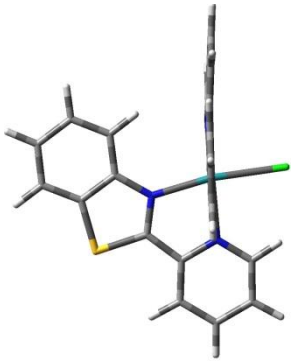	**C3**	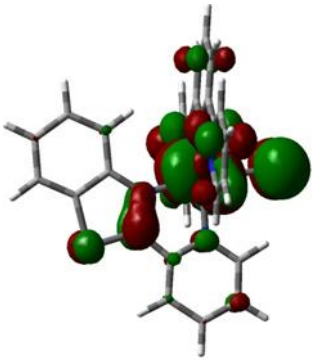	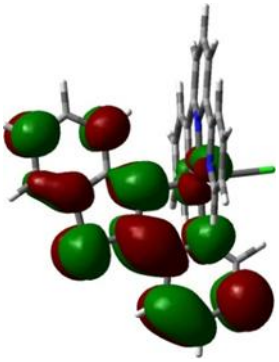
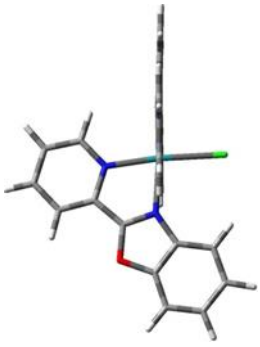	**C4**	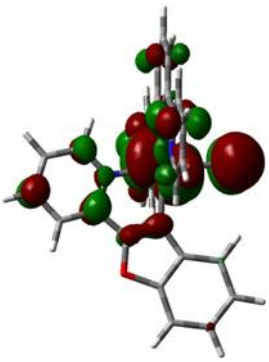	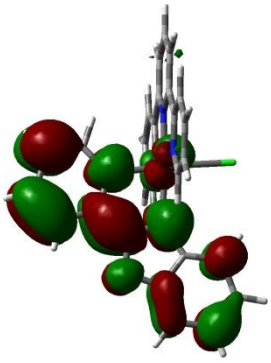

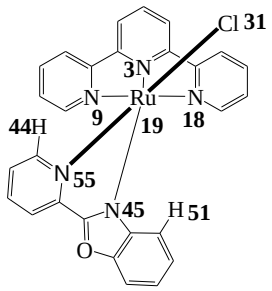

Figure 6. 2 Structure of **C4** showing atomic numbering used in Table 6.2 and the orientation of **L4** relative to the chloride. The numbering is adopted from DFT optimised structural atomic numbering

Table 6. 2 Summary of DFT calculated data for the complexes investigated

Parameters	**C1**	**C2**	**C3**	**C4**
Bond lengths (Å)				
Ru19-Cl31	2.53	2.54	2.52	2.53
Ru19-N3	1.98	1.98	2.00	1.99
Ru19-N9	2.10	2.10	2.10	2.10
H51-Cl31	-	2.66	2.59	2.73
Bond angles (°)				
N9-Ru19-N18	159.1	159.2	158.8	159.1
N45-Ru19-Cl31	93.4	97.3	93.4	96.5
N55-Ru19-Cl31	171.6	175.2	171.4	174.5
N3-Ru19-Cl31	89.9	87.1	85.5	88.0
N3-Ru19-N18	79.5	79.6	79.4	79.6
N3-Ru19-N45	176.6	175.5	178.9	175.5
NBO charges				
Ru19	0.664	0.659	0.667	0.661
Orbital energy/eV				
HOMO	-5.623	-5.661	-5.780	-5.811
LUMO	-2.622	-2.653	-2.938	-2.894
$\Delta E_{HOMO-LUMO}$	3.001	3.008	2.843	2.916
Global chemical reactivity indices				
η/eV	1.500	1.504	1.421	1.458
μ/eV	-4.122	-4.157	-4.359	-4.352
ω/eV	5.662	5.744	6.684	6.496

Where; η = Chemical Hardness μ = Electronic chemical potential ω = Electrophilicity index

The HOMO-LUMO energy gap can predict accurately the relative kinetic inertness and chemical reactivity of a family of structurally related compounds. Compounds whose energy gap is wide are kinetically inert and less reactive.[34] The electronic and steric characteristics of the auxillary ligands **L1**, **L2**, **L3** and **L4** coordinated onto the Ru(tpy)Cl core affect the lability of the chloride. Crystallographic data[35] for **C2-C4** has shown that the auxillary ligands; **L1**, **L2** and **L4** are bonded onto the Ru(II)(tpy)Cl via the azole nitrogen (N45) and the pyridyl nitrogen (N55) with the labile chloride ligand *trans* to the pyridyl as shown in **Figure 6.2.** However, **L3** coordinates somehow differently in that the chloride is *trans* to the azole nitrogen as shown in Figure 6.3.

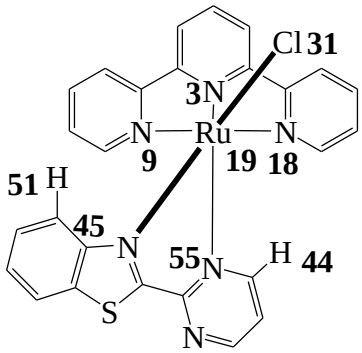

Figure 6. 3 Structure of **C3** showing the coordination of the azole ligand on the Ru(II) metal centre. The numbering is adopted from DFT optimised structural atomic numbering

The terpyridine ligand is coordinated to the metal centre in the expected meridional fashion giving rise to geometric constraints reflected in the *trans*-angles (N9-Ru19-N18) of 159 ° instead of the expected 180 °. The central Ru19-N3 bond length is about 0.1 Å shorter than the terminal Ru19-N18 and Ru19-N9 and this is also observed in the crystal structure data [35] causing smaller bite angles of the tridentate. The Ru(II) metal centre in these complexes is in a distorted octahedral typical of (tpy)(N-N)Ru(II) complexes.[36] [37]

The distortion of the octahedral geometry arises from geometrical constraints of the terpyridine ligand as a result of the smaller bite angles (N3-Ru19-N18, 79.5°, N55-Ru19-N45, 78.1°, N3-Ru19-N9, 78.5°) and *trans*-angles (N9-Ru-19-N18, 159.1°, Cl31-Ru19-N55, 174° and N3-Ru19-N45, 175.5°). Compound **C3** has its Ru19-N3 distance a little longer than the rest because the axillary ligand is attached to the Ru metal centre with the benzothiazole *trans* to the chloro ligand (Figure 6.3) as described earlier on. This difference in the

coordination of the bidentate on Ru(II) has been observed in literature[38] [39] [40] and the DFT calculated bond distances confirm the same. There is intramolecular hydrogen bonding interactions in the compounds based on the DFT calculated H51-Cl31 and H44-N3 distances that are within typical hydrogen bond distances of 1-3 Å.[41] [42]

A closer look at the geometry of the complexes from the DFT-optimized structures reveals that the plane of the bidentate ligand (i.e. azole ligand) and that of the terpyridine ligand are almost perpendicular to each other. The chloride ligand lies in the same plane as the bidentate azole ligands. The conformations of the complexes are constrained in this arrangement to minimize the steric repulsions between the equatorial hydrogens on the two ligands. The consequence of this is that the lability of the chloride ligand is principally controlled by the electronic or steric characteristics of the azole based ligands.

6.3.2 Kinetic results

Kinetic measurements were done under *pseudo* first-order conditions, using at least 10 fold excess of nucleophile in methanol with an ionic strength of 0.1 M, provided by adding 0.01 M LiCl and 0.09 M $NaClO_4$ in dry methanol. The chloride ions from LiCl suppressed any possibility of solvolysis of the complexes. The perchlorate ion is such a poor nucleophile and cannot competitively substitute the co-labile ligand ahead of the incoming thiourea ligands.[28] Kinetic solutions were prepared by dissolving required amounts of Ru(II) complexes in the methanolic solution. Nucleophile stock solutions were prepared at 50 times the concentration of the respective complex and diluted to afford concentrations of 40, 30, 20 and 10 times the concentration of the complexes for kinetic analysis

The rate of substituting the chloro ligand was investigated spectrophotometrically by following the change in absorbance with time using the UV-Vis spectrophotometer for conventional and slower reactions or stopped flow technique for ultrafast reactions. Spectral changes due to the reactions were observed over the wavelength range 200-800 nm to establish a suitable wavelength at which the respective reaction for each metal complex could be followed. All reactions were thermostated within ± 0.1 °C of the set value. The changes in absorbance accompanying the reactions were analysed graphically using the software package OriginPro 9.1. An example of such spectral changes for the reaction of **C1** with thiourea nucleophile (DMTU) is shown in Figure 6.4. The inset to figure 6.4 is the kinetic trace of the reaction at 316 nm.

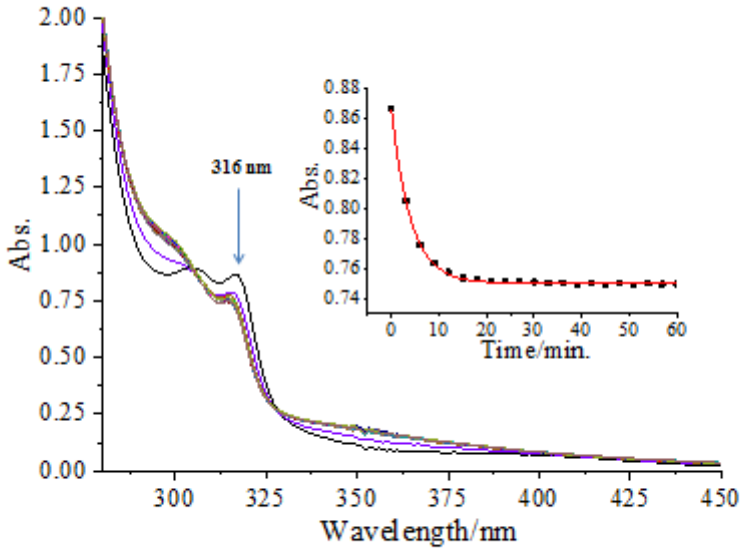

Figure 6. 4 Absorbance spectra for the reaction of **C1** and DMTU at 298 K (*inset* is the kinetic trace obtained for the reaction at 316 nm)

The observed first order rate constant, k_{obs}, were obtained from the fitted data consistent with equation 6.1 using OriginPro 9.1 program.

$$A_t = A_\circ + (A_\circ - A_\infty) \exp(-k_{obs}\, t) \tag{6.1}$$

where; A_0 is initial absorbance of the mixture, A_t is absorbance of the reaction mixture at time, t and A_∞ is final absorbance.

The rate of nucleophilic attack by the thiourea nucleophiles was measured at different concentrations of the nucleophile, [Nu], in excess of the complex's at 25° C. The average value of the observed rate constant, k_{obs}, were plotted against [Nu] according to Equation 6.2. Linear plots of k_{obs} verses $[Nu]$ were obtained for all reactions and typical plots are shown in Figure 6.5 for the substitution reactions of **C4** with the thiourea nucleophiles at 298 K

$$k_{obs} = k_2[Nu] + k_s \approx k_2[Nu] \tag{6.2}$$

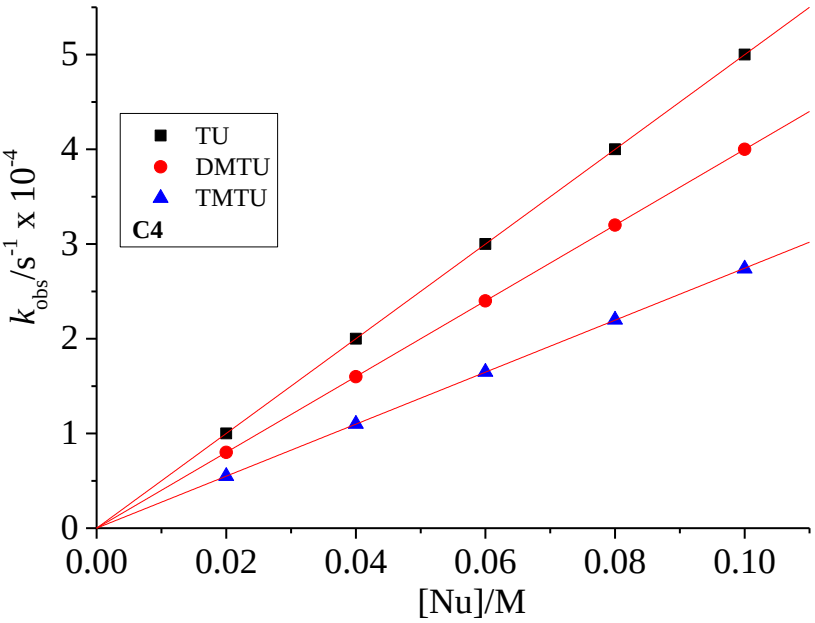

Figure 6. 5 Concentration dependence plot of k_{obs} verses [Nu] for the substitution reaction of **C4** with the thiourea nucleophiles at 298 K

The slopes give the second order rate constants, k_2, of the reaction of the respective nucleophile with **C4.** Other similar plots are presented in the supplementary information Figures SI 6.14, 6.16, 6.18 and 6.20. Tables of k_{obs} and respective nucleophile concentrations are also given in the supplementary information Tables SI 6.1, 6.3, 6.5 and 6.7.

Mechanism of substitution

Based on the kinetic data, the proposed mechanism of chloride substitution in the compounds under investigation can be represented by Scheme 6.1

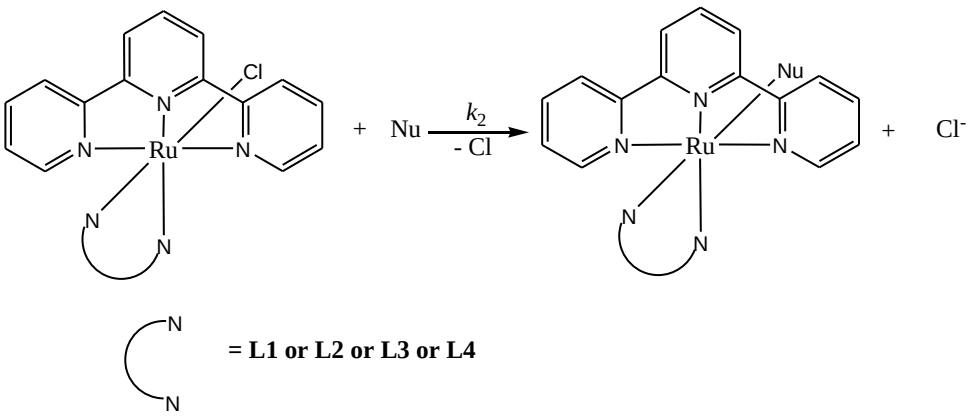

Scheme 6. 1 Proposed mechanisms of chloride substitution for the Ru complexes

The rate constants were also measured over the temperature range of 25-45 °C in increments of 5° C. Graphs of $\ln(k_2/T)$ verses $1/T$ were plotted in accordance to the Eyring equation (Equation 6.3). Typical Eyring plots are shown in Figure 6.6 for the reaction of **C2** with the thiourea nucleophiles.

$$\ln\left(\frac{k_{exp}}{T}\right) = \frac{-\Delta H^{\neq}}{R}.\frac{1}{T} + \left[23.8 + \frac{\Delta S^{\neq}}{R}\right] \qquad (6.3)$$

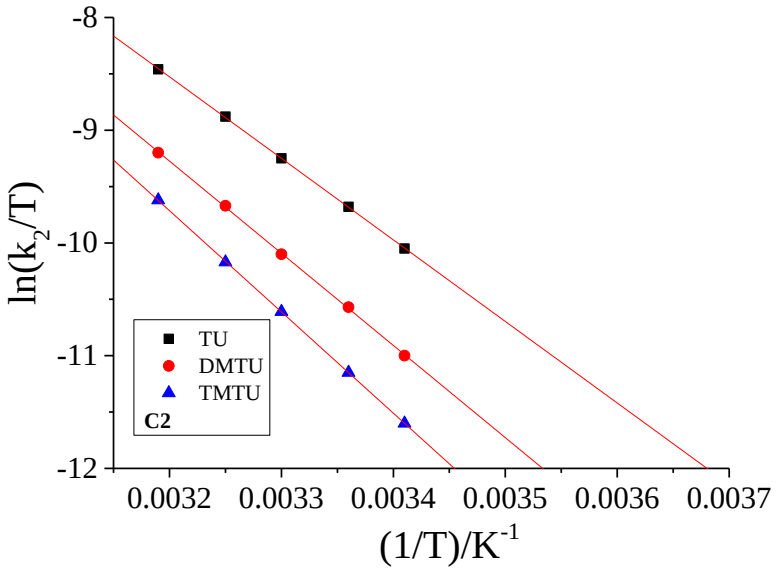

Figure 6. 6 Eyring plots for the reaction of **C2** with the thiourea nucleophiles

Other Eyring plots are presented in the supplementary information Figures SI 6.15, 6.17, 6.19, and 6.21. Data tables of $\ln(k_2/T)$ and $1/T$ are in the supplementary information Tables SI 6.2, 6.4, 6.6 and 6.8. The enthalpy of activation, $\Delta H^{\neq}$, and entropy of activation, $\Delta S^{\neq}$, were calculated from the slope and the intercept of the Eyring plots respectively. The values of the rate constants, $k_{2,}$ and activation parameters are summarised in Table 6.3.

Table 6. 3 Rate constants and activation parameters for the substitution reactions investigated

Complexes		Nu.	k_1 /M^{-1} s^{-1} x 10^{-4}	$\Delta H_1^{\neq}$ /kJ mol^{-1}	$\Delta S_1^{\neq}$ /$K^{-1}mol^{1-1}$
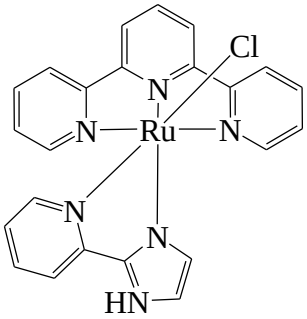	**C1**	TU	321 ± 0.5	53 ± 3	-99 ±7
		DMTU	251 ± 0.4	59 ± 2	-84 ± 5
		TMTU	147 ± 0.2	63 ± 1	-71 ± 3
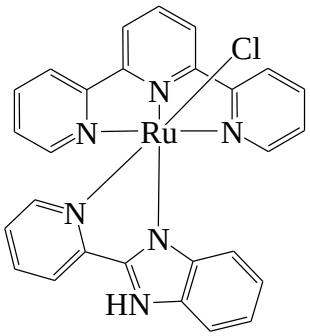	**C2**	TU	173 ± 0.3	60 ± 2	-76 ± 5
		DMTU	83 ± 0.2	68 ± 1	-57 ± 3
		TMTU	57 ± 0.3	75 ± 2	-40 ± 5
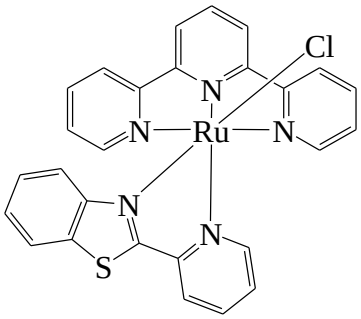	**C3**	TU	50 ± 0.1	73 ± 1	-48 ± 3
		DMTU	40 ± 0.2	73 ± 2	-42 ± 7
		TMTU	28 ± 0.1	83 ± 1	-11 ± 3
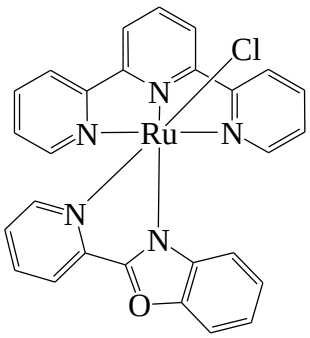	**C4**	TU	30 ± 0.2	79 ± 2	-28 ± 5
		DMTU	32 ± 0.1	76 ± 1	-35 ± 3
		TMTU	20 ± 0.2	85 ± 3	-10 ± 7

6.4 Discussion

The rate of substitution from the Ru(II) complexes decreases in the order: **C1** > **C2** > **C3** > **C4**. The substitution reaction of **C1** is higher than **C2**, as shown by the magnitude of the second order rate constant values in Table 6.3. Ru imidazole and benzimidazole complexes have increased electron density on the Ru metal centre which indirectly comes from the hydrogen bonding interactions between the N-H bond (Hydrogen donor) in the complex and solvent molecules/ions.[43] [44] [45] The increased electron density on the Ru can be qualitatively interpreted by an increase in the proportion of an ionic resonance form B (Scheme 6.2). The high electron density on Ru is supported by the lower DFT calculated electrophilicity indices for **C1** and **C2** compared to the other Ru complexes (Table 6.2). This caused a rise in the dπ orbital which is supported by higher HOMO energies and hence wider HOMO-LUMO energy gap for **C1** and **C2** compared to **C3** and **C4** (Table 6.2). The increased electron density on the Ru metal centre repels the negatively charged chloride coligand resulting in *trans*-effect.

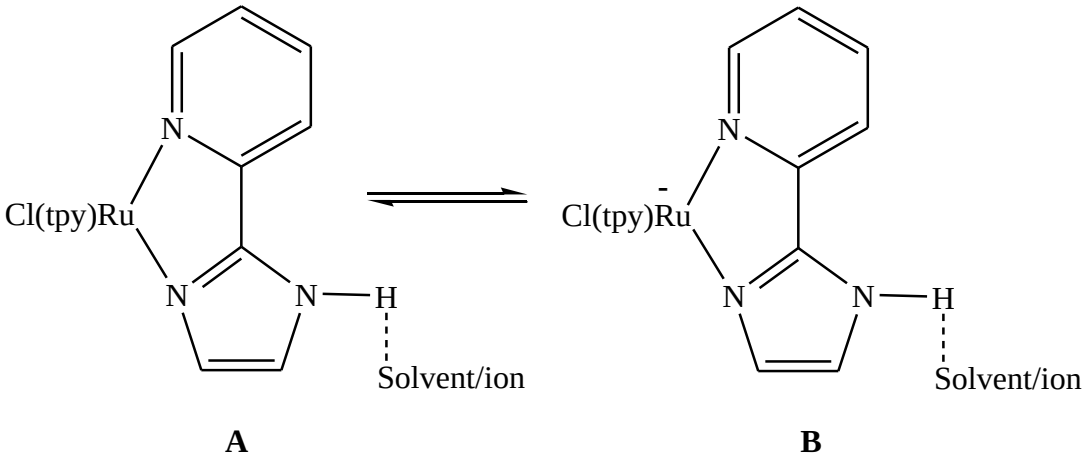

Scheme 6. 2 Structural illustration of outer sphere interactions in Ru complexes

C2 is less reactive than **C1** because the addition of the phenyl ring to the imidazolyl moiety of the 2-(1*H*-Imidazol-2-yl)pyridine ligand in **C1** increases the π-surface which increases the π-acceptor (weakens its *trans*-influence) ability of the ligand as supported by the higher electrophilicity index of **C2** (5.744) compared to that of **C1** (5.662) but reduces *trans*-effect in **C2**. Additionally, the added phenyl ring in **C2** enlarges the overall ligand size on one side of the metal centre hindering the approach of the incoming nucleophile. This also introduces H-bonding between the H51 and Cl13 atoms as observed from the H51---Cl13 distance of

2.66 Å that is within the literature defined range of hydrogen bonding distance.[46] The hydrogen bonding interaction makes **C2** relatively more stable in ground state and hence less reactive than **C1**.

Since the sulphur and oxygen atoms in 2-(2-Pyridyl)benzothiazole and 2-(2-Pyridyl)-benzoxazole ligands in **C3** and **C4** respectively are highly electronegative, there is a withdrawal of electrons by the atoms from the ligands. The ligands consequently withdraw electron density from the metal due to their enhanced π-acceptor ability compared to the ligands in **C1** and **C2**.[47] The higher rates of substitution of **C1** and **C2** compared to **C3** and **C4** is due to the greater magnitude of the *trans*-effect force operating in the former complexes than the π-back bonding force working in the later Ru complexes. The reactivity of **C1** is particularly much higher due to less hindrance at the Ru metal centre in this complex as explained in the previous section.

C3 has higher reactivity than **C4** because of greater π-bacbonding in **C3** that withdraws electron density from the Ru metal centre increasing its positive charge making it easily accommodate the extra electron density from the incoming nucleophile in the transition state. The greater π-acceptor capacity of the ligand in **C3** compared to **C4** is supported by literature information where thiazole rings are said to be more planar and aromatic and characterized by larger π-electron delocalization than the corresponding oxazoles and have therefore greater aromaticity.[47] This explains the greater π-back-bonding experienced in **C3** compared to **C4** which is supported by higher electrophilicity index of **C3** (6.684) than **C4** (6.496). Additionally, it is worth noting that the ancillary ligand in **C4** is coordinated to the Ru with the pyridyl *trans* to the chloro ligand while in **C3** the coordination is such that the thiazole end of the ligand is *trans* to the leaving group. This means that the azole end of the ligand in **C3** directly influences the chloro ligand. This is another possible reason why there is greater π-backbonding in **C3** than **C4** (Figure 6.2 and 6.3). This trend in reactivity is further supported by the lower HOMO-LUMO energy gap of **C2** (3.008), for **C3** (2.843) compared to **C4** (2.916).

The reactivity of the thiourea nucleophiles decreased in the order: TU > DMTU > TMTU consistent with their steric bulkiness. In all the complexes, entropy of activation, $\Delta S^{\#}$, values are negative, suggesting that the activation process is strongly dominated by bond-making. The small values of enthalpy of activation, $\Delta H^{\#}$, and negative values of activation entropy,

$\Delta S^{\#}$, clearly support the associative mechanism for the substitution processes. Similar mechanisms have been observed in other reactions of organometallic Ru(II) complexes with biologically relevant nucleophiles. [48] [18] [49]

6.5 Conclusions

It has been shown that the nature, orientation and bulkiness of the bidentate auxiliary ligand attached to the Ru(tpy)Cl moiety dictates the rate of substitution from the Ru(II) complexes. The reactivity of the complexes under investigation reveals two electronic forces at play, π-donation in **C1** and **C2** and π-back-donation in **C3** and **C4.** The 2-(1*H*-Imidazol-2-yl)pyridine ligand has been observed to be a strong electron donor resulting in strong *trans*-effect that makes **C1** most reactive. The addition of the benzene on 2-(1*H*-Imidazol-2-yl)pyridine ligand to form 2-(2-Pyridyl)benzimidazole in **C2** extents the π-space lowering the electron donor strength hence the lower reactivity of **C2** compared to **C1**. Additionally, the extended size of the ligand in **C2** introduces hindrance at the metal centre also lowering reactivity. The *trans* effect experienced in **C1** and **C2** has greater magnitude and effect on reactivity than the π-back-bonding effect in **C3** and **C4** hence the higher reactivity of the former complexes. There is greater aromaticity in the 2-(2-Pyridyl)benzothiazole ligand in **C3** than in the 2-(2-Pyridyl)benzoxazole ligand in **C4** that accounts for the higher reactivity of **C3** compared to **C4**. This is supported by higher DFT calculated electrophiliciy index in **C3** than in **C4**. The greater π-acceptor capacity of **C3** is also brought about by having the azole end of the ancillary ligand *trans* to the leaving group which is not the case in **C4**. The nature of the hetero-atom in the azole ligand has been observed to influence the acceptor ability of the ligands and subsequently the electrophilicity of the metal centre which is manifested in the rate of reaction of the complexes. The small values of $\Delta H^{\#}$ and negative values of $\Delta S^{\#}$ clearly support the associative mechanism for the substitution process.

6.6 References

[1] J. Reedijk, *Proceedings of the National Academy of Sciences* **2003**, *100*, 3611.

[2] V. Brabec, O. Nováková, *Drug Resistance Updates* **2006**, *9*, 111-122.

[3] C. Metcalfe, J. A. Thomas, *Chemical Society Reviews* **2003**, *32*, 215-224.

[4] K. K.-W. Lo, T. K.-M. Lee, *Inorganic Chemistry* **2004**, *43*, 5275-5282.

[5] M. R. Gill, J. A. Thomas, *Chemical Society reviews* **2012**, *41*, 3179-3192.

[6] T. Gianferrara, I. Bratsos, E. Alessio, *Dalton transactions* **2009**, 7588-7598.

[7] N. Yamamoto, S. Danos, P. D. Bonnitcha, T. W. Failes, E. J. New, T. W. Hambley, *Journal of Biological Inorganic Chemistry* **2008**, *13*, 861.

[8] aD. C. Monteiro, R. M. Phillips, B. D. Crossley, J. Fielden, C. E. Willans, *Dalton Transactions* **2012**, *41*, 3720-3725; bE. Wachter, A. Zamora, D. K. Heidary, J. Ruiz, E. C. Glazer, *Chemical Communications* **2016**, *52*, 10121-10124; cA. Herman, J. M. Tanski, M. F. Tibbetts, C. M. Anderson, *Inorganic Chemistry* **2008**, *47*, 274-280; dB. Therrien, W. H. Ang, F. Chérioux, L. Vieille-Petit, L. Juillerat-Jeanneret, G. Süss-Fink, P. J. Dyson, *Journal of Cluster Science* **2007**, *18*, 741-752; eB. Therrien, G. Süss-Fink, P. Govindaswamy, A. K. Renfrew, P. J. Dyson, *Angewandte Chemie International Edition* **2008**, *47*, 3773-3776.

[9] aF. R. Svensson, M. Abrahamsson, N. Strömberg, A. G. Ewing, P. Lincoln, *The journal of physical chemistry letters* **2011**, *2*, 397-401; bF. M. Foley, F. R. Keene, J. G. Collins, *Journal of the Chemical Society, Dalton Transactions* **2001**, 2968-2974; cV. Gonzalez, T. Wilson, I. Kurihara, A. Imai, J. A. Thomas, J. Otsuki, *Chemical communications* **2008**, 1868-1870; dD. A. Lutterman, A. Chouai, Y. Liu, Y. Sun, C. D. Stewart, K. R. Dunbar, C. Turro, *Journal of the American Chemical Society* **2008**, *130*, 1163-1170; eJ. A. Smith, J. L. Morgan, A. G. Turley, J. G. Collins, F. R. Keene, *Dalton Transactions* **2006**, 3179-3187; fC. Rajput, R. Rutkaite, L. Swanson, I. Haq, J. A. Thomas, *Chemistry-A European Journal* **2006**, *12*, 4611-4619; gS. P. Foxon, M. A. H. Alamiry, M. G. Walker, A. J. H. M. Meijer, I. V. Sazanovich, J. A. Weinstein, J. A. Thomas, *The Journal of Physical Chemistry A* **2009**, *113*, 12754-12762; hY. Sun, L. E. Joyce, N. M. Dickson, C. Turro, *Chemical Communications* **2010**, *46*, 2426-2428.

[10] T. Chen, W.-J. Mei, Y.-S. Wong, J. Liu, Y. Liu, H.-S. Xie, W.-J. Zheng, *Medicinal Chemistry Communication* **2010**, *1*, 73-75.

[11] T. Chen, Y. Liu, W.-J. Zheng, J. Liu, Y.-S. Wong, *Inorganic Chemistry* **2010**, *49*, 6366-6368.

[12] G. M. R., D. Hanan, S. C. G. W., B. Giuseppe, T. J. A., *ChemBioChem* **2011**, *12*, 877-880.

[13] O. Novakova, J. Kasparkova, O. Vrana, P. M. van Vliet, J. Reedijk, V. Brabec, *Biochemistry* **1995**, *34*, 12369-12378.

[14] P. M. van Vliet, S. M. S. Toekimin, J. G. Haasnoot, J. Reedijk, O. Nováková, O. Vrána, V. Brabec, *Inorganica Chimica Acta* **1995**, *231*, 57-64.

[15] P. M. van Vliet, J. G. Haasnoot, J. Reedijk, *Inorganic Chemistry* **1994**, *33*, 1934-1939.

[16] F. Zobi, M. Hohl, I. Zimmermann, R. Alberto, *Inorganic Chemistry* **2004**, *43*, 2771-2772.

[17] aC.-C. Cheng, W.-L. Lee, J.-G. Su, C.-L. Liu, *Journal of the Chinese Chemical Society* **2000**, *47*, 213-220; bE. Corral, A. C. G. Hotze, D. M. Tooke, A. L. Spek, J. Reedijk, *Inorganica Chimica Acta* **2006**, *359*, 830-838; cK. Karidi, A. Garoufis, N. Hadjiliadis, M. Lutz, A. L. Spek, J. Reedijk, *Inorganic Chemistry* **2006**, *45*, 10282-10292; dE. Corral, A. C. G. Hotze, A. Magistrato, J. Reedijk, *Inorganic Chemistry* **2007**, *46*, 6715-6722; eE. Corral, A. C. G. Hotze, H. den Dulk, A. Leczkowska, A. Rodger, M. J. Hannon, J. Reedijk, *Journal of Biological Inorganic Chemistry* **2009**, *14*, 439-448.

[18] A. Rilak, I. Bratsos, E. Zangrando, J. Kljun, I. Turel, Ž. D. Bugarčić, E. Alessio, *Inorganic Chemistry* **2014**, *53*, 6113-6126.

[19] A. A. W., R. T. Nageswara, W. C. G., *Journal of Heterocyclic Chemistry* **1983**, *20*, 1481-1484.

[20] D. Osman, D. Serkan, K. İbrahim, Ç. Bekir, *Applied Organometallic Chemistry* **2012**, *26*, 663-670.

[21] R. A. Gaussian, *Inc., Wallingford CT* **2009**, *121*, 150-166.

[22] P. J. Hay, W. R. Wadt, *The Journal of chemical physics* **1985**, *82*, 270-283.

[23] C. Lee, W. Yang, R. G. Parr, *Physical Review B* **1988**, *37*, 785.

[24] A. D. Becke, *The Journal of chemical physics* **1993**, *98*, 5648-5652.

[25] M. Okamura, M. Yoshida, R. Kuga, K. Sakai, M. Kondo, S. Masaoka, *Dalton Transactions* **2012**, *41*, 13081-13089.

[26] M. Cossi, N. Rega, G. Scalmani, V. Barone, *Journal of computational chemistry* **2003**, *24*, 669-681.

[27] T. Le Bahers, T. Pauporté, G. Scalmani, C. Adamo, I. Ciofini, *Physical Chemistry Chemical Physics* **2009**, *11*, 11276-11284.

[28] A. Shaira, D. Jaganyi, *Journal of Coordination Chemistry* **2014**, *67*, 2843-2857.

[29] P. K. Chattaraj, U. Sarkar, M. Elango, R. Parthasarathi, V. Subramanian, *arXiv preprint physics/0509089* **2005**.

[30] A. Cedillo, R. Contreras, *Journal of the Mexican Chemical Society* **2012**, *56*, 257-260.

[31] E. Seifert, American Chemical Society Publications, **2014**.

[32] R. G. Parr, W. Yang, Oxford University Press, New York, **1989**.

[33] P. Geerlings, F. De Proft, W. Langenaeker, *Chemical Reviews* **2003**, *103*, 1793-1874.

[34] S. B. Jensen, S. J. Rodger, M. D. Spicer, *Journal of Organometallic Chemistry* **1998**, *556*, 151-158.

[35] N. Chanda, D. Paul, S. Kar, S. M. Mobin, A. Datta, V. G. Puranik, K. K. Rao, G. K. Lahiri, *Inorganic Chemistry* **2005**, *44*, 3499-3511.

[36] F. Zeng, Z. Yu, *Organometallics* **2009**, *28*, 1855-1862.

[37] A. Singh, B. Chetia, S. M. Mobin, G. Das, P. K. Iyer, B. Mondal, *Polyhedron* **2008**, *27*, 1983-1988.

[38] B. Mondal, H. Paul, V. G. Puranik, G. K. Lahiri, *Journal of the Chemical Society, Dalton Transactions* **2001**, 481-487.

[39] N. Chanda, S. M. Mobin, V. G. Puranik, A. Datta, M. Niemeyer, G. K. Lahiri, *Inorganic Chemistry* **2004**, *43*, 1056-1064.

[40] H. Hadadzadeh, M. C. DeRosa, G. P. A. Yap, A. R. Rezvani, R. J. Crutchley, *Inorganic Chemistry* **2002**, *41*, 6521-6526.

[41] S. Sarkar, B. Sarkar, N. Chanda, S. Kar, S. M. Mobin, J. Fiedler, W. Kaim, G. K. Lahiri, *Inorganic Chemistry* **2005**, *44*, 6092-6099.

[42] P. O. Ongoma, D. Jaganyi, *Dalton transactions* **2013**, *42*, 2724-2734.

[43] B. H. Kim, D. N. Lee, H. J. Park, J. H. Min, Y. M. Jun, S. J. Park, W.-Y. Lee, *Talanta* **2004**, *62*, 595-602.

[44] M.-A. Haga, A. Tsunemitsu, *Inorganica Chimica Acta* **1989**, *164*, 137-142.

[45] H. Yi, J. A. Crayston, J. T. S. Irvine, *Dalton Transactions* **2003**, 685-691.

[46] J. J. Dannenberg, *Journal of the American Chemical Society* **1998**, *120*, 5604-5604.

[47] J. D. Wales, in *WIKIPEDIA The Free Encylopedia*, **2001**.

[48] A. Rilak, I. Bratsos, E. Zangrando, J. Kljun, I. Turel, Z. D. Bugarcic, E. Alessio, *Dalton Transactions* **2012**, *41*, 11608-11618.

[49] A. Rilak, B. Petrović, S. Grgurić-Šipka, Ž. Tešić, Ž. D. Bugarčić, *Polyhedron* **2011**, *30*, 2339-2344.

6.7 Supporting information

Included in the supplementary information are NMR spectra, mass spectra, tables, and various kinetic graphs for the synthetic and kinetic analysis of the complexes; **C1, C2, C3** and **C4** investigated in this study.

6.7.1 Synthesis

Figure SI 6.1 TOF-MS of benzoxazole ligand **L4**

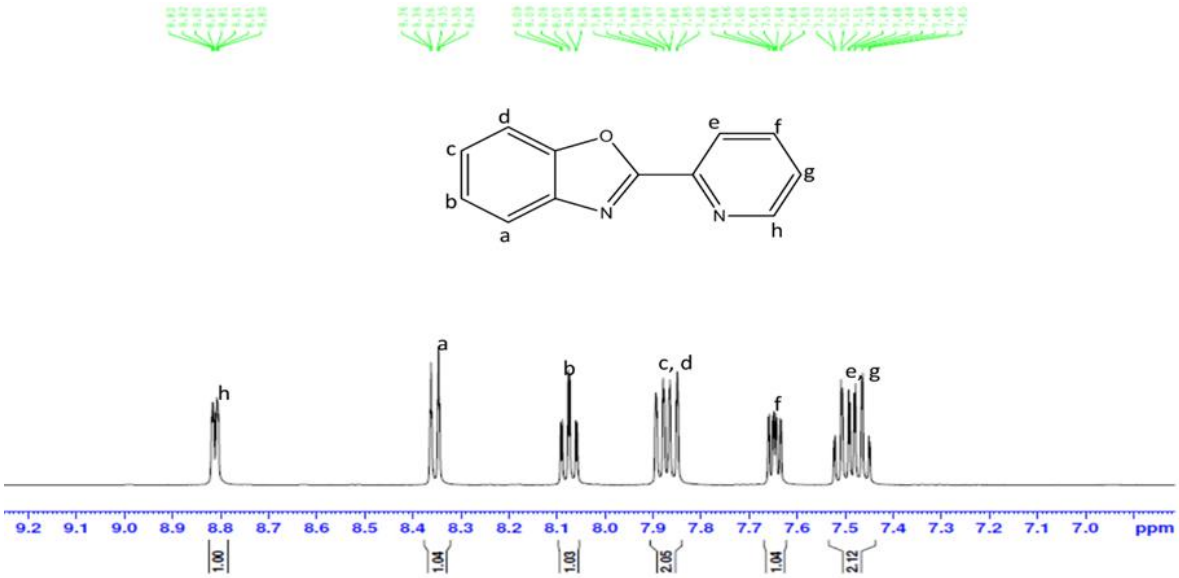

Figure SI 6.2 ^{1}H NMR spectra of benzoxazole ligand **L4**

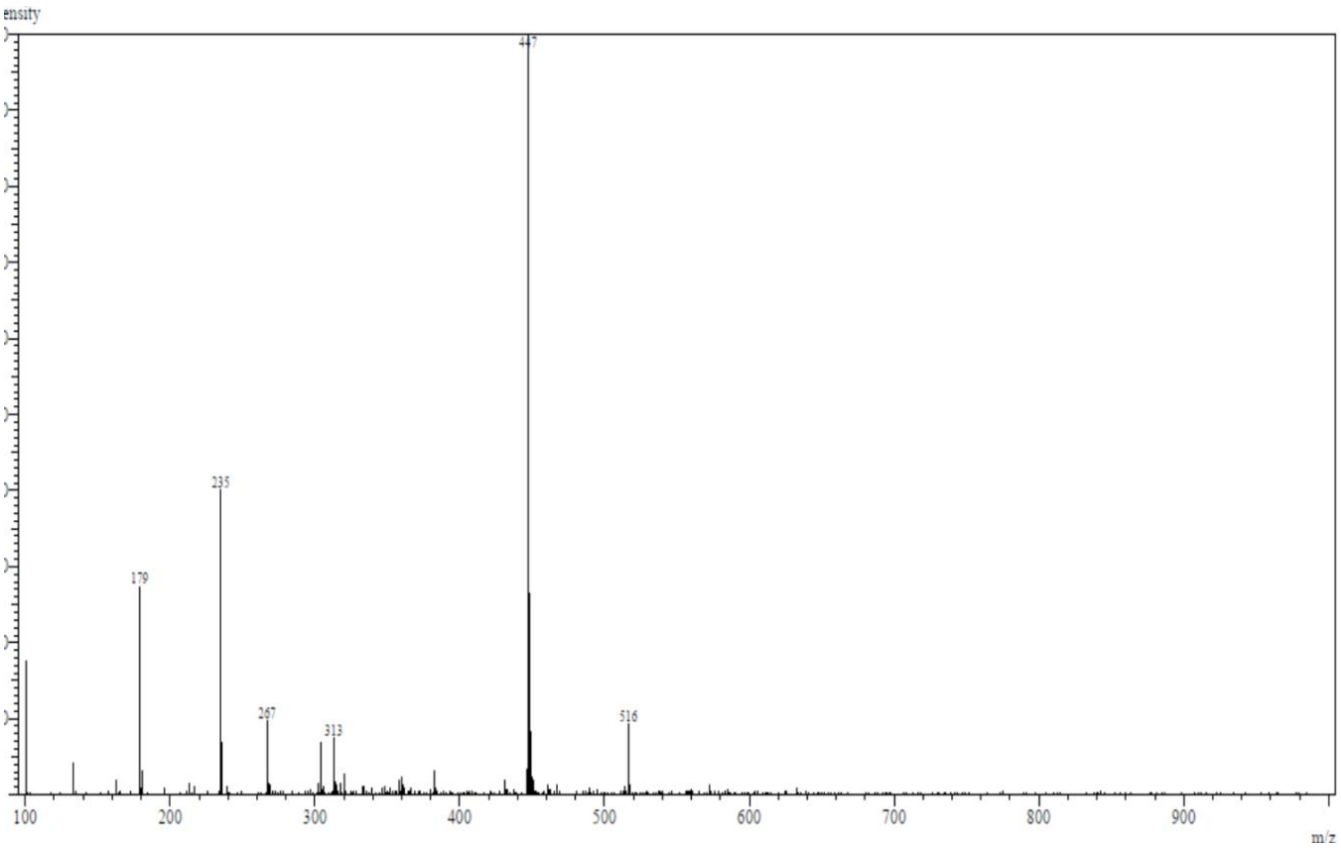

Figure SI 6.3 LCMS of benzothiazole **L3**

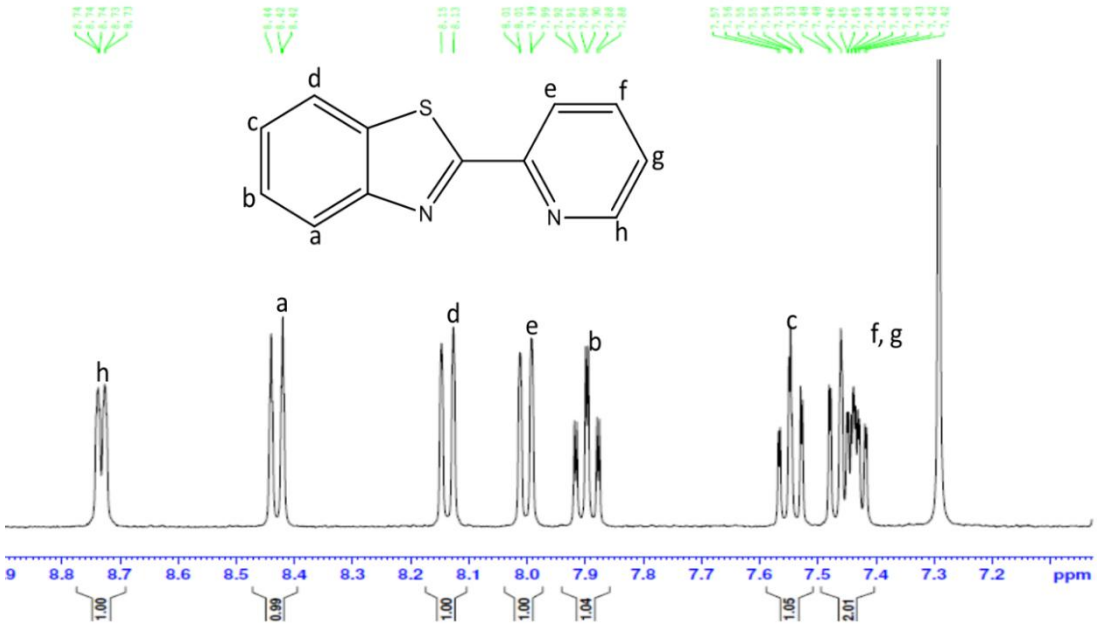

Figure SI 6.4 ^{1}H NMR spectrum of benzothiazole **L3**

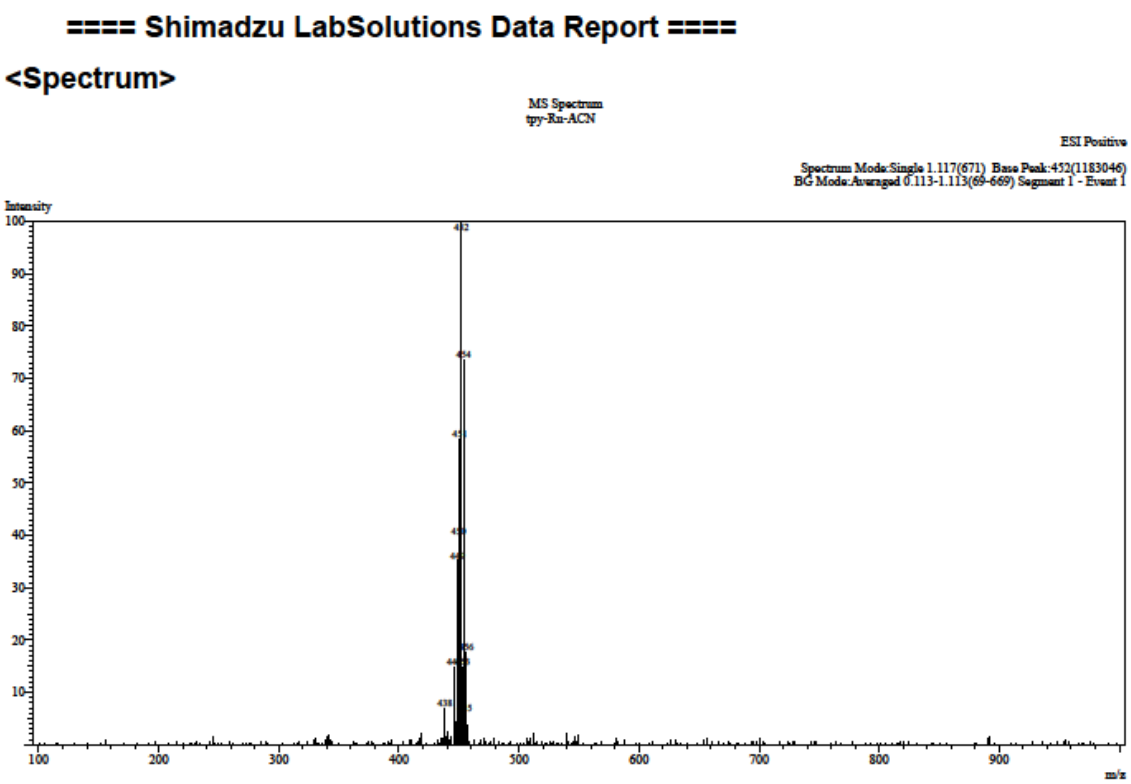

Figure SI 6.5 LCMS of **[$RuCl_2$(tpy)(CH_3CN)]**

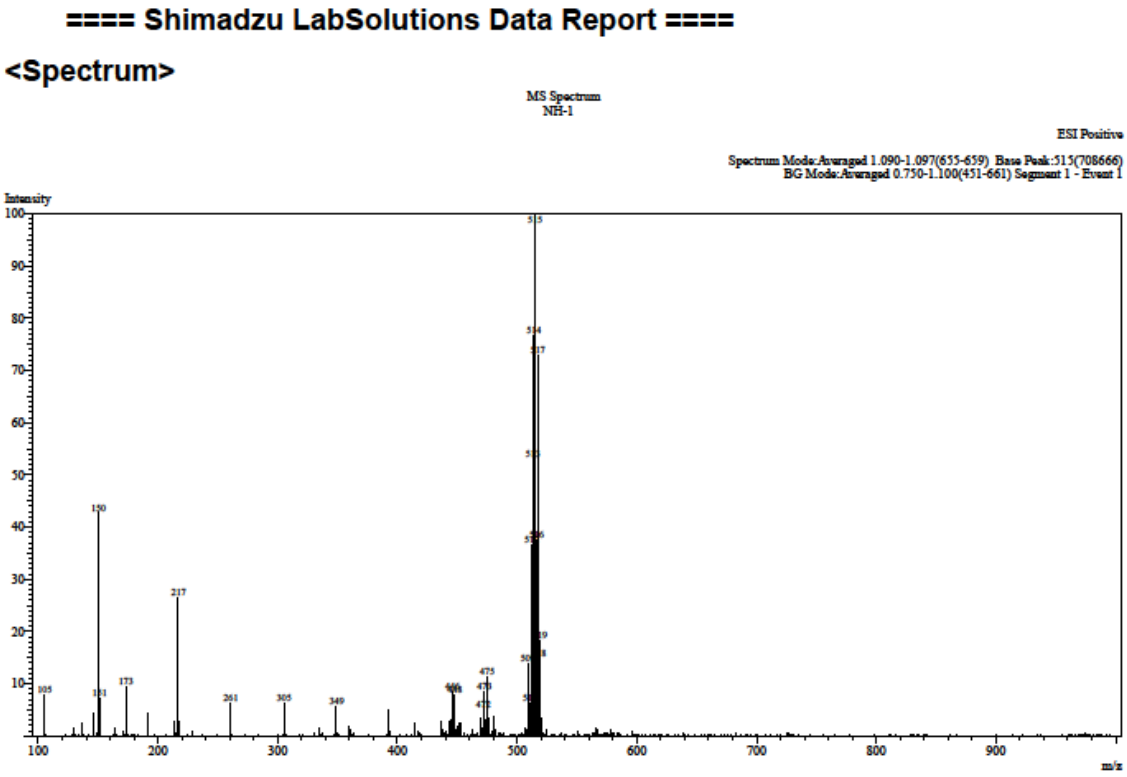

Figure SI 6.6 LCMS of **C1**

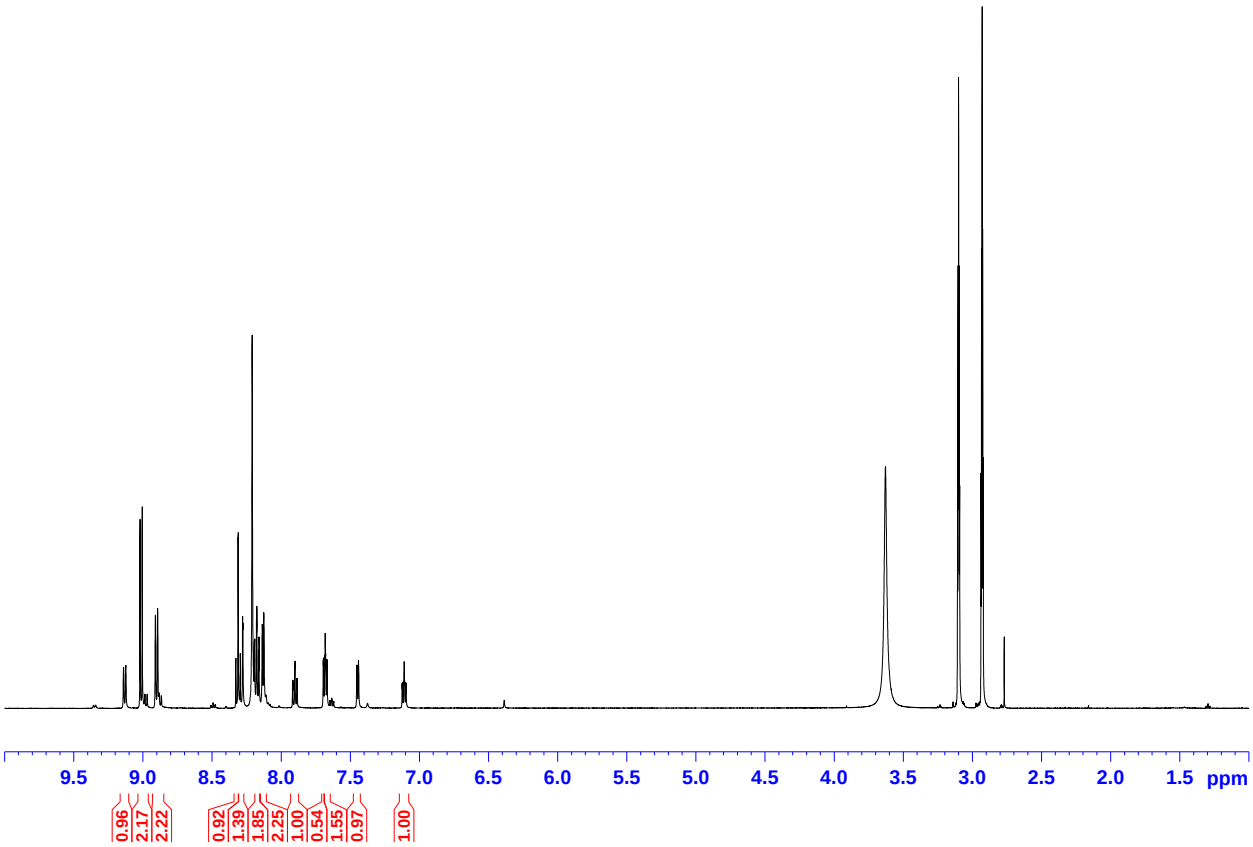

Figure SI 6.7 ^{1}H NMR spectra of **C1**

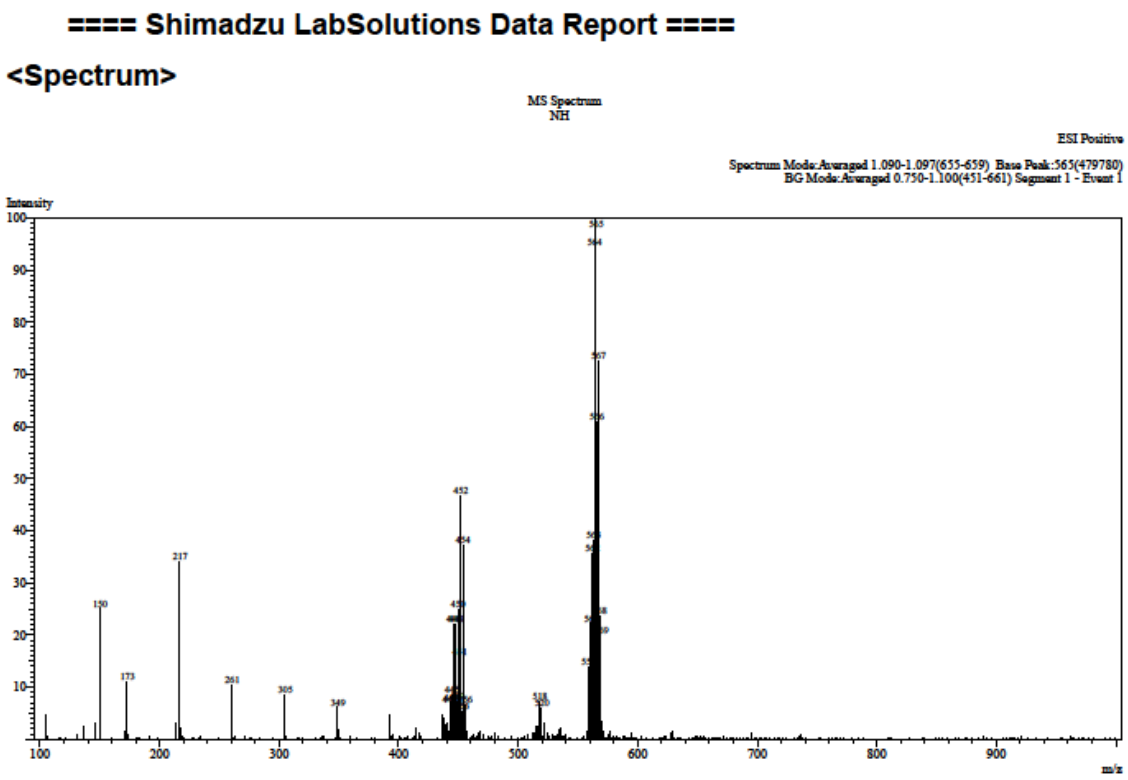

Figure SI 6.8 LCMS of **C2**

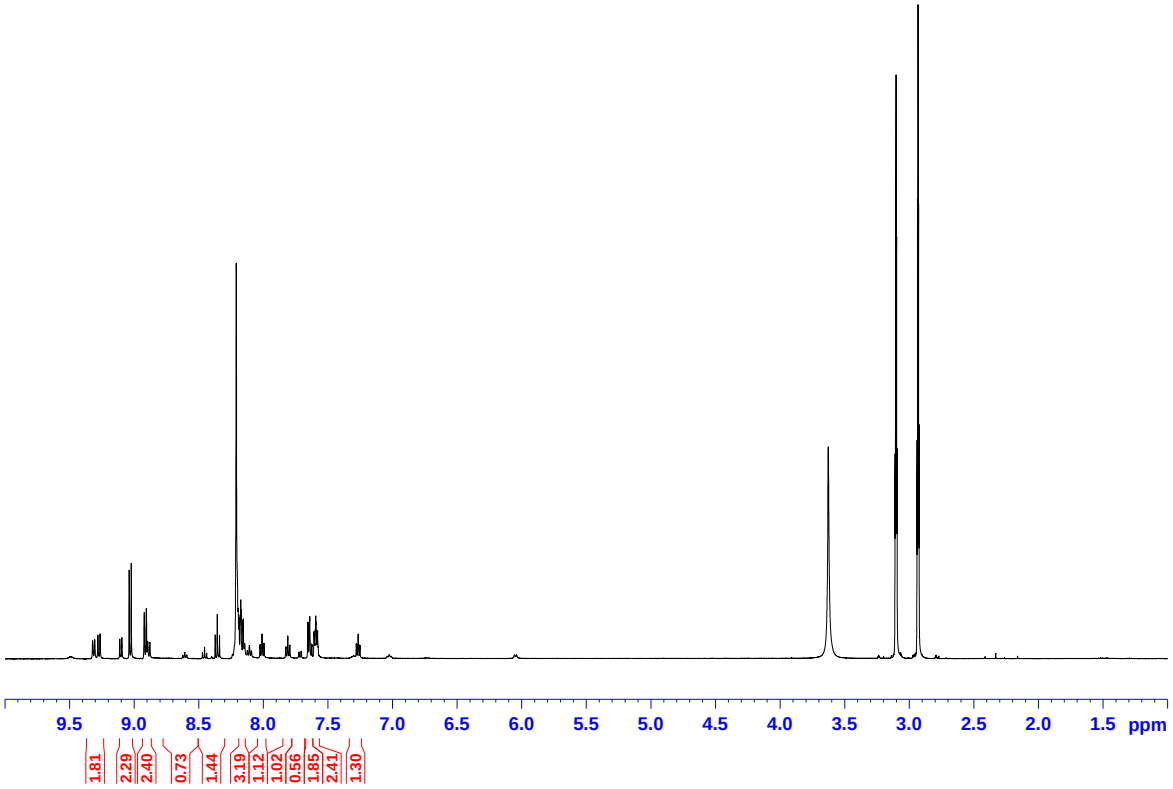

Figure SI 6.9 ^{1}H NMR spectra of **C2**

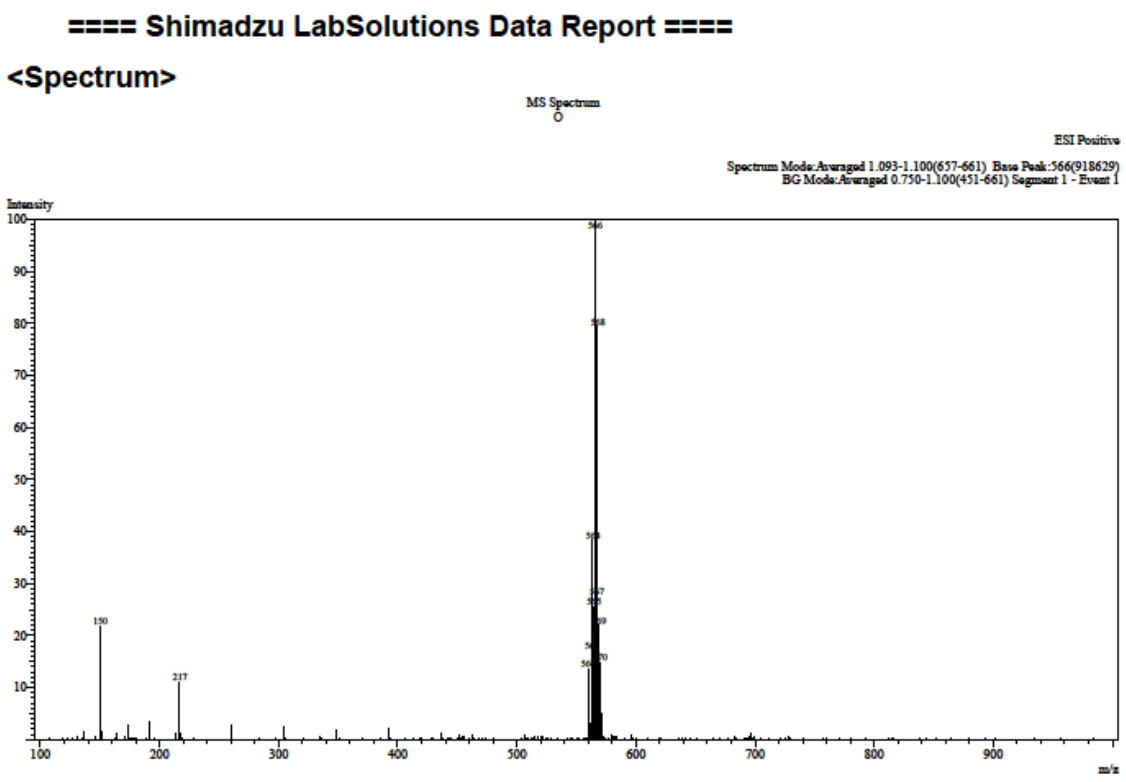

Figure SI 6.10 LCMS of **C4**

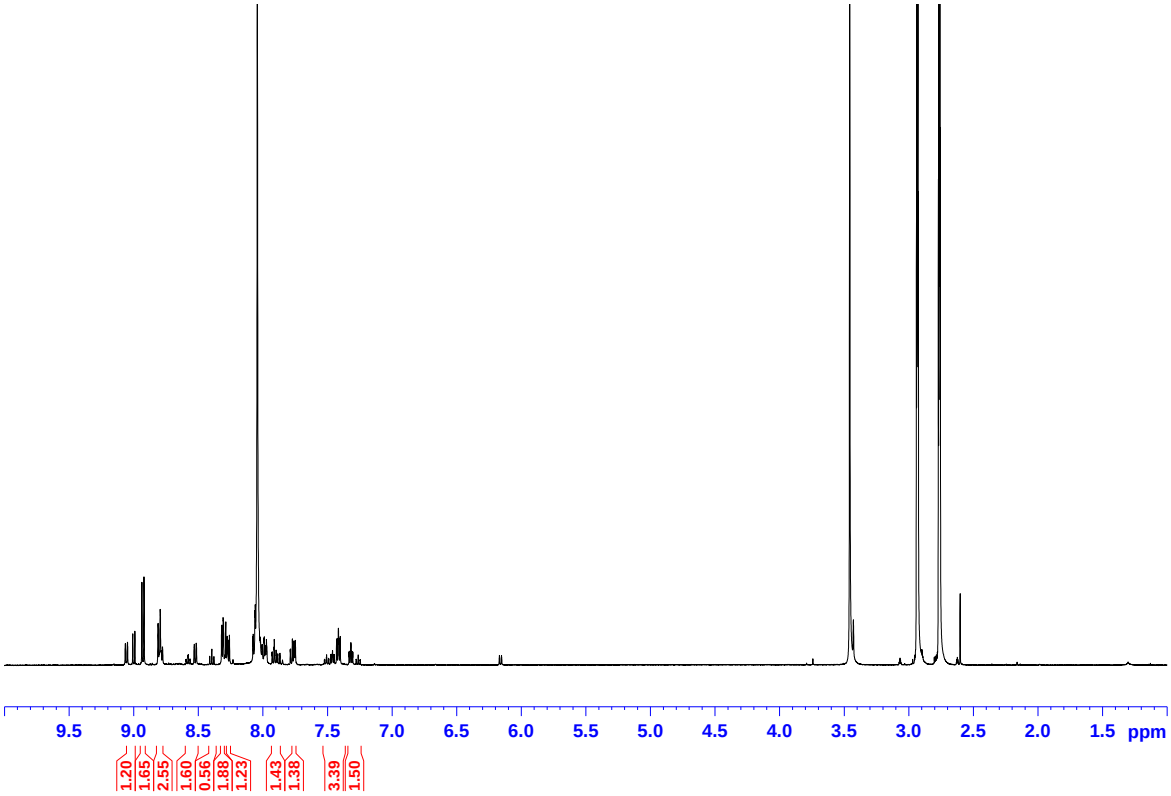

Figure SI 6.11 ^{1}H NMR spectra of **C4**

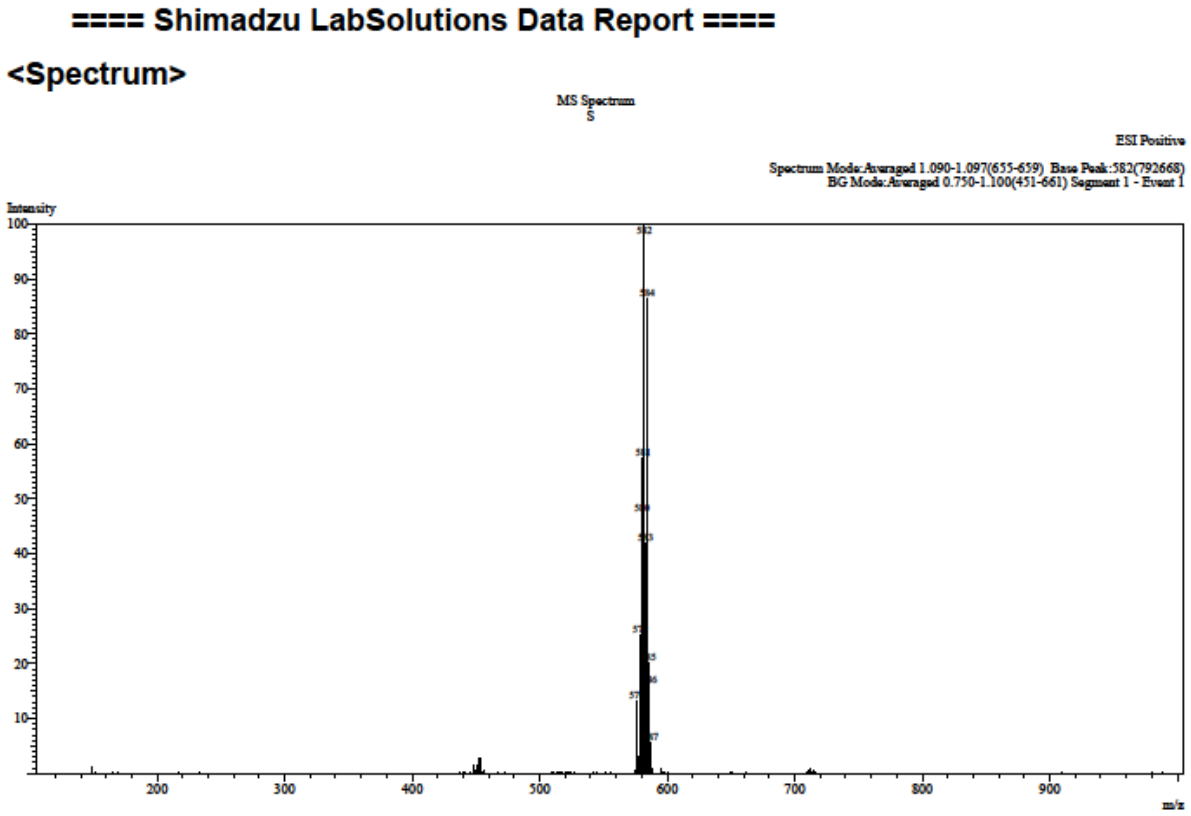

Figure SI 6.12 LCMS of **C3**

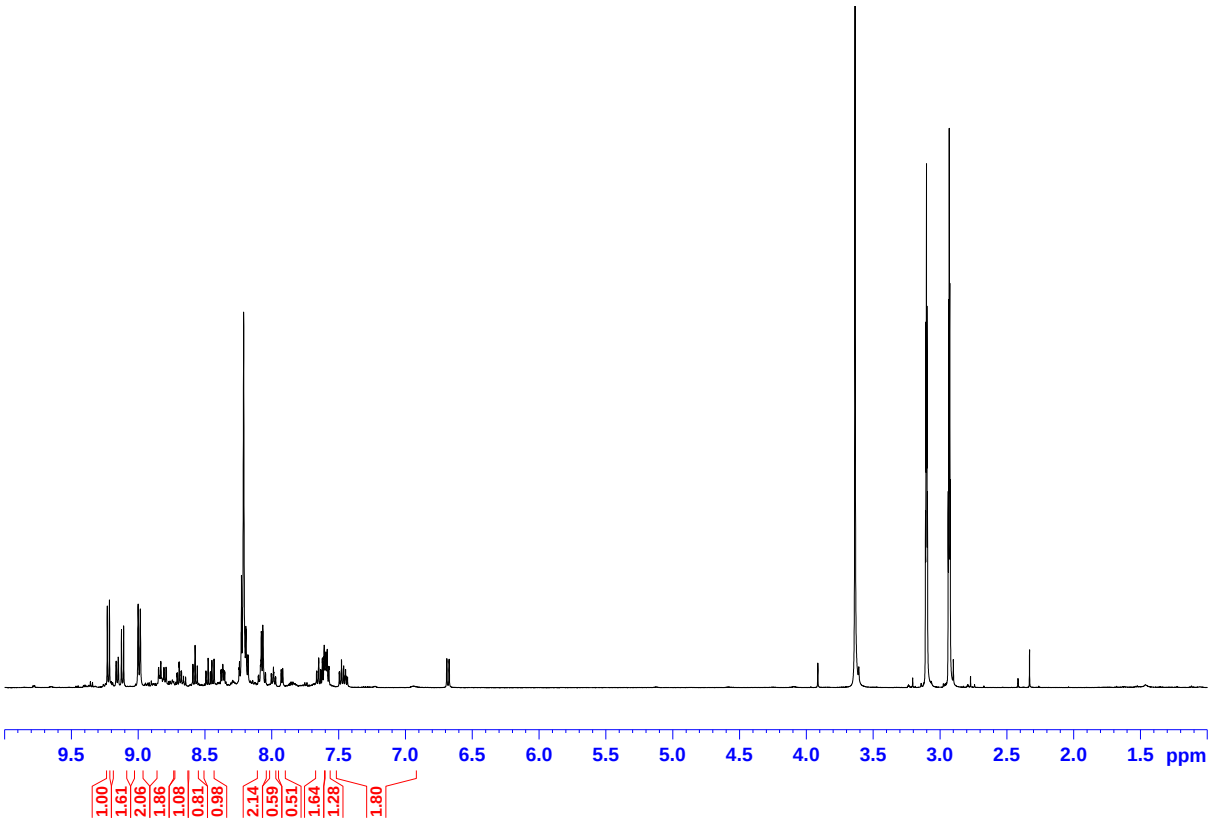

Figure SI 6.13 ^{1}H NMR spectra of **C3**

6.7.2 Kinetic data

1. 2, 2': 6', 2''-terpyridineruthenium(II)-2-(1*H*-Imidazol-2-yl)pyridine dichloride (C1)

Table SI 6.1 Observed rate constants and the corresponding nucleophile concentrations for complex **C1**

[Nu]/M	**k_{obs}/s^{-1} TU**	**k_{obs} / s^{-1} DMTU**	**k_{obs} / s^{-1} TMTU**
0.01	3.2E-4	0.00025	0.000145
0.02	6.4E-4	0.00050	0.000295
0.03	9.62E-4	0.00075	0.000441
0.04	0.00128	0.001	0.00059
0.05	0.00161	0.00126	0.000735

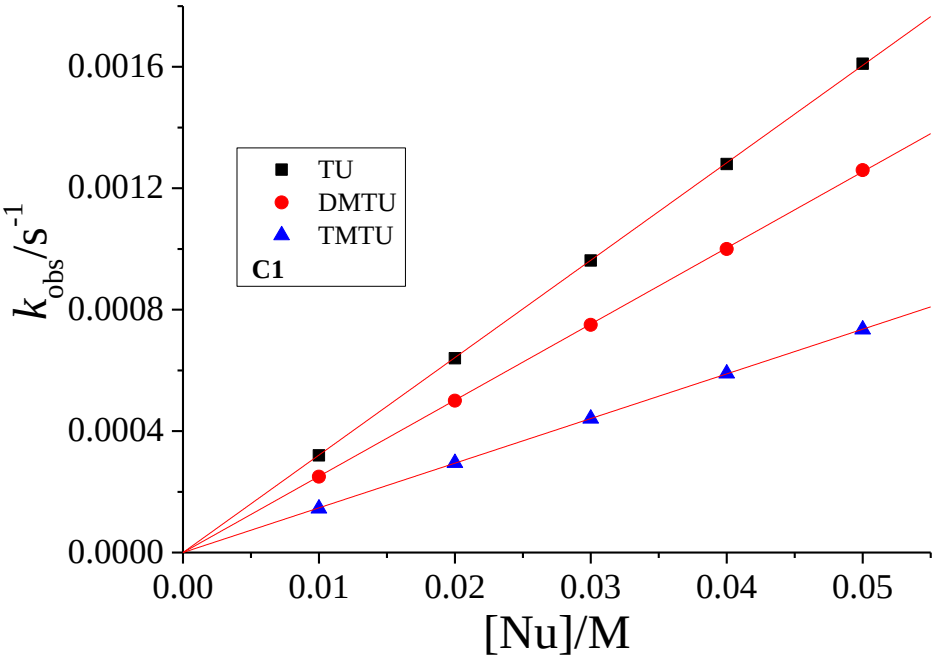

Figure SI 6.14 Concentration dependence plots for the reaction of **C1** with thiourea nucleophiles at 298 K

Table SI 6.2 Data of $\ln(k_2/T)$ and 1/T for complex **C1**

1/T	**$\ln(k_2/T)$ TU**	**$\ln(k_2/T)$ DMTU**	**$\ln(k_2/T)$ TMTU**
0.00341	-9.8	-10.25	-10.7
0.00336	-9.5	-9.9	-10.33
0.0033	-9.1	-9.48	-9.87
0.00325	-8.8	-9.13	-9.48
0.00319	-8.4	-8.7	-9.03

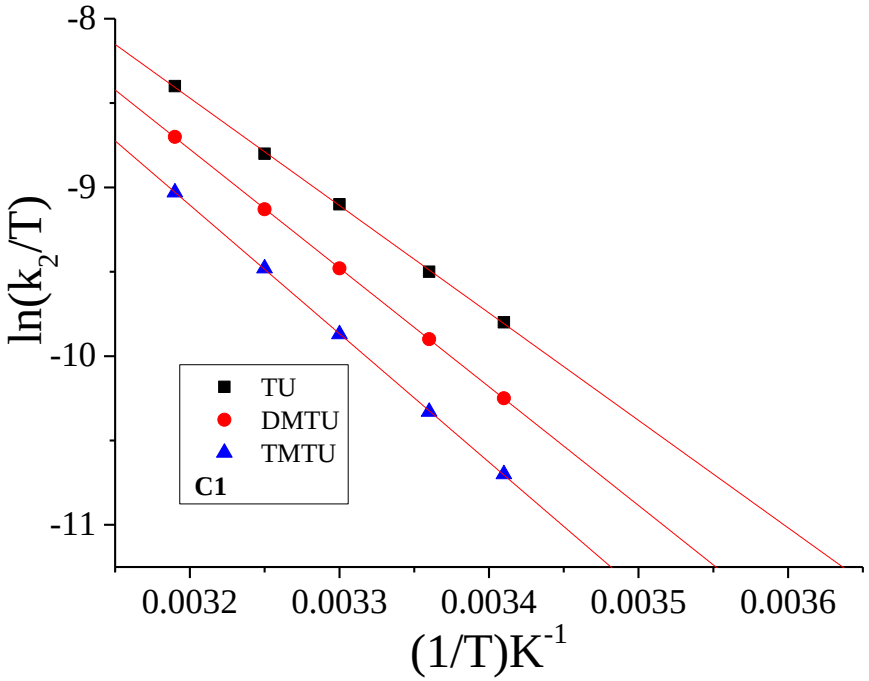

FigureSI 6.15 Eyring plots for the reaction of **C1** with thiourea nucleophiles

2. 2, 2': 6', 2''-terpyridineruthenium(II)-2-(2-pyridyl)-1*H*-benzimidazole dichloride (C2)

Table SI 6.3 Observed rate constants and the corresponding nucleophile concentrations for complex **C2**

[Nu]/M	k_{obs}/s^{-1} **TU**	k_{obs} / s^{-1} **DMTU**	k_{obs} / s^{-1} **TMTU**
0.015	2.6E-4	8.5E-5	1.25E-4
0.03	5.2E-4	1.7E-4	2.5E-4
0.045	7.8E-4	2.55E-4	3.75E-4
0.06	0.00104	3.4E-4	5E-4
0.075	0.0013	4.25E-4	6.25E-4

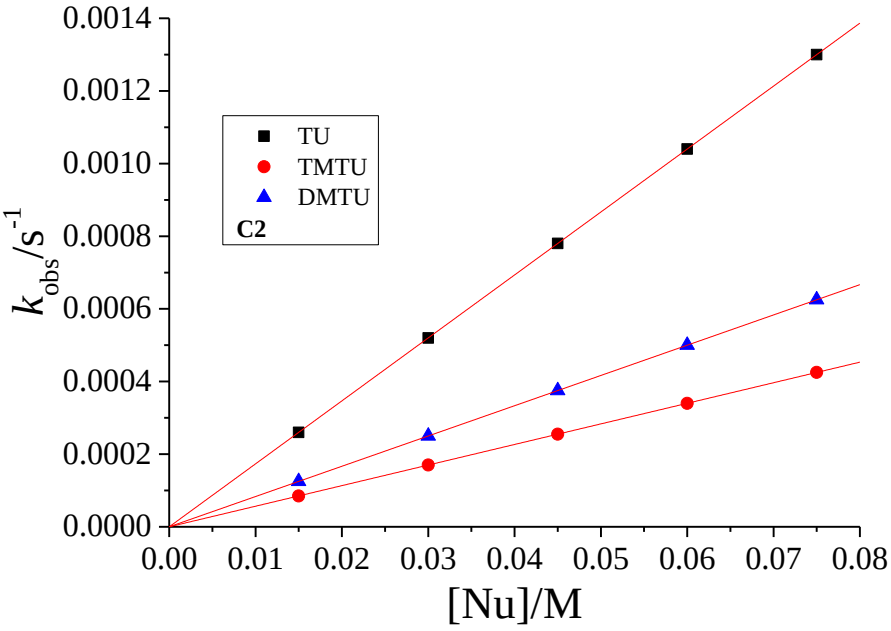

Figure SI 6.16 Concentration dependence plots for the reaction of **C2** with thiourea nucleophiles at 298 K

Table 6.4 Data of ln(k_2/T) and 1/T for complex **C2**

1/T	**ln(k_2/T) TU**	**ln(k_2/T) DMTU**	**ln(k_2/T) TMTU**
0.00341	-10.05	-11	-11.6
0.00336	-9.68	-10.57	-11.15
0.0033	-9.25	-10.1	-10.61
0.00325	-8.88	-9.67	-10.17
0.00319	-8.46	-9.2	-9.62

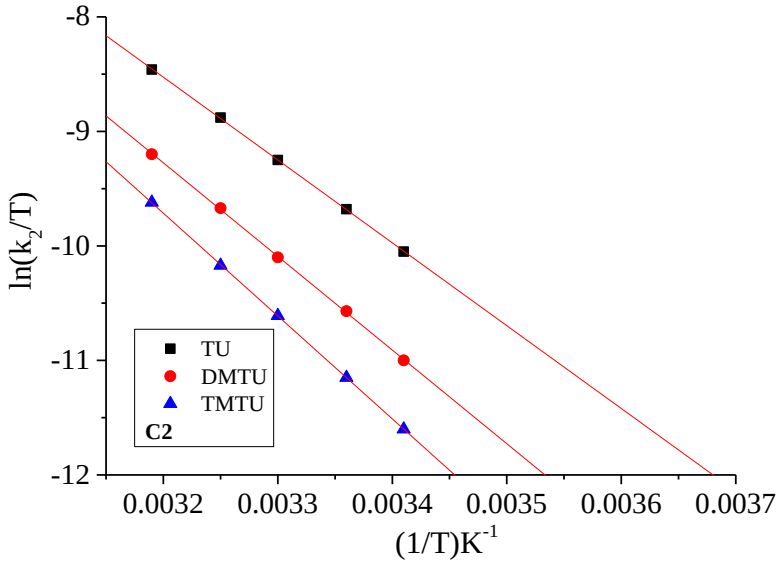

Figure SI 6.17 Eyring plots for the reaction of **C2** with thiourea nucleophiles

2, 2': 6', 2''-terpyridineruthenium(II)-2-(pyridyl)benzoxale dichloride (C4)

Table 6.5 Observed rate constants and the corresponding nucleophile concentrations for complex **C4**

[Nu]/M	k_{obs}/s^{-1} **TU**	k_{obs} / s^{-1} **DMTU**	k_{obs} / s^{-1} **TMTU**
0.017	5E-5	5.5E-5	4E-5
0.034	1E-4	1.1E-4	8E-5
0.051	1.5E-4	1.65E-4	1.2E-4
0.068	2E-4	2.2E-4	1.6E-4
0.085	2.5E-4	2.75E-4	2E-4

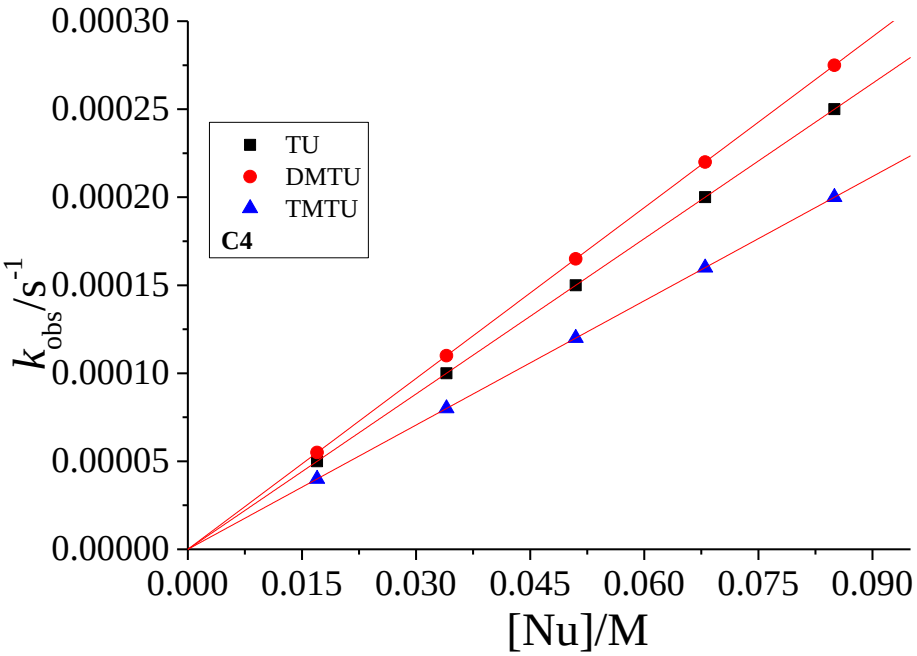

Figure SI 6.18 Concentration dependence plots for the reaction of **C4** with thiourea nucleophiles at 298 K

Table 6.6 Data of $\ln(k_2/T)$ and 1/T for complex **C4**

1/T	**$\ln(k_2/T)$ TU**	**$\ln(k_2/T)$ DMTU**	**$\ln(k_2/T)$ TMTU**
0.00341	-11.8	-11.4	-12.2
0.00336	-11.3	-10.95	-11.7
0.0033	-10.78	-10.4	-11.1
0.00325	-10.3	-9.95	-10.58
0.00319	-9.7	-9.4	-9.95

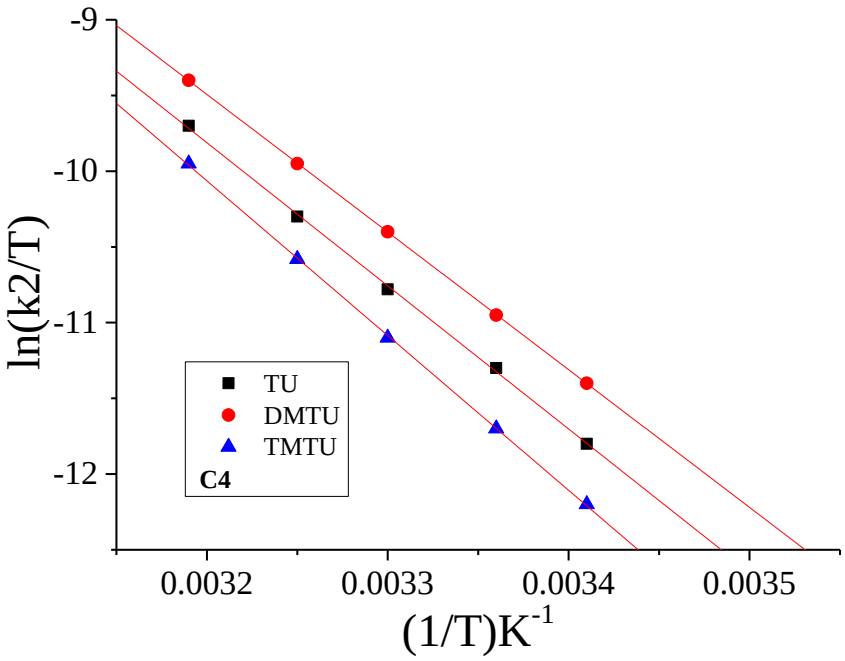

Figure SI 6.19 Eyring plots for the reaction of **C4** with thiourea nucleophiles

2, 2': 6', 2''-terpyridineruthenium(II)-2-(pyridyl)benzothiazole dichloride (C3)

Table 6.7 Observed rate constants and the corresponding nucleophile concentrations for complex **C3**

[Nu]/M	k_{obs}/s^{-1} **TU**	k_{obs} / s^{-1} **DMTU**	k_{obs} / s^{-1} **TMTU**
0.02	1E-4	8E-5	5.5E-5
0.04	2E-4	1.6E-4	1.1E-4
0.06	3E-4	2.4E-4	1.65E-4
0.08	4E-4	3.2E-4	2.2E-4
0.1	5E-4	4E-4	2.74E-4

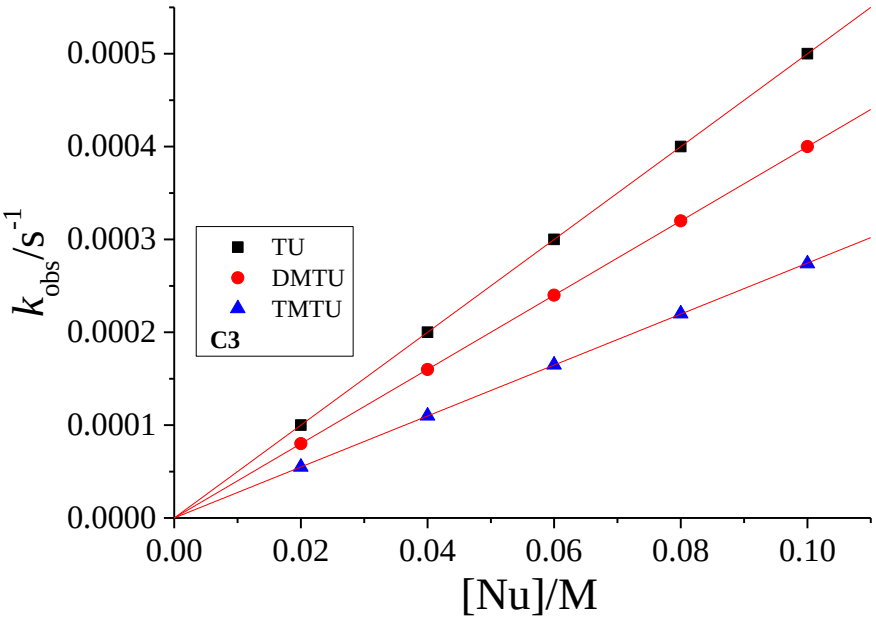

Figure 6.20 Concentration dependence plots for the reaction of **C3** with thiourea nucleophiles at 298 K

Table 6.8 Data of $\ln(k_2/T)$ and 1/T for complex **C3**

1/T	**$\ln(k_2/T)$ TU**	**$\ln(k_2/T)$ DMTU**	**$\ln(k_2/T)$ TMTU**
0.00341	-12.15	-11	-11.7
0.00336	-11.7	-10.6	-11.2
0.0033	-11.2	-10.05	-10.6
0.00325	-10.72	-9.6	-10.1
0.00319	-10.21	-9.1	-9.5

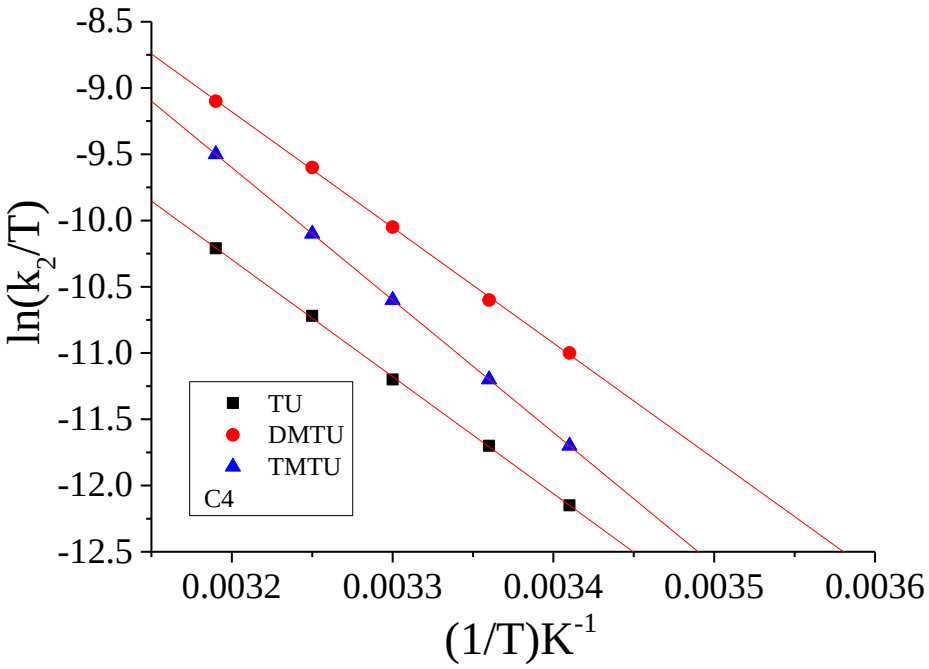

Figure 6.21 Eyring plots for the reaction of **C3** with thiourea nucleophiles

Chapter 7

Substituent effect on the rate of substitution from (Dichloro)((4-substituted)terpyridine)(triphenylphosphino)Ru(II) complexes

7.0 Abstract

The study of rates of substitution of the labile chloro ligands from Ru(II) complexes (**C1-C6**) of the form $[Ru(\kappa^3\text{-}L)(PPh_3)Cl_2]$ (L = 2,2′:6′,2″-terpyridine (tpy) (**L1**) or 4'-(4-methylphenyl)- 2,2′:6′,2″-terpyridine (**L2**) or 4,4'4''-tri-tert-butyl-2,2′:6′,2″-terpyridine (**L3**) or 4'-(4-Chlorophenyl)- 2,2′:6′,2″-terpyridine (**L4**) or 4-chloro-2,2′:6′,2″-terpyridine (**L5**) or 2,6-bis(2-pyrazolyl)pyridine (**L6**)) by thiourea nucleophiles. This was carried out under *pseudo* first order conditions in 0.1 M $NaClO_4$/LiCl methanol solution as a function of nucleophile concentrations and temperature. The UV-Visible Spectrophotometer or Stopped Flow Spectrophotometer for ultrafast reactions was used to study the reactions. The observed *pseudo* first order rate constants are consistent with the rate law, $k_{obs/obs'} = k_{2/2'}[Nu]$. The chloro ligands are substituted in two steps. The trend in the reactivity of the complexes in both the steps is in the order; **C3** > **C2** > **C4** > **C5** > **C1** > **C6.** There are two competing electronic forces in these complexes, inductive electron donation towards the metal centre by *trans*-effect and the donation from the filled *d* orbitals to the π* antibonding ligand orbitals by π-back-bonding effect. The complexes **C2** and **C3** having donor substituents on the tpy backbone experience *trans*-effect that makes them more reactive than **C1**. Electron donation towards the metal centres which leads to *trans*-effect is confirmed by their lower global electrophilcity indices and NBO charges compared to **C1**. Complexes **C4** and **C5** are more reactive than **C1** due to their enhanced π-back-bonding brought about by electron withdrawing substituents on their tpy ligand backbones which is confirmed by their higher electrophilicity indices and NBO charges. The reactivity of **C4** is higher than **C5** due to the greater electron acceptor capacity of the chlorophenyl ligand than the chloro ligand in **C5**. The 2,6-bis(pyrazolyl)pyridine ligand in **C6** sharply retards the reactivity at the Ru(II) metal centre compared to **C1** due to the *cis*-donor effect of the pyrazole ligands that is confirmed by reduced electophilicity index and NBO charges on the Ru. The reactivity of the complexes in this study is associative for all the nucleophiles in step one and only thiourea nucleophile in step two. The substitution reactions for the rest of the nucleophiles in step two occur via the dissociatively activated interchange mechanism. The reactivity of the nucleophiles follows the order; TU > DMTU > TMTU.

7.1 Introduction

The coordination chemistry of Ru(II) has been a centre of focus due to its versatile applications particularly in the area of DNA intercalation and protein binding. [1] Tridentate ligands such as 2,2′:6′,2″-terpyridine (tpy) and its derivatives have been used extensively by Thorp *et. al.* in the synthesis of Ru complexes.[2] The tpy ligand and its derivatives have been widely studied as chelating ligands because they form strong σ-bonds with metals.[3] Their complexes have found many applications. The tpy type ligands have also shown cytotoxicity against several human tumour cell lines.[4] A number of complexes incorporating these ligands have been reported to interact with DNA through electrostatic interaction, intercalation and groove binding.[5] [6]

Majority of Ru(tpy) complexes are potent DNA intercalators. For example, the activity of tpyRu(III)Cl_3 against L1210 leukemia cells compares to that of cisplatin.[7] The physical and chemical properties and DNA binding capacity of Ru(tpy) complexes and hence their interaction with DNA can be varied by the introduction of different substituents on the tpy ligand.[8] Turro and co-workers reported DNA photocleavage by Ru(tpy)-3-(pyrid-2-yl)dipyrido(3,2,-a:2',3'-c)phenazine in the presence of oxygen.[9] The substituent ensured favourable intercalating interactions by the planar groups at the sites of DNA cleavage. Complexes incorporating tpy and N-N bidentate ligands like $[Ru(tpy)(bipyridine)O]^{2+}$ and $Ru(tpy)(bipyridin)OH]^{2+}$ were also found to be efficient DNA photocleaving agents.[10] The DNA cleavage of $[Ru(tpy)N,N,N,N\text{-tetramethylenediamine})OH_2]^{2+}$ was also confirmed by cyclic voltammetry.[11] In a similar manner, heteroleptic Ru(III) complexes [Ru(tpy)(2-(2-benzimidazole)-1,10-phenanthroline] and [Ru(tpy)(2(2-napthoimidazole)-1,10-phenanthroline] interact with DNA by electrostatic interactions and intercalation respectively.[6]

Further studies on aryl modified $(tpy)_2Ru$ complexes have been reported to photophysically generate $^1O_2$ for cleaving DNA.[12] Aryl substituted tpy complexes interact with DNA through the intercalation of their aryl group substituent between the DNA bases.[5] The complexes $[Ru(\kappa^3\text{-}L)(PPh_3)_2\text{-}Cl]^+$ (L = tpy or 2,4,6-tris(2-pyridyl)-1,3,5-triazine ligands) have been reported to have biocatalytic properties.[13] Replacement of one of the triphenyl ligands by a chloride ligand gave Ru(II) complexes of the form, $[Ru(\kappa^3\text{-}L)(PPh_3)Cl_2]$ (L = tpy or 2,4,6-tris(2-pyridyl)-1,3,5-triazine ligands) which lowers the steric hindrance and increase DNA binding. The less hindered $Ru(\kappa^3\text{-}tptz)(PPh_3)Cl_2]$ inhibit activity of Topo II towards its

interaction with DNA of filarial parasite.[1] Data on the biochemical interactions of (tpy)Ru(II) complexes cover mainly their binding interaction with DNA yet anti-cancer metal complexes interact with all sorts of bionucleophiles in a biological environment. This study focuses on the rate of chloride substitution reactions from neutral Ru(II) complexes where the metal centre is coordinated to the tpy ligand or its derivatives and a triphenylphosphine ligand. Their general formula is $[Ru(\kappa^3\text{-L})(PPh_3)Cl_2]$ (L = 2,2′:6′,2″-terpyridine (**L1**), 4'-(4-methylphenyl)- 2,2′:6′,2″-terpyridine (**L2**), 4,4'4''-tri-tert-butyl-2,2′:6′,2″-terpyridine (**L3**), 4'-(4-chlorophenyl)- 2,2′:6′,2″-terpyridine (**L4**), 4-chloro-2,2′:6′,2″-terpyridine (**L5**), and 2,6-bis(2-pyrazolyl)pyridine (**L6**)). Information on the rate of substitution of potential anti-cancer agents is important to infer on their interactions with biological nucleophiles. The chemical structures of the complexes investigated are shown in Figure 7.1.

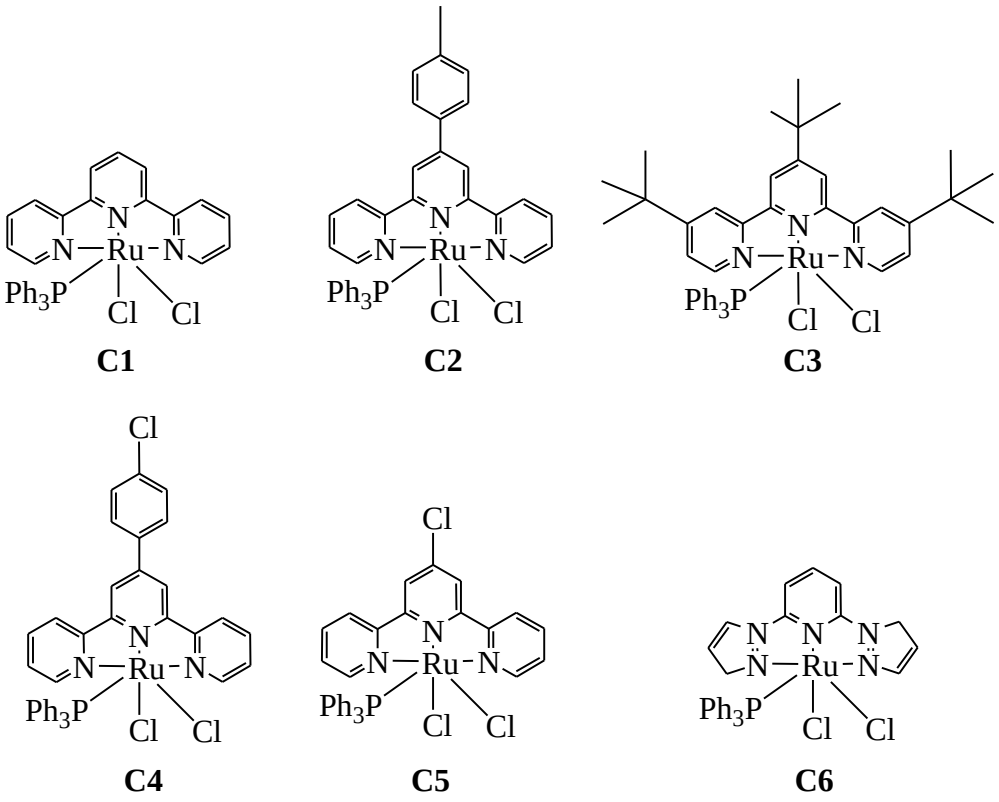

Figure 7. 1 Chemical structure of the neutral Ru complexes under investigation

7.2 Experimental

7.2.1 Materials

Solvents and other reagents including **L1**, **L2**, **L3**, **L4**, **L5**, **L6** and tris(triphenylphosphine)-Ru(II)dichloride were obtained from Sigma Aldrich and used as received.

7.2.2 Synthesis of the Complexes

The synthesis of the complexes was carried out according to modified standard literature method.[1] [14]

Dichloro(2,2′:6′,2′′-terpyridine)(triphenylphosphine)ruthenium(II) (**C1**)

Ligand, **L1** (46.65 mg, 0.2 mmol), and tris(triphenylphosphine)Ru(II)dichloride (191.77 mg, 0.2 mmol) were mixed in 30 mL of benzene and the mixture heated under reflux for 6 hours. After cooling to room temperature, the precipitate was collected by filtration, washed several times with cold benzene and diethyl ether then dried. Yield: 90.11 mg, (67.5 %), brown solid. ^{1}H NMR (400 MHz, DMF) δ/ppm: δ = 9.51 (d, 2H); 8.44 (m, 2H); 8.07 (t, 2H); 7.80 (m, 1H); 7.72 (t, CH, 2H); 7.54 (m, 8H); 7.39 (m, 9H). ^{31}P NMR (400 MHz, DMF) δ/ppm = 41.18. ^{13}C NMR (400 MHz, DMF), δ/ppm: 121.98, 126.36, 128.39, 132.77, 135.90, 154.49, 159.93. TOF MS-ES^{+}, m/z: 667.53. *Anal. Calc. For* $C_{33}H_{26}Cl_2N_3PRu.2.5H_2O$: C 55.62, N 5.90, H 4.39. *Found*: C 55.64, N 5.99, H 4.17.

Dichloro(4'-(4-methylphenyl)-2,2′:6′,2′′-terpyridine)(triphenylphosphino)ruthenium(II) (**C2**)

C2 was synthesized in the same way as **C1** using **L2** (64.67 mg, 0.2 mmol), and tris(triphenylphosphine)Ru(II)dichloride (191.77 mg, 0.2 mmol). Yield: 109.86 mg, (72.5 %), red-brown solid. ^{1}H NMR (400 MHz, DMF) δ/ppm: δ = 9.36 (d, 2H); 8.67 (m, 2H); 8.51 (d, 2H); 8.41 (s, 2H); 7.94 (m, 9H); 7.58 (t, 2H); 7.43 (t, 6H); 2.47 (s, 3H). ^{31}P NMR (400 MHz, DMF) δ/ppm = 40.67. ^{13}C NMR (400 MHz, DMF), δ/ppm: 20.51, 119.51, 122.31, 126.18, 127.35, 127.7, 129.05, 129.84, 132.37, 132.7, 132.96, 134.92, 135.7, 139.19, 143.25, 154.37, 159.86. TOF MS-ES^{+}, m/z: 757.65. *Anal. Calc. For* $C_{40}H_{32}Cl_2N_3PRu.2H_2O$: C 60.52, N 5.29, H 4.57. *Found*: C 60.13, N 5.29, H 4.46.

Dichloro(triphenylphosphino)(4,4',4''-tri-tert-butyl-2,2′:6′,2′′-terpyridine)ruthenium-(II) (**C3**)

C3 was synthesized in the same way as **C1** using **L3** (80.31 mg, 0.2 mmol), and tris(triphenylphosphine)Ru(II)dichloride (191.77 mg, 0.2 mmol). Yield: 104.48 mg, (62.5 %), red solid. ^{1}H NMR (400 MHz, DMF) δ/ppm: δ = 9.16 (d, 2H); 8.85 (d, 2H); 8.24 (s, 2H); 7.52 (d, 9H); 7.28 (m, 3H); 7.14 (t, 2H); 1.38 (m, 27H). ^{31}P NMR (400 MHz, DMF) δ/ppm = 43.71. ^{13}C NMR (400 MHz, DMF), δ/ppm: 29.47, 34.61, 119.30, 123.01, 127.61, 128.66, 132.83, 153.74, 155.69, 159.5, 165.03. TOF MS-ES^{+}, m/z: 835. *Anal. Calc. For* $C_{45}H_{50}Cl_2N_3PRu$: C 64.66, N 5.03, H 6.03. *Found*: C 64.51, N 5.14, H 6.33.

Dichloro(4'-(4-Chlorophenyl)-2,2′:6′,2′′-terpyridine)(triphenylphosphino)ruthenium(II) (**C4**)

C4 was synthesized in the same way as **C1** using **L4** (68.76 mg, 0.2 mmol), and tris(triphenylphosphine)Ru(II)dichloride (191.77 mg, 0.2 mmol). Yield: 109.71 mg, (70.5 %), red solid. ^{1}H NMR (400 MHz, DMF) δ/ppm: δ = 9.55 (d, 2H); 8.67 (d, 2H); 8.61 (s, 2H); 8.30 (d, 2H); 8.11 (m, 2H); 7.86 (t, 2H); 7.76 (t, 2H); 7.59 (m, 6H); 7.38 (m, 9H). ^{31}P NMR(400 MHz, DMF) δ/ppm = 40.29. ^{13}C NMR (400 MHz, DMF), δ/ppm: 119.79, 122.53, 126.44, 127.97, 129.34, 132.85, 134.62, 135.92, 136.82, 141.80, 154.52, 160.07. TOF MS-ES^{+}, m/z: 778.07. *Anal. Calc. For* $C_{39}H_{29}Cl_3N_3PRu$: C 60.20, N 5.40, H 3.76. *Found*: C 59.90, N 5.30, H 4.15.

Dichloro(4-chloro-2,2′:6′,2′′-Terpyridine)(triphenylphosphino)ruthenium(II) (**C5**)

C5 was synthesized in the same way as **C1** using **L5** (53.54 mg, 0.2 mmol), and tris(triphenylphosphine)Ru(II)dichloride (191.77 mg, 0.2 mmol). Yield: 83.67 mg, (59.6 %), red solid. ^{1}H NMR (400 MHz, DMF) δ/ppm: δ = 9.39 (d, 2H); 8.40 (d, 2H); 8.29 (s, 2H); 7.96 (t, 2H); 7.63 (t, 6H); 7.42 (m, 9H); 7.29 (m, 2H). ^{31}P NMR (400 MHz, DMF) δ/ppm = 39.39. ^{13}C NMR (75 MHz, DMF), δ/ppm: 122.40, 126.80, 127.89, 132.91, 135.93, 137.06, 154.42, 158.74, 160.96. TOF MS-ES^{+}, m/z: 701.97. *Anal. Calc. For* $C_{33}H_{25}Cl_3N_3PRu$: C 56.46, N 5.99, H 3.59. *Found*: C 56.80, N 6.33, H 3.20.

Dichloro(2,6-bis(2-pyrazolyl)pyridine)(triphenylphosphino)ruthenium(II) (**C6**)

C6 was synthesized in the same way as **C1** using **L6** (42.64 mg, 0.2 mmol), and tris(triphenylphosphine)Ru(II)dichloride (191.77 mg, 0.2 mmol). Yield: 56.07 mg, (43.3 %),

yellow solid. ^{1}H NMR (400 MHz, DMF) δ/ppm: δ = 9.79 (d, 1H); 9.02 (m, 4H); 7.95 (m, 9H); 7.69 (m, 2H); 7.43 (m, 6H); 6.36 (m, 2H). ^{31}P NMR (400 MHz, DMF) δ/ppm = 50.34. ^{13}C NMR (400 MHz, DMF), δ/ppm: 106.61, 110.33, 128.42, 130.13, 132.75, 137.51, 162.27. TOF MS-ES^{+}, m/z: 645.48. *Anal. Calc. For* $C_{29}H_{24}Cl_2N_3PRu$: C 53.96, N 10.85, H 3.75. *Found*: C 53.80, N 10.84, H 3.70.

All compounds gave ^{1}H, ^{31}P and ^{13}C NMR spectra corresponding to the proposed structures and elemental analysis data consistent with their formulations. Mass spectrometric data gave peaks corresponding to the masses of the complexes. The spectra for NMR and mass analyses are placed in the supporting information Figures SI 7.1-7.24

7.2.3 Instrumentation and measurement

NMR spectroscopy were recorded on a Bruker Avance DPX 400 MHz spectrophotometer at 303 K using $Si(CH_3)_4$ as a reference. Low resolution electron spray ionization (ESI^{+}) mass spectra were recorded on the Waters Micromass LCT Premier Spectrometer or Shimadzu LCMS 2020. Elemental analyses were done on a ThermoScientific Flash 2000 elemental analyser. Kinetic measurements for ultrafast reactions were performed on an Applied Photophysics SX20 Stopped Flow instrument coupled with an online data acquisition system whose temperature is controlled within ± 0.1 °C. The slow reactions were monitored using Varian Cary 100 Bio UV-Visible Spectrophotometer to an attached Varian Peltier temperature controller and online kinetic application. The UV-Visible Spectrophotometer was also used to pre-determine the wavelengths at which the reactions were monitored.

7.2.4 Computational modelling

The computations were done by Density Functional Theory (DFT) run on Gaussian 09 suite of programs.[15] The structures were optimised using the hybrid Becke, 3-parameter, Lee-Young-Parr (B3LYP) method with LANL2DZ (Los Alamos National Laboratory 2 double ζ) basis sets having inner core electrons of the Ru atom replaced by relativistic effective core potential (ECP).[16] [17] [18] DFT applies to physically observable electron density over a wave function in the determination of the properties of a system. Los Alamos National Laboratory 2 double ζ basis set exploits relativistic effective core potentials to account for effect of inner core 28 electrons ([Ar]3d^{10}) in Ru.[19] [20] To take into account of the solvent effects, the complexes were fully optimised in methanol using the conductor polarizable continuum model (C-PCM).[21] [22] The singlet state was used due to the low electronic spin state of

Ru(II) complexes. The complexes were considered to have an overall charge of +1. The chemical potential (μ) and molecular hardness (η) for each structure were calculated from the HOMO and LUMO energies. The global electrophilicities (ω) were determined by the relationship $\omega = \mu^2/2\eta$.[23] [24] The charge on each atom is expressed as a natural bond orbitals (NBO) .[25]

7.3 Results

7.3.1 Computational results

DFT calculated quantities (Table 7.2) have been used in literature to explain kinetic behaviour. [26] [27] For example, electronic chemical potential, μ, chemical hardness, η, and electrophilicity index, ω, have been used to support observed trends in the rates of substitution reactions.[28] [29] In this study, computational calculations and optimisation were carried out to gain information on the electronic and structural properties of the complexes. The DFT optimized structures of the complexes are shown in Table 7.1 and a summary of selected DFT parameters are presented in Table 7.2. The DFT calculated frontier molecular orbitals (Table 7.1) show that the HOMO are located mainly on the Ru metal centre and partially on the chloro ligands while the LUMO on the N-N-N ligands as has also been observed in literature.[30]

Table 7. 1 DFT minimum energy structures and frontier molecular orbitals of the complexes

Optimised Structures		HOMO	LUMO
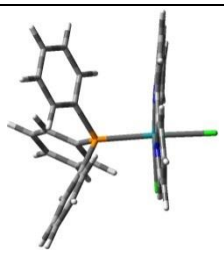	**C1**	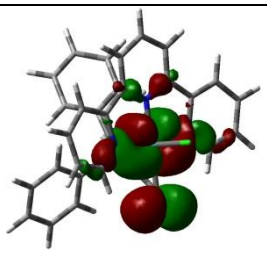	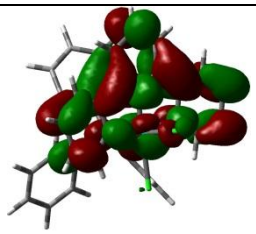
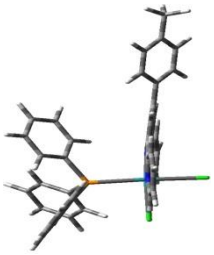	**C2**	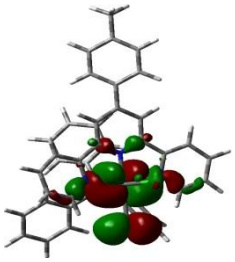	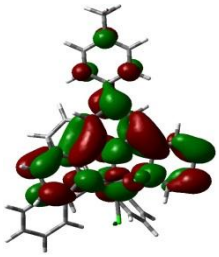
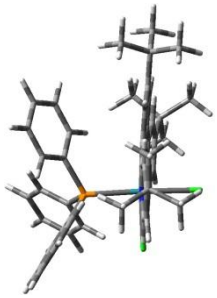	**C3**	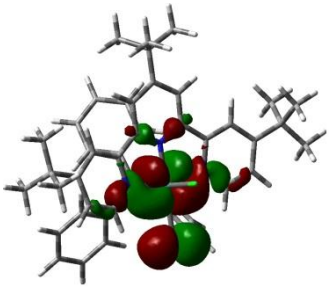	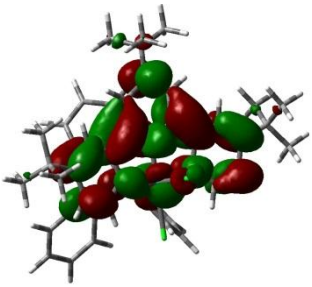
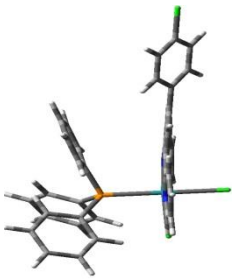	**C4**	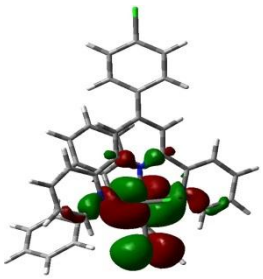	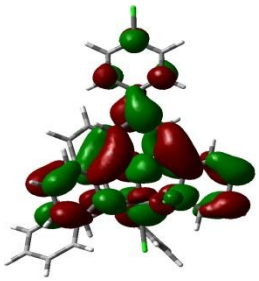
	**C5**	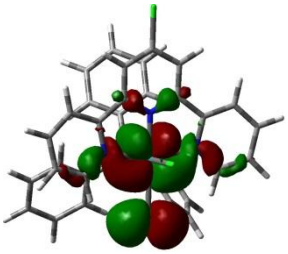	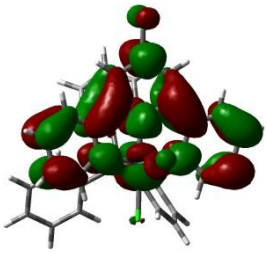
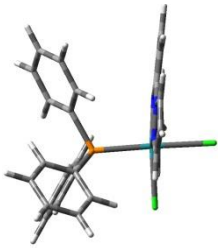	**C6**	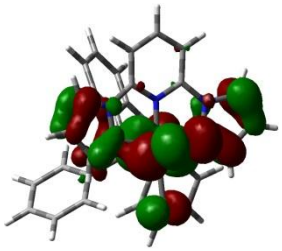	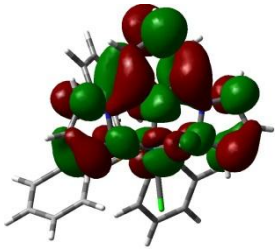

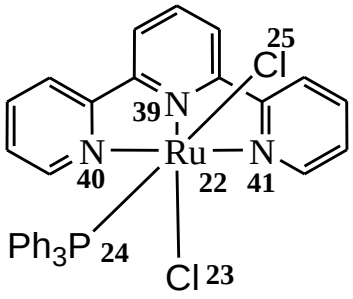

Figure 7. 2 Structure of **C1** illustrating numbering of atoms and the spatial orientation of the ligands around the Ru(II) metal centre

Table 7. 2 Summary of DFT calculated data for the complexes investigated

Parameters	**C1**	**C2**	**C3**	**C4**	**C5**	**C6**
Distances/Å						
Ru22-Cl23	2.58	2.59	2.59	2.59	2.57	2.56
Ru22-Cl25	2.56	2.55	2.56	2.48	2.55	2.56
Ru22-N39	1.97	1.97	1.97	1.97	1.96	1.99
Ru22-N40	2.10	2.10	2.10	2.10	2.10	2.10
Ru22-N41	2.10	2.10	2.10	2.10	2.10	2.10
Angles/ °						
N41-Ru22-N40	159.2	159.0	158.6	159.1	159.1	157.9
N40-Ru22-N39	79.8	79.7	79.5	79.8	79.8	79.3
Cl23-Ru22-Cl25	89.4	89.7	89.7	89.3	89.4	90.2
NBO charges/eV						
Ru(22)	0.171	0.164	0.151	0.176	0.173	0.133
Orbital energy/eV						
HOMO	-5.488	-5.471	-5.360	-5.525	-5.571	-5.620
LUMO	-2.479	-2.514	-2.289	-2.568	-2.604	-2.180
$\Delta E_{HOMO-LUMO}$	3.009	2.957	3.070	2.957	2.967	3.440
Global chemical reactivity indices						
η/eV	1.504	1.478	1.535	1.484	1.478	1.720
μ/eV	-3.984	-3.992	-3.824	-4.088	-4.047	-3.900
ω/eV	5.275	5.389	4.763	5.633	5.539	4.422

Where; η = Chemical Hardness μ = Electronic chemical potential ω = Electrophilicity index

The HOMO-LUMO energy gap has been used to predict the kinetic stability and chemical reactivity of compounds. Compounds with wider energy gap (Table 7.2) are likely to be kinetically stable and chemically less reactive.[31] The coordination geometry about the Ru(II) metal centre in these complexes (Figure 7.1) is a distorted octahedral. The angle N40-Ru22-N39 (79.8) and N41-Ru22-N40 (159.2) is smaller than the expected 90° and 180°, respectively. The angle Cl23-Ru22-Cl25 is 90 ° confirming that the chloride groups are in *cis* orientation. The data of calculated DFT parameters in Table 7.2 is in agreement with the literature findings on similarly structured Ru(II) complexes.[32] [33] [34] [35] [36] The DFT results reveal that the distances of the axial nitrogen atoms from the Ru(II) metal centre (Ru22-N39) are shorter than those of the equatorial ones (Ru22-N40/41). This further attest to the distortion in the coordination geometry of the Ru(II) complexes.

7.3.2 Kinetic Analyses

The chloride ions from LiCl suppressed any possibility of solvolysis of the complexes.[22] The perchlorate ion is such a poor nucleophile and cannot competitively substitute the co-labile ligand ahead of the incoming thiourea ligands.[22] The rate of substitution was measured under *pseudo* first-order conditions. Kinetic solutions were prepared by dissolving the required amount of complex in in 0.1 M ionic solution consisting of 0.01 M LiCl and 0.09 M $NaClO_4$ in dry methanol to achieve a specific concentration. Nucleophile stock solutions were prepared at 100 times higher than the concentration of the respective complex and diluted to afford those that were 80, 60, 40 and 20 times.

The rate of substitution of the chloride ligands was measured spectrophotometrically by following the change in absorbance with time using a UV-Visible Spectrophotometer for the slow reactions or a Stopped Flow spectrophotometer for ultrafast reactions. Spectral changes due to the reactions were observed over the wavelength range 200-800 nm to establish a suitable wavelength at which the respective reaction for each metal complex could be followed. All reactions were thermostated within ± 0.1 ° C of the set value. The changes in absorbance accompanying the reactions were analysed graphically using the software package OriginPro 9.1. An example of such spectral changes for the reaction of **C4** with DMTU is shown in Figure 7.3. The inset to figure 3 is the kinetic trace of the reaction at 317 nm.

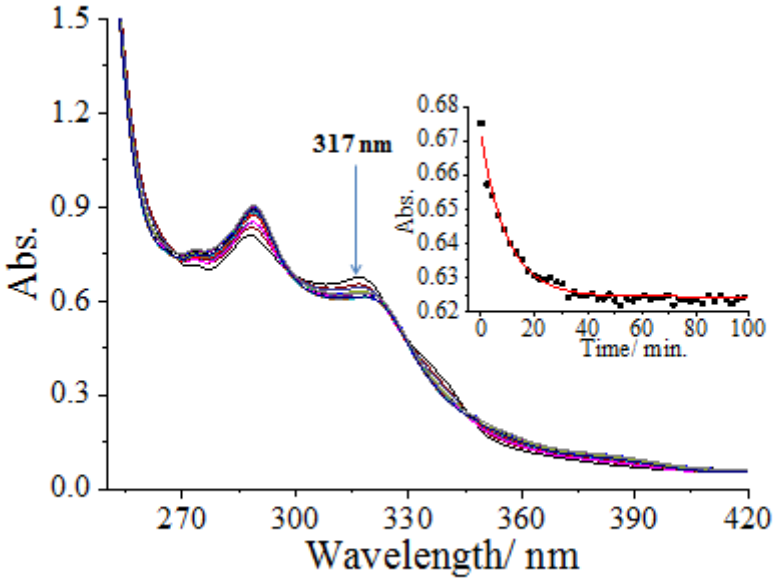

Figure 7. 3 Absorbance spectra for the reaction of **C4** and DMTU at 298 K (*Inset* is the kinetic trace obtained for the reaction at 317 nm)

The observed first order rate constants, $k_{obs/obs'}$, were obtained from the fitted data consistent with equation 7.1 [22] using OriginPro 9.1 program.

$$A_t = A_\circ + (A_\circ - A_\infty) \exp(-k_{obs/obs'} t) \quad (7.1)$$

where; A_0 is initial absorbance of the mixture, A_t is absorbance of the reaction mixture at time, t and A_∞ is final absorbance.

The rate of nucleophilic attack by the thiourea nucleophiles was calculated from the observed rate constant measured by varying the concentration of the nucleophile at 25° C. The average values of the observed rate constant, $k_{obs/obs'}$, for the first or second step of the reaction were plotted against [Nu], according to Equation 7.2. Linear plots of $k_{obs/obs'}$ verses $[Nu]$ were obtained for all reactions and typical plots are shown in Figure 7.4 for the substitution reactions of **C3** with the thiourea nucleophiles at 298 K

$$k_{obs/obs'} = k_{2/2'}[Nu] + k_{s/s'} \approx k_{2/2'}[Nu] \quad (7.2)$$

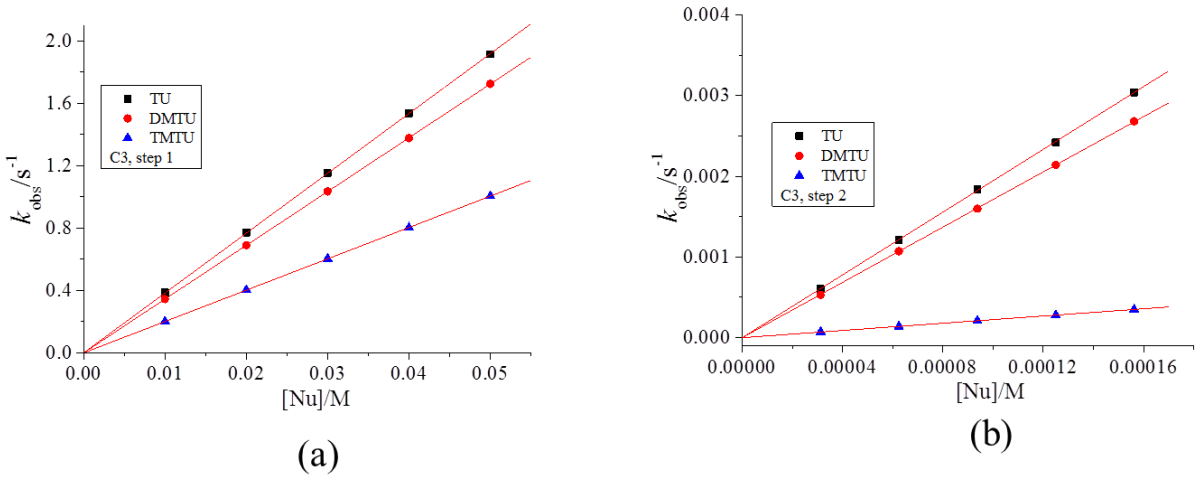

Figure 7. 4 Plots of k_{obs} (a) and $k_{obs'}$ (b) versus [Nu] for the reactions of **C3** with the thiourea nucleophiles at 298 K

The slopes represent the second order rate constants, k_2 (a) and $k_{2'}$ (b), respectively**.** Other similar plots are placed in the supplementary information, Figures SI 7.25, 7.26, 7.28, 7.30, 7.32, 7.33 and 7.35. Tables of $k_{obs/obs'}$ and respective nucleophile concentrations are presented in supplementary information, Tables SI 7.1, 7.2, 7.5, 7.6, 7.9, 7.10, 7.13, 7.14, 7.17 and 7.19.

Confirmation of substitution mechanism by ^{31}P NMR

The ^{31}P NMR spectra in Figure 7.5 illustrate the substitution from **C2** by the thiourea nucleophile.

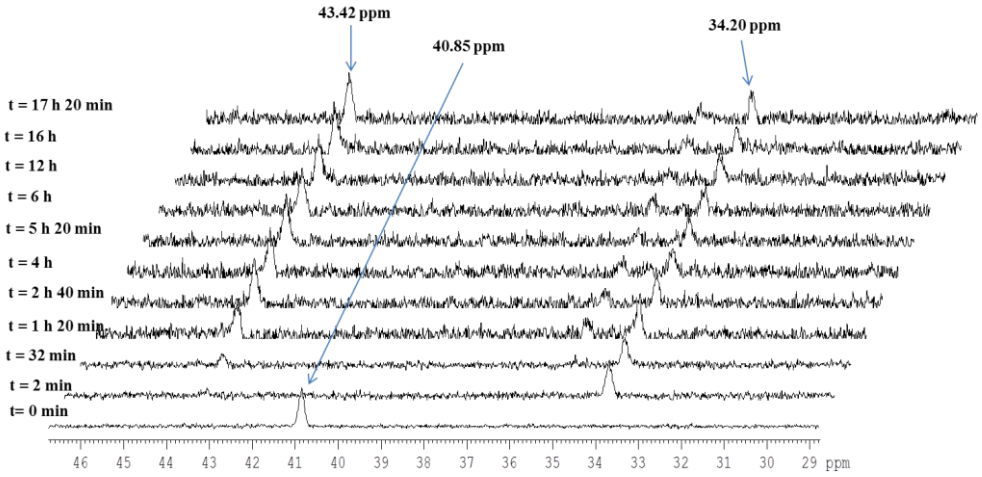

Figure 7. 5 ^{31}P NMR spectra array for the reaction of **C2** with thiourea (Tu)

The ^{31}P NMR spectrum of **C2** shows a single chemical shift peak at 40.85 ppm. On mixing the complex with Tu a new peak at 34.2 ppm appears within 2 minutes with a concomitant disappearance of the 40.85 ppm resonance peak. The first chloride substitution from **C2** produced an intermediate coordinated with one chloro and Tu ligand. This intermediate reacts with another Tu nucleophile at a much slower rate as evidenced by a decrease in its resonance at 34.20 ppm and concomitant growing of a resonance peak at 43.42 ppm after 32 min. This resonance is due to $Ru(\kappa^3\text{-tptz})(PPh_3)Tu_2$ species.[37] The ^{31}P NMR peak characteristic of the free triphenylphosphine ligand (Figure 7.6) was not observed during the course of the substitution reaction.

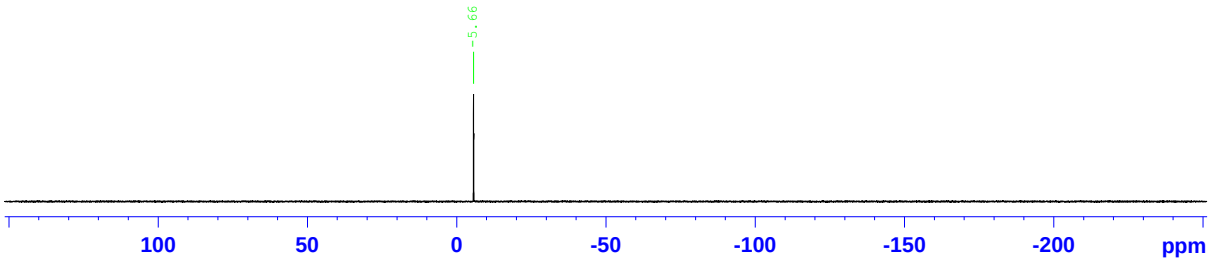

Figure 7. 6 ^{31}P NMR spectra for the free triphenylphosphine ligand

Based on the kinetic data and ^{31}P NMR kinetics analysis, the proposed mechanism of chloride substitution in the compounds under investigation can be represented by Scheme 7.1

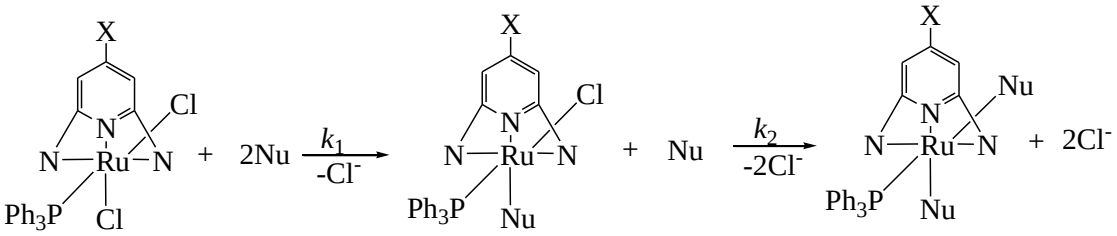

X, N = H, 2-Pyridyl (**L1**), 4-methylphenyl, 2-pyridyl (**L2**), tert-butyl, 4-tert-butyl-2-pyridyl (**L3**), 4-Chlorophenyl, 2-pyridyl (**L4**), Chloro, 2-pyridyl (**L5**) or H, 2-pyrazolyl (**L6**)

Scheme 7. 1 Proposed mechanisms of substitution from the Ru(II) complexes

The rate constants were also measured WITH the temperature range of 25-45 °C in increments of 5° C. Graphs of ln $k_{2/2'}$/T verses 1/T were plotted in accordance to the Eyring equation (Equation 7.3). Typical Eyring plots are shown in Figure 7.7 for the reaction of **C4** with the thiourea nucleophiles.

$$\ln\left(\frac{k_{\exp}}{T}\right) = \frac{-\Delta H^{\neq}}{R}.\frac{1}{T} + \left[23.8 + \frac{\Delta S^{\neq}}{R}\right] \qquad (7.3)$$

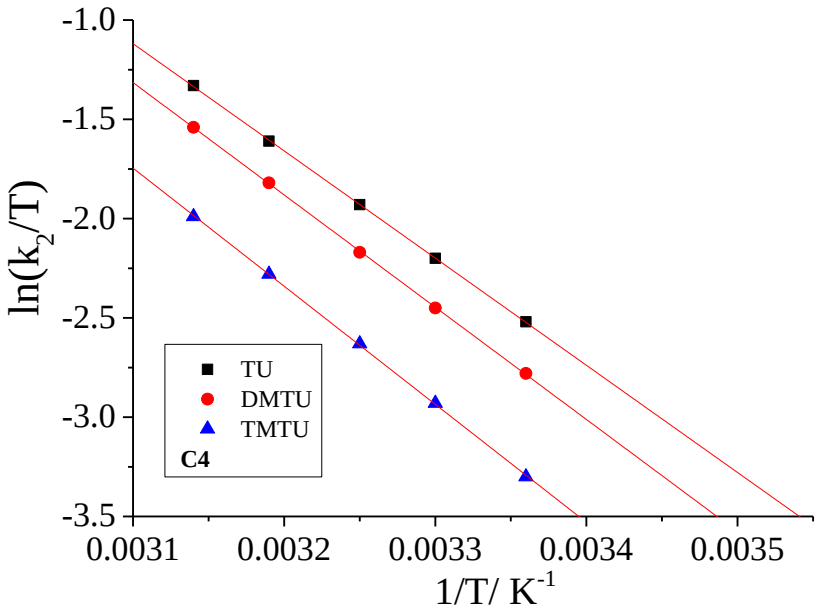

Figure 7. 7 Eyring plots for the reactions of **C4** with the thiourea nucleophiles

Other Eyring plots are presented in the supplementary information Figures SI 7.27, 7.29, 7.31 and 7.34. The tables of $\ln(k_2/T)$ and $1/T$ are provided in the supplementary information Tables SI 7.3 7.4, 7.7, 7.8, 7.11, 7.12, 7.15, 7.16 and 7.19. The enthalpy of activation ($\Delta H^{\neq}$), and entropy of activation, ($\Delta S^{\neq}$) were calculated from the slope and the intercept of the Eyring plots respectively. The rate constants ($k_{2/2'}$) and activation parameters ($\Delta H^{\neq}$, $\Delta H'^{\neq}$, $\Delta S^{\neq}$ and $\Delta S'^{\neq}$) for the first and second substitution steps are summarised in Table 7.3-7.4.

Table 7. 3 Second order rate constants and activation parameters for the first substitution

Complexes		Nu	k_2 / M^{-1} s^{-1}	$\Delta H^{\neq}$ / kJ mol^{-1}	$\Delta S^{\neq}$ / $JK^{-1}mol^{1}$
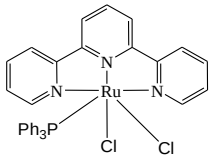	**C1**	TU	19.9 ± 0.05	56 ± 2	-27 ± 5
		DMTU	17.4 ± 0.01	58 ± 0.5	-22 ± 1.6
		TMTU	9.7 ± 0.05	67 ± 3	-3 ± 7
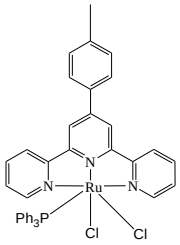	**C2**	TU	26.1 ± 0.20	30 ± 1	-116 ± 2.5
		DMTU	23.5 ± 0.07	37 ± 2	-96 ± 5
		TMTU	13.8 ± 0.04	58 ± 4	-31 ± 9
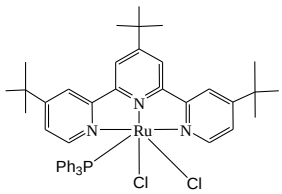	**C3**	TU	38.4 ± 0.04	28 ± 1.2	-121 ± 3.5
		DMTU	34.4 ± 0.02	29 ± 3	-118 ± 7
		TMTU	20.2 ± 0.01	55 ± 0.7	-34 ± 2
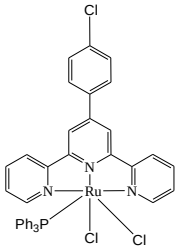	**C4**	TU	23.2 ± 0.08	45 ± 2	- 68 ± 6
		DMTU	19.5 ± 0.03	47 ± 1.3	- 63 ± 4
		TMTU	10.0 ± 0.05	61 ± 2	- 29 ± 5
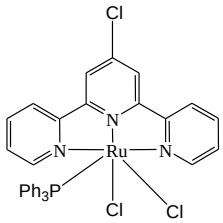	**C5**	TU	22.6 ± 0.1	40 ± 3	- 85 ± 7
		DMTU	18.8 ± 0.1	58 ± 1	- 90 ± 3
		TMTU	11.4 ± 0.1	60 ± 3	- 40 ± 7
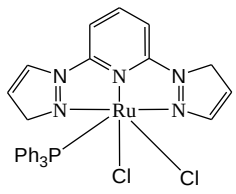	**C6**	TU	0.008 ± 0.0001	80 ± 1.8	-20 ± 6
		DMTU	0.007 ± 0.0001	90 ± 2.5	-15 ± 8
		TMTU	0.005 ± 0.0001	120 ± 1	-6 ± 3

Table 7. 4 Second order rate constants and activation parameters for the second substitution

Complexes		Nu	$k_{2'}$ / $M^{-1}\ s^{-1}$ X 10^{-1}	$\Delta H'^{\neq}$ / kJ mol^{-1}	$\Delta S'^{\neq}$ / $JK^{-1}mol^{1}$
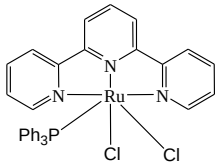	**C1**	TU	108.2 ± 0.2	62 ± 1	-24 ± 3
		DMTU	22.8 ± 0.04	78 ± 2	26 ± 4
		TMTU	2.5 ± 0.001	118 ± 1.2	140 ± 3.5
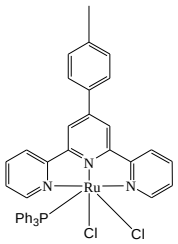	**C2**	TU	166.4 ± 0.01	36 ± 3	-99 ± 7
		DMTU	64.0 ± 0.01	74 ± 2.5	19 ± 7
		TMTU	6.5 ± 0.001	106 ± 3	108 ± 9
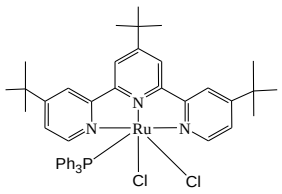	**C3**	TU	194.7 ± 0.4	34 ± 1.5	-102 ± 5
		DMTU	171.2 ± 0.2	49 ± 0.3	-58 ± 1
		TMTU	22.4 ± 0.001	98 ± 0.2	89 ± 0.5
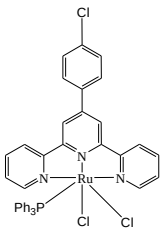	**C4**	TU	142.5 ± 0.04	47 ± 2	-59 ± 7
		DMTU	32.2 ± 0.001	76 ± 0.5	24 ± 1.2
		TMTU	2.7 ± 0.003	112 ± 2	121 ± 5
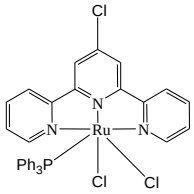	**C5**	TU	124.0 ± 0.03	50 ± 3	-56 ± 7
		DMTU	28.3 ± 0.001	77 ± 2	25 ± 5
		TMTU	2.5 ± 0.001	114 ± 0.3	130 ± 1
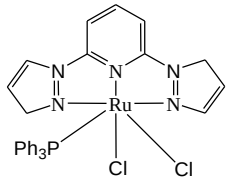	**C6**	TU	0.03 ± 0.0002	92 ± 2	-10 ± 6
		DMTU	0.001 ± 0.0001	110 ± 3	28 ± 8
		TMTU	0.0004 ± 0.0001	129 ± 2	146 ± 5

7.4 Discussion

The stepwise substitutions of the chloride ligands follow the order: **C3** > **C2** > **C4** > **C5** > **C1** > **C6.** The differences in the rate of substitution from all the complexes investigated is due to differences substituents on the tpy have as reported for square planar Pt(II) complexes.[38] In analysing the results, a clear understanding of the role substituent(s) on the tpy ligand has is very important because it changes the electronic properties of the ligand thereby influencing the reactivity of the Ru(II) metal centre. Both π-back-bonding and σ-*trans*-effect have been found to control reactivity of (tpy) Pt(II) complexes depending on the nature of the substituent(s) attached on the tpy.[38] [39] [40] [41]. The σ-*trans*-effect and π-back-bonding both lead to higher rate of substitution in octahedral transition metal complexes.[42]

The introduction of the electron donating[43] methylphenyl ligand at the 4'-position of the tpy ligand in **C1** to form **C2** and addition of the strongly electron donating[38] [44] tert-butyl substituents at the 4'-*trans* and *cis* positions of **C1** to form **C3** results in increased rate of substitution. The increase in the rate of substitution with the addition of electron donating substituents follows the order: **C1** < **C2** < **C3**. The oxidation potentials of these comlexes increased as follows: 0.98 V **(C3**) < 1.01 V (**C2**) < 1.02 V (**C1**).[45] The oxidation potentials inversely correlate to their the electron donating ability of the substituents on the ligands implying that there is highest donation of electrons towards the Ru(II) metal centre in **C3**.[45] [46] [47]

The trend in the rate of substitution increases in the same way as the electron donor strength indicating that the reactivity is driven by *trans*-effect where electron density donated to the Ru(II) metal centre repels the electrons in the chloride ligand stretching and thus weakening the Ru-Cl bond resulting in increased reactivity. The strength of the *trans*-effect increases from **C1**-**C3** in line with the trend in the reactivity. Evidence in supported of electron donation going from **C1** to **C3** is indicated by decrease in DFT calculated NBO charges in the order: 0.171 **(C1)** > 0.164 **(C2)** > 0.151 **(C3)** confriming that **C3** is the least electrophilic. Further evidence of electron donation in these complexes is seen in the raising of the HOMO energy as donor effect increases (-5.488 **(C1**) < -5.471 **(C2**) < -5.360 **(C3**). It has been reported in literature that strong electron donors raise the HOMO energy.[48] [49] [50] The very high *trans*-effect in **C3** results in unusually high reactivity compared to **C1** and **C2** which is due to donation of electrons from both *cis* and *trans* positions. The trans-effect phenomenon has been observed in a number of studies.[42] [51] [52] [53] [54]

The addition of chlorophenyl and chloro ligands at the 4'-position of the tpy ligand in **C1** forms **C4** and **C5** respectively resulting in increase in reactivity as follows: **C1** < **C5** < **C4.** A chloro substituent withdraws electron density by π resonance[55] and this enhances the π-back-donation of electron density from the Ru(II) orbitals into the π anti-bonding molecular orbitals of the tpy ligand. There is increase in the positive charge on the Ru(II) metal centre that makes it more reactive to the incoming nucleophiles. This observation is supported by the increase in DFT calculated NBO charges on addition of the electron withdrawing substituents as follows: 0.171 **(C1**) < 0.173 **(C5**) < 0.176 (**C4**). This is an indication that **C4** and **C5** have enhanced π-back-bonding which makes it easier for electron shift from the filled metal Ru *d* orbitals into the empty ligand *π**-orbitals hence higher reactivity. The fact that **C4** is more reactive than **C5** indicates that the chlorophenyl substituent is a stronger electron acceptor than the chloro ligand in line with what has been observed in literature.[56] [57]

Notably, **C2** and **C4** only differ in the substituent on the phenyl at the 4'-position of the tpy. **C2** has an overall electron donating substituent (methyl substituent) while **C4** has electron accepting substituent (chloro substituent). This is clearly supported by their respective DFT calculated quantities as already discussed. The higher reactivity of **C2** compared to **C4** shows that *trans*-effect due to the methyl substituent in **C2** in this study has a greater substitution effect than the π-back-bonding due to the chloro group in **C4**. The relative higher influence of trans-effect compared to the π-back-bonding effect has been observed in other studies. [58] [59] [60] [61]

The replacement of the *cis* positioned pyridyl ligands in **C1** with pyrazolyl ligands to form **C6** resulted in a sharp decrease in the reactivity. The replacement of pyridyl ligands lowers the π-back-bonding ability of the overall ligand system leading to a less electropositive metal centre and hence lower reactivity. As shown in literature, pyrazole ligands are effective donors in transition metals.[62] Further, pyrazole has a lower basicity (pK_a = 2.47) compared to that of pyridine (pK_a = 5.23)[63] [64] [65] which causes it to bind metals more weakly than pyridine. The donor effect of the pyrazolyl ligands is supported by the lower DFT calculated NBO charge for **C6 (**0.133) compared to **C1 (**0.171) confirming that **C1** is more electropositive. This is further corroborated by the higher electrophilicity index of **C1**, 5.275 compared to **C6**, 4.422. In addition the HOMO-LUMO energy gap and chemical hardness values for **C1** are smaller than those of **C6** in support of the higher rate of substitution from **C1**. Further, the LUMO of **C6** (-2.180) is raised compared to that of **C1** (-2.479), making it

difficult for π-back-donation. On the other hand the higher π-back-bonding capabilities of the conjugated pyridine rings in **C1** readily accept electron density from the Ru(II) metal centre compared to the pyrazole rings that are π-electron rich due to an extra pyrollic-N within the chelate ring and hence better π-donors.[66] [67] [68] [69] [70]

The rate constants, k_2', for the substitution of the second chloride for all the complexes are lower than those of the first step, k_2, due to decrease in the electrophilicity of the metal centre upon coordination of the first thiourea nucleophile in complexes where π-back-bonding is dominant.[71] [72] [73] The reduction of the electrophilicity of Ru(II) results from the donation of electrons by the incoming electron rich thiourea nucleophile to the electron deficient metal centre lowering its charge. Further, the coordinated nucleophile introduces steric hindrance at the Ru(II) metal centre hindering the approach of the second incoming nucleophile.

The first substitution occurs at the chloride which is within the plane of the tpy ligand framework, Cl23, followed by Cl25 which is perpendicular to the ligand plane. The chloro ligand, Cl23, being within the plane of the ligand is most influenced by the electronic changes of the tpy ligand. This is supported by the DFT calculated bond distances between the metal centres and the chloro ligands showing that Ru-Cl23 bonds are slightly longer than Ru-Cl25 by about 0.03Å, hence easier to break. In addition, since Cl25 is *trans* to a different type of ligand (triphenylphosphine) which is a donor,[74] [75] the rate substitution of the chloro ligand varies for a given Ru(II) complex.

Based on the large negative values of entropies and positive enthalpies of activation for all nucleophiles in step one and thiourea nucleophile only in step two it can be concluded that the reaction proceed via associative reaction pathway in which a seven coordinate intermediate pathway is formed. Ru(II) associative mode of reactivity has been observed in literature.[76] [77] However, the substitution of the second chloride by DMTU and TMTU was observed to have positive values of entropy which shows that these reactions proceeded via the dissociatively activated interchange pathway. This is most probably due to the steric bulkiness of the ligands that could not allow for the easy formation of the full seven coordinate intermediate transition state. The trend in reactivity of the nucleophiles was; TU > DMTU > TMTU. This can be accounted for in terms of the steric factors where reactivity decreases with increase in steric hindrance of the nucleophile.

7.5 Conclusions

The rate of substitutions in the current study are electronically driven either through *trans*-effect or π-back-donation effects. The groupings **C2**, **C3** and **C4**, **C5** are more reactive than **C1** because of enhanced *trans*-effect and π-back-donation respectively. The reactivity of **C4** is higher than **C5** due to the presence of a chlorophenyl substituent on the tpy ligand in **C4** that is a stronger π-acceptor than the chloro ligand in **C5**. It has been shown that the *trans*-effect in **C2** influences the reactivity more strongly than the π-back-donation in **C4**. The *cis* electron donation by 2,6-bis(pyrazolyl)pyridine ligand in **C6** retards significantly the reactivity of the Ru(II) metal centre compared to **C1** hence it can be used to tune the reactivity of Ru(II) complexes. It has generally been observed that the reactivity of Ru(II) complexes is more strongly affected by the electron donating ligands (*trans*-effect) than ligands that enhance π-back-donation. The *tert*-butyl substituents in **C3** are very strong donor ligands whose donation from both the *cis* and *trans* positions strongly accelerates the reactions. The trend in the DFT calculated data supports the observed reactivity of the complexes. The reactivity of the complexes in this study proceeds by the associative mechanism for all the nucleophiles in step one and in step two with the thiourea nucleophile only. The substitution reactions proceed via the dissociatively activated interchange mechanism for the rest of the nucleophiles in the second step.

7.6 References

[1] S. Sharma, S. K. Singh, D. S. Pandey, *Inorganic Chemistry* **2008**, *47*, 1179-1189.

[2] C. Metcalfe, S. Spey, H. Adams, J. A. Thomas, *Journal of the Chemical Society, Dalton Transactions* **2002**, 4732-4739.

[3] E. C. Constable, in *Advances in Inorganic Chemistry, Vol. 30*, Elsevier, **1986**, pp. 69-121.

[4] L.-X. Zhao, T. S. Kim, S.-H. Ahn, T.-H. Kim, E.-k. Kim, W.-J. Cho, H. Choi, C.-S. Lee, J.-A. Kim, T. C. Jeong, *Bioorganic & Medicinal Chemistry Letters* **2001**, *11*, 2659-2662.

[5] K. K. Patel, E. A. Plummer, M. Darwish, A. Rodger, M. J. Hannon, *Journal of Inorganic Biochemistry* **2002**, *91*, 220-229.

[6] C.-W. Jiang, H. Chao, H. Li, L.-N. Ji, *Journal of Inorganic Biochemistry* **2003**, *93*, 247-255.

[7] P. M. van Vliet, S. M. Toekimin, J. G. Haasnoot, J. Reedijk, O. Nováková, O. Vrána, V. Brabec, *Inorganica chimica acta* **1995**, *231*, 57-64.

[8] A. Jain, C. Slebodnick, B. S. Winkel, K. J. Brewer, *Journal of Inorganic Biochemistry* **2008**, *102*, 1854-1861.

[9] Y. Liu, R. Hammitt, D. A. Lutterman, R. P. Thummel, C. Turro, *Inorganic Chemistry* **2007**, *46*, 6011-6021.

[10] B. T. Farrer, H. H. Thorp, *Inorganic Chemistry* **2000**, *39*, 44-49.

[11] N. Grover, N. Gupta, P. Singh, H. H. Thorp, *Inorganic Chemistry* **1992**, *31*, 2014-2020.

[12] H.-Y. Ding, X.-S. Wang, L.-Q. Song, J.-R. Chen, J.-H. Yu, B.-W. Zhang, *Journal of Photochemistry and Photobiology A: Chemistry* **2006**, *177*, 286-294.

[13] S. Sharma, M. Chandra, D. S. Pandey, *European Journal of Inorganic Chemistry* **2004**, *2004*, 3555-3563.

[14] B. P. Sullivan, J. M. Calvert, T. J. Meyer, *Inorganic Chemistry* **1980**, *19*, 1404-1407.

[15] R. A. Gaussian, *Inc., Wallingford CT* **2009**, *121*, 150-166.

[16] P. J. Hay, W. R. Wadt, *The Journal of chemical physics* **1985**, *82*, 270-283.

[17] C. Lee, W. Yang, R. G. Parr, *Physical Review B* **1988**, *37*, 785.

[18] A. D. Becke, *The Journal of chemical physics* **1993**, *98*, 5648-5652.

[19] M. Okamura, M. Yoshida, R. Kuga, K. Sakai, M. Kondo, S. Masaoka, *Dalton Transactions* **2012**, *41*, 13081-13089.

[20] M. Cossi, N. Rega, G. Scalmani, V. Barone, *Journal of computational chemistry* **2003**, *24*, 669-681.

[21] T. Le Bahers, T. Pauporté, G. Scalmani, C. Adamo, I. Ciofini, *Physical Chemistry Chemical Physics* **2009**, *11*, 11276-11284.

[22] A. Shaira, D. Jaganyi, *Journal of Coordination Chemistry* **2014**, *67*, 2843-2857.

[23] P. K. Chattaraj, U. Sarkar, M. Elango, R. Parthasarathi, V. Subramanian, *arXiv preprint physics/0509089* **2005**.

[24] A. Cedillo, R. Contreras, *Journal of the Mexican Chemical Society* **2012**, *56*, 257-260.

[25] E. Seifert, American Chemical Society Publications, **2014**.

[26] R. G. Parr, W. Yang, Oxford University Press, New York, **1989**.

[27] P. Geerlings, F. De Proft, W. Langenaeker, *Chemical Reviews* **2003**, *103*, 1793-1874.

[28] R. G. Parr, W. Yang, *Journal of the American Chemical Society* **1984**, *106*, 4049-4050.

[29] W. Yang, W. J. Mortier, *Journal of the American Chemical Society* **1986**, *108*, 5708-5711.

[30] S. Sangilipandi, D. Sutradhar, K. Bhattacharjee, W. Kaminsky, S. R. Joshi, A. K. Chandra, K. M. Rao, *Inorganica Chimica Acta* **2016**, *441*, 95-108.

[31] S. B. Jensen, S. J. Rodger, M. D. Spicer, *Journal of Organometallic Chemistry* **1998**, *556*, 151-158.

[32] S. B. Billings, M. T. Mock, K. Wiacek, M. B. Turner, W. S. Kassel, K. J. Takeuchi, A. L. Rheingold, W. J. Boyko, C. A. Bessel, *Inorganica Chimica Acta* **2003**, *355*, 103-115.

[33] R. A. Leising, S. A. Kubow, M. R. Churchill, L. A. Buttrey, J. W. Ziller, K. J. Takeuchi, *Inorganic Chemistry* **1990**, *29*, 1306-1312.

[34] H. J. Lawson, T. S. Janik, M. R. Churchill, K. J. Takeuchi, *Inorganica Chimica Acta* **1990**, *174*, 197-204.

[35] M. R. Churchill, L. M. Krajkowski, L. F. Szczepura, K. J. Takeuchi, *Journal of Chemical Crystallography* **1996**, *26*, 853-859.

[36] M. R. Churchill, R. F. See, C. A. Bessel, K. J. Takeuchi, *Journal of Chemical Crystallography* **1996**, *26*, 543-551.

[37] T. Ben-Hadda, C. Mountassir, H. Le Bozec, *Polyhedron* **1995**, *14*, 953-955.

[38] D. Reddy, K. J. Akerman, M. P. Akerman, D. Jaganyi, *Transition Metal Chemistry* **2011**, *36*, 593-602.

[39] J. Deogratius, H. Andreas, v. E. Rudi, *Angewandte Chemie International Edition* **2001**, *40*, 1680-1683.

[40] A. Hofmann, D. Jaganyi, O. Q. Munro, G. Liehr, R. van Eldik, *Inorganic Chemistry* **2003**, *42*, 1688-1700.

[41] D. Jaganyi, D. Reddy, J. A. Gertenbach, A. Hofmann, R. van Eldik, *Dalton Transactions* **2004**, 299-304.

[42] B. J. Coe, S. J. Glenwright, *Coordination Chemistry Reviews* **2000**, *203*, 5-80.

[43] A. Jain, C. Slebodnick, B. S. J. Winkel, K. J. Brewer, *Journal of Inorganic Biochemistry* **2008**, *102*, 1854-1861.

[44] S. B. Billings, M. T. Mock, K. Wiacek, M. B. Turner, W. S. Kassel, K. J. Takeuchi, A. L. Rheingold, W. J. Boyko, C. A. Bessel, *Inorganica Chimica Acta* **2003**, *355*, 103-115.

[45] A. Jain, J. Wang, E. R. Mashack, B. S. J. Winkel, K. J. Brewer, *Inorganic Chemistry* **2009**, *48*, 9077-9084.

[46] T. B. Hadda, H. Le Bozec, *Polyhedron* **1988**, *7*, 575-577.

[47] T. Ben Hadda, H. Le Bozec, *Inorganica Chimica Acta* **1993**, *204*, 103-107.

[48] D. Reddy, D. Jaganyi, *Dalton transactions* **2008**, 6724-6731.

[49] M. Maestri, N. Armaroli, V. Balzani, E. C. Constable, A. M. W. C. Thompson, *Inorganic Chemistry* **1995**, *34*, 2759-2767.

[50] C. A. Mebi, *Journal of Chemical Sciences* **2011**, *123*, 727-731.

[51] K. M. Anderson, A. G. Orpen, *Chemical Communications* **2001**, 2682-2683.

[52] F. Guégan, V. Tognetti, L. Joubert, H. Chermette, D. Luneau, C. Morell, *Physical Chemistry Chemical Physics* **2016**, *18*, 982-990.

[53] M. Maestri, N. Armaroli, V. Balzani, E. C. Constable, A. M. C. Thompson, *Inorganic Chemistry* **1995**, *34*, 2759-2767.

[54] A. Rilak, I. Bratsos, E. Zangrando, J. Kljun, I. Turel, Ž. D. Bugarčić, E. Alessio, *Inorganic Chemistry* **2014**, *53*, 6113-6126.

[55] D. Reddy, D. Jaganyi, *Dalton Transactions* **2008**, 6724-6731.

[56] M. M. Milutinović, A. Rilak, I. Bratsos, O. Klisurić, M. Vraneš, N. Gligorijević, S. Radulović, Ž. D. Bugarčić, *Journal of Inorganic Biochemistry* **2017**, *169*, 1-12.

[57] M. M. Milutinović, S. K. C. Elmroth, G. Davidović, A. Rilak, O. R. Klisurić, I. Bratsos, Ž. D. Bugarčić, *Dalton Transactions* **2017**, *46*, 2360-2369.

[58] E. Shustorovich, M. Porai-Koshits, Y. A. Buslaev, *Coordination Chemistry Reviews* **1975**, *17*, 1-98.

[59] J. K. Burdett, T. A. Albright, *Inorganic Chemistry* **1979**, *18*, 2112-2120.

[60] P. D. Lyne, D. M. P. Mingos, *Journal of organometallic chemistry* **1994**, *478*, 141-151.

[61] P. D. Lyne, D. M. P. Mingos, *Journal of the Chemical Society, Dalton Transactions* **1995**, 1635-1643.

[62] D. L. Jameson, J. K. Blaho, K. T. Kruger, K. A. Goldsby, *Inorganic Chemistry* **1989**, *28*, 4312-4314.

[63] J. Catalan, J. Elguero, in *Advances in Heterocyclic Chemistry, Vol. 41* (Ed.: A. R. Katritzky), Academic Press, **1987**, pp. 187-274.

[64] C. Wijnberger, C. L. Habraken, *Journal of Heterocyclic Chemistry* **1969**, *6*, 545-551.

[65] D. L. Jameson, K. A. Goldsby, *The Journal of Organic Chemistry* **1990**, *55*, 4992-4994.

[66] J. M. Holland, J. A. McAllister, C. A. Kilner, M. Thornton-Pett, A. J. Bridgeman, M. A. Halcrow, *Journal of the Chemical Society, Dalton Transactions* **2002**, 548-554.

[67] T. Astley, A. J. Canty, M. A. Hitchman, G. L. Rowbottom, B. W. Skelton, A. H. White, *Journal of the Chemical Society, Dalton Transactions* **1991**, 1981-1990.

[68] T. Astley, J. M. Gulbis, M. A. Hitchman, E. R. T. Tiekink, *Journal of the Chemical Society, Dalton Transactions* **1993**, 509-515.

[69] M. A. Halcrow, *Coordination Chemistry Reviews* **2005**, *249*, 2880-2908.

[70] X. Zhang, N. Xing, F. Bai, L. Wan, H. Shan, Y. Hou, Y. Xing, Z. Shi, *Crystal Engeneering Communication* **2013**, *15*, 9135-9147.

[71] B. B. Khusi, A. Mambanda, D. Jaganyi, *Journal of Coordination Chemistry* **2016**, *69*, 2121-2135.

[72] W. M. Mthiyane, A. Mambanda, D. Jaganyi, *Transition Metal Chemistry* **2017**, *42*, 739-751.

[73] M. W. M., M. Allen, J. Deogratius, *International Journal of Chemical Kinetics* **2018**, *50*, 531-543.

[74] T. Karlen, P. Dani, D. M. Grove, P. Steenwinkel, G. van Koten, *Organometallics* **1996**, *15*, 5687-5694.

[75] C. A. Tolman, *Journal of the American Chemical Society* **1970**, *92*, 2953-2956.

[76] H. K. Mandal, P. K. Ghosh, A. Mahapatra, *Polyhedron* **2010**, *29*, 2867-2874.

[77] A. Rilak, R. Puchta, Ž. D. Bugarčić, *Polyhedron* **2015**, *91*, 73-83.

7.7 Supporting information

Included in the supplementary information are NMR spectra, mass spectra, tables, and various kinetic graphs for the synthetic and kinetic analysis of the complexes; **C1, C2, C3, C4, C5** and **C6** investigated in this study.

7.7.1 Synthesis

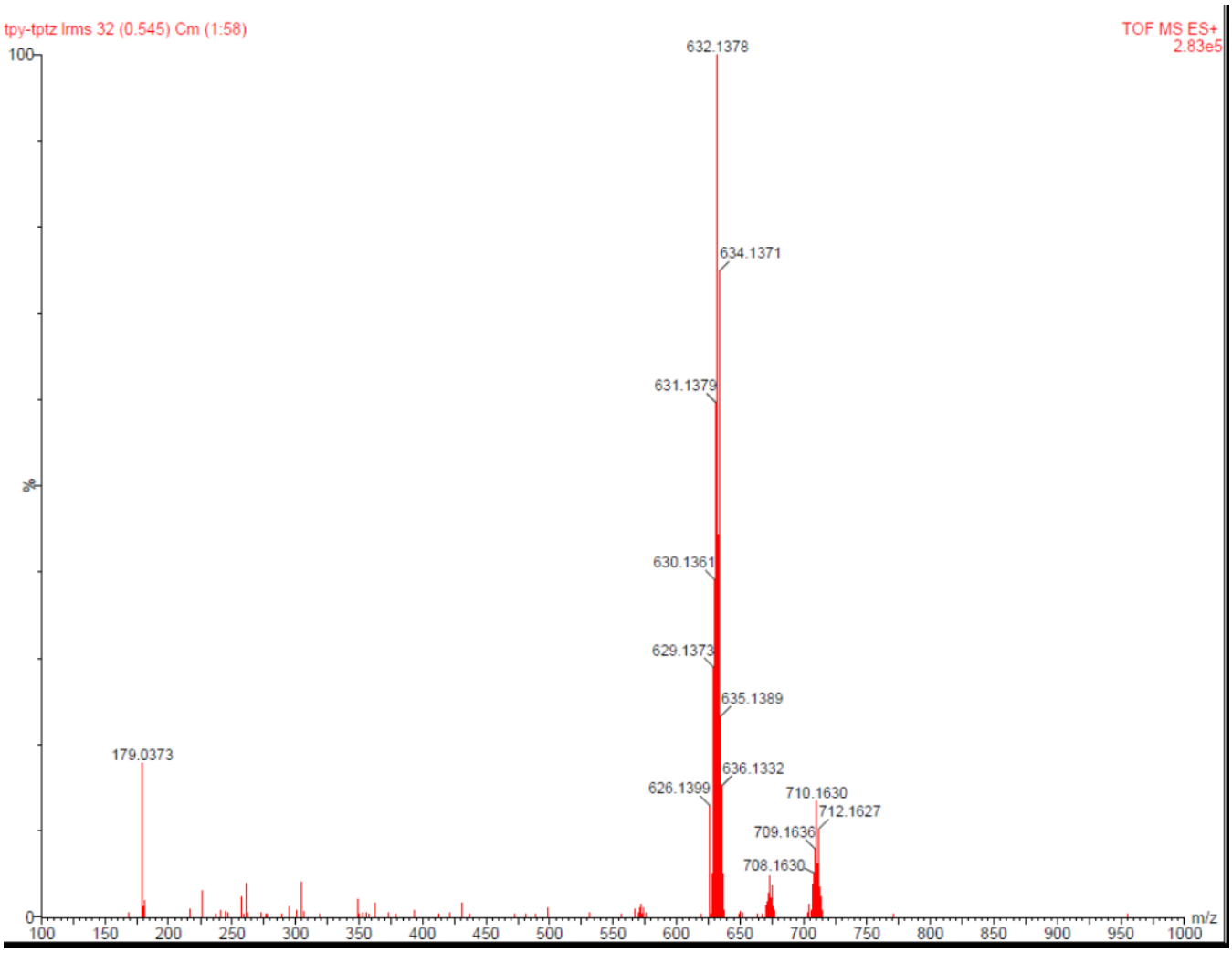

Figure SI 7.1 Low-Res Mass spectrum for **C1**

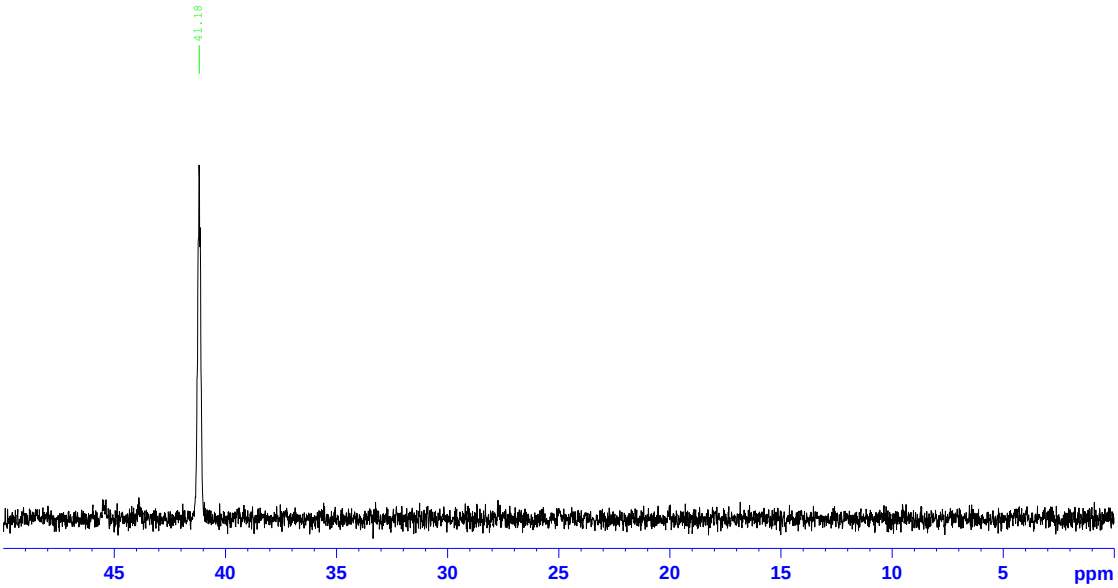

Figure SI 7.2 ^{31}P NMR spectrum for **C1**

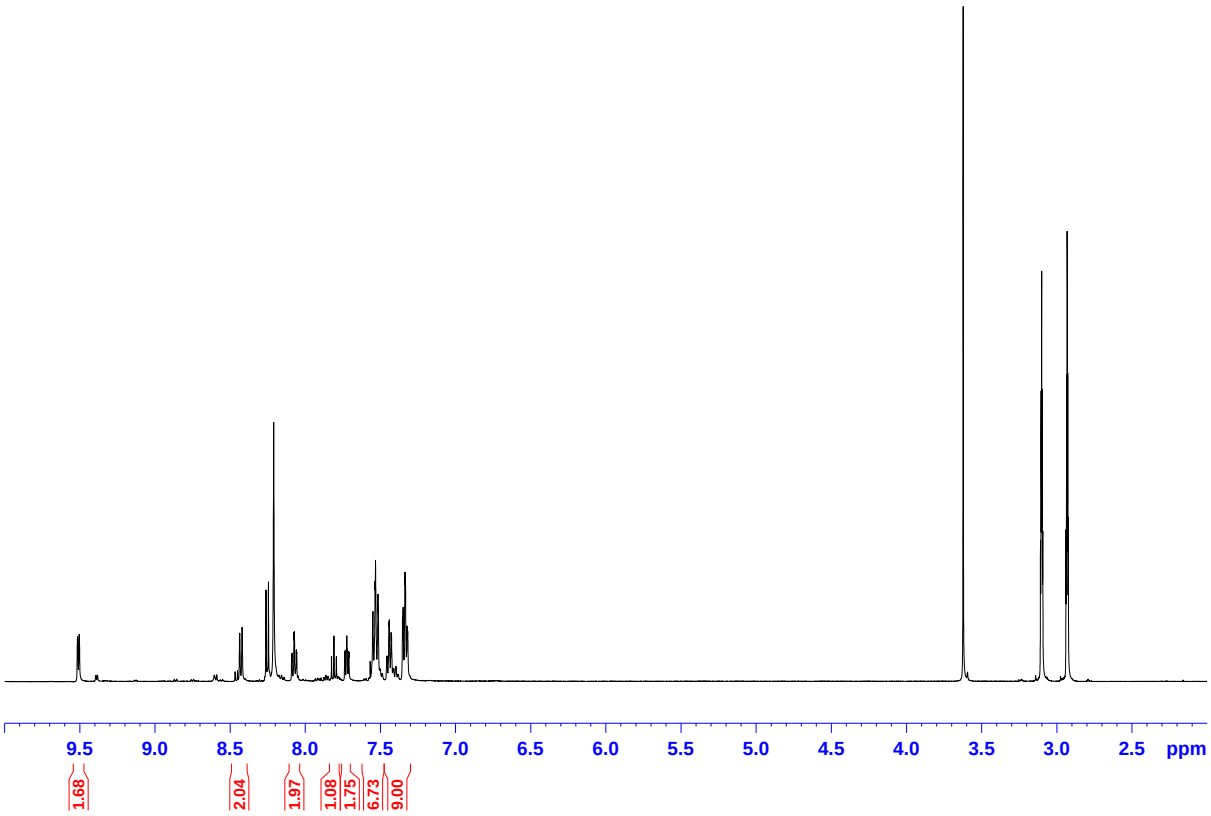

Figure SI 7.3 ^{1}H NMR spectra of **C1**

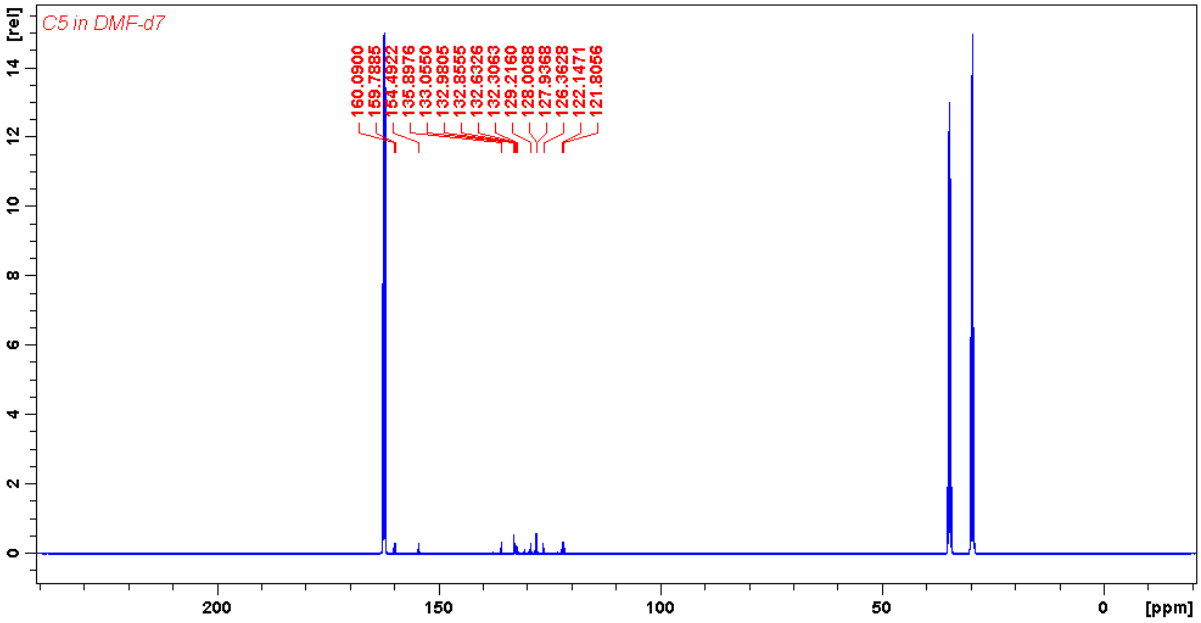

Figure SI 7.4 ^{13}C NMR spectrum for **C1**

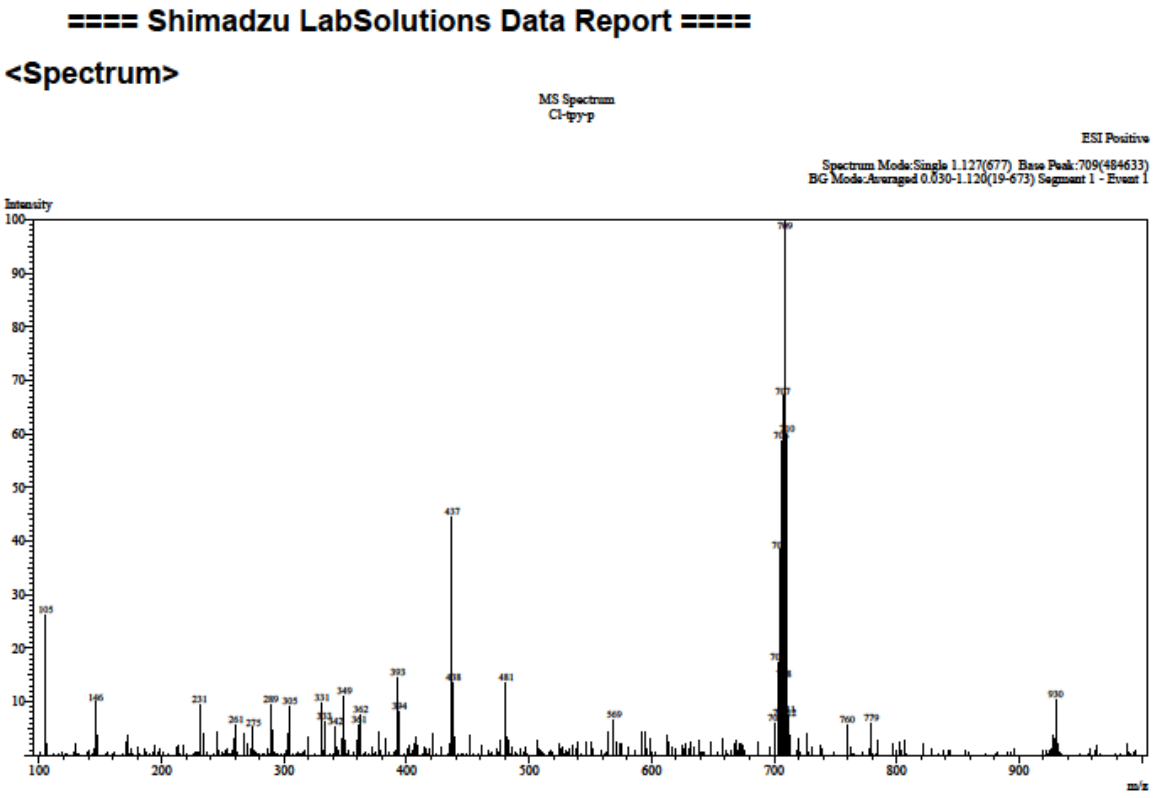

Figure SI 7.5 Low-Res Mass spectrum for **C5**

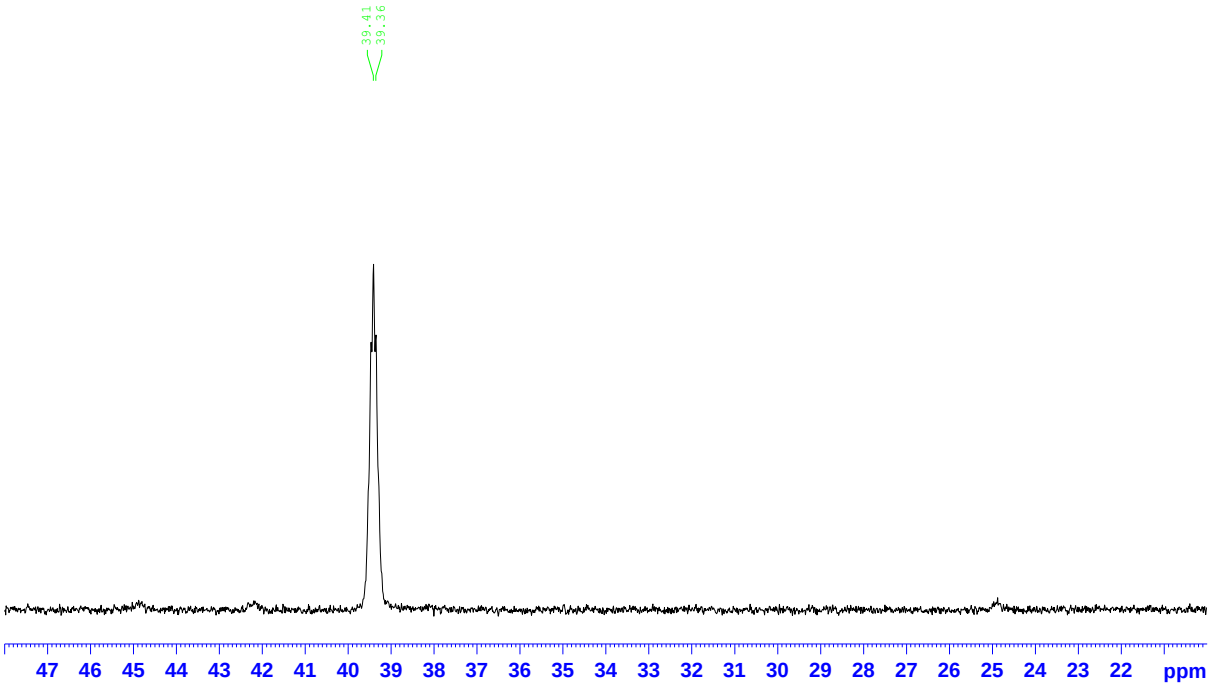

Figure SI 7.6 ^{31}P NMR spectrum for **C5**

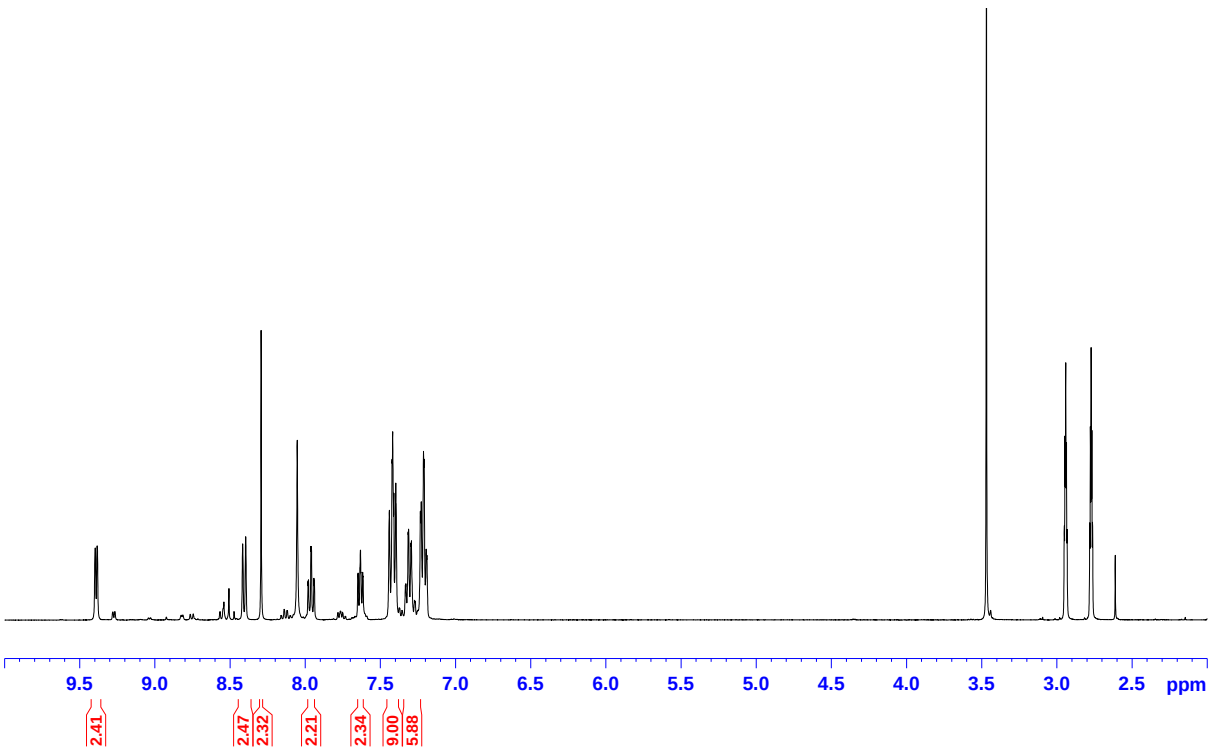

Figure SI 7.7 ^{1}H NMR spectra of **C5**

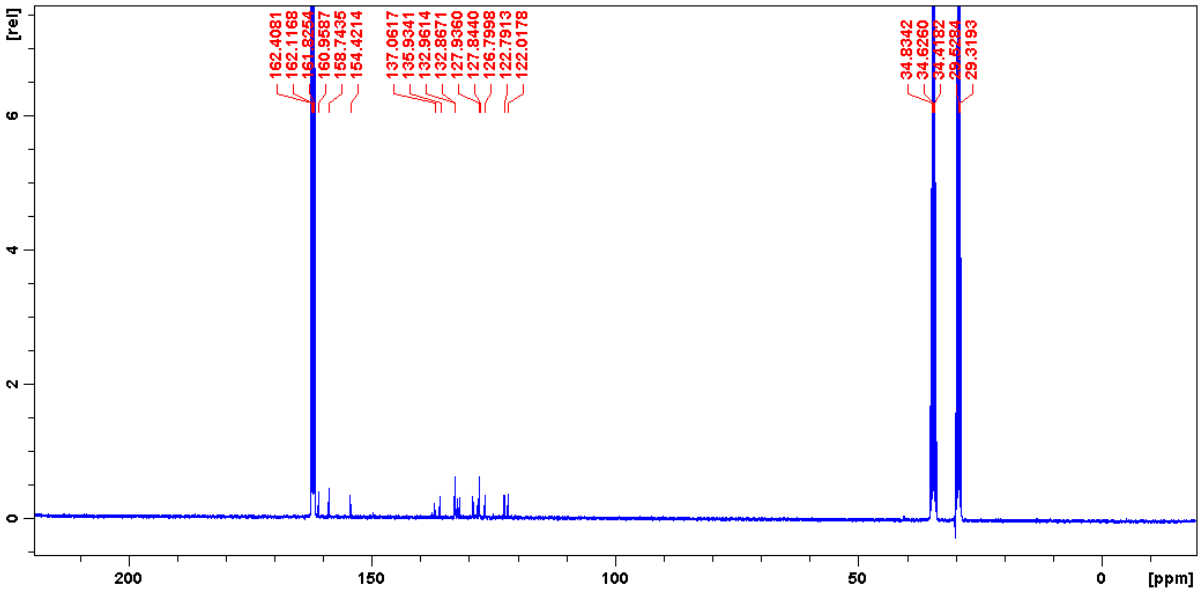

Figure SI 7.8 ^{13}C NMR spectrum for **C5**

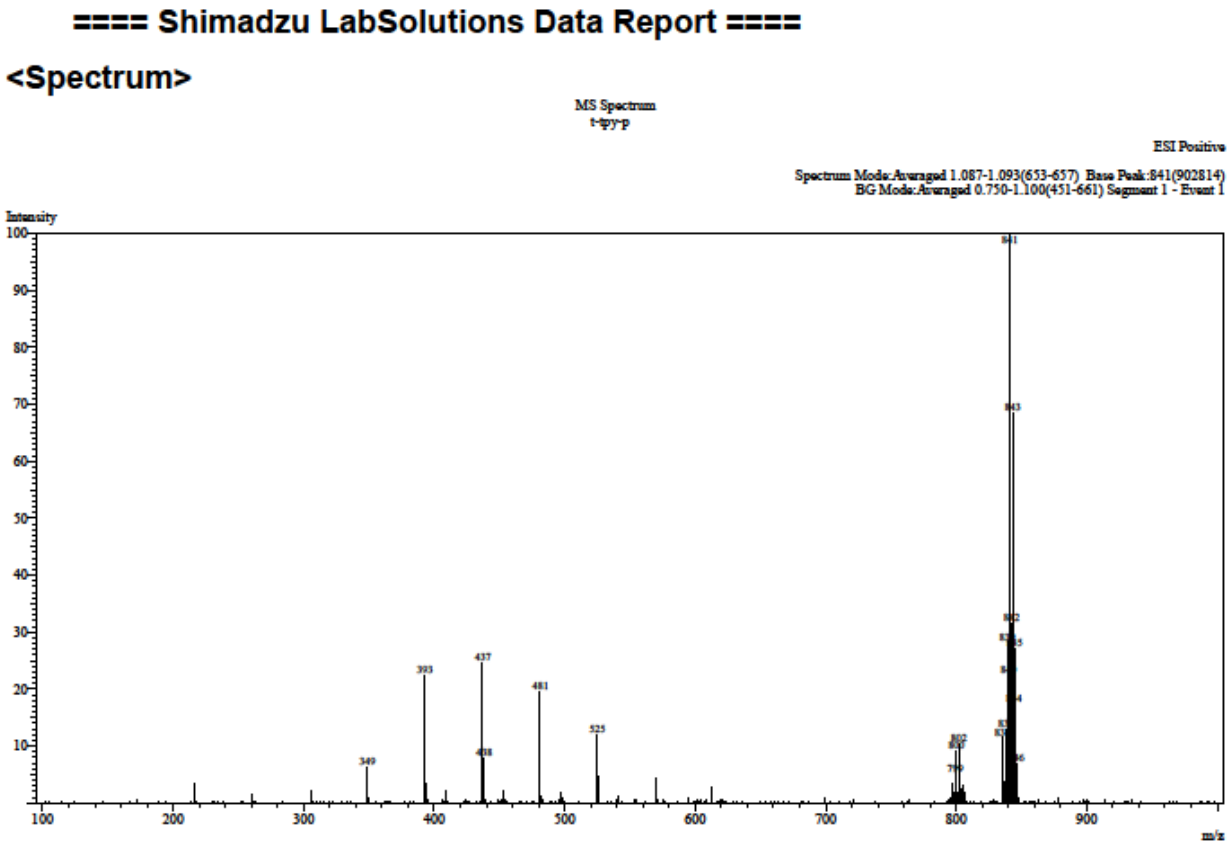

Figure SI 7.9 Low-Res Mass spectrum for **C3**

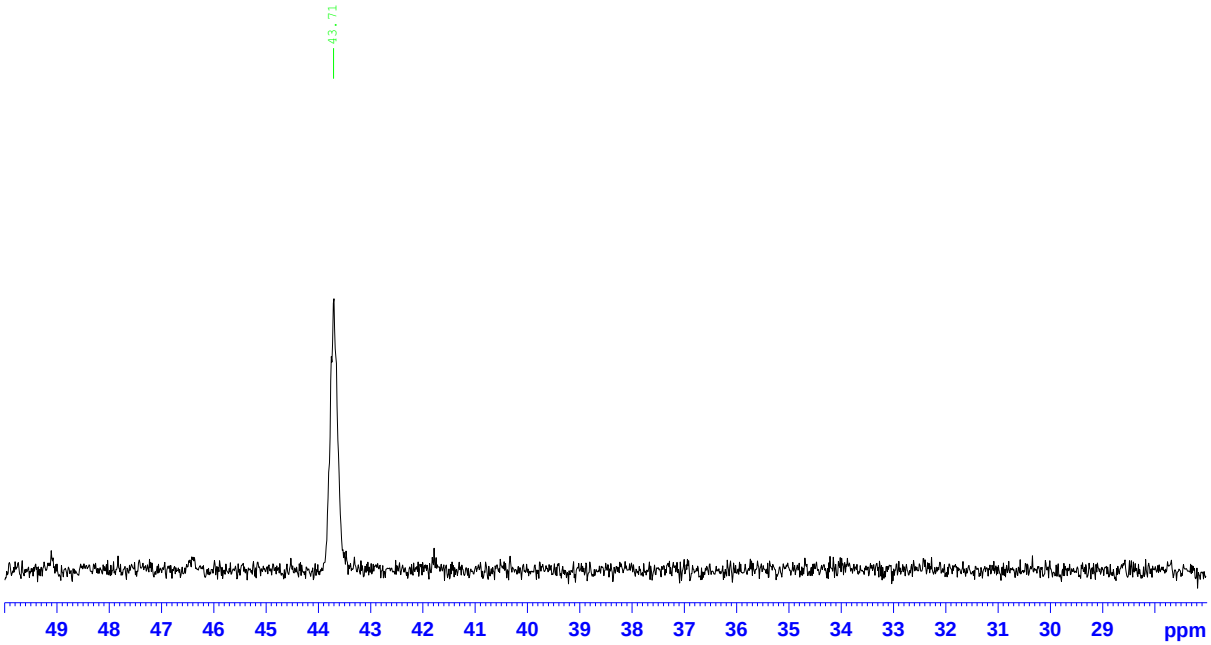

Figure SI 7.10 ^{31}P NMR spectrum for **C3**

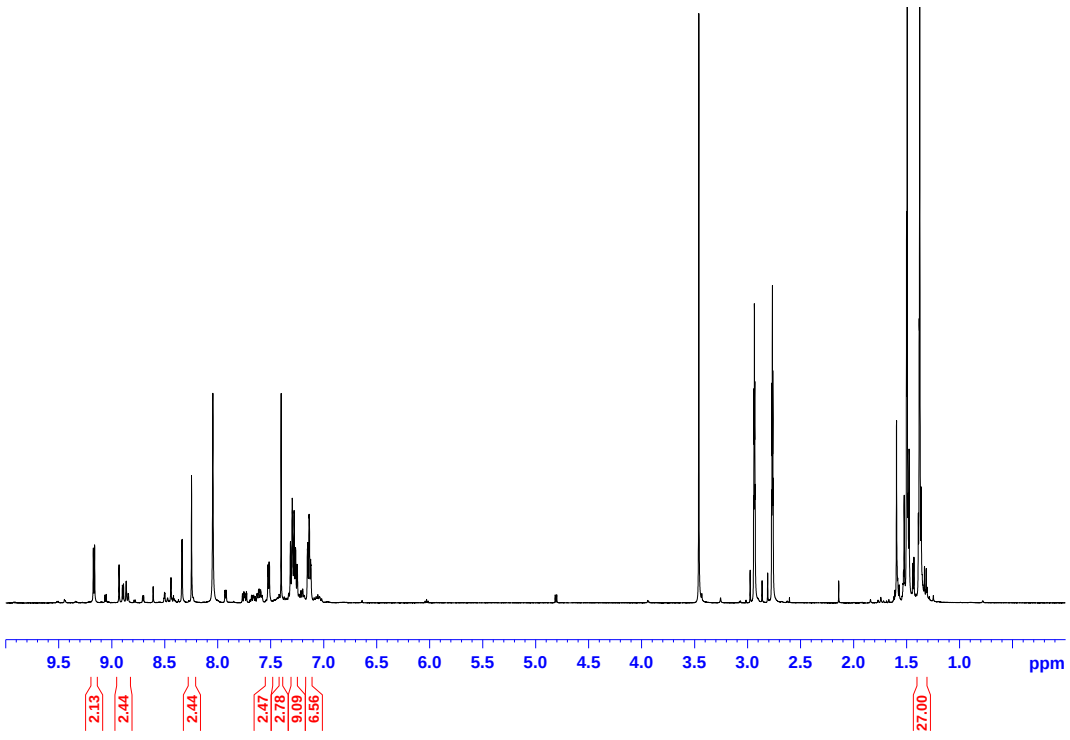

Figure SI 7.11 ^{1}H NMR spectra of **C3**

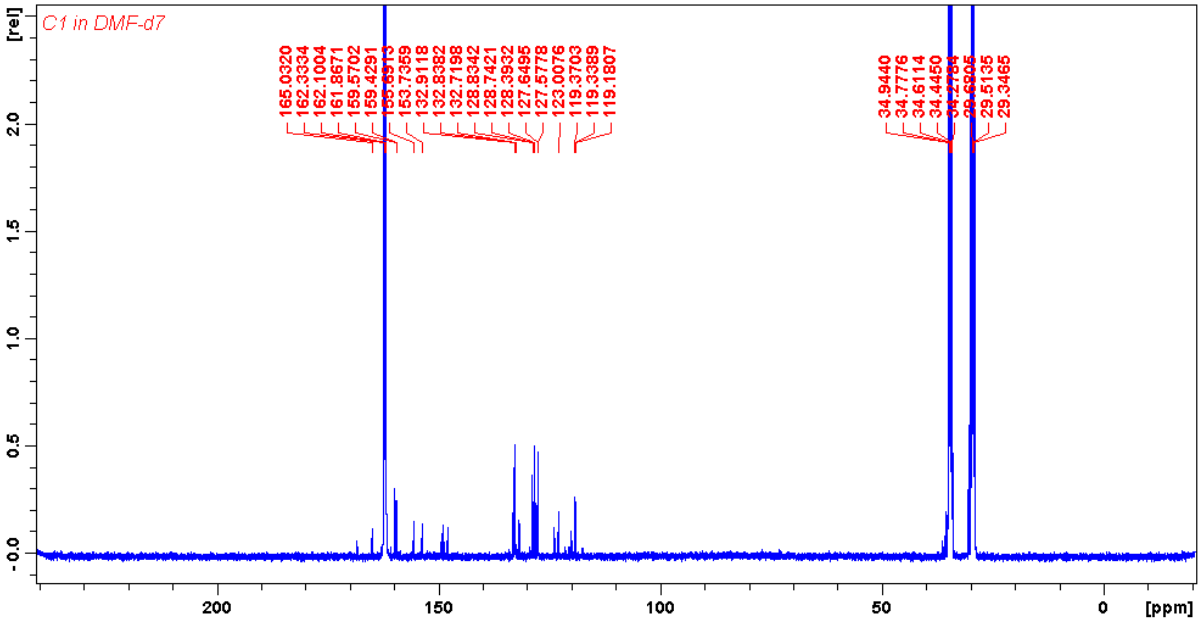

Figure SI 7.12 ^{13}C NMR spectrum for **C3**

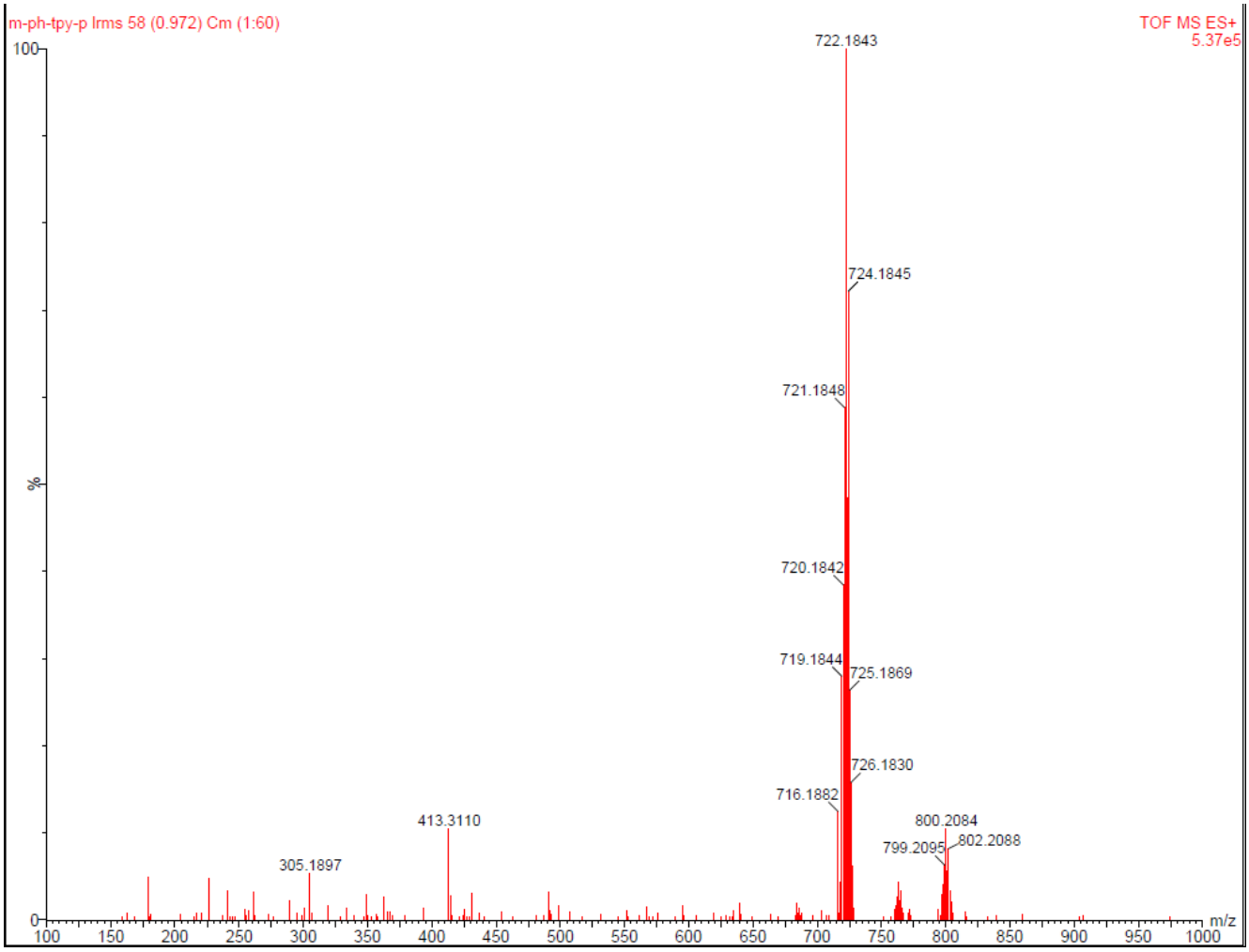

Figure SI 7.13 Low-Res Mass spectrum for **C2**

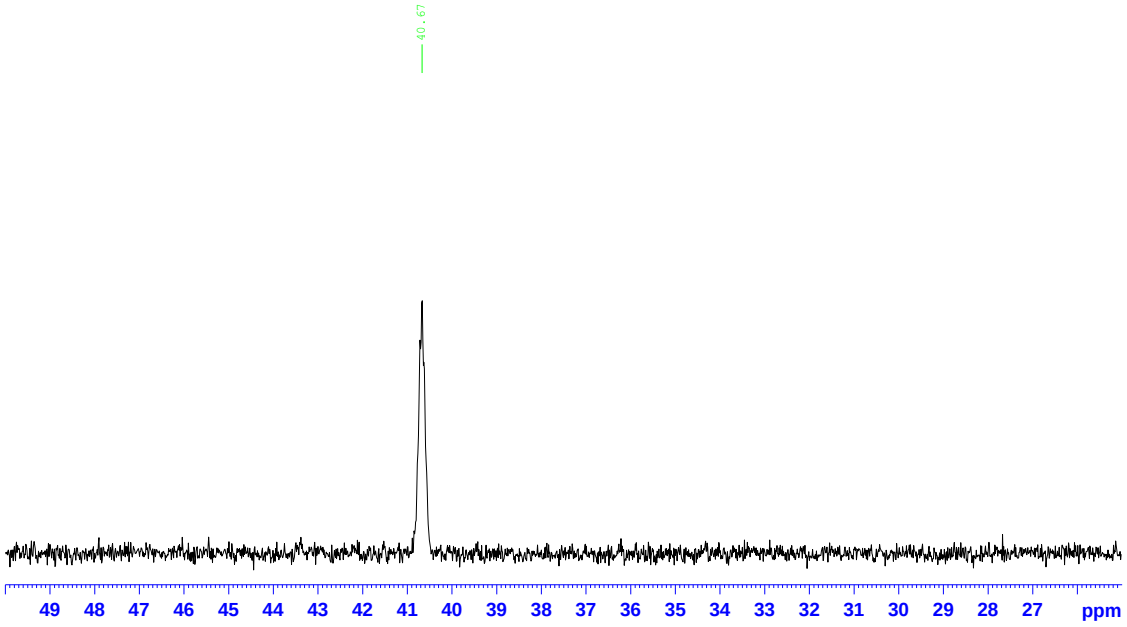

Figure SI 7.14 ^{31}P NMR spectrum for **C2**

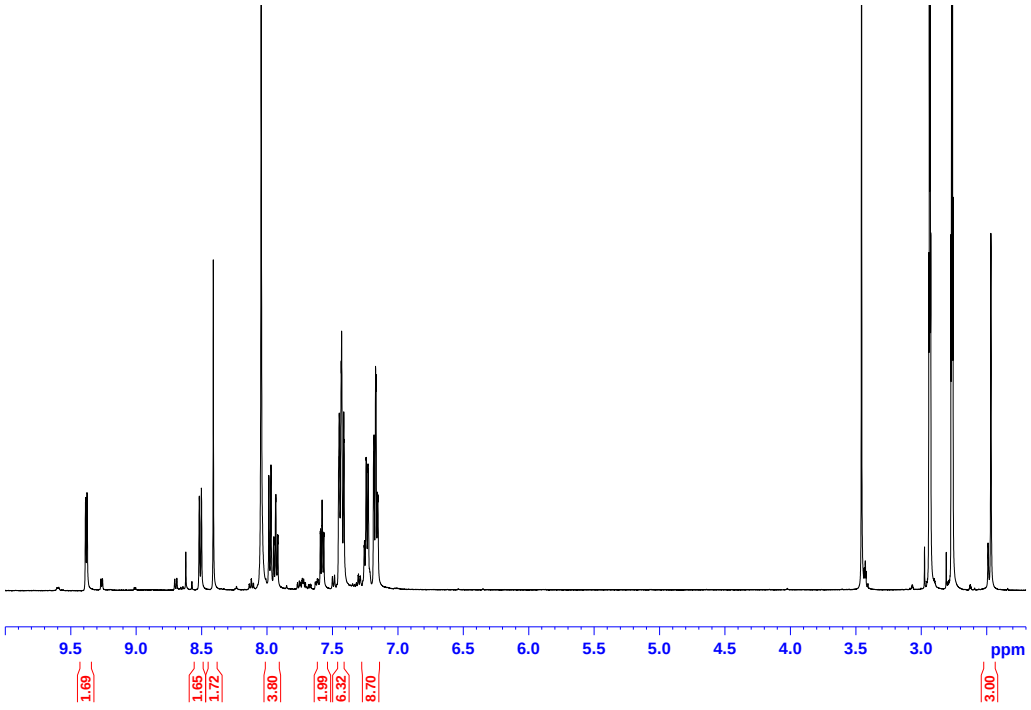

Figure SI 7.15 ^{1}H NMR spectra of **C2**

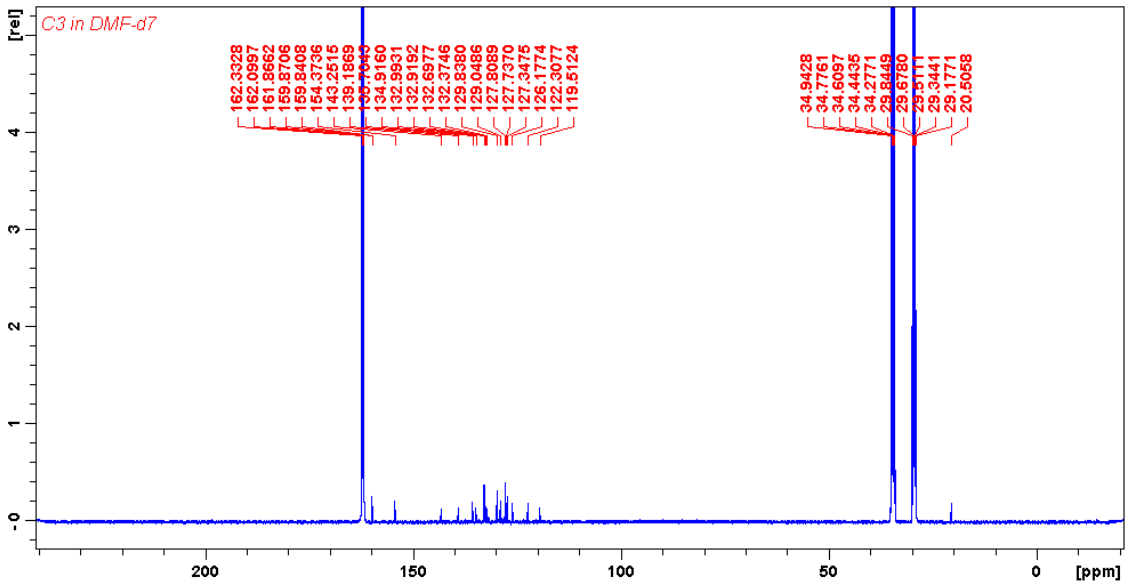

Figure SI 7.16 ^{13}C NMR spectrum for **C2**

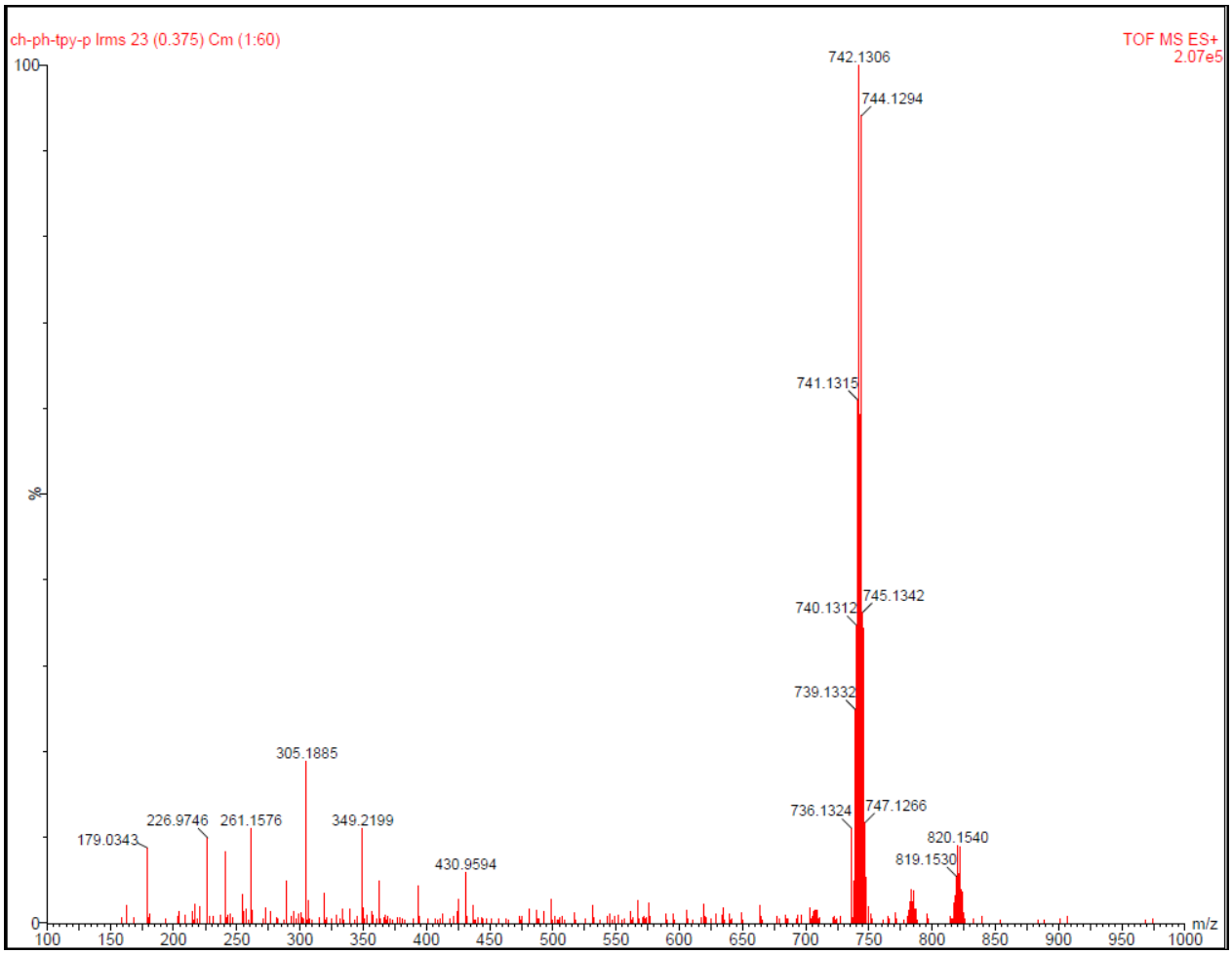

Figure SI 7.17 Low-Res Mass spectrum for **C4**

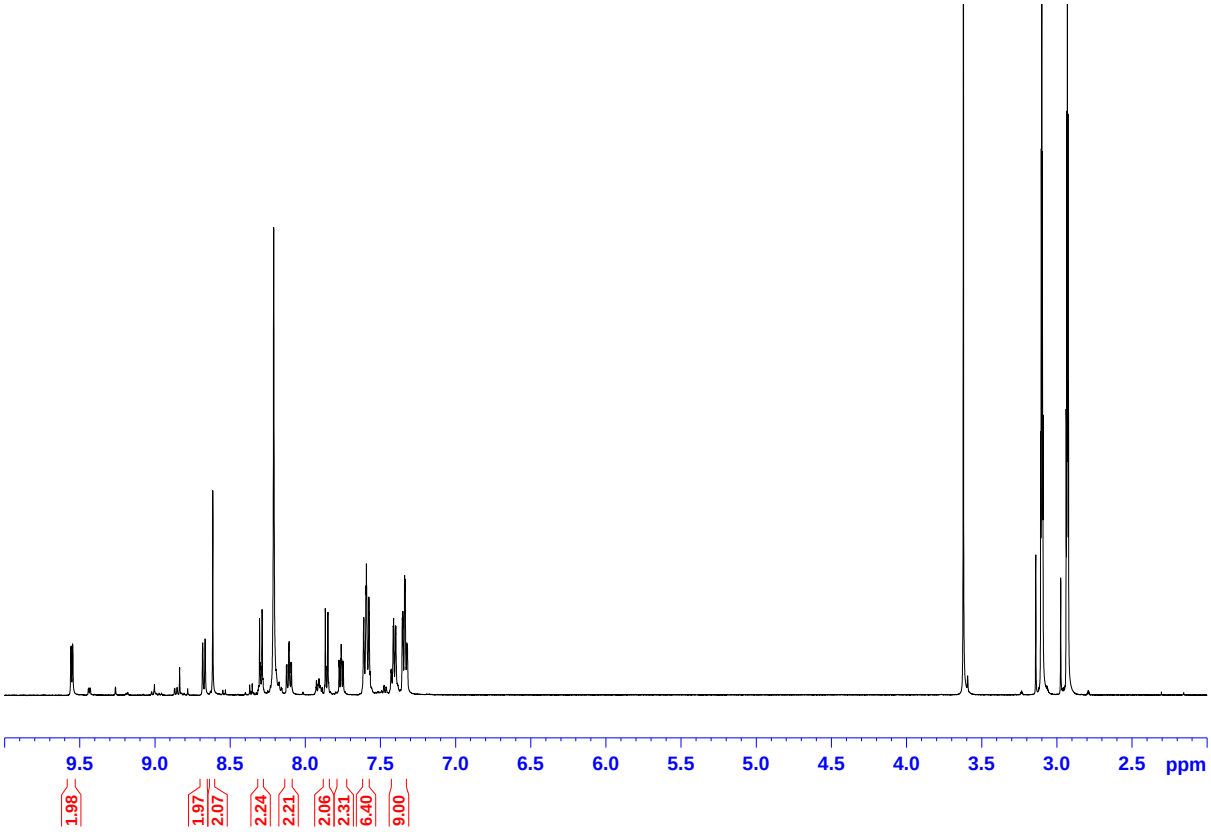

Figure SI 7.18 ^{1}H NMR spectra of **C4**

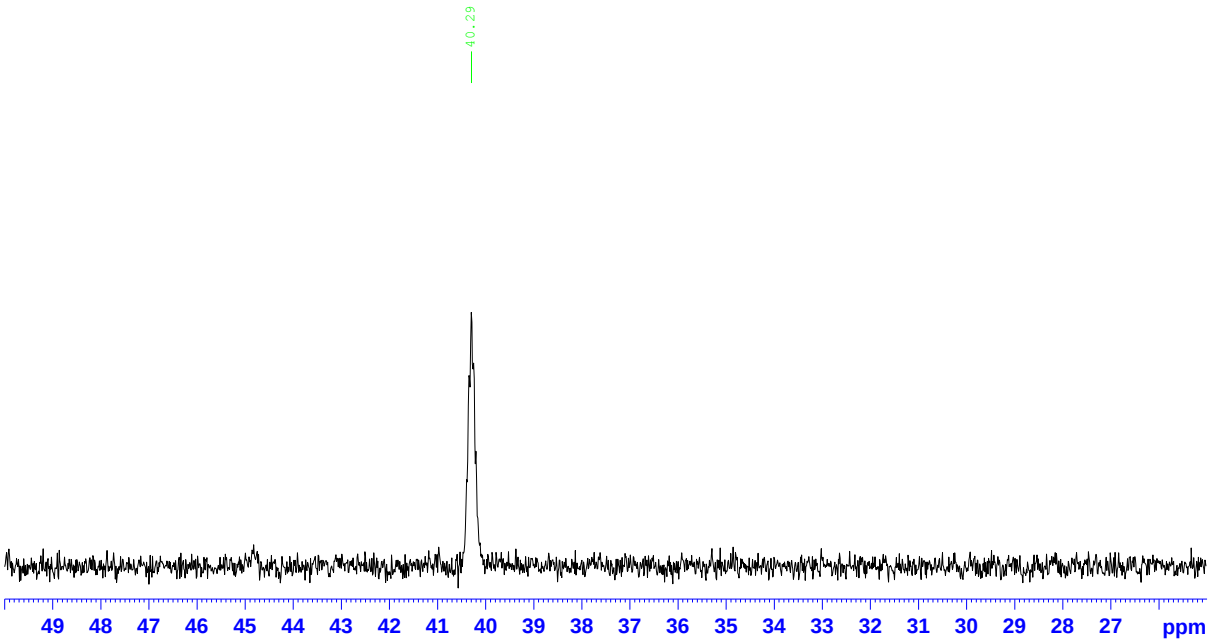

Figure SI 7.19 ^{31}P NMR spectrum for **C4**

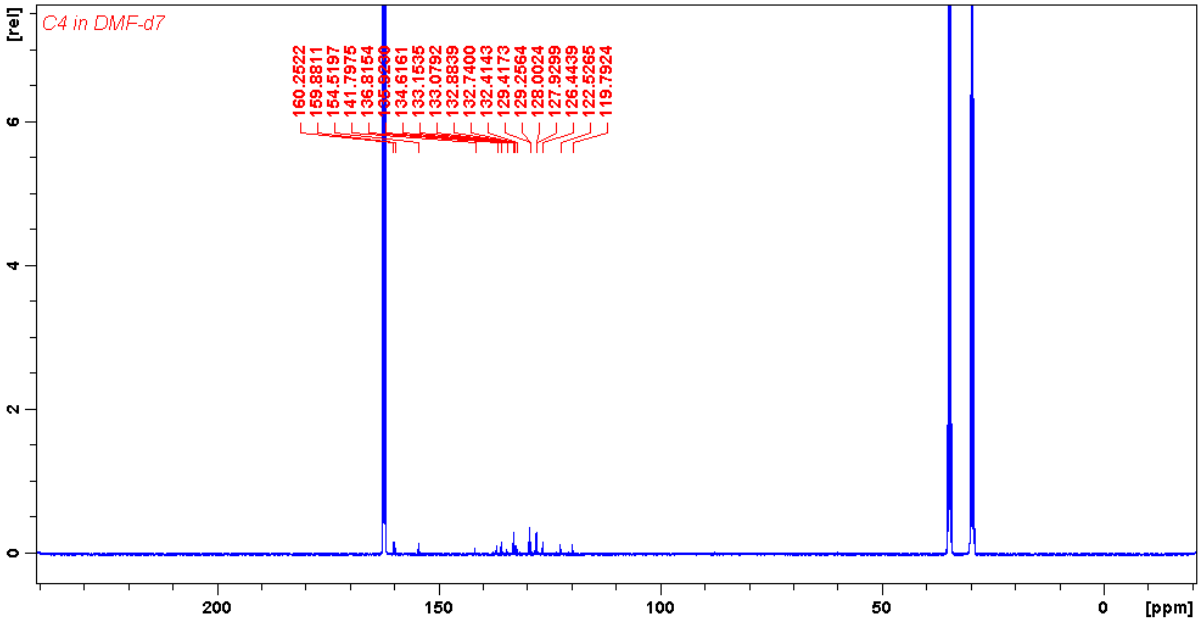

Figure SI 7.20 ^{13}C NMR spectrum for **C4**

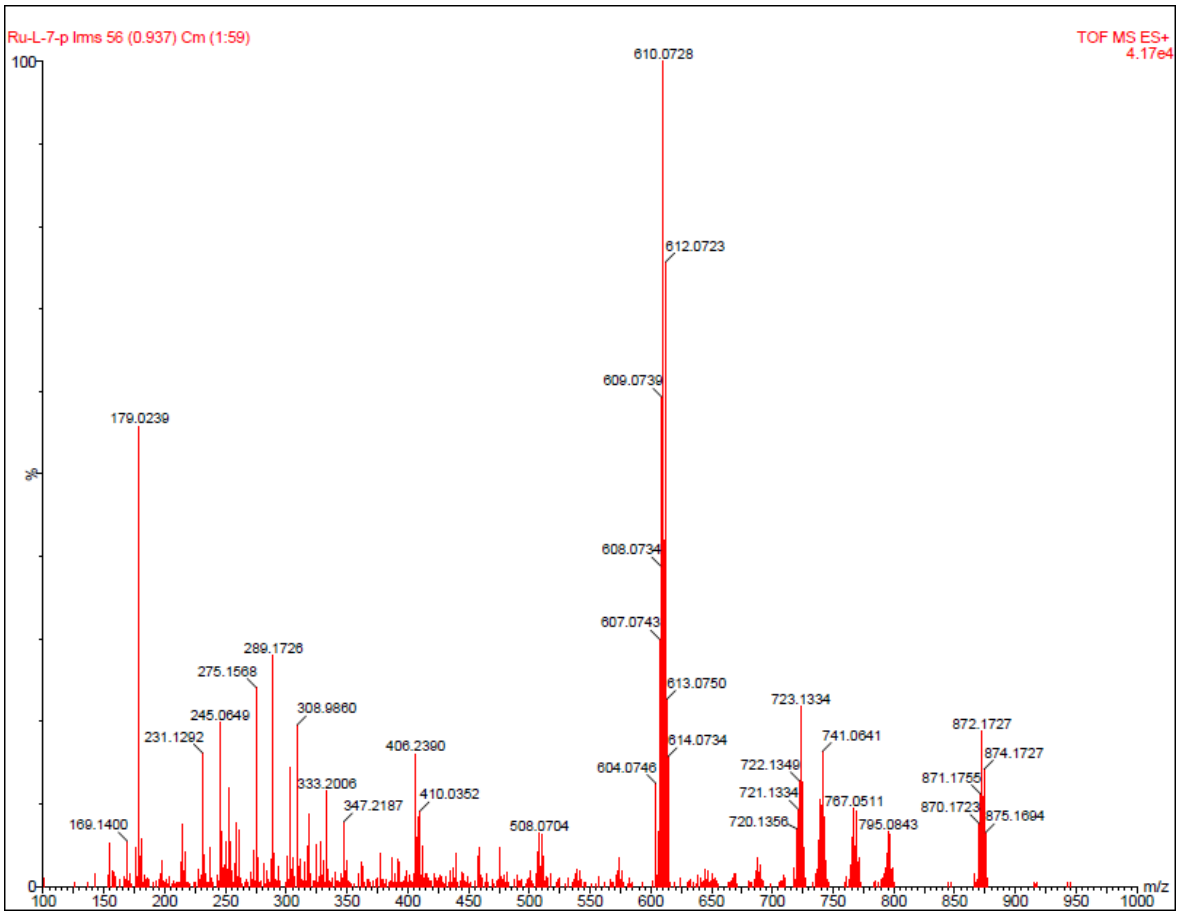

Figure SI 7.21 Low-Res Mass spectrum for **C6**

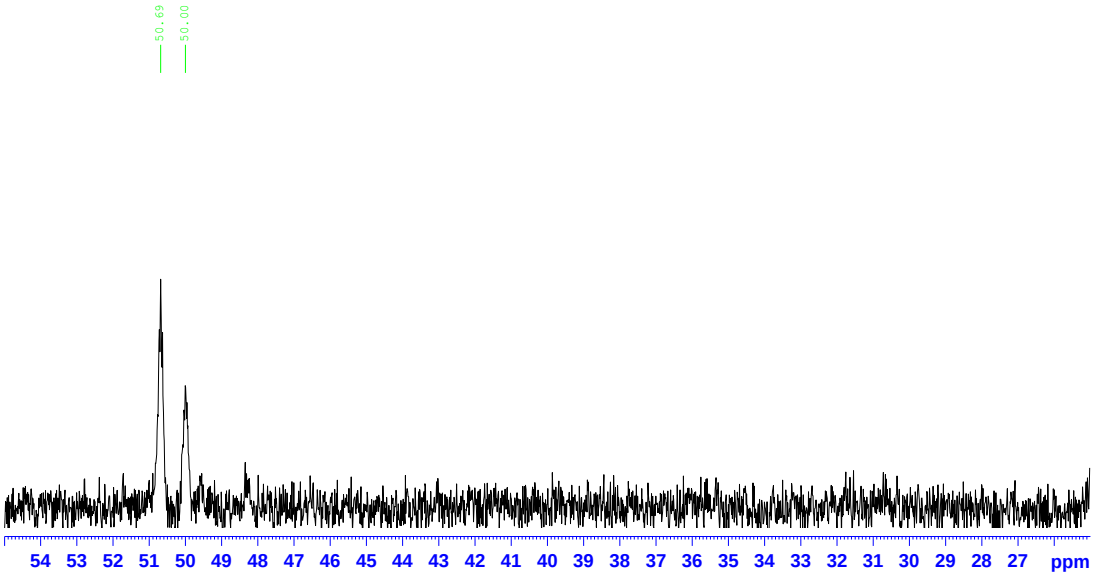

Figure SI 7.22 ^{31}P NMR spectrum for **C6**

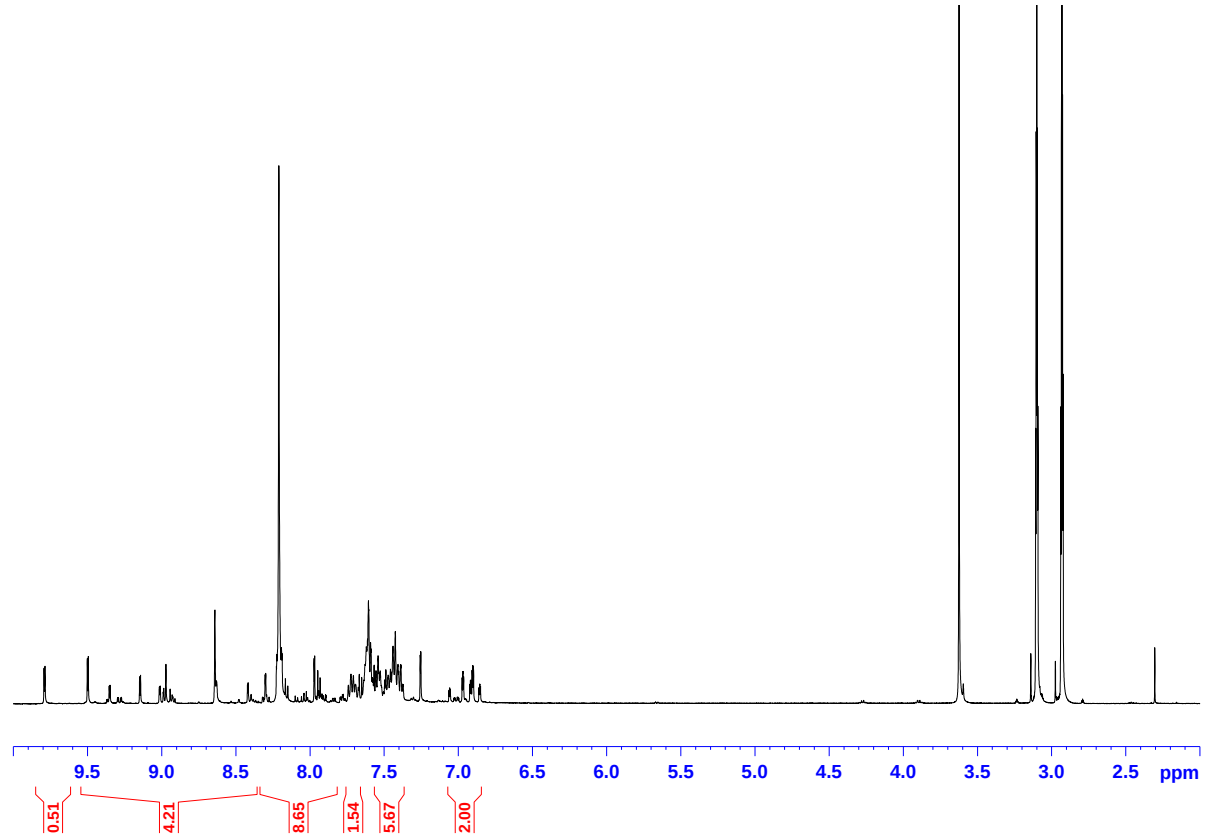

Figure SI 7.23 ^{1}H NMR spectra of **C6**

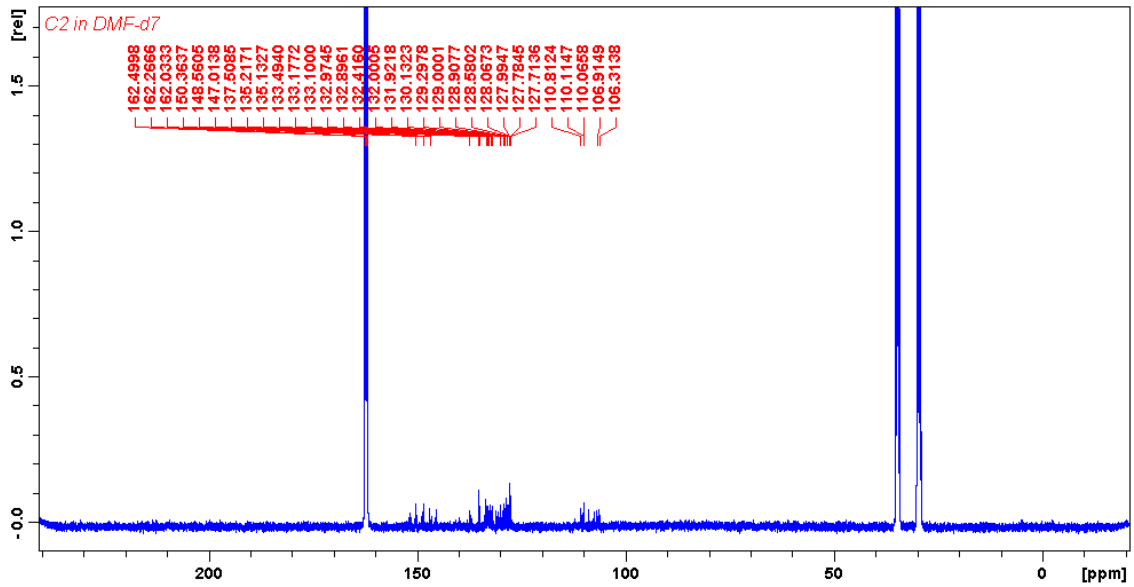

Figure SI 7.24 ^{13}C NMR spectrum for **C6**

7.7.2 Kinetic data

Dichloro(4'-(4-Chlorophenyl)-2,2′:6′,2″-terpyridine)(triphenylphosphino)ruthenium(II) (**C4**)

Table SI 7.1 Step 1 observed rate constants and the corresponding nucleophile concentrations for complex **C4**

[Nu]/M	k_{obs}/s^{-1} TU	[Nu]/M	k_{obs} / s^{-1} DMTU	[Nu]/M	k_{obs} / s^{-1} TMTU
0.01	0.279	0.02	0.445	0.028	0.354
0.02	0.535	0.04	0.908	0.056	0.709
0.03	0.789	0.06	1.363	0.084	1.082
0.04	1.045	0.08	1.831	0.112	1.448
0.05	1.287	0.10	2.297	0.140	1.794

Table SI 7.2 Step 2 observed rate constants and the corresponding nucleophile concentrations for complex **C4**

[Nu]/M	k_{obs}/ s^{-1} TU	k_{obs} / s^{-1} DMTU	k_{obs} / s^{-1} TMTU
0.000125	0.00178	4.03E-4	3.43E-5
2.5E-4	0.00356	8.06E-4	6.85E-5
3.75E-4	0.00534	0.00121	1.028E-4
0.5E-3	0.00712	0.00161	1.37E-4
0.000625	0.00892	0.00201	1.7E-4

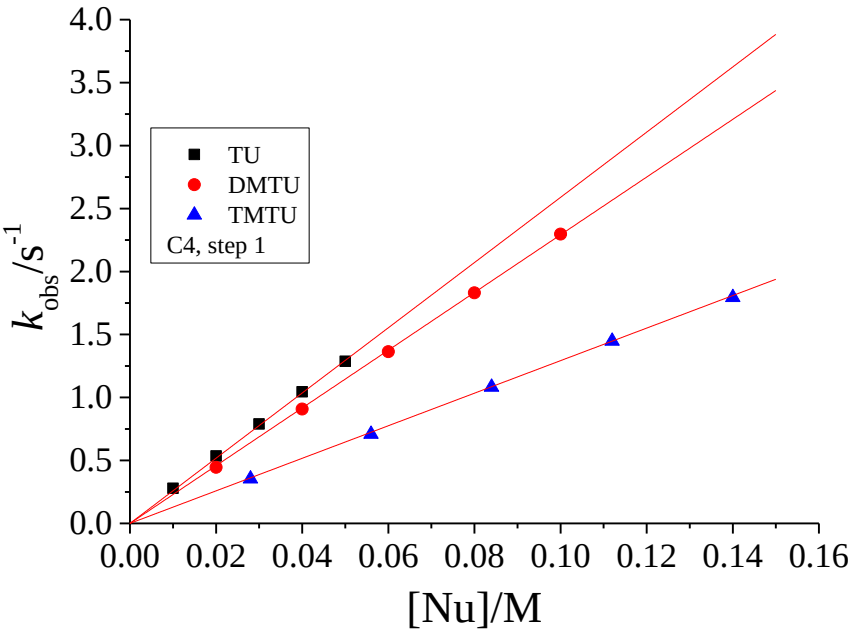

Figure SI 7.25 Step 1 concentration dependence plots for the reaction of **C4** with thiourea nucleophiles at 298 K

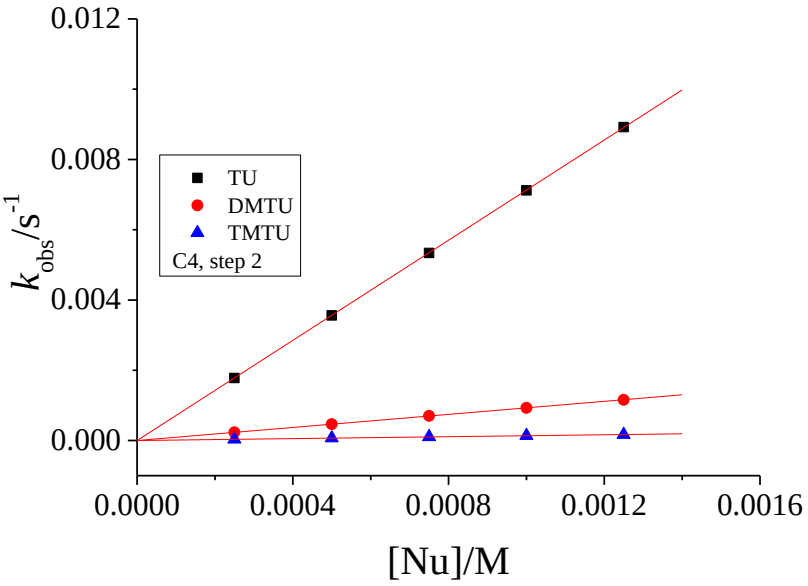

Figure SI 7.26 Step 2 concentration dependence plots for the reaction of **C4** with thiourea nucleophiles at 298 K

Table SI 7.3 Step 1 data of $\ln(k_2/T)$ and 1/T for complex **C4**

1/T	**$\ln(k_2/T)$ TU**	**$\ln(k_2/T)$ DMTU**	**$\ln(k_2/T)$ TMTU**
0.00336	-2.45	-2.58	-3.14
0.0033	-2.23	-2.32	-2.72
0.00325	-2.04	-2.09	-2.37
0.00319	-1.82	-1.83	-1.96
0.00314	-1.65	-1.61	-1.6

Table SI 7.4 Step 2 data of ln(k_2/T) and 1/T for complex **C4**

1/T	**ln(k_2/T) TU**	**ln(k_2/T) DMTU**	**ln(k_2/T) TMTU**
0.00336	-2	-4.21	-7.04
0.0033	-1.73	-3.66	-6.2
0.00325	-1.51	-3.2	-5.53
0.00319	-1.24	-2.65	-4.73
0.00314	-1.01	-2.19	-4.06

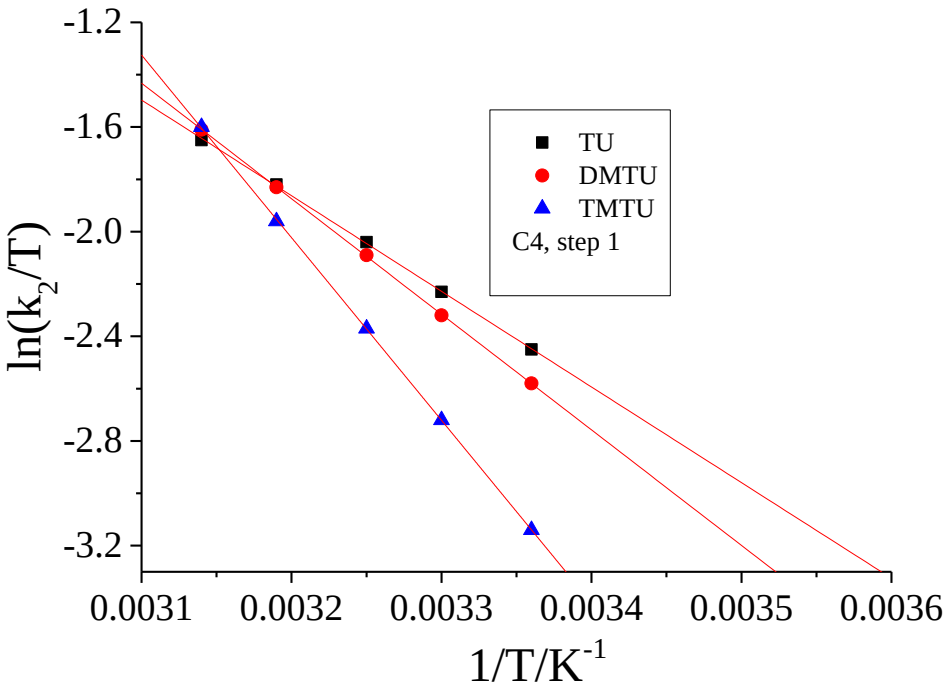

Figure SI 7.27 Step 1 temperature dependence plots for the reaction of **C4** with the thiourea nucleophiles

Dichloro(4-chloro-2,2′:6′,2′′-Terpyridine)(triphenylphosphino)ruthenium(II) (**C5**)

Table SI 7.5 Step 1 observed rate constants and the corresponding nucleophile concentrations for **C5**

[Nu]/M	**k_{obs}/s^{-1} TU**	**[Nu]/M**	**k_{obs} / s^{-1} DMTU**	**[Nu]/M**	**k_{obs} / s^{-1} TMTU**
0.01	0.24	0.04	0.775	0.028	0.321
0.02	0.469	0.08	1.574	0.056	0.625
0.03	0.686	0.12	2.354	0.084	0.930
0.04	0.926	0.16	3.121	0.112	1.237
0.05	1.16	0.20	3.895	0.140	1.53

Table SI 7.6 Step 2 observed rate constants and the corresponding nucleophile concentrations for **C5**

[Nu]/M	**k_{obs} /s^{-1} TU**	**k_{obs} / s^{-1} DMTU**	**k_{obs} / s^{-1} TMTU**
0.000125	0.00135	2.85E-4	3.1E-5
2.5E-4	0.0027	5.7E-4	6.2E-5
3.75E-4	0.0041	8.6E-4	9.3E-5
0.5E-3	0.0054	0.00114	1.24E-4
0.000625	0.00675	0.00142	1.55E-4

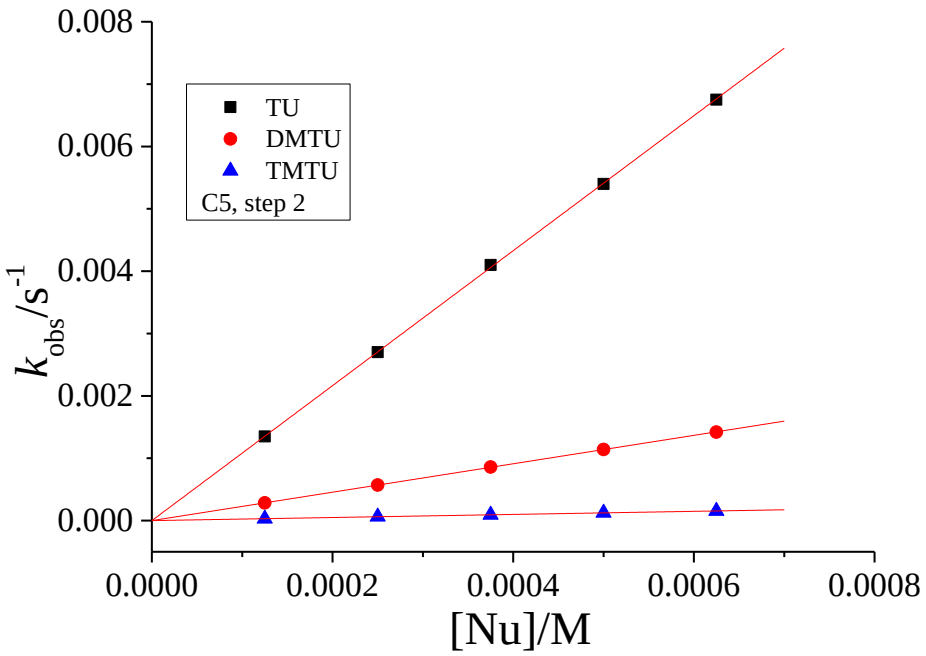

Figure SI 7.28 Step 2 concentration dependence plots for the reaction of **C5** with thiourea nucleophiles at 298 K

Table SI 7.7 Step 1 data of ln(k_2/T) and 1/T for complex **C5**

1/T	**ln(k_2/T) TU**	**ln(k_2/T) DMTU**	**ln(k_2/T) TMTU**
0.00336	-2.52	-2.78	-3.3
0.0033	-2.2	-2.45	-2.93
0.00325	-1.93	-2.17	-2.63
0.00319	-1.61	-1.82	-2.28
0.00314	-1.33	-1.54	-1.99

Table SI 7.8 Step 2 data of ln(k_2/T) and 1/T for complex **C5**

1/T	ln(k_2/T) TU	ln(k_2/T) DMTU	ln(k_2/T) TMTU
0.00336	-3.33	-4.72	-6.93
0.0033	-3.03	-4.16	-6.08
0.00325	-2.77	-3.68	-5.39
0.00319	-2.47	-3.12	-4.51
0.00314	-2.22	-2.65	-3.82

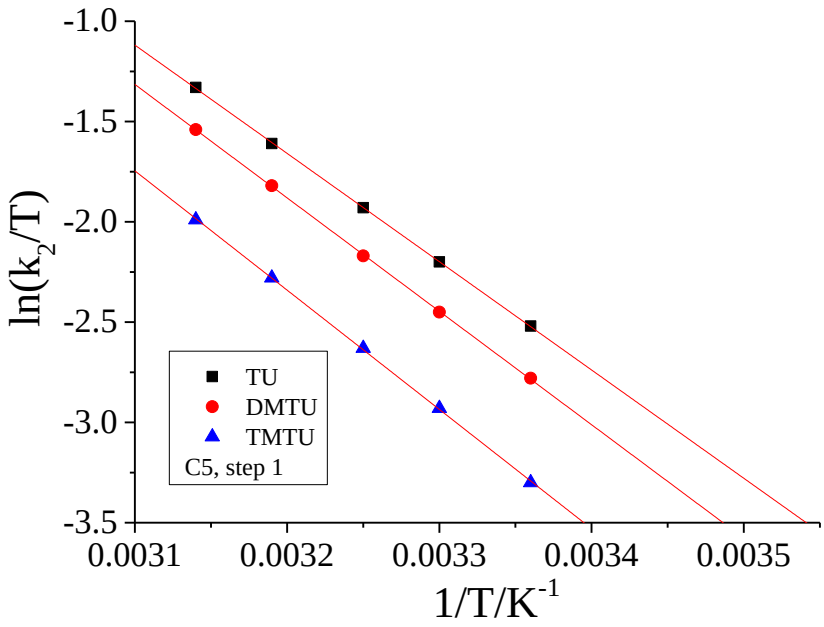

Figure SI 7.29 Step 1 temperature dependence plots for the reaction of **C5** with the thiourea nucleophiles

Dichloro(2,2′:6′,2″-terpyridine)(triphenylphosphine)ruthenium(II) (**C1**)

Table SI 7.9 Step 1 observed rate constants and the corresponding nucleophile concentrations for **C1**

[Nu]/M	k_{obs}/s^{-1} **TU**	k_{obs} / s^{-1} **DMTU**	k_{obs} / s^{-1} **TMTU**
0.0133	0.335	0.298	0.156
0.0266	0.67	0.596	0.312
0.0399	1.005	0.894	0.468
0.0532	1.34	1.192	0.624
0.0665	1.676	1.488	0.78

Table SI 7.10 Step 2 observed rate constants and the corresponding nucleophile concentrations for complex **C1**

[Nu]/M	k_{obs}/ s^{-1} **TU**	**[Nu]/M**	k_{obs} / s^{-1} **DMTU**	**[Nu]/M**	k_{obs} / s^{-1} **TMTU**
1.5625E-5	2.6E-4	3.125E-5	2E-4	1.25E-4	8.1E-5
3.125E-5	5.2E-4	6.25E-5	4E-4	2.5E-4	1.62E-4
4.6875E-5	7.8E-4	9.375E-5	6E-4	3.75E-4	2.43E-4
6.25E-5	0.00104	1.25E-4	8E-4	5E-4	3.24E-4
7.8125E-5	0.0013	1.5625E-4	1E-3	6.25E-4	4.05E-4

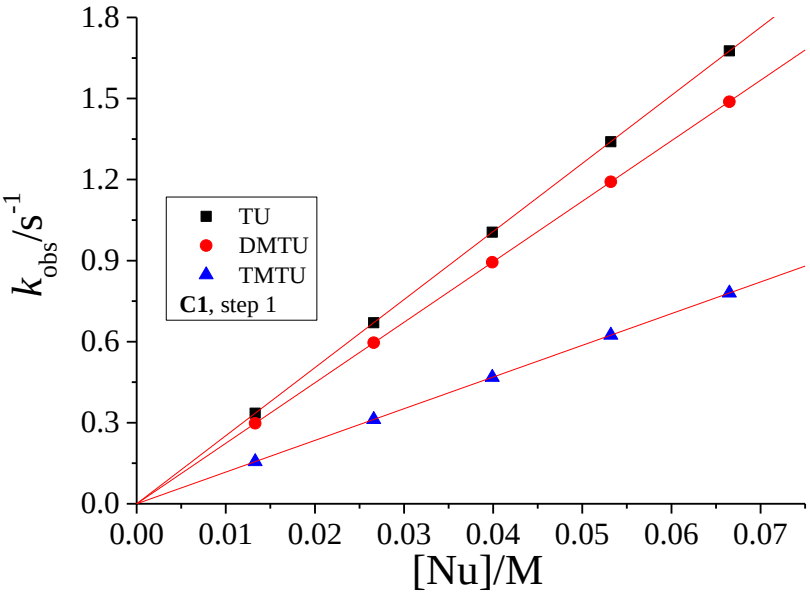

Figure SI 7.30 Step 1 concentration dependence plots for the reaction of **C1** with thiourea nucleophiles at 298 K

Table SI 7.11 Step 1 data of ln(k_2/T) and 1/T for complex **C1**

1/T	**ln(k_2/T) TU**	**ln(k_2/T) DMTU**	**ln(k_2/T) TMTU**
0.00336	-2.17	-2.32	-3.4
0.0033	-1.76	-1.9	-2.92
0.00325	-1.43	-1.55	-2.5
0.00319	-1.02	-1.13	-2.04
0.00314	-0.68	-0.78	-1.64

Table SI 7.12 Step 2 data of ln(k_2/T) and 1/T for complex **C1**

1/T	**ln(k_2/T) TU**	**ln(k_2/T) DMTU**	**ln(k_2/T) TMTU**
0.00336	-2.89	-3.84	-6.25
0.0033	-2.63	-3.31	-5.48
0.00325	-2.41	-2.85	-4.84
0.00319	-2.14	-2.33	-4.06
0.00314	-1.93	-1.88	-3.44

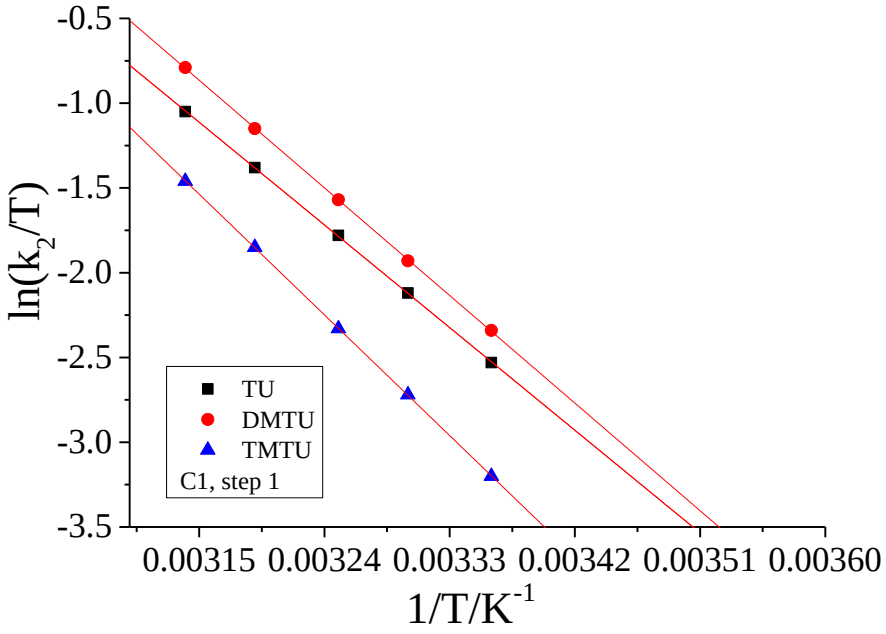

Figure SI 7.31 Step 1 temperature dependence plots for the reaction of **C1** with the thiourea nucleophiles

Dichloro(triphenylphosphino)(4,4',4''-tri-tert-butyl-2,2′:6′,2″-terpyridine)-ruthenium(II) (C3)

Table SI 7.13 Step 1 observed rate constants and the corresponding nucleophile concentrations for complex **C3**

[Nu]/M	**k_{obs}/s^{-1} TU**	**k_{obs} / s^{-1} DMTU**	**k_{obs} / s^{-1} TMTU**
0.01	0.386	0.3445	0.201
0.02	0.771	0.6895	0.4025
0.03	1.153	1.035	0.6038
0.04	1.535	1.3765	0.8025
0.05	1.914	1.724	1.005

Table SI 7.14 Step 2 observed rate constants and the corresponding nucleophile concentrations for complex **C3**

[Nu]/M	k_{obs}/ s^{-1} TU	k_{obs} / s^{-1} DMTU	k_{obs} / s^{-1} TMTU
3.125E-5	6.06E-4	5.3E-4	3.5E-4
6.25E-5	0.00121	0.00107	2.8E-4
9.375E-5	0.00184	0.0016	2.1E-4
1.25E-4	0.00242	0.00214	1.4E-4
1.5625E-4	0.00304	0.00268	7E-5

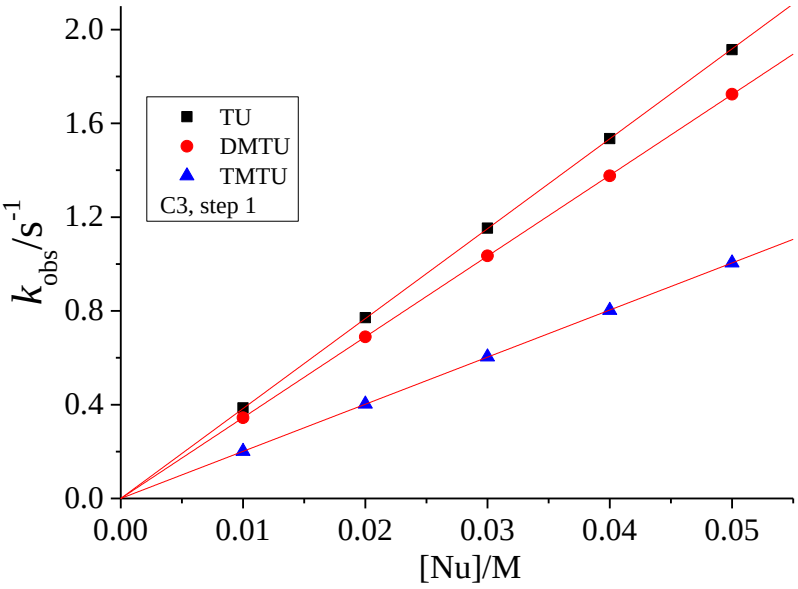

Figure SI 7.32 Step 1 concentration dependence plots for the reaction of **C3** with thiourea nucleophiles at 298 K

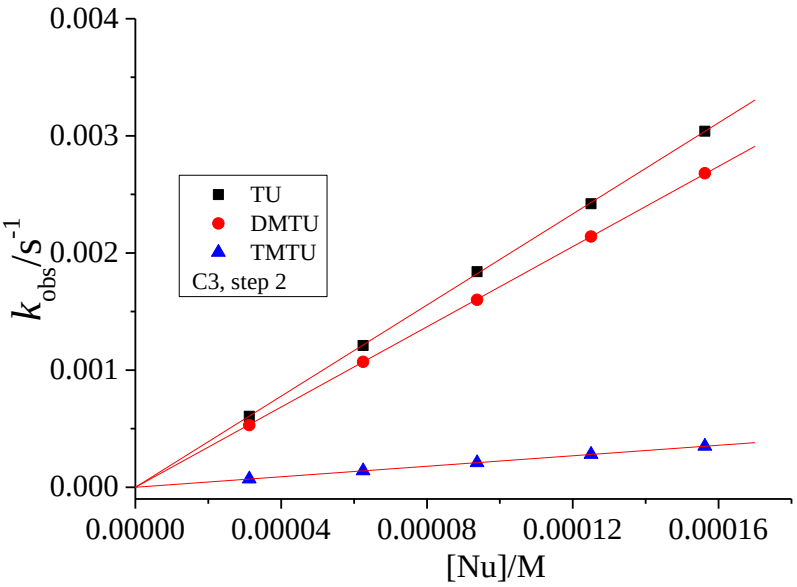

Figure SI 7.33 Step 2 concentration dependence plots for the reaction of **C3** with thiourea nucleophiles at 298 K

Table SI 7.15 Step 1 data of ln(k_2/T) and 1/T for complex **C3**

1/T	**ln(k_2/T) TU**	**ln(k_2/T) DMTU**	**ln(k_2/T) TMTU**
0.00336	-1.93	-2.16	-2.7
0.0033	-1.73	-1.95	-2.3
0.00325	-1.56	-1.77	-1.97
0.00319	-1.36	-1.57	-1.57
0.00314	-1.2	-1.39	-1.24

Table SI 7.16 Step 2 data of ln(k_2/T) and 1/T for complex **C3**

1/T	**ln(k_2/T) TU**	**ln(k_2/T) DMTU**	**ln(k_2/T) TMTU**
0.00336	-2.22	-2.87	-4.95
0.0033	-1.98	-2.52	-4.25
0.00325	-1.77	-2.22	-3.66
0.00319	-1.52	-1.88	-2.96
0.00314	-1.32	-1.58	-2.37

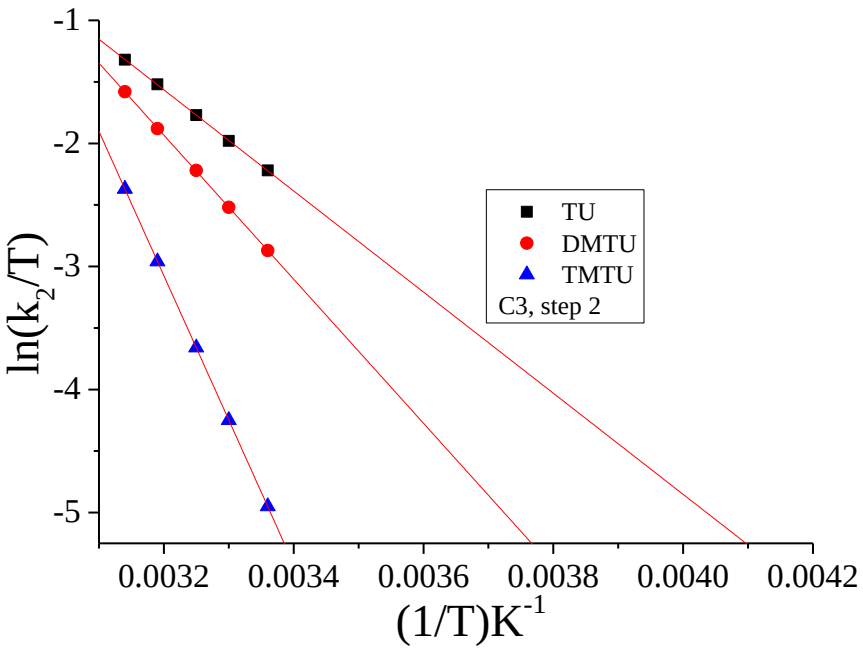

Figure SI 7.34 Step 2 temperature dependence plots for the reaction of **C3** with the thiourea nucleophiles

Dichloro(2,6-bis(2-pyrazolyl)pyridine)(triphenylphosphino)ruthenium(II) (**C6**)

Table SI 7.17 Step 1 observed rate constants and the corresponding nucleophile concentrations for complex **C6**

[Nu]/M	k_{obs}/s^{-1} TU	[Nu]/M	k_{obs} / s^{-1} DMTU	[Nu]/M	k_{obs} / s^{-1} TMTU
0.008	6.6E-5	0.02	1.35E-4	0.02	1.1E-4
0.016	1.3E-4	0.04	2.69E-4	0.04	2.1E-4
0.024	1.95E-4	0.06	4.1E-4	0.06	3.16E-4
0.032	2.58E-4	0.08	5.4E-4	0.08	4.22E-4
0.04	3.24E-4	0.1	6.8E-4	0.1	5.2E-4

Dichloro(4'-(4-methylphenyl)-2,2′:6′,2″-terpyridine)(triphenylphosphino)ruthenium(II) (**C2**)

Table SI 7.18 Step 1 observed rate constants and the corresponding nucleophile concentrations for complex **C2**

[Nu]/M	k_{obs} /s^{-1} TU	k_{obs} / s^{-1} DMTU	k_{obs} / s^{-1} TMTU
0.01	0.23	0.18	0.115
0.02	0.46	0.37	0.23
0.03	0.68	0.56	0.34
0.04	0.9	0.76	0.45
0.05	1.13	0.94	0.565

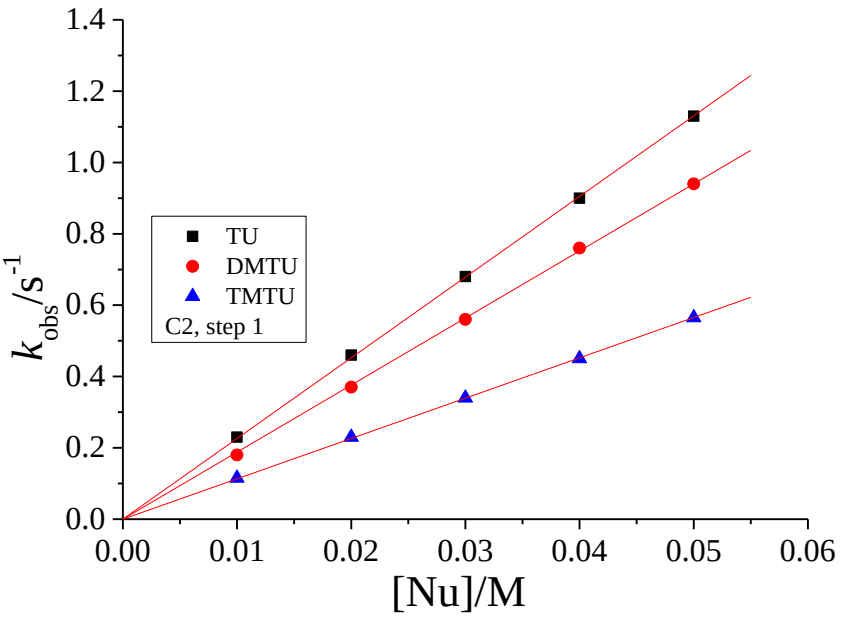

Figure SI 7.35 Step 1 concentration dependence plots for the reaction of **C2** with thiourea nucleophiles at 298 K

Table SI 7.19 Step 1 data of ln(k_2/T) and 1/T for complex **C2**

1/T	**ln(k_2/T) TU**	**ln(k_2/T) DMTU**	**ln(k_2/T) TMTU**
0.00336	-2.67	-3.14	-3.920
0.0033	-2.38	-2.70	-3.500
0.00325	-2.14	-2.36	-3.140
0.00319	-1.85	-1.96	-2.700
0.00314	-1.61	-1.60	-2.346

Chapter 8

Conclusions

The objective of this study was to investigate the rate and mechanisms of substitution from Ru(II) complexes bearing different kinds of ligands. The study was done with biologically relevant thiourea nucleophiles. The complexes have potential as anticancer agents hence knowing their interaction with the nucleophile provides understanding of their behaviour in the biological environment. The focus of the study was on how the electronic and steric properties of a variety of ligands influence the rate of substitution from the Ru(II) metal centres. The substitution reactions were undertaken as a function of concentration and temperature under *pseudo* first-order conditions. The outcome of this study provides useful information that will be the basis for the design and development of effective anticancer drugs, with reduced toxicity and improved uptake.

The nature of ligands coordinated on the Ru metal centres enabled the study of how ligand electronic properties, bulkiness or spatial orientation can affect the overall rate and mechanism of substitution. A series of neutral biologically relevant thiourea nucleophiles (TU, DMTU and TMTU) with varying steric demands were used for the substitution reactions. The results and the discussions of this study are reported in Chapters 3-7 of this thesis. The structural formulae of the complexes studied are reported in the figures 8.1- 8.5.

Chapter 1 presented an introduction showing a chronological order of research events that led to the discovery of the anticancer agent cisplatin and further efforts towards finding an improved drug. The weakness of cisplatin led to the development of other Pt compounds although without much success as cisplatin remained the best among all. The second part of this chapter shows how further search efforts were directed towards Ru complexes as the possible better alternative with an insight into the biological features of Ru that make its complexes as potential biological probes and therapeutic agents. It also deals with applications in photodynamic therapy, DNA binding including postulated mechanism of action of Ru anticancer agents and the substitution reactions. The conclusion of this chapter outlines the importance of investigating the kinetic and mechanistic behaviour of potential anti-cancer agents.

Chapter 2 discusses substitution reactions, the general factors influencing the ligand substitution reactions using ruthenium complexes as some of the examples. There was a

further elaborate discussion on the relevant kinetic theory including the techniques employed in investigating the ligand substitution reactions and the instrumentation that facilitate study of substitution reactions.

The investigation of the role of the arene ligand and introduction of the 2, 2'-bipyridyl ligand to the Ru(II)arenetri-aqua complexes on the kinetics and mechanism of reaction was discussed in **chapter 3**. It was determined that the reactivity of the complexes under this study is driven by electronic factors and steric effects. Complex **C1** is more reactive than **C2** because it has a more electropositive metal centre. This is due to less electron donation towards the Ru(II) metal centre by the less electron rich benzene in **C1** compared to the mesitylene ligand in **C2**. The tri-aqua complexes **C1** and **C2** have trigonal pyramidal orientation that precludes any possibility of *trans*-effect. The addition of the bipyridyl ligand to the tri-aqua complexes, **C1** and **C2** to form the mono-aqua complexes **C3** and **C4** respectively changes the orientation from trigonal pyramidal to one where the aqua group is *trans* to the arene ligand bringing at play *trans*-effect which is the key factor influencing the reactivity in **C3, C4, C5** and **C6.** Complexes with arenes having alkyl substituents have higher electron density thereby exhibiting stronger *trans*-effect that results in higher reactivity. However this orientation introduces steric hindrance at the Ru(II) metal centre in the later complexes lowering their reactivity. The mode of substitution in these complexes is associative in nature. The complexes reported in chapter 3 are represented by figure 8.1.

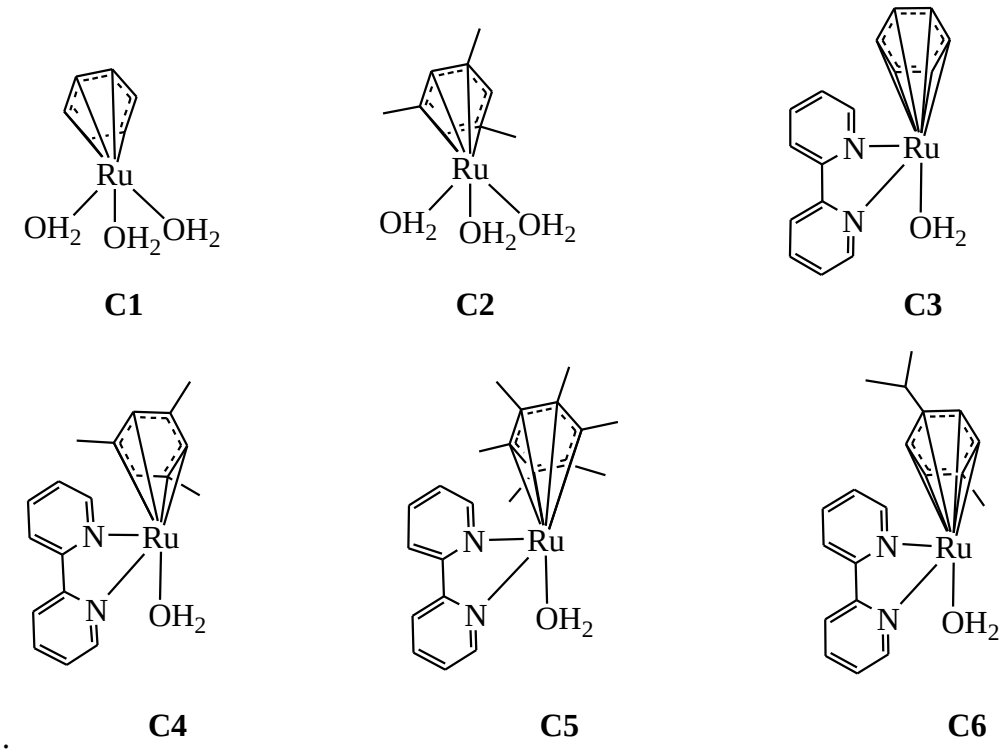

Figure 8. 1 Chemical structures of the complexes investigated in chapter 3

In **chapter 4** the role of non-labile arene and phosphane ligands on the kinetic and mechanistic behaviour of some arene phosphorruthenium(II) complexes was investigated. It was found that the two main factors controlling the reactivity of the complexes in this study are the electronic nature and steric hindrance due to the spectator ligands. Varying the nature of the arene on the ruthenium complexes from benzene to cyclopentadienyl as happens from **C1** and **C3** lowers electron density donated towards the metal centre. This also reduces the space occupied by the arene by narrowing the cone angle, B. The result is lower reactivity for **C1** than **C2** due to a more negatively charged metal centre in **C1.** Introduction of the bis(diphenylphosphino)methane ring around the ruthenium decreases the phosphorus-phosphorus separation and angle A between the phosphorus atoms. This results in the narrowing of the path of the incoming nucleophile which slows the reactivity. In enlarging the size of the ring around the phosphine atoms, the reactivity increases. This is due to the increase in P-P distance and the expansion of angle A. This decreases the steric hindrance and results in the creation of a trough that traps the nucleophiles enhancing the reactivity. These observed results are supported by DFT calculations. The mode of mechanism of reactivity of these complexes is dissociative in nature, which is mostly due to the steric nature around the

Ru complex. The structural formulas for the complexes investigated in chapter 4 are shown in figure 8.2.

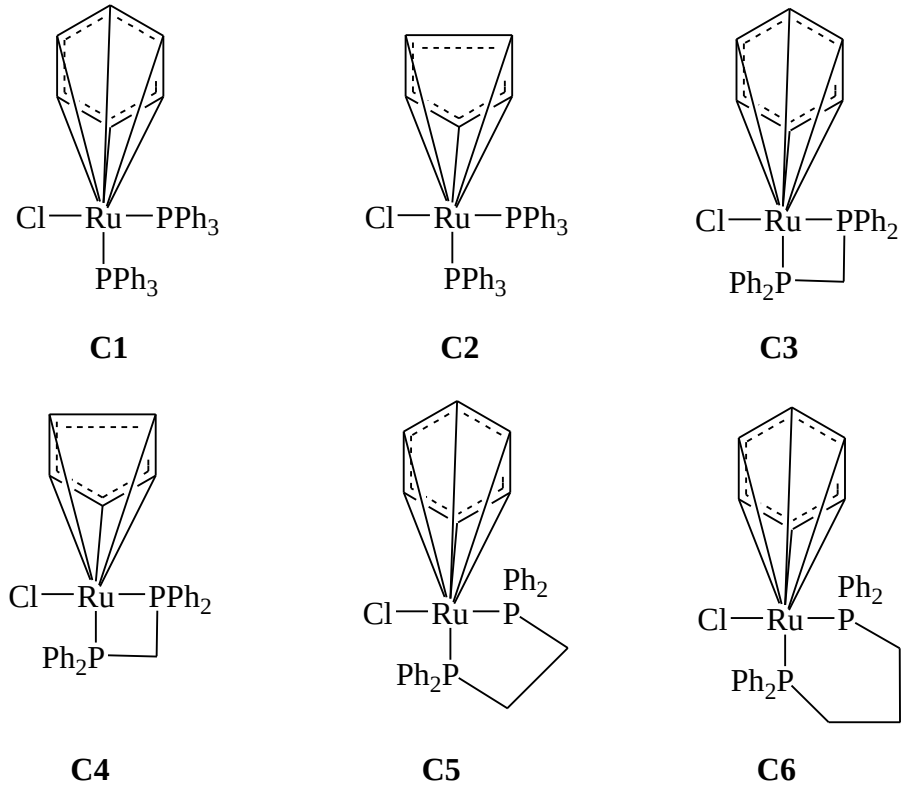

Figure 8. 2 Chemical structures of the complexes investigated in chapter 4

The study in **chapter 5** sought to understand how the rate of substitution from 2,4,6-tris(2-pyridyl)-1,3,5-triazineRu(PPh3)(Cl) and analogous complexes is affected by the substituents on the centrosymmetric 1,2,3-triazine ligand. The study has shown that increasing π-conjugation of the C_3 symmetric tris(2-pyridyl)-1,3,5-triazine by introduction of the quinolyl in place of the pyridyl substituents increases π-back-bonding of the resultant chelate backbone making the Ru(II) metal centre more electrophilic, thereby accelerating the substitution reactivity of the compound as observed for the reaction of **C3** compared to **C1**. The methyl substituents on the 2-pyridyl substituents of the triazine ligand chelate increase electron density into the triazine ring by σ-induction effects. This lowers π-acceptor ability of the chelate which results in a less electrophilic metal centre. As a result, it reacts slightly slower as observed in the relative reactivity of **C2** in comparison to the reference complex **C1**. The introduction of the phenyl in the 2,4,6-positions on the 2-pyridyl rings of the triazine ligand, increases the steric demands of the resultant triazine chelate ligand **L4,** forcing it to assume a trough like orientation at the metal centre. This facilitates the trapping of incoming

nucleophiles increasing reactivity. The study also revealed that the substituents on the pyridyl ligand at the 4-positions of the C_3-centrosymmetric 1,2,3-triazine ligands are far removed from the metal centres and therefore have negligible effect on the rate of the substitution reactions. This is supported by the DFT comparative data (Table 5.3). The substitution reactions proceeds via two steps and the trend for both decreases in the order: **C3** > **C4** > **C1** > **C3**. The reactivity of the second step is about 10^3 lower than the first step. Both reaction steps proceed via the associative mode of substitution.

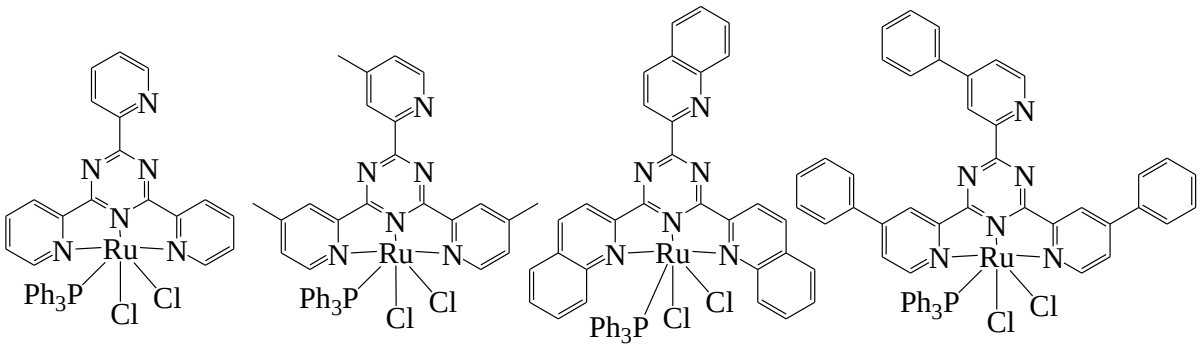

C1 **C2** **C3** **C4**

Figure 8. 3 Chemical structures of the complexes investigated in chapter 5

The study in **chapter 6** seeks to establish how hetero-atoms affect the overall electronic properties of the bidentate 2-(2-Pyridyl)azole based ancillary ligands which affects the rate of chloride substitution from $[Ru^{II}(tpy)(L)(Cl)]^+$ complexes. It has been shown that the nature of hetero atom (N, S or O), orientation and bulkiness of these bidentate auxiliary ligands attached to the Ru(tpy)Cl moiety dictates the rate of substitution from the Ru(II) complexes. The reactivity of the complexes under investigation reveals two electronic forces at play, π-donation in **C1** and **C2** and π-back-donation in **C3** and **C4.** The 2-(1*H*-Imidazol-2-yl)pyridine ligand in **C1** is a strong electron donor resulting in strong *trans*-effect that makes **C1** most reactive. The addition of the benzene on 2-(1*H*-Imidazol-2-yl)pyridine ligand to form 2-(2-Pyridyl)benzimidazole in **C2** extents the π-space lowering the electron donor strength hence the lower reactivity of **C2** compared to **C1**. Additionally, the extended size of the ligand in **C2** introduces hindrance at the metal centre also lowering reactivity. The *trans*-effect experienced in **C1** and **C2** has greater magnitude and effect on reactivity than the π-back-bonding effect in **C3** and **C4** hence the higher reactivity of the former complexes. There is greater aromaticity in the 2-(2-Pyridyl)benzothiazole ligand in **C3** than in the 2-(2-

Pyridyl)benzoxazole ligand in **C4** that accounts for the higher reactivity of **C3** compared to **C4**. This is supported by higher DFT calculated electrophiliciy index in **C3** compared to **C4**. The greater π-acceptor capacity of **C3** is also brought about by having the azole end of the ancillary ligand *trans* to the leaving group which is not the case in **C4**. The nature of the hetero-atom in the azole ligand has been observed to influence the electronic properties of the ligands and subsequently the rate of substitution. The small values of $\Delta H^{\#}$ and negative values of $\Delta S^{\#}$ clearly support the associative mechanism for the substitution process.

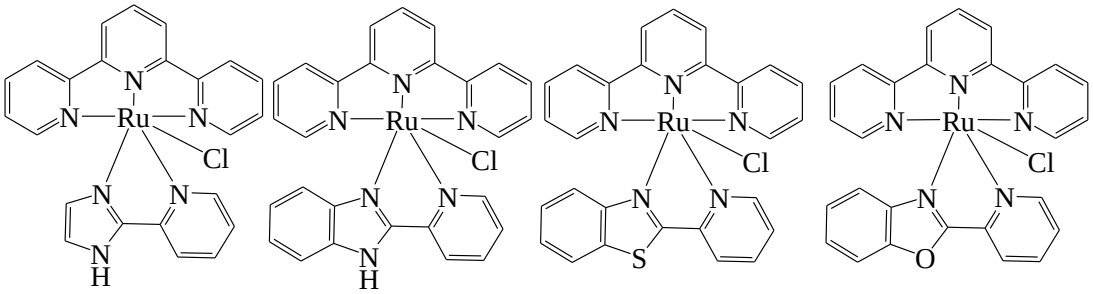

Figure 8. 4 Chemical structures of the complexes investigated in chapter 6

The tpy ligand and its analoques have been widely explored especially with the Pt metal as the coordinating metal because of their versatility. The study in **chapter 7** sought to understand the role of substituents on the rate of substitution from Ru(II) complexes bearing tpy or tpy analogues and a tertiary phosphine ligand. It was determined that the rate of substitutions from these complexes are electronically driven either through *trans*-effect or π-back-donation. **C2** and **C3** have electron donating substituents (methyl and methylphenyl) that increase electron density on the Ru metal centre enhancing *trans*-effect and hence higher reactivity compared to **C1**. Further on, **C4** and **C5** have the electron withdrawing substituents namely chloro and chlorophenyl substituents respectively that increase the electrophilicity of their metal centres thereby increasing their reactivity compared to that of **C1**. The reactivity of **C4** is higher than **C5** due to the presence of a chlorophenyl substituent in **C4** that is a stronger π-acceptor than the chloro ligand in **C5**. It has been shown that the *trans*-effect in **C2** influences the reactivity more strongly than the π-back-donation in **C4**. The *cis* electron donation by 2,6-bis(pyrazolyl)pyridine ligand in **C6** significantly retards the reactivity of the Ru(II) metal centre compared to **C1** hence it can be used to tune the reactivity of Ru(II) complexes. It has generally been observed that the reactivity of Ru(II) complexes is more strongly affected by the electron donating ligands (*trans*-effect) than ligands that enhance π-

back-donation. The *tert*-butyl substituents in **C3** are very strong donor ligands whose donation from both the *cis* and *trans* positions strongly accelerates the reactions. The trend in the DFT calculated data supports the observed reactivity of the complexes. The reactivity of the complexes in this study proceeds by the associative mechanism for all the nucleophiles in step one and the thiourea nucleophile only in step two. The substitution reactions proceed via the dissociatively activated interchange mechanism for the rest of the nucleophiles in the second step.

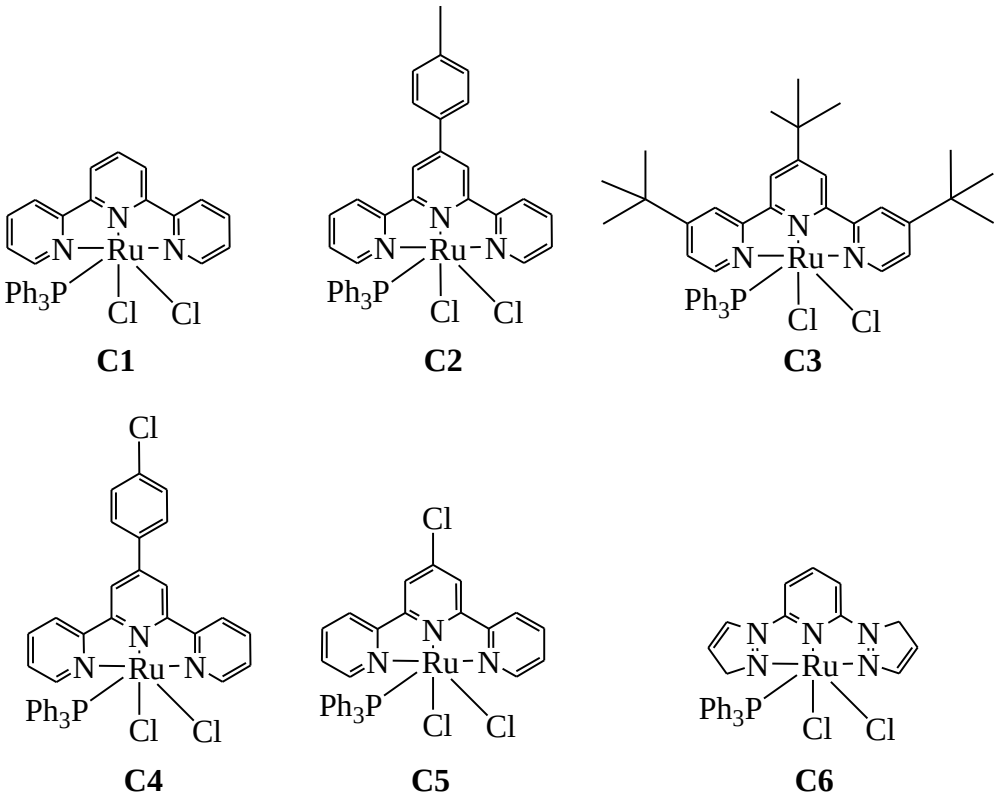

Figure 8. 5 Chemical structures of the complexes investigated in chapter 7

The reactivity of the nucleophiles was influenced purely by steric demands with the order of reactivity as follows: TU > DMTU > TMTU. The trend in reactivity of the nucleophiles was replicated in all the complexes studied

Chapter 9

Future investigations on the rate of substitution from azine-bridged Ru(II)-Pt(II) complexes

9.0 Introduction

In preparation for future study on the rate of substitution from hetero-bimetallic Ru-Pt complexes, extra work on the synthesis of two schemes of the complexes has been done. The first scheme has a variation in the π-surface of the bridging ligand while the second scheme has terminal ligands with different electronic properties. Polynuclear coordination is an attractive idea for anti-cancer applications because of their high cytotoxicity and versatile activity. They can be homo or hetero di or tri nuclear complexes. The latter feature two or more different metal ions bridged by one or two ligands. In heterometallic polynuclear complexes, the different metal coordination sites offer selective specificity and reactivity at each metal centre. Di-nuclear complexes of Ru and Pt have a promising anti-cancer activity because mononuclear complexes of each are known for their antitumor activity.[1] Little is known about Ru–Pt anticancer activity and substitution reactivity and these complexes have generated great interest. Only a few compounds with a rigid bridging ligand have been studied so far.[2] [3] The complexes consist of a Ru(II) cationic species as a light-absorbing unit linked to a reactive Pt(II) centre by a short, rigid polyazine bridging ligand. These complexes have attracted attention for decades due to their ability to photocleave DNA .[4] [5] [6]

It has been reported that incorporating the tpy as a terminal ligand (Figure 9.1) on the Ru centre causes it to interacte with DNA electrostatically or by intercalation between base pairs or by groove binding.[7] [8] The DNA photocleavage activity of $[Ru(tpy)(pydppz)]^{2+}$ (pydppz = 3-(pyrid-2'-yl)dipyrido-(3,2-a:2',3'-c]phenazine) in the presence of oxygen has been reported in literature.[9] Thorp and co-workers[10] examined the DNA cleavage activity of $[Ru(tpy)(tmen)(OH_2)]^{2+}$(tmen = N,N,N',N'-tetramethylethylenediamine) by cyclicvoltammetry. The mixed metal complexes, consisting of Ru light absorbers and a cisplatin unit, represent an emerging class of bioactive molecules of interest as anticancer agents. They exhibit enhanced covalent binding compared to cisplatin.[11] [12] The DNA-binding properties and anti-microbial properties of the heteronuclear bimetallic complex (tpy)Ru(dpp)Pt has been reported.[2] It shows rapid binding to plasmid DNA with significant retardation of migration of the DNA through agarose gels as compared to that of cisplatin, no photo

cleavage was observed. The heterobimetallic complexes could have a varying terminal or bridging ligands. Firstly, the DNA-binding properties of the heteronuclear bimetallic complexes whose bridging ligand is varying, [(tpy)RuCl(BL)$PtCl_2$](PF_6) (BL = 2,3-bis(2-pyridyl)pyrazine (dpp), 2,3-bis(2-pyridyl)quinoxaline (dpq), or 2,3-bis(2-pyridyl)benzo-quinoxaline (dpb)), have been reported.[5] Secondly, the coupling of [(TL)RuCl(dpp)] (TL= tpy, t-tpy, m-ph-tpy, p-cy or Cl-ph-tpy) subunits to a cis-Pt(II)Cl_2 moiety[13] which has been synthesised in literature gives the second type of heterobimetallic complexes with different terminal ligands. Their potential to bind to DNA at more than one site offer a better prospect and thus superior anti-cancer therapy with possibility to overcome the shortcomings of cisplatin. The short distance dinuclear Ru-Pt complexes bridged by polyazine ligands offer some advantages. The polyazine bridging ligands are good π-acceptors hence imparting interesting and useful spectroscopic and redox properties to the complexes. complexes of the type $[(bpy)_2Ru\text{-}(BL)PtCl2]^{2+}$ (where BL= dpp, dpq, dpb, or bpm (bpm = 2,2-bipyrimidine) and nitrogen dendrimeric ligands have shown that coordination of the Pt(II) centre to the remote nitrogens of the BL(Bridging Ligand) stabilizes the bridging ligand $\eth^*$ orbitals.[14] [15] The $(NH_3)_2$Pt(II) moeity, which is known to exert anti-cancer activity in mononuclear Pt(II) complexes such as cisplatin through binding to DNA provide the basic cyto effect of the Ru-Pt complexes assisted synergistically by the covalent/non-covalent attachment of the octahedral Ru unit.[16] The DNA-binding property of the Pt(II) centre has been shown to be maintained when it is combined with Ru.[17] In this study, the two sets of heterobimetallic Ru(II)-Pt(II) complexes have been synthesised and characterised. The structures of the complexes synthesized and characterised are shown in Figure 9.1 and Figure 9.2.

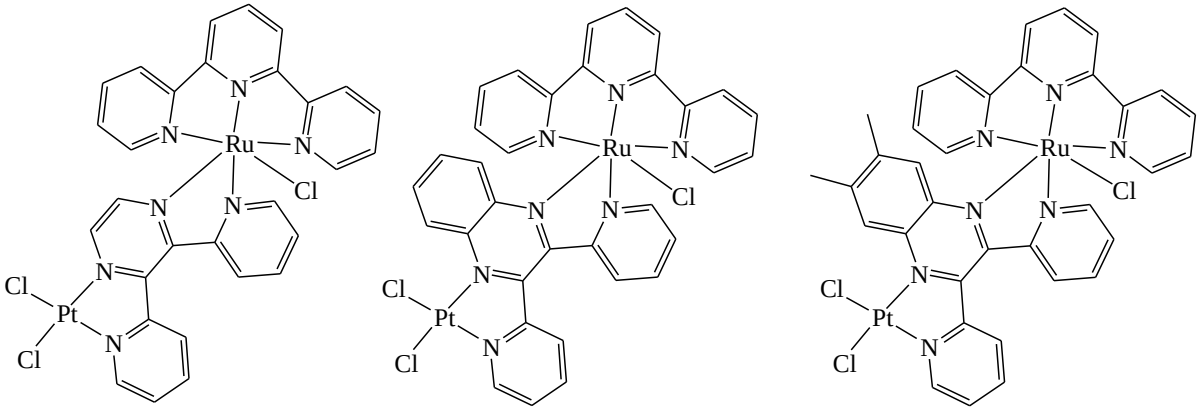

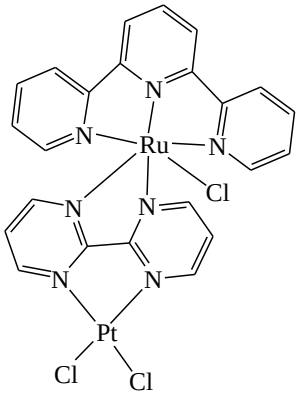

Figure 9. 1 Structures of the Ru-Pt complexes with varying bridging ligands

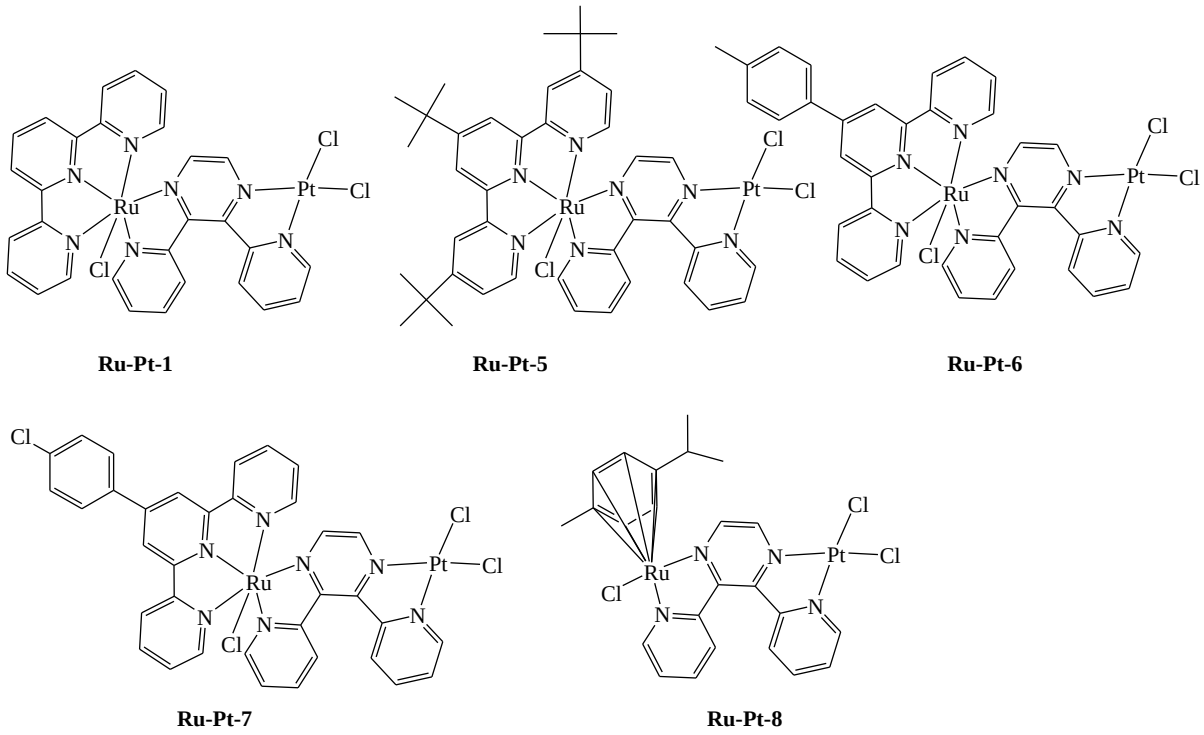

Figure 9. 2 Structures of the Ru-Pt complexes with varying terminal ligands

9.1 Experimental

9.1.1 Materials

Sigma Aldrich chemical Co. supplied the following chemicals; Ligands: 2,3-Bis(2-pyridyl)pyrazine (**dpp**), 2,3-Bis-(2'-pyridy1)-quinoxalie (**dpq**), 6,7-Dimethyl-2,3-di(2-pyridyl)quinoxaline (**mdpq**), 2,2′;6,2″-terpyridine (**tpy**), 4′-(4-Methylphenyl)-2,2′:6′,2″-terpyridine (**m-ph-tpy**), 4′-(4-Chlorophenyl)-2,2′:6′,2″-terpyridine (**Cl-ph-tpy**), 4,4′,4″-Tri-*tert*-Butyl-2,2′:6′,2″-terpyridine (**t-tpy**), and 2,2'-bipyrimidine (**bpm**). Ruthenium trichloride hydrate, *cis*-Dichlorobis(dimethyl sulfoxide)platinum(II), Dichloro(*p*-cymene)ruthenium(II) dimer, alumina, Potassium hexaflorophosphate, triethylamine, Lithium chloride, 2,2'-pyridil, o-phenylenediamine, silver perchlorate and all the solvents used. All the chemicals were used as received. The ligand, 2, 3-Bis-(2 '-pyridy1)-quinoxalie (**dpq**) was prepared following literature methods.[18] The complexes $Ru(L)RuCl_3$ (where L = **tpy**, **m-ph-tpy**, **Cl-ph-tpy** or **t-tpy)** were prepared as previously reported.[19]

9.1.2 Physical measurements and instrumentation

Low resolution electron spray ionization (ESI^+) mass spectra were recorded on the Waters Micromass LCT Premier Spectrometer or Shimadzu LCMS 2020. Elemental analyses were

done on a ThermoScientific Flash 2000 elemental analyser. The sample spectra for mass and elemental analysis are placed in the supporting information.

9.1.3 Synthesis of ligand

2, 3-Bis-(2 '-pyridy1)-quinoxalie (dpq).

A solution of o-phenylenediamine (1.08g, 0.00999mol) in ethanol (8 ml.) was added to a solution of 2,2'-pyridil (2.12 g, 0.00999mol) in ethanol (12 ml.) and the mixture refluxed for 30 min. On cooling, light brown cubes of the product separated from ethanol. Yield: 90% (2.556g, 0.000899). 1H NMR (500 MHz, CH3CN), (ppm): 8.29 (d, 1H), 8.24 (q, 1H), 8.018 (d, 1H), 7.97 (m, 2H), 7.37 (m, 1H). *Anal.* Calcd. for $C_{I8}H_{12}N_4$: C, 76.04; H, 4.25; N, 19.71 Found: C, 76.05 ; H, 4.23; N, 19.84

9.1.4 Synthesis of Ru Precursors

Chloro-2,2';6,2''-terpyridine-2,3-Bis(2-pyridyl)pyrazineruthenium(II) hexaflorophosphate (Ru1)

Ru1 was prepared by a modified literature method, Ru(tpy)Cl_3 (824.11 mg, 1.87 mmol), **dpp** (599.71 mg, 2.56 mmol) and LiCl (100.89 mg, 2.38mmol) were refluxed overnight under Nitrogen atmosphere in 100 mL 2:1 ethanol/deionized solution. Triethylamine was added at the start of the reaction to facilitate reduction of Ru(III) to Ru(II). The reaction mixture was cooled to room temperature and precipitated by addition of an aqueous saturated solution of potassium hexaflorophosphate then the crude product obtained by vacuum filtration. The pure product was obtained by alumina chromatography using 3:2 toluene/acetonitrile. The first coloured red band was collected, evaporated to dryness, dissolved in a minimum amount of acetonitrile and precipitated in cold diethyl ether then filtered to get the final pure product. Yield: 50.0% (700.5 mg), FAB (nitrobenzyl alcohol matrix), *m/z*: 604.05, $[M - PF_6]^+$

Chloro-2,2';6,2''-terpyridine-2,3-Bis-(2-pyridy1)-quinoxalineruthenium(II) hexaflorophosphate (Ru2)

Ru2 was prepared in the same manner as **Ru1** using the **dpq** ligand (727.83 mg, 2.56 mmol). The purification was as above with the first purple band being collected. Yield: 35.4 %, (528.97 mg). FAB (nitrobenzyl alcohol matrix), *m/z*: 654.11, $[M - PF_6]^+$

Chloro-2,2';6,2''-terpyridine-6,7-Dimethyl-2,3-di(2-pyridyl)quinoxaline ruthenium(II) hexaflorophosphate (Ru3)

Ru3 was prepared in the same manner as **Ru1** using the **mdpq** ligand (799.67 mg, 2.56 mmol). The purification was as above with the first purple band being collected. Yield: 30.3 %, (468.65 mg). FAB (nitrobenzyl alcohol matrix), *m/z*: 682.16, $[M - PF_6]^+$.

Chloro-2,2';6,2''-terpyridine-2,2'-bipyrimidineruthenium(II)hexaflorophosphate (Ru4)

Ru4 was prepared in the same way as **Ru1** using the **bpm** ligand (404.89 mg, 2.56 mmol). The purification was as above with the first purple band being collected. Yield: 58.9 %, (741.17 mg). FAB (nitrobenzyl alcohol matrix), *m/z*: 527.99, $[M - PF_6]^+$

Chloro-4,4′,4″-Tri-*tert*-Butyl-2,2′:6′,2″-terpyridine-2,3-Bis(2-pyridyl)pyrazineruthenium(II) hexaflorophosphate (Ru5)

Ru5 was prepared in the same way as **Ru1** using Ru(**t-tpy**)Cl_3 (1.1389 g, 1.87 mmol) in the place of Ru(**tpy**)Cl_3. The purification was as above with the first red band being collected. Yield: 29.2 %, (506.26 mg). FAB (nitrobenzyl alcohol matrix), *m/z*: 772.21, $[M]^+$

Chloro- 4′-(4-Methylphenyl)-2,2′:6′,2″-terpyridine -2,3-Bis(2-pyridyl)pyrazineruthenium(II) hexaflorophosphate (Ru6).

Ru6 was prepared in the same way as **Ru1** using Ru(**m-ph-tpy**)Cl_3 (992.63 mg, 1.87 mmol) in the place of Ru(**tpy**)Cl_3. The purification was as above with the first brown band being collected. Yield: 40.1 %, (629.23 mg). FAB (nitrobenzyl alcohol matrix), *m/z*: 694.05, $[M - PF_6]^+$

Chloro- 4′-(4-Chlorophenyl)-2, 2′:6′, 2″-terpyridine -2,3-Bis(2-pyridyl)pyrazineruthenium(II) hexaflorophosphate (Ru7)

Ru7 was prepared in the same way as **Ru1** using Ru(**Cl-ph-tpy**)Cl_3 (1.0308 g, 1.87 mmol) in the place of Ru(**tpy**)Cl_3. The purification was as above with the first yellow band being collected. Yield: 38.6 %, (620.44 mg). FAB (nitrobenzyl alcohol matrix), *m/z*: 714.04, $[M - PF_6]^+$

Chloro-*p*-cymene-2,3-Bis(2-pyridyl)pyrazineruthenium(II) tetrafloroborate (Ru8)

Ru8 was prepared in the same way as **Ru1** using Dichloro(*p*-cymene)ruthenium(II) dimer (286.3 mg, 0.5 mmol) in the place of Ru(**tpy**)Cl_3. The purification was as above with the first

yellow band being collected. Yield: 49.5 %, (145.47 mg). FAB (nitrobenzyl alcohol matrix), *m/z*: 505.07, $[M - PF_6]^+$

The structures of the synthesised precursor complexes are shown in figure 9.3 and figure 9.4.

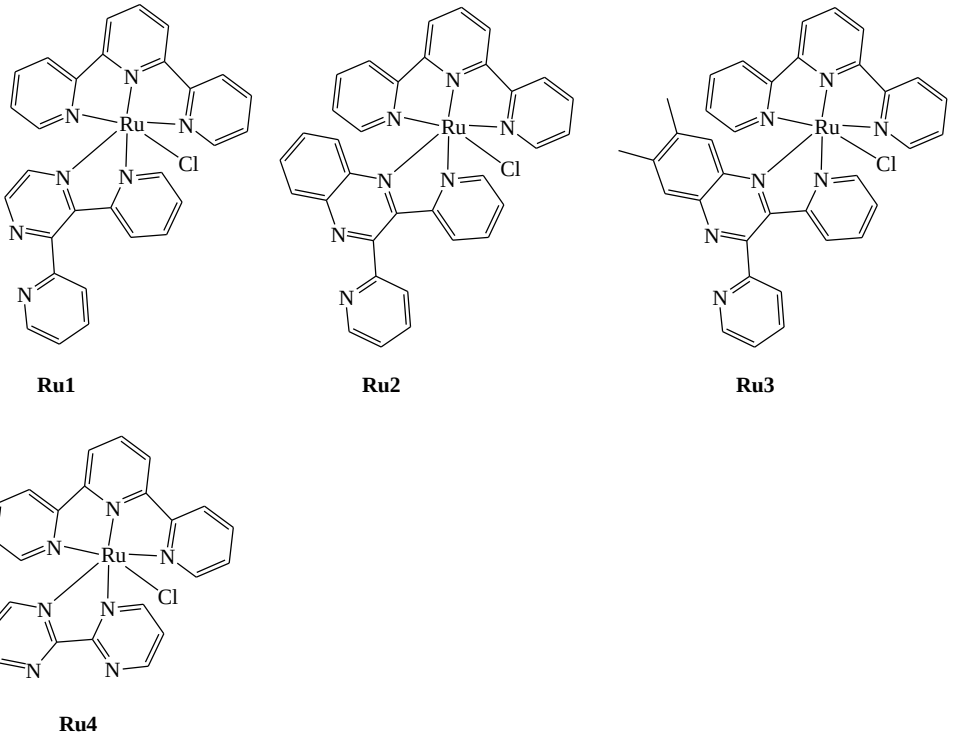

Figure 9. 3 Structures of Ru precursor complexes with varying bridging ligands

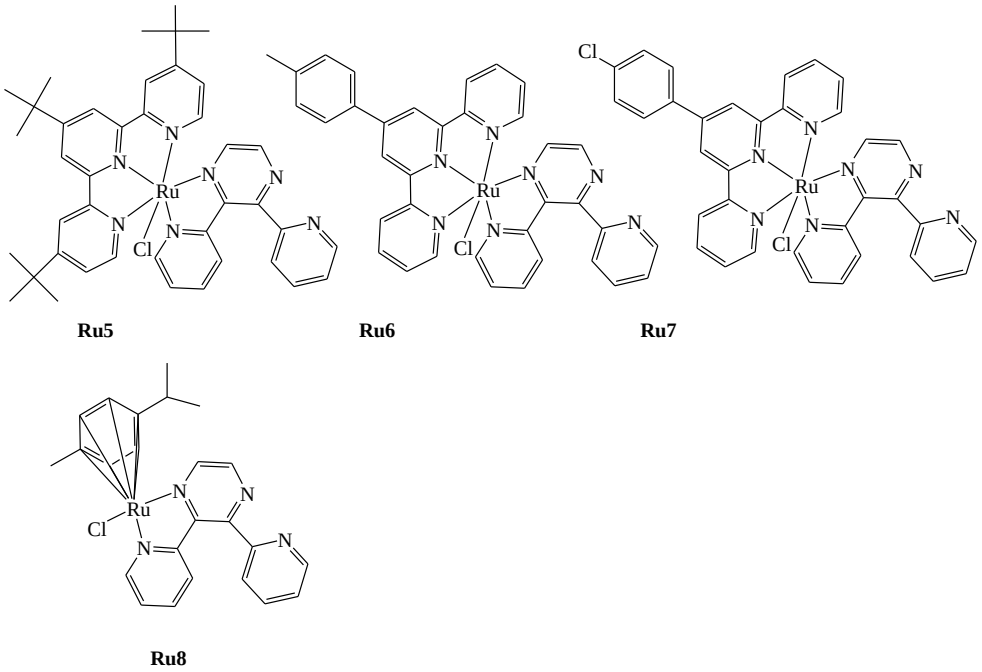

Figure 9. 4 Structural formulae of Ruthenium precursor complexes with varying terminal ligands

9.1.5 Synthesis of Ru-Pt complexes

2,3-Bis(2-pyridyl)pyrazine(2,2';6,2''-terpyridine)(trichloro)ruthenium(II)platinum(II) hexaflorophosphate (Ru-Pt-1)

Ru-Pt-1 was prepared by a modified previously published method.[35] **Ru1** (149.80 mg, 0.2 mmol) and $Pt(DMSO)_2Cl_2$ (88.67 mg, 0.21 mmol) were heated in 10 mL of 95% ethanol for one hour. After cooling to room temperature, the purple precipitate was filtered then washed with 10 mL ethanol and 10 mL chloroform then dissolved in about 30 mL acetonitrile, filtered, reduced in volume to about 15 mL and then flash precipitated in 60 mL COLD diethyl ether. Yield 82.1 % (166.66 mg), FAB (nitrobenzyl alcohol matrix), *m/z*: 869.98, $[M - PF_6]^+$ Anal calcd for $C_{29}H_{21}Cl_3F_6N_7PPtRu$: C, 34.31; H, 2.09; N, 9.66 Found. C, 34.22; H, 2.16; N, 9.21

2,3-Bis-(2-pyridy1)-quinoxaline(2,2';6,2''-terpyridine)(trichloro)ruthenium(II)platinum(II) hexaflorophosphate (Ru-Pt-2)

Ru-Pt-2 was prepared in the same way as **Ru-Pt-1** using **Ru2** (159.81 mg, 0.2 mmol) in the place of **Ru1**. A blue product was obtained. Yield 73.2 % (155.92 mg), FAB (nitrobenzyl

alcohol matrix), *m/z*: 920.01, $[M - PF_6]^+$. Anal calcd for $C_{33}H_{23}Cl_3F_6N_7PPtRu$: C, 37.21; H, 2.18; N, 9.21 Found. C, 37.51; H, 2.27; N, 8.99

6,7-Dimethyl-2,3-di(2-pyridyl)quinoxaline(2,2';6,2''-terpyridine)(trichloro) ruthenium(II)platinum(II) hexaflorophosphate (Ru-Pt-3)

Ru-Pt-3 was prepared in the same way as **Ru-Pt-1** using **Ru3** (165.42 mg, 0.2 mmol) in the place of **Ru1**. A blue product was obtained. Yield 66.8 % (146.04 mg), FAB (nitrobenzyl alcohol matrix), *m/z*: 948.03, $[M - PF_6]^+$. Anal calcd for $C_{35}H_{27}Cl_3F_6N_7PPtRu$: C, 38.46; H, 2.49; N, 8.97. Found. C, 38.07; H, 2.30; N, 8.65

2,2'-bipyrimidine(2,2';6,2''-terpyridine)(trichloro)ruthenium(IIplatinum(II)) hexaflorophosphate (Ru-Pt-4)

Ru-Pt-4 was prepared in the same way as **Ru-Pt-1** using **Ru4** (134.58 mg, 0.2 mmol) in the place of **Ru1**. A blue product was obtained. Yield 59.5 % (111.73 mg), FAB (nitrobenzyl alcohol matrix), *m/z*: 793.96, $[M - PF_6]^+$. Anal calcd for $C_{23}H_{17}Cl_3F_6N_7PPtRu$: C, 29.42; H, 1.83; N, 10.44. Found. C, 29.27; H, 1.90; N, 10.17

2,3-Bis(2-pyridyl)pyrazine(4,4′,4″-Tri-*tert*-Butyl-2,2′:6′,2″-terpyridine)(trichloro)ruthenium(II)platinum(II) hexaflorophosphate (Ru-Pt-5)

Ru-Pt-5 was prepared in the same way as **Ru-Pt-1** using **Ru5** (183.47 mg, 0.2 mmol) in the place of **Ru1**. A blue product was obtained. Yield 63.8 % (151.00 mg), FAB (nitrobenzyl alcohol matrix), *m/z*: 1038.14, $[M - PF_6]^+$. Anal calcd for $C_{41}H_{45}Cl_3F_6N_7PPtRu.3.5H_2O$: C, 39.51; H, 4.21; N, 7.87. Found. C, 39.34; H, 4.00; N, 7.57

2,3-Bis(2-pyridyl)pyrazine(4′-(4-Methylphenyl)-2,2′:6′,2″-terpyridine)(trichloro)ruthenium(II)platinum(II) hexaflorophosphate (Ru-Pt-6)

Ru-Pt-6 was prepared in the same way as **Ru-Pt-1** using **Ru6** (167.83 mg, 0.2 mmol) in the place of **Ru1**. A blue product was obtained. Yield 68.1 % (150.52 mg), FAB (nitrobenzyl alcohol matrix), *m/z*: 960.05, $[M - PF_6]^+$. Anal calcd for $C_{36}H_{27}Cl_3F_6N_7PPtRu.3.5H_2O$: C, 37.01; H, 2.93; N, 8.39. Found. C, 37.43; H, 2.44; N, 8.03

2,3-Bis(2-pyridyl)pyrazine(4′-(4-Chlorophenyl)-2, 2′:6′, 2″-terpyridine)(trichloro) ruthenium(II)platinum(II) hexaflorophosphate(Ru-Pt-7)

Ru-Pt-7 was prepared in the same way as **Ru-Pt-1** using **Ru7** (171.91 mg, 0.2 mmol) in the place of **Ru1**. A blue product was obtained. Yield 59.2 % (133.26 mg), FAB (nitrobenzyl

alcohol matrix), *m/z*: 979.95, $[M - PF_6]^+$. Anal calcd for $C_{35}H_{24}Cl_4F_6N_7PPtRu.3.5H_2O$: C, 35.37; H, 2.63; N, 8.25. Found. C, 35.01; H, 2.50; N, 8.44

2,3-Bis(2-pyridyl)pyrazine(*p*-cymene)(trichloro)ruthenium(II)platinum(II) tetrafloroborate(Ru-Pt-8)

Ru-Pt-8 was prepared in the same way as **Ru-Pt-1** using **Ru8** (117.55 mg, 0.2 mmol) in the place of **Ru1**. A blue product was obtained. Yield 70.1 % (119.70 mg), FAB (nitrobenzyl alcohol matrix), *m/z*: 770.99, $[M - BF_4]^+$. Anal calcd for $C_{24}H_{24}BCl_3F_6N_4PtRu$: C, 33.60; H, 2.82; N, 6.53. Found. C, 33.25; H, 2.84; N, 6.16

9.2 Building block synthesis

The supramolecular mixed metal-ligand complexes were prepared in good yields using the building block approach. The method allows for the construction of the desired molecule by first binding the terminal ligand, TL, (TL = **tpy**, **m-ph-tpy**, **Cl-ph-tpy** or **t-tpy**) to the Ru metal centre. The resultant complex is then attached to a bridging ligand, BL, (BL = **dpp**, **dpq**, **mdpq** or **bpm**). This is then followed by column chromatography to remove minor unwanted Ru bimetallic impurity. Finally the Pt(II) chloride is then attached to the complexes to form the hetero-bimetallic complexes. The TOF mass spectra of the monometallic and bi-metallic complexes produced are consistent with the molecular ion and loss of PF_6^- counter ion (BF_4^- for **Ru-Pt-8**). The elemental analysis was consistent with their respective formulations. NMR measurements could not be applied in the characterisation due to the isomeric nature of the bulky complexes. The building block synthesis is illustrated in scheme 9.1 using **Ru-Pt-3**.

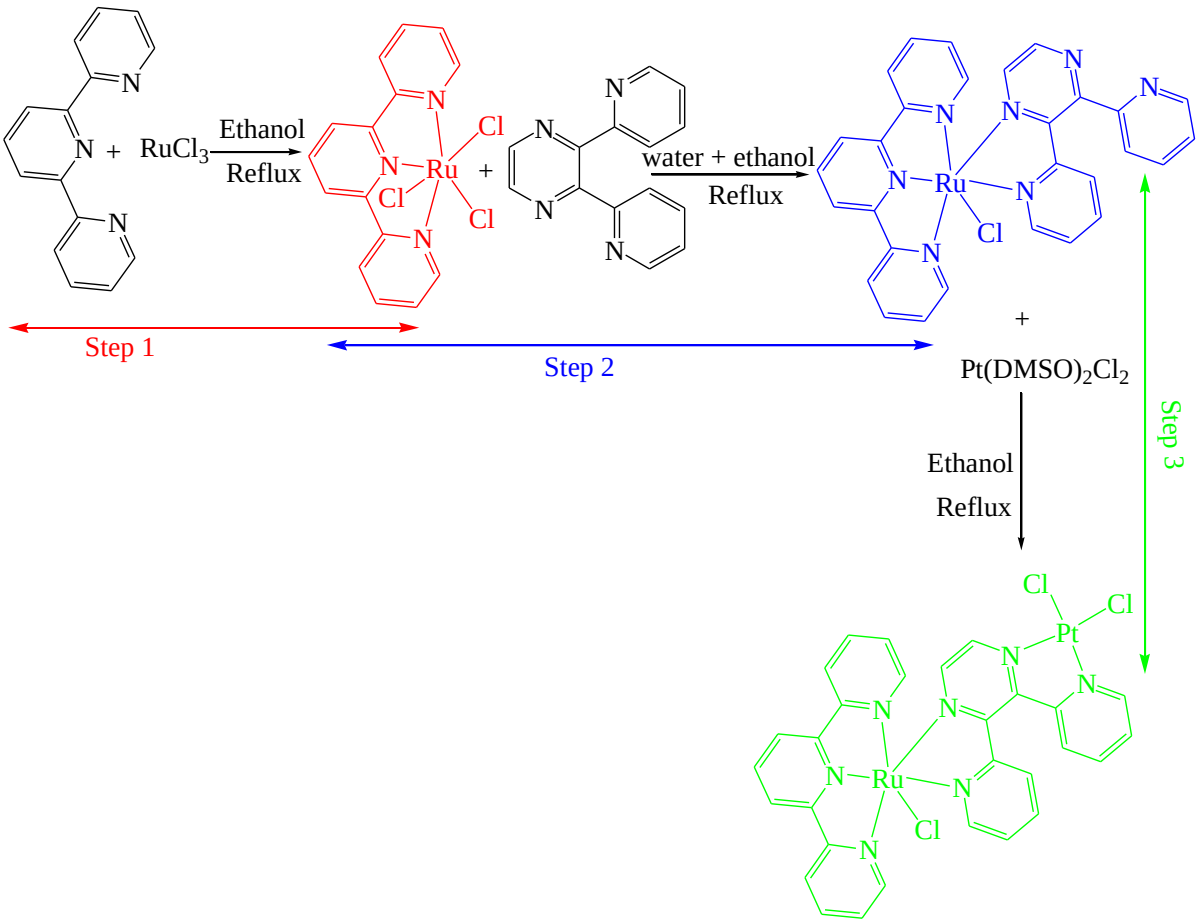

Red = First precursor, Blue = Second precursor, Green = Final complex

Scheme 9. 1 Illustration of the building block approach synthetic method using **Ru-Pt-3**

9.3 Future work

It will be interesting to investigate the rate of substitution from the **Ru-Pt** complexes to get insight on competitive reactivity and determine to what extent bridging ligands (Figure 9.1) and terminal ligands (Figure 9.2) affect the rate at which the chloride ligands are substituted from the Pt and Ru metal centres respectively. It is interesting to determine to what extent increasing the π-ligand surface around the Ru metal centre raises the rate of substitution from the R(II) metal centre relative to the Pt(II) metal centre. More importantly, due to the potential of these complexes to be applied in cancer treatment, understanding their reactivity with S-donor ligands which mimics S-biomolecules will help in understanding their interaction when placed in biological systems.

9.4 References

[1] M. J. Clarke, *Coordination Chemistry Reviews* **2002**, *232*, 69-93.

[2] R. L. Williams, H. N. Toft, B. Winkel, K. J. Brewer, *Inorganic Chemistry* **2003**, *42*, 4394-4400.

[3] M. Milkevitch, H. Storrie, E. Brauns, K. J. Brewer, B. W. Shirley, *Inorganic Chemistry* **1997**, *36*, 4534-4538.

[4] K. Kalyanasundaram, *Coordination Chemistry Reviews* **1982**, *46*, 159-244.

[5] M. J. Clarke, *Coordination Chemistry Reviews* **2002**, *232*, 69-93.

[6] B. T. Farrer, H. H. Thorp, *Inorganic Chemistry* **2000**, *39*, 44-49.

[7] K. K. Patel, E. A. Plummer, M. Darwish, A. Rodger, M. J. Hannon, *Journal of Inorganic Biochemistry* **2002**, *91*, 220-229.

[8] C.-W. Jiang, H. Chao, H. Li, L.-N. Ji, *Journal of Inorganic Biochemistry* **2003**, *93*, 247-255.

[9] Y. Liu, R. Hammitt, D. A. Lutterman, R. P. Thummel, C. Turro, *Inorganic Chemistry* **2007**, *46*, 6011-6021.

[10] N. Grover, N. Gupta, P. Singh, H. H. Thorp, *Inorganic Chemistry* **1992**, *31*, 2014-2020.

[11] A. Jain, B. S. J. Winkel, K. J. Brewer, *Journal of Inorganic Biochemistry* **2007**, *101*, 1525-1528.

[12] M. Milkevitch, E. Brauns, K. J. Brewer, *Inorganic Chemistry* **1996**, *35*, 1737-1739.

[13] A. Jain, J. Wang, E. R. Mashack, B. S. J. Winkel, K. J. Brewer, *Inorganic Chemistry* **2009**, *48*, 9077-9084.

[14] C.-W. Jiang, H. Chao, X.-L. Hong, H. Li, W.-J. Mei, L.-N. Ji, *Inorganic Chemistry Communications* **2003**, *6*, 773-775.

[15] M. Sommovigo, G. Denti, S. Serroni, S. Campagna, C. Mingazzini, C. Mariotti, A. Juris, *Inorganic Chemistry* **2001**, *40*, 3318-3323.

[16] S. T. Sullivan, A. Ciccarese, F. P. Fanizzi, L. G. Marzilli, *Journal of the American Chemical Society* **2001**, *123*, 9345-9355.

[17] V. W.-W. Yam, V. W.-M. Lee, K.-K. Cheung, *Organometallics* **1997**, *16*, 2833-2841.

[18] H. Blaschko, P. J. Friedman, R. Hawes, K. Nilsson, *The Journal of Physiology* **1959**, *145*, 384-404.

[19] B. P. Sullivan, J. M. Calvert, T. J. Meyer, *Inorganic Chemistry* **1980**, *19*, 1404-1407.

9.5 Supporting information

Included in the supplementary information are sample NMR spectra, mass spectra, and elemental analysis spectra for the synthesised compounds.

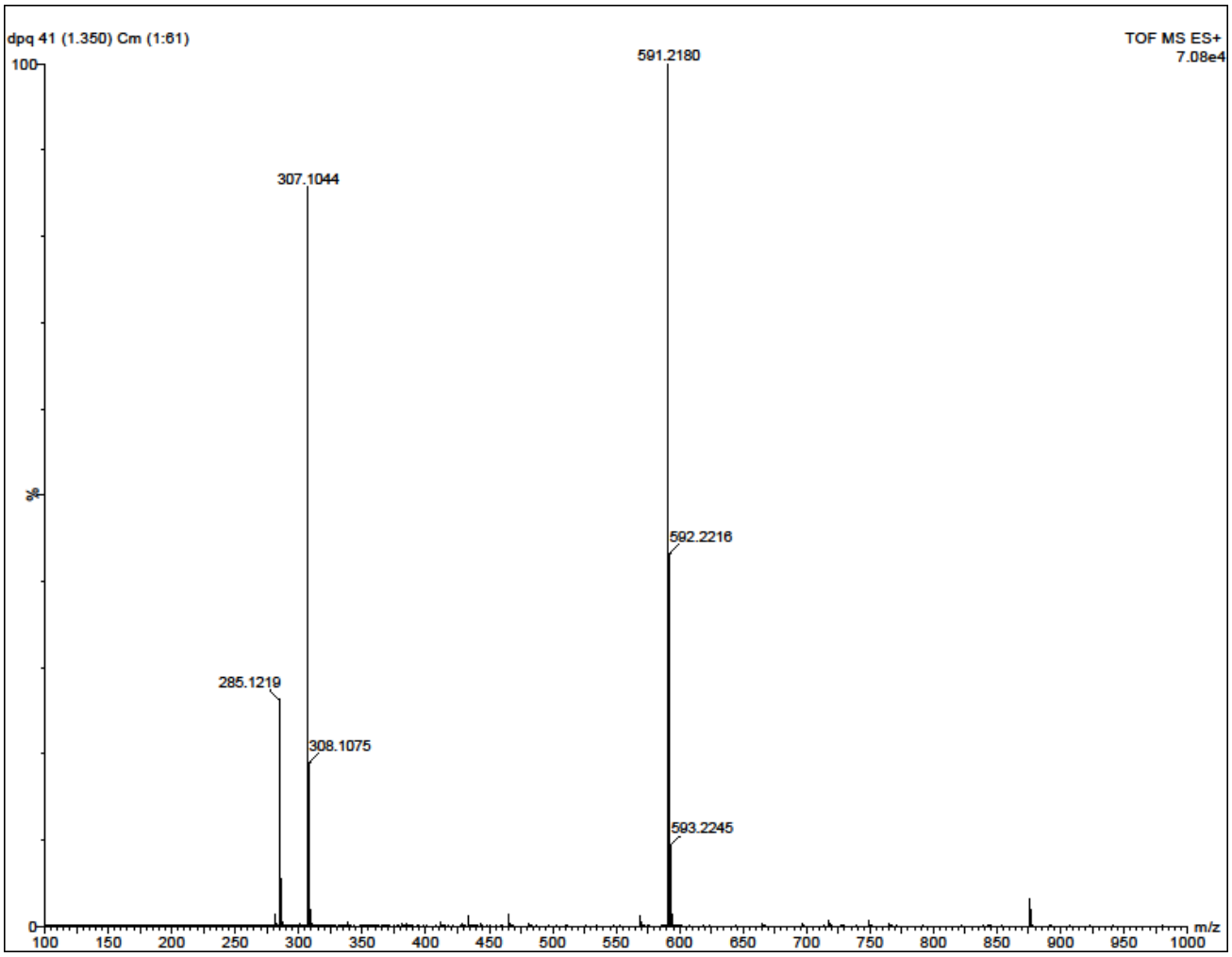

Figure SI 1 TOF mass spectrum for **dpq** ligand

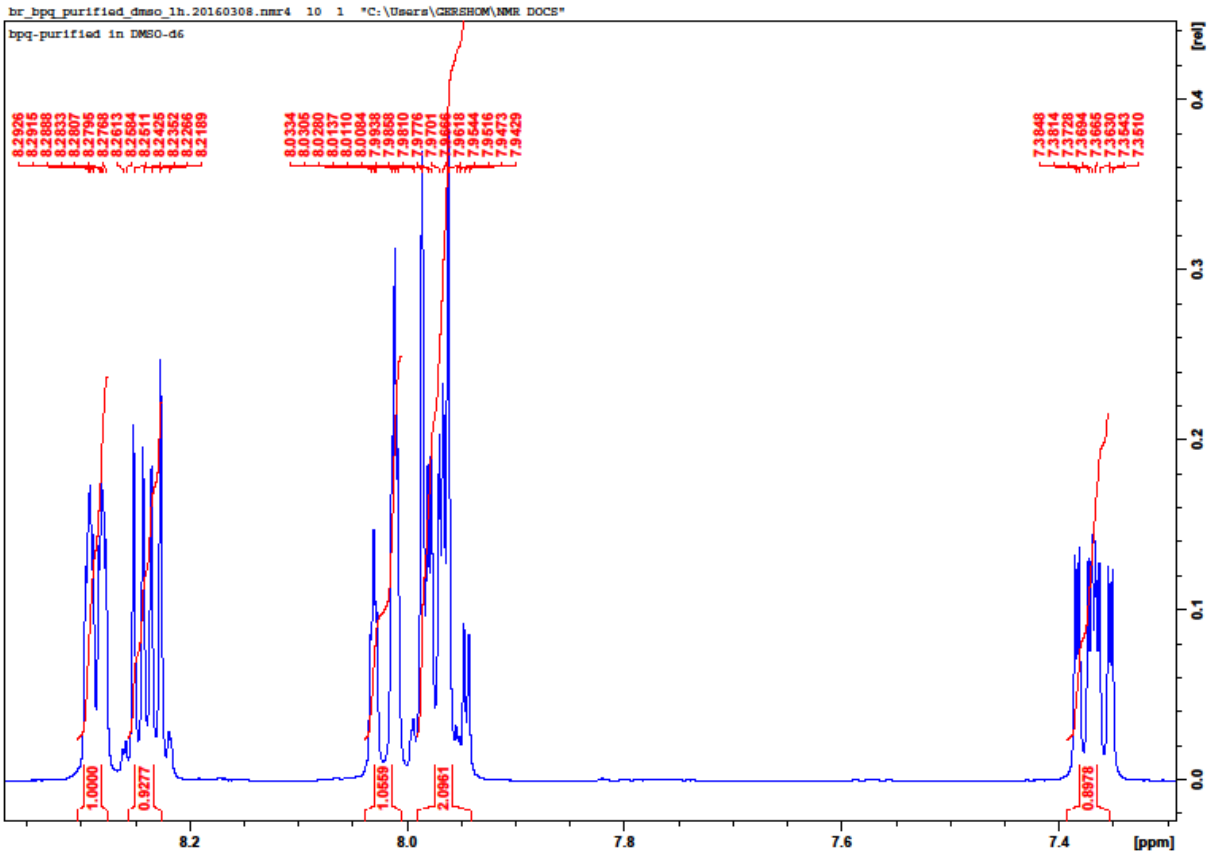

Figure SI 2 ^{1}H NMR spectrum for **dpq** ligand

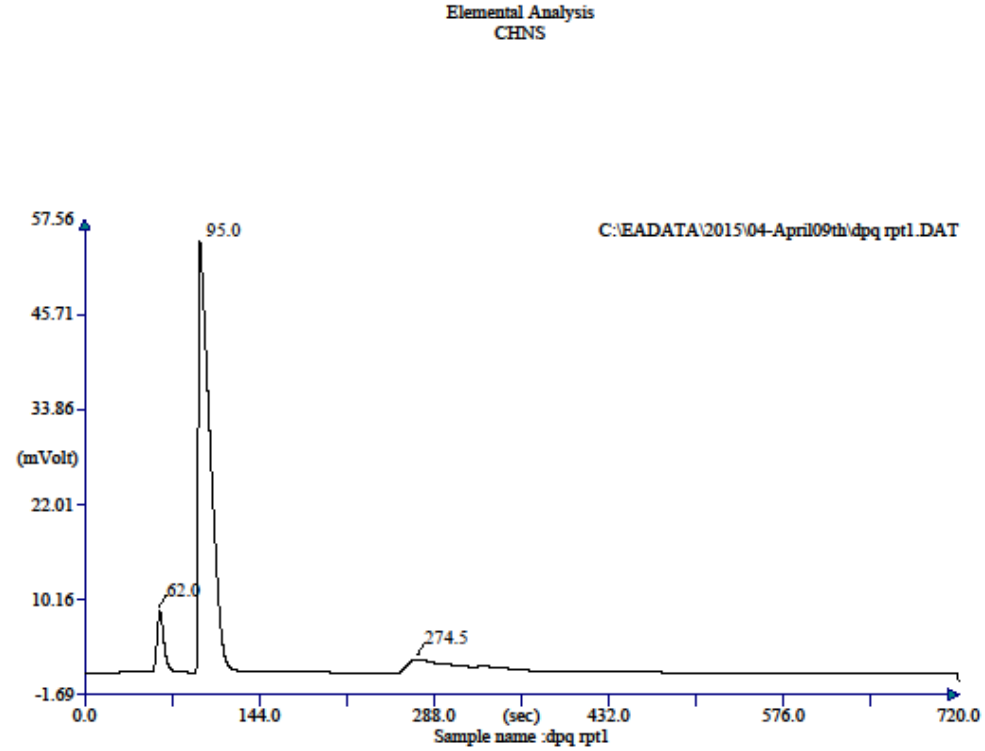

Retention Time (min)	Element Name	Element %
1.033	Nitrogen	8.394
1.583	Carbon	38.186
4.575	Hydrogen	2.269
		48.849

Warning Chromatogram has been subjected to manual inte

Figure SI 3 CHN elemental analysis spectrum for **dpq** ligand

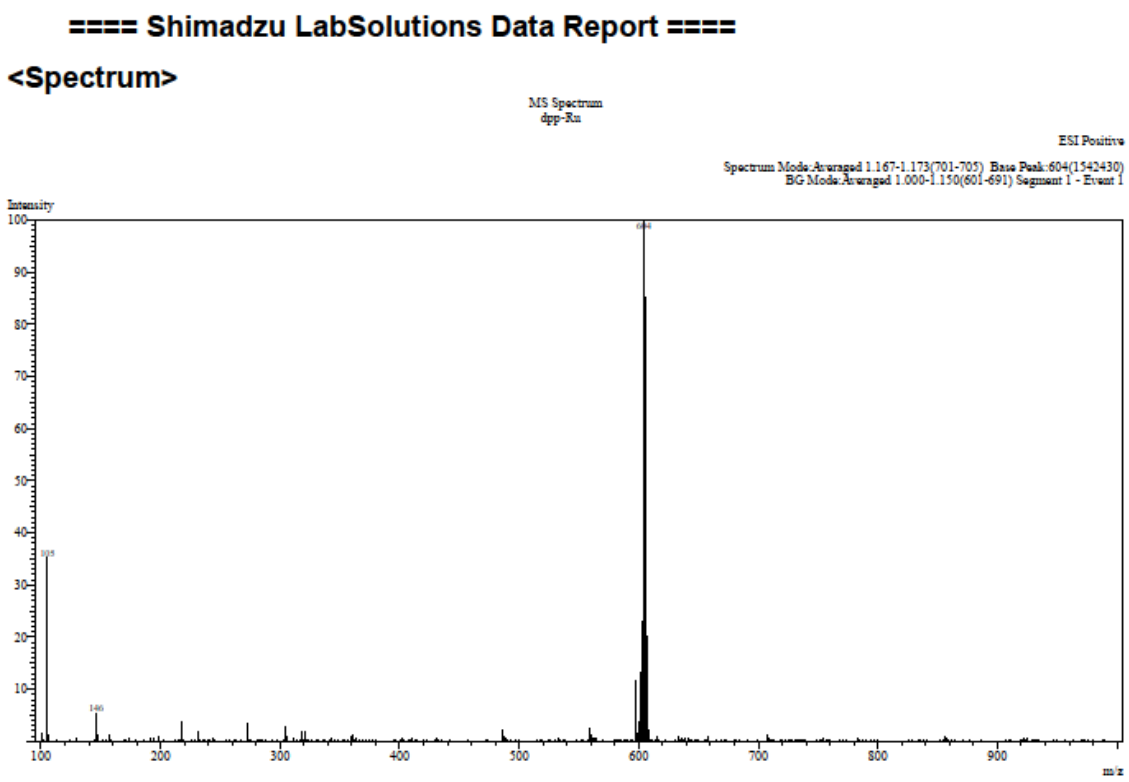

Figure SI 4 LC Mass spectrum for **Ru1**

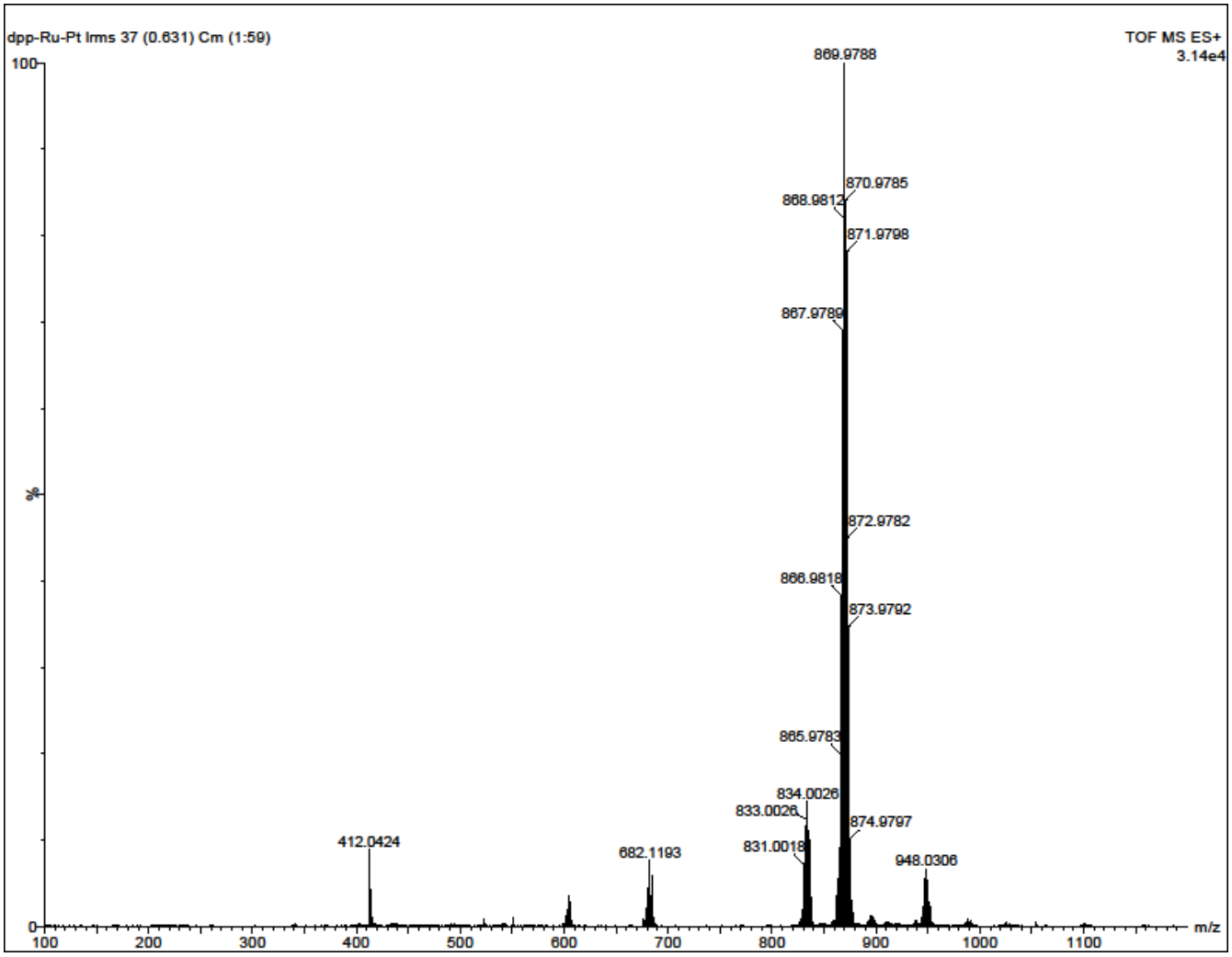

Figure SI 5 TOF Mass spectrum for **Ru-Pt-1**

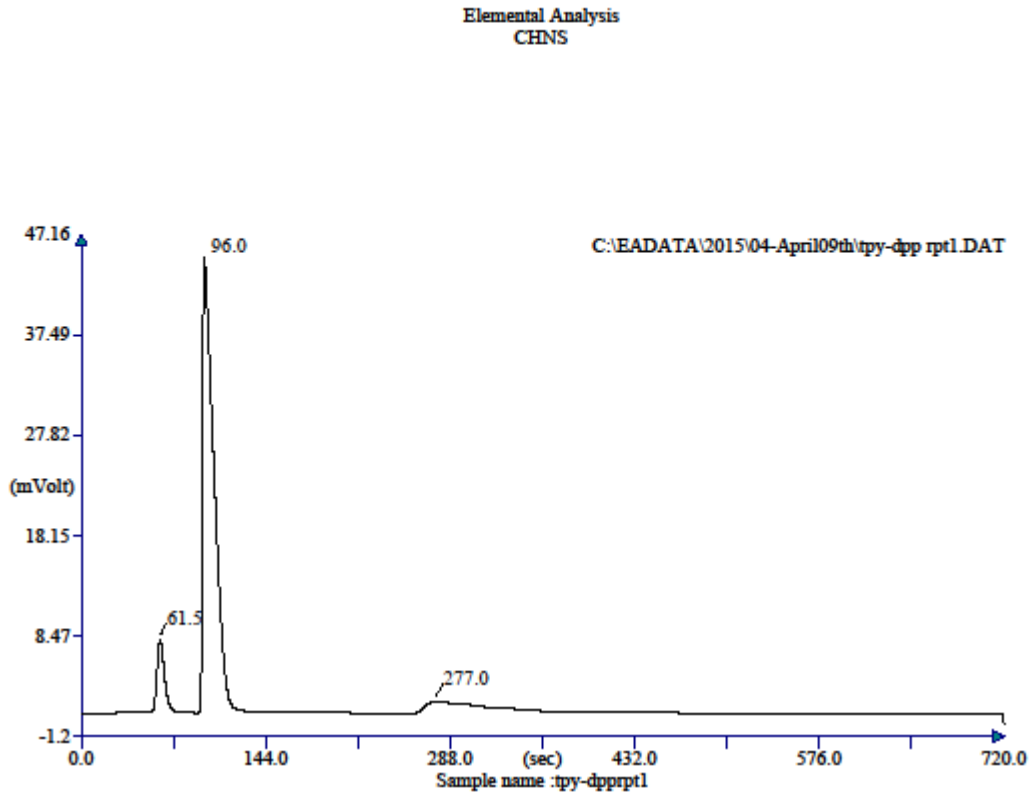

Retention Time (min)	Element Name	Element %
1.025	Nitrogen	9.206
1.600	Carbon	34.216
4.617	Hydrogen	2.158
		45.580

Warning Chromatogram has been subjected to manual inte

Figure SI 6 CHN elemental analysis spectrum for **Ru-Pt-1**

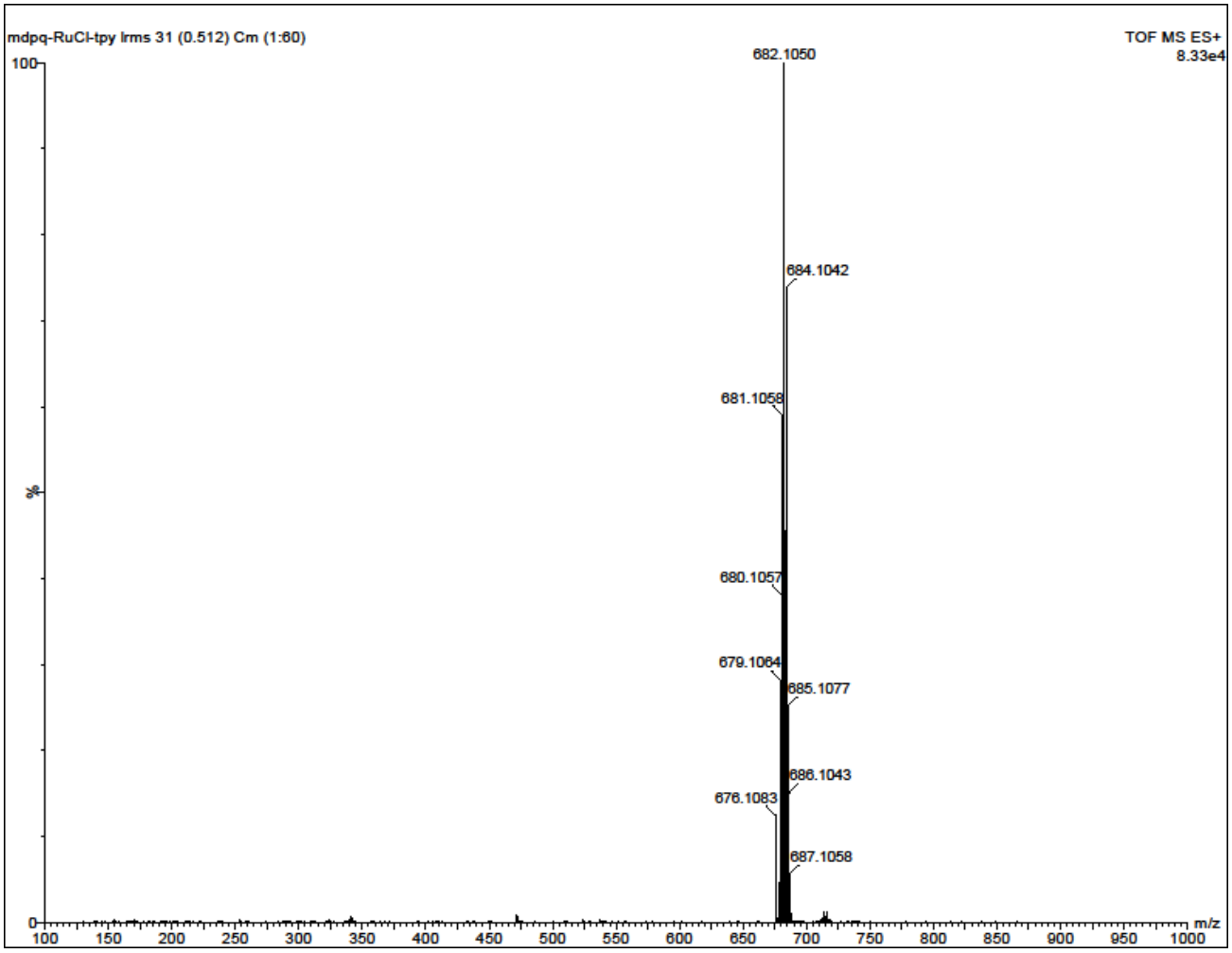

Figure SI 7 TOF Mass spectrum for **Ru3**

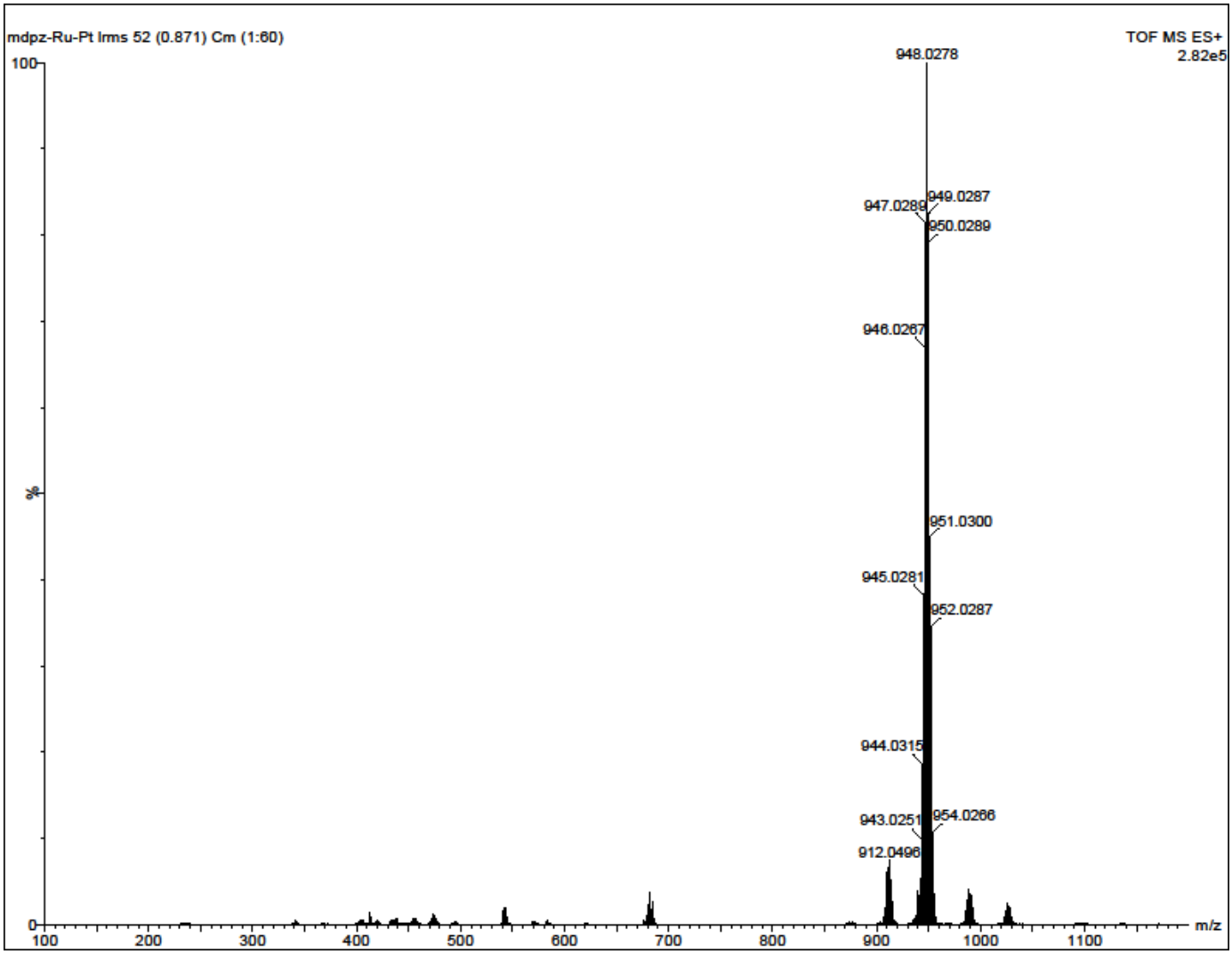

Figure SI 8 TOF Mass spectrum for **Ru-Pt-3**

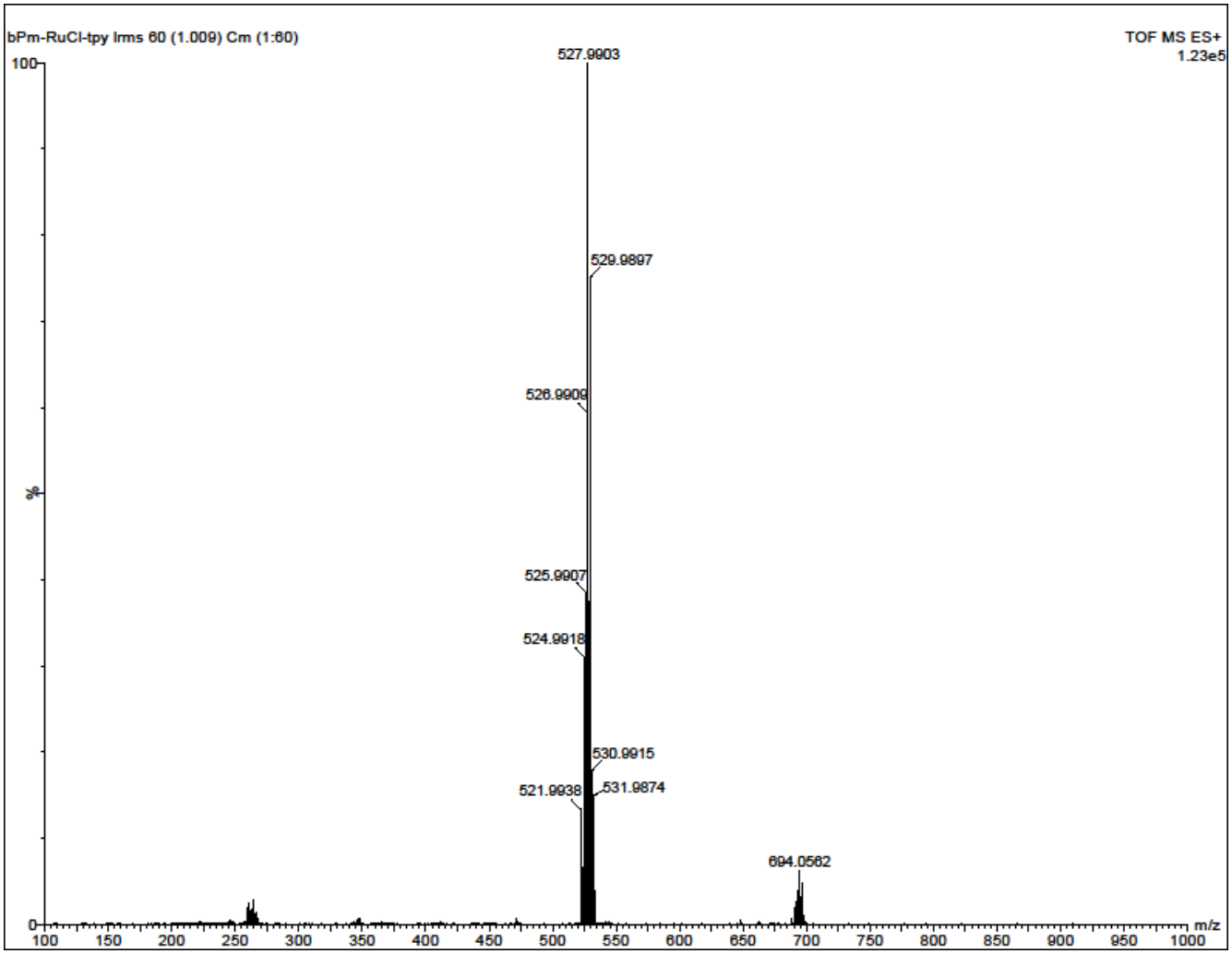

Figure SI 9 TOF Mass spectrum for **Ru4**

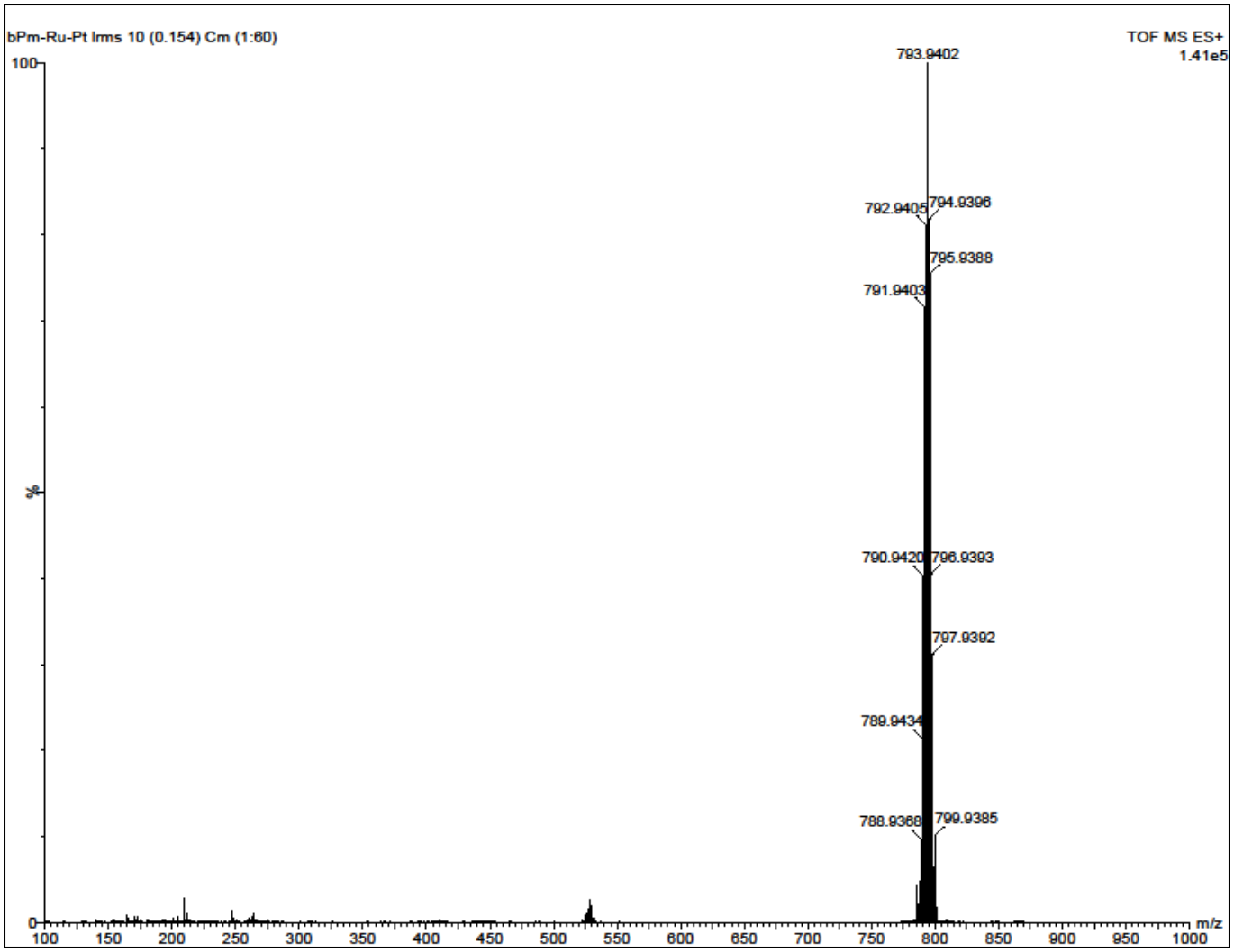

Figure SI 10 TOF Mass spectrum for **Ru-Pt-4**

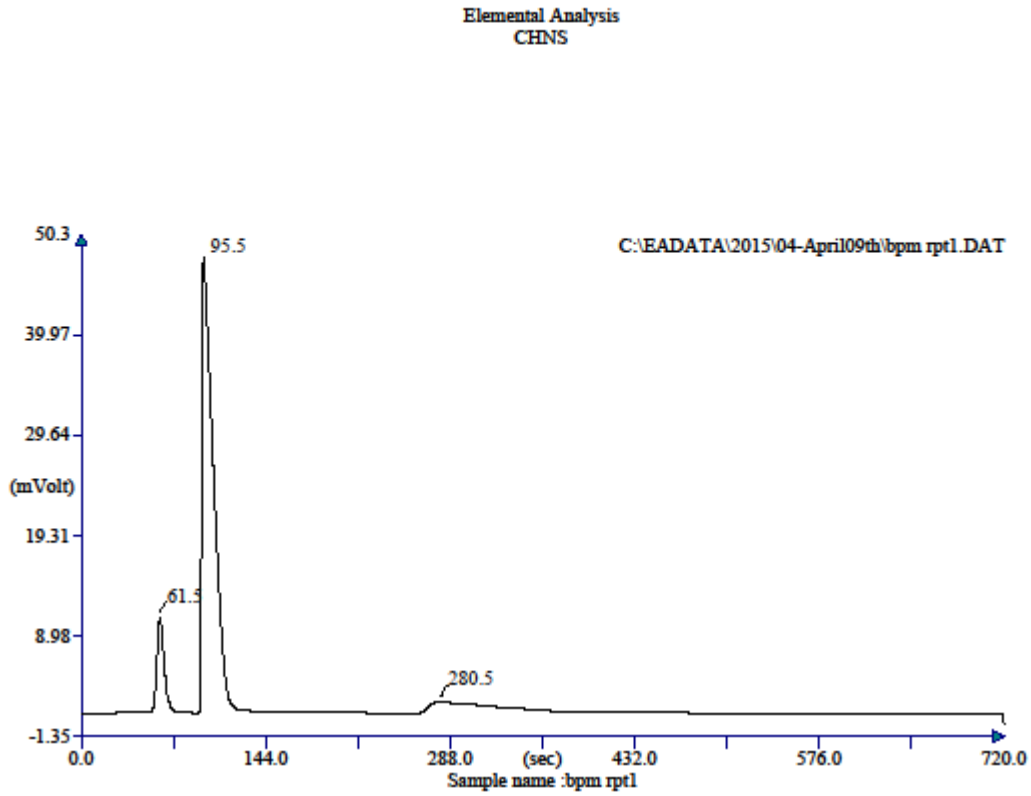

Retention Time (min)	Element Name	Element %
1.025	Nitrogen	10.169
1.592	Carbon	29.271
4.675	Hydrogen	1.900
		41.339

Warning Chromatogram has been subjected to manual inte

Figure SI 11 CHN elemental analysis spectrum for **Ru-Pt-4**

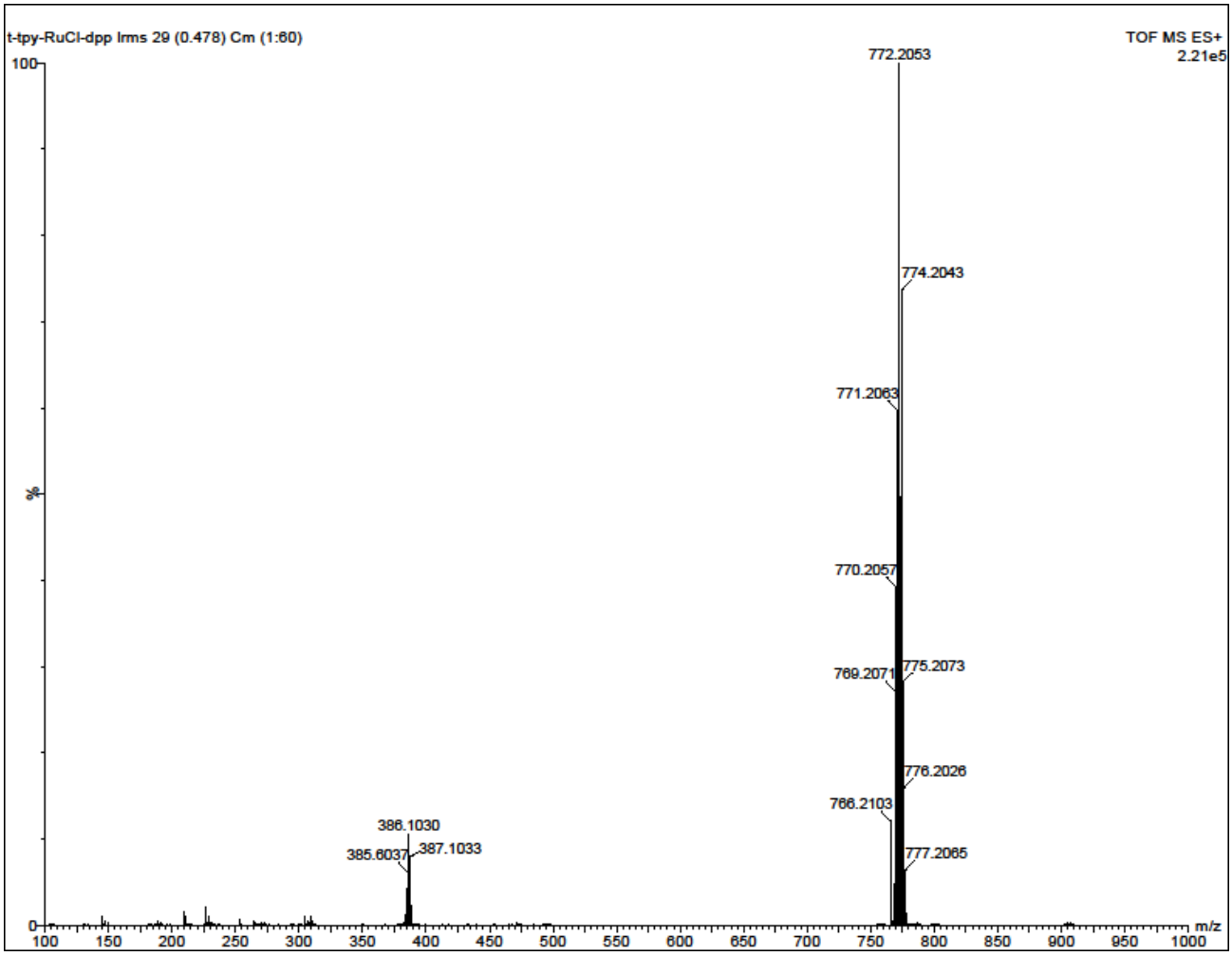

Figure SI 12 TOF Mass spectrum for **Ru5**

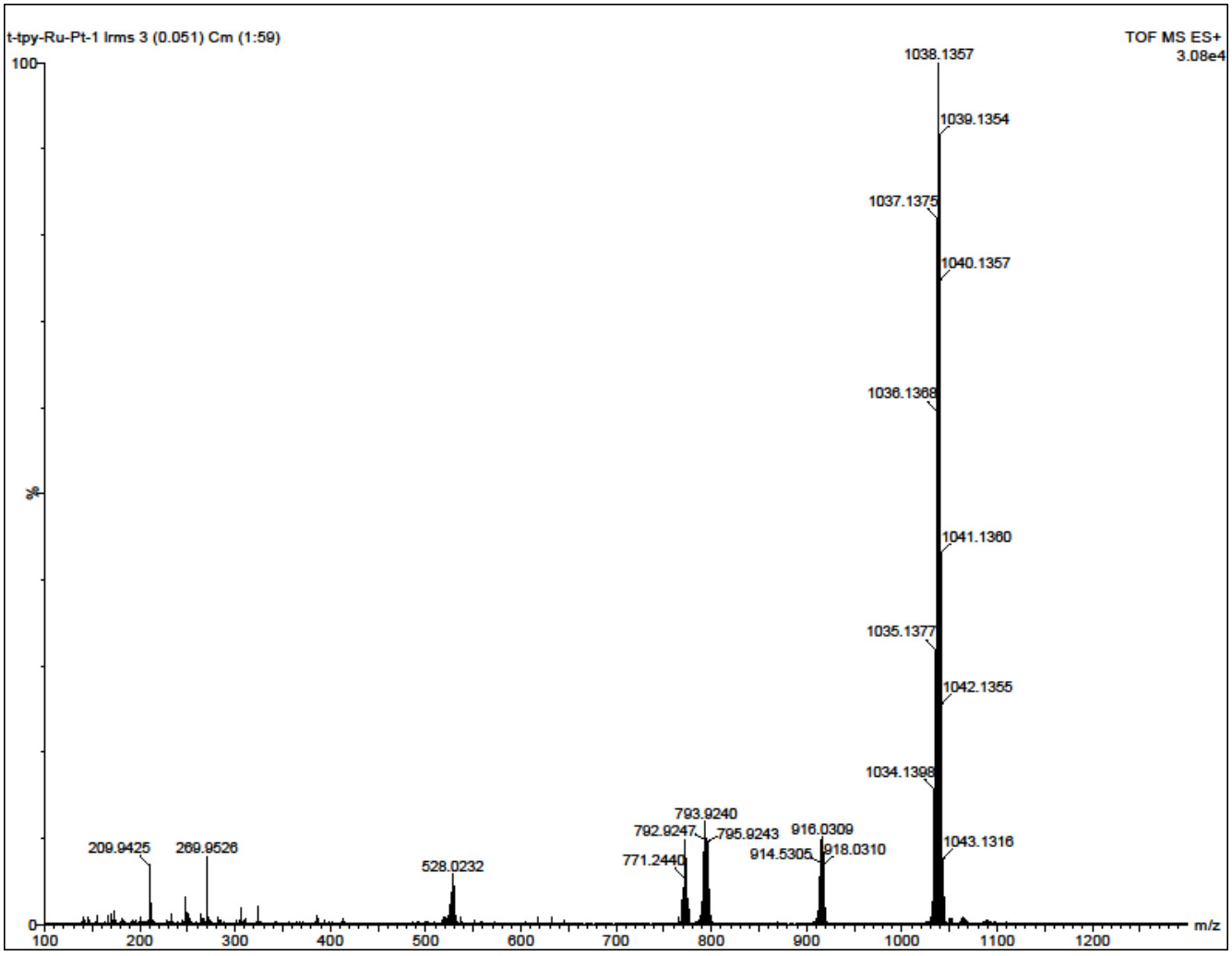

Figure SI 13 TOF Mass spectrum for **Ru-Pt-5**

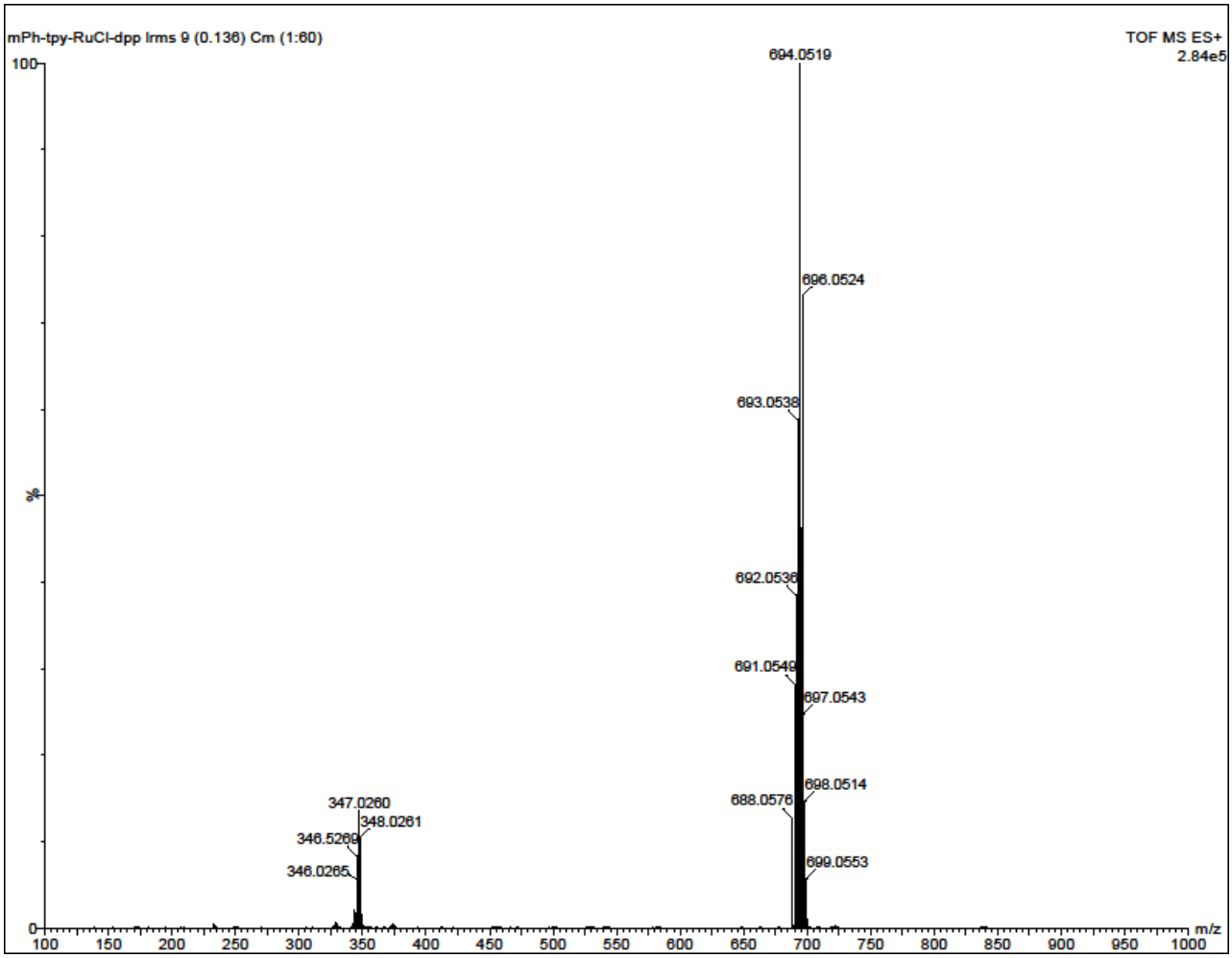

Figure SI 14 TOF Mass spectrum for **Ru6**

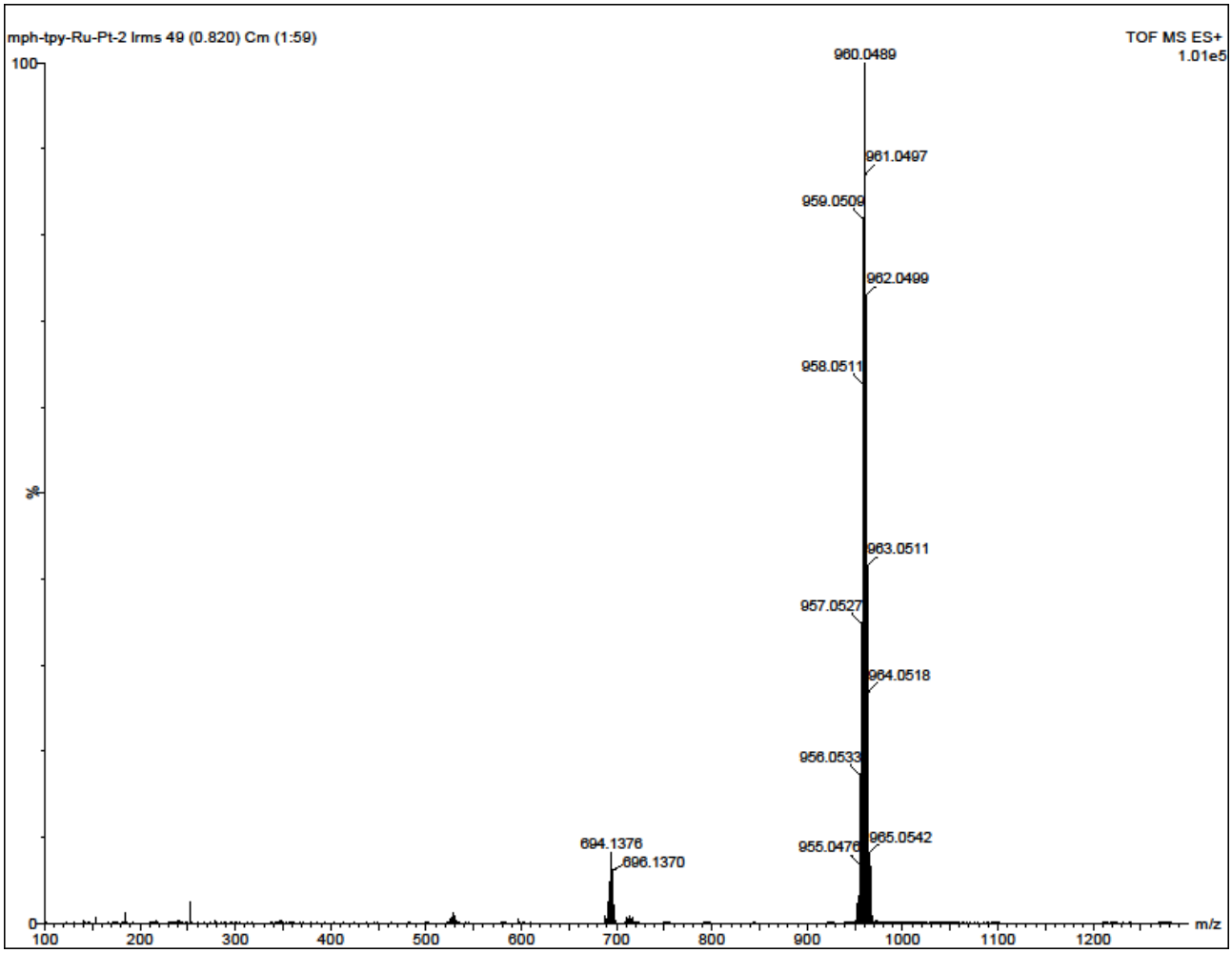

Figure SI 15 TOF Mass spectrum for **Ru-Pt-6**

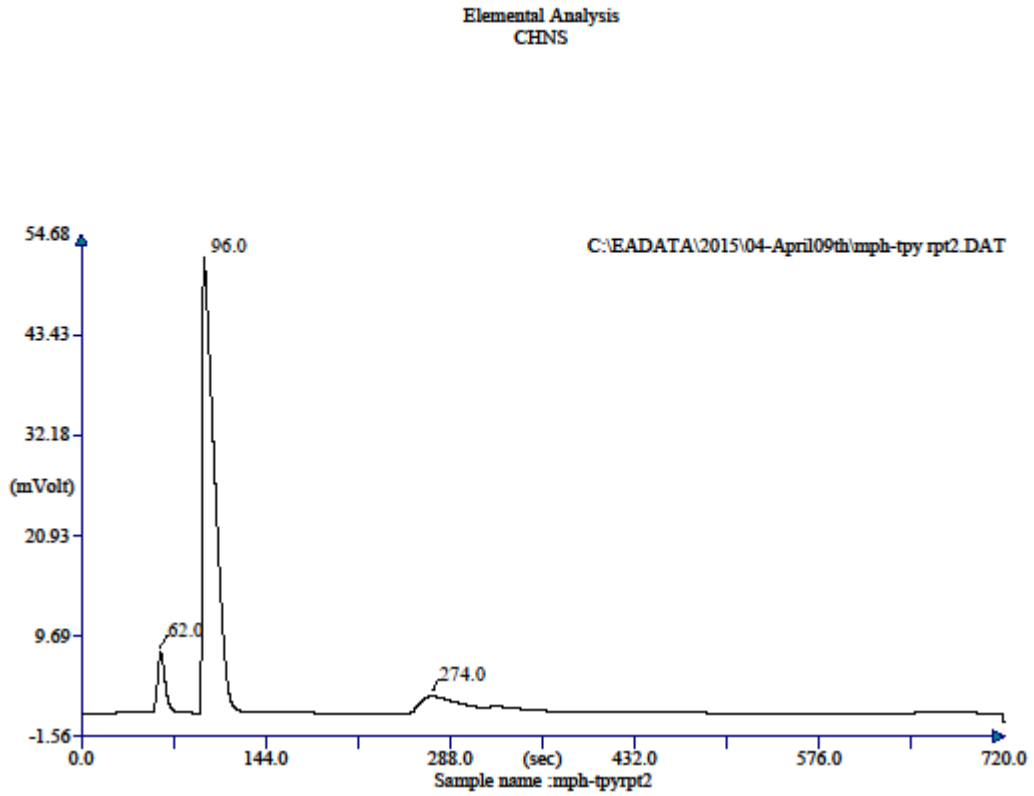

Retention Time (min)	Element Name	Element %
1.033	Nitrogen	8.034
1.600	Carbon	37.430
4.567	Hydrogen	2.438
		47.902

Warning Chromatogram has been subjected to manual inte

Figure SI 16 CHN elemental analysis spectrum for **Ru-Pt-6**

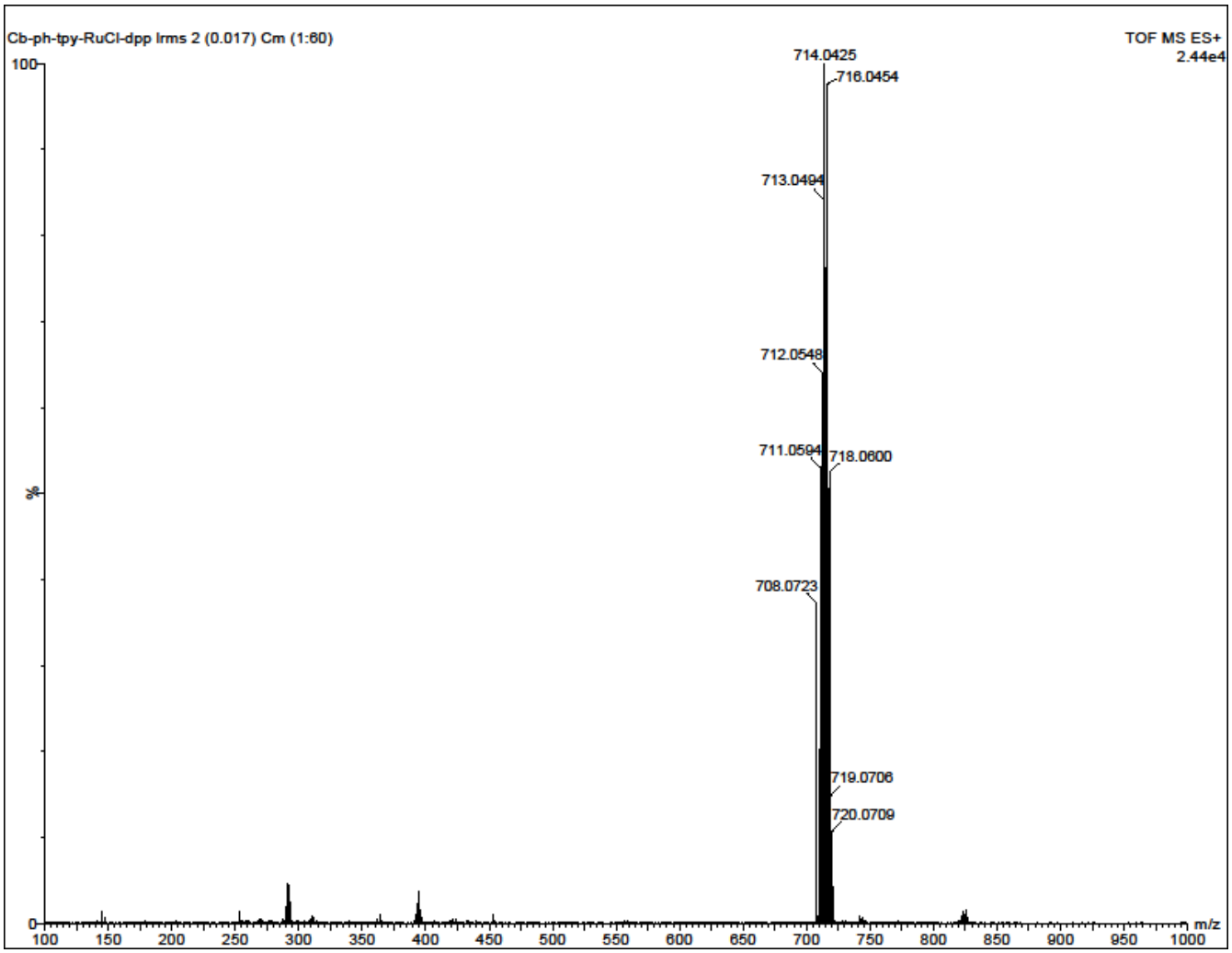

Figure SI 17 TOF Mass spectrum for **Ru7**

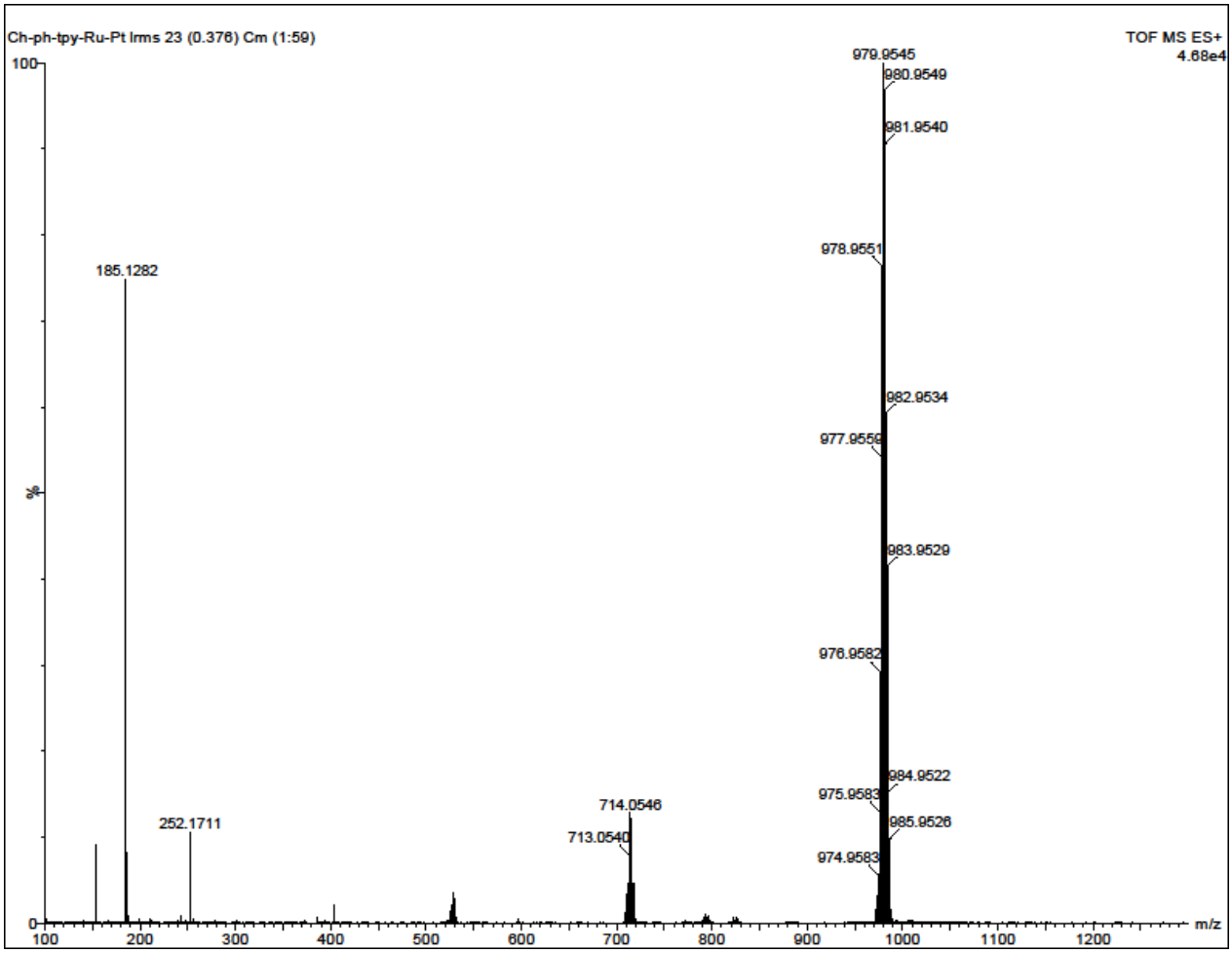

Figure SI 18 TOF Mass spectrum for **Ru-Pt-7**

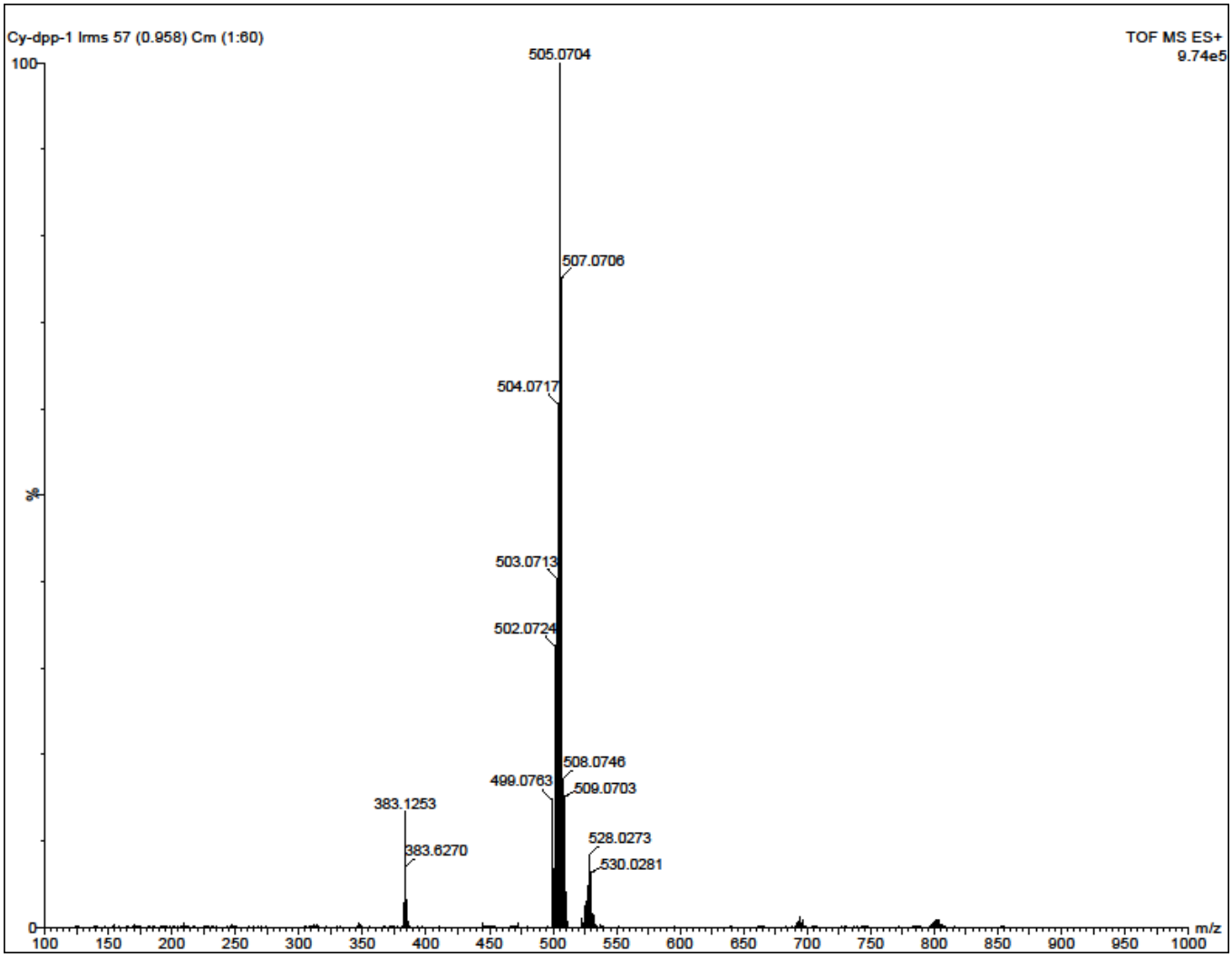

Figure SI 19 TOF Mass spectrum for **Ru8**

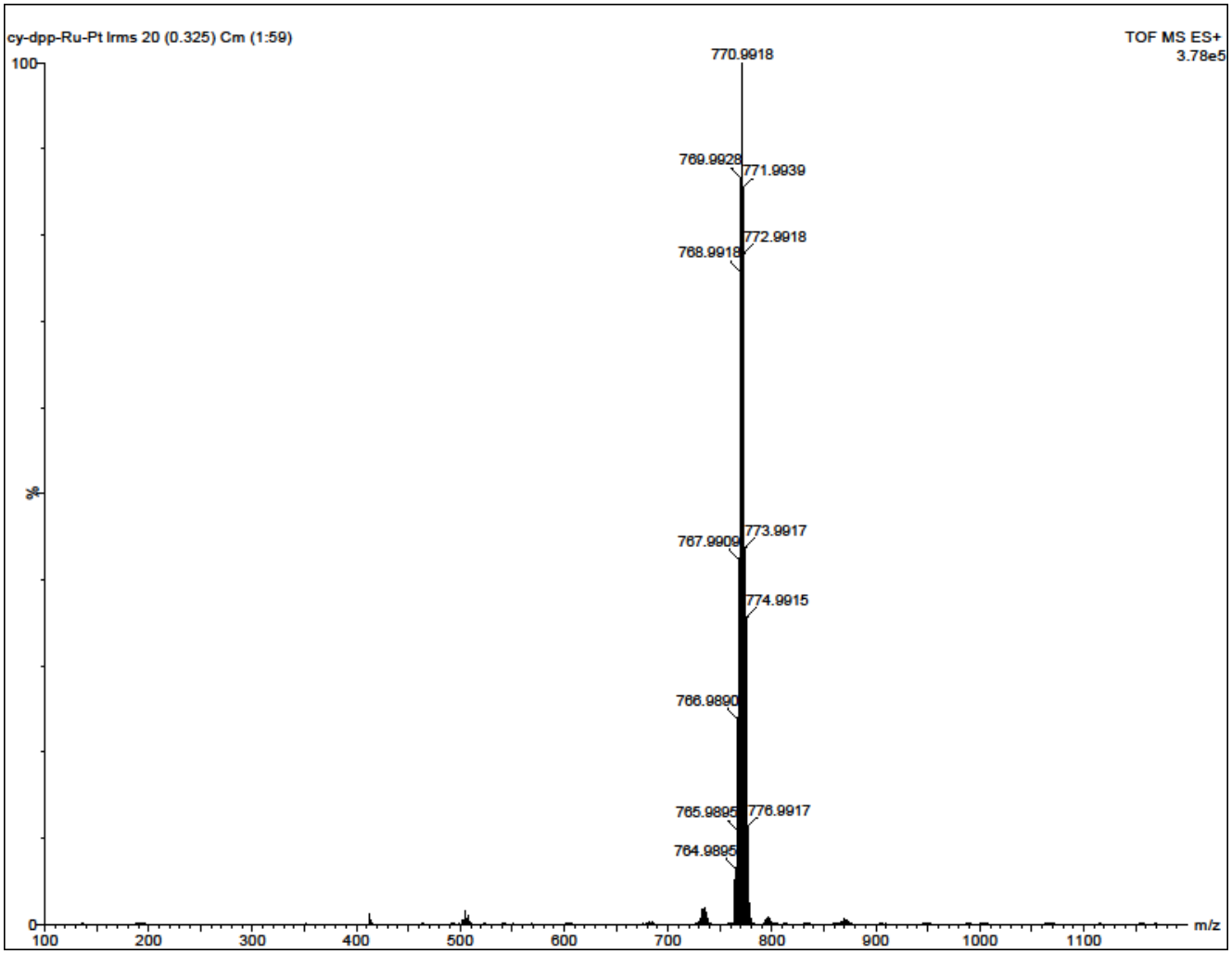

Figure SI 20 TOF Mass spectrum for **Ru-Pt-8**

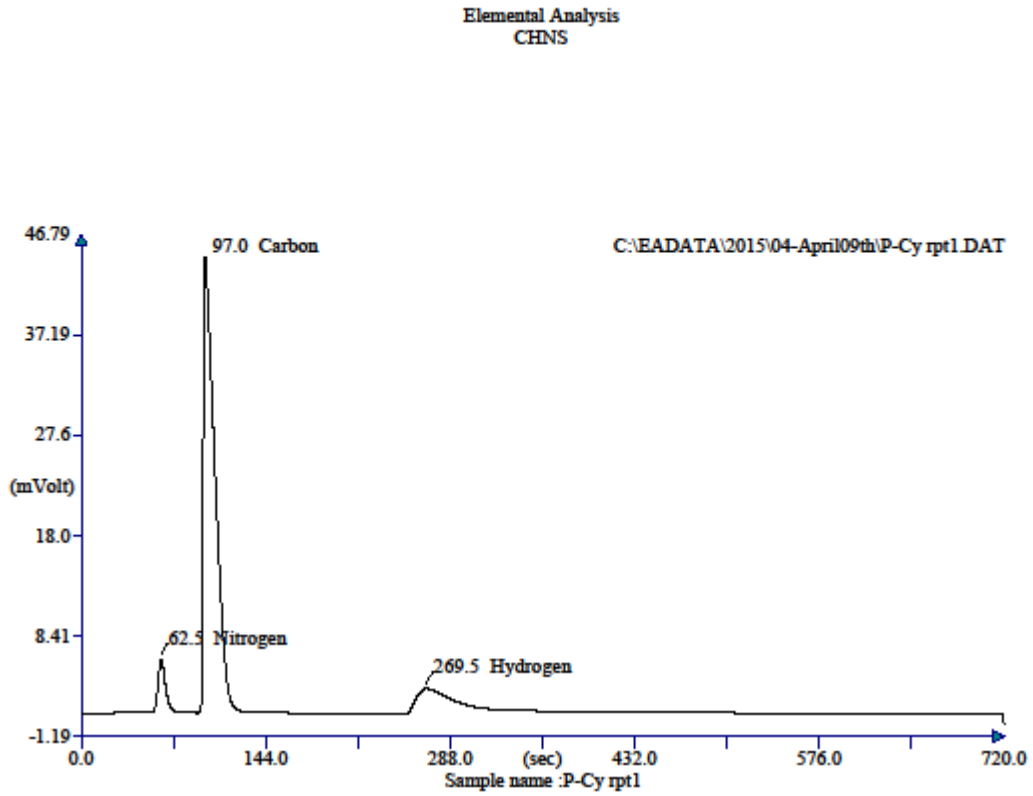

Retention Time (min)	Element Name	Element %
1.042	Nitrogen	6.167
1.617	Carbon	33.248
4.492	Hydrogen	2.835
		42.250

Figure SI 21 CHN elemental analysis spectrum for **Ru-Pt-8**